The structural performance of GFRP-reinforced seawater sea-sand fiber reinforced concrete culverts

by

Amirhesam Mashayekhi

M.Sc.

For the fulfilment of the requirement for the degree of

Doctor of Philosophy

UniSA STEM



University of South Australia

March 2025

Contents

Contents ..... **ii**
List of Figures ..... **viii**
List of Tables ..... **xii**
Notations ..... **xiii**
Publications ..... **xvii**
Abstract ..... **xviii**
Declaration ..... **xx**
Acknowledgments ..... **xxi**
1 Introduction and general overview **1**
1.1 Background of research 1
1.2 Research objectives and questions 3
1.3 Thesis outline 5
1.4 Research Approach 7
1.4.1 Fiber selection and hybridization 7
1.4.2 Mechanical properties testing 8
1.4.3 Concrete culvert 9
2 Literature review **15**
2.1 Introduction 15
2.2 Seawater sea-sand concrete (SWSSC) 15
2.3 Fresh and hardened characteristics of SWSSC 16
2.3.1 Fresh properties 17
2.3.2 Mechanical properties 17
2.4 Properties of FR-SWSSC 17
2.5 Structural behaviour of concrete culverts 19
2.5.1 Effect of Backfill and Installation methods 20
2.6 Application of FRP bars in SWSSC structures 21
2.7 Summary 23
3 Synergistic effects of fiber hybridization on the mechanical performance of seawater sea-sand concrete **33**
Abstract 33
Keywords 34
3.1 Introduction 34
3.2 Materials and experiments 37

3.2.1 Materials 37
3.2.2 Mixture proportions and test methods 38
3.3 Results and discussion 41
3.3.1 Fresh concrete properties 41
3.3.2 Compressive strength 44
3.3.3 Elastic modulus 49
3.3.4 Splitting tensile strength 50
3.3.5 Stress–strain results and discussions 52
3.3.6 Empirical constitutive model of FR-SWSS in compression 59
3.3.7 Synergistic impact of hybrid fiber 60
3.4 Conclusion 63
4 Synergistic effects of fiber hybridization on the fracture toughness of seawater sea-sand concrete 72
Abstract 72
Keywords 72
4.1 Introduction 73
4.2 Test Program 76
4.2.1 Materials 76
4.2.2 Mix design, and specimens preparation 77
4.2.3 Test specimens and methods 77
4.3 Results and discussion 78
4.3.1 Load–CMOD curves 79
4.3.2 Fracture energy (G_F) 82
4.3.3 Fracture toughness (K_{IC}) 85
4.3.4 Analysis of fracture behaviour 92
4.3.5 Post-crack performance evaluation using guidelines 95
4.4 Synergistic effects of fiber hybridization 98
4.5 Conclusion 100
5 Cyclic flexural performance of seawater sea-sand concrete reinforced with hybrid fibers 109
Abstract 109
Keywords 110
5.1 Introduction 110
5.2 Experimental work 114
5.2.1 Material properties 114
5.2.2 Mix proportions and test specimens 116
5.2.3 Cyclic flexural test setup and procedure 117

5.3 Results and discussions 119
5.3.1 Cyclic flexural behaviour of FR-SWSSC 119
5.3.2 Damage characteristics 136
5.4 Summary and conclusion 144
6 Shear performance of fibre reinforced seawater sea-sand concrete - fibre hybridization and synergy effects 158
Abstract 158
Keywords 158
6.1 Introduction 159
6.2 Experimental program 162
6.2.1 Materials 162
6.2.2 Specimen preparation and mix proportions 165
6.2.3 Shear strength test setup and specimen 167
6.2.4 Finite element method (FEM) 170
6.3 Test results and discussion 171
6.3.1 Evaluation of the modified JSCE-SF6 using finite element 171
6.3.2 Failure mode 178
6.3.3 Load–deflection curves 179
6.3.4 Shear strength and toughness 184
6.3.5 The synergy effect of fibers 187
6.4 Conclusion 189
7 Structural behaviour of small GFRP-reinforced seawater sea-sand fiber reinforced concrete culverts 201
Abstract 201
Keywords 202
7.1 Introduction 202
7.2 Experimental program 206
7.2.1 Material properties and mixture proportions 206
7.2.2 Test specimens and preparation 208
7.3 Test results and observations 211
7.3.1 Behaviour of SWSS concrete 211
7.3.2 Behaviour of GFRP-reinforced SWSS concrete culverts 212
7.4 Discussion 218
7.4.1 Group Ⅰ: Effect of mono and hybrid fibers 218
7.4.2 Group Ⅱ: Effect of compression reinforcement 224
7.4.3 Group Ⅲ: Effect of crown thickness 226

7.4.4 Group Ⅳ: Effect of haunches....227
7.4.5 Group Ⅴ: Effect of SWSS concrete strength....228
7.5 Shear capacity prediction models....230
7.5.1 Method-1: ACI 440.1R-15/RILEM TC-162....230
7.5.2 Method-2: AS 5100.5....231
7.5.3 Method-3: AS 1597.2-2013....232
7.5.4 Method-4: AASHTO LRFD 2020....233
7.5.5 Method-5: ACI 440.1R-15 punching shear strength....234
7.5.6 Comparison of the shear capacity prediction models....235
7.5.7 Proposed shear capacity prediction model....236
7.6 Summary and conclusion....237
8 Cyclic performance of GFRP-reinforced seawater sea-sand concrete culverts reinforced with synthetic fibers....245
Abstract....245
Keywords....246
8.1 Introduction....246
8.2 Experimental program....250
8.2.1 Raw materials....250
8.2.2 Mix design and specimen preparation....252
8.2.3 Test setup, instrumentation, and testing procedure....254
8.3 Results and discussion....257
8.3.1 Load-deflection behaviour under cyclic loading....257
8.3.2 Backbone curve....260
8.3.3 Failure mode and damage mechanism....264
8.3.4 Relative leg-opening....267
8.3.5 Damage evaluation....270
8.3.6 Energy dissipation....274
8.3.7 Hysteretic damping ratio....276
8.4 Prediction models for shear capacity....278
8.4.1 ACI 440.1R-15/RILEM TC-162....279
8.4.2 ACI 440.1R-15....280
8.4.3 AASHTO LRFD....280
8.4.4 AS 1597.2-2013....282
8.4.5 AS 5100.5....283
8.4.6 Assessing the accuracy of different shear capacity prediction models....283
8.5 Summary and conclusion....285
9 Conclusions and future research recommendations....295

9.1 Conclusions 295
9.2 Phase I: Synergistic effects of fiber hybridization on material characteristics 296
9.2.1 Study 1: Mechanical properties 296
9.2.2 Study 2: Fracture toughness 299
9.2.3 Study 3: Cyclic flexural performance 300
9.2.4 Study 4: Shear performance 302
9.3 Phase Ⅱ: Structural performance of GFRP-reinforced SWSSC culverts incorporating hybrid fibers 304
9.3.1 Study 5: Structural behaviour of small GFRP-reinforced FR-SWSSC culverts 304
9.3.2 Study 6: Cyclic performance of GFRP-reinforced FR-SWSSC culverts 307
9.4 Future research 309
Appendix A Supplementary Information for Chapter 7 312
A.1 Behaviour of SWSS concrete 312
A.1.1 Compressive stress-strain behaviour 312
A.1.2 Splitting tensile strength 314
A.1.3 Flexural strength 316
Appendix B Copyright permissions 320
B.1 Copyright permission for Chapter 3 320
B.2 Copyright permission for Chapter 4 321
B.3 Copyright permission for Chapter 5 322
B.4 Copyright permission for Chapter 7 323
B.5 Copyright permission for Chapter 8 324
Appendix C Statements of authorship 324

List of Figures

Figure 1-1 Thesis framework 11
Figure 3-1 SEM image, shape, and dimension of different types of fibers, a) PPS, b) PVA, c) BF, d) PPL, and e) TPPL 41
Figure 3-2 The values of slump for all the mono and hybrid mixtures 42
Figure 3-3 Air content results for all mixes 43
Figure 3-4 Compressive strength (fcm) results for all mixes 45
Figure 3-5 SEM images of the micro-fibers in SWSS concrete 46
Figure 3-6 SEM images of BF corrosion and the formation of calcium silicate ($CaSiO3$) in SWSS 47
Figure 3-7 Synergistic effects of PVA/BF hybridization in SWSS concrete 49
Figure 3-8 Elastic modulus (Ec) results for all mixes 50
Figure 3-9 Splitting tensile strength (fst) results for all mixes 52
Figure 3-10 Synergistic effects of PPL/PVA and TPPL/PVA hybridization in SWSS concrete 52
Figure 3-11 Typical stress-strain curves of FR-SWSS concrete under compression 53
Figure 3-12 Compressive toughness index (CTI) and residual strength ($fres$) results for all mixes 57
Figure 3-13 SEM images of the plain concrete mixtures (FWNS and SWSS) 58
Figure 3-14 Comparison between the experimental and proposed stress-strain curves. 62
Figure 3-15 Synergistic coefficients (SC) of the mechanical properties of the hybrid FR-SWSS. 62
Figure 3-16 The combined mechanical performance (CMP) of fiber reinforced SWSS (FR-SWSS). 63
Figure 4-1 Grading curves for NS and SS coarse aggregates. 78
Figure 4-2 Characterization of various fibers: shape, dimensions, and SEM images. 79
Figure 4-3 Schematic of the fracture toughness test setup. 79
Figure 4-4 Typical fracture toughness failure mode. 80
Figure 4-5 Load-CMOD curves of flexural strength test for different fiber types: (a) Mono-fibers, (b) Hybrid micro-fibers, (c) Hybrid micro- and macro-fibers. 81
Figure 4-6 Comparison of load reduction factor (LRF) values for different concrete mixes. 83
Figure 4-7 The SEM images of hybrid PPL/PVA and TPPL/PVA fibers. 83
Figure 4-8 Comparison of fracture energy for different concrete mixes. 84
Figure 4-9 Stress distribution of DKFM method. 86
Figure 4-10 The fracture toughness properties (initial and unstable) based on DKFM method. 89
Figure 4-11 The microstructure of plain concrete mixtures (FWNS and SWSS) using SEM images. 90
Figure 4-12 The cohesion toughness ($KICC$) parameter based on DKFM method. 91
Figure 4-13 Load-CMOD curves for various SWSSC mixes. 93
Figure 4-14 Schematic of the crack development process in hybrid FR-SWSSC. 94
Figure 4-15 Flexural behaviour of FRC: Nominal stress vs. CMOD. 96
Figure 4-16 The peak flexural strength of FR-SWSSC. 97
Figure 4-17 The post-peak residual flexural strength of FR-SWSSC. 98
Figure 4-18 Synergistic coefficients derived from fracture parameters of hybrid FR-SWSSC. 100
Figure 4-19 The combined mechanical performance (CMP) of FR-SWSSC. 100
Figure 5-1 SEM analysis of a) sea-sand and b) natural sand. 115

Figure 5-2 Cyclic flexural test setup. 119
Figure 5-3 Cyclic loading protocol. 121
Figure 5-4 Load-deflection curves of FR-SWSSC mixtures with different fiber reinforcements, (a) mono-fibers, (b) hybrid micro-fiber, and (c) hybrid macro/micro-fiber. 122
Figure 5-5 Backbone curves of load-deflection behaviour in FR-SWSSC with different fiber reinforcements: (a) mono-fiber, (b) hybrid micro-fiber, and (c) hybrid macro/micro-fiber. 123
Figure 5-6 Microstructure of SWSSC and FWNS using SEM images. 124
Figure 5-7 Microstructure of FR-SWSSC reinforced with micro-fibers using SEM images. 124
Figure 5-8 Microstructure of PPL/PVA and TPPL/PVA hybridization using SEM images. 125
Figure 5-9 Energy dissipation of FR-SWSSC mixtures per cycle and cumulative with varying fiber reinforcements: (a) mono-fibers, (b) hybrid micro-fibers, and (c) hybrid macro/micro-fibers. 126
Figure 5-10 Hysteretic damping ratio of FR-SWSSC mixtures per cycle with varying fiber reinforcements: (a) mono-fibers, (b) hybrid micro-fibers, and (c) hybrid macro/micro-fibers. 128
Figure 5-11 Monotonic and cyclic load-deflection behaviour of FR-SWSSC reinforced with PPL fibers and their hybridization with micro-fibers in flexural testing. 130
Figure 5-12 Monotonic and cyclic load-deflection behaviour of FR-SWSSC reinforced with TPPL fibers and their hybridization with micro-fibers in flexural testing. 131
Figure 5-13 Characterization of peak load and energy absorption capacity ($T600D$ and $T150D$) in typical backbone load-deflection behaviour. 132
Figure 5-14 Energy absorption parameters of FR-SWSSC mixtures from backbone curves. 133
Figure 5-15 Flexural strength, residual strength, and equivalent flexural strength of all mixtures. 134
Figure 5-16 Cyclic damage parameters. 137
Figure 5-17 Damage index (DI) of FR-SWSSC mixtures per cycle with varying fiber reinforcements: (a) mono-fibers, (b) hybrid micro-fibers, and (c) hybrid macro/micro-fibers. 140
Figure 5-18 Strength degradation ratio (SDR) of FR-SWSSC mixtures per cycle with varying fiber reinforcements: (a) mono-fibers, (b) hybrid micro-fibers, and (c) hybrid macro/micro-fibers. 141
Figure 5-19 Degree of reversibility (R) of FR-SWSSC mixtures per cycle with varying fiber reinforcements: (a) mono-fibers, (b) hybrid micro-fibers, and (c) hybrid macro/micro-fibers. 142
Figure 5-20 Heatmap of all investigated normalized parameters for different hybrid FR-SWSS mixes. 146
Figure 6-1 The sieve analysis of the aggregates. 163
Figure 6-2 Abrasion test of basalt fibers using mortar and pestle. 166
Figure 6-3 BF testing in NaOH solution using a magnetic stirrer and aggregate-shaped outcomes. 166
Figure 6-4 Typical concrete shear test methods: (a) FIB, (b) JSCE-SF6, (c) modified JSCE-G553, (d) ASTM D5607, (e) Z-type pushoff specimen, and (f) L-type specimen. 168
Figure 6-5 Modified JSCE-SF6 concrete shear test setup. 171
Figure 6-6 Stress distribution in various states. 174

Figure 6-7 Comparison of FEM modeling and experimental results for the FWNS concrete specimen at peak load using the proposed shear test method. 175
Figure 6-8 Stress distribution of FWNS concrete specimen in the modified JSCE-SF6 shear test method: (a) low friction coefficient, (b) high friction coefficient. 176
Figure 6-9 The effect of support location on stress distribution in FWNS concrete specimen using the modified JSCE-SF6 shear test method. 176
Figure 6-10 Stress distribution of FWNS concrete specimen using the modified JSCE-SF6 shear test method: (a) with released upward movement, (b) with fixed upward movement. 177
Figure 6-11 Typical shear failure mode of the specimens: a) plain SWSS concrete, b) PPL reinforced specimen. 179
Figure 6-12 The typical stress-deflection curves of the shear strength test: a) Mono-fibers, b) Hybrid micro-fibers, and c) Hybrid macro- and micro-fibers. 180
Figure 6-13 The typical load-displacement curves of the shear strength test. 181
Figure 6-14 SEM images of micro-fibers, including BF, PVA, and PPS. 183
Figure 6-15 SEM images of PVA hybrid fibers combined with TPPL, PPL, and BF. 183
Figure 6-16 Comparison of mean shear strength (τC) for all mixtures. 186
Figure 6-17 Comparison of mean shear toughness ($K\tau$) for all mixtures. 186
Figure 6-18 Synergistic effects of fiber hybridization on shear strength and toughness of FR-SWSS mixes. 188
Figure 6-19 The combined mechanical performance (CMP) of FR-SWSS mixes. 189
Figure 7-1 The application of small culverts. 202
Figure 7-2 The details of culverts, a) group I, II, and V, b) group III, and c) group IVTest setup, instrumentation, and testing procedure 210
Figure 7-3 The fabrication of culvert specimens, (a) plywood formwork sealed with silicone, (b) GFRP cage secured in formwork using plastic chairs and ties, and (c) casted SWSS concrete culverts. 211
Figure 7-4 Test setup. 212
Figure 7-5 Failure mode of the fiber-reinforced SWSS concrete culverts, a) group I, b) group II, c) group III, d) group IV, and e) group V. 215
Figure 7-6 The load versus mid-span deflection curves for all culvert groups. 217
Figure 7-7 The maximum strain of GFRP bars for all culvert groups. 218
Figure 7-8 Typical distribution of stress and strain within the crown cross-section of GFRP fiber-reinforced culverts. 219
Figure 7-9 The ultimate strength of culverts for all groups. 222
Figure 7-10 Synergistic hybridization of PPL/PVA and PVA/BA in SWSS concrete. 222
Figure 7-11 The cracking strength (Pcr) of culverts for all groups. 222
Figure 7-12 The energy dissipation ($Etot$) of culverts for all groups (the values in each column represent the percentage of pre-peak energy dissipation to the total energy dissipation). 223
Figure 7-13 The ductility index (μe) of culverts for all groups. 225
Figure 7-14 Influence of crown thickness on ductility index (μe) for various fibers. .228
Figure 7-15 Comparison of experimental and predicted shear capacity for GFRP reinforced concrete culverts. 235
Figure 8-1 The application of concrete culverts. 246
Figure 8-2 Dimensions and reinforcement details of the specimens. 254
Figure 8-3 Test setup and instrumentations along with cyclic loading pattern. 257
Figure 8-4 Load-deflection behaviour of GFRP-reinforced SWSS concrete culvert (GFSS). 259

Figure 8-5 Hysteretic behaviour of culverts: Effects of (a) fiber incorporation and (b) SWSS concrete and GFRP reinforcement. 260
Figure 8-6 Backbone curves of all investigated culverts with (b) peak capacity and (c) peak deflection. 262
Figure 8-7 Microstructure analysis of SWSS and FWNS concrete. 263
Figure 8-8 Shear transfer mechanism at the crown. 263
Figure 8-9 Typical failure mode of the investigated culverts. 264
Figure 8-10 Strain values in reinforcement per cycle: (a) top bar, and (b) bottom bar. 266
Figure 8-11 Concrete compressive strain of the culverts per cycle. 267
Figure 8-12 Hysteresis behaviour of concrete strain. 268
Figure 8-13 Hysteresis behaviour of leg-opening in the culverts. 269
Figure 8-14 Leg-opening of the culverts per cycle. 270
Figure 8-15 Cyclic damage parameters. 271
Figure 8-16 Damage parameters (a) damage index (DI), (b) stress deterioration ratio (SDR), and (c) self-resetting capacity (R). 272
Figure 8-17 Energy dissipation (a) per cycle, and (b) cumulatively. 275
Figure 8-18 Hysteretic damping ratio parameters. 277
Figure 8-19 Hysteretic damping ratio (ζ) of the culverts per cycle. 278
Figure 8-20 Experimental vs. predicted shear capacity of concrete culverts. 284
Figure A-9-1 Cyclic loading regime used in flexural testing. 313
Figure A-9-2 Compressive strength of concrete samples. 313
Figure A-9-3 Compressive behaviour of FR-SWSS concrete: a) stress-strain curves and b) key parameters (e.g., strain values and ductility). 315
Figure A-9-4 Splitting tensile strength of concrete samples. 315
Figure A-9-5 Visualizing the bonding of PPL and TPPL fibers in SWSS concrete through SEM images. 316
Figure A-9-6 Modulus of rupture values of concrete samples under flexural test. 316
Figure A-9-7 Comparison between flexural behaviour of a) PPL, b) TPPL, c) hybrid PPL/PVA, and d) hybrid PVA/BF under monotonic and cyclic loading. 318
Figure A-9-8 Energy absorption under monotonic and cyclic flexural tests. 319
Figure B-1 Copyright permission for Chapter 3 320
Figure B-2 Copyright permission for Chapter 4 321
Figure B-3 Copyright permission for Chapter 5 322
Figure B-4 Copyright permission for Chapter 7 323
Figure B-5 Copyright permission for Chapter 8 324

List of Tables

Table 3-1 Physical properties of different fibers 38
Table 3-2 Mix design of concrete mixes and their fresh properties 40
Table 3-3 The mechanical and compressive stress-strain properties of concrete specimens, and fitting curves parameters (α and β) 56
Table 3-4 Empirical constitutive model parameters of FR-SWSS 61
Table 4-1 Physical properties of the aggregates. 76
Table 4-2 Physical properties of different fibers. 77
Table 4-3 Concrete mix design and their 28-day compressive strengths. 88
Table 5-1 Physical properties of fibers. 116
Table 5-2 Concrete mix design. 118
Table 5-3 The synergistic actions of fibers in the hybrid system of FR-SWSSC. 147
Table 6-1 Chemical compositions of OPC and GGBS (Vafaei et al. 2022a). 163
Table 6-2 Physical properties of coarse and fine aggregates (Mashayekhi et al. 2024d). 163
Table 6-3 Concentration of elements determined from ICP-OES test. 164
Table 6-4 Physical characteristics of various fibers (Mashayekhi et al. 2024a). 169
Table 6-5 Concrete mix designs and corresponding 28-day compressive strengths (Mashayekhi et al. 2024d). 173
Table 7-1 Physical properties of different fibers. 207
Table 7-2 Physical properties of GFRP bars. 208
Table 7-3 Mix proportions of SWSS concrete. 208
Table 7-4 Mechanical properties of different FR-SWSS concrete mixes. 208
Table 7-5 Summary of culvert specimens. 209
Table 7-6 Values of key parameters in Figure 7-8. 221
Table 8-1 Mix proportions of SWSS concrete. 251
Table 8-2 Physical properties of different fibers. 253
Table 8-3 Mechanical properties of reinforcing bars. 253
Table 8-4 Summary of culvert specimens. 255
Table A-1 Material level test methods used to determine concrete mechanical properties. 317

Notations

A	Area of the sliding plane
A_0	Pre-peak area from zero stress to the peak point
A_{GFRP}	GFRP reinforcement area
A_l	Area enclosed by the loop
A_{lig}	Ligament area
A_s	Area of reinforcement within the design width
B	Width of the beams
C_C	Compression force of concrete
C_i	Initial compliance ($CMOD_i/P_i$)
CMP	Combined mechanical performance
CTI	Compressive toughness index
DI	Damage index
D_{max_i}	Maximum displacement during each loading cycle (i)
$D_{residuc}$	Residual deflection during each loading cycle (i)
E	Elastic modulus
E_0	Initial modulus
E_c	Compressive elastic modulus
E_d	Dissipated energy within the loop
E_{d_i}	Damage modulus
E_{el}	Elastic energy dissipated
E_{GFRP}	Elastic modulus of GFRP
E_{hys}	Dissipated energy within the loop
E_s	Elastic modulus of steel bars
E_{tot}	Energy dissipation capacity
E_{tot}	Total energy under the load-deflection curve
F_{be}	Bond efficiency of the fiber (varies from 1.0 to 1.2)
F_D	Depth factor
F_l	Maximum force experienced by the loop
F_N	Axial thrust factor
FPZ	Fracture process zone

F_{rel_i}	Reloading strength for each cycle (i)
f_{st}	Tensile strength
F_{unl_i}	Unloading strength for each cycle (i)
g	Gravity acceleration
G_F	Fracture energy
H_0	Thickness of the knife edges
k	Ratio of depth of neutral axis to depth of flexural reinforcement
k_1	Size effect
k_f	Contributions of the flanges in a T-section
K_{IC}^{C}	Cohesion toughness
K_{IC}^{ini}	Initial fracture toughness
K_{IC}^{un}	Unstable fracture toughness
k_v	Coefficient measuring the extent of concrete contribution to shear strength
K_τ	Shear toughness
L	Specimen length
l_{fiber}	Fiber length
m	Specimen mass
M_u	Factored moment at the section
NI	Nonlinearity index
P_1	First peak load
P_{cr}	Cracking strength
P_i	Load at the initial linear segment of the P-CMOD curve
P_{ini}	Initial cracking load
P_{max}	Peak load
P_{rel_i}	Reloading strength
P_{unl_i}	Unloading strength
R	Degree of reversibility
$R_{e,3}$	Equivalent flexural strength
$R_{hybrid,}^{\square}$	Fracture toughness properties of hybrid FR-SWSSC
RI	Reinforcing index
R_{mono}	Fracture properties of mono-fibers
S	Loading span

SC	Synergistic coefficient
SDR	Strength deterioration ratio
s_x	Crack spacing parameter
s_{xe}	Crack spacing parameter influenced by aggregate size
T_{150}^{D}	Energy absorption capacity at deflection = 2 mm (1/150 of the beam span)
T_{600}^{D}	Energy absorption capacity at deflection = 0.50 mm (1/600 of the beam span)
T_{FRC}	Tensile force across all fibers
t_{top}	Crown thickness
V_0	Ratio of initial crack length to specimen depth ($^{a_0}/_{W}$)
V_{AI}	Inclined shear stress from aggregate interlocking
v_b	Nominal basic shear strength for locations where $\frac{M_u}{\emptyset V_u d} \geq 3.0$
V_C	Span-to-height ratio of the beams ($^{a_C}/_{W}$)
V_{cc}	Uncracked concrete compression zone
V_d	Dowel force from tension reinforcement
V_{exp}	Experimental shear strength
V_f	Fiber volume fraction
V_{fc}	Shear resistance of fibers
V_{fi}	Fiber volume fraction
V_n	Shear strength of fiber-reinforced concrete without stirrups
V_{pre}	Predicted shear strength
V_u	Ultimate shear capacity
V_{uf}	Vertical components of the fiber pull-out force
W	Height of the beams
W_0	Energy consumed at CMOD=3.5 mm
W_1	Work of self-weight of the specimen and equipment
α	Parameter controlling the shape of the ascending branch of the stress-strain curve
β	Parameter controlling the shape of the descending branch of the stress-strain curve
ε_c^p	Peak strain
ε_c^u	Ultimate strain
ε_s	Net longitudinal tensile strain within the section at the centroid of the tension reinforcement

θ_v	Angle between the axis of the concrete compression strut and the longitudinal axis of the member
μ_e	Ductility factor
ξ_{hys}	Hysteretic damping
ρ_{fiber}	Fiber volume fraction (percent by volume)
τ_C	Mean shear strength
$\tau_{C,max}$	Maximum shear strength
τ_{fd}	Shear strength due to fibers

Publications

Journal articles:

1. **Mashayekhi, A**, Hassanli, R, Zhuge, Y, Ma, X & Chow, CW 2024a, 'Synergistic effects of fiber hybridization on the mechanical performance of seawater sea-sand concrete', Construction and Building Materials, vol. 416, p. 135087.
2. **Mashayekhi, A**, Hassanli, R, Zhuge, Y, Ma, X, Chow, CW, Bazli, M & Manalo, A 2024c, 'Synergistic effects of fiber hybridization on the fracture toughness of seawater sea-sand concrete', Construction and Building Materials, vol. 444, p. 137845.
3. **Mashayekhi, A**, Hassanli, R, Zhuge, Y, Ma, X, Chow, CW, Bazli, M & Manalo, A 2024d, 'Cyclic flexural performance of seawater sea-sand concrete reinforced with hybrid fibers', Construction and Building Materials, vol. 449, p. 138480.
4. **Mashayekhi, A**, Hassanli, R, Zhuge, Y, Ma, X, W. K. Chow, C, Bazli, M & Manalo, A 2024, 'Structural behaviour of small GFRP-reinforced seawater sea-sand fiber reinforced concrete culverts', Structures, vol. 69, p. 107492.
5. **Mashayekhi, A**, Hassanli, R, Zhuge, Y, Ma, X, W. K. Chow, C, Bazli, M & Manalo, A 2025, 'Cyclic performance of GFRP-reinforced seawater sea-sand concrete culverts reinforced with synthetic fibers', Structures, vol. 72, p. 108262.

Abstract

Concrete culverts are essential for stormwater management and infrastructure continuity but face durability issues due to steel reinforcement corrosion. Glass fiber-reinforced polymer (GFRP) bars offer a corrosion-resistant alternative, enhancing tensile strength, and service life while reducing maintenance costs. Despite proven load-bearing capacity, knowledge gaps remain regarding their performance under varied loading conditions. Additionally, conventional concrete use raises ecological concerns due to high resource consumption and carbon emissions. SWSS (Seawater Sea-Sand) concrete, made from abundant natural resources, offers a sustainable alternative by conserving freshwater and reducing transport costs. While its chloride content poses challenges for steel reinforcement, GFRP provides a viable solution, especially for coastal construction. However, the application of SWSS concrete in culverts remains underexplored, as does the impact of hybrid fibers on its performance and durability. Therefore, this study aims to evaluate the performance of GFRP-reinforced SWSS concrete culverts with hybrid fibers through experimental investigation. Micro-fibers—such as polypropylene (PPS), polyvinyl alcohol (PVA), and basalt (BF)—and macro-fibers, including long polypropylene (PPL) and twisted polypropylene (TPPL), were used to examine the combined effects of fiber size and type on the mechanical properties of SWSS concrete. Hybrid-fiber reinforcements were applied in two configurations: micro-fibers only and a mix of micro- and macro-fibers. Ground granulated blast furnace slag (GGBS) was also used to reduce the environmental impact of concrete by lowering CO_2 emissions. This thesis consists of two phases: Phase I investigates the mechanical and fresh properties of hybrid fiber-reinforced SWSS concrete (FR-SWSSC) with a total fiber volume fraction of 0.25%, including slump, air content, compressive strength, stress-strain behaviour, tensile strength, elastic modulus, fracture toughness, cyclic flexural performance, and direct shear behaviour. Phase II evaluates the structural performance of GFRP-reinforced culverts with hybrid fibers, assessing both small- and large-size culverts to determine their effectiveness across diverse applications. Fiber hybridization enhanced the mechanical properties of FR-SWSSC, with macro/micro-fiber combinations showing the significant improvements. TPPL/PVA hybridization increased cumulative energy dissipation by 105% and 664% over mono TPPL and PVA, respectively. PPL/PVA hybridization improved initial fracture toughness by 32% and cumulative energy dissipation by 260% compared to mono PVA. It also increased the ultimate strength of

GFRP-reinforced culverts by 47% and 30% over plain SWSSC and mono PPL fibers. The strong chemical bonding of PVA fibers reinforced the concrete matrix, enhancing macro-fiber effectiveness in crack bridging and load bearing, leading to improved energy dissipation and damping under cyclic loading.

Declaration

This thesis presents work carried out by myself and does not incorporate without acknowledgment any material previously submitted for a degree or diploma in any university; to the best of my knowledge it does not contain any materials previously published or written by another person except where due reference is made in the text; and all substantive contributions by others to the work presented, including jointly authored publications, are clearly acknowledged.

Amirhesam Mashayekhi

15/03/2025



Acknowledgments

Completing this doctoral thesis has been a journey filled with challenges, growth, and incredible support. I would like to express my heartfelt gratitude to those who have contributed to this achievement.

First and foremost, I would like to extend my deepest appreciation to my principal supervisor, Reza Hassanli, for his invaluable guidance, encouragement, and expertise throughout the course of this research. His unwavering support and insightful feedback have been instrumental in shaping this work and my academic growth. I am also immensely grateful to my co-supervisors, Prof. Yan Zhuge, Prof. Xing Ma, Prof. Christopher W.K. Chow, Dr. Milad Bazli, and Prof. Allan Manalo, whose expertise and constructive suggestions have greatly enriched this study. Their dedication to my progress has been truly inspiring.

A special thanks goes to the concrete laboratory team at the University of South Australia. I am profoundly thankful for the assistance provided by the technical staff, particularly Mr. Tim Golding, Mrs. Michelle Plew, Dr. Henry Senko, Mr. Craig Sweetman, Mr. Gregory O'Neil, Mr. Stewart Lloyd, and Mr. Ian Whitehead, whose expertise and dedication ensured that all experimental work was conducted smoothly and safely. Their support in the preparation and testing phases was indispensable.

I also extend my gratitude to Adelaide Brighton Cement Ltd and Independent Cement and Lime Pty Ltd for their generous donations of OPC and GGBS, respectively, and TEXO for supplying fibers. I am also grateful to Mr. Adam Bromley for his support. Furthermore, I am thankful to Mr. Jason Quinn, Dr. Murray Townsend, and Mr. Mojtaba Karbasi from the Department for Environment and Water (DEW), as well as Mr. Spiros Dimas from the Department for Infrastructure and Transport (DIT) in the Government of South Australia, for their invaluable support in providing sea-sand. My sincere thanks also go to Inconmat Australia for supplying the GFRP reinforcement used in this project. Additionally, I recognize the valuable instrumentation and expertise provided by Microscopy Australia at the Future Industries Institute, University of South Australia.

I am also deeply grateful to the University of South Australia, whose financial assistance made it possible to access the necessary resources and equipment for the experimental work.

To my family and friends, thank you for your unconditional love, patience, and encouragement. Your belief in me has been a source of strength during moments of doubt and fatigue.

Finally, I dedicate this thesis to my parents for their unwavering faith in my abilities and for inspiring me to pursue this path. Their sacrifices, encouragement, and unconditional love have been the foundation of my success. I am forever grateful for their constant support, which gave me the strength to overcome every challenge and strive for excellence.

This thesis would not have been possible without the collective efforts of all these individuals and organizations. To each and every one of you, thank you from the bottom of my heart.

1 Introduction and general overview

1.1 Background of research

The construction industry reliance on conventional concrete is increasingly being questioned due to environmental concerns. These include the depletion of natural resources and carbon emissions from concrete production (Amran *et al.* 2020); Xiong *et al.* (2021). The extraction of freshwater and river sand, essential in conventional concrete, has caused significant ecological damage, including river ecosystem degradation (Xiong *et al.* 2021). In response, seawater sea-sand concrete (SWSSC) has been proposed as a promising alternative to mitigate these challenges. SWSSC uses abundant seawater (SW) and sea-sand (SS), conserving freshwater, reducing carbon footprints, and improving durability in marine environments (Cao *et al.* 2008; Tjaronge *et al.* 2015; Xiong *et al.* 2021). SWSSC is well-suited for coastal, offshore, and environmental projects, such as artificial reefs, habitat restoration, and coastal infrastructure (Tjaronge *et al.* 2015; Mashayekhi *et al.* 2024a). It offers excellent resistance to harsh marine conditions and is cost-effective in areas where freshwater and high-quality aggregates are scarce (Mashayekhi *et al.* 2024e). Replacing steel reinforcement with non-corrosive materials can also mitigate corrosion risks, a major concern in SWSS concrete applications (Vafaei *et al.* 2021b; Kaidi *et al.* 2023).

Fiber-reinforced polymers (FRP) are particularly suitable as an alternative to steel reinforcement due to their non-corrosive nature, high tensile strength, and durability in harsh marine environments (Yuntao *et al.* 2020; Dong *et al.* 2021; Chen *et al.* 2022; Zeng *et al.* 2022; Zhihao *et al.* 2022; Hassanli *et al.* 2023; Vafaei *et al.* 2023; Mashayekhi *et al.* 2024a; Mashayekhi *et al.* 2024e). FRP bars demonstrate excellent resistance to chlorides, sulfates, and other aggressive agents found in marine conditions, which makes them ideal for SWSSC applications (Kim *et al.* 2008; Wu, Weiwei *et al.* 2023). Studies have shown that GFRP (Glass Fiber Reinforced Polymer) bars, a common type of FRP,

maintain their microstructural integrity and mechanical properties over long-term exposure, making them highly effective for enhancing the durability of SWSS concrete (Kim *et al.* 2008; Bertola *et al.* 2017; Khatibmasjedi *et al.* 2017; Wang, Zhihao *et al.* 2023; Wu, Weiwei *et al.* 2023).

Given the unique characteristics of SWSS concrete, crack control is essential to ensure long-term durability, particularly in marine environments where aggressive agents such as chlorides and sulfates accelerate degradation. Fiber reinforcement has proven to be effective in controlling crack initiation and propagation, enhancing the structural integrity and overall performance of SWSS concrete (Vafaei *et al.* 2021a; Ahmad *et al.* 2022; Li, Yan *et al.* 2022; Vafaei *et al.* 2022b). Synthetic fibers, including polyvinyl alcohol (PVA) and polypropylene (PP), have gained popularity for their cost-effectiveness, resistance to corrosion, and positive impact on concrete properties (Vafaei *et al.* 2021a; Vafaei *et al.* 2022b; Kaidi *et al.* 2023). Investigations into the effects of these fibers have demonstrated significant improvements in tensile strength and compressive strength, making them suitable for use in aggressive environments (Vafaei *et al.* 2021a; Kaidi *et al.* 2023).

However, mono-fibers have inherent limitations in terms of crack control, tensile strength, toughness, and distribution within the concrete matrix (Pakravan *et al.* 2017; Chenggong *et al.* 2023; Kaidi *et al.* 2023; Mashayekhi *et al.* 2024a). Fiber hybridization, which combines different types of fibers, has emerged as an effective approach to enhance the properties of SWSS concrete. Carefully selected hybrid fibers can improve the ductility and overall performance of both conventional and SWSS concrete (Ahmed *et al.* 2011; Chenggong *et al.* 2023; Kaidi *et al.* 2023). Studies on hybrid fiber-reinforced concrete have reported synergistic effects, where combining micro- and macro-fibers has led to enhanced compressive strength, tensile strength, and fracture energy compared to using mono-fibers alone (Ahmed *et al.* 2011; Pakravan *et al.* 2018; Ling *et al.* 2019; Çelik *et al.* 2020a; Ríos *et al.* 2020; Şükrü *et al.* 2021; Abbas *et al.* 2022; Mehran *et al.* 2022; Nguyen *et al.* 2022; Abdel-Karim *et al.* 2023; Chenggong *et al.* 2023; Kai *et al.* 2023; Kaidi *et al.* 2023; Mashayekhi *et al.* 2024a). Despite the promising findings, research on the hybridization of fibers, particularly in SWSSC, remains limited.

This study aims to comprehensively assess the potential of using mono and hybrid fibers in SWSSC culverts reinforced with GFRP bars, with a focus on enhancing its overall structural performance. Limited studies are available on FRP-reinforced elements,

particularly in culverts, which necessitates further research to evaluate their performance under harsh environmental conditions. Concrete culverts play a critical role in managing stormwater, reducing flooding, and ensuring proper drainage in infrastructure systems. These culverts often experience harsh environments, including constant exposure to moisture, chlorides, and other aggressive agents that can lead to degradation. GFRP bars are particularly beneficial in culverts due to their non-corrosive nature, high tensile strength, and excellent durability in such challenging conditions, including marine and coastal areas. By employing mono-fibers, hybrid micro-fibers, hybrid combinations of micro- and macro-fibers, this study investigates the synergistic effects of hybrid fibers on the fresh and hardened properties of SWSSC. Ultimately, the findings contribute to the development of sustainable concrete solutions that address both environmental and structural challenges, making SWSSC an attractive alternative for coastal, offshore, environmental, and culvert applications.

1.2 Research objectives and questions

Concrete culverts are often subjected to harsh conditions from both the surrounding water and soil. Field studies of steel-reinforced concrete culverts have shown that steel bars are highly susceptible to corrosion. Additionally, concerns about the depletion of natural resources—freshwater and river sand—in the construction industry have led to the exploration of alternative materials such as SW and SS for use in concrete production. However, SW and SS can potentially accelerate the corrosion of steel reinforcement. Therefore, using non-corrosive alternatives such as GFRP bars and fibers—both synthetic and natural—is necessary to improve the sustainability and durability of SWSSC culverts. As a result, the behaviour of fiber incorporation and their hybrid synergy in GFRP-reinforced concrete culverts should be investigated.

To the best of the authors' knowledge, the mechanical properties of SWSSC reinforced with different types of fibers—both micro and macro—and their combinations have not been thoroughly examined. Therefore, further studies are needed to better understand the mechanical properties, especially the shear strength, of hybrid fiber-reinforced SWSSC. Furthermore, no previous investigation has focused on the application of GFRP bars in concrete culverts in conjunction with different fiber types. This study aims to evaluate the mechanical performance of hybrid fiber-reinforced (HFR) SWSSC and its application in GFRP-reinforced concrete culverts.

The primary objectives of this study are as follows:

- Develop a new type of fiber-reinforced concrete using SW, SS, and hybrid fibers.
- Evaluate the effect of fiber hybridization on the mechanical behaviour—including compressive, splitting tensile, shear, and flexural strength—of SWSSC mixtures.
- Investigate the fracture toughness of SWSSC reinforced with both mono and hybrid fibers.
- Investigate the cyclic flexural performance of SWSSC reinforced with both mono and hybrid fibers.
- Assess the effect of hybrid fiber synergy on the shear performance of SWSSC.
- Evaluate the structural behaviour of SWSSC culverts reinforced with GFRP bars and hybrid fibers through full-scale experimental studies on both small and large specimens under monotonic and cyclic loading.

This research aims to explore the following research questions:

- What is the effect of fiber synergy on the mechanical properties of SWSSC?
- What are the impacts of mono and hybrid fiber reinforcement on the cyclic flexural performance of SWSSC?
- How does the use of mono and hybrid fibers influence the fracture toughness of SWSSC?
- How does the shear strength of SWSSC mixtures change with the addition of different types of micro and macro fibers?
- What is the structural behaviour of GFRP hybrid fiber-reinforced concrete using SW and SS?
- What is the structural behaviour of SWSSC culverts reinforced with GFRP bars and the effect of hybrid fiber synergy?
- How does the structural performance of SWSSC culverts reinforced with GFRP bars compare to conventional steel-reinforced culverts under dynamic loading conditions?

1.3 Thesis outline

The framework of this thesis is illustrated in **Figure 1-1**. The thesis comprises nine chapters, divided into two phases: Phase I, focusing on material-level testing, and Phase II, on structural-level testing. Chapter 1 provides an overview of SWSSC and outlines the thesis structure. Chapter 2 presents a comprehensive literature review related to the research topics and objectives.

Phase I, covering material-level testing, focusing on hybrid fiber synergy, is detailed in Chapters 3 to 6. Phase II, focusing on structural-level testing of GFRP-reinforced SWSSC culverts using hybrid fibers, is presented in Chapters 7 and 8.

Chapter 3 examines the impact of hybrid fibers and their synergistic effects on the mechanical properties of SWSSC, including compressive strength, elastic modulus, splitting tensile strength, compressive stress-strain behaviour, ductility, slump, and air content. The study investigates two hybridization approaches: micro-fibers (different fiber types) and a combination of micro- and macro-fibers (varying fiber lengths). The hybrid fibers used are polypropylene (PPS), polyvinyl alcohol (PVA), basalt (BF), polypropylene macro-fiber (PPL), and twisted polypropylene (TPPL), at a total volume fraction of 0.25%. Additionally, an empirical constitutive model for fiber-reinforced SWSSC in compression is presented, based on its stress-strain behaviour. The results of this research have been published in Construction and Building Materials journal.

Chapter 4 focuses on the fracture behaviour of fiber-reinforced SWSSC, specifically the impact of fiber hybridization on fracture toughness and potential synergistic effects. The study evaluates fracture parameters, such as fracture toughness and fracture energy, as well as initial, unstable, and cohesive fracture toughness. The chapter also assesses the post-crack performance of fiber-reinforced SWSSC based on existing guidelines. The results have been published in Construction and Building Materials journal.

Chapter 5 investigates the effect of fiber hybridization on the cyclic flexural behaviour of fiber-reinforced SWSSC using four-point cyclic bending tests. The study includes hybrid-fiber reinforcements in two configurations: micro-fibers only and a combination of micro- and macro-fibers. Key parameters analysed include hysteretic damping ratio, energy absorption, flexural tensile strength, damage index, strength deterioration ratio, and

degree of reversibility. The results are published in Construction and Building Materials journal.

Chapter 6 explores the synergistic effects of fiber hybridization on the shear performance of SWSSC. A modified direct shear test method, based on JSCE-SF6, was developed to achieve more accurate pure shear testing through experimental work and finite element modeling. The method was tailored for beam specimens according to Australian standards. Parameters such as concrete-steel plate friction, support positioning, and bolt prestressing were investigated experimentally and through finite element analysis. The chapter also presents the results of shear strength, toughness, and Inductively Coupled Plasma Optical Emission Spectroscopy (ICP-OES) analysis of SW and SS. This work is currently under review at the Construction and Building Materials journal.

Chapter 7 presents the structural behaviour of fiber-reinforced SWSSC culverts reinforced with GFRP bars. Eighteen small-scale concrete culverts, with widths of 470 mm and two heights (425 mm and 365 mm), conforming to Australian standards, were subjected to experimental evaluation. The study examines parameters such as fiber type (PPL, TPPL, PVA, and BF), fiber hybridization, GFRP compression reinforcement, crown thickness, haunches, and concrete compressive strength. A comprehensive analysis of culvert behaviour is provided, covering load at first crack, crack propagation, load-displacement response, ultimate load capacity, energy dissipation, ductility, and failure modes. The results have been published in Structures journal.

Chapter 8 examines the cyclic behaviour of GFRP-reinforced SWSSC culverts with synthetic fibers. Five full-scale culverts incorporating mono and hybrid fibers (PPL and PVA) were tested under cyclic loading. Additionally, two reference culverts (steel- and GFRP-reinforced FWNS concrete without fibers) were evaluated to determine the effects of concrete and reinforcement types. The study investigated failure mechanisms, load-deflection response, ultimate capacity, energy dissipation, hysteretic damping, damage parameters, strength degradation ratio, and self-resetting capacity. This work has been published in Structures journal.

Finally, Chapter 9 presents the conclusions and recommendations for future work.

1.4 Research Approach

This section outlines key research decisions regarding fiber selection, mechanical properties testing, and concrete culverts. It provides insights into the rationale behind material choices, experimental procedures, and analytical approaches, ensuring a clear understanding of the methodology adopted in this study.

1.4.1 Fiber selection and hybridization

The hybridization of fibers in this study is based on combining fibers according to their size (micro/macro-fiber hybrids) and type (micro-fiber hybrids). To achieve this, micro-fibers—including polypropylene (PPS), polyvinyl alcohol (PVA), and basalt (BF)—as well as macro-fibers—including polypropylene macro-fiber (PPL) and twisted polypropylene (TPPL)—were selected. This study employed both synthetic fibers (PPS, PVA, PPL, and TPPL) and a natural fiber (BF). BF was chosen for its eco-friendly nature and sustainability benefits in concrete applications. It is derived from naturally occurring volcanic rock without requiring chemical processing or additives. As an inorganic natural fiber, its production involves melting basalt rock and extruding it into continuous fibers, making it a mineral-based, environmentally friendly material.

A total fiber dosage of 0.25% was selected for Phase 1 (material level testing) of this study, based on its impact on structural performance, strength improvement, and workability, as determined through preliminary trials and existing literature. While determining the optimal fiber content for practical applications and design considerations would require a comprehensive analysis, this was beyond the scope of this research. Instead, the study focused on the performance and synergy of hybrid fibers in SWSS concrete and their application in concrete culverts. Consequently, the investigation prioritized different fiber types and their combinations over defining an optimal fiber content.

For fiber combinations, mix proportions of 33% and 66% were chosen for the hybrid system, resulting in two different hybridizations per system. For example, in the PVA/PPL hybridization, two mix designs were used: 0.33PVA/0.66PPL and 0.66PVA/0.33PPL. This approach aimed to effectively evaluate fiber synergy, as doubling the dosage of each fiber in the hybrid system allows for a clearer assessment of their individual and combined effects. These proportions were also validated through

initial trials, which demonstrated their distinct contributions to the overall performance of the hybrid system.

1.4.2 Mechanical properties testing

To investigate the mechanical performance of FR-SWSSC, different properties have been investigated by utilizing different standard test methods including compressive stress-strain, compressive elastic modulus, splitting tensile strength, fracture toughness, cyclic flexural behaviour, and shear strength. This approach provides a comprehensive investigation of the performance of FR-SWSSC and their application in concrete culverts.

The compressive elastic modulus and stress-strain was selected due to its widespread use in structural design, as defined by major design codes (e.g., ACI, Eurocode), where it serves as a key parameter for evaluating structural stiffness. While synthetic fibers may reduce compressive strength, the modulus remains relevant for assessing overall compressive behaviour. Additionally, compressive tests are more standardized and reproducible compared to tensile modulus tests, which require specialized setups and are prone to variability. Moreover, the fracture behaviour and flexural response of the specimens, which provide insights into tensile performance, are extensively discussed in Chapter 4.

The stress-strain curve from the compression test was preferred due to its standardized methodology, relevance to concrete culverts, and comparability with existing studies. A true (dog-bone) tensile test was not conducted due to equipment constraints, testing complexity, and the preference for flexural testing as a practical alternative for assessing tensile performance.

The discussion in Chapter 3 focuses on compressive behaviour. While an indirect tensile test was considered, the fracture toughness test is a more comprehensive method for assessing tensile behaviour, as it provides detailed calculations of crack propagation and resistance. A more in-depth analysis of fracture and flexural behaviour, including energy absorption and ultimate strength, is provided in Chapters 4 and 5 using displacement control testing. Therefore, Chapter 3 prioritizes compressive parameters to maintain consistency with its scope.

The cyclic flexural test was conducted to evaluate the performance of FR-SWSSC under repeated loading, relevant to culverts subjected to dynamic stresses from vehicular traffic

and environmental factors. While this test does not fully replicate seismic conditions due to the absence of a push-pull mechanism, it provides valuable insight into the material's durability and crack resistance under cyclic bending stresses. This assessment serves as a preliminary evaluation of the ability of FR-SWSSC to withstand fatigue-induced stresses, contributing to its long-term performance in culvert applications.

1.4.3 Concrete culvert

According to the Australian Standard AS 1597.1:2010 – Precast Reinforced Concrete Box Culverts, Part 1: Small Culverts, small concrete culverts (SCC) are defined as having internal spans ranging from 300 mm to 1,200 mm and heights from 225 mm to 1,200 mm. This classification differentiates them from larger culverts, which are specified in AS 1597.2:2013 – Large Culverts.

The culverts investigated in this study align with the definition of small culverts but include two different sizes to examine the effect of hybrid FR-SWSSC on their performance. The selected spans, 320 mm and 1,160 mm, represent the lower and upper limits of the small culvert classification, allowing for a comprehensive analysis across the defined range.

Based on the results obtained from Phase 1: Material-level testing of FR-SWSSC, the hybrid systems with superior mechanical properties and performance have been selected for Phase 2: Structural-level testing, where they have been incorporated into GFRP-reinforced concrete culverts. Considering the findings from the literature review and initial trials—evaluating both strength and workability—a total fiber volume of 0.66% has been found effective in enhancing the structural performance of concrete elements. Therefore, in this study, a 0.66% total fiber dosage has been adopted for the hybrid systems without the use of a comprehensive optimization technique. Additionally, fiber combinations of 33% and 66% within the hybrid system have also been considered.

To calculate the tensile stress distribution along the tension part of the crown section using Eq. (7-1), the length and diameter of each fiber type were considered separately, with volume fractions of 33% and 66% of the total 0.66%. The equation also accounts for fiber synergy in enhancing bonding strength, making it a reliable approach for estimating the tensile strength of fiber-reinforced concrete. While this method simplifies the analysis of

hybrid fiber systems, a more comprehensive assessment of their tensile strength should be explored in future studies.

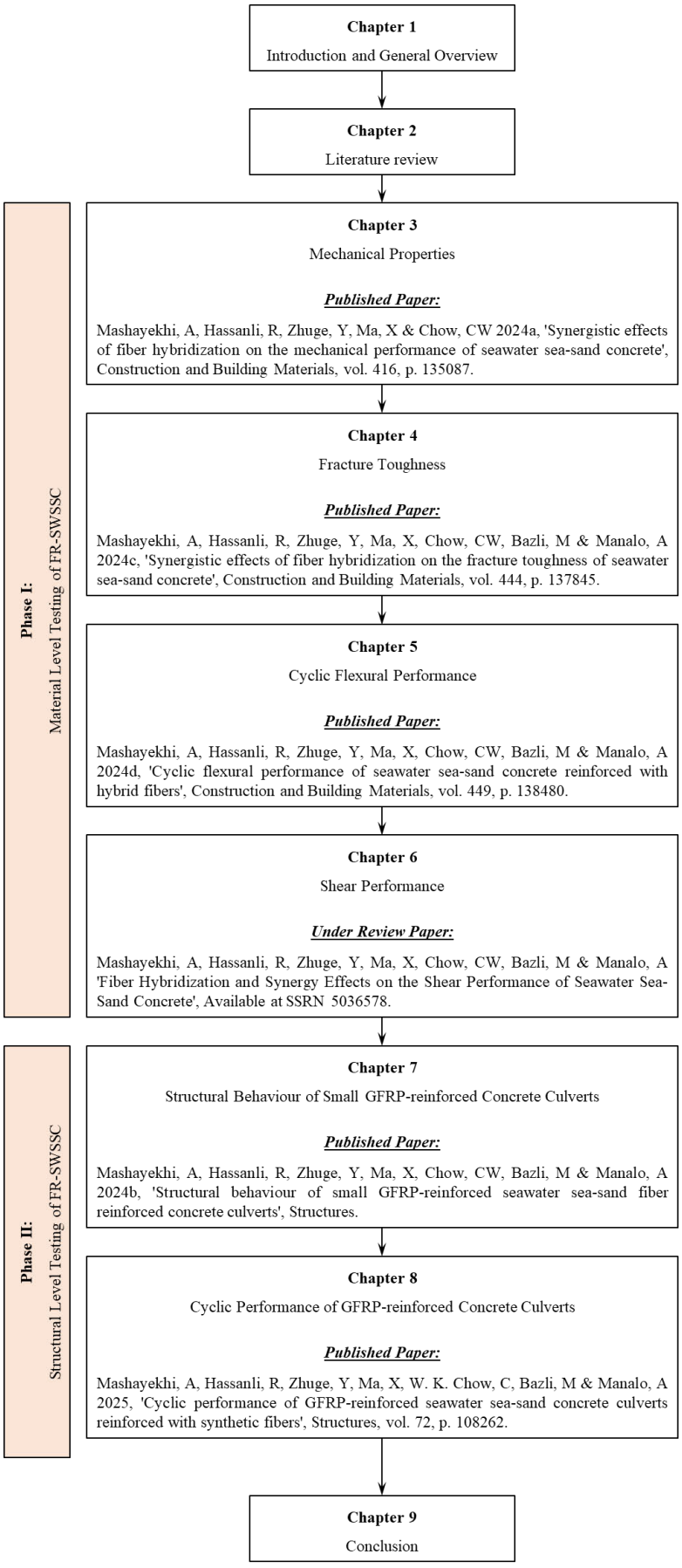


Figure 1-1 Thesis framework

Chapter 1 References

Abbas, YM, Hussain, LA & Khan, MI 2022, 'Constitutive compressive stress–strain behavior of hybrid steel-PVA high-performance fiber-reinforced concrete', Journal of Materials in Civil Engineering, vol. 34, no. 1, p. 04021401.

Abdel-Karim, AH, Khalil, GI, Ewis, AE & Makhlouf, MH 2023, 'Impact of developed hybrid polypropylene fiber inclusion on the flexural performance of concrete beams reinforced with innovative hybrid bars', Construction and Building Materials, vol. 409, p. 134113.

Ahmad, J, González-Lezcano, RA, Majdi, A, Ben Kahla, N, Deifalla, AF & El-Shorbagy, MA 2022, 'Glass fibers reinforced concrete: Overview on mechanical, durability and microstructure analysis', Materials, vol. 15, no. 15, p. 5111.

Ahmed, SFU & Mihashi, H 2011, 'Strain hardening behavior of lightweight hybrid polyvinyl alcohol (PVA) fiber reinforced cement composites', Materials and structures, vol. 44, no. 6, pp. 1179-91.

Amran, YM, Soto, MG, Alyousef, R, El-Zeadani, M, Alabduljabbar, H & Aune, V 2020, 'Performance investigation of high-proportion Saudi-fly-ash-based concrete', Results in Engineering, vol. 6, p. 100118.

Bertola, F, Canonico, F & Nanni, A 2017, SEACON Project: sustainable concrete using seawater, salt-contaminated aggregates, and non-corrosive reinforcement, XIV DBMC-14th International Conference on Durability of Building Materials and Components.

CAO, X-q, ZHANG, Y, HE, Y-j, JIANG, Y-c & YUAN, X-j 2008, 'Retrospect and discussion of surveys for construction sand in China offshore area', Marine Geology & Quaternary Geology, vol. 28, no. 3, pp. 121-25.

Çelik, Z & Bingöl, AF 2020, 'Fracture properties and impact resistance of self-compacting fiber reinforced concrete (SCFRC)', Materials and structures, vol. 53, no. 3, pp. 1-16.

Chen, Z, Li, S, Zhou, J, Xu, R & Dai, S 2022, 'Flexural behavior of GFRP bars reinforced seawater sea sand concrete beams exposed to marine environment: Experimental and numerical study', Construction and Building Materials, vol. 349, p. 128784.

Chenggong, Z, Zhiyuan, W, Zhenyu, Z, Qiuyu, G, Xinrui, W & Renda, Z 2023, 'Research on different types of fiber reinforced concrete in recent years: An overview', Construction and Building Materials, vol. 365, p. 130075.

Dong, S, Li, C & Xian, G 2021, 'Environmental impacts of glass-and carbon-fiber-reinforced polymer bar-reinforced seawater and sea sand concrete beams used in marine environments: An LCA case study', Polymers, vol. 13, no. 1, p. 154.

Hassanli, R, Manalo, A, Vafaei, D, Yekrangnia, M, Elchalakani, M & Noël, M 2023, 'Cyclic behavior of GFRP-reinforced concrete one-way slabs with synthetic fibers', Journal of Building Engineering, vol. 65, p. 105741.

Kai, C, Lihua, X, Tao, T, Le, H, Jian, L, Jian, H, Huan, L & Yin, C 2023, 'Mechanical behavior of multiscale hybrid fiber reinforced recycled aggregate concrete subject to uniaxial compression', Journal of Building Engineering, vol. 71, p. 106504.

Kaidi, J, Xin, W, Lining, D, Zhiyuan, C, Huang, H, Xia, L, Jianxun, L & Zhishen, W 2023, 'Mechanical properties of multi-scale mono/hybrid non-metallic fiber-reinforced ultra-high performance seawater sea-sand concrete', Construction and Building Materials, vol. 401, p. 132922.

Khatibmasjedi, M & Nanni, A 2017, Durability of GFRP reinforcement in SEACON, The Fifth International Conference on Durability of Fiber Reinforced Polymer (FRP) Composites for Construction and Rehabilitation of Structures (CDCC 2017).

Kim, H-Y, Park, Y-H, You, Y-J & Moon, C-K 2008, 'Short-term durability test for GFRP rods under various environmental conditions', Composite Structures, vol. 83, no. 1, pp. 37-47.

Li, Y, Zhang, J, He, Y, Huang, G, Li, J, Niu, Z & Gao, B 2022, 'A review on durability of basalt fiber reinforced concrete', Composites Science and Technology, vol. 225, p. 109519.

Ling, Y, Zhang, P, Wang, J & Chen, Y 2019, 'Effect of PVA fiber on mechanical properties of cementitious composite with and without nano-SiO2', Construction and Building Materials, vol. 229, p. 117068.

Mashayekhi, A, Hassanli, R, Zhuge, Y, Ma, X & Chow, CW 2024a, 'Synergistic effects of fiber hybridization on the mechanical performance of seawater sea-sand concrete', Construction and Building Materials, vol. 416, p. 135087.

Mashayekhi, A, Hassanli, R, Zhuge, Y, Ma, X, Chow, CW, Bazli, M & Manalo, A 2024b, 'Structural behaviour of small GFRP-reinforced seawater sea-sand fiber reinforced concrete culverts', Structures.

Mehran, K, Mingli, C, Chaopeng, X & Majid, A 2022, 'Effectiveness of hybrid steel-basalt fiber reinforced concrete under compression', Case Studies in Construction Materials, vol. 16, p. e00941.

Nguyen, D-L, Thai, D-K & Lam, MN-T 2022, 'Synergy in Flexure of High-Performance Fiber-Reinforced Concrete with Hybrid Steel Fibers', Journal of Materials in Civil Engineering, vol. 34, no. 6, p. 04022090.

Pakravan, H, Jamshidi, M & Latifi, M 2018, 'The effect of hydrophilic (polyvinyl alcohol) fiber content on the flexural behavior of engineered cementitious composites (ECC)', The Journal of The Textile Institute, vol. 109, no. 1, pp. 79-84.

Pakravan, HR, Latifi, M & Jamshidi, M 2017, 'Hybrid short fiber reinforcement system in concrete: A review', Construction and Building Materials, vol. 142, 2017/07/01/, pp. 280-94.

Ríos, J, Cifuentes, H, Leiva, C, Ariza, M & Ortiz, M 2020, 'Effect of polypropylene fibers on the fracture behavior of heated ultra-high performance concrete', International Journal of Fracture, vol. 223, no. 1, pp. 173-87.

Şükrü, Ö & Ömer, Ç 2021, 'The hybrid effects of basalt and PVA fiber on properties of a cementitious composite: Physical properties and non-destructive tests', Construction and Building Materials, vol. 312, p. 125292.

Tjaronge, MW & Irfan, UR 2015, 'Porosity, pore size and compressive strength of self compacting concrete using sea water', Procedia Engineering, vol. 125, pp. 832-37.

Vafaei, D, Hassanli, R, Ma, X, Duan, J & Zhuge, Y 2021a, 'Sorptivity and mechanical properties of fiber-reinforced concrete made with seawater and dredged sea-sand', Construction and Building Materials, vol. 270, p. 121436.

Vafaei, D, Ma, X, Hassanli, R & Zhuge, Y 2021b, Effects of seawater and sea-sand on concrete properties: A review paper, EASEC16: Proceedings of The 16th East Asian-Pacific Conference on Structural Engineering and Construction, 2019.

Vafaei, D, Ma, X, Hassanli, R, Duan, J & Zhuge, Y 2022, 'Microstructural behaviour and shrinkage properties of high-strength fiber-reinforced seawater sea-sand concrete', Construction and Building Materials, vol. 320, p. 126222.

Vafaei, D, Ma, X, Hassanli, R, Duan, J & Zhuge, Y 2023, 'Experimental study on cyclic flexural behaviour of GFRP-reinforced seawater sea-sand concrete slabs with synthetic fibres', Ocean Engineering, vol. 273, p. 114014.

Wang, Z, Xie, J, Mai, Z, Liu, P, Lu, Z & Li, L 2023, 'Durability of GFRP bar-reinforced seawater–sea sand concrete beams: Coupled effects of sustained loading and exposure to a chloride environment', Engineering Structures, vol. 283, p. 115814.

Wu, W, He, X, Yang, W, Wei, B & Alam, MS 2023, 'Durability and microstructure degradation mechanism of FRP-seawater seasand concrete structures: A review', Construction and Building Materials, vol. 391, p. 131825.

Xiong, Z, He, S, Kwan, A, Li, L & Zeng, Y 2021, 'Compressive behaviour of seawater sea-sand concrete containing glass fibres and expansive agents', Construction and Building Materials, vol. 292, p. 123309.

Yuntao, H, Shiping, Y & Zhangtao, P 2020, 'Crack development and calculation method for the flexural cracks in BFRP reinforced seawater sea-sand concrete (SWSSC) beams', Construction and Building Materials, vol. 255, p. 119328.

Zeng, J-J, Liao, J, Zhuge, Y, Guo, Y-C, Zhou, J-K, Huang, Z-H & Zhang, L 2022, 'Bond behavior between GFRP bars and seawater sea-sand fiber-reinforced ultra-high strength concrete', Engineering Structures, vol. 254, p. 113787.

Zhihao, W, Jianhe, X, Jianglin, L, Peng, L, Cuiqing, S & Zhongyu, L 2022, 'Flexural behaviour of seawater–sea sand concrete beams reinforced with GFRP bars: Effects of the reinforcement ratio, stirrup ratio, shear span ratio and prestress level', Journal of Building Engineering, vol. 54, p. 104566.

2 Literature review

2.1 Introduction

This chapter presents an in-depth review of seawater sea-sand concrete (SWSSC), including its fresh and hardened properties and structural performance, particularly in applications involving fiber-reinforced polymers (FRP). It explores the environmental benefits of SWSSC, its mechanical and durability characteristics, and its suitability for coastal infrastructure. Furthermore, the chapter discusses the role of FRP bars in mitigating the corrosion challenges associated with conventional steel reinforcement in SWSSC. Additionally, it presents the influence of fibers on the mechanical properties and durability of SWSSC, highlighting their effectiveness in enhancing crack control and toughness. The structural behaviour of concrete culverts, including their shear performance, backfill effects, and failure mechanisms, is also reviewed to understand their design implications in practice. The chapter concludes by identifying existing knowledge gaps and providing directions for future research and advancements in the field.

2.2 Seawater sea-sand concrete (SWSSC)

Concrete is one of the most widely used construction materials, but its production poses significant environmental challenges, such as high water consumption, depletion of natural sand, and considerable CO_2 emissions (Interior 2020). SWSS concrete, utilizing abundant seawater and sea-sand resources, presents a promising solution for sustainable construction, particularly in coastal regions. With an estimated 388 billion cubic meters of sea-sand available along China's coastline (Cao *et al.* 2008) and seawater constituting 97% of the Earth's water supply (Tjaronge *et al.* 2015), SWSS concrete offers a significant opportunity to conserve freshwater and reduce carbon emissions (Xiong *et al.* 2021). The use of seawater and sea-sand in concrete began in the 1960s and has since gained traction globally (Griffin *et al.* 1964; Chapman 1968; Newman 1968). This type of concrete provides several benefits, including excellent resistance to marine environments, reduced transportation and maintenance costs, and affordability in remote areas where freshwater and high-quality aggregates are scarce (Xiao *et al.* 2017; Dhondy *et al.* 2019; Guo *et al.* 2020; Li *et al.* 2021; Ge *et al.* 2023; Zhu *et al.* 2023; Li *et al.* 2024).

Life cycle assessments further demonstrate that SWSS concrete has significantly lower environmental impacts compared to traditional concrete used in marine applications, with reductions in environmental impact categories ranging from 26.3% to 48.6% (Dong *et al.* 2021). Although there is a concern about steel reinforcement corrosion due to chloride ions (Zongao *et al.* 2024), this issue can be addressed by incorporating non-corrosive materials (Vafaei *et al.* 2021b; Kaidi *et al.* 2023), such as fiber-reinforced polymers (FRP) (Yuntao *et al.* 2020; Dong *et al.* 2021; Chen *et al.* 2022; Zeng *et al.* 2022; Zhihao *et al.* 2022; Hassanli *et al.* 2023; Vafaei *et al.* 2023; Mashayekhi *et al.* 2024e), which enhances the durability of SWSS concrete structures (Micelli *et al.* 2004; Kamal *et al.* 2011; Al-Salloum *et al.* 2013; Hu *et al.* 2022). With proper planning and a comprehensive understanding of its properties, SWSS concrete is a sustainable, cost-effective, and durable alternative for coastal and environmental projects, including artificial reefs, habitat restoration, and coastal infrastructure development (Tjaronge *et al.* 2015).

2.3 Fresh and hardened characteristics of SWSSC

The presence of various ions in SWSSC, including sodium (Na^+), potassium (K^+), chloride (Cl^-), sulphate (SO_4^{2-}), calcium (Ca^{2+}), and magnesium (Mg^{2+}), can impact the properties of both fresh and hardened SWSSC compared to freshwater normal sand concrete (FWNSC). Additionally, in the aggressive environment of SWSSC, crack control is paramount for the long-term performance and structural integrity of concrete structures due to the presence of these ions (Vafaei *et al.* 2021a; Ahmad *et al.* 2022; Li, Yan *et al.* 2022; Vafaei *et al.* 2022b). The penetration of Cl^- into the cement hydration products differs considerably from the direct addition of Cl^-. Furthermore, their reduction is an ongoing process that accelerates cement hydration over time (Xiao *et al.* 2017). In terms of durability, the incorporation of SW and SS into concrete significantly reduces water absorption, sorptivity, and porosity compared to traditional concrete (Etxeberria *et al.* 2016a; Etxeberria *et al.* 2016b; Ting *et al.* 2020b; Vafaei *et al.* 2021a). However, it also leads to increased autogenous and drying shrinkage (Katano *et al.* 2013; Etxeberria *et al.* 2016b; Younis *et al.* 2018). Despite the potential durability concerns caused by high salt concentrations and harmful ions, the use of supplementary cementitious materials (SCMs) can effectively address these challenges while enhancing the mechanical properties of SWSS concrete (Li *et al.* 2015; Zhao *et al.* 2021).

2.3.1 Fresh properties

Previous studies reported that both initial and final setting time of the fresh concrete decreased by using SW and SS (Etxeberria *et al.* 2016b; Khatibmasjedi 2018; Younis *et al.* 2018). In addition, most of the previous studies indicated that using SW had no significant effect on slump and air content of fresh concrete (Etxeberria *et al.* 2016b; Khatibmasjedi 2018; Younis *et al.* 2018).

2.3.2 Mechanical properties

The mechanical properties of SWSSC have been the subject of extensive research, with mixed results regarding compressive, flexural, and tensile strengths. At early ages, most studies indicated an increase in the compressive strength of SWSSC compared to FWNS concrete, primarily due to the chloride ions in SW and SS that accelerate cement hydration (Shi *et al.* 2015; Etxeberria *et al.* 2016a; Khatibmasjedi 2018; Younis *et al.* 2018; Li, Peiran *et al.* 2020b; Sikora *et al.* 2020; Ting *et al.* 2020a; Ting *et al.* 2020b; Vafaei *et al.* 2021a). However, the long-term compressive strength showed inconsistent results—some studies reported higher 28-day compressive strength compared to conventional concrete (Limeira *et al.* 2012), while others observed either a decrease or no significant change (Limeir *et al.* 2012; Hong *et al.* 2013; Girish *et al.* 2015). Notably, the strength deterioration factor (SDF) in SWSSC has been found to vary between 24% and 90%, depending on factors such as the water-to-binder (W/B) ratio, the quality of the sea-sand, and the use of SCMs (Zhao *et al.* 2021). Most studies suggested that the use of SW and SS has little to no effect on the elastic modulus of concrete (Limeir *et al.* 2012; Hong *et al.* 2013; Etxeberria *et al.* 2016b; Yang *et al.* 2020; Vafaei *et al.* 2021b; Zhao *et al.* 2021). The impact on flexural strength was less conclusive—some research suggested that SWSSC exhibited lower flexural strength compared to FWNS concrete (Sun *et al.* 2016), whereas other studies found no significant difference (Limeir *et al.* 2012; Limeira *et al.* 2012; Etxeberria *et al.* 2016b; Lv *et al.* 2020). As for tensile strength, it was widely reported that SWSSC tends to have lower tensile strength compared to FWNS concrete (Younis *et al.* 2018; Ting *et al.* 2020a; Ting *et al.* 2020b; Vafaei *et al.* 2021a; Yifan *et al.* 2021).

2.4 Properties of FR-SWSSC

Crack control is essential for the long-term performance and structural integrity of SWSSC, particularly in harsh environments. While FRP bars eliminate the risk of steel

reinforcement corrosion, crack control remains crucial to prevent the ingress of aggressive agents such as water, chlorides, and sulfates, which accelerate degradation and compromise the performance of SWSSC. This highlights the importance of fiber reinforcement in minimizing crack initiation and propagation, thereby enhancing durability and performance. However, the use of steel fibers in SWSS concrete is impractical due to corrosion risks from elevated ion concentrations in SW and SS (Kaidi *et al.* 2023). Therefore, researchers have focused on synthetic fibers like polyvinyl alcohol (PVA) and polypropylene (PP), which offer corrosion resistance, cost-effectiveness, and positive effects on concrete properties in aggressive environments (Vafaei *et al.* 2021a; Vafaei *et al.* 2022b; Kaidi *et al.* 2023). For example, adding 0.3% micro PVA and PP fibers has been shown to increase splitting tensile strength by 17% and 23%, respectively (Vafaei *et al.* 2021a). Incorporating 3% macro basalt fiber (BF) improved the compressive strength of ultra-high performance (UHP) SWSSC by approximately 26%, with no adverse effects on compressive strength from micro PP or BF additions (Kaidi *et al.* 2023).

While mono-fibers such as PVA, PP, or BF enhanced specific properties of SWSS concrete, they have inherent limitations in crack control, tensile strength, toughness, and bonding due to chemical and mechanical constraints, particularly at high doses (Pakravan *et al.* 2017; Chenggong *et al.* 2023; Kaidi *et al.* 2023). Hybrid fiber-reinforced concrete (HFRC) systems, which combine micro and macro fibers based on type, volume, aspect ratio, and bonding interface, can overcome these limitations, resulting in improved mechanical properties, ductility, and durability (Ahmed *et al.* 2011; Chenggong *et al.* 2023; Kaidi *et al.* 2023). For example, increasing the content of thicker hybrid PVA fibers has been shown to improve ductility (Ahmed *et al.* 2011). In UHP-SWSS concrete, combining micro and macro fibers increased compressive strength, although a high dosage of micro-fibers slightly reduced it (Kaidi *et al.* 2023). In HFRC, higher-modulus fibers primarily enhanced strength, while lower-modulus fibers contribute to improved ductility (Pakravan *et al.* 2017). Studies have also demonstrated that combining micro and macro fibers in SWSSC created synergistic effects, where micro-fibers primarily enhanced first-cracking strength, and macro fibers improved post-cracking behaviour (Kaidi *et al.* 2023). For instance, hybrid micro BF/PP systems in SWSS mortars improved flexural, compressive, direct tensile, and splitting tensile strengths, with optimal results observed at a fiber dosage of 0.4% for each type (Yang *et al.* 2024b).

2.5 Structural behaviour of concrete culverts

The shear behaviour of concrete culverts with varying fill heights has been a subject of ongoing debate among researchers. According to AASHTO (2005), shear transfer devices are required at joints if the distribution width exceeds the distance between joints, whereas earlier versions of AASHTO (1998 and 2002) did not apply this requirement to culverts, a stance that some researchers did not support (Abolmaali *et al.* 2008a). Several studies have shown that the shear strength of concrete culverts exceeds estimates provided by various codes (Yee 2004; Garg *et al.* 2007; Abolmaali *et al.* 2008b; Garg *et al.* 2009). One study used experimental and numerical modeling to examine the shear capacity of precast reinforced concrete (RC) box culverts, finding that the shear capacity determined by ACI equations surpassed the factored critical shear force obtained from finite element (FE) modeling (Garg *et al.* 2009).

Another investigation into the shear capacity of precast RC box culverts found that shear strength was higher than predicted by AASHTO provisions, with shear not being a primary failure mode (Abolmaali *et al.* 2008b). Findings were also confirmed in a study showing that the shear strength of four box culverts was 1.5 to 2 times the design live load, with minimal deflection of the top slab (Garg *et al.* 2007). However, some researchers reported that shear failure was the predominant failure mode in certain cases, using FE modeling to evaluate the shear strength of deeply buried RC box culverts. Their results indicated that the shear strength predicted by AASHTO (2017) was significantly higher than FE model results, with failure modes including flexural, shear, and combined failures (Ghahremannejad *et al.* 2019a).

A study comparing the shear strength of RC box culverts with the ACI 318-14 formulation found it to be conservative and recommended a 25% increase in shear strength (Ghahremannejad *et al.* 2019b). Another investigation showed that code formulations generally underestimated shear strength (Yee 2004). Prior research indicated that joint shear transfer was not significant in culverts with zero fill depth, as deflections and strains were minimal at service loads (James 1983; Frederick *et al.* 1988). The impact of live load positioning was explored, which led to a revised load distribution formula in AASHTO (2005) (McGrath *et al.* 2005).

The use of synthetic fibers in concrete culverts has also been evaluated, with significant increases in shear strength, flexural strength, and toughness observed due to the addition

of fibers. The failure mode for all investigated culverts was identified as punching shear of the top slab (Mostafazadeh *et al.* 2019). Also, FE results suggested that shear capacity could be increased by up to 67% with a 0.52% macro-PP fiber dosage, recommending synthetic fibers as an alternative to increasing slab thickness or using transverse shear reinforcement (Mostafazadeh *et al.* 2019).

In summary, the shear performance of concrete culverts remains a contentious issue, with significant variation among studies regarding the shear capacity of RC box culverts. No studies have examined the shear behaviour of FRP-reinforced culverts, with most focusing on steel reinforcement. Synthetic fibers have shown promise in enhancing shear and flexural strength, potentially transforming failure modes from brittle shear failure to more ductile flexural failure.

2.5.1 Effect of Backfill and Installation methods

Reinforced concrete (RC) culverts can be installed using various methods, including embankment installation (EI), trench installation (TI), and trapezoidal trench installation (TTI). Studies have shown that the installation method significantly influences soil pressure, which is a crucial factor in the structural performance of RC box culverts. This review summarizes the impact of backfill and installation methods on vertical and horizontal earth pressures acting on RC culverts.

The soil-structure interaction (SSI) of deeply buried RC box culverts has been analysed using FE analysis, highlighting the substantial effect of sloping trench walls on SSI (Kim *et al.* 2005). Sidewall frictional forces were found to be higher in imperfect trench installation (ITI) compared to embankment installation, with uncompacted side fills resulting in higher earth pressures than compacted fills (Kang *et al.* 2008). Field tests comparing EI and TI methods showed that the vertical earth pressure on the TI culvert was 39% lower, while horizontal earth pressure was 49% higher compared to the EI culvert. A yielding foundation was also found to reduce vertical earth pressure (Oshati *et al.* 2012). In the TTI method, the vertical earth pressure differed significantly from other techniques, and reducing vertical pressure could be achieved by using a high slope and a narrow trench bottom (Chen *et al.* 2014). Reducing the stiffness difference between the foundation and embankment can also lower vertical load, as demonstrated in studies on soft foundation box culverts under high embankments (Zhang *et al.* 2015).

Geofoam has been shown to effectively reduce vertical stress on culverts, with less stiff and thinner geofoam providing more pronounced effects. Experimental results correlated well with analytical studies (Al-Naddaf *et al.* 2019). Field tests on sections of a long arc culvert showed that more compressible geofoam was particularly effective in reducing soil pressure (Wang, Junqi *et al.* 2021). Mathematical models confirmed that geosynthetics with sufficient stiffness significantly reduce vertical pressure, and the modulus of compressible material is crucial for the force exerted on the top slab (Ma *et al.* 2021). Geofoam as a backfill material also reduced lateral deformation by 63.3% and total deformation by 73.3% (Kumar *et al.* 2020).

The use of recycled materials as backfill has been explored to reduce earth pressure and address environmental concerns. Recycled tire chips and expanded polystyrene (EPS) were shown to reduce dynamic earth pressure by 70% and 23%, respectively, with tire chips proving more efficient due to their higher damping ratio and lower stiffness (Lee *et al.* 2007). Recycled concrete aggregate (RCA) as backfill exhibited similar friction angles to natural sand and gravel but had a lower density (Sohrabpour *et al.* 2021).

In conclusion, installation methods significantly affect earth pressures on concrete culverts, and compressible materials like geofoam and recycled materials can effectively reduce these pressures.

2.6 Application of FRP bars in SWSSC structures

FRPs have emerged as a promising alternative to steel reinforcement in concrete structures due to their lightweight nature, high tensile strength, and excellent corrosion resistance (Manalo *et al.* 2021; Xiao *et al.* 2023b; Mostafa *et al.* 2024). These attributes effectively reduce corrosion-related issues, thereby extending the service life of concrete elements, particularly in harsh environments (Zhang, Pu *et al.* 2022). Among FRP types, glass fiber-reinforced polymer (GFRP) is gaining popularity as a cost-effective reinforcement solution (Amran 2018; Xiao *et al.* 2023b).

Research on GFRP-reinforced culverts demonstrated their satisfactory load-carrying capacity, maintaining acceptable deflection, crack width, and long-term structural integrity over extended periods (Alkhrdaji *et al.* 2001; Gooranorimi *et al.* 2017b; Hassanli *et al.* 2022). The stability of GFRP bars in saltwater, chemical, and alkaline environments make it a suitable reinforcement for sustainable concrete alternatives like SWSSC (Wang

et al. 2017b; D'Antino *et al.* 2018; Wang, Zike *et al.* 2018). Despite extensive research on FRP bars in various SWSSC elements, studies specifically on SWSSC culverts with FRP reinforcement are limited. Existing literature indicates that GFRP outperforms basalt fiber-reinforced polymer (BFRP) in terms of durability in SWSSC (Wang *et al.* 2017b; Wang, Zike *et al.* 2018). Experimental investigations on slabs and beams confirm that GFRP bars offer comparable shear behaviour to steel reinforcement and increased load-carrying capacity with higher reinforcement ratios and shear span ratios (Wang, Zhihao *et al.* 2022; Vafaei *et al.* 2023; Zhou *et al.* 2023) . However, marine exposure negatively impacted the bond behaviour, resulting in reduced stiffness, ductility, and bond strength (Vafaei *et al.* 2023; Zhou *et al.* 2023).

Recent advancements have improved the economic and environmental feasibility of GFRP bars, contributing to its increasing adoption as an alternative to conventional steel reinforcement for concrete culverts (Hassanli *et al.* 2023). GFRP reinforcement significantly reduces maintenance costs by mitigating corrosion-related issues, thereby extending the lifespan of culverts. Design considerations for GFRP-reinforced concrete culverts should emphasize serviceability aspects, such as deflection and crack control, rather than focusing solely on ultimate strength (Hassanli *et al.* 2022). A long-term study on a precast GFRP-RC box culvert revealed no signs of microstructural degradation after 16 years in service, validating the suitability of GFRP bars for precast applications in corrosive environments (Gooranorimi *et al.* 2017a).

Experimental studies suggest that chloride ions have minimal impact on FRP durability, though exposure to moisture, extreme temperatures, or chemical environments may still degrade mechanical properties (ACI Committee 440 2012; Ahmed *et al.* 2020). Field investigations have confirmed that FRP bars offer strong resistance to chloride penetration from seawater and sea-sand (Raman *et al.* 2018), although combined effects of sustained stress, corrosion, and elevated temperatures may accelerate FRP degradation in SWSSC (Wang, Zike *et al.* 2018). GFRP-reinforced SWSSC beams have shown enhanced durability in chloride-rich environments (Wang, Zhihao *et al.* 2023), with field assessments revealing no significant deterioration in GFRP bars after accelerated marine exposure (Bertola *et al.* 2017; Khatibmasjedi *et al.* 2017). GFRP bars have been found to be highly durable in marine environments (Kim *et al.* 2008; Wu, Weiwei *et al.* 2023), although they demonstrate lower interlaminar shear strength compared to BFRP and carbon fiber-reinforced polymer (CFRP) bars (Wang *et al.* 2017a). Despite this, no

microstructural changes were detected in GFRP bars after several years of field exposure, suggesting they retained their tensile strength (Wang *et al.* 2017b). Studies also indicate that SWSSC exhibits higher bond strength with FRP bars compared to ordinary concrete, likely due to microparticles in SW filling voids within the matrix (Sena-Cruz *et al.* 2018; Wu, Weiwei *et al.* 2023). Water absorption and expansion contribute to increased bond strength between FRP and SWSSC, temporarily enhancing structural performance. Over long-term corrosive exposure, FRP-reinforced SWSSC beams demonstrate better performance than steel-reinforced beams, highlighting their potential for SWSSC applications (Hu *et al.* 2022).

Field monitoring of GFRP-reinforced concrete box culverts up to 20 months after construction revealed minimal deflection and elastic behaviour without residual deformation, indicating no significant stiffness degradation (Alkhrdaji *et al.* 2001). The results suggested that the ACI 440 design approach may be overly conservative (Alkhrdaji *et al.* 2001). A long-term evaluation of GFRP bars used in concrete culverts confirmed their mechanical, chemical, and physical stability. Despite chloride and carbonation penetration, microscopic examination found no evidence of degradation, with fiber content and cross-sectional area remaining unchanged. After 15 years in service, GFRP bars retained their microstructural integrity, affirming their long-term durability (Gooranorimi *et al.* 2017b; Benzecry *et al.* 2021).

2.7 Summary

This chapter provided a comprehensive review of seawater sea-sand concrete (SWSSC), focusing on its fresh and hardened properties, structural performance, and potential applications in coastal and marine environments. The environmental benefits of SWSSC were discussed, highlighting its role in reducing freshwater consumption, minimizing CO_2 emissions, and utilizing abundant seawater and sea-sand resources. Additionally, the mechanical and durability characteristics of SWSSC were analysed, emphasizing its performance compared to conventional concrete.

A critical aspect reviewed was the role of fiber-reinforced polymers (FRP) and synthetic fibers in enhancing the structural integrity of SWSSC. FRP reinforcement was shown to effectively mitigate corrosion-related challenges, while fiber addition improved crack control, tensile strength, and overall durability. The chapter also examined the structural behaviour of concrete culverts, particularly in terms of shear performance, backfill

effects, and failure mechanisms, providing insights into optimizing their design and material selection.

Despite these advancements, several knowledge gaps remain. Limited research exists on the effects of hybrid fiber reinforcement on the mechanical properties of SWSSC. Additionally, the cyclic performance of fiber-reinforced SWSSC remains unexplored, which is crucial for its application in marine environments and structures such as concrete culverts. Furthermore, the impact of fiber hybridization on the shear performance of SWSSC has not been thoroughly investigated. The application of FRP bars and SWSSC reinforced with mono and hybrid fibers in concrete culverts, particularly under cyclic loading, also requires further study. Addressing these gaps will support the wider adoption of SWSSC as a sustainable, durable, and cost-effective solution for marine and coastal infrastructure.

In this study, a two-phase approach was undertaken to investigate the material- and structural-level behaviour of hybrid fiber-reinforced seawater sea-sand concrete (SWSSC), particularly in culvert applications. Phase I focused on material-level testing (Chapters 3–6), examining the synergistic effects of hybrid fibers on the mechanical, fracture, cyclic flexural, and shear behaviour of SWSSC. Hybridization approaches included micro-fibers and combinations of micro- and macro-fibers, using polypropylene (PPS, PPL, TPPL), polyvinyl alcohol (PVA), and basalt fibers (BF). The study evaluated fracture toughness and energy and introduced a modified direct shear test method tailored to Australian standards. Phase II (Chapters 7–8) advanced to structural-level testing, assessing the behaviour of GFRP-reinforced SWSSC culverts under monotonic and cyclic loading. Concrete culverts with different sizes were tested to analyze crack propagation, load-displacement response, energy dissipation, ductility, and failure modes. The findings contribute to a deeper understanding of fiber-reinforced SWSSC as a viable alternative for marine and coastal infrastructure, offering insights into material performance, structural reliability, and design optimization for enhanced durability and sustainability.

Chapter 2 references

Abolmaali, A & Garg, A 2008a, 'Shear behavior and mode of failure for ASTM C1433 precast box culverts', Journal of Bridge Engineering, vol. 13, no. 4, pp. 331-38.

Abolmaali, A & Garg, AK 2008b, 'Effect of wheel live load on shear behavior of precast reinforced concrete box culverts', Journal of Bridge Engineering, vol. 13, no. 1, pp. 93-99.

ACI Committee 440 2012, Guide test methods for fiber-reinforced polymer (FRP) composites for reinforcing or strengthening concrete and masonry structures.

Ahmad, J, González-Lezcano, RA, Majdi, A, Ben Kahla, N, Deifalla, AF & El-Shorbagy, MA 2022, 'Glass fibers reinforced concrete: Overview on mechanical, durability and microstructure analysis', Materials, vol. 15, no. 15, p. 5111.

Ahmed, A, Guo, S, Zhang, Z, Shi, C & Zhu, D 2020, 'A review on durability of fiber reinforced polymer (FRP) bars reinforced seawater sea sand concrete', Construction and Building Materials, vol. 256, p. 119484.

Ahmed, SFU & Mihashi, H 2011, 'Strain hardening behavior of lightweight hybrid polyvinyl alcohol (PVA) fiber reinforced cement composites', Materials and structures, vol. 44, no. 6, pp. 1179-91.

Al-Naddaf, M, Han, J, Xu, C & Rahmaninezhad, SM 2019, 'Effect of geofoam on vertical stress distribution on buried structures subjected to static and cyclic footing loads', Journal of Pipeline Systems Engineering and Practice, vol. 10, no. 1, p. 04018027.

Al-Salloum, YA, El-Gamal, S, Almusallam, TH, Alsayed, SH & Aqel, M 2013, 'Effect of harsh environmental conditions on the tensile properties of GFRP bars', Composites Part B: Engineering, vol. 45, no. 1, pp. 835-44.

Alkhrdaji, T & Nanni, A 2001, 'Design, construction, and field-testing of an RC Box Culvert Bridge reinforced with GFRP bars', Non-Metallic Reinforcement for Concrete Structures-FRPRCS, vol. 5.

Amran, YM, Alyousef, Rayed, Rashid, Raizal SM, Alabduljabbar, Hisham, Hung, Chung-Chan 2018, Properties and applications of FRP in strengthening RC structures: A review, Structures.

Benzecry, V, Al-Khafaji, AF, Haluza, RT, Bakis, CE, Myers, JJ & Nanni, A 2021, 'Durability Assessment of 15-to 20-Year-Old GFRP Bars Extracted from Bridges in the US. I: Selected Bridges, Bar Extraction, and Concrete Assessment', Journal of Composites for Construction, vol. 25, no. 2, p. 04021007.

Bertola, F, Canonico, F & Nanni, A 2017, SEACON Project: sustainable concrete using seawater, salt-contaminated aggregates, and non-corrosive reinforcement, XIV DBMC-14th International Conference on Durability of Building Materials and Components.

CAO, X-q, ZHANG, Y, HE, Y-j, JIANG, Y-c & YUAN, X-j 2008, 'Retrospect and discussion of surveys for construction sand in China offshore area', Marine Geology & Quaternary Geology, vol. 28, no. 3, pp. 121-25.

Chapman, G 1968, The sea-dredged sand and gravel industry of Great Britain, Proceedings of a Symposium: Sea-dredged aggregates for concrete. Buckinghamshire.

Chen, B & Sun, L 2014, 'Performance of a Reinforced Concrete Box Culvert Installed in Trapezoidal Trenches', Journal of Bridge Engineering, vol. 19, no. 1, pp. 120-30.

Chen, Z, Li, S, Zhou, J, Xu, R & Dai, S 2022, 'Flexural behavior of GFRP bars reinforced seawater sea sand concrete beams exposed to marine environment: Experimental and numerical study', Construction and Building Materials, vol. 349, p. 128784.

Chenggong, Z, Zhiyuan, W, Zhenyu, Z, Qiuyu, G, Xinrui, W & Renda, Z 2023, 'Research on different types of fiber reinforced concrete in recent years: An overview', Construction and Building Materials, vol. 365, p. 130075.

D'Antino, T, Pisani, M & Poggi, C 2018, 'Effect of the environment on the performance of GFRP reinforcing bars', Composites Part B: Engineering, vol. 141, pp. 123-36.

Dhondy, T, Remennikov, A & Shiekh, MN 2019, 'Benefits of using sea sand and seawater in concrete: a comprehensive review', Australian Journal of Structural Engineering, vol. 20, no. 4, pp. 280-89.

Dong, S, Li, C & Xian, G 2021, 'Environmental impacts of glass-and carbon-fiber-reinforced polymer bar-reinforced seawater and sea sand concrete beams used in marine environments: An LCA case study', Polymers, vol. 13, no. 1, p. 154.

Etxeberria, M, Fernandez, JM & Limeira, J 2016a, 'Secondary aggregates and seawater employment for sustainable concrete dyke blocks production: Case study', Construction and Building Materials, vol. 113, pp. 586-95.

Etxeberria, M, Gonzalez-Corominas, A & Pardo, P 2016b, 'Influence of seawater and blast furnace cement employment on recycled aggregate concretes' properties', Construction and Building Materials, vol. 115, pp. 496-505.

Frederick, G, Ardis, C, Tarhini, K & Koo, B 1988, 'Investigation of the structural adequacy of C 850 box culverts', Transportation Research Record, no. 1191.

Garg, AK, Abolmaali, A & Fernandez, R 2007, 'Experimental investigation of shear capacity of precast reinforced concrete box culverts', Journal of Bridge Engineering, vol. 12, no. 4, pp. 511-17.

Garg, AK & Abolmaali, A 2009, 'Finite-element modeling and analysis of reinforced concrete box culverts', Journal of Transportation Engineering, vol. 135, no. 3, pp. 121-28.

Ge, L, Feng, Z, Sayed, U & Li, H 2023, 'Research on the performance of seawater sea-sand concrete: A review', Construction and Building Materials, vol. 409, p. 133921.

Ghahremannejad, M & Abolmaali, A 2019a, 'Shear capacity of reinforced concrete box culverts compared with AASHTO shear equation', Journal of Bridge Engineering, vol. 24, no. 5, p. 04019032.

Ghahremannejad, M, Abolmaali, A & Mahdavi, M 2019b, 'Shear strength of top slab of reinforced concrete box culverts', ACI Structural Journal, vol. 116, no. 6, pp. 63-74.

Girish, C, Tensing, D & Priya, K 2015, 'Dredged offshore sand as a replacement for fine aggregate in concrete', International Journal of Engineering Sciences & Emerging Technologies, vol. 8, no. 3, pp. 88-95.

Gooranorimi, O, Myers, J & Nanni, A 2017a, GFRP reinforcements in box culvert bridge: A case study after two decades of service, Symposium on Concrete Pipe and Box Culverts.

Gooranorimi, O & Nanni, A 2017b, 'GFRP Reinforcement in Concrete after 15 Years of Service', Journal of Composites for Construction, vol. 21, no. 5, p. 04017024.

Griffin, DF & Henry, RL 1964, The effect of salt in concrete on compressive strength, water vapor transmission, and corrosion of reinforcing steel, US Naval Civil Engineering Laboratory Port Hueneme, CA,

Guo, M, Hu, B, Xing, F, Zhou, X, Sun, M, Sui, L & Zhou, Y 2020, 'Characterization of the mechanical properties of eco-friendly concrete made with untreated sea sand and seawater based on statistical analysis', Construction and Building Materials, vol. 234, p. 117339.

Hassanli, R, Youssf, O, Manalo, A, Najafgholipour, MA, Elchalakani, M, del Rey Castillo, E & Lutze, D 2022, 'An experimental study of the behavior of GFRP-reinforced precast concrete culverts', Journal of Composites for Construction, vol. 26, no. 5, p. 04022043.

Hassanli, R, Manalo, A, Vafaei, D, Yekrangnia, M, Elchalakani, M & Noël, M 2023, 'Cyclic behavior of GFRP-reinforced concrete one-way slabs with synthetic fibers', Journal of Building Engineering, vol. 65, p. 105741.

Hong, CJ, Fan, Y, Zhang, RH & Wu, HT 2013, Research on the properties of sea sand concrete, Applied Mechanics and Materials.

Hu, X, Xiao, J, Zhang, K & Zhang, Q 2022, 'The state-of-the-art study on durability of FRP reinforced concrete with seawater and sea sand', Journal of Building Engineering, vol. 51, p. 104294.

Interior, USGSDd 2020, 'Mineral commodity summaries 2020', 06.02. 2020, Reston, VA; https://pubs. er. usgs. gov/publication/mcs2020.

James, RW 1983, Behavior of ASTM C 850 concrete box culverts without shear connectors, Texas Transportation Institute, the Texas A & M University System,

Kaidi, J, Xin, W, Lining, D, Zhiyuan, C, Huang, H, Xia, L, Jianxun, L & Zhishen, W 2023, 'Mechanical properties of multi-scale mono/hybrid non-metallic fiber-reinforced ultra-high performance seawater sea-sand concrete', Construction and Building Materials, vol. 401, p. 132922.

Kamal, A & Boulfiza, M 2011, 'Durability of GFRP rebars in simulated concrete solutions under accelerated aging conditions', Journal of Composites for Construction, vol. 15, no. 4, pp. 473-81.

Kang, J, Parker, F, Kang, YJ & Yoo, CH 2008, 'Effects of frictional forces acting on sidewalls of buried box culverts', International Journal for Numerical and Analytical Methods in Geomechanics, vol. 32, no. 3, pp. 289-306.

Katano, K, Takeda, N, Ishizeki, Y & Iriya, K 2013, Properties and application of concrete made with sea water and un-washed sea sand, Proceedings of Third International conference on Sustainable Construction Materials and Technologies.

Khatibmasjedi, M & Nanni, A 2017, Durability of GFRP reinforcement in SEACON, The Fifth International Conference on Durability of Fiber Reinforced Polymer (FRP) Composites for Construction and Rehabilitation of Structures (CDCC 2017).

Khatibmasjedi, M 2018, 'Sustainable concrete using seawater and glass fiber reinforced polymer bars', University of Miami.

Kim, H-Y, Park, Y-H, You, Y-J & Moon, C-K 2008, 'Short-term durability test for GFRP rods under various environmental conditions', Composite Structures, vol. 83, no. 1, pp. 37-47.

Kim, K & Yoo, CH 2005, 'Design loading on deeply buried box culverts', Journal of Geotechnical and Geoenvironmental Engineering, vol. 131, no. 1, pp. 20-27.

Kumar, A, Ahirwar, SK & Mandal, J 2020, 'Behavior of box culvert with geofoam as a backfill material in Highway', Transportation Research Procedia, vol. 48, pp. 3642-47.

Lee, HJ & Roh, HS 2007, 'The use of recycled tire chips to minimize dynamic earth pressure during compaction of backfill', Construction and Building Materials, vol. 21, no. 5, pp. 1016-26.

Li, P, Li, W, Yu, T, Qu, F & Tam, VWY 2020, 'Investigation on early-age hydration, mechanical properties and microstructure of seawater sea sand cement mortar', Construction and Building Materials, vol. 249, 2020/07/20/, p. 118776.

Li, P, Li, W, Sun, Z, Shen, L & Sheng, D 2021, 'Development of sustainable concrete incorporating seawater: A critical review on cement hydration, microstructure and mechanical strength', Cement and Concrete Composites, vol. 121, p. 104100.

Li, Q, Geng, H, Shui, Z & Huang, Y 2015, 'Effect of metakaolin addition and seawater mixing on the properties and hydration of concrete', Applied Clay Science, vol. 115, pp. 51-60.

Li, Y, Zhang, J, He, Y, Huang, G, Li, J, Niu, Z & Gao, B 2022, 'A review on durability of basalt fiber reinforced concrete', Composites Science and Technology, vol. 225, p. 109519.

Li, Y, Liu, W, Mi, T, Ding, X, Tang, L & Xing, F 2024, 'Durability study of seawater and sea-sand concrete under the combined effects of carbonation and chloride redistribution', Journal of Building Engineering, p. 109294.

Limeir, J, Agulló, L & Etxeberria, M 2012, 'Dredged marine sand as construction material', European journal of environmental and civil engineering, vol. 16, no. 8, pp. 906-18.

Limeira, J, Agulló, L & Etxeberria, M 2012, 'Dredged marine sand as a new source for construction materials', Materiales de Construcción, vol. 62, no. 305, pp. 7-24.

Lv, W, Sun, Z & Su, Z 2020, 'Study of seawater mixed one-part alkali activated GGBFS-fly ash', Cement and Concrete Composites, vol. 106, p. 103484.

Ma, Q, Zheng, J-J & Xiao, H-l 2021, 'Analysis of pressure on the roof of a culvert underneath a ditch with compressible material covered by a geosynthetic layer', European journal of environmental and civil engineering, vol. 25, no. 6, pp. 1025-41.

Manalo, A, Mendis, P, Bai, Y, Jachmann, B & Sorbello, C 2021, 'Fiber-reinforced polymer bars for concrete structures: State-of-the-practice in Australia', Journal of Composites for Construction, vol. 25, no. 1, p. 05020007.

Mashayekhi, A, Hassanli, R, Zhuge, Y, Ma, X, Chow, CW, Bazli, M & Manalo, A 2024, 'Structural behaviour of small GFRP-reinforced seawater sea-sand fiber reinforced concrete culverts', Structures.

McGrath, TJ, Liepins, AA & Beaver, JL 2005, 'Live load distribution widths for reinforced concrete box sections', Transportation Research Record: Journal of the Transportation Research Board, no. CD 11-S.

Micelli, F & Nanni, A 2004, 'Durability of FRP rods for concrete structures', Construction and Building Materials, vol. 18, no. 7, pp. 491-503.

Mostafa, IT, Mousa, S, Mohamed, HM & Benmokrane, B 2024, 'Experimental and Analytical Behavior of GFRP-Reinforced Concrete Box Girders under Pure Torsion', Journal of Composites for Construction, vol. 28, no. 1, p. 04023064.

Mostafazadeh, M, Abolmaali, A & Ghahremannejad, M 2019, 'Shear Strength of Synthetic Fiber-Reinforced Concrete Box Culverts', Journal of Bridge Engineering, vol. 24, no. 6, p. 04019039.

Newman, K 1968, Sea-dredged Aggregates for Concrete: Proceedings of a Symposium, Buckinghamshire: Sand and Gravel Association Great Britain.

Oshati, OS, Valsangkar, AJ & Schriver, AB 2012, 'Performance of two cast-in-place box culverts under high embankments', Canadian geotechnical journal, vol. 49, no. 12, pp. 1331-46.

Pakravan, HR, Latifi, M & Jamshidi, M 2017, 'Hybrid short fiber reinforcement system in concrete: A review', Construction and Building Materials, vol. 142, 2017/07/01/, pp. 280-94.

Raman, RS, Guo, F, Al-Saadi, S, Zhao, X-L & Jones, R 2018, 'Understanding fibre-matrix degradation of FRP composites for advanced civil engineering applications: an overview', Corrosion and Materials Degradation, vol. 1, no. 1, pp. 27-41.

Sena-Cruz, J, Pereira, E, Freitas, N, Pereira, E & Soares, SRR 2018, 'Bond behaviour between GFRP rods and concrete produced with seawater: an experimental research'.

Shi, Z, Shui, Z, Li, Q & Geng, H 2015, 'Combined effect of metakaolin and sea water on performance and microstructures of concrete', Construction and Building Materials, vol. 74, pp. 57-64.

Sikora, P, Cendrowski, K, Abd Elrahman, M, Chung, S-Y, Mijowska, E & Stephan, D 2020, 'The effects of seawater on the hydration, microstructure and strength development of Portland cement pastes incorporating colloidal silica', Applied Nanoscience, vol. 10, no. 8, pp. 2627-38.

Sohrabpour, AH & Long, M 2021, 'Behaviour of intermediate stiffness culverts with recycled concrete aggregate backfill', Tunnelling and Underground Space Technology, vol. 115, p. 104061.

Sun, W, Liu, J, Yan, J & Dai, Y 2016, 'Study on the influence of chloride ions content on the sea sand concrete performance', Am. J. Civ. Eng, vol. 4, pp. 50-54.

Ting, MZY, Wong, KS, Rahman, ME & Joo, MS 2020a, 'Mechanical and durability performance of marine sand and seawater concrete incorporating silicomanganese slag as coarse aggregate', Construction and Building Materials, vol. 254, p. 119195.

Ting, MZY, Wong, KS, Rahman, ME & Selowara Joo, M 2020b, 'Mechanical and durability performance of marine sand and seawater concrete incorporating silicomanganese slag as coarse aggregate', Construction and Building Materials, vol. 254, 2020/09/10/, p. 119195.

Tjaronge, MW & Irfan, UR 2015, 'Porosity, pore size and compressive strength of self compacting concrete using sea water', Procedia Engineering, vol. 125, pp. 832-37.

Vafaei, D, Hassanli, R, Ma, X, Duan, J & Zhuge, Y 2021a, 'Sorptivity and mechanical properties of fiber-reinforced concrete made with seawater and dredged sea-sand', Construction and Building Materials, vol. 270, p. 121436.

Vafaei, D, Ma, X, Hassanli, R & Zhuge, Y 2021b, Effects of seawater and sea-sand on concrete properties: A review paper, EASEC16: Proceedings of The 16th East Asian-Pacific Conference on Structural Engineering and Construction, 2019.

Vafaei, D, Ma, X, Hassanli, R, Duan, J & Zhuge, Y 2022, 'Microstructural behaviour and shrinkage properties of high-strength fiber-reinforced seawater sea-sand concrete', Construction and Building Materials, vol. 320, p. 126222.

Vafaei, D, Ma, X, Hassanli, R, Duan, J & Zhuge, Y 2023, 'Experimental study on cyclic flexural behaviour of GFRP-reinforced seawater sea-sand concrete slabs with synthetic fibres', Ocean Engineering, vol. 273, p. 114014.

Wang, J & Huang, J 2021, 'Full-scale field study of using geofoam to reduce earth pressures on buried concrete culverts', Geotextiles and Geomembranes.

Wang, Z, Zhao, X-L, Xian, G, Wu, G, Raman, RS & Al-Saadi, S 2017a, 'Durability study on interlaminar shear behaviour of basalt-, glass-and carbon-fibre reinforced polymer (B/G/CFRP) bars in seawater sea sand concrete environment', Construction and Building Materials, vol. 156, pp. 985-1004.

Wang, Z, Zhao, X-L, Xian, G, Wu, G, Raman, RS, Al-Saadi, S & Haque, A 2017b, 'Long-term durability of basalt-and glass-fibre reinforced polymer (BFRP/GFRP) bars in seawater and sea sand concrete environment', Construction and Building Materials, vol. 139, pp. 467-89.

Wang, Z, Zhao, X-L, Xian, G, Wu, G, Raman, RS & Al-Saadi, S 2018, 'Effect of sustained load and seawater and sea sand concrete environment on durability of basalt-and glass-fibre reinforced polymer (B/GFRP) bars', Corrosion science, vol. 138, pp. 200-18.

Wang, Z, Xie, J, Li, J, Liu, P, Shi, C & Lu, Z 2022, 'Flexural behaviour of seawater–sea sand concrete beams reinforced with GFRP bars: effects of the reinforcement ratio, stirrup

ratio, shear span ratio and prestress level', Journal of Building Engineering, vol. 54, p. 104566.

Wang, Z, Xie, J, Mai, Z, Liu, P, Lu, Z & Li, L 2023, 'Durability of GFRP bar-reinforced seawater–sea sand concrete beams: Coupled effects of sustained loading and exposure to a chloride environment', Engineering Structures, vol. 283, p. 115814.

Wu, W, He, X, Yang, W, Wei, B & Alam, MS 2023, 'Durability and microstructure degradation mechanism of FRP-seawater seasand concrete structures: A review', Construction and Building Materials, vol. 391, p. 131825.

Xiao, J, Qiang, C, Nanni, A & Zhang, K 2017, 'Use of sea-sand and seawater in concrete construction: Current status and future opportunities', Construction and Building Materials, vol. 155, pp. 1101-11.

Xiao, L, Hu, H, Peng, S, Du, Z & Xu, C 2023, 'Compression behavior of GFRP reinforced hybrid fibre reinforced concrete short columns subjected to eccentric loading', Construction and Building Materials, vol. 393, p. 131985.

Xiong, Z, He, S, Kwan, A, Li, L & Zeng, Y 2021, 'Compressive behaviour of seawater sea-sand concrete containing glass fibres and expansive agents', Construction and Building Materials, vol. 292, p. 123309.

Yang, S, Zang, C, Xu, J & Fan, G 2020, 'Determination of Fracture Parameters of Seawater Sea Sand Concrete Based on Maximum Fracture Load', Journal of Materials in Civil Engineering, vol. 32, no. 1, p. 04019315.

Yang, Z, Zhan, X, Zhu, H, Zhang, B, Li, R, Dong, Z & Kua, HW 2024, 'Eco-sustainable design of seawater sea-sand slag-based geopolymer mortars incorporating ternary solid waste', Construction and Building Materials, vol. 431, p. 136512.

Yee, RA 2004, 'Shear behaviour of concrete box culverts', Dept. of Civil Engineering, Univ. of Toronto, Toronto.

Yifan, Z, Xiang, H, Caijun, S, Zuhua, Z & Deju, Z 2021, 'A review on seawater sea-sand concrete: Mixture proportion, hydration, microstructure and properties', Construction and Building Materials, vol. 295, p. 123602.

Younis, A, Ebead, U, Suraneni, P & Nanni, A 2018, 'Fresh and hardened properties of seawater-mixed concrete', Construction and Building Materials, vol. 190, pp. 276-86.

Yuntao, H, Shiping, Y & Zhangtao, P 2020, 'Crack development and calculation method for the flexural cracks in BFRP reinforced seawater sea-sand concrete (SWSSC) beams', Construction and Building Materials, vol. 255, p. 119328.

Zeng, J-J, Liao, J, Zhuge, Y, Guo, Y-C, Zhou, J-K, Huang, Z-H & Zhang, L 2022, 'Bond behavior between GFRP bars and seawater sea-sand fiber-reinforced ultra-high strength concrete', Engineering Structures, vol. 254, p. 113787.

Zhang, J-h, Yao, Y-s, Zheng, J-l & Zhang, T 2015, 'Centrifugal model test and numerical simulation of vertical earth pressure on soft foundation box culvert', Journal of Central South University, vol. 22, no. 9, pp. 3556-63.

Zhang, P, Shang, J, Liu, Y, Shao, J, Gao, D, Dong, Z & Sheikh, SA 2022, 'Flexural behavior of GFRP bar-reinforced concrete beams with U-shaped UHPC stay-in-place formworks', Journal of Building Engineering, vol. 45, p. 103403.

Zhao, Y, Hu, X, Shi, C, Zhang, Z & Zhu, D 2021, 'A review on seawater sea-sand concrete: Mixture proportion, hydration, microstructure and properties', Construction and Building Materials, vol. 295, p. 123602.

Zhihao, W, Jianhe, X, Jianglin, L, Peng, L, Cuiqing, S & Zhongyu, L 2022, 'Flexural behaviour of seawater–sea sand concrete beams reinforced with GFRP bars: Effects of the reinforcement ratio, stirrup ratio, shear span ratio and prestress level', Journal of Building Engineering, vol. 54, p. 104566.

Zhou, L, Zheng, Y, Di, B, Lv, J & Taylor, SE 2023, Shear behaviour of SWSS-SCC beams reinforced with GFRP bars and Stirrups: Experimental and analytical investigations, Structures.

Zhu, M, Chen, B, Wu, M & Han, J 2023, 'Preparation and mechanical characterization of cost-effective low-carbon engineered cementitious composites with seawater and sea-sand', Cement and Concrete Composites, vol. 136, p. 104883.

Zongao, L, Fuming, D, Hui, Q, Peifan, Q & Yifei, S 2024, 'Shear performance of seawater sea-sand concrete beams reinforced with shape memory alloy longitudinal and stirrup bars', Construction and Building Materials, vol. 421, p. 135685.

3 Synergistic effects of fiber hybridization on the mechanical performance of seawater sea-sand concrete

Reprinted and reformatted (including changes to the referencing style) with permission from Elsevier Ltd (see Appendix B).

Mashayekhi, A, Hassanli, R, Zhuge, Y, Ma, X & Chow, CW 2024a, 'Synergistic effects of fiber hybridization on the mechanical performance of seawater sea-sand concrete', Construction and Building Materials, vol. 416, p. 135087.

Abstract

This study investigated the effect of hybrid fibers and their synergic interactions on the mechanical properties of seawater sea-sand (SWSS) concrete. These properties include compressive strength, elastic modulus, splitting tensile strength, compressive stress-strain behaviour, and ductility, as well as slump and air content. Two hybridizations were incorporated: hybrid micro-fibers (hybridization of the type of fibers) and hybrid micro- and macro-fibers (hybridization of the length of fibers). The hybrid fibers comprised three micro-fibers—polypropylene (PPS), polyvinyl alcohol (PVA), basalt (BF)—and two macro-fibers—polypropylene (PPL), and twisted polypropylene (TPPL)—with a total volume fraction of 0.25%. The findings revealed that if designed properly hybrid micro-fibers can outperform mono-fibers in mechanical properties and ductility, bridging micro-cracks. This study revealed that incorporating PVA/PPS and BF/PPS hybrid micro-fibers enhanced both interlocking, facilitated by the chemical bonding of PVA and BF, and elongation, enabled by PPS. This synergistic effect led to a significant 33-35% increase in compressive elastic modulus compared to mono PPS fibers. At the same total dosage of fibers, PVA/BF hybridization significantly improved SWSS concrete total energy absorption and residual strength under compression by 44% and 181% over mono BF incorporation. Increasing BF in hybrid fibers significantly reduced ductility and increased brittleness. In PVA/PPL hybridization, PVA fiber improved PPL bonding strength and tensile capacity through chemical bonding with concrete, enhancing ductility and residual strength under compression by 59% and 65% over mono PPL fiber. Overall, hybrid fibers improved the mechanical properties and ductility of SWSS over mono-fibers. This was due to positive synergy and inter-fiber performance due to mechanical and chemical

bonding, overcoming individual fiber type limitations (e.g., poor bonding, tensile strength, or ductility). This effect was more pronounced with micro- and macro-fiber hybridization. The findings of this study can be used to provide an improved performance for SWSS concrete by adding hybrid fibers to the mix considering the synergic interactions of fibers.

Keywords

Fiber-reinforced concrete, Seawater, Sea-sand, Stress-strain behaviour, Basalt fiber, Hybrid fibers, Mechanical properties.

3.1 Introduction

The building and infrastructure industries heavily rely on concrete, a primary material whose consumption increases with industry growth. This widespread use has depleted natural resources like freshwater and river sand, leading to harm inflicted upon river ecosystems (Xiong *et al.* 2021). Globally, annual concrete and cement consumption, around 25 and 3.3 billion tons respectively, generates substantial carbon dioxide, contributing significantly to emissions (Amran *et al.* 2020). Developing eco-friendly concrete is vital for engineering sustainability. Seawater sea-sand (SWSS) concrete, from abundant resources, offers a promising alternative. As much as 388 billion cubic meters of sea-sand (SS) could serve as fine aggregate on China coastline alone (Cao *et al.* 2008). Additionally, seawater (SW), constituting 97% of water on Earth (Tjaronge *et al.* 2015). SWSS concrete has advantages including conserving freshwater, reducing carbon footprints (Xiong *et al.* 2021), and excellent resistance in marine environments. It is ideal for coastal, offshore, environmental projects like reefs, and habitat restoration. Additionally, it is cost-effective in areas with scarce freshwater and high-quality aggregates. Previous study demonstrated viability of slag-based alkali-activated materials (AAMs) as alternatives for ordinary Portland cements (OPCs) with sea-sand and coral aggregate in SWSS concretes, resulted in reduced CO_2 emission, cost, and improved interfacial transition zone (ITZ) density for crack resistance (Yang *et al.* 2023). With proper planning, SWSS concrete can potentially be a valuable, sustainable, and durable alternative to traditional concrete in harsh environments. Additionally, using non-corrosive materials can potentially mitigate the risk of steel corrosion, a major issue with SWSS concrete (Vafaei *et al.* 2021b; Kaidi *et al.* 2023).

In comparison to normal concrete, research studies have consistently shown that early-stage compressive strength of SW and SS blended concrete is higher (Younis *et al.* 2018; Ting *et al.* 2020a), thanks to the chloride present in these materials that speeds up cement hydration. However, there is conflicting evidence in the literature regarding the long-term compressive strength (Vafaei *et al.* 2021a). Earlier study has suggested that the strength deterioration factor (SDF) in SWSS concrete range from 24% to 90% which declines over time (Zhao *et al.* 2021). The variation in compressive strength between SWSS and conventional concrete is influenced mainly by three key factors: the water-to-binder (W/B) ratio, properties of sea-sand, and supplementary cementitious materials (SCMs) (Zhao *et al.* 2021). Elastic modulus studies of SWSS concrete have generally shown that SW and SS have no significant impact (Yang *et al.* 2020; Vafaei *et al.* 2021b; Zhao *et al.* 2021). However, most investigations have reported that SW and SS can adversely affect concrete tensile strength (Ting *et al.* 2020a; Vafaei *et al.* 2021a; Yifan *et al.* 2021).

Crack control in concrete is crucial for long-term performance and structural integrity, especially in harsh environments like those encountered by seawater and sea-sand. While fiber reinforced polymer (FRP) bars eliminate the specific concern of steel reinforcement corrosion in SWSS structures compared to conventional RC, crack control remains crucial for ensuring their long-term performance and robustness in harsh environments. Cracks facilitate ingress of aggressive agents like water, chlorides, and sulfates, accelerating degradation and compromising robustness of SWSS concrete. This underscores the importance of fiber reinforcement in SWSS concrete, as it effectively minimizes crack initiation and propagation, leading to enhanced long-term performance and structural integrity. Furthermore, replacing steel reinforcement with FRP bars can potentially reduce both crack formation and deflection. Additionally, incorporating FRP tubes significantly enhances concrete durability by providing a confinement effect. This confinement effect mitigates the brittle behaviour characteristic of over-reinforced concrete, leading to improved overall performance (Benny *et al.* 2023). In SWSS concrete, with elevated ion concentration from seawater and sea-sand (Zhao *et al.* 2021), using steel fibers, common in normal concrete, are infeasible due to corrosion risk (Kaidi *et al.* 2023). Consequently, researchers have focused on synthetic fibers such as polyvinyl alcohol (PVA) and polypropylene (PP) because of their cost-effectiveness, corrosion resistance, and favorable impact on concrete properties in aggressive environments, including SWSS concrete (Vafaei *et al.* 2021a; Vafaei *et al.* 2022b; Kaidi *et al.* 2023).

Investigations into the effects of mono-fibers on SWSS concrete have demonstrated that adding 0.3% micro PVA and PP fibers can enhance splitting tensile strength by 17% and 23%, respectively (Vafaei *et al.* 2021a). Moreover, adding 3% macro basalt fiber (BF) significantly improved the compressive strength of ultra-high performance (UHP) SWSS concrete by approximately 26%, while micro PP and BF additions had no adverse impact on compressive strength (Kaidi *et al.* 2023).

Mono-fibers, whether micro or macro, pose limitations in crack control, tensile strength, toughness, and bonding due to chemical and mechanical constraints and challenges in uniform distribution at high doses. This restricts their applicability and potential to enhance mechanical properties broadly (Pakravan *et al.* 2017; Chenggong *et al.* 2023; Kaidi *et al.* 2023). Research indicates that micro- and macro-fibers hybridization by meticulous fiber selection based on criteria like type, volume, aspect ratio, and interface bonding can enhance the mechanical properties, ductility, and durability of both normal and SWSS concrete (Ahmed *et al.* 2011; Chenggong *et al.* 2023; Kaidi *et al.* 2023), overcoming the limitations of mono-fibers. Higher mono-fiber content in concrete risks clumping and reduced mechanical properties. Replacing some in a hybrid system with a similar fiber volume, improves distribution due to diverse fiber properties, including size and geometry, ultimately leading to enhanced mechanical performance. For instance, investigations on hybrid PVA fibers showed increasing thicker fibers content improved ductility (Ahmed *et al.* 2011). It was shown that in UHP-SWSS concrete, combining micro- and macro-fibers increased compressive strength with increasing fiber content, but a high micro-fiber dosage (0.6 vol%) slightly reduced it (Kaidi *et al.* 2023). Additionally, hybrid PP fibers, monofilament and staple, improved concrete properties compared to mono-fibers due to the high elastic modulus of the monofilament fiber and the stress concentration reduction of the staple one (Hsie *et al.* 2008). A similar outcome was observed when hybridizing steel fibers with PP or PVA fibers (Lawler *et al.* 2002; Banthia *et al.* 2004). Studies found a 75% PVA and 25% PP blend optimal for enhancing flexural strength (Pakravan *et al.* 2016). Although research on size-based hybridization (micro and macro) in SWSS concrete is limited, it often overlooks the critical aspect of micro-fiber hybridization. This is notable given the heightened chemical reactivity of SWSS concrete compared to normal concrete (Yifan *et al.* 2021). Research on micro-fiber hybridization in normal concrete demonstrated the significant influence of distinct chemical and mechanical properties on strength and ductility. Combining PVA/BF in

normal concrete improved mechanical and physical properties compared to mono-fibers. BF outperformed PVA in enhancing the fiber-matrix interface due to superior distribution (Özkan *et al.* 2020; Şükrü *et al.* 2021; Zhuang *et al.* 2022).

There is limited research on hybridizing fibers, especially micro-fibers, in normal-strength SWSS concrete. Prior studies on conventional concrete indicated that fiber complementarity enhances strength and ductility over mono-fibers. The substantial chemical reactivity in SWSS concrete can potentially affect fiber synergies and interfacial bonding, critical for the performance of fibers. This study aims to comprehensively evaluate the potential of hybrid fibers and their interactions for enhancing the mechanical properties—compressive and tensile strength— and the ductility of SWSS concrete. These characteristics are considered critical for the enhancement of the structural performance and durability of SWSS concrete elements. Both the fresh and hardened characteristics of hybrid fiber-reinforced SWSS (HFR-SWSS) concrete will be assessed using mono-fibers, hybrid micro-fibers, and hybrid micro- and macro-fibers, and the synergic interaction between fibers will be discussed.

3.2 Materials and experiments

3.2.1 Materials

In this study, cementitious materials consisted of ordinary Portland cement (OPC) and ground granulated blast furnace slag (GGBS). Seawater from Adelaide coastal waters, with high chloride and sulphate levels (360 and 76 times tap water, respectively), was stored in a sealed container to prevent evaporation and contamination. Potable water from Adelaide water supply network was used for traditional concrete. Fine aggregates were natural sand (NS) and sea-sand (SS) with 2.5 mm and 0.3 mm maximum sizes, respectively. SS had a smooth, rounded surface. The specific gravity, bulk density, and fineness modulus of the coarse aggregate, NS, and DSS were 2.71 kg/m^3, 2.66 kg/m^3, and 2.57 kg/m^3 respectively, 1560 kg/m^3, 1628 kg/m^3 and 1578 kg/m^3 respectively, and 6.92, 1.97, and 1.38 respectively. Inductively Coupled Plasma Optical Emission Spectroscopy (ICP-OES) was used to assess heavy metal levels in sand and water. Sea sand had significantly higher lead (Pb) and selenium (Se) concentrations than natural sand, with Pb levels of 1.05 mg/kg and Se levels of 2.80 mg/kg, respectively. Natural sand had lower Pb and Se levels, at 0.08 mg/kg and 0.17 mg/kg, respectively. These

levels are all below the hazardous regulatory limit for landfills based on the European standard (Decision 2003).

The research used a mix of synthetic and natural fibers to reinforce SWSS concrete, with micro-fibers (PPS, PVA, and BF) and macro-fibers (PPL and TPPL) employed without added treatments to minimize expenses. **Figure 3-1** displays the dimensions of the fibers and shapes using a scanning electron microscope (SEM), and **Table 3-1** describes their attributes. The macro-fibers with similar lengths, but different aspect ratios and stiffness, were used to study their impact. In addition, an eco-friendly PPL fiber was used, which was made from recycled plastic and is readily available in the Australian market, as they resist harsh and corrosive environments. BF was also investigated due to its high tensile strength, cost-effectiveness, and eco-friendliness. Micro-fiber length was kept consistent to avoid its effect on results. Various micro-fibers were used based on different tensile strengths, young modulus, and aspect ratios. Physical properties of different fibers.

Table 3-1 Physical properties of different fibers

Property	PPS[1]	PVA[2]	BF[3]	PPL[4]	TPPL[5]
Specific gravity	0.91	1.3	1.57	0.91	0.91
Length (mm)	6	8	7	47	54
Diameter (μm)	180	38	15	—	800
Thickness (μm)	—	—	—	<500	—
Tensile strength (MPa)	600	1600	2900	400	620
Young's modulus (GPa)	9.5	40	85	6	9.5
Chemical resistance	Excellent	Excellent	Excellent	Excellent	Excellent
Melting point (°C)	160	225	1450	160	160
Water absorption (% by weight)	<1	<1	<1	Nil	Nil
Alkali resistance	Excellent	Excellent	—	Excellent	Excellent
Corrosion resistance	Excellent	Excellent	—	Excellent	Excellent

[1] short polypropylene, [2] polyvinyl alcohol, [3] basalt fiber, [4] long polypropylene, [5] long twisted polypropylene.

3.2.2 Mixture proportions and test methods

In this study, a wide range of mixes were considered to comprehensively understand the synergistic effects of fibers, based on their type and size, on the strength and ductility of SWSS concrete. A total of 23 concrete mixes (target compressive strength= 25 MPa, design slump=150-200 mm) were prepared at the University of South Australia. **Table 3-2** provide the mix proportions of these mixes. As shown, Series I used plain normal and SWSS, Series II employed 0.25% mono-fibers, Series III used 0.25% micro-fiber hybridization, and Series IV combined micro- and macro-fibers at 0.25%. To ensure

proper mixing and avoid any detrimental impact on sample performance, a 0.25% fiber dosage was adopted. This dosage has been previously utilized in research to examine the influence of fibers on FRC properties (Pakravan *et al.* 2017; Vafaei *et al.* 2022b). Excessive fiber content can lead to non-uniform fiber dispersion and clumping tendencies, thereby hindering workability, and potentially compromising the synergistic benefits anticipated from the combination of different fibers. The hybrid mixtures were made up of two ratios, 33% and 66% of each component. For instance, two hybrid mixtures of PPL and PVA fibers were tested: 0.33PPL and 0.66PVA, and 0.66PPL and 0.33PVA.

The fresh characteristics of FR-SWSS concrete were determined using air content and slump tests in accordance with AS 1012.4.2 (Australia 2014b) and AS1012.3.1 (Standard 2014) standards. The slump test investigated four water-to-binder (W/B) ratios (0.59, 0.64, 0.67, 0.71) on fiber-reinforced (FR_SWSS) concrete workability. Mechanical properties, including compressive strength, splitting tensile strength, and elastic modulus, were examined following AS 1012.9 (Committe 2014) , AS 1012.10 (Australia, Standards 2000), and AS 1012.17 (AS 2005). Nine standard 100×200 mm concrete cylinders were prepared for every mix, amounting to 207 samples in total. Samples were cured at 23°C ± 2°C for 28 days in a lime-saturated water bath. Compressive strength tests were conducted on days 7, 28, and 365, while splitting tensile strength and elastic modulus tests were performed on day 28. Three samples were conducted to each test and the mean values are reported here. A 100-kN universal testing device applied loading rates of 20 MPa/min, 1.5 MPa/min, and 15 MPa/min, per Australian standards (Australia, Standards 2000; AS 2005; Committe 2014) for compressive strength, splitting tensile strength, and elastic modulus, respectively.

To explore the stress-strain properties, 365-day old concrete cylinders were tested for compression using an 1800-kN compression machine. The test followed the RILEM standard (Committee 1970), applying an axial load at a constant displacement ratio of 0.001 mm/s. The axial shortening of the cylinder during compression was measured with linear variable displacement transducers (LVDT) set between the platens, ensuring data integrity by avoiding contact with the specimen and preventing interference from specimen cracking and spalling. Loading was terminated when either the strain reached approximately 0.0065 or the load dropped to 20% of maximum load.

Table 3-2 Mix design of concrete mixes and their fresh properties

Concrete mix			Mix proportions (kg/m^3)												Slump (mm)	Air content %	Reinforcing index (RI)				
			Fiber					Binder		Gravel	Sand		Water				Fiber				
			PPS	PVA	BF	PPL	TPPL	OPC	GGBS		PPS	PPS	PPS	PPS			PPS	PVA	BF	PPL	TPPL
Series I	Plain	FWNS	—	—	—	—	—	126	234	995	785	—	256	—	210	2.3	—	—	—	—	—
		SWSS	—	—	—	—	—				—	785	—	256	185	3.7	—	—	—	—	—
Series II	Mono-fibers	PPS	2.28	—	—	—	—	126	234	995	—	785	—	256	85	5.1	0.14	—	—	—	—
		PVA	—	3.25	—	—	—								140	4.3	—	0.53	—	—	—
		BF	—	—	6.63	—	—								115	5.6	—	—	0.10	—	—
		PPL	—	—	—	2.28	—								185	4.4	—	—	—	0.25	—
		TPPL	—	—	—	—	2.28								175	3.8	—	—	—	—	0.14
Series III	Micro-fiber Hybridization	0.33PPS+0.66BF	0.76	—	4.41	—	—	126	234	995	—	785	—	256	95	5.6	0.05	—	0.07	—	—
		0.66PPS+0.33BF	1.52	—	2.21	—	—								73	5.5	0.09	—	0.03	—	—
		0.66PVA+0.33BF	—	2.17	2.21	—	—								145	5	—	0.35	0.03	—	—
		0.33PVA+0.66BF	—	1.08	4.41	—	—								115	4.2	—	0.17	0.07	—	—
		0.33PPS+0.66PVA	0.76	2.17	—	—	—								115	4.9	0.05	0.35	—	—	—
		0.66PPS+0.33PVA	1.52	1.08	—	—	—								85	5.2	0.09	0.17	—	—	—
Series IV	Micro- and Macro-fiber Hybridization	0.33PPL+0.66PPS	1.52	—	—	0.76	—	126	234	995	—	785	—	256	95	5.2	0.09	—	—	0.08	—
		0.66PPL+0.33PPS	0.76	—	—	1.52	—								135	4.7	0.05	—	—	0.17	—
		0.66PPL+0.33PVA	—	1.08	—	1.52	—								165	4.2	—	0.17	—	0.17	—
		0.33PPL+0.66PVA	—	2.17	—	0.76	—								145	4.7	—	0.35	—	0.08	—
		0.33PPL+0.66BF	—	—	4.41	0.76	—								120	5.5	—	—	0.07	0.08	—
		0.66PPL+0.33BF	—	—	2.21	1.52	—								170	5.1	—	—	0.03	0.17	—
		0.33TPPL+0.66PVA	—	2.17	—	—	0.76								145	4.1	—	0.35	—	—	0.05
		0.66TPPL+0.33PVA	—	1.08	—	—	1.52								165	3.8	—	0.17	—	—	0.09
		0.33TPPL+0.66BF	—	—	4.41	—	0.76								125	4.4	—	—	0.07	—	0.05
		0.66TPPL+0.33BF	—	—	2.21	—	1.52								140	3.6	—	—	0.03	—	0.09



Figure 3-1 SEM image, shape, and dimension of different types of fibers, a) PPS, b) PVA, c) BF, d) PPL, and e) TPPL

3.3 Results and discussion

3.3.1 Fresh concrete properties

3.3.1.1 Slump

Concrete with a higher slump is easier to pump and place, making it more capable for a variety of applications. In this study, FWNS concrete was targeted to have a slump of 150-200 mm, without the use of plasticizers, to avoid their chemical impact on the results. The study examined the impact of mono and hybrid fibers of different types and lengths on SWSS concrete slump using four water-to-binder (W/B) ratios (0.59, 0.64, 0.67, 0.71) with varying water levels and consistent binder content. Slump values for all mixtures appear in **Figure 3-2**. As shown, workability decreased in SWSS versus FWNS at all W/B ratios. This is due to dissolved salt and mineral content in SWSS which aligns with previous research (Ting *et al.* 2020a; Vafaei *et al.* 2021a). Finer SS particles and stronger particle bonding from accelerated cement hydration resulted in higher solid content and lower SWSS slump (Wang, Junjie *et al.* 2018). As W/B ratios increased, the slump difference between plain SWSS and FWNS decreased due to higher cohesion in lower ratios but decreased with increased water content.

A significant slump reduction occurred with added fibers in all W/B ratios, except for macro-fibers (PPL and TPPL). This can be attributed to better micro-fiber (PVA, PPS, and BF) dispersion, enhancing flow resistance and lowering slump by interlocking the particles. Also, micro-fibers possess higher surface area per unit volume than macro-

fibers, causing friction with surrounding concrete particles, greater water absorption on their surfaces, further impeding flow. Notably, PVA fiber concrete showed a sharp slump increase with higher water content, which can be attributed to its hydrophilic nature and greater water absorption capacity. For lower water content, PVA fiber absorbed water significantly and got saturated, while increasing water content increased the slump. Conversely, incorporation PPL and TPPL fiber in lower water content mixes increased slump compared with plain SWSS, due to decreased interlocking of particles in SWSS. More water decreased interlocking in plain SWSS concrete, narrowing the slump difference between plain SWSS and macro FR-SWSS concrete.

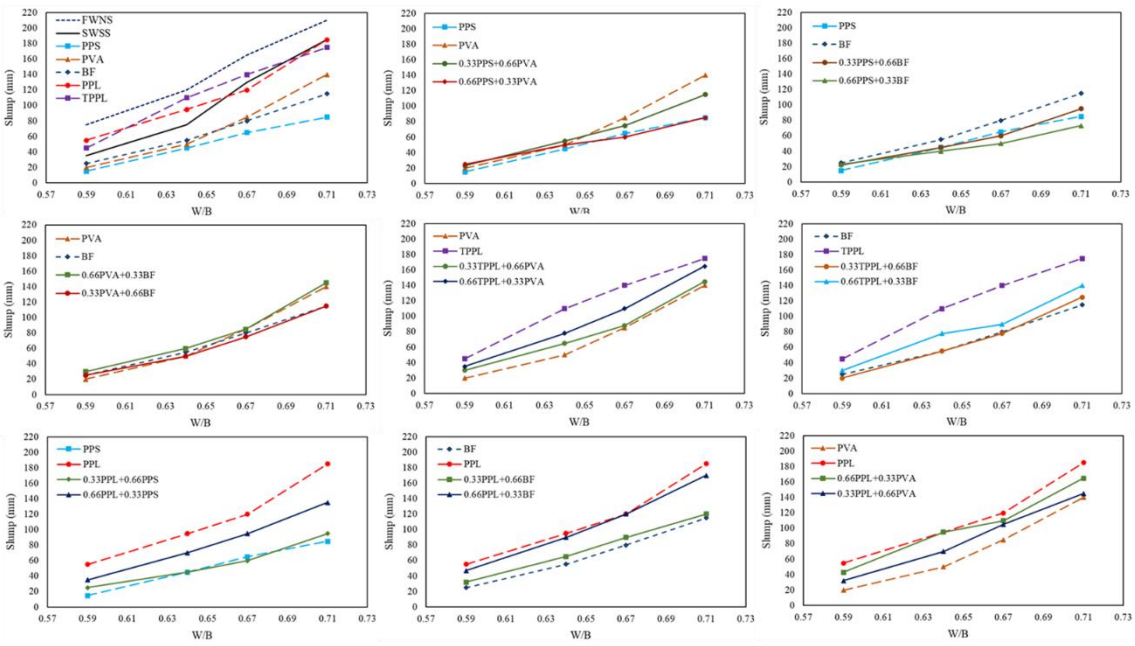


Figure 3-2 The values of slump for all the mono and hybrid mixtures

The micro-fiber hybridization exhibited a similar trend, with PPS fibers having a greater impact on the slump compared to other fibers. This reduction in slump at higher W/B ratios resulted from the synergistic water-trapping effect of PPS and BF, unlike PVA and BF fibers, which had positive impact on slump values compared to mono-fibers. Hybridizing macro- and micro-fibers, especially PPS fiber, yielded lower slump values than separately using PPL and TPPL fibers. Increasing micro-fiber volume intensified slump reduction. TPPL and PVA or BF fibers complemented each other, further reducing slump by enhancing water trapping, while PPL and micro-fiber combinations were less sensitive to W/B ratio due to reduced fiber interaction.

3.3.1.2 Air Content

High air content in concrete reduces strength and increases permeability by forming microcracks and weakening interparticle bonding. **Figure 3-3** shows air content results for concrete mixes. SWSS concrete had 60% more air content than FWNS concrete, consistent with prior studies (Nishida *et al.* 2015; Vafaei *et al.* 2021a), due to the more porous nature of SS, resulting in enhanced air entrapment during the mixing process. Adding mono PPS and BF to SWSS increased air content by 38% and 54%, more than PVA fiber, which increased it by 16%. PVA fibers displace air voids by absorbing water during mixing, thanks to its hydrophilic nature, while PPS and BF, being hydrophobic, repel water, and hence creating air pockets (Vafaei *et al.* 2021a). PPS/BF combination raised air content by 10% compared to mono PPS, displaying a negative synergy effect. Conversely, PVA/BF hybridization had the lowest air content among hybrid micro-fiber mixtures, indicating a positive synergy. Here, the hydrophilic nature of PVA allowed air to escape, while PPS fibers, hydrophobic, negatively affected PVA fibers, increasing air entrapment.

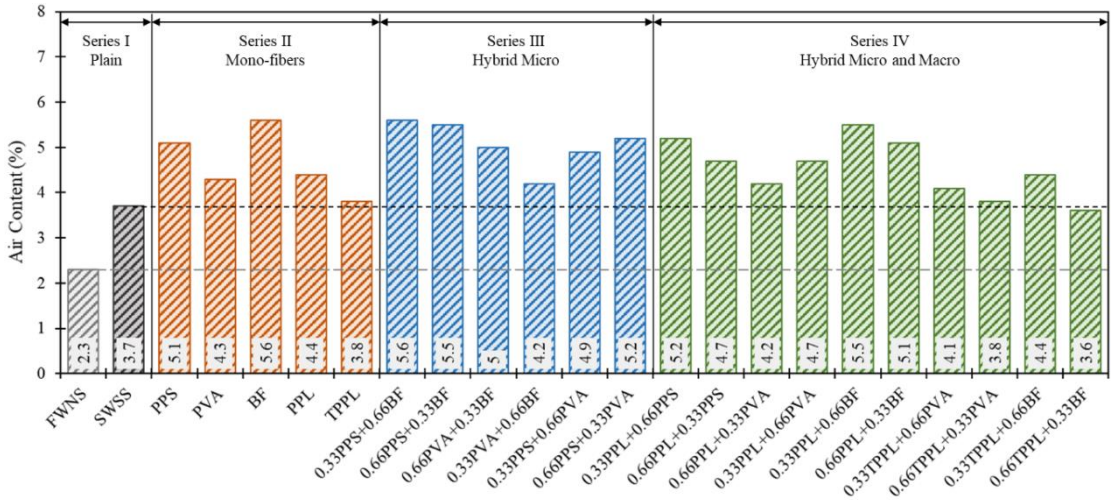


Figure 3-3 Air content results for all mixes

The air content was increased by 19% with the incorporation of mono PPL fibers and by 3% with TPPL fibers compared to SWSS concrete. This difference can be attributed to the lower flexibility of PPL fibers, which makes them challenging to orient and distribute, leading to the entrapment of more air voids in the fresh concrete. When micro- and macro-fibers were combined in SWSS concrete, the air content was elevated, but the dosage of micro-fiber had a direct impact on the resulting air content. Notably, the hybrid mix

consisting of 66% TPPL and 33% PVA or BF exhibited positive synergy and resulted in the lowest air content among all hybrid mixes.

3.3.2 Compressive strength

Figure 3-4 displays compressive strength results for all concrete mixes at 7, 28, and 365 days, with error bars indicating standard deviations. The study found that SWSS concrete exhibited 46% higher early-age compressive strength than FWNS concrete, attributed to chloride ions in SW and SS. The ions accelerating cement hydration (Younis *et al.* 2018; Matthew Zhi Yeon *et al.* 2020; Vafaei *et al.* 2021a) and forming calcium chloride ($CaCl_2$) by the reaction of sodium chloride ($NaCl$) with calcium hydroxide ($Ca(OH)_2$), as described by Eq. (3-1). In early stages, SWSS concrete exhibits significantly higher hydration product concentrations than FWNS concrete due to $CaCl_2$ accelerating cement hydration (Younis *et al.* 2018; Vafaei *et al.* 2021a), resulting in denser calcium silicate hydrate (C-S-H) needle microstructures in SWSS compared to the less compact and dispersed ones in FWNS (Younis *et al.* 2019).

$$Ca(OH)_2 + 2NaCl \rightarrow CaCl_2 + 2Na^+ + 2OH^- \quad (3\text{-}1)$$

In contrast to early-age strength, SWSS concrete showed similar compressive strength to FWNS concrete at 28 days, but slightly higher strength (about 5%) after 365 days, consistent with previous findings (Li *et al.* 2013; Vafaei *et al.* 2021b). This difference is attributed to inherent chemical process variations in SWSS and FWNS. Although both used similar materials, it was initially expected they would have equivalent chemical potential—the chemical energy per mole of the concrete—to reach ultimate strength. As discussed, SWSS has a faster chemical reaction rate initially, but by 28 days, both reached similar chemical potential consumption and strength levels. After 365 days, the quicker reaction rate of SWSS led to slightly higher strength. This pattern likely recurs, eventually converging to equal maximum strength, explaining contradictory literature observations regarding the long-term compressive strength of SWSS concrete compared to FWNS. Furthermore, factors like the presence of organic content in SS and its smoother surface, which affect the bonding between concrete elements, can also be responsible for the decrease in strength observed in SWSS when compared to FWNS. Additionally, micro-crack formation due to salt crystallization from SW and SS, and calcium hydroxide (CH)

dissolution induced by $MgCl_2$, can also contribute to reduce SWSS compressive strength (Matthew Zhi Yeon *et al.* 2020).

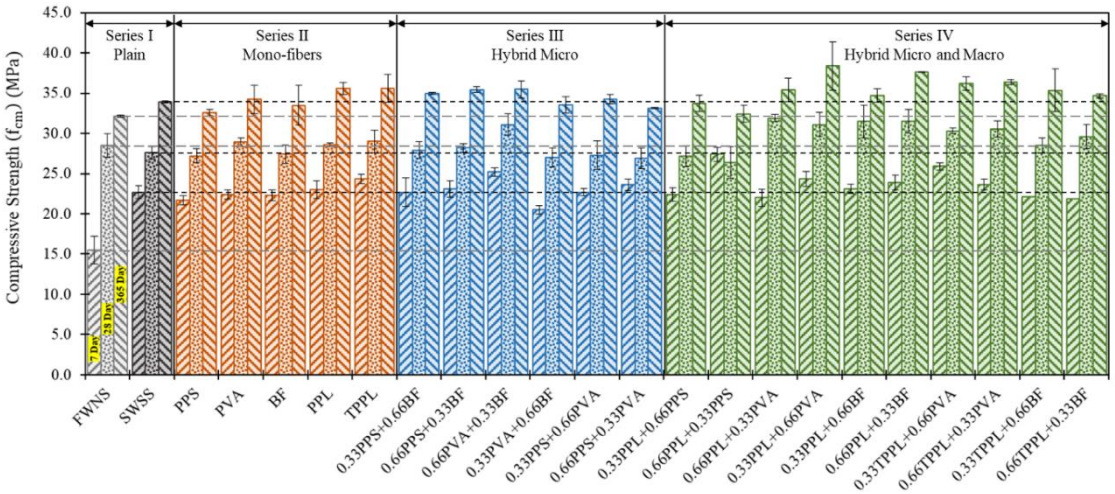
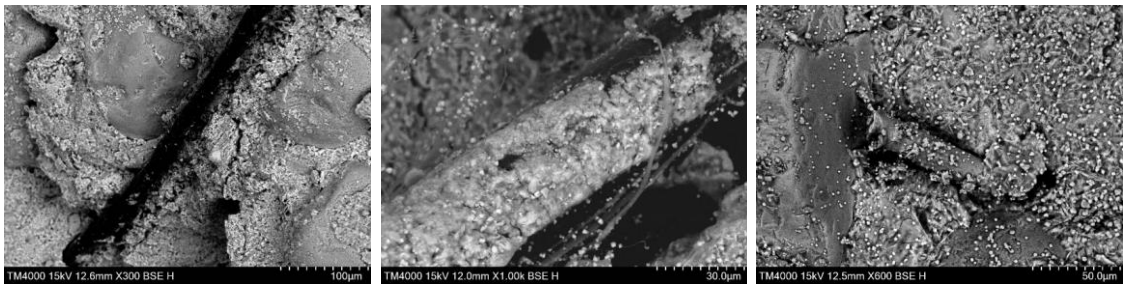


Figure 3-4 Compressive strength (f_{cm}) results for all mixes

Incorporating micro-fibers slightly reduced compressive strength (f_{cm}) except for PVA fiber, which increased it at 28 and 365 days. **Figure 3-5** presents SEM images of micro-fibers. The analysis revealed that PVA fibers form strong chemical bonds with the cement paste during the hydration process, aligning with prior research findings (Amin *et al.* 2013; Vafaei *et al.* 2021a; Chenggong *et al.* 2023). The presence of hydroxyl groups (OH) within PVA fibers facilitates the formation of hydrogen bonds between individual molecules. This intermolecular interaction significantly enhances the surface bond strength between PVA fibers and the surrounding matrix (Bo *et al.* 2010; Amin *et al.* 2013). The elevated OH content of SWSS concrete, as evidenced by Eq. (3-1), presents a potential advantage over conventional concrete by facilitating stronger chemical bonding between PVA fibers and the concrete matrix. This superior bonding capacity of PVA fibers allowed for the efficient utilization of their tensile strength in reinforcing the concrete mixture. In contrast to PPS, PVA fibers significantly enhance specimen reinforcement due to their high tensile strength, elastic modulus, and elongation characteristics (Amin *et al.* 2013), contributing to fiber breakage. Conversely, PPS fibers exhibited a tendency for pull-out, due to their comparatively weaker bonding strength.

Figure 3-5 displays the microstructure of BF-containing concrete, revealing fiber breakage and non-uniform distribution. This phenomenon was consistently observed

during the incorporation of BF where fibers were not easily discernible after mixing. This is caused by brittleness of BF, resulting from mechanical abrasion and shear forces during mixing caused by the interaction with other components, making them vulnerable to fracture. Also, previous studies have reported BF corrosion caused by exposure to alkaline ($NaOH$) and cement ($Ca(OH)_2$) solutions (Wang, Qingxuan *et al.* 2021; Li, Meng *et al.* 2022), which was also observed in this study. **Figure 3-6** shows that corrosion occurred on the surface of BF in SWSS concrete, but the fiber diameter reduction was not significant.



PPS PVA BF

Figure 3-5 SEM images of the micro-fibers in SWSS concrete

BF corrosion in concrete occurs in two distinct stages (Wang, Qingxuan *et al.* 2021). The first stage involves surface flaw formation due to the action of hydroxide (OH^-) ions present in the cement solution (Li, Meng *et al.* 2022). These ions attack the Si-O-Si and Al-O-Al bonds within the fiber structure, leading to the formation of soluble silicate and aluminosilicate compounds, as described by Eqs. (3-2) and (3-3) (Li, Meng *et al.* 2022; Benny *et al.* 2023). Notably, the inherently higher OH^- concentration in SWSS concrete compared to FWNS concrete (Eq. 3-1) accelerates this flaw formation. In seawater environments, the degradation of BF further intensifies due to the presence of chloride (Cl^-) ions. Previous studies have identified the reaction between Fe^{2+} ions within the basalt fibers and Cl^- as a key contributor to this enhanced degradation compared to freshwater immersion. This reaction, detailed in Eqs. (3-4) and (3-5), results in more severe surface flaws and overall weakening of the fiber (Xie *et al.* 2022). Additionally, the presence of Na^+ and K^+ in sea-sand can potentially enhance the reaction between alkaline and silica components in BF fibers (Xie *et al.* 2022). In stage 2, a protective layer of calcium silicate ($CaSiO_3$) forms on the fiber surface by the combination of hydrated calcium hydroxide and silicon dioxide (SiO_2) (Eq. 3-6), slowing corrosion (Wang, Qingxuan *et al.* 2021). However, excessive flaws can lead to breakdown and reduced

tensile strength, resulting in a dense and brittle mixture (Özkan *et al.* 2020; Wang, Qingxuan *et al.* 2021). Previous study (Kai *et al.* 2023) also reported that higher dosage of BF (0.4%) slightly increased f_{cm} in UHP-SWSS concrete, likely due to the strength of concrete and dosage of BF.

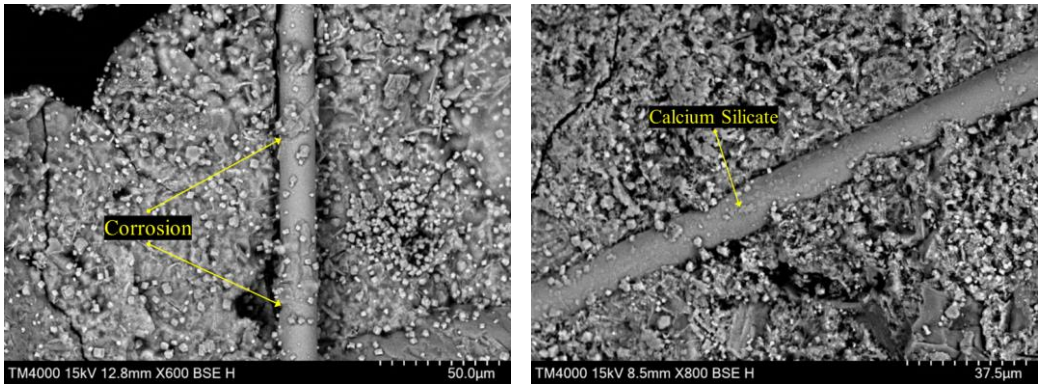


Figure 3-6 SEM images of BF corrosion and the formation of calcium silicate ($CaSiO_3$) in SWSS

$$[-Si-O-Si-] + OH^- \rightarrow [-Si-O]^- + [HO-Si-] \quad (3\text{-}2)$$

$$[-Al-O-Si-] + OH^- \rightarrow [-Al-O]^- + [HO-Si-] \quad (3\text{-}3)$$

$$Fe^{2+} + Cl^- \rightarrow [FeCl\ complex]^- \quad (3\text{-}4)$$

$$[FeCl\ complex]^- + OH^- \rightarrow FeOH_2 + Cl^- \quad (3\text{-}5)$$

$$Ca(OH)_2 + SiO_2 \rightarrow CaSiO_3 \downarrow + H_2O \quad (3\text{-}6)$$

The weakness of BF due to corrosion and brittleness was effectively addressed through hybridization with PVA, significantly increasing f_{cm}. The presence of hydroxide ions (OH^-) on PVA fibers presents a potential for hydrogen bonding (Bo *et al.* 2010) with the surface of BF under sufficient interfacial contact area. Additionally, the inherent roughness of PVA fibers facilitates mechanical interlocking with the smooth surface of BF fibers, further contributing to some degree of mechanical adhesion. The SEM analysis, as depicted in **Figure 3-7**, revealed a synergistic effect of PVA/BF hybridization. In this hybrid, the tensile strength and elongation of PVA facilitated stress transfer and micro-crack bridging, while BF improved PVA bonding, enhancing interlocking mechanism. It was reported that BF had nine times higher strength reduction than PVA fiber [43] and 87.6% higher chemical bonds [21]. This study revealed that due

to the brittleness of BF, most of the fibers were unable to attain a sufficient length for effective transfer of tensile stress, even with their considerable bonding strength, resulting in fiber pull-out. PVA fibers, in contrast to BF, exhibited flexibility in their filaments, allowing for a dual mechanism of mechanical and chemical bonding. Conversely, BF, characterized by its circular and rigid structure, primarily depended on chemical bonding strength. Optimal PVA to BF ratio was 66:33, resulting in an 11% increase at 7-day and 12.7% at 28-day in f_{cm}. This contradicts (Du *et al.* 2022), that proposed higher BF proportions with PVA enhance the compressive strength of FWNS concrete. Nevertheless, this divergence was attributed to the accelerated corrosion rate and brittleness of BF in SWSS compared to FWNS. It is also reported that BF increases microcracks and pores at the interface transition zone (ITZ), while filling large matrix pores, reducing their volume fraction (Zhuang *et al.* 2022). Similarly, PPS and BF had a comparable effect, with PPS as stress transferors and BF for providing bonding strength, improving fiber complementarity, stress distribution, and reinforcement in the concrete matrix. A higher PPS percentage was more effective than BF in the hybrid system, notably with age, a 66:33 BF:PPS leading to a remarkable 9% f_{cm} increase compared to mono PPS.

When examining macro-fibers, PPL and TPPL inclusion increased f_{cm} for both 28- and 365-day measurements. Additionally, when hybridized with bonding-enhancing micro-fibers like PVA and BF, a positive f_{cm} impact occurred. Notably, PVA/PPL combination significantly improved both 28- and 365-day compressive strength, with ~13% enhancement over plain SWSS. Furthermore, a 66:33 PPL:PVA ratio proved more effective at 28 days, while 33:66 worked better at 365 days. Over time, PVA fibers in the concrete matrix promoted increased chemical bonding. Greater PVA fiber content led to improved complementarity with PPL after 365 days, enhancing adhesion and interlocking, also attributed to its higher elastic modulus (Kaidi *et al.* 2023). Conversely, 66:33 PPL:BF was more effective than 33:66, due to BF corrosion and breakage, reducing PPL bonding over time. Consequently, a higher PPL percentage showed superior mechanical bonding compared to a higher BF percentage. The results affirm that combining PPL with PVA or BF fibers enhanced inter-fiber bonding, interlocking, and FR-SWSS concrete compressive strength. In contrast, hybridizing TPPL with PVA or BF fibers showed no substantial impact on compressive strength over time when compared to mono TPPL.

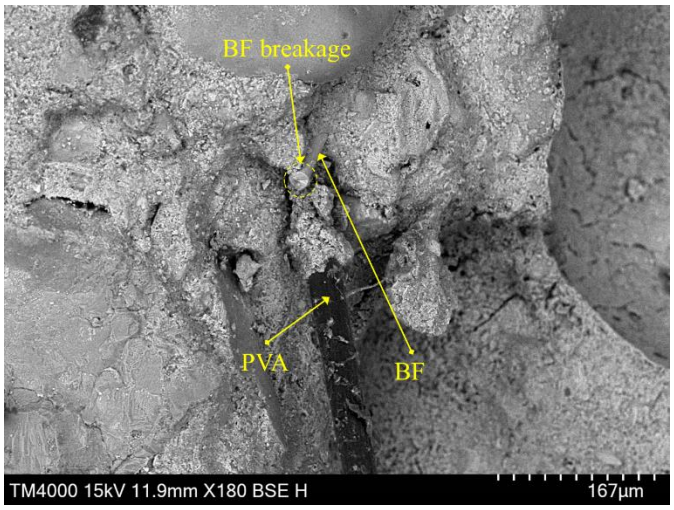


Figure 3-7 Synergistic effects of PVA/BF hybridization in SWSS concrete

3.3.3 Elastic modulus

Figure 3-8 illustrates 28-day concrete specimen compressive elastic modulus (E_c) before cracking, evaluated at a 0.4 f_c' stress level. SWSS concrete showed an 8% E_c higher compared to FWNS due to superior adhesion, mechanical reinforcement, and SS particle stiffness. Micro-fibers reduced E_c by increasing air voids, acting as stress concentrators, and decreasing concrete stiffness. This is consistent with the finding of (Vafaei *et al.* 2021a) on the effects of PVA and PPS fibers on reduced E_c of SWSS concrete. PPS fiber exhibited the lowest E_c, 30% less than SWSS, due to its lower elastic modulus and bonding strength, which reduced matrix stiffness (Kaidi *et al.* 2023). On the contrary, hybrid micro-fibers improved stiffness and E_c when compared to mono micro-fibers. Mono PVA and BF decreased E_c by approximately 14%, but a 66:33 ratio (PVA:BF) in hybridization achieved an E_c close to SWSS, mitigating weaknesses through better chemical bonding, in line with (Şükrü *et al.* 2021). However, increasing BF dosage had a detrimental effect due to its corrosion in SWSS concrete, unlike PVA/BF hybridization in normal concrete (Şükrü *et al.* 2021). Prior studies (Zhuang *et al.* 2022) also reported similar E_c values for PVA/BF hybridization in normal concrete, but this study revealed a significant E_c enhancement in SWSS due to PVA/BF chemical reactions. Hybridization of PPS/PVA and PPS/BF, significantly enhanced E_c, exceeding that of the mono PPS fibers by about 33% and 35%, respectively. In summary, micro-fiber hybridization significantly affects the E_c of the hybrid system, emphasizing the importance of high elastic modulus, tensile strength, and bonding strength of fibers, especially when combining PPS fiber with PVA/BF, resulting in increased stiffness.

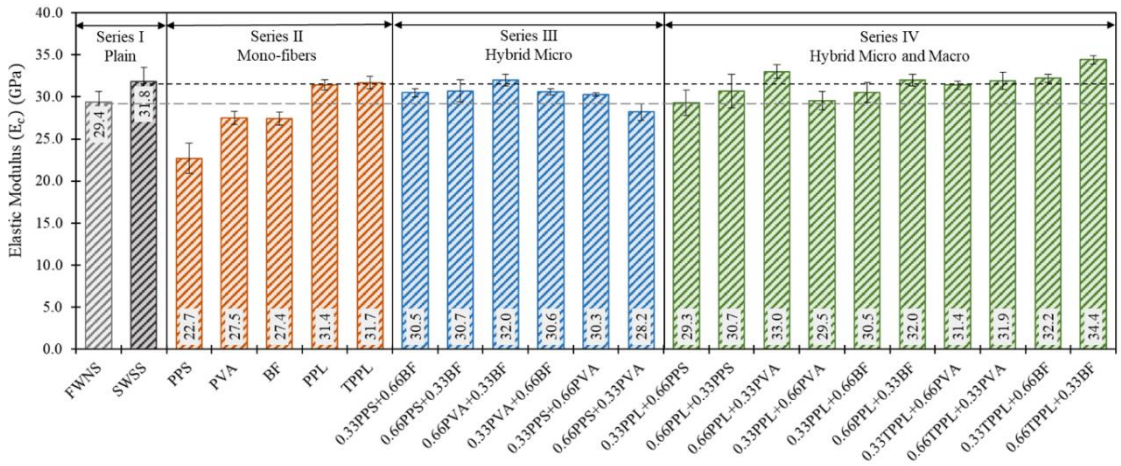


Figure 3-8 Elastic modulus (E_c) results for all mixes

Concerning macro-fibers (PPL and TPPL), their impact on E_c was minimal, also reported in (Kaidi *et al.* 2023), but their hybridization with micro-fibers (PVA/BF), which enhanced their bonding strength, slightly increased stiffness. The improved mechanical and chemical bonding of PPL or TPPL fibers increased elasticity and provided reinforcement in various directions. The complementarity of micro and macro-fibers elevated stiffness and adhesion at both micro and macro levels within the concrete matrix. The optimal dosage achieved was 66% macro-fibers and 33% micro-fibers. It is worth noting that an excess of micro-fibers caused corrosion and air voids in SWSS concrete. Results indicated that TPPL outperformed PPL due to higher flexibility, elastic modulus, and better distribution.

3.3.4 Splitting tensile strength

The tensile strength (f_{st}) of specimens was assessed after 28 days. **Figure 3-9** displays the results with standard deviation error bars. As shown, SWSS had a slightly lower f_{st} than FWNS, consistent with prior studies (Ting *et al.* 2020b; Vafaei *et al.* 2021a). Micro-fibers increased f_{st} slightly, except for BF which decreased it. This was despite earlier research (Pakravan *et al.* 2017; Özkan *et al.* 2020) showing that tensile strength and fiber elongation influence f_{st}, but both factors decreased in SWSS concrete due to PVA and BF chemical reactions. Conversely, PPS fiber incorporation was more effective than others due to its superior chemical resistance in SWSS concrete. Tensile strength depends on factors such as fiber volume, length, shape, distribution, and concrete strength (Pakravan *et al.* 2017; Chenggong *et al.* 2023). Previous research (Vafaei *et al.* 2021a)

demonstrated that in high-strength SWSS concrete using PP fibers (19 mm, fibrillated) had lower f_{st} compared to PVA fibers (8 mm, monofilament), but this study yielded different results, possibly due to similar PPS and PVA fiber lengths and better distribution.

Although BF slightly decreased f_{st}, PPS/BF hybridization increased it compared to both mono BF and control SWSS concrete, likely due to higher elongation of PPS fibers bridging micro-cracks; using a higher PPS fiber percentage than BF was more effective. Despite increasing compressive strength by combining BF/PVA fibers but it had no notable impact on f_{st}, possibly due to increased air voids and brittleness from BF corrosion in SWSS concrete, in line with previous study (Özkan *et al.* 2020). The 66:33 ratio of PPS/PVA fibers yielded the most pronounced positive f_{st} effect among micro-fiber hybridizations, thanks to PVA fiber enhancing the bonding strength of PPS fibers, facilitating utilization of their tensile and elongation capacity. As reported previously (Özkan *et al.* 2020; Zhuang *et al.* 2022), increasing the dosage of BF in the hybridization, reduced the tensile strain and elongation of cementitious composites. This study confirmed that increased micro-fiber corrosion (especially BF) in SWSS concrete negatively affect tensile strength and mixture ductility.

Regarding micro- and macro-fiber hybridization, the optimal ratio was found to be 33% micro-fibers and 66% macro-fibers, improving f_{st} compared to mono-fibers and plain SWSS. Microstructural analysis (**Figure 3-10**) revealed that PVA fibers reinforced the region around macro-fibers, improving bonding strength, while longer macro-fibers enhanced mechanical bonding, increasing f_{st}. Micro- and macro-fibers complementarily reinforced micro-cracks before ultimate strength, but BF fiber breakage and corrosion in SWSS concrete increased micro-cracks, negatively impacting f_{st} compared to mono-fibers. Furthermore, TPPL fibers, with a lower aspect ratio, greater flexibility, and better distribution were more influenced by micro-fiber type and dosage. **Figure 3-10** also shows that TPPL fibers, due to their flexibility, greater length, and filaments, provided better mechanical bonding than PPL fibers. However, these characteristics also increased the initiation and development of micro-cracks surrounding the filaments, which weakened the concrete's tensile strength. Hybrid TPPL/PVA fibers outperformed mono-fibers in terms of f_{st} by providing chemical bonding of PVA fibers and bridging micro-cracks around TPPL fiber filaments.

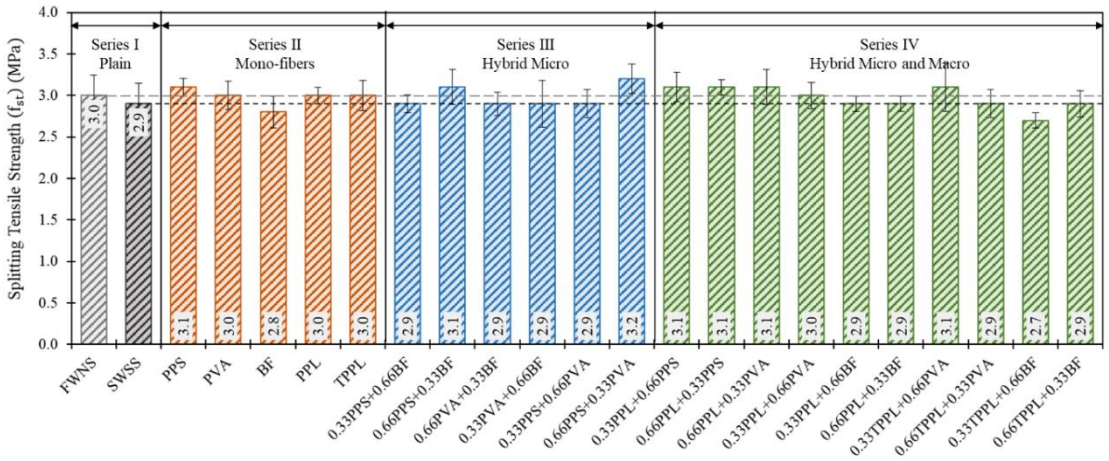
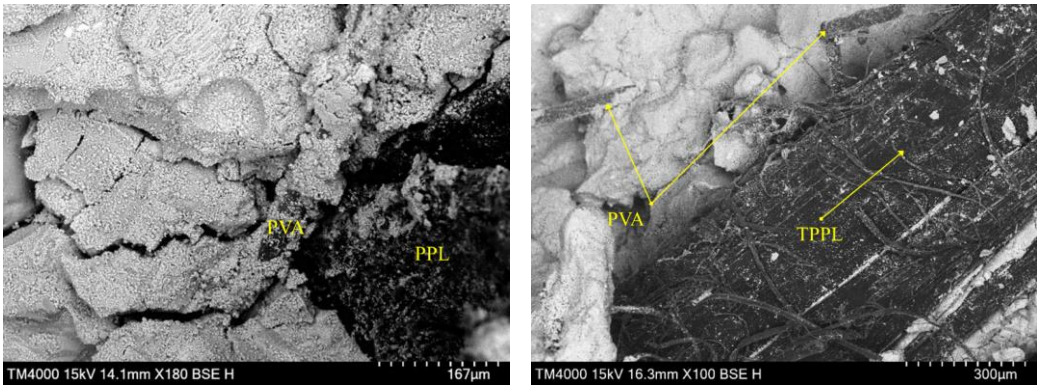


Figure 3-9 Splitting tensile strength (f_{st}) results for all mixes



PPL/PVA TPPL/PVA

Figure 3-10 Synergistic effects of PPL/PVA and TPPL/PVA hybridization in SWSS concrete

3.3.5 Stress–strain results and discussions

3.3.5.1 Stress–strain curves

Figure 3-11 illustrates the standard stress-strain curves for fiber-reinforced SWSS concrete under compression. Each curve reveals distinct stages, as reported in prior research (Zhou *et al.* 2015; Abbas *et al.* 2022): stage I, the linear elastic ascending stage; stage II, the nonlinear ascending stage; stage III, the cracking stage; and stage IV, the residual softening stage. As shown in **Figure 3-11**, stages I and II correspond to the pre-peak phase, while stages III and IV relate to the post-peak phase.

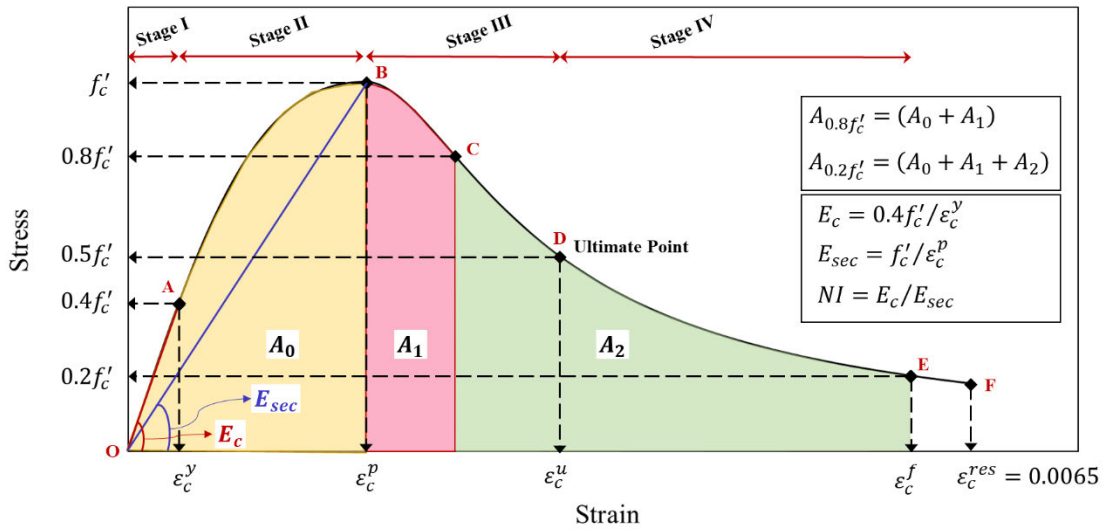


Figure 3-11 Typical stress-strain curves of FR-SWSS concrete under compression

During stage I, specimens behaved elastically as stress increased. When the applied load reached about 40% of the compressive strength (Khaloo *et al.* 2008; Zhou *et al.* 2015; Concrete *et al.* 2022), the curves shifted from linearity to nonlinearity up to peak stress, due to the formation and propagation of microcracks during loading. The pre-peak behaviour (stages I and II) was similar for plain and fiber-reinforced SWSS concrete, suggesting that fibers had a limited impact on elasticity due to their minimal influence on uncracked concrete, as reported in prior studies (Xijun *et al.* 2020; Abbas *et al.* 2022).

The nonlinearity of plain and fiber-reinforced SWSS concrete in the pre-peak phase was compared using a previously established nonlinearity index (NI) (Khaloo *et al.* 2008). The NI quantifies the extent of nonlinearity, with higher values indicating more nonlinear behaviour. It is calculated as the ratio of the elastic modulus (E_c) to the secant elastic modulus (E_{sec}), as showed in **Figure 3-11**. The results showed that incorporating BF, as mono- or hybrid-fibers, decreased the NI during the pre-peak phase. This could be attributed to the breakage and corrosion of BF in SWSS, which led to a denser and more brittle structure, decreasing E_c and causing an abrupt transition from linear (stage I) to nonlinear behaviour (stage II) by propagating micro-cracks under compression. Hybridizing BF with other fibers (micro- or macro-fibers) increased E_c over mono BF concrete, which increased the NI. This could be attributed to their lower chemical reactions in SWSS and higher elongation, which prevented an abrupt transition from

linear to nonlinear behaviour by bridging micro-cracks and increasing concrete strain under compression. Hybridizing the other fibers did not significantly change the NI.

After the peak stress, the curves showed varying slopes due to the fibers' ability to bridge macro-cracks. At $0.5f_c'$ stress level, the stress-strain curve inflected. Beyond this point, the residual softening stage (stage IV), stress consistently decreased as strain increased, leading to failure (Khaloo *et al.* 2008; Zhou *et al.* 2015; Abbas *et al.* 2022). Fibers with high bonding strength and elongation resulted in more ductile post-peak behaviour (stage III and stage IV). During the rapid transition from point B to C, PVA fiber was more effective than others to bridge micro- and macro-cracks due to its bonding strength, tensile strength, and elongation. Hybridizing PPL fibers with micro-fibers improved its bonding strength and better kept the micro-cracks compared to mono PPL concrete.

During the transition from point C to E, fibers with higher elongation, such as PPS and PVA, were more effective in bridging cracks. Hybridizing BF/PVA (33:66) increased crack resistance and ductility compared to mono-fibers. Here, BF increased PVA bonding strength, allowing PVA fibers to bridge cracks more effectively due to its high tensile strength. Hybridizing PPL/PVA fiber (66:33) increased the bridging effect compared to mono PPL fiber. This may result from the effect of PVA fibers to increase the bonding strength of PPL fibers. TPPL fibers required more PVA fiber to improve bonding strength and ductility over mono-fibers. Conversely, BF negatively affected both PPL and TPPL, likely due to its corrosion in SWSS concrete.

3.3.5.2 Comparison of strain values (peak and ultimate)

The peak strain (ε_c^p) and ultimate strain (ε_c^u) are presented in **Table 3-3**. The results revealed that ε_c^p was not significantly affected by fiber addition, as reported in previous studies (Syed Minhaj Saleem *et al.* 2019; Haobo *et al.* 2023). This is because micro-cracks form under compression just before the ultimate stress (point B), so fibers cannot effectively contribute to improving deformation capacity before the peak point. Conversely, ε_c^u is significantly affected by fiber addition, as fibers can bridge macro-cracks that form after micro-cracks. PPS and PVA fibers, with high tensile strength, elongation, and bonding strength, which are the most important parameters for the transition from ε_c^p to ε_c^u, were the most effective mono-fibers for improving ε_c^u. Although BF had a high tensile strength and chemical bonding strength, its ε_c^u was lower than other mono-fibers due to corrosion in SWSS concrete. Hybridizing BF/PVA increased

ε_c^u by 17%, with the optimal dosage of 66:33 PVA/BF and overcame the weakness of BF.

PPL fibers did not affect ε_c^u as mono-fibers, due to their low bonding strength for the transition from the ε_c^p to the ε_c^u under the sudden failure. However, hybridizing PPL/PVA increased ε_c^u by 16% over mono PPL, with the optimal dosage of 66:33 PPL/PVA. Conversely, mono TPPL fibers were more effective than hybridized TPPL fibers, due to the reduction in dosage when combined with other fibers, which led to decreased ductility up to ε_c^u.

3.3.5.3 Energy absorption capacity

The area under the stress-strain curve is a parameter for quantifying energy absorption capacity or toughness in fiber-reinforced concrete under compression (Poon *et al.* 2004). This study employs the compressive toughness index (CTI) to explore the influence of fibers on SWSS concrete, as outlined below.

3.3.5.4 Compressive toughness index (*CTI*)

CTI is a critical parameter for assessing the compressive characteristics of concrete, indicating its capacity to absorb energy and ductile behaviour. This study used the dimensionless CTI_N to evaluate the ductile properties of FR-SWSS concrete. CTI_N is calculated as the ratio of the area under the stress-strain curve from zero stress to the point where stress reaches N% of f_c' during the post-peak stage to the pre-peak area from zero stress to the peak point (A_0), as shown in **Figure 3-11** and Eq. (3-7) (Zhou *et al.* 2015; Qiuhong *et al.* 2022). To investigate the influence of fibers on both small and large deformations under compressive loads, this analysis considered two post-peak thresholds, 80% and 20%, as N.

$$CTI_N = \frac{A_{Nf_c'}}{A_0}; (N = 0.8\ and\ 0.2) \quad (3\text{-}7)$$

Figure 3-12 shows that SWSS and FWNS concrete had similar $CTI_{0.2}$, but SWSS had 16% lower $CTI_{0.8}$, indicating lower energy absorption in small deformations beyond the peak-point. **Figure 3-13** compares the microstructures of SWSS and FWNS concrete using SEM. SWSS concrete had a denser structure, consistent with previous studies (Wang, Junjie *et al.* 2018; Vafaei *et al.* 2022b). This is because SWSS had a significantly higher concentration of portlandite, which filled gaps and pores. Additionally, ettringite

Table 3-3 The mechanical and compressive stress-strain properties of concrete specimens, and fitting curves parameters (α and β)

Concrete Mix			f_{cm}^{7}	f_{cm}^{28}	f_{cm}^{365} (MPa)	f_{st}	f_{res}	E_c^{28}	E_c^{365} (GPa)	E_{sec}	Nonlinearity index (NI)	ε_c^p	ε_c^u	α	β
Series I	Plain	FWNS	15.5	28.5	32.2	3.0	4.2	29.4	30.1	16.8	1.80	0.0019	0.0040	0.946	1.984
		SWSS	22.7	27.6	33.9	2.9	6.1	31.8	31.9	17.4	1.84	0.0020	0.0039	0.940	2.234
Series II	Mono-fibers	PPS	21.7	27.2	32.6	3.1	12.2	22.7	22.5	12.2	1.85	0.0027	0.0053	0.939	1.839
		PVA	22.4	28.9	34.2	3.0	11.0	27.5	27.8	15.6	1.78	0.0022	0.0052	0.918	1.367
		BF	22.3	27.4	33.5	2.8	3.9	27.4	27.2	16.1	1.69	0.0021	0.0040	0.952	2.310
		PPL	23.0	28.6	35.6	3.0	8.0	31.4	31.5	16.8	1.87	0.0021	0.0039	0.970	2.435
		TPPL	24.3	29.0	35.6	3.0	8.6	31.7	31.3	17.7	1.77	0.0020	0.0044	0.940	1.696
Series III	Micro-fiber Hybridization	0.33PPS+0.66BF	22.7	27.9	35.0	2.9	6.4	30.5	29.6	16.3	1.81	0.0021	0.0033	0.949	4.040
		0.66PPS+0.33BF	23.1	28.2	35.4	3.1	8.2	30.7	30.2	16.6	1.82	0.0021	0.0038	0.946	2.520
		0.66PVA+0.33BF	25.2	31.1	35.5	2.9	11.0	32.0	31.2	17.0	1.84	0.0021	0.0047	0.952	1.568
		0.33PVA+0.66BF	20.5	27.0	33.5	2.9	9.0	30.6	31.0	17.0	1.82	0.0020	0.0042	0.954	1.643
		0.33PPS+0.66PVA	22.7	27.3	34.3	2.9	7.9	30.3	30.1	16.4	1.84	0.0021	0.0042	0.941	2.327
		0.66PPS+0.33PVA	23.6	26.9	33.1	3.2	8.6	28.2	28.7	15.8	1.82	0.0021	0.0037	0.946	2.113
Series IV	Micro- and Macro-fiber Hybridization	0.33PPL+0.66PPS	22.4	27.2	33.7	3.1	10.4	29.3	29.2	16.3	1.79	0.0021	0.0047	0.938	1.380
		0.66PPL+0.33PPS	27.4	26.4	32.4	3.1	8.2	30.7	30.3	17.4	1.74	0.0019	0.0045	0.953	1.416
		0.66PPL+0.33PVA	22.0	31.9	35.4	3.1	13.1	33.0	33.5	18.9	1.77	0.0019	0.0045	0.946	1.002
		0.33PPL+0.66PVA	24.3	31.1	38.4	3.0	9.0	29.5	29.3	17.5	1.67	0.0022	0.0044	0.952	2.089
		0.33PPL+0.66BF	23.1	31.5	34.7	2.9	7.9	30.5	29.7	16.8	1.77	0.0021	0.0042	0.946	2.097
		0.66PPL+0.33BF	23.9	31.5	37.6	2.9	6.7	32.0	32.2	17.6	1.83	0.0021	0.0039	0.943	3.245
		0.33TPPL+0.66PVA	25.9	30.3	36.2	3.1	11.1	31.4	31.4	17.4	1.80	0.0021	0.0043	0.941	1.379
		0.66TPPL+0.33PVA	23.6	30.5	36.4	2.9	8.4	31.9	31.7	17.3	1.83	0.0021	0.0040	0.934	2.261
		0.33TPPL+0.66BF	22.1	28.5	35.3	2.7	7.1	32.2	32.2	18.9	1.70	0.0019	0.0037	0.946	2.096
		0.66TPPL+0.33BF	21.9	29.6	34.7	2.9	8.2	34.4	35.1	19.1	1.84	0.0018	0.0039	0.942	1.615

formation was significantly higher in SWSS than in FWNS due to the use of seawater (Wang, Junjie *et al.* 2018), which also helped to fill pores and create a more uniform structure. The denser structure made SWSS more brittle than FWNS, resulting in lower ductility and energy absorption.

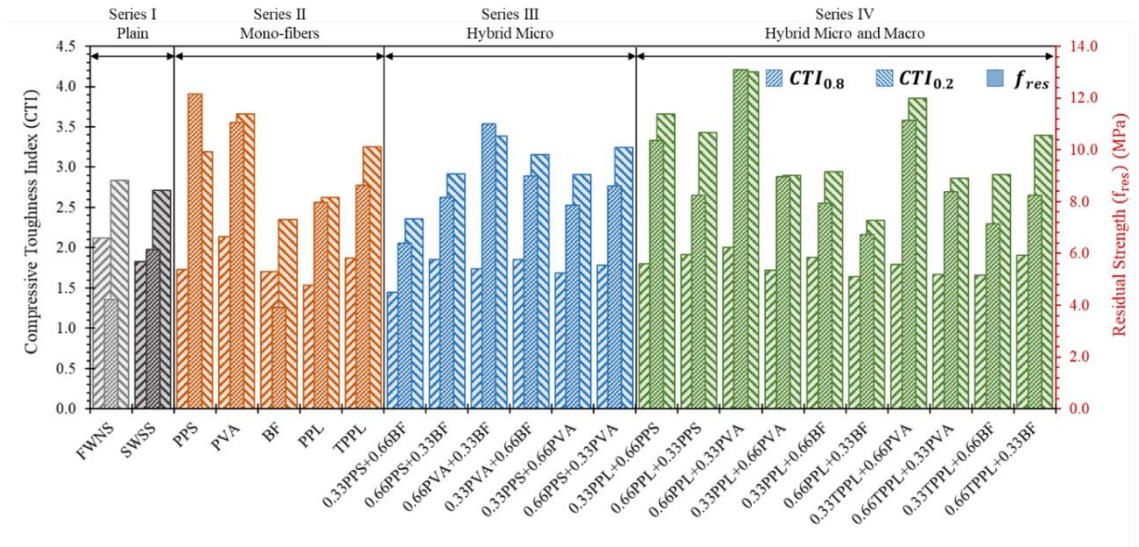
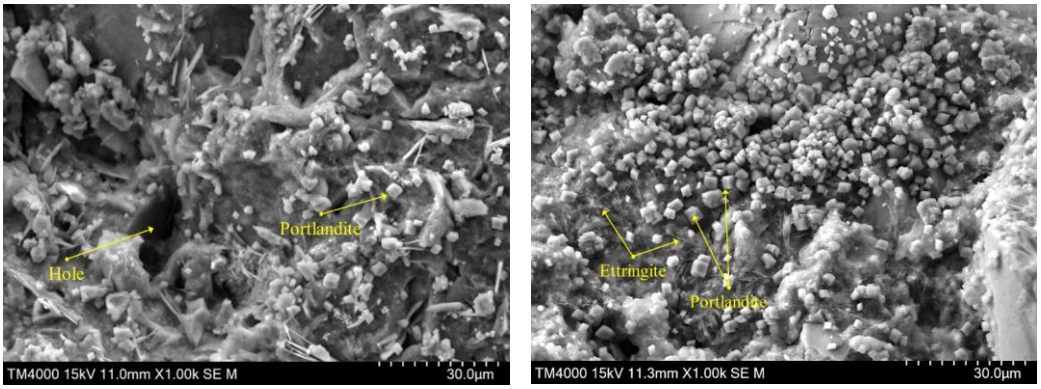


Figure 3-12 Compressive toughness index (CTI) and residual strength (f_{res}) results for all mixes

The addition of fibers did not significantly affect the $CTI_{0.8}$ except for PVA fiber, which increased it by 17%. Fibers did not impact energy absorption significantly after the peak point, due to rapid transition from the point B to C. PVA fiber significantly increased the $CTI_{0.2}$, by 35% due to its elongation, bonding, and tensile strength. BF diminished ductility and energy absorption at both levels. This could be due to breakage and corrosion of BF and increased cohesion, which led to increased brittleness. Hybridizing BF/PVA fibers significantly increased the $CTI_{0.2}$, by providing more ductility at high deformations. The optimal PVA/BF combination was 66:33, which increased the $CTI_{0.2}$, by 44% compared to mono BF. The 33:66 PVA/BF combination increased the $CTI_{0.2}$, by 34%. The brittle behaviour and higher cracking strength of BF compared to PVA, as well as its higher bonding strength, likely contributed to this (Choi *et al.* 2015).

Hybridizing micro- and macro-fibers increased energy absorption under compression for $CTI_{0.2}$ and $CTI_{0.8}$ compared to mono-fibers. Combining PPL/PVA fiber increased $CTI_{0.2}$ by 59% and combining TPPL/PVA fiber increased $CTI_{0.2}$ by 18%, over mono PPL and TPPL, with the optimal PVA fiber content being 33% for PPL and 66% for TPPL. This

difference might be due to the different properties of TPPL and PPL fibers. TPPL fibers had a more even distribution, larger diameter and length, and higher elastic modulus than PPL fibers, which provided better reinforcement in different orientations at a lower dosage. Therefore, more PVA fiber was needed to improve the bonding strength of TPPL fiber at a lower dosage.



FWNS SWSS

Figure 3-13 SEM images of the plain concrete mixtures (FWNS and SWSS)

3.3.5.5 Residual strength

The residual strength (f_{res}) is the stress level at 0.0065 strain in the post-peak region (point F in **Figure 3-11**). The results are depicted in **Figure 3-12**. SWSS had a 45% higher f_{res} than FWNS due to its denser structure and higher interlocking strength. PPS and PVA fibers increased f_{res} compared to macro-fibers due to their bonding strength, which helped distribute compression stress and maintain micro-cracks. BF corroded in SWSS concrete and could not reach its tensile capacity, reducing f_{res} by 36% compared to plain SWSS. Hybridizing BF/PVA significantly increased f_{res} compared to mono BF and overcame its tensile weakness caused in SWSS. When the PVA fiber content was twice that of BF, f_{res} increased by 181% compared to mono BF.

Similarly, PVA mitigated the bonding strength weaknesses of PPL/TPPL and increased f_{res} compared to mono-fibers. The optimized micro-fiber content in the hybridization was 66% PVA for 33% PPL fiber, which increased f_{res} by 65% and 19% over mono PPL and PVA mixes, respectively. The optimum PVA/TPPL fiber content in the hybrid form was 66:33, due to the difference in PPL and TPPL fiber properties mentioned before.

3.3.6 Empirical constitutive model of FR-SWSS in compression

In this section the stress-strain model proposed by Code GB50010-2010 (GB 50010 2010) was modified using fiber properties to predict the stress-strain relationship of FR-SWSS concrete. The model is as follows:

$$\sigma = (1 - d)E\varepsilon \tag{3-8}$$

where σ and ε are the axial stress and strain of FR-SWSS, respectively; E_c stands for the elastic modulus; d denotes the elastic damage evolution parameter, ranging from 0 to 1, whose expression is as follows (Kai *et al.* 2023):

$$d = \begin{cases} 1 - \dfrac{\alpha\rho n}{\alpha n - 1 + x^{\alpha n}};\ (0 \le x \le 1) \\ 1 - \dfrac{\rho}{\beta(x-1)^2 + x};\ (x > 1) \end{cases} \tag{3-9}$$

$$n = \frac{1}{1 - \dfrac{E_{sec}}{E_c}}, \rho = \frac{f_c'}{E_c \varepsilon_c^p}, x = \frac{\varepsilon}{\varepsilon_c^p}$$

The peak stress and strain are denoted by f_c' and ε_c^p, respectively, and the parameters controlling the shape of the ascending and descending branch of the stress-strain curve are denoted by α and β, respectively. The fitting results are listed in **Table 3-3**. The parameters α and β are mainly associated with the reinforcing index (RI), is determined by its volume fraction V_{fi}, length L_i, and diameter d_i, as defined in Eq. (3-10). An empirical equation is recommended as follows:

$$\alpha, \beta = af(RI_i) + bf\left(RI_j\right) + cRI_j + d \tag{3-10}$$

$$f(RI) = RI^{1.3} \tag{3-11}$$

$$RI_i = V_{fi}\frac{L_i}{d_i} \tag{3-12}$$

where a, b, c, and d, are the coefficients provided in **Table 3-4**, and RI_i and RI_j are the reinforcing index of fiber i and j in the hybrid or mono form, provided in **Table 3-2**. **Figure 3-14** compares the proposed constitutive model to some test results and their R-squared values, indicating that the proposed equations accurately predicted the stress-strain curves for both ascending and descending parts.

3.3.7 Synergistic impact of hybrid fiber

The success of hybridization relies on achieving synergy among fibers. This study quantifies mechanical properties and ductility-related parameters of hybrid FR_SWSS, comparing them with single fibers. Synergy, quantified by the synergistic coefficient (SC) in Eq. (3-13) (Hoan *et al.* 2019; Nguyen *et al.* 2022), is based on compressive strength, splitting tensile strength, elastic modulus, and energy absorption of hybrid FR_SWSS concrete ($R_{hybrid,a+b}$) and mono-fibers ($R_{mono,a}$ and $R_{mono,b}$), all with V_f = 0.25%. **Figure 3-15**displays synergy results; a positive SC value indicates successful hybridization and superior hybrid fiber performance over mono-fibers.

$$SC = \frac{R_{hybrid,a+b}^{(V_f)} - \max\left(R_{mono,a}^{(V_f)}, R_{mono,b}^{(V_f)}\right)}{\max\left(R_{mono,a}^{(V_f)}, R_{mono,b}^{(V_f)}\right)} \quad (3\text{-}13)$$

3.3.7.1 Micro-fiber hybridization

Though mono PPS and PVA fibers enhanced SWSS concrete ductility, only PPS/BF hybridization had positive synergy on $CTI_{0.8}$, while all micro-fiber hybridizations, including PPS/BF, negatively affected $CTI_{0.2}$ and f_{res}. This could result from reduced fiber dosage of high elongation and tensile strength (PPS and PVA) when combined with BF, along with BF breakage and corrosion in SWSS concrete negatively impacting synergy, increasing brittleness. In addition, micro-fiber hybridization improved SWSS concrete stiffness and had positive synergy on E_c. Partial PPS fiber replacement with PVA or BF had positive synergy on f_{st} by improving bonding strength, particularly with PVA fiber. Despite enhancing $f_{cm,365}$ and E_c with a 66:33 PVA/BF combination, which improved interlocking through complementarity, it compromised SWSS concrete ductility by increasing brittleness. SEM analysis (**Figure 3-7**) demonstrated a beneficial chemical bond between PVA fibers and SWSS concrete, leading to enhanced tensile capacity utilization within the concrete matrix. Furthermore, when PVA was combined with other microfibers, particularly BF, it contributed to improved bonding strength for the fibers. This effect arose from PVA effectively reinforcing the surrounding zone of the other fibers, resulting in a positive synergistic effect through both chemical and mechanical interfacial bonding. To sum up, selecting suitable micro-fibers combination, considering critical properties—elongation, tensile strength, and bonding strength—enhanced stress transfer through micro-cracks, improved cohesion and ductility over mono-fibers.

Table 3-4 Empirical constitutive model parameters of FR-SWSS

RI_i	RI_j	α				β			
		a	b	c	d	a	b	c	d
PPS	PVA	-1.476	-0.106	-0.170	1.054	-184.5	20.2	-44.7	16.2
PPS	BF	0.254	-0.821	0.735	0.919	-604.4	735.3	-822.9	48.8
PPS	PPL	-0.968	1.158	-0.941	1.014	113.2	-7.3	42.3	-7.0
PVA	BF	0.378	-7.557	5.754	0.753	18.9	-125.1	152.2	-6.9
PVA	PPL	1.474	-4.734	5.899	0.276	101.9	-275.5	363.5	-43.0
PVA	TPPL	0.806	-6.373	6.194	0.567	-56.1	307.7	-342.7	25.8
BF	PPL	6.680	-1.153	2.222	0.605	-659.0	211.0	-275.9	36.6
BF	TPPL	-0.295	0.518	-0.487	0.968	173.7	-107.4	119.7	-6.7

3.3.7.2 Micro- and macro-fiber hybridization

Combining PPL/PPS fibers negatively impacted f_{cm}^{365} and E_c but positively affected f_{st}, and ductility ($CTI_{0.2}$ and $CTI_{0.8}$) by improving stress transfer across micro- and macro-cracks while reducing stiffness and interlocking. Additionally, the pull-out of PPS fiber, which negatively affected strength, improved ductility in the hybrid system. PPL/PVA hybridization (66:33) improved f_{res}, unlike PPL/PPS, likely due to the stronger bonding strength of PVA fiber, as observed in SEM images. Despite f_{cm}^{365} being negatively affected by PPL/PVA, it contributed positively to f_{st}, and E_c, thereby improving compression energy absorption ($CTI_{0.2}$). PPL/ (PPS or PVA) combination showed positive synergy on tensile strength (f_{st}), but PPL/BF caused increased brittleness due to BF breakage and corrosion in SWSS concrete, resulting in negative synergy. The 33:66 PPL/BF hybridization negatively impacted f_{cm}^{365} and E_c, but enhanced compression ductility ($CTI_{0.2}$ and $CTI_{0.8}$). Conversely, the 66:33 PPL/BF combination improved synergy for f_{cm}^{365} and E_c, but negatively impacted compression ductility ($CTI_{0.2}$ and $CTI_{0.8}$). This could be explained by BF breakage and corrosion reduced compressive strength, increased porosity, and weakened micro-crack stress transfer, while higher BF dosage enhanced PPL bonding to bridge macro-cracks and energy absorption.

TPPL/PVA fiber showed positive synergy on f_{cm}^{365}, while TPPL/BF had negative synergy on it due to BF breakage and corrosion increasing porosity around TPPL fibers, weakening stress transfer. TPPL/BF positively affected E_c, enhancing SWSS concrete stiffness. Partially replacing TPPL with BF caused negative synergy in f_{st} and f_{res} due to increased brittleness. TPPL/PVA (33:66) showed positive synergy for f_{res} and $CTI_{0.2}$, while the opposite occurred for 66:33 incorporation. SEM analysis (**Figure 3-10**) revealed the crucial role of the chemical bonding of PVA fibers in enhancing the bonding strength of macro-fibers (PPL and TPPL). This improvement stemmed from the PVA

fibers reinforcing the surrounding concrete matrix of macro-fibers, leading to a synergistic effect on overall fiber-matrix interaction. Greater PVA bonding strength and TPPL distribution promoted enhanced inter-fiber bonding, bridging macro-cracks, and improving energy absorption and residual strength.

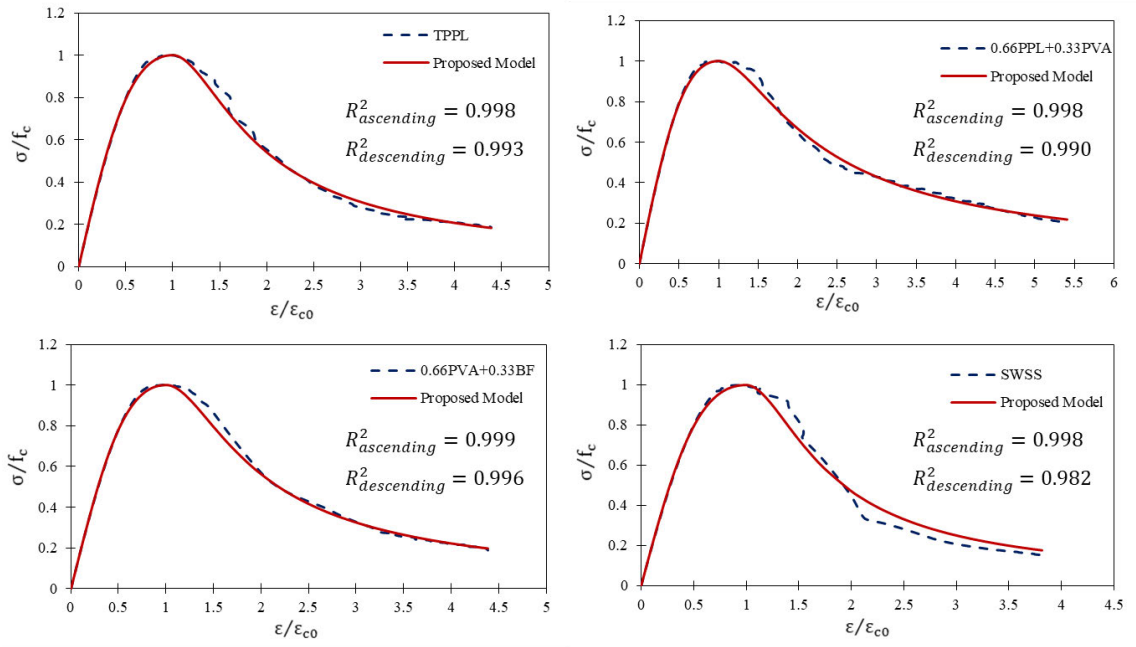


Figure 3-14 Comparison between the experimental and proposed stress-strain curves.

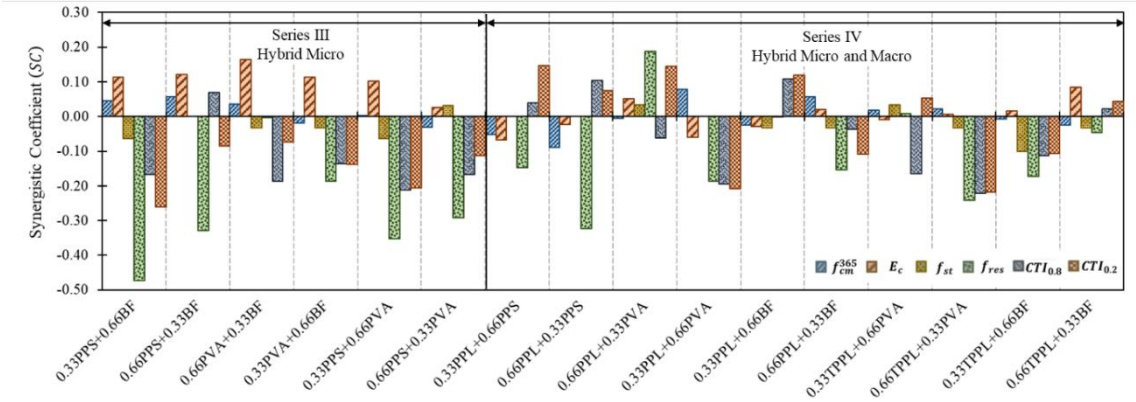


Figure 3-15 Synergistic coefficients (SC) of the mechanical properties of the hybrid FR-SWSS.

3.3.7.3 Combined mechanical performance (CMP)

Varied synergistic coefficients emphasize the importance of selecting the most effective fiber type or combination for overall performance. Using the Combined Mechanical Performance (CMP) (Ali 2022), mixtures were compared to plain SWSS concrete in Eq.

(3-14) with equal weighting given to all investigated properties. A value above one indicates superior performance.

$$CMP = \frac{1}{n}\sum_{i=1}^{n}\left(\frac{P_{i,fiber}}{P_{i,SWSS}}\right) \quad (3\text{-}14)$$

$$P_i = f_{cm}^{365}, f_{st}, E_c, f_{res}, CTI_{0.8}, CTI_{0.2}$$

Figure 3-16 displays CMP analysis results for SWSS concrete with various fibers. PVA had the highest CMP at 1.2 among mono-fibers, while BF had a lower 0.87 CMP, indicating a negative impact. Replacing 33% of PVA with BF resulted in a CMP of 1.45, significantly increasing it by 19% and 64% over mono PVA and BF, respectively. Substituting 66% of PVA with PPL resulted in a 1.65 CMP, 36% and 59% higher than mono PVA and PPL, respectively. Hybridizing BF notably mitigated its corrosion-induced weakness in SWSS, with PVA and TPPL achieving the most effective enhancement, resulting in a 64% and 48% CMP increase over mono BF.

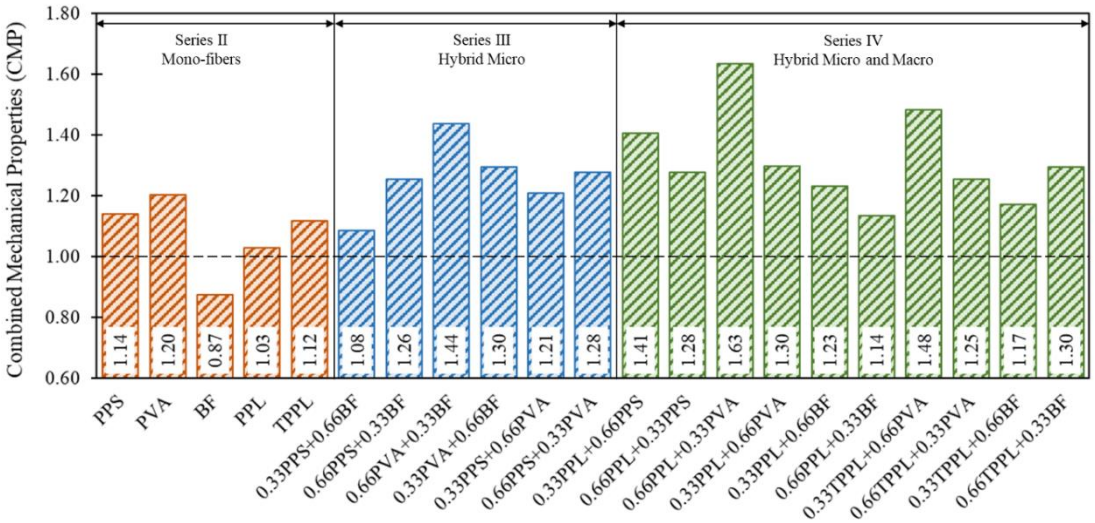


Figure 3-16 The combined mechanical performance (CMP) of fiber reinforced SWSS (FR-SWSS).

3.4 Conclusion

This study investigated the impact of hybrid fibers on the compressive stress-strain behaviour, tensile strength (f_{st}), and elastic modulus (E_c) of sustainable SWSS concrete. Micro-fibers—polypropylene (PPS), polyvinyl alcohol (PVA), basalt (BF)—and macro-fibers—polypropylene (PPL), and twisted polypropylene (TPPL)—at 0.25% volume

fraction were employed. Three fiber incorporation forms (mono-fibers, hybrid micro-fibers, and hybrid micro- and macro-fibers) were assessed for their synergistic effect on fiber-reinforced SWSS (FR-SWSS) performance. Principal conclusions follow:

- Adding fibers reduced slump, except for macro-fibers. Micro-fibers reduced slump more due to their even distribution, higher surface area, and water absorption. PVA/BF fibers synergy had minimal impact on slump, improving workability over the mono-fibers. PPL/micro-fiber combinations were less affected by W/B ratio due to reduced fiber interaction. The 66:33 PPL/ (PVA or BF) combination displayed good workability synergy.

- PPS and BF increased air content due to their hydrophobic nature, creating air pockets. Replacing part of BF with PVA fibers (66:33) reduced air content by 33% over mono BF due to the hydrophilic nature of PVA, preventing the formation of air pockets and facilitating air release. The flexibility of TPPL improved synergy with micro-fibers, resulting in better air release than PPL fiber. The TPPL/ (PVA or BF) (66:33) combination had the lowest air content among hybrid mixtures.

- BF in SWSS concrete decreased 28-day and 365-day compressive strength (f_{cm}) due to corrosion, while PVA fibers increased them due to high tensile strength, elastic modulus, and chemical bonding, enhancing interlocking. PVA/BF hybridizing overcame the weakness of BF and significantly increased f_{cm}. The optimal 66:33 PVA/BF combination increased f_{cm} by 13% over plain SWSS.

- Combining PPL/ (PVA or BF) improved f_{cm}, by 13%-16% over plain SWSS, due to enhanced bonding and stress transfer. The optimal PPL/PVA ratio shifted from 66:33 to 33:66 over 365 days, due to increased chemical bonding facilitated by PVA fiber. Conversely, PPL/BF combinations showed a reverse trend due to BF corrosion, suggesting that lower BF concentrations enhance bonding.

- After 365 days, PVA fibers increased compressive energy absorption by 17% ($CTI_{0.8}$) and 35% ($CTI_{0.2}$), while BF reduced ductility and energy absorption due to corrosion, increasing brittleness. Replacing 66% of BF with PVA fibers increased $CTI_{0.2}$ by 44%. While PPL fiber had no impact on energy absorption, combining PPL/PVA fibers (66:33) raised $CTI_{0.2}$ by 59% over mono PPL fiber.

- Fibers notably impact the residual strength (f_{res}) of SWSS concrete. PPS and PVA fibers increased f_{res} by 98% and 80%, respectively, while BF reduced it by 36% due to corrosion. A PVA/BF hybrid (66:33) significantly raised f_{res} by 181% over mono BF. While PPL fibers had a weaker impact on f_{res} than PVA fibers due to low bonding strength under high compression strain, partially substituting 66% of PPL with PVA increased f_{res} by 65% and 19% over mono PPL and PVA fibers, respectively.

- The impact of micro-fiber hybridization on compressive elastic modulus (E_c) highlighted the importance of fibers with high elastic modulus, tensile strength, and bonding. Micro-fibers reduced E_c by increasing air voids and reducing stiffness. While mono PVA and BF reduced E_c by 14%, a 66:33 PVA:BF hybridization nearly matched plain SWSS E_c by countering individual weaknesses through better chemical inter-bonding. A 33:66 micro- and macro-fiber combination enhanced stiffness and adhesion at micro and macro levels within the matrix, resulting in E_c improvement.

- The splitting tensile strength (f_{st}) of SWSS concrete was minimally affected by hybrid micro-fibers compared to mono-fibers. However, a positive synergy emerged with PPS/ (PVA or BF) (66:33) hybridization due to the enhanced elongation of PPS properties and the robust bonding of PVA or BF fibers, enhancing inter-fiber bonding and crack-bridging ability. Increased micro-fiber corrosion in SWSS concrete impacted tensile strength and ductility. Additionally, the optimal combination of 33% micro-fibers and 66% macro-fibers notably improved f_{st} over mono-fibers and plain SWSS.

- CMP analysis showed that all mono-fiber concretes had CMP > 1.0 except BF (CMP = 0.87), with PVA fiber having the highest CMP at 1.20. Hybrid PVA/BF (66:33) had the highest CMP (1.44) of all micro-fiber combinations. Hybrid, PPL/PVA (66:33) had the highest CMP among FR-SWSS concretes. Conversely, TPPL fiber exhibited superior synergy with 66% PVA fiber, due to its better distribution and higher flexibility. Thus, increasing PVA dosage enhanced TPPL bonding strength, improving strength and ductility.

Hybrid fibers in SWSS concrete significantly improved strength and ductility over mono-fiber mixtures. Micro-fiber chemical reactions had a considerable impact on their complementary. Further research is needed to determine the optimal fiber content for

various environments and evaluate its long-term performance and durability. In addition, more studies are needed to investigate the potential impact of varying fiber dosages on the analytical outcomes of this study.

Acknowledgements

The authors gratefully acknowledge the University of South Australia for providing laboratory and financial support. We also thank the technicians of the concrete laboratory at the University of South Australia for their assistance, as well as Adelaide Brighton Cement Ltd and Independent Cement and Lime Pty Ltd for donating OPC and GGBS, respectively. We also appreciate the donation of PPS and TPPL fibers from TEXO company, and the support of Mr. Adam Bromley. The authors acknowledge the instruments and expertise of Microscopy Australia at the Future Industries Institute (FII), University of South Australia, enabled by NCRIS, university, and state government support.

Chapter 3 References

Abbas, YM, Hussain, LA & Khan, MI 2022, 'Constitutive compressive stress–strain behavior of hybrid steel-PVA high-performance fiber-reinforced concrete', Journal of Materials in Civil Engineering, vol. 34, no. 1, p. 04021401.

Ahmed, SFU & Mihashi, H 2011, 'Strain hardening behavior of lightweight hybrid polyvinyl alcohol (PVA) fiber reinforced cement composites', Materials and structures, vol. 44, no. 6, pp. 1179-91.

Ali, B 2022, 'Development of environment-friendly and ductile recycled aggregate concrete through synergetic use of hybrid fibers', Environmental Science and Pollution Research, vol. 29, no. 23, pp. 34452-63.

Amin, N, Bijan, S & Kirk, V 2013, 'Effect of polyvinyl alcohol (PVA) fibre on dynamic and material properties of fibre reinforced concrete', Construction and Building Materials, vol. 49, pp. 374-83.

Amran, YM, Soto, MG, Alyousef, R, El-Zeadani, M, Alabduljabbar, H & Aune, V 2020, 'Performance investigation of high-proportion Saudi-fly-ash-based concrete', Results in Engineering, vol. 6, p. 100118.

AS, SA 2005, Methods of Testing Concrete. Method 17: Determination of the Static Chord Elastic Modulus and Poisson's Ratio of Concrete Specimens, Standards Australia Sydney, Australia.

Australia, S 2000, AS 1012.10 Methods for Testing Concrete: Determination of Indirect Tensile Strength of Concrete Cylinders (Brazil or Splitting Test), Standards Australia Strathfield, NSW, Australia.

Australia, S 2014, Methods of Testing Concrete, Method 4.2: Determination of Air Content of Freshly Mixed Concrete—Measuring Reduction in Air Pressure in Chamber Above Concrete, AS 1012.4. 2, Standards Australia Limited Sydney, Australia.

Banthia, N & Gupta, R 2004, 'Hybrid fiber reinforced concrete (HyFRC): fiber synergy in high strength matrices', Materials and structures, vol. 37, no. 10, pp. 707-16.

Benny, B, Bazli, M, Rajabipour, A & Arashpour, M 2023, 'Durability of tubular sea water sea sand concrete and fibre-reinforced polymer hybrid structures: Mechanisms and effective parameters: Critical overview and discussion', Construction and Building Materials, vol. 366, p. 130206.

Bo, X, Houssam, AT & John, G 2010, 'Impact resistance of poly(vinyl alcohol) fiber reinforced high-performance organic aggregate cementitious material', Cement and concrete Research, vol. 40, no. 2, pp. 347-51.

CAO, X-q, ZHANG, Y, HE, Y-j, JIANG, Y-c & YUAN, X-j 2008, 'Retrospect and discussion of surveys for construction sand in China offshore area', Marine Geology & Quaternary Geology, vol. 28, no. 3, pp. 121-25.

Chenggong, Z, Zhiyuan, W, Zhenyu, Z, Qiuyu, G, Xinrui, W & Renda, Z 2023, 'Research on different types of fiber reinforced concrete in recent years: An overview', Construction and Building Materials, vol. 365, p. 130075.

Choi, J-I & Lee, BY 2015, 'Bonding properties of basalt fiber and strength reduction according to fiber orientation', Materials, vol. 8, no. 10, pp. 6719-27.

Committe, SA 2014, AS 1012.9 Methods of Testing Concrete-Method 9: Determination of the Compressive Strength of Concrete Specimens, Australian Standards Sydney.

Committee, RCF 1970, 'Test and specifications of reinforcements for reinforced and prestressed concrete. Four recommendations of the RILEM/CEB/FIP Committee–Bond stress for reinforcing steel–1 Beam test–2 Pull-out test', Mater. Struct, vol. 3, no. 15, pp. 169-78.

Concrete, AICCo & Aggregates, C 2022, Standard Test Method for Static Modulus of Elasticity and Poisson's Ratio of Concrete in Compression, Astm international,

Decision, C 2003, 'Council Decision 2003/33/EC of 19 December 2002 establishing criteria and procedures for the acceptance of waste at landfills pursuant to Article 16 and Annex II to Directive 1999/31/EC', Official Journal of the European Communities, vol. 16, no. 2003, pp. 27-49.

Du, X, Li, Y, Si, Z, Huang, L & Chen, X 2022, 'Effects of basalt fiber and polyvinyl alcohol fiber on the properties of recycled aggregate concrete and optimization of fiber contents', Construction and Building Materials, vol. 340, p. 127646.

GB 50010 2010, 'Code for design of concrete structures', Standardization Administration of China: Beijing, China.

Haobo, B, Yuanzhen, L, Yaodong, G, Yi, L & Wenjuan, S 2023, 'Investigating stress–strain relationship and damage constitutive model of basalt fiber reinforced concrete under uniaxial compression', Journal of Building Engineering, vol. 73, p. 106789.

Hoan, PT & Thuong, NT 2019, 'Shear resistance of ultra-high-performance concrete reinforced with hybrid steel fiber subjected to impact loading', Journal of Science and Technology in Civil Engineering (STCE)-HUCE, vol. 13, no. 1, pp. 12-20.

Hsie, M, Tu, C & Song, P 2008, 'Mechanical properties of polypropylene hybrid fiber-reinforced concrete', Materials Science and Engineering: A, vol. 494, no. 1-2, pp. 153-57.

Kai, C, Lihua, X, Tao, T, Le, H, Jian, L, Jian, H, Huan, L & Yin, C 2023, 'Mechanical behavior of multiscale hybrid fiber reinforced recycled aggregate concrete subject to uniaxial compression', Journal of Building Engineering, vol. 71, p. 106504.

Kaidi, J, Xin, W, Lining, D, Zhiyuan, C, Huang, H, Xia, L, Jianxun, L & Zhishen, W 2023, 'Mechanical properties of multi-scale mono/hybrid non-metallic fiber-reinforced ultra-high performance seawater sea-sand concrete', Construction and Building Materials, vol. 401, p. 132922.

Khaloo, AR, Dehestani, M & Rahmatabadi, P 2008, 'Mechanical properties of concrete containing a high volume of tire–rubber particles', Waste management, vol. 28, no. 12, pp. 2472-82.

Lawler, JS, Zampini, D & Shah, SP 2002, 'Permeability of cracked hybrid fiber-reinforced mortar under load', Materials Journal, vol. 99, no. 4, pp. 379-85.

Li, M, Xing, D, Zheng, Q-B, Li, H, Hao, B & Ma, P-C 2022, 'Variation on the morphology and tensile strength of basalt fiber processed in alkali solutions', Construction and Building Materials, vol. 335, p. 127512.

Li, YT, Zhou, L, Jiang, M, Zhang, Y & Shao, J 2013, 'Experimental study on mechanical property of concrete based on seawater and sea sand', Advanced Materials Research, vol. 641, pp. 574-77.

Matthew Zhi Yeon, T, Kwong Soon, W, Muhammad Ekhlasur, R & Meheron 2020, 'Mechanical and durability performance of marine sand and seawater concrete incorporating silicomanganese slag as coarse aggregate', Construction and Building Materials, vol. 254, p. 119195.

Nguyen, D-L, Thai, D-K & Lam, MN-T 2022, 'Synergy in Flexure of High-Performance Fiber-Reinforced Concrete with Hybrid Steel Fibers', Journal of Materials in Civil Engineering, vol. 34, no. 6, p. 04022090.

Nishida, T, Otsuki, N, Ohara, H, Garba-Say, ZM & Nagata, T 2015, 'Some considerations for applicability of seawater as mixing water in concrete', Journal of Materials in Civil Engineering, vol. 27, no. 7, p. B4014004.

Özkan, Ş & Demir, F 2020, 'The hybrid effects of PVA fiber and basalt fiber on mechanical performance of cost effective hybrid cementitious composites', Construction and Building Materials, vol. 263, p. 120564.

Pakravan, HR, Latifi, M & Jamshidi, M 2016, 'Ductility improvement of cementitious composites reinforced with polyvinyl alcohol-polypropylene hybrid fibers', Journal of Industrial Textiles, vol. 45, no. 5, pp. 637-51.

Pakravan, HR, Latifi, M & Jamshidi, M 2017, 'Hybrid short fiber reinforcement system in concrete: A review', Construction and Building Materials, vol. 142, 2017/07/01/, pp. 280-94.

Poon, CS, Shui, Z & Lam, L 2004, 'Compressive behavior of fiber reinforced high-performance concrete subjected to elevated temperatures', Cement and concrete Research, vol. 34, no. 12, pp. 2215-22.

Qiuhong, Z, Youqun, W, Meng, X & Baoshan, H 2022, 'Experimental study on mechanical behavior of steel fiber reinforced geopolymeric recycled aggregate concrete', Construction and Building Materials, vol. 356, p. 129267.

Standard, A 2014, 'Methods of testing concrete, method 3.1: Determination of properties related to the consistency of concrete–slump test', AS, vol. 1012, pp. 1-2014.

Şükrü, Ö & Ömer, Ç 2021, 'The hybrid effects of basalt and PVA fiber on properties of a cementitious composite: Physical properties and non-destructive tests', Construction and Building Materials, vol. 312, p. 125292.

Syed Minhaj Saleem, K, Muhammad Junaid, M, Yu-Fei, W, Indubhushan, P, Yingwu, Z & Feng, X 2019, 'Axial stress-strain behavior of macro-synthetic fiber reinforced recycled aggregate concrete', Cement and Concrete Composites, vol. 97, pp. 341-56.

Ting, MZY, Wong, KS, Rahman, ME & Joo, MS 2020a, 'Mechanical and durability performance of marine sand and seawater concrete incorporating silicomanganese slag as coarse aggregate', Construction and Building Materials, vol. 254, p. 119195.

Ting, MZY, Wong, KS, Rahman, ME & Selowara Joo, M 2020b, 'Mechanical and durability performance of marine sand and seawater concrete incorporating silicomanganese slag as coarse aggregate', Construction and Building Materials, vol. 254, 2020/09/10/, p. 119195.

Tjaronge, MW & Irfan, UR 2015, 'Porosity, pore size and compressive strength of self compacting concrete using sea water', Procedia Engineering, vol. 125, pp. 832-37.

Vafaei, D, Hassanli, R, Ma, X, Duan, J & Zhuge, Y 2021a, 'Sorptivity and mechanical properties of fiber-reinforced concrete made with seawater and dredged sea-sand', Construction and Building Materials, vol. 270, p. 121436.

Vafaei, D, Ma, X, Hassanli, R & Zhuge, Y 2021b, Effects of seawater and sea-sand on concrete properties: A review paper, EASEC16: Proceedings of The 16th East Asian-Pacific Conference on Structural Engineering and Construction, 2019.

Vafaei, D, Ma, X, Hassanli, R, Duan, J & Zhuge, Y 2022, 'Microstructural behaviour and shrinkage properties of high-strength fiber-reinforced seawater sea-sand concrete', Construction and Building Materials, vol. 320, p. 126222.

Wang, J, Liu, E & Li, L 2018, 'Multiscale investigations on hydration mechanisms in seawater OPC paste', Construction and Building Materials, vol. 191, pp. 891-903.

Wang, Q, Ding, Y & Randl, N 2021, 'Investigation on the alkali resistance of basalt fiber and its textile in different alkaline environments', Construction and Building Materials, vol. 272, p. 121670.

Xie, J, Li, Y, Lu, Z, Fan, Z, Li, J & Li, S 2022, 'Effects of immersion in water, alkaline solution, and seawater on the shear performance of basalt FRP bars in seawater–sea sand concrete', Journal of Composites for Construction, vol. 26, no. 2, p. 04021071.

Xijun, S, Philip, P, Younho, R, Kaijian, H & Chungwook, S 2020, 'Constitutive behaviors of steel fiber reinforced concrete under uniaxial compression and tension', Construction and Building Materials, vol. 233, p. 117316.

Xiong, Z, He, S, Kwan, A, Li, L & Zeng, Y 2021, 'Compressive behaviour of seawater sea-sand concrete containing glass fibres and expansive agents', Construction and Building Materials, vol. 292, p. 123309.

Yang, S, Zang, C, Xu, J & Fan, G 2020, 'Determination of Fracture Parameters of Seawater Sea Sand Concrete Based on Maximum Fracture Load', Journal of Materials in Civil Engineering, vol. 32, no. 1, p. 04019315.

Yang, Z, Zhan, X, Zhu, H, Zhang, B, Feng, P, Li, H & Kua, HW 2023, 'Performance-based alkali-activated seawater sea-sand concrete: Mixture optimization for mechanical, environmental, and economical objectives', Construction and Building Materials, vol. 409, p. 134156.

Yifan, Z, Xiang, H, Caijun, S, Zuhua, Z & Deju, Z 2021, 'A review on seawater sea-sand concrete: Mixture proportion, hydration, microstructure and properties', Construction and Building Materials, vol. 295, p. 123602.

Younis, A, Ebead, U, Suraneni, P & Nanni, A 2018, 'Fresh and hardened properties of seawater-mixed concrete', Construction and Building Materials, vol. 190, pp. 276-86.

Younis, A, Ebead, U, Suraneni, P & Nanni, A 2019, Microstructure investigation of seawater vs. freshwater cement pastes, Proceedings, 10th International Structural Engineering and Construction Conference: Interdependence between Structural Engineering and Construction Management (ISEC 2019).

Zhao, Y, Hu, X, Shi, C, Zhang, Z & Zhu, D 2021, 'A review on seawater sea-sand concrete: Mixture proportion, hydration, microstructure and properties', Construction and Building Materials, vol. 295, p. 123602.

Zhou, J, Pan, J & Leung, CK 2015, 'Mechanical behavior of fiber-reinforced engineered cementitious composites in uniaxial compression', Journal of Materials in Civil Engineering, vol. 27, no. 1, p. 04014111.

Zhuang, J, Shen, S, Yang, Y, Xu, K & Ni, P 2022, 'Mechanical performance of basalt and PVA fiber reinforced hybrid-fiber engineered cementitious composite with superimposed basalt fiber content', Construction and Building Materials, vol. 353, p. 129183.

4 Synergistic effects of fiber hybridization on the fracture toughness of seawater sea-sand concrete

Reprinted and reformatted (including changes to the referencing style) with permission from Elsevier Ltd (see Appendix B).

Mashayekhi, A, Hassanli, R, Zhuge, Y, Ma, X, Chow, CW, Bazli, M & Manalo, A 2024c, 'Synergistic effects of fiber hybridization on the fracture toughness of seawater sea-sand concrete', Construction and Building Materials, vol. 444, p. 137845.

Abstract

This study investigates the fracture behaviour of fiber-reinforced seawater sea-sand concrete (FR-SWSSC), focusing on the impact of fiber hybridization on fracture toughness properties and potential synergistic effects. The study employed micro-fibers including short polypropylene (PPS), polyvinyl alcohol (PVA), basalt fibers (BF), and macro-fibers consisting long polypropylene (PPL) and twisted polypropylene (TPPL) fibers. The results indicated that macro-fibers, PPL and TPPL, significantly enhanced the post-peak behaviour of SWSSC, increasing fracture energy by 144% and 93% respectively, while micro-fibers alone showed negligible impact on the post-peak behaviour. Micro-fiber hybridization significantly enhanced both flexural strength and fracture energy of SWSSC, with hybrid PPS/BF and PPS/PVA demonstrated notably improved fracture energy by 176% and 290%, respectively, compared to mono PPS. Hybrid combinations of micro/macro-fibers demonstrated a synergistic effect on fracture toughness, where PPL and TPPL fibers bridged larger cracks, activating micro-fibers for enhanced energy dissipation. Moreover, the strong interfacial bond of PVA and BF fibers with the concrete matrix improved macro-fiber bonding strength and overall fracture resistance. By exploring the synergistic effect of hybrid discrete fibers in enhancing the fracture performance of FR-SWSSC, this research promotes sustainable construction practices by addressing inherent challenges of SWSSC.

Keywords

Fiber-reinforced concrete, Seawater, Sea-sand, Fracture toughness, Hybrid fiber, Synergy.

4.1 Introduction

Concrete production significantly impacts the environment due to high water consumption and river sand/gravel extraction (Miller *et al.* 2018; Li *et al.* 2024). This is particularly concerning with the looming global water crisis, with predictions of water scarcity for over half the population by 2050 (Slowey 2018). River sand extraction further exacerbates ecological disruption in river ecosystems. Additionally, cement production, a key component of concrete, generates significant CO_2 emissions, which reached to 2.8 billion tons in 2019 (Interior 2020). Consequently, research prioritizes identifying more sustainable concrete materials to reduce greenhouse gas emissions (Li, Ying *et al.* 2020; Gholampour *et al.* 2021; Gupta *et al.* 2021). Seawater (SW) and sea-sand (SS) emerge as promising replacements for freshwater (FW) and normal river sand (NS) due to their abundance and ease of extraction and transport, particularly in coastal projects and remote areas with limited access to high-quality materials due to scarcity or transportation costs (Xiao *et al.* 2017; Dhondy *et al.* 2019; Li *et al.* 2021; Li *et al.* 2024). The utilization of seawater sea-sand concrete (SWSSC) presents a promising approach for sustainable construction, particularly for coastal structures. However, to ensure its successful implementation as a viable alternative, a thorough understanding of its properties is crucial.

The presence of various ions in SWSSC, including sodium (Na^+), potassium (K^+), chloride (Cl^-), sulphate (SO_4^{2-}), calcium (Ca^{2+}), and magnesium (Mg^{2+}), can impact the properties of both fresh and hardened SWSSC compared to freshwater normal sand concrete (FWNSC). The presence of chloride in SW and SS accelerates cement hydration (Etxeberria *et al.* 2016a; Younis *et al.* 2018), resulting in higher compressive strength at an early age of SWSSC (Shi *et al.* 2015; Younis *et al.* 2018; Li, Peiran *et al.* 2020b; Sikora *et al.* 2020; Ting *et al.* 2020b; Vafaei *et al.* 2021a). Furthermore, most studies have shown that the tensile and flexural strength of SWSSC is lower than FWNSC (Etxeberria *et al.* 2016b; Younis *et al.* 2018; Lv *et al.* 2020; Ting *et al.* 2020b). Additionally, the use of SW and SS, containing chloride ions, can lead to carbonation of the concrete and corrosion of steel in steel reinforced concrete structures, negatively impacting their long-term performance (Liu *et al.* 2021; Li *et al.* 2024). To improve the durability of SWSS-RC structures, it is crucial to enhance crack resistance and understand the fracture behaviour of SWSSC.

Previous studies employed fibers (natural or synthetic) to improve the crack resistance of both SWSSC and FWNSC, leading to improve long-term performance (Vafaei *et al.* 2021a; Ahmad *et al.* 2022; Li, Yan *et al.* 2022; Vafaei *et al.* 2022b). Fiber-reinforced concrete (FRC) exhibited improved energy absorption and ductility compared to normal concrete (Gholampour *et al.* 2019; Ameri *et al.* 2020; Lin *et al.* 2020; Prasad *et al.* 2021). Synthetic fibers (e.g. polypropylene (PP) and polyvinyl alcohol (PVA)) are popular FRC choices due to their affordability, positive influence on concrete properties, and environmental resilience (Feng *et al.* 2019; Ling *et al.* 2019; Vafaei *et al.* 2021a). Studies showed that the mechanical bonding between PP fibers and concrete resulted in fiber pull-out, whereas PVA fibers exhibited rupture due to their chemical bond with the concrete matrix (Vafaei *et al.* 2022a). Research on FRC using micro-PP and PVA fibers in SWSSC demonstrated significant improvements in flexural strength, fracture energy, and post-peak behaviour (Vafaei *et al.* 2022a). Both PP and PVA fiber inclusion transformed SWSSC failure mode from brittle to ductile under compression (Vafaei *et al.* 2021a; Mashayekhi *et al.* 2024a). Incorporation of PP and PVA fibers also increased splitting tensile strength by 17% and 23% compared to plain SWSSC (Vafaei *et al.* 2021a). Incorporation of basalt fiber (BF) into SWSSC demonstrated that a fiber length of 12 mm and a volume fraction of 0.6% constitute optimal parameters. Under these conditions, compressive strength increased by 9% and splitting tensile strength by 7% compared to control specimens (Yang *et al.* 2024a).

Fiber incorporation improves SWSSC strength and ductility, but the impact of hybrid fibers, particularly on flexural and fracture behaviour, remains unexamined. While mono-fibers reinforce concrete, their limitations—length, tensile strength, and bonding strength— in crack control of concrete are well-documented (Chenggong *et al.* 2023; Kaidi *et al.* 2023; Mashayekhi *et al.* 2024a). A meticulously designed hybrid fiber system, combining micro and macro-fibers based on specific properties, has the potential to overcome these limitations and enhance the overall mechanical performance, ductility, and durability of FWNSC (Ahmed *et al.* 2011; Şükrü *et al.* 2021; Abbas *et al.* 2022; Mehran *et al.* 2022; Nguyen *et al.* 2022; Abdel-Karim *et al.* 2023; Kai *et al.* 2023). Hybrid fiber-reinforced concrete (HFRC) offers superior strength, ductility, toughness, and energy absorption (Pakravan *et al.* 2018; Ling *et al.* 2019; Çelik *et al.* 2020a; Ríos *et al.* 2020). In HFRC, higher-modulus fibers enhance strength, while lower-modulus fibers improve ductility (Pakravan *et al.* 2017). Studies demonstrate the synergistic effect of

fiber hybridization in SWSSC. PVA-basalt fiber (BF) hybridization significantly improved total energy absorption and residual compressive strength compared to mono-BF at the same fiber content (44% and 181% increase, respectively) (Mashayekhi *et al.* 2024a). Similarly, PVA-long PP (PPL) hybridization exhibited substantially higher ductility and residual compressive strength (59% and 65% increase, respectively) compared to mono-PPL (Mashayekhi *et al.* 2024a). Furthermore, adding 3% macro-BF significantly increased ultra-high performance (UHP) SWSSC compressive strength by 26%, while micro-PP and BF additions maintained compressive strength (Kaidi *et al.* 2023). Hybridization of micro-BF/PP fibers in SWSS mortars demonstrated the potential to enhance flexural, compressive, direct tensile, and splitting tensile strengths compared to incorporating mono-fibers. Optimal results were observed with a fiber dosage of 0.4% for each fiber type in the hybrid system (Yang *et al.* 2024b).

Fiber-reinforced SWSSC (FR-SWSSC), a relatively new sustainable construction material, requires further investigation to understand its properties and industrial applications. Existing research on its mechanical properties (splitting tensile strength, elastic modulus, compressive strength, etc.) is limited and mostly focused on single fiber types (Vafaei *et al.* 2021a, 2022a; Vafaei *et al.* 2022b; Kaidi *et al.* 2023; Mashayekhi *et al.* 2024a). SWSSC exhibits distinct physical and chemical properties compared to conventional concrete. This substantial chemical reactivity in SWSSC can potentially influence fiber synergies and interfacial bonding, both of which are critical for the performance of hybrid fiber mixes. Additionally, fracture toughness, a crucial property of concrete that reveals crack resistance and propagation, ductility, and post-crack behaviour, all of which are valuable for both design optimization and durability assessment of concrete structures, needs thorough evaluation for FR-SWSSC as well. This study comprehensively investigates the potential effects of hybrid fibers on the fracture toughness of FR-SWSSC. The hybrid fibers employed micro and macro fibers, combining them based on size and type, and then compared their impact on the fracture performance of FR-SWSSC with the mixes containing mono fibers. The findings of this study contribute to sustainability in the construction industry by addressing common problems associated with SWSSC.

4.2 Test Program

4.2.1 Materials

In line with previous findings on the benefits of ground granulated blast furnace slag (GGBS) in lowering CO_2 emissions and enhancing material properties (Zhang *et al.* 2013; Fattah *et al.* 2017; Yang *et al.* 2020), this study employed a similar approach. A combination of 35% ordinary Portland cement (OPC) and 65% GGBS was used as the cementitious material in all investigated mixes. Ion chromatography (IC) analysis revealed significantly elevated chloride (Cl^-) and sulphate (SO_4^{2-}) concentrations in seawater compared to tap-water (Vafaei *et al.* 2021a). Chloride levels in seawater were approximately 360 times higher than those in tap water, measuring 19,809.7 mg/L and 54.9 mg/L, respectively. Similarly, sulfate concentrations were 76 times greater in seawater (2,824.4 mg/L) than in tap-water (36.8 mg/L). The physical properties of coarse aggregate, normal sand, and sea-sand are listed in **Table 4-1**. The corresponding sieve analysis for the aggregates is shown in **Figure 4-1**.

Table 4-2 provides the physical properties of the fibers employed in this study. A combination of synthetic fibers (PP and PVA) and a natural fiber (BF) was used to reinforce SWSSC. The purpose of using these fibers was their readily availability in Australian market and to reduce manufacturing costs while utilizing their high performance. The selection of BF stemmed from its excellent mechanical properties, high-temperature resistance, acid/alkali resistance, readily available raw materials, and eco-friendly processing (Zheng *et al.* 2022; Dou *et al.* 2023). Two fiber sizes were investigated including micro-fibers (PPS, PVA, and BF) and macro-fibers (PPL and TPPL), as shown in **Table 4-2**. Additionally, recycled plastic-based PPL fibers were incorporated for eco-friendliness. Fiber morphology was characterized using scanning electron microscope (SEM) and presented in **Figure 4-2**.

Table 4-1 Physical properties of the aggregates.

Material	Specific Gravity (kg/m^3)	Bulk Density (kg/m^3)	Fineness Modulus
Coarse Aggregate	2.71	1560	6.92
Normal Sand	2.66	1628	1.97
Sea-Sand	2.57	1578	1.38

4.2.2 Mix design, and specimens preparation

A total of 23 concrete mixes (target compressive strength = 25 MPa) were prepared including two plain concrete (FWNS and SWSS), and 21 FR-SWSSC. The mix proportions and their 28-day compressive strengths (average of three standard cylinders) are presented in **Table 4-3**. All concrete mixes shared the same base proportions, with variations only in fiber type and the use of SW and SS. The study incorporated micro-fibers (PPS, PVA, and BF) and macro-fibers (PPL and TPPL) at a total volume of 0.25%, used in both mono and hybrid configurations (detailed in **Table 4-3**). This relatively lower fiber dosage ensured that the performance of samples would not be adversely affected by improper mixing. This percentage aligns with previous studies examining the impact of fibers on various properties of FRC for both FWNSC and SWSSC (Vafaei *et al.* 2021a, 2022a; Vafaei *et al.* 2022b). Hybrid mixtures incorporated these fibers at ratios of 33% and 66% each. For instance, two mixtures were prepared to examine the hybrid behaviour of PPL and PVA fibers: 0.33PPL/0.66PVA, and 0.66PPL/0.33PVA. To facilitate the placement of the concrete for the structural applications, a highly workable mix was designed to reach a slump value of 150-200 mm without the use of any superplasticizer.

Table 4-2 Physical properties of different fibers.

Property	PPS	PVA	BF	PPL	TPPL
Specific gravity	0.91	1.3	1.57	0.91	0.91
Length (mm)	6	8	7	47	54
Diameter (μm)	180	38	15	—	800
Thickness (μm)	—	—	—	<500	—
Tensile strength (MPa)	600	1600	2900	400	620
Young's modulus (GPa)	9.5	40	85	6	9.5
Chemical resistance	Excellent	Excellent	Excellent	Excellent	Excellent
Melting point (°C)	160	225	1450	160	160
Water absorption (% by weight)	<1	<1	<1	Nil	Nil
Alkali resistance	Excellent	Excellent	—	Excellent	Excellent
Corrosion resistance	Excellent	Excellent	Excellent	Excellent	Excellent

4.2.3 Test specimens and methods

Three concrete beam specimens were prepared according to Australian Standard AS 1012.2 (Australia 1994) with dimensions of 100 mm × 100 mm × 350 mm. After casting, beam samples were demolded at 24 hours and cured in a moist environment at 23 ± 2°C for one day. Subsequently, they were immersed in a lime-saturated water bath for 28 days, following the same curing procedure as the cylinder samples. After curing, all samples

were pre-cracked with a length of 30 mm and a width of 5 mm using a cutting saw, creating a defined notch. To determine the fracture toughness properties, three-point bending test was employed, which have been used widely in previous studies (Faraj *et al.* 2019; Çelik *et al.* 2020a; Vafaei *et al.* 2022a; Mukhtar 2024; Zhang *et al.* 2024). Details regarding the beam geometry and support configuration are provided in **Figure 4-3**. The experiments were conducted with a 100-kN displacement-control testing machine at a loading rate of 0.05 mm/min. A dynamic extensometer and linear variable displacement transducers (LVDT) (see **Figure 4-3**) were used to measure the crack mouth opening displacement (CMOD) and deflection at the mid-span of the beams, respectively. Data were recorded using a data acquisition system, and the test was terminated when CMOD reached 3.5 mm.

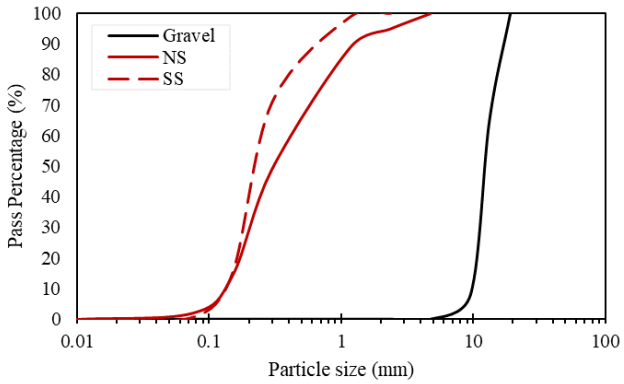


Figure 4-1 Grading curves for NS and SS coarse aggregates.

4.3 Results and discussion

Figure 4-4 shows typical failures of the specimens. As expected, all specimens exhibited a major crack forming at the mid-span notch point. With increasing concentrated load, the crack at the concrete mid-span propagated upward, and all specimens exhibited similar Mode I fracture (fracture opening in tension), as anticipated. A detailed analysis of the fracture properties, including load–CMOD curves, fracture energy, and fracture toughness, along with the overall behaviour of the specimens, is presented and compared in subsequent sections.

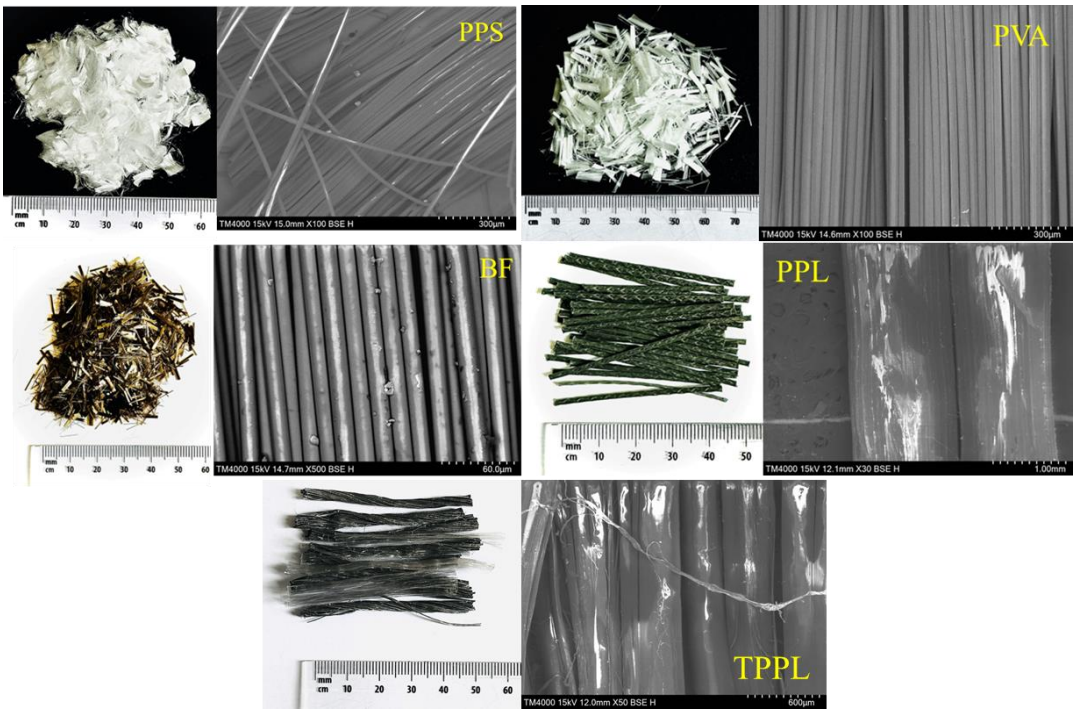


Figure 4-2 Characterization of various fibers: shape, dimensions, and SEM images.

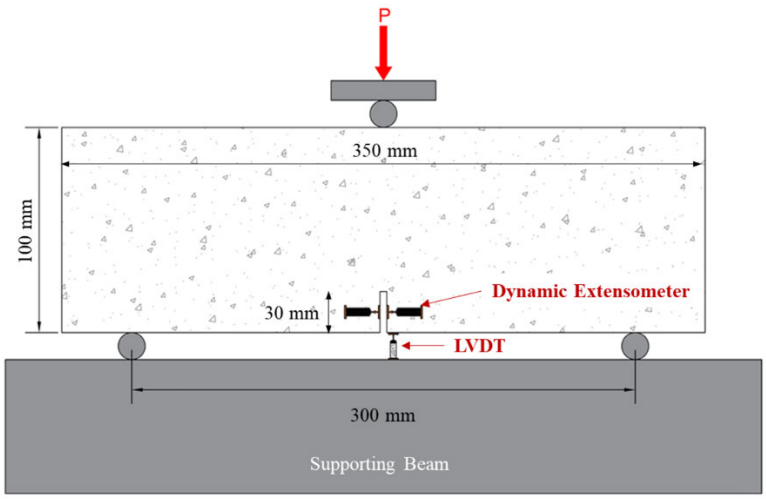


Figure 4-3 Schematic of the fracture toughness test setup.

4.3.1 Load–CMOD curves

Figure 4-5a-c presents load-CMOD curves for concrete mixes reinforced with mono-, hybrid micro-, and hybrid macro/micro-fibers, respectively. As shown in **Figure 4-5**a, plain concretes (SWSS and FWNS) showed similar pre-peak behaviour with comparable strengths but exhibited brittle failure after cracking (sudden strength loss). All FR-SWSSC mixes exhibited approximately similar initial pre-peak behaviour, suggesting minimal fiber contribution in the pre-cracking stage, aligning with prior research findings

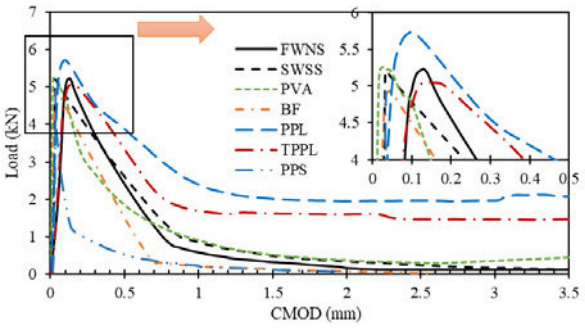
(Çelik *et al.* 2020a; Vafaei *et al.* 2022a). **Figure 4-6** presents the load reduction factor (LRF), defined as the ratio of the peak load to the residual load at 0.8 mm of CMOD. The LRF represents the percentage reduction in load capacity between the peak point and the point where the CMOD reaches 0.8 mm. Both SWSS and FWNS concretes exhibited significant strength loss, exceeding 80% at 0.8 mm CMOD, with negligible residual strength (defined as post-peak flexural strength) remaining at 2.5 mm CMOD. Macro fiber addition (PPL and TPPL) significantly improved post-cracking behaviour in SWSSC, maintaining approximately 50% and 38% of peak load at 0.8 mm CMOD, respectively. Among the micro-fibers investigated (PVA, PPS, and BF), PVA exhibited the best post-crack performance (**Figure 4-5**a and **Figure 4-6**), potentially due to strong chemical bonding with the matrix, as reported in previous studies (Amin *et al.* 2013; Kaidi *et al.* 2023; Mashayekhi *et al.* 2024a).



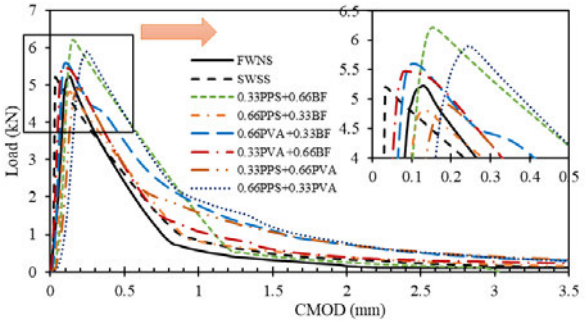
Figure 4-4 Typical fracture toughness failure mode.

In comparison, as shown in **Figure 4-5**b, the post-cracking behaviour of hybrid micro-fiber mixes showed improvement specially when PVA fibers were incorporated in the hybrid system. According to **Figure 4-5**b, the hybrid PVA/PPS fibers significantly improved LRF compared to both mono PVA and PPS fibers. In this case, incorporating 0.66PPS/0.33PVA was more effective. Additionally, compared to mono BF, PVA/BF and PPS/BF hybridization significantly improved LRF and maintained the load drop after peak point. At a CMOD of 0.8 mm, hybrid 0.66PVA/0.33BF fibers showed a great enhancement of strength, with an approximately 185% and 55% increase compared to

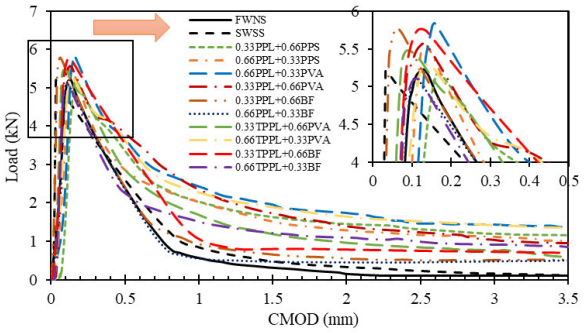
mono BF and plain SWSSC, respectively. This improvement can be attributed to the chemical bonding between PVA and BF fibers (Amin *et al.* 2013; Chenggong *et al.* 2023; Mashayekhi *et al.* 2024a), which enhanced the strength of the mixture by increasing its cohesion and overall strength, resulting in improved peak-load and post-cracking performance.



(a)



(b)



(c)

Figure 4-5 Load-CMOD curves of flexural strength test for different fiber types: (a) Mono-fibers, (b) Hybrid micro-fibers, (c) Hybrid micro- and macro-fibers.

Micro/macro fiber hybridization (**Figure 4-5**a) improved both peak and post-cracking performance in all fiber mixtures. This is attributed to macro-fibers bridging cracks,

enhancing the load-carrying capacity of SWSSC. Their longer length allows macro-fibers to limit crack width more effectively than micro-fibers. Among the hybrids, 0.66PPL/0.33PVA improved flexural strength by 10% compared to mono PVA, while 0.33PPL/0.66BF yielded a 20% increase compared to mono BF. **Figure 4-6** demonstrates significant improvement in LRF and post-peak behaviour of SWSSC due to hybrid macro/micro fiber incorporation. PPL/PPS hybridization yielded the greatest improvement in LRF, with a 193%–273% enhancement compared to mono PPS fibers. This superior performance stems from the effectiveness of long PPL fibers in bridging post-peak macro cracks. Compared to mono PVA and BF, both hybrid PPL/PVA and PPL/BF significantly enhanced the ratio by 47-77%, while TPPL/PVA and TPPL/BF achieved a 55-115% improvement. This enhancement was likely attributed to the improved bonding strength of PPL and TPPL fibers achieved through hybridization with PVA and BF fibers. Considering the SEM images in **Figure 4-7**, the hybrid PPL/PVA and TPPL/PVA fibers appear to exhibit synergistic effects. This stems from the strong chemical bonds between PVA and BF and the SWSSC matrix, as reported previously (Vafaei *et al.* 2022a; Mashayekhi *et al.* 2024a). Notably, TPPL/PVA exhibited the highest improvement, likely due to superior TPPL fiber distribution and flexibility compared to PPL.

4.3.2 Fracture energy (G_F)

In this study Eq. (4-1), (Standard 2003) was adopted to calculate fracture energy (G_F). Researchers commonly employ this equation to quantify total energy dissipation per unit crack area from load-CMOD curves (Rasheed *et al.* 2018; Kazemian *et al.* 2019; Xie, Chaopeng *et al.* 2021).

$$G_F = \frac{0.75W_0 + W_1}{A_{lig}} \tag{4-1}$$

In Eq. (4-1), W_0 denotes the energy consumed at CMOD=3.5 mm and A_{lig} represents the ligament area. The work W_1, due to self-weight of the specimen and equipment (e.g., steel rod), is calculated as:

$$W_1 = 0.75 \times \frac{S}{L} m \times g \times CMOD_c \tag{4-2}$$

with S as the loading span, L the specimen length, m the specimen mass, and g representing the gravity acceleration, and $CMOD_c$ =3.5 mm.

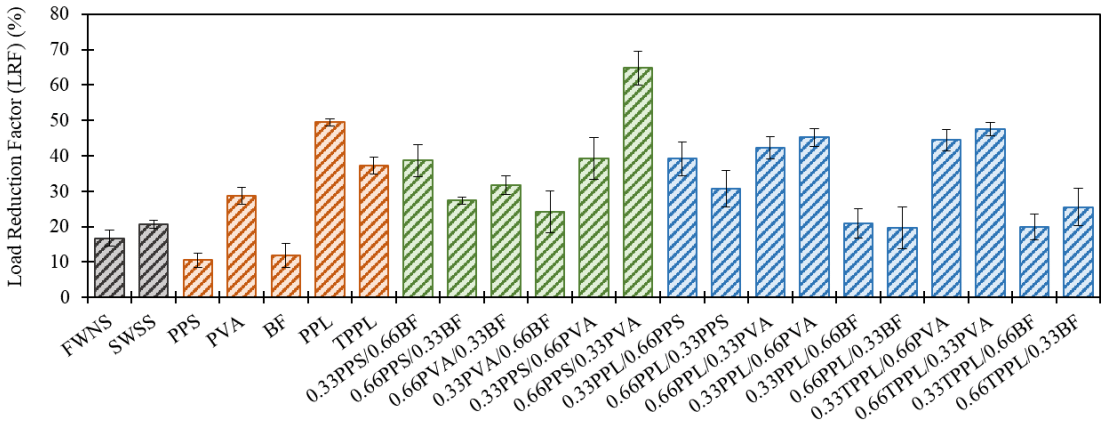


Figure 4-6 Comparison of load reduction factor (LRF) values for different concrete mixes.

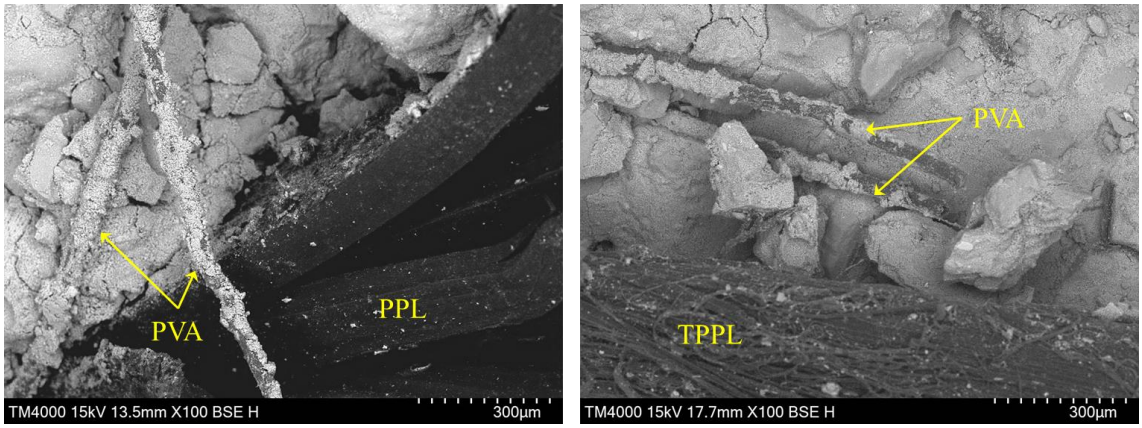


Figure 4-7 The SEM images of hybrid PPL/PVA and TPPL/PVA fibers.

Figure 4-8 presents the mean G_F values for all investigated concrete mixes at CMOD values of 0.5, 1.0, and 3.5 mm. The results demonstrated approximately similar G_F values for both FWNS and SWSSC across all CMOD values. The incorporation of mono fibers exhibited a dependence on fiber type, with increases or decreases in G_F observed. Notably, mono fibers were more effective at higher CMOD values due to their ability to bridge the load across cracked concrete. For example, PPS and BF fiber incorporation significantly decreased G_F, while PPL and TPPL fibers significantly improved it. PPL and TPPL fibers demonstrably increased G_F by approximately 144% and 93%, respectively, compared with plain SWSSC at a CMOD of 3.5 mm. Mono PVA fiber incorporation resulted in lower G_F at lower CMOD values, but it increased at a CMOD

of 3.5 mm by about 11%. The observed behaviour could be due to the crack-bridging capability of PVA fibers, which stems from their superior bonding and tensile strengths. However, their effectiveness in this regard is demonstrably lower compared to PPL and TPPL fibers, likely due to a difference in fiber length.

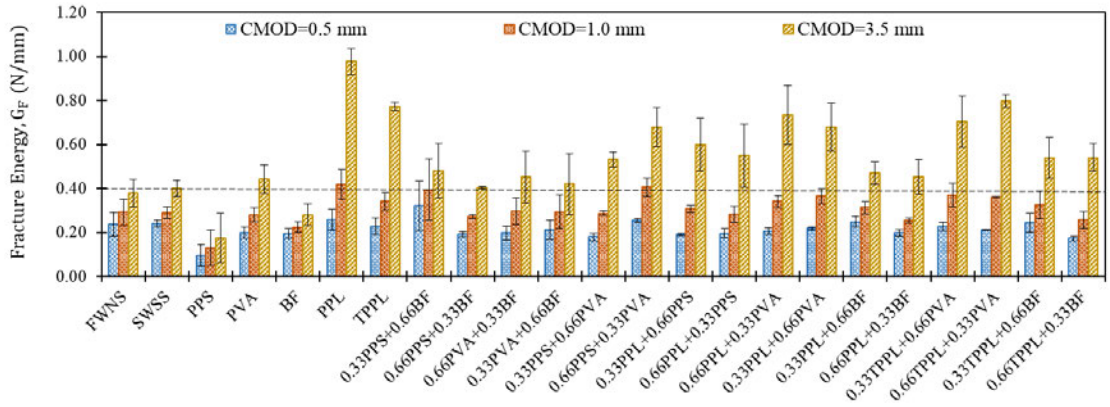


Figure 4-8 Comparison of fracture energy for different concrete mixes.

The combination of micro-fibers significantly influenced G_F and exhibited a synergistic effect compared to mono fibers. Hybridizing PPS with BF or PVA significantly improved G_F at CMOD 3.5 mm by approximately 176% and 290%, respectively, compared to mono PPS. Additionally, hybrid PPS/PVA fiber was more effective than hybrid PPS/BF fiber, which led to an increased G_F at CMOD 3.5 mm by 53% over mono PVA. Notably, a higher dosage of BF in the hybrid system with PPS fibers (0.33PPS/0.66BF) proved more effective, while for PVA and PPS hybridization, a higher dosage of PPS fibers (0.66PPS/0.33PVA) yielded better results. These observations can be attributed to the ability of PVA and BF fibers to enhance the bonding strength of PPS fibers. While BF exhibited slight corrosion in SWSSC (Mashayekhi *et al.* 2024a), leading to their lower contribution to improved bonding compared to PVA fibers, a higher dosage of BF was required in the hybrid system. When it comes to the PVA/BF hybrid, G_F at CMOD 3.5 mm improved by 62% compared to mono BF incorporation. In this case, 0.66PVA/0.33BF was more effective.

A significant improvement in G_F was observed for all CMOD values when macro/micro fiber hybridization was employed compared to mono PPS and BF. This enhancement was attributed to the bridging effect of macro fibers across larger cracks, with its effectiveness increasing with higher CMOD values. Specifically, hybridization of PPL fibers with PPS,

PVA, or BF resulted in increases of 244%, 66%, and 68% in G_F at a CMOD of 3.5 mm, respectively, compared to only micro-fibers. Similarly, hybridization of TPPL with PVA or BF led to enhancements of 80% and 93% in G_F at a CMOD of 3.5 mm, respectively. Notably, a fiber volume fraction of 0.66TPPL/0.33PVA (or BF) and 0.66PPL/0.33PVA (or BF) proved to be more effective.

In summary, the fracture energy analysis revealed a positive correlation with increasing CMOD value. This trend was attributed to the enhanced contribution of macro-fibers (due to their extended length and mechanical bonding) and micro-fibers (particularly PVA and BF with superior chemical bonding and tensile strength) in arresting crack propagation. Notably, fiber length emerged as the most crucial parameter influencing G_F improvement.

4.3.3 Fracture toughness (K_{IC})

In three-point bending fracture tests, concrete undergoes three stages including crack initiation, stable crack propagation, and critical unstable fracture. The double-K fracture model (DKFM), a two-parameter method for assessing concrete fracture behaviour (Xu *et al.* 1999b, 1999a, 2000; Zhang, Peng *et al.* 2022), treats it as a brittle elastic-plastic material. It defines K_{IC}^{ini} (initial fracture toughness) as the energy for crack initiation influenced by cohesive strength, and K_{IC}^{un} (unstable fracture toughness) as the energy for continued crack propagation governed by tensile strength. DKFM allows evaluation of concrete fracture behaviour under varying loads and the influence of reinforcement. This study employs DKFM to calculate fracture parameters of the investigated mixtures, with results presented in this section.

According to the DKFM (**Figure 4-9**), the K_{IC}^{ini} can be calculated using Eq. (4-3).

$$K_{IC}^{ini} = \frac{3(P_{ini} + \frac{mg}{2})\, S\sqrt{a_0}}{W^2 B}\, f(V_0) \tag{4-3}$$

where S denotes the span length. For S/W values of 2.5 and 4.0, the function $f(V_0)$ can be determined using equations (4-4) and (4-5), respectively. Interpolation techniques can then be employed to estimate $f(V_0)$ for intermediate S/W ratios.

$$f(V_0) = \frac{1.83 - 1.65V_0 + 4.76{V_0}^2 - 5.3{V_0}^3 + 2.51{V_0}^4}{(1 + 2V_0)(1 - V_0)^{3/2}} \tag{4-4}$$

$$f(V_0) = \frac{1.99 - V_0(1 - V_0)\left(2.15 - 3.93V_0 + 2.7{V_0}^2\right)}{(1 + 2V_0)(1 - V_0)^{3/2}} \quad (4\text{-}5)$$

where P_{ini} represents the initial cracking load; W denotes the height of the beams; B represents the width of the beams; a_0 represents the length of the initial crack; and V_0 represents the ratio of the initial crack length to the depth of the specimen (a_0/W).

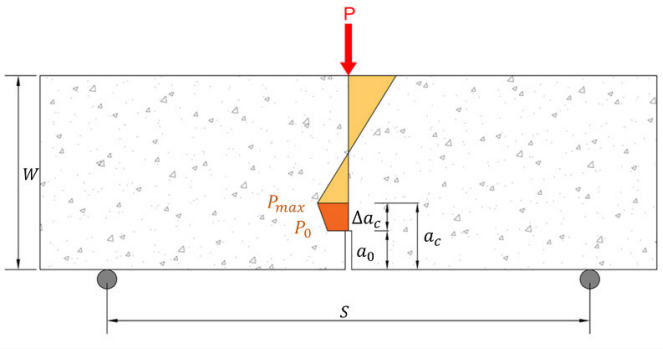


Figure 4-9 Stress distribution of DKFM method.

Using Eq. (4-6), K_{IC}^{un} can be calculated.

$$K_{IC}^{un} = \frac{3(P_{max} + \frac{mg}{2})\, S\sqrt{a_C}}{W^2 B}\, f(V_C) \quad (4\text{-}6)$$

where a_C represents the critical effective crack length, and it can be calculated using Eq. (4-7) as follows:

$$a_C = \frac{2}{\pi}(W + H_0)arctg\sqrt{\frac{B.E.CMOD_C}{32.6P_{max}} - 0.1135} - H_0 \quad (4\text{-}7)$$

where P_{max} represents the peak load, $CMOD_C$ represents the critical crack mouth opening displacement, H_0 refers to the thickness of the knife edges, and E denotes the elastic modulus, which can be calculated using Eq. (4-8).

$$E = \frac{1}{BC_i}\left[3.7 + 32.6\, tan^2\left(\frac{\pi}{2}\frac{a_0 + H_0}{W + H_0}\right)\right] \quad (4\text{-}8)$$

where, C_i, representing the initial compliance, can be expressed as $CMOD_i/P_i$, and P_i is the load at the initial linear segment of the P-CMOD curve. When $S/W = 2.5$ and 4.0,

$f(V_C)$ can be calculated using Eqs. (4-9) and (4-10), respectively (Shah 1990; Hiroshi *et al.* 2000; Xu *et al.* 2000; Zhang, Peng *et al.* 2022).

$$f(V_C) = \frac{1.83 - 1.65V_C + 4.76{V_C}^2 - 5.3{V_C}^3 + 2.51{V_C}^4}{(1 + 2V_C)(1 - V_C)^{3/2}} \quad (4\text{-}9)$$

$$f(V_C) = \frac{1.99 - V_C(1 - V_C)\left(2.15 - 3.93V_C + 2.7{V_C}^2\right)}{(1 + 2V_C)(1 - V_C)^{3/2}} \quad (4\text{-}10)$$

The span-to-height ratio of the beams, denoted as V_C, can be calculated by taking the ratio of a_C/W. In this study, the span-to-height ratio (S/W) of the specimen used in the fracture test was designed to be 3.0. As a result, $f(V_0)$ and $f(V_C)$ must be obtained through linear interpolation using the values calculated using S/W values of 2.5 and 4.

The cohesion toughness, represented by K_{IC}^{C}, can be considered as the energy absorbed in the progressive expansion of the fracture process zone. As such, it can be evaluated by utilizing the following straightforward relationship:

$$K_{IC}^{ini} = K_{IC}^{un} - K_{IC}^{C} \quad (4\text{-}11)$$

where K_{IC}^{C} represents the cohesion toughness that arises from the cohesive force within the fracture process zone (FPZ), a region around the crack tip where there is localized damage.

Figure 4-10 depicts higher initial fracture toughness (K_{IC}^{ini}) for SWSSC compared to FWNS concrete (by approximately 7%), likely due to its denser pore structure as supported by (Wang, Junjie *et al.* 2018; Vafaei *et al.* 2022b; Mashayekhi *et al.* 2024a), which may reduce initial microcracking. The SEM analysis in **Figure 4-11** provides further evidence for the denser structure of SWSSC compared to FWNS. As K_{IC}^{ini} reflects inherent toughness at crack initiation, this denser structure likely reduces microcracking at the initial stages, potentially explaining the increased K_{IC}^{ini}. However, K_{IC}^{un} results indicate a 12% lower value for SWSSC. Similarly, **Figure 4-12** shows a significant reduction (by approximately 96%) in K_{IC}^{C} for SWSS compared to FWNS. These findings suggest that while the denser structure in SWSS enhanced initial crack resistance, it may also promote a more brittle fracture behaviour within the FPZ, leading to lower K_{IC}^{C}.

Table 4-3 Concrete mix design and their 28-day compressive strengths.

Groups	Concrete Mix	Binder (kg/m^3)		Gravel (kg/m^3)	Sand (kg/m^3)		Water (kg/m^3)		Fiber (kg/m^3)					28-day f_c' (MPa)
		OPC	GGBS		NS	SS	FW	SW	PPS	PVA	BF	PPL	TPPL	
Plain	FWNS	126	234	995	785	—	256	—	—	—	—	—	—	28.5
	SWSS	126	234	995	—	785	—	256	—	—	—	—	—	27.6
Mono	PPS	126	234	995	—	785	—	256	2.28	—	—	—	—	27.2
	PVA	126	234	995	—	785	—	256	—	3.25	—	—	—	28.9
	BF	126	234	995	—	785	—	256	—	—	6.63	—	—	27.4
	PPL	126	234	995	—	785	—	256	—	—	—	2.28	—	28.6
	TPPL	126	234	995	—	785	—	256	—	—	—	—	2.28	29.0
Hybrid micro	0.33PPS/0.66BF	126	234	995	—	785	—	256	0.76	—	4.41	—	—	27.9
	0.66PPS/0.33BF	126	234	995	—	785	—	256	1.52	—	2.21	—	—	28.2
	0.66PVA/0.33BF	126	234	995	—	785	—	256	—	2.17	2.21	—	—	31.1
	0.33PVA/0.66BF	126	234	995	—	785	—	256	—	1.08	4.41	—	—	27.0
	0.33PPS/0.66PVA	126	234	995	—	785	—	256	0.76	2.17	—	—	—	27.3
	0.66PPS/0.33PVA	126	234	995	—	785	—	256	1.52	1.08	—	—	—	26.9
Hybrid macro/micro	0.33PPL/0.66PPS	126	234	995	—	785	—	256	1.52	—	—	0.76	—	27.2
	0.66PPL/0.33PPS	126	234	995	—	785	—	256	0.76	—	—	1.52	—	26.4
	0.66PPL/0.33PVA	126	234	995	—	785	—	256	—	1.08	—	1.52	—	31.9
	0.33PPL/0.66PVA	126	234	995	—	785	—	256	—	2.17	—	0.76	—	31.1
	0.33PPL/0.66BF	126	234	995	—	785	—	256	—	—	4.41	0.76	—	31.5
	0.66PPL/0.33BF	126	234	995	—	785	—	256	—	—	2.21	1.52	—	31.5
	0.33TPPL/0.66PVA	126	234	995	—	785	—	256	—	2.17	—	—	0.76	30.3
	0.66TPPL/0.33PVA	126	234	995	—	785	—	256	—	1.08	—	—	1.52	30.5
	0.33TPPL/0.66BF	126	234	995	—	785	—	256	—	—	4.41	—	0.76	28.5
	0.66TPPL/0.33BF	126	234	995	—	785	—	256	—	—	2.21	—	1.52	29.6

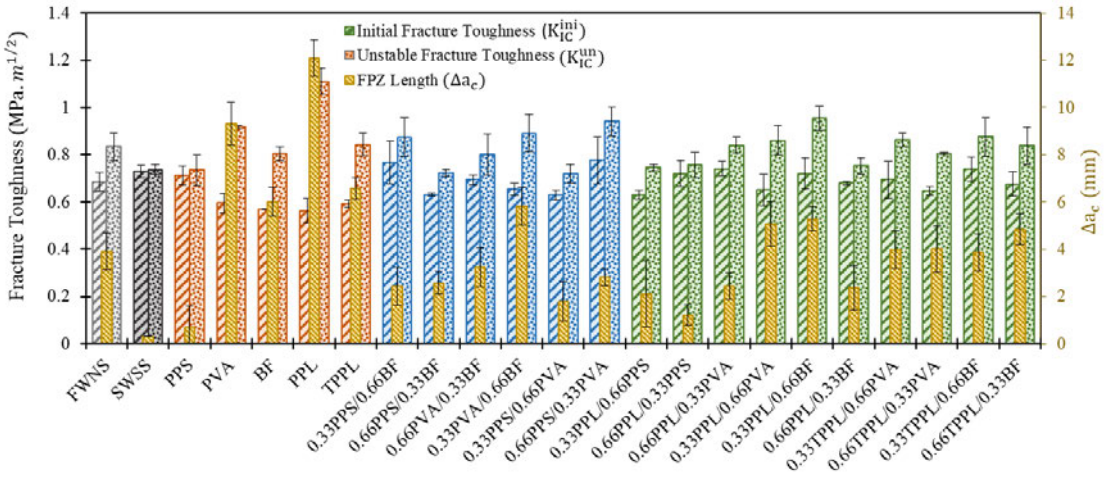


Figure 4-10 The fracture toughness properties (initial and unstable) based on DKFM method.

Mono-fiber mixtures exhibited lower K_{IC}^{ini} compared to plain SWSSC, with PPS fibers showing the least reduction. This is likely due to microcrack formation within the matrix, which weakens the dense structure of plain SWSSC. However, these microcracks can dissipate stress and prevent larger cracks, leading to significantly higher K_{IC}^{un}—a measure of total toughness near failure—with mono PVA and PPL fibers increasing it by 24% and 51%, respectively, compared to plain SWSSC. PPS fiber incorporation demonstrated the least reduction in initial fracture toughness (K_{IC}^{ini}) but proved ineffective for ultimate fracture toughness (K_{IC}^{un}). This behaviour likely arises from the inherent properties of PPS fibers. Their lower stiffness and tensile strength compared to other fibers might improve initial crack resistance through microcrack bridging, but hinder crack arrest and strength enhancement due to weak concrete-fiber bonding, promoting fiber pull-out instead of breakage. Conversely, strong chemical bonding in PVA fibers and superior mechanical interlocking in PPL and TPPL fibers with the concrete matrix resulted in higher K_{IC}^{un}. This is further supported by the K_{IC}^{C} results in **Figure 4-12**, where PPS fiber exhibited the lowest value. Overall, fiber addition significantly improved the K_{IC}^{C} of SWSSC, with PVA and PPL fibers being most effective, leading to approximately 54 and 93 times higher K_{IC}^{C}, respectively.

Micro-fiber hybridization significantly increased K_{IC}^{ini} compared to mono-fiber mixtures. Notably, 0.66PVA/0.33BF hybridization yielded the greatest improvement, surpassing

both BF and PVA by 22% and 17%, respectively. This is attributed to the positive synergy of PVA/BF in SWSSC, enhancing chemical bonding with the matrix and promoting more efficient reinforcing. Hybridizing PPS with BF or PVA significantly improved fracture behaviour compared to mono PPS. Hybrid 0.33PPS/0.66BF and 0.66PPS/0.33PVA increased K_{IC}^{ini} (by about 8% and 9%), K_{IC}^{un} (by about 19% and 28%), and K_{IC}^{C} (by about 362% and 616%), respectively, over mono PPS. This improvement likely stemmed from enhanced bonding strength of PPS fibers, a key weakness, due to the incorporation of PVA or BF, which exhibit strong adhesion to the concrete matrix. Incorporation of hybrid 0.33PPS/0.66BF and 0.66PPS/0.33PVA fibers led to increases in K_{IC}^{ini} (by about 35% and 31%) and K_{IC}^{un} (by about 9% and 3%) compared to mono BF and PVA fibers. Conversely, a significant decrease in K_{IC}^{C} (by about 55% and 49%) was observed compared to mono BF and PVA fibers. This suggests that BF and PVA fibers enhance the bonding of PPS fibers within the concrete matrix, resulting in improved energy absorption, crack bridging capacity, and overall fracture behaviour.

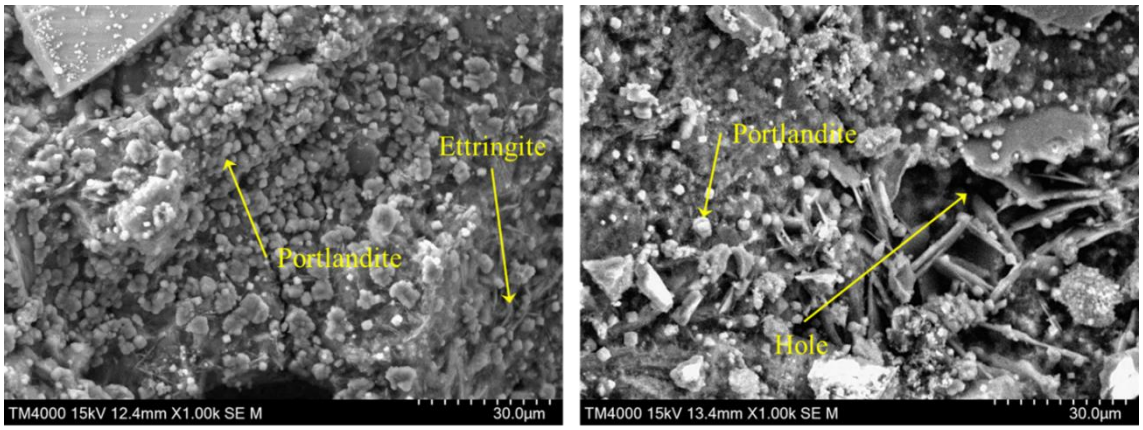


Figure 4-11 The microstructure of plain concrete mixtures (FWNS and SWSS) using SEM images.

Macro/micro-fiber hybridization significantly increased K_{IC}^{ini} compared to mono-fiber. PPL or TPPL combined with BF or PVA fibers showed the most pronounced effect. For example, 0.66PPL/0.33PVA hybridization increased K_{IC}^{ini} by 25% and 32% over mono-PVA and PPL, respectively. Similarly, 0.33PPL/0.66BF increased K_{IC}^{ini} by 27% and 28% over mono-BF and PPL, respectively. The results showed that 0.33PVA was more effective in the PPL fiber-containing hybrid system, while 0.66BF proved more effective

in the combined PPL/BF system. Notably, both micro-fiber type and dosage significantly influenced the initial crack strength. The difference in effectiveness between PVA and BF in SWSS is attributed to their bonding behaviour. PVA fibers exhibited strong chemical bonding (Vafaei *et al.* 2021a; Mashayekhi *et al.* 2024a), enhancing the adhesion of PPL fibers by reinforcing the surrounding matrix. Consequently, a lower dosage (0.33%) of PVA fibers is sufficient to improve PPL fiber bonding and achieve superior fracture toughness compared to a higher PVA dosage in the hybrid system. Conversely, previous research suggested that BF corrosion in SWSSC can compromise its bridging capability (Wang, Qingxuan *et al.* 2021; Li, Meng *et al.* 2022; Mashayekhi *et al.* 2024a). This necessitates a higher BF content for effective PPL fiber bonding and positive synergy within the hybrid system. Considering the results of K_{IC}^{un}, it was found that macro-fiber type significantly impacted K_{IC}^{un}. A 0.33TPPL/0.66BF configuration yielded 9% and 4% greater K_{IC}^{un} compared to mono-fiber and TPPL configurations, respectively. The improved performance may be attributed to a superior distribution of TPPL fibers, enhancing their bond strength with the concrete matrix, particularly when combined with PVA or BF. The results of K_{IC}^{C} indicated that macro/micro-fiber hybridization significantly reduced K_{IC}^{C} compared to mono fibers. The positive synergy between micro and macro fibers enhanced crack resistance across a broad spectrum and improved energy absorption during crack propagation.

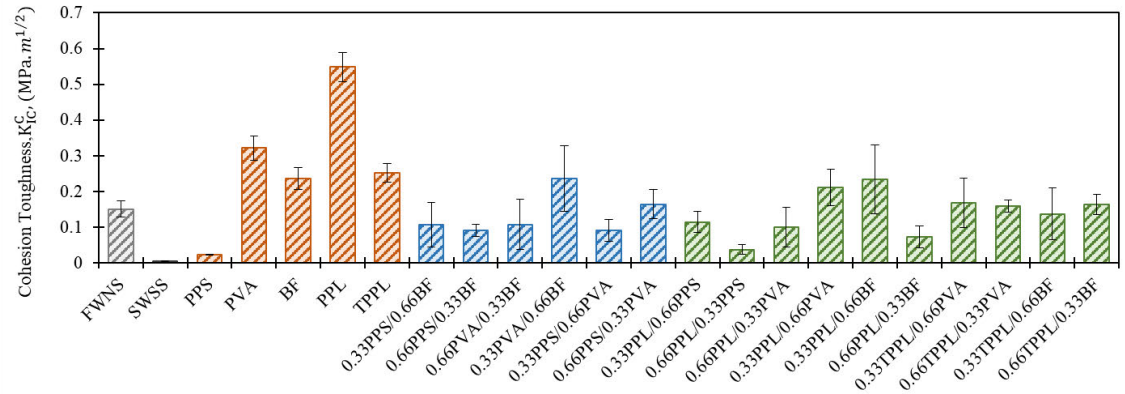


Figure 4-12 The cohesion toughness (K_{IC}^{C}) parameter based on DKFM method.

FWNS concrete exhibited a 12.6-fold increase in fracture process zone length (Δa_C) compared to SWSSC. This suggests a more brittle behaviour and lower damage tolerance for SWSSC. Materials with shorter Δa_C lack the capacity to absorb stress in the surrounding crack zone, potentially leading to rapid crack growth and brittle failure. This

may be attributed to the denser microstructure of SWSSC (Mashayekhi *et al.* 2024a), which enhances crack initiation resistance but accelerates subsequent propagation. Mono-fiber addition significantly enhanced Δa_C compared to plain SWSSC. PVA, BF, PPL, and TPPL fibers were particularly effective, increasing Δa_C by 30, 19, 39, and 21 times, respectively. This suggests fibers improved the fracture toughness of SWSSC, transitioning its behaviour from brittle to ductile, leading to enhanced damage tolerance and plastic deformation, due to fiber bridging, as corroborated by prior research (Çelik *et al.* 2020b; Zhang *et al.* 2020; Vafaei *et al.* 2022a; Zhang, Peng *et al.* 2022). Fiber hybridization further increased Δa_C for PPS fibers, addressing their inherent weakness in bonding with the concrete matrix.

4.3.4 Analysis of fracture behaviour

To investigate the fracture behaviour of plain concrete and fiber-reinforced SWSSC mixes, load-CMOD curves for previously identified promising mixes are analysed and presented in **Figure 4-13**. These mixes were selected based on prior fracture analysis results. To further visualize the fracture behaviour, schematic failure mode is illustrated in **Figure 4-14**. For improved clarity, the fracture behaviour in **Figure 4-13** is categorized into six stages, which are comprehensively discussed in the following section.

- O-A: Linear-elastic phase
- A-B: Crack initiation stage and Crack propagation stage
- B: Peak load stage
- B-C: Post-peak stage
- C-D: Continuation of the post-peak stage
- D-E: Concrete failure stage

Between points O and A (60-80% ultimate strength), plain and FR-SWSSC demonstrated linear-elastic behaviour with minimal cracks. While both exhibited this behaviour, the underlying mechanisms differed. The slope for plain SWSSC reflected its slightly higher elastic modulus than normal concrete by about 8% due to sea-sand (Mashayekhi *et al.* 2024a). Conversely, FR-SWSSC exhibited a load-CMOD slope dependent on fiber characteristics (type, volume fraction, aspect ratio, distribution, and hybridization).

Though fibers potentially increased tensile strength in both plain and FR-SWSSC, they primarily influenced crack behaviour in FR-SWSSC by delaying initiation and reducing initial width. During this initial stage, no fibers were activated, and overall behaviour (except stiffness) remained similar.

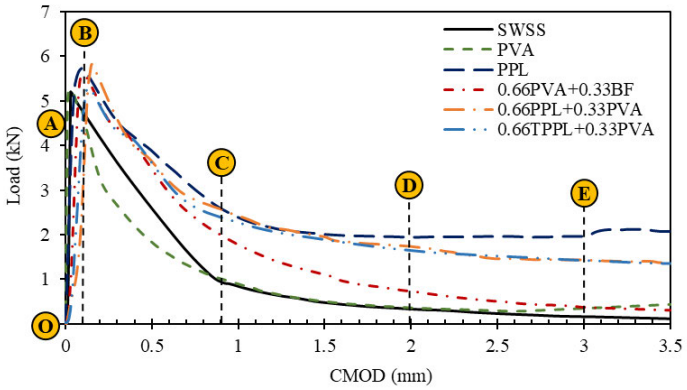


Figure 4-13 Load-CMOD curves for various SWSSC mixes.

The concrete specimens exhibited a transition from the linear elastic to crack initiation and propagation stages (A-B). Both SWSS and FR-SWSSC displayed non-linear behaviour with increasing crack width (CMOD). SWSSC deviated from linearity during crack initiation due to its lower tensile strength, resulting in rapid crack growth during propagation as the material could not sustain the load. The load-CMOD curve of FR-SWSSC exhibited a deviation from linearity during crack initiation. This behaviour can be attributed to the influence of fiber type, volume fraction, aspect ratio, distribution, and hybridization. These fibers bridged crack tips, delaying initiation, and resulting in a slight load increase and reduced initial crack width. Fibers inhibited crack growth during propagation, significantly reducing crack width and increasing peak load. PVA fibers exhibited stronger bonding with concrete matrix, while PPL fibers, with their superior length, enhanced bridging, and fracture energy. Notably, all hybrid mixtures displayed a higher ultimate load compared to those containing only PVA fibers. Additionally, replacing 33% of PVA with BF fibers significantly improved fracture behaviour during this stage. This improvement could stem from the positive synergy of PVA/BF hybridization, where BF enhanced the bonding strength of PVA fibers by reinforcing the surrounding concrete matrix, thereby facilitating greater contribution from the PVA fibers. This complementary mechanism can be observed in **Figure 4-14** through SEM imaging.

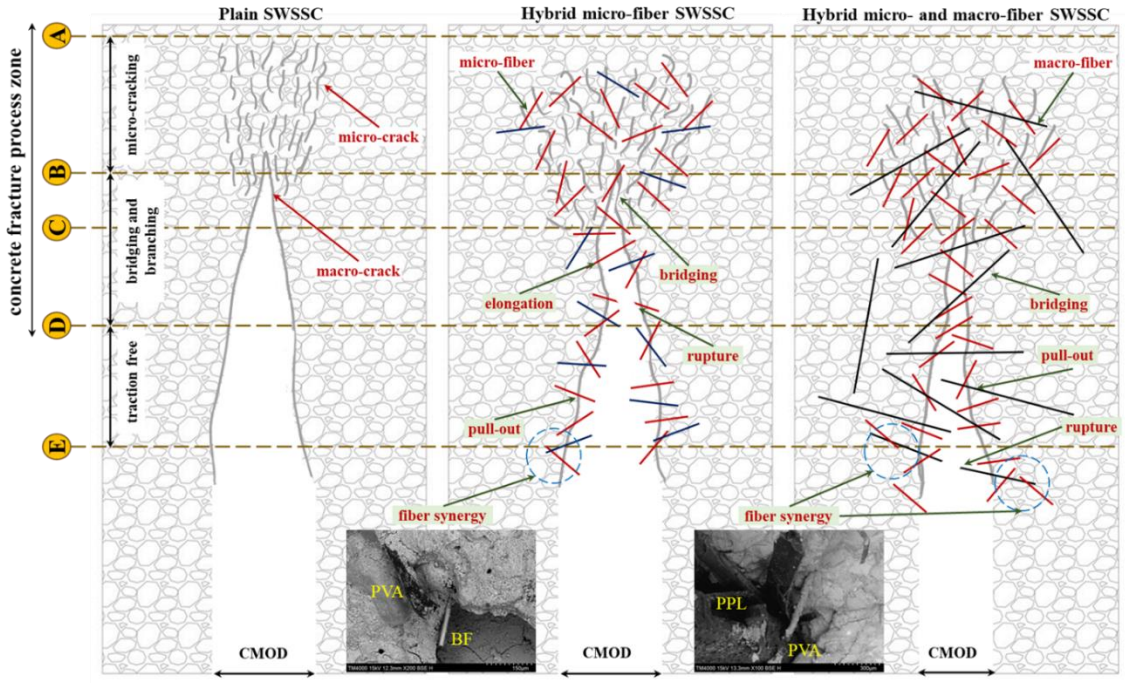


Figure 4-14 Schematic of the crack development process in hybrid FR-SWSSC.

Following the peak load stage, concrete specimens transitioned to the post-peak stage (B-C), marked by a sudden localization and propagation of a macrocrack through the beam, leading to a significant loss in flexural strength. Plain SWSSC displayed a post-peak decrease in load capacity and load-CMOD curve, driven by its low tensile strength. Aggregate bridging acted as the main toughening mechanism. With diminishing load resistance, the crack width continued to increase. The post-peak stage in FR-SWSSC also exhibited a decrease in load capacity, although the rate of decrease was influenced by fiber type. Fibers enhanced the tensile strength of SWSSC, leading to a higher residual strength at Point C and a reduced rate of crack width increase compared to plain concrete. Fiber hybridization significantly improved load-bearing capacity compared to mono PVA fibers. Notably, the 0.66PVA/0.33BF combination enhanced both bonding strength and the bridging effect within the hybrid system, leading to a higher load capacity. Similarly, a 0.33PVA content in hybrids with 0.66PPL or 0.66TPPL improved the bonding of macro-fibers (PPL and TPPL), consequently resulting in a significantly enhanced bridging effect. The strong chemical bonding strength of PVA fibers significantly reinforced the surrounding concrete of macro-fibers (**Figure 4-14**). Furthermore, the higher mechanical bonding strength of PPL fibers compared to TPPL fibers, attributed to their rough surface, resulted in a better synergistic effect with PVA fibers, enhancing the

ultimate capacity relative to TPPL/PVA hybridization. Moreover, the residual strength of Point C highlighted the crucial role of macro-fibers in maintaining post-peak load.

Specimens with macro-fibers exhibited a slower load-CMOD reduction and reached stability during transition from point C to D. This extended softening, attributed to crack-bridging and branching, contrasted with the failure-prone behaviour of plain SWSSC due to its loosely connected aggregates, leading to rupture or pull-out of fibers. Conversely, the 0.66 PVA/0.33BF mix, displayed rapid crack widening and reduced load capacity, attributed to lacking elongation-providing fibers like PPL or TPPL. However, its higher capacity compared to plain SWSSC can be explained by a strong bond between PVA, BF, and the concrete matrix. At large CMOD values during this phase, macro-fibers exhibited a more pronounced influence on crack propagation arrest and stabilization due to their greater length. However, their synergistic interaction with microfibers, particularly PVA and basalt BF, yielded superior performance compared to micro-fibers alone. The incorporation of mono micro-fibers proved inadequate in sustaining crack growth at large CMOD values, owing to their limited length and tensile strength.

During the failure stage (D to E and after), SWSSC and FR-SWSSC exhibited distinct failure mechanisms under load. SWSSC experienced a sudden, brittle failure with complete load-bearing capacity loss and minimal energy dissipation. The failure mode was typically tensile, with concrete fracturing along cracks. On the other hand, FR-SWSSC failure can be impacted by fiber properties, potentially experiencing delays due to increased energy absorption within the fibers. These fibers also altered the failure mode from brittle to ductile, allowing concrete deformation before catastrophic failure. Among the fiber types, macro-fibers offered consistent load-bearing capacity, while single PPL fibers exhibited enhanced energy absorption and a slight improvement in load-bearing. The PVA/BF hybrid, however, reached its minimum load capacity due to short length and inability to bridge macrocracks. These findings highlight the crucial role of macro-fibers in enhancing the ductility of FR-SWSSC.

4.3.5 Post-crack performance evaluation using guidelines

The post-crack behaviour of FR-SWSSC was investigated in this study to elucidate its residual strength and brittleness, providing more insights to informing the design and evaluation of FR-SWSSC structures. Established methods outlined in the Fib Model Code (Code 2010), European standard EN 14651 (Institution 2008), and RILEM TC 162-TDF

(TC162-TDF 2003) are employed. The study focused on determining residual strength corresponding to specific CMOD of 0.5, 1.5, 2.5, and 3.5 mm, following the Fib Model Code [69] (**Figure 4-15**). Residual strength was evaluated using f_{R1} and f_{R3} for both serviceability (SLS) and ultimate (ULS) limit states. Moreover, the f_{R3}/f_{R1} ratio assessed material brittleness. The potential for FR-SWSSC to partially replace ULS reinforcement if it meets $f_{R1}/f_L > 0.4$ and $f_{R3}/f_{R1} > 0.5$ (Di Prisco *et al.* 2009; Code 2010). f_L, defined by RILEM TC 162-TDF (TC162-TDF 2003) and EN 14651 (CEN 2005) (Institution 2008), is the peak load within 0-0.05 mm of CMOD. The flexural strengths were calculated using:

$$f_r = \frac{3}{2}\frac{F \times S}{b \times h_{sp}^2} \tag{4-12}$$

where F represents load values from tests, b is the specimen width (100 mm), and h_{sp} is the distance from notch tip to the top of the cross-section (70 mm).

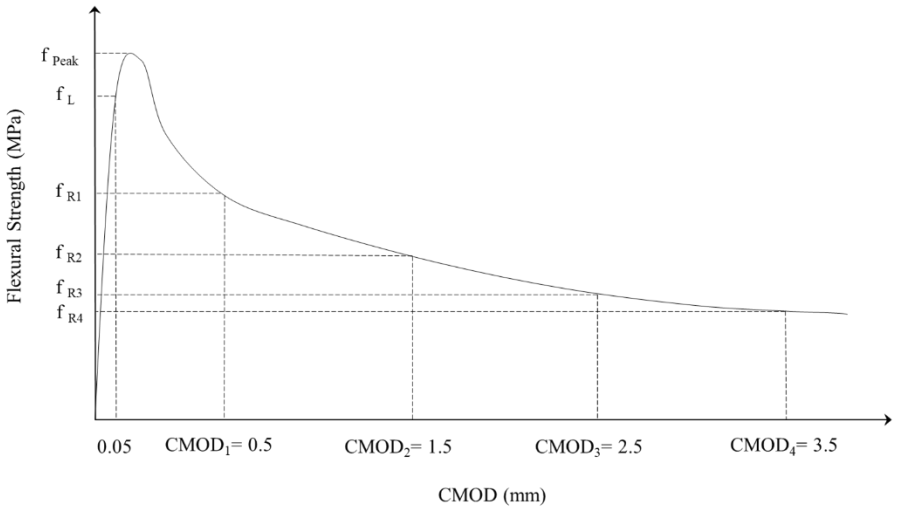


Figure 4-15 Flexural behaviour of FRC: Nominal stress vs. CMOD.

Figure 4-16 presents the flexural strength of all investigated mixtures. FWNS and SWSS measured 4.94 MPa and 4.79 MPa, respectively. Mono fiber addition to SWSS minimally affected peak strength, except for PPL fibers, which increased it by 10%. Micro-fiber hybridization with 0.66PPS/0.33PVA achieved the highest strength (5.74 MPa), exceeding mono PPS and PVA by 26% and 22%, respectively. This was likely due to the superior chemical bonding of PVA fibers, enhancing the bonding strength of PPS fibers

within the concrete matrix. Incorporation of hybrid micro- and macro-fibers including 0.66PPL/0.33PVA, 0.33PPL/0.66BF, and 0.33TPPL/0.66BF, significantly enhanced SWSS flexural strength by about 8%, 14%, and 8%, respectively, compared to plain SWSS. These mixtures also exhibited greater strength than mono PVA and BF.

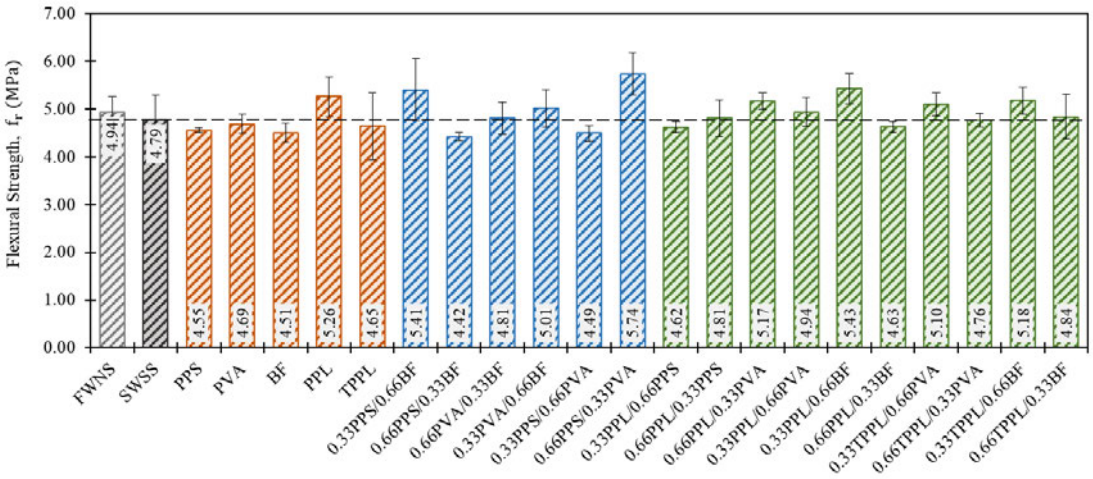


Figure 4-16 The peak flexural strength of FR-SWSSC.

Figure 4-17 shows the residual strength ratios (f_{R3}/f_{R1} and f_{R1}/f_L), with f_{R3}/f_{R1} indicating material brittleness. Mono PPL and TPPL fibers increased f_{R3}/f_{R1} by 317% and 278%, respectively, compared to plain SWSSC, resulting in significantly more ductile behaviour. Among the micro-fibers, only PVA resulted in a 45% higher f_{R3}/f_{R1} ratio compared to the control (SWSS). PPS and BF, conversely, exhibited a decrease in f_{R3}/f_{R1} and a shift towards brittle behaviour. Micro-fiber hybridization of BF with either PPS or PVA fibers significantly enhanced f_{R3}/f_{R1} and promoted ductile behaviour. Micro- and macro-fiber hybridization significantly enhanced ductility compared to mono micro-fibers, as evidenced by the increased f_{R3}/f_{R1} ratio. Hybrids 0.66PPL/0.33PVA and 0.66PPL/0.33BF increased f_{R3}/f_{R1} by 114% and 466% over PVA and BF, respectively. Notably, 0.66TPPL/0.33BF achieved the most significant improvement, surpassing both mono TPPL and BF by 24% and 679%, respectively. This is attributed to enhanced bonding of TPPL fibers due to partial replacement with BF, leading to improved reinforcement of the TPPL surrounding concrete.

Micro-fiber hybridization significantly enhanced the f_{R1}/f_L ratio compared to mono fibers in all hybrid mixtures. Among these, the 0.66PPS/0.33PVA hybrid achieved the most pronounced improvement by about 244% and 80% over mono-PPS and -PVA,

respectively. Micro/macro fiber hybridization significantly improved f_{R1}/f_L compared to micro-fibers alone, but negatively impacted compared to mono macro-fibers. Notably, only the PPL fiber achieved f_{R1}/f_L > 0.4 and f_{R3}/f_{R1} > 0.5, demonstrating adequate reinforcement in SWSSC. While hybridization offers potential, a higher total dosage is needed to meet reinforcement substitution requirements.

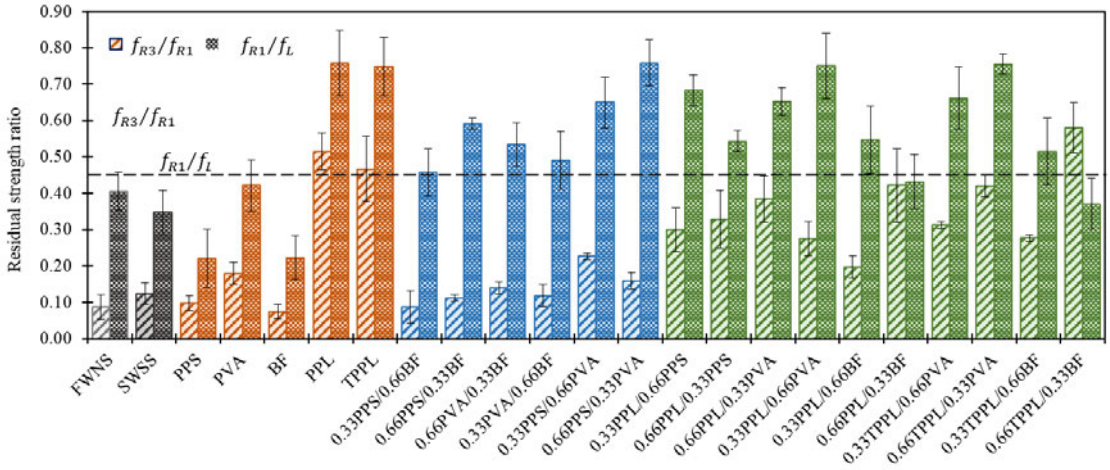


Figure 4-17 The post-peak residual flexural strength of FR-SWSSC.

4.4 Synergistic effects of fiber hybridization

Synergistic effects of various fibers in hybrid system determine hybridization success. This study employed the synergistic coefficient (SC) to evaluate the fracture performance of these combinations relative to single fibers. The *SC* was calculated using Eq. (4-13) (Hoan *et al.* 2019; Nguyen *et al.* 2022) at a constant fiber volume fraction (V_f) of 0.25%. A positive value indicates improved performance relative to the individual fibers.

$$SC = \frac{R_{hybrid,a+b}^{(V_f)} - \max\left(R_{mono,a}^{(V_f)}, R_{mono,b}^{(V_f)}\right)}{\max\left(R_{mono,a}^{(V_f)}, R_{mono,b}^{(V_f)}\right)} \quad (4\text{-}13)$$

where $R_{hybrid,a+b}$ is the fracture toughness properties—flexural strength, fracture energy and two fracture parameters (K_{IC}^{ini}, and K_{IC}^{un})— of hybrid FR-SWSSC, $R_{mono,a}$ and $R_{mono,b}$ are the fracture properties of mono-fibers, respectively.

The synergistic coefficients in **Figure 4-18** indicate that the incorporation of fibers in all hybrid systems resulted in a significant increase in the K_{IC}^{ini} and showed positive synergy.

However, the specific fiber type and dosage are critical factors influencing the positive synergy observed for ultimate fracture toughness (K_{IC}^{un}). Hybridizing 0.33PPS/0.66BF and 0.66PPS/0.33BF fibers exhibited positive synergy in all fracture toughness parameters compared to mono-fibers. PPS/BF and PPS/PVA hybrids exhibited enhanced G_F and positive synergy, likely due to PVA and BF improving bonding strength and PPS fibers enhancing elongation, ultimately leading to increased fracture energy. Incorporation of PPL fibers with BF, PPS, and PVA generally resulted in decreased G_F and flexural strength. However, the 0.33PPL/0.66BF combination exhibited a synergistic enhancement in flexural strength. This positive synergy was attributed to the ability of BF to improve the bonding strength of PPL fibers with concrete matrix. Conversely, increasing BF content within the hybrid system led to heightened brittleness due to BF corrosion in SWSSC, resulting in a negative synergistic effect on energy dissipation. Furthermore, the influence of PPL fiber content on the energy dissipation mechanisms within the PPL/micro-fiber hybrid system was pronounced. TPPL hybridization with PVA or BF resulted in positive synergy for flexural strength, likely due to the superior flexibility and distribution of TPPL fibers compared to PPL, leading to improved synergy within the hybrid system. Notably, only the 0.66TPPL/0.33PVA combination displayed positive synergy for G_F, possibly due to the superior bonding strength of PVA fibers compared to BF. This stronger bonding reinforced the surrounding concrete matrix of TPPL, promoting fiber rupture and enhancing energy dissipation. Additionally, TPPL/BF hybridization exhibited positive synergy for K_{IC}^{un}, whereas TPPL/PVA displayed a negative effect.

Synergistic coefficient analysis revealed that fiber addition differentially impacted properties. Selecting the optimal fiber type or mix based on maximized overall fracture performance was therefore critical. To achieve this, the combined mechanical performance (CMP) of all mixes, calculated using Eq. (4-14) [68], was compared to plain SWSSC. A CMP exceeding 1.0 indicated superior overall fracture behaviour. This study assigned equal weight to all fracture parameters, neglecting their individual significance.

$$CMP = \frac{1}{4} \times \left(\frac{f_{r,fiber}}{f_{r,SWSS}} + \frac{G_{F,fiber}}{G_{F,SWSS}} + \frac{K_{IC,fiber}^{ini}}{K_{IC,SWSS}^{ini}} + \frac{K_{IC,fiber}^{un}}{K_{IC,SWSS}^{un}} \right) \quad (4\text{-}14)$$

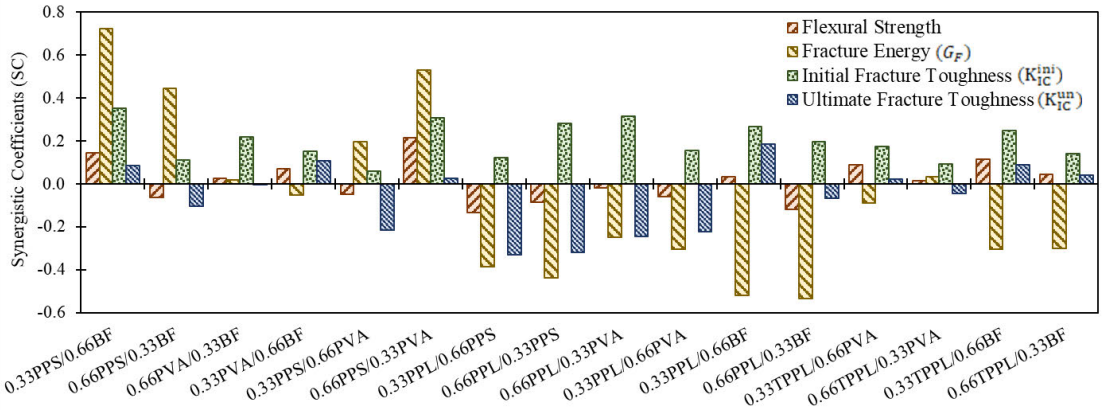


Figure 4-18 Synergistic coefficients derived from fracture parameters of hybrid FR-SWSSC.

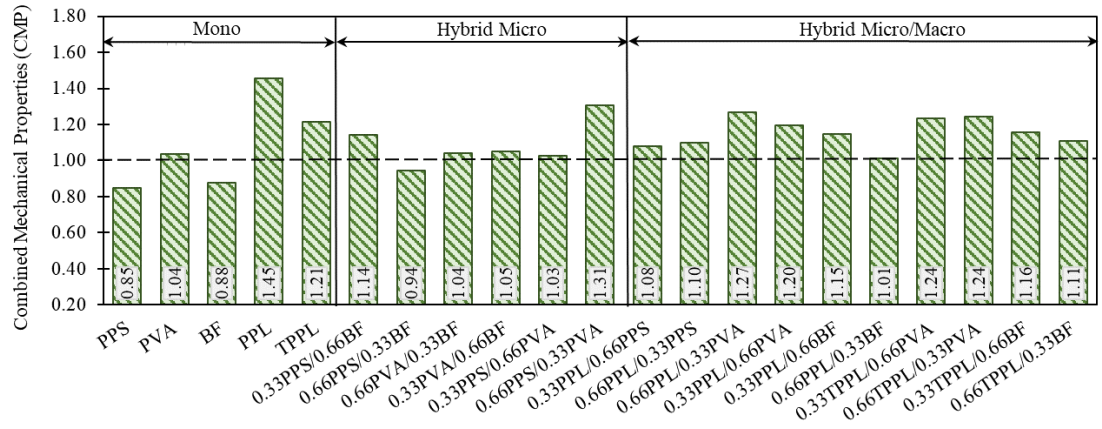


Figure 4-19 The combined mechanical performance (CMP) of FR-SWSSC.

The results of the CMP study for FR-SWSSC mixes were compared with those of plain SWSSC and are illustrated in **Figure 4-19**. The results showed that PPS and BF fibers had the lowest CMP value, while mono PPL and TPPL mixtures had the highest. It was found that hybrid micro-fiber mixes had a CMP value greater than 1.0, except for 0.66PPS/0.33BF mixture. 0.66PPS/0.33PVA exhibited the greatest CMP value among micro-fiber hybrids. Among all micro and macro fiber hybridizations, hybrid PPL/PVA and TPPL/PVA resulted in the highest CMP value.

4.5 Conclusion

This study investigated the influence of hybrid fibers on fracture properties of fiber-reinforced seawater sea-sand concrete. Five fiber types were incorporated: micro-polypropylene (PPS), polyvinyl alcohol (PVA), and basalt (BF) alongside macro-

polypropylene (PPL) and twisted polypropylene (TPPL), all at 0.25% volume fraction. These were added to plain SWSSC in mono, hybrid micro, and hybrid micro-macro combinations to assess the hybridization effect. The findings offer valuable insights into how hybrid fibers can improve the fracture resistance of FR-SWSSC. Key results are presented below:

- Macro-fiber incorporation (PPL and TPPL) significantly improved the post-peak behaviour of SWSSC. PPL and TPPL fibers increased fracture energy by 144% and 93%, respectively compared to the plain SWSSC at CMOD 3.5 mm. The enhanced performance was attributed to the length of macro-fibers, which effectively bridged macro-cracks at post-peak stages due to superior mechanical bonding strength.

- Micro-fiber inclusion in SWSSC marginally affected post-crack behaviour, but hybridization significantly enhanced fracture performance. Hybridizing PPS with BF or PVA increased fracture energy at CMOD 3.5 mm by 176% and 290%, respectively, compared to mono PPS. This improvement likely stemmed from the weak bonding strength of PPS fibers, which PVA and BF effectively addressed, and their synergistic action in mitigating micro-cracks.

- Hybridizing PPL fibers with PPS, PVA, or BF significantly increased fracture energy at a CMOD of 3.5 mm compared to mono micro-fibers by 244%, 66%, and 68%, respectively. Similarly, TPPL hybridization with PVA or BF enhanced fracture energy by 80% and 93%, respectively. The ability of PPL and TPPL fibers to bridge macro-cracks activated micro-fibers for synergistic behaviour. Additionally, the strong chemical bonding of PVA and BF effectively reinforced the surrounding concrete matrix and improved macro-fiber bonding.

- The fracture process zone length (Δa_C) of SWSSC significantly increased with PVA, BF, PPL, and TPPL fibers, enhancing it by about 30, 19, 39, and 21 times, respectively. Fiber inclusion significantly enhanced cohesion toughness (K_{IC}^{C}), with PVA and PPL fibers yielding the most improvements, by about 54 and 93 times, respectively. This can be attributed to fiber bridging of micro-cracks, distributing tensile stress, and engaging a larger section compared to plain SWSSC, resulting in higher Δa_C and K_{IC}^{C}.

- Fiber hybridization significantly improved initial fracture toughness (K_{IC}^{ini}). The 0.66PVA/0.33BF combination exhibited the greatest enhancement in micro-fiber hybrids, surpassing both BF and PVA by 22% and 17%, respectively. This was attributed to the synergy of PVA/BF in SWSSC, enhancing matrix bonding and promoting reinforcement efficiency. 0.66PPL/0.33PVA hybridization increased K_{IC}^{ini} by 25% and 32% relative to mono PVA and PPL, respectively. This synergy between the fibers resulted in enhanced bonding strength and concrete reinforcement, allowing PPL fibers to better resist crack initiation.

The study revealed that fiber hybridization in SWSSC showed promise for enhancing its fracture properties. Synergistic effects enhanced fracture performance compared to mono-fiber configurations, making it a promising material for coastal and offshore structures. Further research is needed to understand the behaviour and optimize fiber content of hybrid FR-SWSSC under varying conditions. Additionally, long-term performance and durability in marine environments require evaluation. Overall, hybrid fibers offer significant potential for more resilient SWSSC structures.

Acknowledgements

The authors gratefully acknowledge the financial and laboratory support provided by the University of South Australia. We thank the technicians of the university's concrete laboratory for their assistance. We extend our appreciation to Adelaide Brighton Cement Ltd and Independent Cement and Lime Pty Ltd for donating OPC and GGBS, respectively, and to TEXO company for donating PPS and TPPL fibers. We are also grateful to Mr. Adam Bromley for his support. Additionally, we acknowledge the instruments and expertise of Microscopy Australia at the Future Industries Institute (FII), University of South Australia.

Chapter 4 References

Abbas, YM, Hussain, LA & Khan, MI 2022, 'Constitutive compressive stress–strain behavior of hybrid steel-PVA high-performance fiber-reinforced concrete', Journal of Materials in Civil Engineering, vol. 34, no. 1, p. 04021401.

Abdel-Karim, AH, Khalil, GI, Ewis, AE & Makhlouf, MH 2023, 'Impact of developed hybrid polypropylene fiber inclusion on the flexural performance of concrete beams reinforced with innovative hybrid bars', Construction and Building Materials, vol. 409, p. 134113.

Ahmad, J, González-Lezcano, RA, Majdi, A, Ben Kahla, N, Deifalla, AF & El-Shorbagy, MA 2022, 'Glass fibers reinforced concrete: Overview on mechanical, durability and microstructure analysis', Materials, vol. 15, no. 15, p. 5111.

Ahmed, SFU & Mihashi, H 2011, 'Strain hardening behavior of lightweight hybrid polyvinyl alcohol (PVA) fiber reinforced cement composites', Materials and structures, vol. 44, no. 6, pp. 1179-91.

Ameri, F, de Brito, J, Madhkhan, M & Taheri, RA 2020, 'Steel fibre-reinforced high-strength concrete incorporating copper slag: Mechanical, gamma-ray shielding, impact resistance, and microstructural characteristics', Journal of Building Engineering, vol. 29, p. 101118.

Amin, N, Bijan, S & Kirk, V 2013, 'Effect of polyvinyl alcohol (PVA) fibre on dynamic and material properties of fibre reinforced concrete', Construction and Building Materials, vol. 49, pp. 374-83.

Australia, S 1994, Methods of testing concrete-Preparation of concrete mixes in the laboratory, AS.

Çelik, Z & Bingöl, AF 2020a, 'Fracture properties and impact resistance of self-compacting fiber reinforced concrete (SCFRC)', Materials and structures, vol. 53, pp. 1-16.

Çelik, Z & Bingöl, AF 2020b, 'Fracture properties and impact resistance of self-compacting fiber reinforced concrete (SCFRC)', Materials and structures, vol. 53, no. 3, pp. 1-16.

Chenggong, Z, Zhiyuan, W, Zhenyu, Z, Qiuyu, G, Xinrui, W & Renda, Z 2023, 'Research on different types of fiber reinforced concrete in recent years: An overview', Construction and Building Materials, vol. 365, p. 130075.

Code, M 2010, 'fib model Code for concrete structures', Structural Concrete, vol. 14.

Dhondy, T, Remennikov, A & Shiekh, MN 2019, 'Benefits of using sea sand and seawater in concrete: a comprehensive review', Australian Journal of Structural Engineering, vol. 20, no. 4, pp. 280-89.

Di Prisco, M, Plizzari, G & Vandewalle, L 2009, 'Fibre reinforced concrete: new design perspectives', Materials and structures, vol. 42, pp. 1261-81.

Dou, H, Bai, J, Lu, H, Zhang, T, Kong, L, Bai, Z & Li, W 2023, 'Effect of TiO2 on preparation condition, mechanical properties and alkali resistance of continuous basalt fibers', Cement and Concrete Composites, vol. 136, p. 104861.

Etxeberria, M, Fernandez, JM & Limeira, J 2016a, 'Secondary aggregates and seawater employment for sustainable concrete dyke blocks production: Case study', Construction and Building Materials, vol. 113, pp. 586-95.

Etxeberria, M, Gonzalez-Corominas, A & Pardo, P 2016b, 'Influence of seawater and blast furnace cement employment on recycled aggregate concretes' properties', Construction and Building Materials, vol. 115, pp. 496-505.

Faraj, RH, Sherwani, AFH & Daraei, A 2019, 'Mechanical, fracture and durability properties of self-compacting high strength concrete containing recycled polypropylene plastic particles', Journal of Building Engineering, vol. 25, p. 100808.

Fattah, KP, Al-Tamimi, AK, Hamweyah, W & Iqbal, F 2017, 'Evaluation of sustainable concrete produced with desalinated reject brine', International Journal of Sustainable Built Environment, vol. 6, no. 1, pp. 183-90.

Feng, J, Su, Y & Qian, C 2019, 'Coupled effect of PP fiber, PVA fiber and bacteria on self-healing efficiency of early-age cracks in concrete', Construction and Building Materials, vol. 228, p. 116810.

Gholampour, A, Hassanli, R, Mills, JE, Vincent, T & Kunieda, M 2019, 'Experimental investigation of the performance of concrete columns strengthened with fiber reinforced concrete jacket', Construction and Building Materials, vol. 194, pp. 51-61.

Gholampour, A, Ozbakkaloglu, T & Ngo, TD 2021, 'Development of a waste-based eco-friendly structural mortar without Portland cement and natural sand', Structural Concrete, vol. 22, pp. E488-E500.

Gupta, N, Siddique, R & Belarbi, R 2021, 'Sustainable and greener self-compacting concrete incorporating industrial by-products: A review', Journal of Cleaner Production, vol. 284, p. 124803.

Hiroshi, T, Paris, P & Irwin, G 2000, 'The stress analysis of cracks handbook', ASME, New York.

Hoan, PT & Thuong, NT 2019, 'Shear resistance of ultra-high-performance concrete reinforced with hybrid steel fiber subjected to impact loading', Journal of Science and Technology in Civil Engineering (STCE)-HUCE, vol. 13, no. 1, pp. 12-20.

Institution, BS 2008, Test Method for Metallic Fibre Concrete: Measuring the Flexural Tensile Strength (limit of Proportionality (LOP), Residual), BSI,

Interior, USGSDd 2020, 'Mineral commodity summaries 2020', 06.02. 2020, Reston, VA; https://pubs. er. usgs. gov/publication/mcs2020.

Kai, C, Lihua, X, Tao, T, Le, H, Jian, L, Jian, H, Huan, L & Yin, C 2023, 'Mechanical behavior of multiscale hybrid fiber reinforced recycled aggregate concrete subject to uniaxial compression', Journal of Building Engineering, vol. 71, p. 106504.

Kaidi, J, Xin, W, Lining, D, Zhiyuan, C, Huang, H, Xia, L, Jianxun, L & Zhishen, W 2023, 'Mechanical properties of multi-scale mono/hybrid non-metallic fiber-reinforced ultra-high performance seawater sea-sand concrete', Construction and Building Materials, vol. 401, p. 132922.

Kazemian, F, Rooholamini, H & Hassani, A 2019, 'Mechanical and fracture properties of concrete containing treated and untreated recycled concrete aggregates', Construction and Building Materials, vol. 209, pp. 690-700.

Li, M, Xing, D, Zheng, Q-B, Li, H, Hao, B & Ma, P-C 2022, 'Variation on the morphology and tensile strength of basalt fiber processed in alkali solutions', Construction and Building Materials, vol. 335, p. 127512.

Li, P, Li, W, Yu, T, Qu, F & Tam, VWY 2020, 'Investigation on early-age hydration, mechanical properties and microstructure of seawater sea sand cement mortar', Construction and Building Materials, vol. 249, 2020/07/20/, p. 118776.

Li, P, Li, W, Sun, Z, Shen, L & Sheng, D 2021, 'Development of sustainable concrete incorporating seawater: A critical review on cement hydration, microstructure and mechanical strength', Cement and Concrete Composites, vol. 121, p. 104100.

Li, Y, Qiao, C & Ni, W 2020, 'Green concrete with ground granulated blast-furnace slag activated by desulfurization gypsum and electric arc furnace reducing slag', Journal of Cleaner Production, vol. 269, p. 122212.

Li, Y, Zhang, J, He, Y, Huang, G, Li, J, Niu, Z & Gao, B 2022, 'A review on durability of basalt fiber reinforced concrete', Composites Science and Technology, vol. 225, p. 109519.

Li, Y, Liu, W, Mi, T, Ding, X, Tang, L & Xing, F 2024, 'Durability study of seawater and sea-sand concrete under the combined effects of carbonation and chloride redistribution', Journal of Building Engineering, p. 109294.

Lin, J-X, Song, Y, Xie, Z-H, Guo, Y-C, Yuan, B, Zeng, J-J & Wei, X 2020, 'Static and dynamic mechanical behavior of engineered cementitious composites with PP and PVA fibers', Journal of Building Engineering, vol. 29, p. 101097.

Ling, Y, Zhang, P, Wang, J & Chen, Y 2019, 'Effect of PVA fiber on mechanical properties of cementitious composite with and without nano-SiO2', Construction and Building Materials, vol. 229, p. 117068.

Liu, W, Li, Y, Tang, L & Xing, F 2021, 'Modelling analysis of chloride redistribution in sea-sand concrete exposed to atmospheric environment', Construction and Building Materials, vol. 274, p. 121962.

Lv, W, Sun, Z & Su, Z 2020, 'Study of seawater mixed one-part alkali activated GGBFS-fly ash', Cement and Concrete Composites, vol. 106, p. 103484.

Mashayekhi, A, Hassanli, R, Zhuge, Y, Ma, X & Chow, CW 2024, 'Synergistic effects of fiber hybridization on the mechanical performance of seawater sea-sand concrete', Construction and Building Materials, vol. 416, p. 135087.

Mehran, K, Mingli, C, Chaopeng, X & Majid, A 2022, 'Effectiveness of hybrid steel-basalt fiber reinforced concrete under compression', Case Studies in Construction Materials, vol. 16, p. e00941.

Miller, SA, Horvath, A & Monteiro, PJ 2018, 'Impacts of booming concrete production on water resources worldwide', Nature Sustainability, vol. 1, no. 1, pp. 69-76.

Mukhtar, F 2024, 'Simulation of fracture behavior in seawater and sea-sand mixed recycled coarse aggregate concrete under three-point bending', Theoretical and Applied Fracture Mechanics, vol. 131, p. 104413.

Nguyen, D-L, Thai, D-K & Lam, MN-T 2022, 'Synergy in Flexure of High-Performance Fiber-Reinforced Concrete with Hybrid Steel Fibers', Journal of Materials in Civil Engineering, vol. 34, no. 6, p. 04022090.

Pakravan, H, Jamshidi, M & Latifi, M 2018, 'The effect of hydrophilic (polyvinyl alcohol) fiber content on the flexural behavior of engineered cementitious composites (ECC)', The Journal of The Textile Institute, vol. 109, no. 1, pp. 79-84.

Pakravan, HR, Latifi, M & Jamshidi, M 2017, 'Hybrid short fiber reinforcement system in concrete: A review', Construction and Building Materials, vol. 142, 2017/07/01/, pp. 280-94.

Prasad, N & Murali, G 2021, 'Exploring the impact performance of functionally-graded preplaced aggregate concrete incorporating steel and polypropylene fibres', Journal of Building Engineering, vol. 35, p. 102077.

Rasheed, MA, Prakash, SS, Raju, G & Kawasaki, Y 2018, 'Fracture studies on synthetic fiber reinforced cellular concrete using acoustic emission technique', Construction and Building Materials, vol. 169, pp. 100-12.

Ríos, J, Cifuentes, H, Leiva, C, Ariza, M & Ortiz, M 2020, 'Effect of polypropylene fibers on the fracture behavior of heated ultra-high performance concrete', International Journal of Fracture, vol. 223, no. 1, pp. 173-87.

Shah, SP 1990, 'Size-effect method for determining fracture energy and process zone size of concrete', Materials and structures, vol. 23, pp. 461-65.

Shi, Z, Shui, Z, Li, Q & Geng, H 2015, 'Combined effect of metakaolin and sea water on performance and microstructures of concrete', Construction and Building Materials, vol. 74, pp. 57-64.

Sikora, P, Cendrowski, K, Abd Elrahman, M, Chung, S-Y, Mijowska, E & Stephan, D 2020, 'The effects of seawater on the hydration, microstructure and strength development of Portland cement pastes incorporating colloidal silica', Applied Nanoscience, vol. 10, no. 8, pp. 2627-38.

Slowey, K 2018, 'Report: Global construction waste will almost double by 2025', Construction Dive.

Standard, J 2003, 'Method of test for fracture energy of concrete by use of notched beam', JCI-S-001e2003, Japan Concrete Institute.

Şükrü, Ö & Ömer, Ç 2021, 'The hybrid effects of basalt and PVA fiber on properties of a cementitious composite: Physical properties and non-destructive tests', Construction and Building Materials, vol. 312, p. 125292.

TC162-TDF, R 2003, 'Test and design methods for steel fibre reinforced concrete', Materials and structures, vol. 36, pp. 560-67.

Ting, MZY, Wong, KS, Rahman, ME & Selowara Joo, M 2020, 'Mechanical and durability performance of marine sand and seawater concrete incorporating silicomanganese slag as coarse aggregate', Construction and Building Materials, vol. 254, 2020/09/10/, p. 119195.

Vafaei, D, Hassanli, R, Ma, X, Duan, J & Zhuge, Y 2021, 'Sorptivity and mechanical properties of fiber-reinforced concrete made with seawater and dredged sea-sand', Construction and Building Materials, vol. 270, p. 121436.

Vafaei, D, Hassanli, R, Ma, X, Duan, J & Zhuge, Y 2022a, 'Fracture Toughness and Impact Resistance of Fiber-Reinforced Seawater Sea-Sand Concrete', Journal of Materials in Civil Engineering, vol. 34, no. 5, p. 04022038.

Vafaei, D, Ma, X, Hassanli, R, Duan, J & Zhuge, Y 2022b, 'Microstructural behaviour and shrinkage properties of high-strength fiber-reinforced seawater sea-sand concrete', Construction and Building Materials, vol. 320, p. 126222.

Wang, J, Liu, E & Li, L 2018, 'Multiscale investigations on hydration mechanisms in seawater OPC paste', Construction and Building Materials, vol. 191, pp. 891-903.

Wang, Q, Ding, Y & Randl, N 2021, 'Investigation on the alkali resistance of basalt fiber and its textile in different alkaline environments', Construction and Building Materials, vol. 272, p. 121670.

Xiao, J, Qiang, C, Nanni, A & Zhang, K 2017, 'Use of sea-sand and seawater in concrete construction: Current status and future opportunities', Construction and Building Materials, vol. 155, pp. 1101-11.

Xie, C, Cao, M, Khan, M, Yin, H & Guan, J 2021, 'Review on different testing methods and factors affecting fracture properties of fiber reinforced cementitious composites', Construction and Building Materials, vol. 273, p. 121766.

Xu, S & Reinhardt, HW 1999a, 'Determination of double-K criterion for crack propagation in quasi-brittle fracture, Part I: Experimental investigation of crack propagation', International Journal of Fracture, vol. 98, no. 2, pp. 111-49.

Xu, S & Reinhardt, HW 1999b, 'Determination of double-K criterion for crack propagation in quasi-brittle fracture, Part II: Analytical evaluating and practical measuring methods for three-point bending notched beams', International Journal of Fracture, vol. 98, pp. 151-77.

Xu, S & Reinhardt, HW 2000, 'A simplified method for determining double-K fracture parameters for three-point bending tests', International Journal of Fracture, vol. 104, pp. 181-209.

Yang, S, Zang, C, Xu, J & Fan, G 2020, 'Determination of Fracture Parameters of Seawater Sea Sand Concrete Based on Maximum Fracture Load', Journal of Materials in Civil Engineering, vol. 32, no. 1, p. 04019315.

Yang, Z, Lu, F, Zhan, X, Zhu, H, Zhang, B, Chen, Z & Zhang, H 2024a, 'Mechanical properties and mesoscopic damage characteristics of basalt fibre-reinforced seawater sea-sand slag-based geopolymer concrete', Journal of Building Engineering, vol. 84, p. 108688.

Yang, Z, Zhan, X, Zhu, H, Zhang, B, Li, R, Dong, Z & Kua, HW 2024b, 'Eco-sustainable design of seawater sea-sand slag-based geopolymer mortars incorporating ternary solid waste', Construction and Building Materials, vol. 431, p. 136512.

Younis, A, Ebead, U, Suraneni, P & Nanni, A 2018, 'Fresh and hardened properties of seawater-mixed concrete', Construction and Building Materials, vol. 190, pp. 276-86.

Zhang, J-c, Li, B-j, Chen, W-y & Guo, R-x 2024, 'Experimental investigations on tensile strength and fracture toughness of a polyoxymethylene fiber reinforced concrete', Theoretical and Applied Fracture Mechanics, vol. 130, p. 104250.

Zhang, P, Yang, Y, Wang, J, Jiao, M & Ling, Y 2020, 'Fracture models and effect of fibers on fracture properties of cementitious composites—A review', Materials, vol. 13, no. 23, p. 5495.

Zhang, P, Yuan, P, Guan, J & Guo, J 2022, 'Fracture behavior of multi-scale nano-SiO2 and polyvinyl alcohol fiber reinforced cementitious composites under the complex environments', Theoretical and Applied Fracture Mechanics, vol. 122, p. 103584.

Zhang, ZH, Sang, ZQ, Zhang, LY, Ma, ZX & Zhang, Y 2013, Experimental research on durability of concrete made by seawater and sea-sand, Advanced Materials Research.

Zheng, Y, Zhang, Y, Zhuo, J, Zhang, Y & Wan, C 2022, 'A review of the mechanical properties and durability of basalt fiber-reinforced concrete', Construction and Building Materials, vol. 359, p. 129360.

5 Cyclic flexural performance of seawater sea-sand concrete reinforced with hybrid fibers

Reprinted and reformatted (including changes to the referencing style) with permission from Elsevier Ltd (see Appendix B).

Mashayekhi, A, Hassanli, R, Zhuge, Y, Ma, X, Chow, CW, Bazli, M & Manalo, A 2024d, 'Cyclic flexural performance of seawater sea-sand concrete reinforced with hybrid fibers', Construction and Building Materials, vol. 449, p. 138480.

Abstract

Fiber-reinforced seawater sea-sand concrete (FR-SWSSC), a sustainable alternative to traditional concrete, requires evaluation of its flexural performance under cyclic loading, critical for coastal and marine structures experiencing repeated loads. This study investigated the effect of fiber hybridization and its potential synergistic effects on the cyclic flexural behaviour of FR-SWSSC. Incremental cyclic loading was employed for testing FR-SWSSC specimens in four-point cyclic bending. This investigation employed micro-fibers—polypropylene (PPS), polyvinyl alcohol (PVA), basalt (BF)—and macro-fibers—long polypropylene (PPL) and twisted polypropylene (TPPL)—to explore the synergistic influence of fiber size and type (synthetic and natural) on the cyclic flexural behaviour. Hybrid-fiber reinforcements were incorporated in two configurations: micro-fibers only and a combination of micro- and macro-fibers. This approach facilitated the evaluation of size-dependent synergy on cyclic flexural properties. According to the results, micro/macro-fiber hybridization significantly improved performance during large deflection cycles. Hybrid TPPL/PVA exhibited 105% and 664% greater energy dissipation compared to mono TPPL and PVA, respectively. Similarly, PPS/PVA hybrids displayed a 79% and 112% increase in hysteretic damping ratio, over mono PVA and PPS fibers, respectively and reduced damage index and improved strength degradation at large deflections compared to mono fibers. This improvement was attributed to enhanced bonding strength of TPPL or PPS by the strong chemical bonding strength of PVA fibers, which strengthened the surrounding concrete matrix and allowed for a greater contribution from the hybrid components. This study addresses a knowledge gap and paves the way for improved material development through the utilization of a potential sustainable alternative concrete.

Keywords

Cyclic loading; Seawater; Sea-sand; Hybrid fibers; Energy dissipation; PVA; Flexural strength; Fiber reinforced concrete.

5.1 Introduction

The reliance of construction industry on conventional concrete presents significant environmental challenges, including high freshwater (FW) consumption, disruption of river ecosystems due to sand extraction, and substantial CO_2 emissions from cement production (Miller *et al.* 2018; Li *et al.* 2024; Zeng *et al.* 2024). This is particularly problematic for the development of marine engineering projects, where traditional materials often lead to increased costs and longer construction times due to transportation needs (Xiao *et al.* 2017; Guo *et al.* 2020; Li *et al.* 2021; Li *et al.* 2024). Developing sustainable alternatives for concrete is critical considering a projected global water crisis (Slowey 2018). Previous studies have investigated the potential of using eco-friendly materials such as recycled aggregate and supplementary cementitious materials, including slag and fly ash, and their effectiveness in producing more sustainable concrete (Lothenbach *et al.* 2011; Yang *et al.* 2015; Yu *et al.* 2024a; Yu *et al.* 2024b). Seawater sea-sand concrete (SWSSC) emerges as a promising solution for sustainable construction in coastal regions, capitalizing on the readily available seawater (SW) and sea-sand (SS) resources (Cao *et al.* 2008; Tjaronge *et al.* 2015; Xiao *et al.* 2017; Dhondy *et al.* 2019; Li *et al.* 2021; Li *et al.* 2024). This innovative material offers a multifaceted approach by promoting freshwater conservation, protecting ecological environments, reducing transportation and material costs, as well as lowering carbon emissions in coastal areas, making it a local, cost-effective, and environmentally friendly solution (Xiong *et al.* 2021).

Concrete structures face substantial durability challenges in marine environments. In terms of durability, incorporating SW and SS into concrete significantly decreased water absorption, sorptivity, and porosity compared to traditional concrete (Etxeberria *et al.* 2016a; Etxeberria *et al.* 2016b; Ting *et al.* 2020b; Vafaei *et al.* 2021a). However, this inclusion also resulted in increased autogenous and drying shrinkage (Katano *et al.* 2013; Etxeberria *et al.* 2016b; Younis *et al.* 2018). Additionally, in the aggressive environment of SWSSC, due to the presence of various ions (Etxeberria *et al.* 2016a; Younis *et al.* 2018), including sodium (Na^+), potassium (K^+), chloride (Cl^-), sulphate (SO_4^{2-}),

calcium (Ca^{2+}), and magnesium (Mg^{2+}), crack control is paramount for the long-term performance and structural integrity of concrete structures (Vafaei *et al.* 2021a; Ahmad *et al.* 2022; Li, Yan *et al.* 2022; Vafaei *et al.* 2022b). While fiber-reinforced polymer (FRP) bars address steel corrosion concerns compared to traditional reinforced concrete (RC), crack mitigation remains crucial (Mashayekhi *et al.* 2024a). Cracks facilitate the ingress of aggressive agents like chlorides and sulfates, accelerating concrete degradation. Here, fiber reinforcement plays a vital role by minimizing crack initiation and propagation, thus enhancing the long-term durability of SWSSC structures. Previous research has demonstrated the effectiveness of both natural and synthetic fibers in improving crack resistance and long-term performance of SWSSC. The addition of polypropylene (PP) fiber to SWSSC reduced water absorption and sorptivity, enhancing its durability (Vafaei *et al.* 2021a). However, steel fibers commonly used in conventional concrete are not suitable for SWSSC due to corrosion susceptibility in the presence of high ion concentrations (Kaidi *et al.* 2023). Among synthetic fibers, polyvinyl alcohol (PVA) and PP fibers are popular choices due to their affordability, positive influence on concrete properties and environmental resilience (Feng *et al.* 2019; Ling *et al.* 2019; Vafaei *et al.* 2021a, 2022a; Vafaei *et al.* 2022b; Kaidi *et al.* 2023; Mashayekhi *et al.* 2024a). Moreover, the investigation into the durability of polymeric fibers revealed that Polyethylene Terephthalate (PET) fibers exhibit low stability in highly alkaline environments, leading to a rapid decline in fiber strength within concrete matrices (Zheng *et al.* 1995; Rostami *et al.* 2020). The degradation of PET fibers in such conditions significantly increases their instability when embedded in a Portland cement matrix (Won *et al.* 2010; Alani *et al.* 2013). The harsh environment of SWSSC, along with its high chemical reactivity, can potentially impact the performance of fibers and their influence on the long-term behaviour of SWSSC, which requires further investigation.

In addition to durability parameters, investigations into the effect of mono-fibers on the strength performance of SWSSC showed a positive impact. The inclusion of fibers, depending on their length, distribution, and bonding strength, can significantly improve the mechanical properties and fracture toughness of SWSSC (Vafaei *et al.* 2021a, 2022a; Mashayekhi *et al.* 2024a; Mashayekhi *et al.* 2024d). While mono-fibers offer benefits, hybrid fiber-reinforced concrete (HFRC) has the potential to overcome the limitations of mono-fibers-length, tensile strength, and bonding strength- by combining micro and macro fibers with specific properties. This can lead to enhanced overall mechanical

performance, ductility, toughness, and energy absorption of concrete (Ahmed *et al.* 2011; Pakravan *et al.* 2018; Ling *et al.* 2019; Çelik *et al.* 2020a; Ríos *et al.* 2020; Şükrü *et al.* 2021; Abbas *et al.* 2022; Mehran *et al.* 2022; Nguyen *et al.* 2022; Abdel-Karim *et al.* 2023; Chenggong *et al.* 2023; Kai *et al.* 2023; Kaidi *et al.* 2023; Mashayekhi *et al.* 2024a). The influence of fiber geometry, specifically shape and dimension, on the mechanical properties of HFRC is well documented (Gu *et al.* 2024; Ma *et al.* 2024). Research suggests that the macroscopic improvement in the mechanical properties of concrete, due to fiber reinforcement stems from the fiber bridging-peeling-slip failure mechanism (Vairagade *et al.* 2023; Ma *et al.* 2024). However, studies have also shown that smooth, short, and straight fibers are readily pulled out during concrete's tensile loading, compromising their effectiveness (Deng *et al.* 2018). Hsieh et al. (Hsie *et al.* 2008) found that combining monofilament and short polypropylene (PP) fibers enhanced the compressive strength, crack resistance, and bending behaviour of concrete compared to using single-fiber reinforcement. The short PP fibers effectively dispersed, controlling early crack growth, while the coarser fibers contributed to stiffness and strength. At sufficient quantities, coarse fibers exhibited behaviour similar to steel fibers (SF) (Hsie *et al.* 2008). An investigation into the influence of hybrid basalt fiber (BF) and PP fiber on the mechanical performance of concrete revealed both positive and negative synergistic effects. The optimal combination, observed at a BF content of 0.15% and PP fiber content of 0.033%, resulted in enhancements of 14.1%, 22.8%, and 48.6% in compressive strength, flexural strength, and splitting tensile strength, respectively (Wang *et al.* 2019). The combination of BF/PVA exhibited a significant synergistic improvement in concrete performance. The optimal combination of fibers was found to be 0.1% PVA and 0.3% BF, resulting in enhanced compressive strength that were 24.6% and 8.54% greater than those of mono PVA and BF, respectively, at the same content (Du *et al.* 2022). Synergistic effects were observed for the combinations of 0.75% BF/0.25%PP and 0.5% BF/0.5% glass fiber (GF) and demonstrated the highest mechanical properties improvement over mono PP and BF fibers (Ahmed *et al.* 2023).

There are limited studies on the effect of fiber hybridization on the mechanical performance of SWSSC. Incorporation of hybrid PVA/BF resulted in a significant improvement in the total energy absorption by 44% and residual compressive strength by 181% in SWSSC compared to the incorporation of mono BF (Mashayekhi *et al.* 2024a). The incorporation of hybrid micro/macro fibers SWSSC demonstrated synergistic effects,

where the combination of micro- and macro-BF fiber hybridization yielded the greatest synergistic improvement. Notably, the inclusion of micro-fibers primarily contributed to an increase in the first-cracking strength, whereas macro-fibers served to enhance the post-cracking behaviour of the composite (Kaidi *et al.* 2023). The synergistic effects from fiber hybridization significantly enhanced the fracture toughness of SWSSC, with PP fibers combined with BF or PVA fibers resulting in 176% and 290% increases in fracture energy, respectively (Mashayekhi *et al.* 2024b). A review of the literature reveals that previous studies have primarily focused on the influence of mono- and hybrid-fibers on the overall performance of SWSSC under monotonic loading conditions.

Unlike monotonic loading to evaluate the mechanical characteristic of concrete, cyclic loading replicates real-world stresses like wind and traffic, or earthquakes, which are inevitable for the RC structures during the service life (Oyguc *et al.* 2018). Furthermore, a critical factor influencing the seismic performance of RC structures is their ductility and their ability to dissipate the accumulated seismic energy (Boulekbache *et al.* 2016). Research by Park and Paulay (Park *et al.* 1991) demonstrated that controlled crack formation is essential for this energy dissipation process. This highlights the importance of fibers in concrete and the need to evaluate their effect on the overall performance of concrete under cyclic loading. Previous study indicated that hooked-end steel and macro-polypropylene hybrid fiber can effectively mitigate the stiffness degradation process under cyclic compressive loading (Feng *et al.* 2023). The cyclic tensile behaviour of concrete was investigated by incorporating hybrid steel-polypropylene fibers. The results demonstrated that the synergistic effect of SF and PP enhanced the overall tensile properties across multiple levels (Wang, Shunan *et al.* 2023). The cyclic compressive stress–strain behaviour of hybrid SF/PP fibers showed that, with confinement, hybrid fibers significantly enhance concrete's mechanical properties, shifting the failure mode from tensile to shear (Meng *et al.* 2021). Additionally, as the number of cycles increased, both plastic strain energy and hysteretic energy consumption increased. During early cyclic loading, the HFRC primarily retained elastic strain energy with minimal hysteretic energy consumption (Wang, Changqing *et al.* 2022). The incorporation of SF resulted in 242% increase in cyclic flexural strength compared to plain concrete (Boulekbache *et al.* 2016). Adding short PP fibers improved the ductility of concrete after peak stress under cyclic compressive loading. It also increased the compressive strength, peak strain, and

residual stress of the concrete. However, the effects on elastic modulus and plastic strain were not significant (Wu, Huiqin *et al.* 2023).

FR-SWSSC presents a promising and sustainable alternative for coastal construction. However, a comprehensive understanding of its flexural behaviour under cyclic loading is crucial for ensuring the safety, serviceability, and efficiency of these structures. Marine environments subject structures to a combination of waves, tides, and seismic events, all of which induce cyclic loading. Previous research suggests that fiber incorporation improves the ductility, energy dissipation, and crack control of concrete under cyclic loads (Boulekbache *et al.* 2016; Sherif *et al.* 2018; De Smedt *et al.* 2020). Utilizing the synergistic effects of hybrid fibers, where combined properties surpass those of individual fibers, researchers can establish reliable design parameters for engineers, ultimately promoting sustainable and efficient coastal construction. Notably, existing research primarily focuses on either the static flexural behaviour of FR-SWSSC (Vafaei *et al.* 2021a, 2022a) or the cyclic response of conventional concrete with hybrid fibers (de Alencar Monteiro *et al.* 2018; Sherif *et al.* 2018; de Souza Castoldi *et al.* 2019). Moreover, the unique chemical reactivity of SWSSC has the potential to influence interfacial bonding and fiber synergy, both of which are critical factors in hybrid fiber performance. This study aims to bridge this knowledge gap by investigating the specific interaction between SWSSC and hybrid fibers under cyclic loading and evaluating the flexural performance of FR-SWSSC. This study comprehensively investigates the effect of hybrid fibers, combining micro and macro fibers, on the cyclic flexural response of FR-SWSSC compared to mono-fibers. These findings contribute to sustainable construction practices by paving the way for further research on hybrid FR-SWSSC.

5.2 Experimental work

5.2.1 Material properties

This research employed a sustainable approach by incorporating ground granulated blast furnace slag (GGBS) as a partial replacement for ordinary Portland cement (OPC) at a 65:35 ratio, thereby reducing CO_2 emissions (Zhang *et al.* 2013; Fattah *et al.* 2017; Yang *et al.* 2020). Seawater (SW), obtained from Adelaide coast and exhibiting elevated chloride and sulphate concentrations (360 and 76 times higher than tap water, respectively), was carefully stored to prevent contamination prior to utilization. Natural sand (NS) and sea-sand (SS) were employed as fine aggregates for FWNS and SWSSC,

respectively, with a maximum particle size of 2.5 mm for NS and 0.5 mm for SS. Scanning electron microscopy (SEM) analysis (**Figure 5-1**) revealed a smooth, rounded morphology for SS particles compared to the rough surface texture of NS. Inductively Coupled Plasma Optical Emission Spectroscopy (ICP-OES) analysis identified higher lead (Pb) and selenium (Se) concentrations in sea-sand compared to natural sand. Specifically, the concentrations of Pb and Se in sea-sand were 1.05 mg/kg and 2.8 mg/kg, respectively, while in natural sand they were 0.084 mg/kg and 0.174 mg/kg, respectively. However, both elements remained below the established landfill hazardous material limits (Decision 2003). Crushed basalt from a local quarry served as the coarse aggregate, with a maximum particle size of 14 mm.

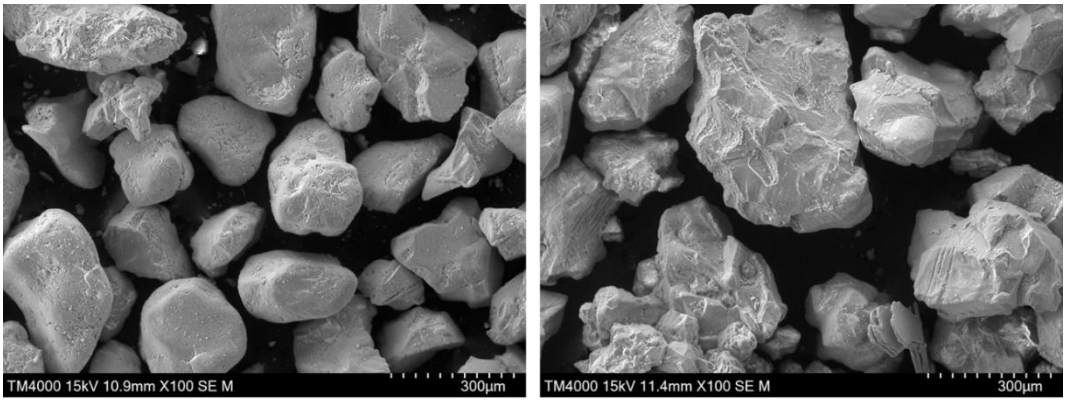


Figure 5-1 SEM analysis of a) sea-sand and b) natural sand.

The selection of fiber types and dosages was carefully considered to balance performance, cost-efficiency, and environmental impact. For fiber reinforcement, a combination of synthetic and natural fibers—including micro-fibers (PPS, PVA, and BF) and macro-fibers (PPL and TPPL)—was employed without surface treatment to maintain cost-efficiency. This selection ensures a diverse range of mechanical properties, including tensile strength and stiffness, that align with the objective of enhancing SWSSC performance. Basalt fibers were implemented for their high tensile strength, cost-effectiveness, and environmental benefits. Details and characteristics of these fibers are presented in **Table 5-1**. Macro-fibers with similar lengths but varying aspect ratios and stiffness were included to analyse their impact. An eco-friendly macro-fiber composed of recycled plastic (PPL) and commercially available in Australia (eMesh by FIBERCON) was incorporated to align with the aim of promoting sustainability in construction

practices. Consistent micro-fiber length was maintained to ensure minimal influence on the results, while a range of micro-fibers with varying tensile strengths, Young's modulus, and aspect ratios were utilized.

Table 5-1 Physical properties of fibers.

Fibers		Specific gravity	Length (mm)	Diameter (μm)	Thickness (μm)	Tensile strength (MPa)	Young's modulus (GPa)	Chemical resistance
Micro	PPS	0.91	6	18	—	600	9.5	Excellent
	PVA	1.3	8	38	—	1600	40	Excellent
	BF	2.8	7	15	—	2900	85	Excellent
Macro	PPL	0.91	47	—	<500	400	6	Excellent
	TPPL	0.91	54	800	—	620	9.5	Excellent

5.2.2 Mix proportions and test specimens

Twenty-three concrete mixes were produced, aiming for a compressive strength of 25 MPa. Details of the mix proportions are provided in **Table 5-2**. To ensure a workable fresh concrete mix suitable for structural applications, a slump of 150-200 mm was targeted without the incorporation of superplasticizers. The experiment was divided into four series. Series I comprised plain concrete (FWNS and SWSSC), which served as the control groups. Series II focused on mono-fiber types, each with a dosage of 0.25%, to explore the effects of different fiber types. Series III utilized combinations of micro-fibers with a total dosage of 0.25%, investigating the synergistic effects of micro-fibers in the hybrid system and their impact on the performance of SWSSC. Series IV examined the effects of combining micro and macro-fibers, also with a total dosage of 0.25%. The choice of a 0.25% fiber dosage was intended to ensure optimal dispersion of fibers throughout the concrete matrix while avoiding workability problems associated with higher fiber contents, as indicated by previous research (Vafaei *et al.* 2021a, 2022a; Vafaei *et al.* 2022b). Trials conducted in this study validated that the 0.25% dosage preserved both workability and suitable fiber distribution, consistent with earlier findings and ensuring the effective performance of the fiber-reinforced concrete. This dosage was considered suitable for practical applications, particularly in scenarios where maintaining a workable concrete mix without superplasticizers is essential. The inclusion of various fiber types and combinations across the series allowed for a detailed investigation of their individual and synergistic effects on the overall performance of SWSSC.

Hybrid fiber mixtures were prepared using two different ratios (33% and 66%) for each component. Adjusting the proportions in these hybrid systems allows for an evaluation of how the distinct mechanical properties—such as tensile strength, stiffness, and bonding behaviour—of the fibers interact within the concrete matrix, resulting in a synergistic effect on performance. For example, the study investigated two PPL/PVA hybrid combinations, designated 0.33PPL/0.66PVA and 0.66PPL/0.33PVA. The 33% PPL and 66% PVA combination highlights the impact of high tensile strength and stiffness of PVA fibers, while still utilizing the sustainability and length benefits of PPL fibers. Conversely, the 66% PPL and 33% PVA mixture emphasizes the mechanical properties of PPL, while exploring the advantages of PVA fibers. This approach effectively demonstrates the influence of fiber types in hybrid systems and their impact on the overall performance of SWSSC.

Two 100 mm × 100 mm × 350 mm prism samples were cast for cyclic and monotonic flexural test for each mixture based on AS 1012.11 (Australia, Standard 2000). Following casting, beam samples were demolded after 24 hours and maintained in a moist curing environment at 23°C ± 2°C for one day before being transferred to a lime-saturated water bath for 28 days, and then air-cured for 365 days to be tested. The specimens were prepared according to AS 1012.2 (Australia 1994).

5.2.3 Cyclic flexural test setup and procedure

The cyclic performance of FR-SWSSC specimens was investigated through four-point cyclic bending following AS 1012.11 (Australia, Standard 2000). The experimental setup is depicted in **Figure 5-2**. A 100 kN Instron testing machine, capable of displacement and load control, was employed for the flexural testing. The beam specimen was simply supported with a 300 mm span between the supports. To achieve pure bending in the beam, two-point loads spaced 150 mm apart were applied simultaneously. Both load and deflection data were collected automatically by a computer system. The mid-span deflection of the beam specimens was monitored using a linear variable differential transducer (LVDT). The loading procedure consisted of two distinct steps: displacement-controlled and load-controlled. During the loading phase,

Table 5-2 Concrete mix design.

Groups	Concrete Mix	Water (kg/m^3)		Gravel (kg/m^3)	Binder (kg/m^3)		Sand (kg/m^3)		Fiber (kg/m^3)					28-day f_c' (MPa)
		FW	SW		OPC	GGBS	NS	SS	PPS	PVA	BF	PPL	TPPL	
Plain	FWNS	256	256	995	126	234	785	—	—	—	—	—	—	28.5
	SWSS	—	—				—	785	—	—	—	—	—	27.6
Mono	PPS	—	256	995	126	234	—	785	2.28	—	—	—	—	27.2
	PVA								—	3.25	—	—	—	28.9
	BF								—	—	6.63	—	—	27.4
	PPL								—	—	—	2.28	—	28.6
	TPPL								—	—	—	—	2.28	29.0
Hybrid micro	0.33PPS/0.66BF	—	256	995	126	234	—	785	0.76	—	4.41	—	—	27.9
	0.66PPS/0.33BF								1.52	—	2.21	—	—	28.2
	0.66PVA/0.33BF								—	2.17	2.21	—	—	31.1
	0.33PVA/0.66BF								—	1.08	4.41	—	—	27.0
	0.33PPS/0.66PVA								0.76	2.17	—	—	—	27.3
	0.66PPS/0.33PVA								1.52	1.08	—	—	—	26.9
Hybrid macro/micro	0.33PPL/0.66PPS	—	256	995	126	234	—	785	1.52	—	—	0.76	—	27.2
	0.66PPL/0.33PPS								0.76	—	—	1.52	—	26.4
	0.66PPL/0.33PVA								—	1.08	—	1.52	—	31.9
	0.33PPL/0.66PVA								—	2.17	—	0.76	—	31.1
	0.33PPL/0.66BF								—	—	4.41	0.76	—	31.5
	0.66PPL/0.33BF								—	—	2.21	1.52	—	31.5
	0.33TPPL/0.66PVA								—	2.17	—	—	0.76	30.3
	0.66TPPL/0.33PVA								—	1.08	—	—	1.52	30.5
	0.33TPPL/0.66BF								—	—	4.41	—	0.76	28.5
	0.66TPPL/0.33BF								—	—	2.21	—	1.52	29.6

displacement control was applied at a constant rate of 0.05 mm/min for all plain and FR-SWSSC specimens. This rate was consistent with those used in previous studies on the flexural performance of fiber-reinforced concrete (de Alencar Monteiro *et al.* 2018; Xie, Faxiang *et al.* 2021; Mashayekhi *et al.* 2024d). Conversely, unloading utilized load control until a near-zero load state was achieved. The specific cyclic loading protocol is illustrated in **Figure 5-3**. This loading protocol effectively incorporates potential real-world experiences of FR-SWSSC structures, which may undergo significant lateral movements due to factors such as seismic events or extreme weather conditions. Additionally, by considering displacement-controlled loading and accommodating higher displacements, the impact of incorporating large fibers can be better investigated.

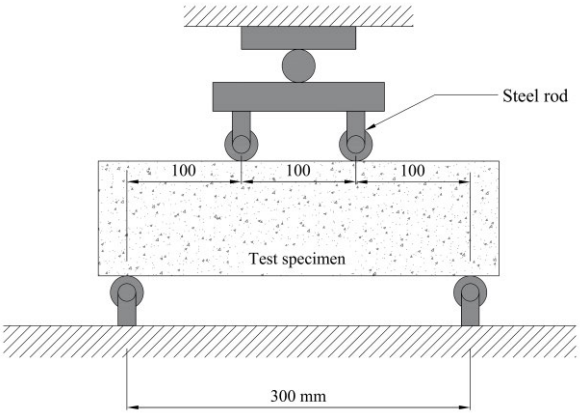


Figure 5-2 Cyclic flexural test setup.

5.3 Results and discussions

5.3.1 Cyclic flexural behaviour of FR-SWSSC

5.3.1.1 Load-mid-span deflection behaviour

Figure 5-4 and **Figure 5-5** illustrate the load-deflection and backbone curves, respectively, resulting from the cyclic flexural behaviour of FR-SWSSC across various concrete mixes. As anticipated, plain SWSSC and FWNS exhibited brittle failure due to a lack of fibers, indicated by a sharp post-peak load drop. Crack initiation and propagation within the concrete at peak point resulted in this behaviour. SWSSC displayed marginally higher peak load and superior post-peak performance compared to FWNS, evidenced by a greater residual load capacity during unloading. SEM images in **Figure 5-6** revealed that SWSSC exhibited a denser structure, consistent with findings from previous studies (Wang, Junjie *et al.* 2018; Vafaei *et al.* 2022b; Mashayekhi *et al.* 2024a). This can be

attributed to the higher concentration of portlandite in SWSS, which effectively filled gaps and pores. Moreover, the formation of ettringite was significantly more pronounced in SWSS than in FWNS, likely due to the use of seawater (Wang, Junjie *et al.* 2018; Mashayekhi *et al.* 2024a), further contributing to pore filling and creating a more uniform structure. As shown in **Figure 5-1**, the smoother, more rounded shape of SS compared to NS may enhance its interfacial bond with the cement paste. In contrast, the irregular and angular shape of NS can potentially create more voids and micro-cracks within the matrix, resulting in a weaker bond with the cement paste. The denser matrix resulted in a stronger interfacial bond between the aggregate and cement paste, which ultimately led to the observed improvements in load capacity and post-peak behaviour for the SWSSC mixture.

The results demonstrated the effectiveness of mono-fiber inclusion in reducing peak deflection. The incorporation of mono PPS and PVA micro-fibers significantly enhanced peak load capacity. This improvement can be explained by a synergistic mechanism involving fiber bridging, pull-out resistance, and early crack control, where the high tensile strength of PVA and BF fibers played a critical role. Prior research reported chemical bonding of PVA and BF within the concrete matrix. This phenomenon was further substantiated by the SEM analysis depicted in **Figure 5-7**, where both PVA and BF displayed chemical bonding with the SWSSC matrix. Notably, PVA fibers exhibited a greater degree of chemical bonding strength compared to BF. Conversely, PPS fibers demonstrated a weak interfacial bond with concrete matrix. Among the microfibers, PPS exhibited the highest peak strength and the lowest peak deflection. Previous studies have shown that the initial fracture toughness of PPS fibers is higher than that of PVA and BF (Mashayekhi *et al.* 2024d). This higher fracture toughness, combined with better distribution and a higher quantity (at a 0.25% dosage), likely contributed to achieving the highest peak strength in this study by providing superior reinforcement before cracking. However, the lower bonding strength and elastic modulus of PPS fibers led to fiber pull-out or breakage after cracking, which limited their bridging effect and inelastic behaviour, resulting in lower deflection. The impact of micro-fibers on post-peak response was minimal, likely due to their short length, which limited their ability to bridge macro-cracks after peak stress. In contrast, macro-fibers such as PPL and TPPL significantly improved post-peak behaviour in comparison to the plain SWSSC mixture. PPL fibers exhibited substantially higher load capacity at larger deformations, attributed to their

superior mechanical bonding facilitated by their length, stiffness, and rough surface. Additionally, micro-fibers, compared to macro-fibers (especially TPPL), showed a greater tendency toward deflection-softening behaviour.

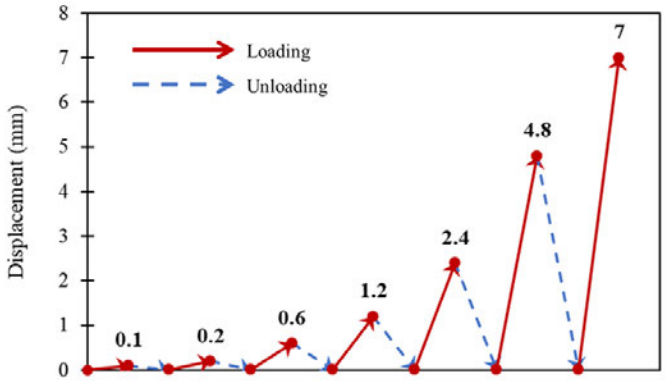


Figure 5-3 Cyclic loading protocol.

The impact of micro-fiber hybridization on SWSSC behaviour under cyclic loading was influenced by the fiber type and dosage in the hybrid system. Hybrid micro-fibers reduced peak deflection compared to mono micro-fibers, attributed to an improved elastic modulus achieved through hybridization (Mashayekhi *et al.* 2024a). Among the micro-fibers studied, BF was the most effective in reducing peak deflection in the hybrid system. The PVA/PPS hybrid increased load-bearing capacity compared to mono-fibers. While peak deflection remained unchanged with PPS/PVA compared to mono PPS, it decreased by 39% versus mono PVA. Specifically, the 0.33PPS/0.66PVA hybrid significantly enhanced peak strength but decreased post-peak strength across subsequent cycles. This was likely due to a synergistic effect, where PVA enhanced PPS fiber bonding, contributing to a more cracking strength and superior strength attainment. However, after crack initiation and reaching the peak point, the absence of fibers capable of crack control and bridging resulted in a substantial decrease in post-peak load-bearing capacity.

Similar observations were made with PPS/BF hybridization, where partial replacement of BF with PPS resulted in a marginal increase in ultimate strength compared to mono BF but exhibited a weaker post-peak response compared to both mono PPS and BF fibers. Hybridizing PPS/BF resulted in lower peak deflection and a decreased pre-peak slope compared to mono fibers. This effect could be attributed to the enhanced elastic modulus of concrete achieved through hybridization, as reported previously (Mashayekhi *et al.*

2024a). The PVA/BF combination in the hybrid system was highly sensitive to the fiber ratio. Notably, 0.33PVA/0.66BF significantly reduced peak deflection (by 56% and 63% compared to single BF and PVA fibers, respectively), whereas the 0.66PVA/0.33BF ratio had minimal effect. Moreover, the 0.66PVA/0.33BF combination improved peak strength compared to both individual PVA and BF fibers but exhibited a weaker post-peak response and lower strength throughout subsequent cycles. Among all micro-fiber hybridizations, the 0.66PVA/0.33BF combination resulted in the highest peak strength. This behaviour could be attributed to the enhanced bonding strength of PVA fibers facilitated by BF fibers, demonstrating the synergistic effect of PVA/BF on bonding strength and elastic modulus, which led to higher strength and improved cracking resistance. However, this combination also increased brittleness, causing a sharp decline in load-bearing capacity beyond the peak point.

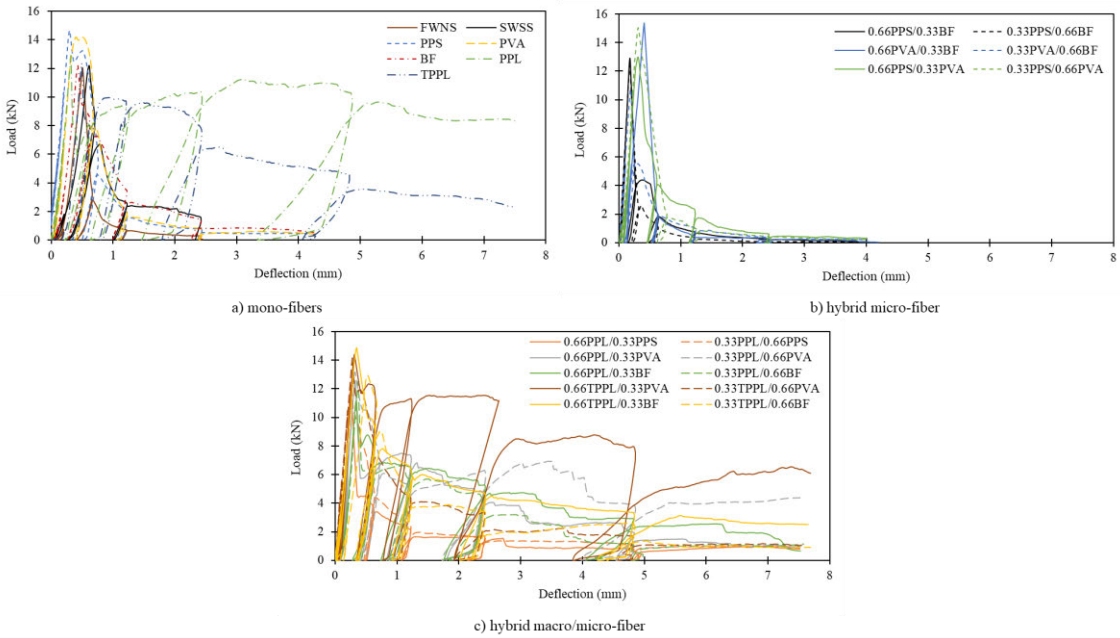


Figure 5-4 Load-deflection curves of FR-SWSSC mixtures with different fiber reinforcements, (a) mono-fibers, (b) hybrid micro-fiber, and (c) hybrid macro/micro-fiber.

Micro/macro fiber hybridization showed that micro-fibers with strong bonding to the concrete matrix (PVA and BF) significantly enhanced the overall bonding strength of macro-fibers in the hybrid system. This improvement resulted from micro-fibers reinforcing the surrounding matrix of macro-fibers, as evidenced by SEM images in **Figure 5-8**. Replacing TPPL fibers with BF increased ultimate strength while reducing

peak deflection, and this combination improved post-peak behaviour compared to mono BF fibers, which endured more cycles. The 0.66TPPL/0.33BF hybrid exhibited superior strength and post-peak performance over mono TPPL and BF, with increases of 49% and 58% in strength, respectively. This was likely due to enhanced bonding strength provided by BF, along with TPPL fiber properties including distribution and flexibility. The TPPL/PVA hybrid outperformed TPPL/BF in post-peak behaviour with minimal impact on ultimate strength. Notably, the 0.66TPPL/0.33PVA combination achieved significantly higher strength at elevated cycles compared to both mono PVA and TPPL fibers. A higher TPPL dosage in hybrid systems proved more effective, showing positive synergy where TPPL bridges macro-cracks and PVA or BF enhances bond strength, resulting in superior overall performance.

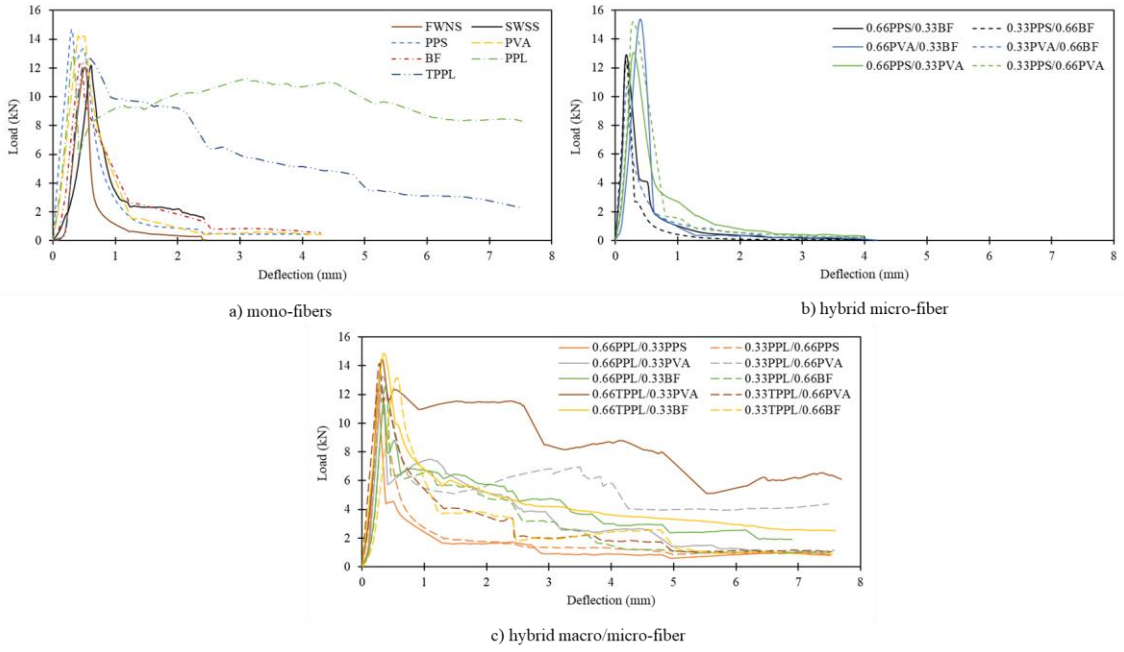


Figure 5-5 Backbone curves of load-deflection behaviour in FR-SWSSC with different fiber reinforcements: (a) mono-fiber, (b) hybrid micro-fiber, and (c) hybrid macro/micro-fiber.

PPL/PPS hybridization did not significantly differ from mono PPS in cyclic performance, with PPL/PPS hybrids showing reduced ultimate strength compared to both PPS and PPL fibers. The post-peak behaviour of PPL/PPS hybrids resembled that of mono PPS, indicating a detrimental synergistic effect of PPL/PPS hybridization. In contrast, PPL/BF and PPL/PVA hybrids improved post-peak performance compared to mono micro-fibers. The strong chemical bonding of PVA and BF fibers enhanced PPL fiber resilience,

preventing pull-out at large deflections and improving the bridging effect and overall load-bearing capacity. PVA fiber dosage notably affected the post-peak behaviour of hybrid PPL/PVA systems. The 0.33PPL/0.66PVA hybrid showed a slight increase in ultimate strength and improved post-peak response compared to 0.66PPL/0.33PVA. Moreover, the 0.66PPL/0.33BF hybrid also demonstrated superior post-peak performance, with approximately 74% higher ultimate strength than the 0.33PPL/0.66BF ratio. This improvement was likely due to the crack-bridging ability of PPL fibers. Higher BF content may enhance cracking strength through its chemical bonding and tensile properties. However, hybridizing with micro-fibers did not enhance the post-peak behaviour of single PPL fibers, likely due to insufficient PPL dosage, which limited crack-bridging capacity and reduced load-bearing capacity under high cyclic loads.

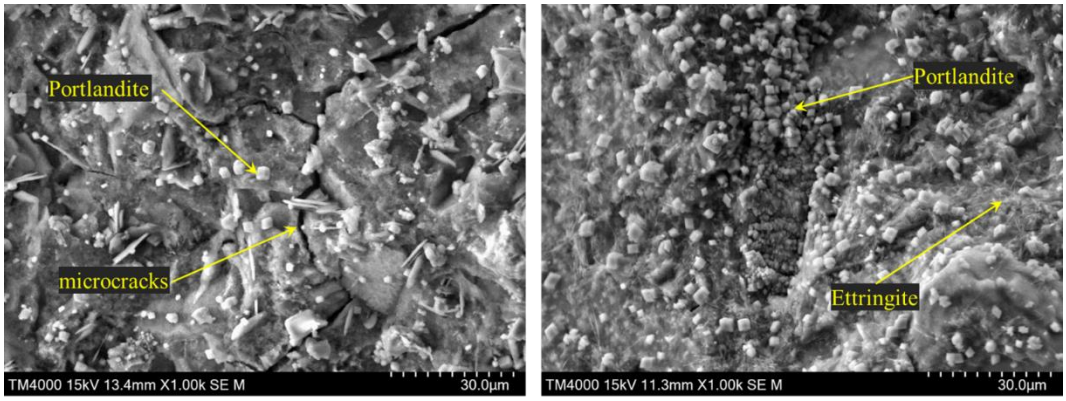


Figure 5-6 Microstructure of SWSSC and FWNS using SEM images.

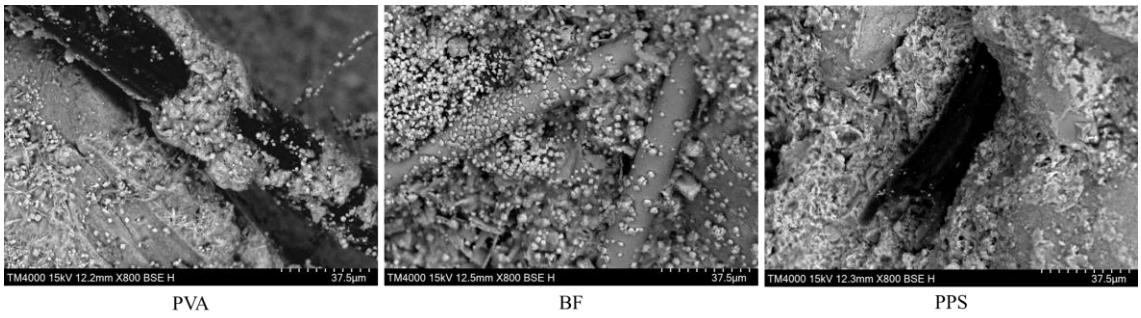
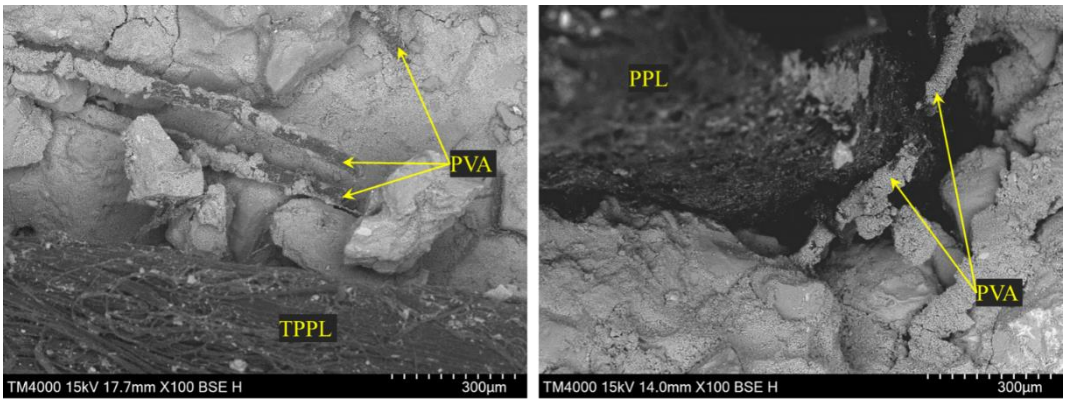


Figure 5-7 Microstructure of FR-SWSSC reinforced with micro-fibers using SEM images.



TPPL/PVA PPL/PVA

Figure 5-8 Microstructure of PPL/PVA and TPPL/PVA hybridization using SEM images.

5.3.1.2 Cyclic energy dissipation

The energy dissipation of FR-SWSSC (per cycle and cumulative) is shown in **Figure 5-9**. Compared to FWNS, SWSSC exhibited about 4.3 times higher dissipation at larger deflections, resulting in much higher cumulative energy dissipation by about 93%. This was likely due to the denser and stronger interlocking of SWSSC (**Figure 5-6**) consistent with previous studies (Wang, Junjie *et al.* 2018; Vafaei *et al.* 2022b; Yang *et al.* 2023). Micro-fiber incorporation significantly increased low-deflection energy dissipation compared to plain SWSSC. Notably, BF maintained 80% higher energy dissipation at high deflections compared to plain SWSSC. This potentially resulted from the uniform BF distribution and strong bonding, promoting crack retention at large deformations. PVA fibers exhibited higher energy dissipation compared to BF fibers at low cycles, leading to consistently higher cumulative dissipated energy across all deflection levels. Notably, the PVA-reinforced mixture achieved a maximum cumulative energy dissipation 36% greater than the plain SWSSC. This enhanced performance could likely be attributed to the strong chemical bonding of PVA fibers, which effectively bridged micro- and macro-cracks. PPL and TPPL fibers surpassed micro-fibers in post-peak energy dissipation, leading to higher cumulative dissipation. PPL fibers were particularly effective, exhibiting 200% and 82% greater energy dissipation at large deflections and cumulative dissipated energy, respectively, compared to TPPL fibers. This was likely due to the higher stiffness and improved mechanical bonding strength of PPL fibers, which limited macro-crack propagation.

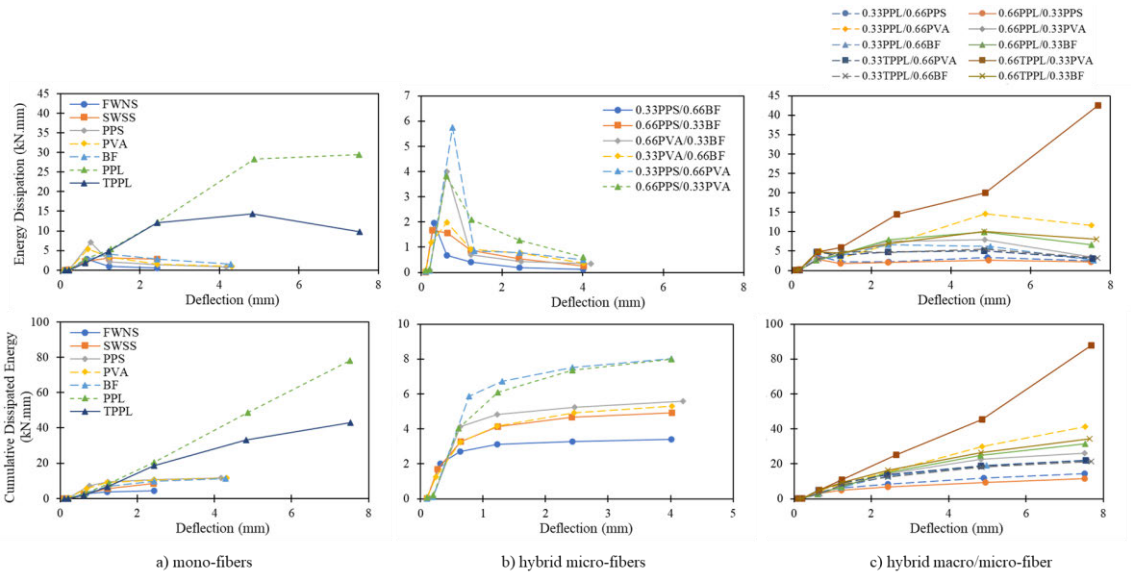


Figure 5-9 Energy dissipation of FR-SWSSC mixtures per cycle and cumulative with varying fiber reinforcements: (a) mono-fibers, (b) hybrid micro-fibers, and (c) hybrid macro/micro-fibers.

Micro-fiber hybridization in FR-SWSSC decreased energy dissipation compared to mono fibers. While it improved energy dissipation at initial cycles, it reduced energy dissipation for larger deflections across all hybrids. This behaviour was likely due to the weak post-peak response of micro-fibers, lacking crack-control and bridging mechanisms, leading to a significant drop in post-peak load-bearing capacity. For example, 0.66PPS/0.33BF resulted in 127% and 89% reductions in maximum cumulative energy dissipation compared to mono BF and PPS, respectively. Hybridizing micro/macro-fibers improved micro-fiber energy dissipation. Hybrid 0.33PPL/0.66PVA exhibited significantly higher cumulative energy dissipation than mono PVA fibers at large deflections by about 260% increase. This approach also yielded an 81% increase over mono PPL fibers at initial cycles. These findings indicated that PVA fibers were more effective for lower deflection energy dissipation, while PPL fibers benefit larger deflections. PPL/BF hybridization (0.66PPL/0.33BF) exhibited superior energy dissipation, with a 181% increase in cumulative dissipated energy compared to mono PPL fibers. This was likely due to the lower dosage of BF, mitigating the corrosion concerns of BF reported in previous studies (Wang, Qingxuan *et al.* 2021; Li, Meng *et al.* 2022; Mashayekhi *et al.* 2024a). While BF corrosion caused reduction in strength and ductility under cyclic loading, a lower dosage could leverage its strong bonding with the concrete matrix to enhance PPL fiber bonding and improve load-bearing capacity at large deflections.

TPPL/PVA hybridization enhanced the energy dissipation capacity at initial cycles. Notably, 0.66TPPL/0.33PVA significantly improved energy dissipation at large deflections compared to both PVA and TPPL fibers. It also resulted in 105% and 664% increase in cumulative dissipated energy over TPPL and PVA, respectively. This could be attributed to strong chemical bonding in PVA fibers (**Figure 5-7**), which likely improved TPPL fiber bonding under cyclic loading and strengthened the mix at large deflection cycles. Like PPL/BF hybridization, TPPL/BF at a combination of 0.66TPPL/0.33BF exhibited greater efficacy, likely due to previously reported BF corrosion. This hybrid resulted in 208% higher cumulative dissipated energy compared to mono BF incorporation.

5.3.1.3 Hysteretic damping ratio

To further investigate the energy dissipation characteristics of FR-SWSSC, hysteretic damping (ξ_{hys}) was evaluated. Hysteretic damping signifies the proportion of energy dissipated relative to the elastic energy stored within the material during deformation. This elastic energy is recovered upon load removal. As defined by (Hassanli *et al.* 2023), hysteretic damping can be expressed as:

$$\xi_{hys} = \frac{1}{4\pi}\frac{E_d}{E_{el}} = \frac{A_l}{\pi F_l d_l} \tag{5-1}$$

where dissipated energy within the loop is denoted by E_d, while E_{el} represents the elastic strain energy, A_l refers to the area enclosed by the loop, and F_l and d_l correspond to the maximum force experienced by the loop and the deflection associated with that force, respectively.

Figure 5-10 demonstrates a significantly higher ξ_{hys} for plain SWSSC compared to FWNS at low deflections by about 67% increase. This aligns with the denser microstructure observed for SWSSC in **Figure 5-6**. Micro-fiber incorporation (PPS, PVA, BF) further elevated ξ_{hys} by 32%, 58%, and 84% over plain SWSSC at low deflections, likely due to their enhanced crack resistance and energy dissipation properties stemming from strong chemical bonding and tensile strength (particularly PVA and BF). PPL fiber incorporation substantially improved ξ_{hys} (by 160% vs. plain SWSSC) while TPPL fibers decreased ξ_{hys} at low deflections. This difference was likely attributed to the

superior stiffness and mechanical bonding strength of PPL, resulting in greater initial cycle resistance and energy damping. During the initial cycles, TPPL fibers may cause micro-crack development and reduce ξ_{hys} compared to plain SWSSC. However, TPPL fibers still contribute to ξ_{hys} at higher deflections due to their ability to bridge cracks over larger deformations.

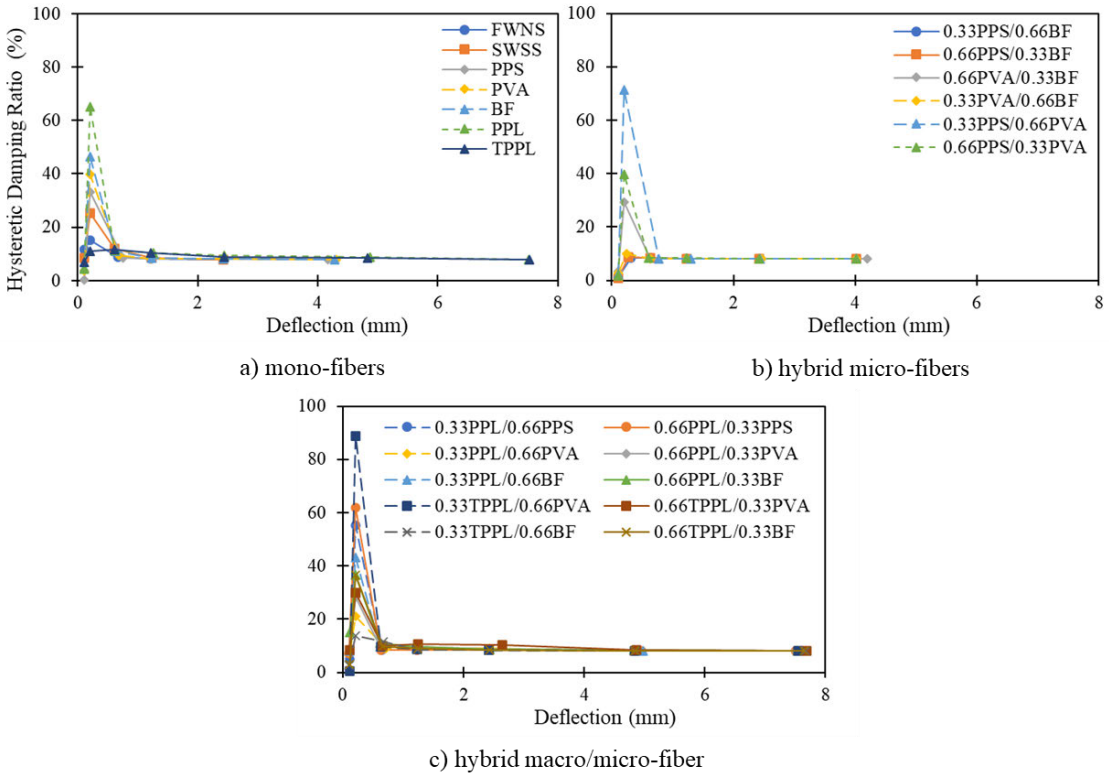


Figure 5-10 Hysteretic damping ratio of FR-SWSSC mixtures per cycle with varying fiber reinforcements: (a) mono-fibers, (b) hybrid micro-fibers, and (c) hybrid macro/micro-fibers.

Micro-fiber hybridization showed that PPS/BF combinations significantly reduced ξ_{hys}, likely due to the weak bonding of PPS fibers (**Figure 5-7**) and BF corrosion, as reported in previous studies (Wang, Qingxuan *et al.* 2021; Li, Meng *et al.* 2022; Mashayekhi *et al.* 2024a), leading to negative synergy. This finding is consistent with previous research on the mechanical properties of PPS/BF hybridizations in SWSSC (Mashayekhi *et al.* 2024a; Mashayekhi *et al.* 2024d). Conversely, PPS/PVA hybrids exhibited improved ξ_{hys}, with the 0.33PPS/0.66PVA combination resulting in 71% of ξ_{hys} at low deflections, representing an increase of 79% and 112% compared to mono PVA and PPS, respectively. This suggested PVA fibers enhanced PPS fiber bonding within the matrix,

leading to greater contribution from PPS fibers in hindering crack initiation and ultimately improving ξ_{hys}. Additionally, the lower stiffness strength of PPS fibers compared to PVA fibers could contribute to elongation and higher strain at failure when bonding was sufficient, further enhancing ξ_{hys}. PVA/BF hybridization decreased ξ_{hys} at low deflections compared to mono PVA and BF. Notably, 0.66PVA/0.33BF exhibited 192% higher ξ_{hys} than 0.33PVA/0.66BF. Higher BF dosage in the hybrid system might be detrimental due to corrosion. This could lead to brittleness in the BF, thereby impeding its positive interaction with PVA fibers.

Micro/macro-fiber hybridization demonstrated that while mono TPPL fibers exhibited low ξ_{hys}, incorporating TPPL/PVA fibers significantly enhanced it. Notably, 0.33TPPL/0.66PVA hybrid displayed a 123% and 656% increase in ξ_{hys} compared to mono PVA and TPPL, respectively. This improvement can be attributed to enhanced TPPL fiber bonding due to PVA addition, alongside improved flexibility, and distribution of TPPL fibers, ultimately leading to more effective energy damping. TPPL/BF hybridization reduced ξ_{hys} compared to mono BF but significantly improved it over mono TPPL fibers. Notably, 0.66TPPL/0.33BF increased ξ_{hys} by 211% at low deflections compared to mono TPPL fibers. However, increasing BF content in the TPPL hybrid system negatively impacted ξ_{hys}, possibly due to BF corrosion. PPL fiber hybridization with PVA or BF resulted in lower ξ_{hys} compared to mono-fibers. The disparity in PPL and TPPL performance stemmed from the superior fiber distribution of TPPL, leading to a more synergistic interaction with micro-fibers. PPL/PPS hybrids exhibited superior ξ_{hys} compared to mono PPS fibers. Notably, 0.66PPL/0.33PPS and 0.33PPL/0.66PPS composites achieved 84% and 65% improvement in ξ_{hys}, respectively, attributed to the ability of PPL fibers to hinder crack initiation and enhance energy damping at lower cycles.

5.3.1.4 Monotonic vs cyclic flexural behaviour

Figure 5-11 and **Figure 5-12** depict the contrasting response of FR-SWSSC reinforced with PPL and TPPL fibers and their respective micro-fiber hybrids, under cyclic and monotonic loading. The inherent rigidity and high tensile strength of PPL fibers resulted in superior performance under monotonic conditions. However, cyclic loading led to a deterioration of the PPL fiber-matrix bond, compromising their effectiveness in subsequent cycles. Conversely, TPPL fibers, characterized by flexibility and appropriate

bond strength, demonstrated superior performance under cyclic loading. This superior behaviour can be attributed to their ability to facilitate efficient stress transfer and effectively bridge micro- and macro-cracks within the concrete matrix.

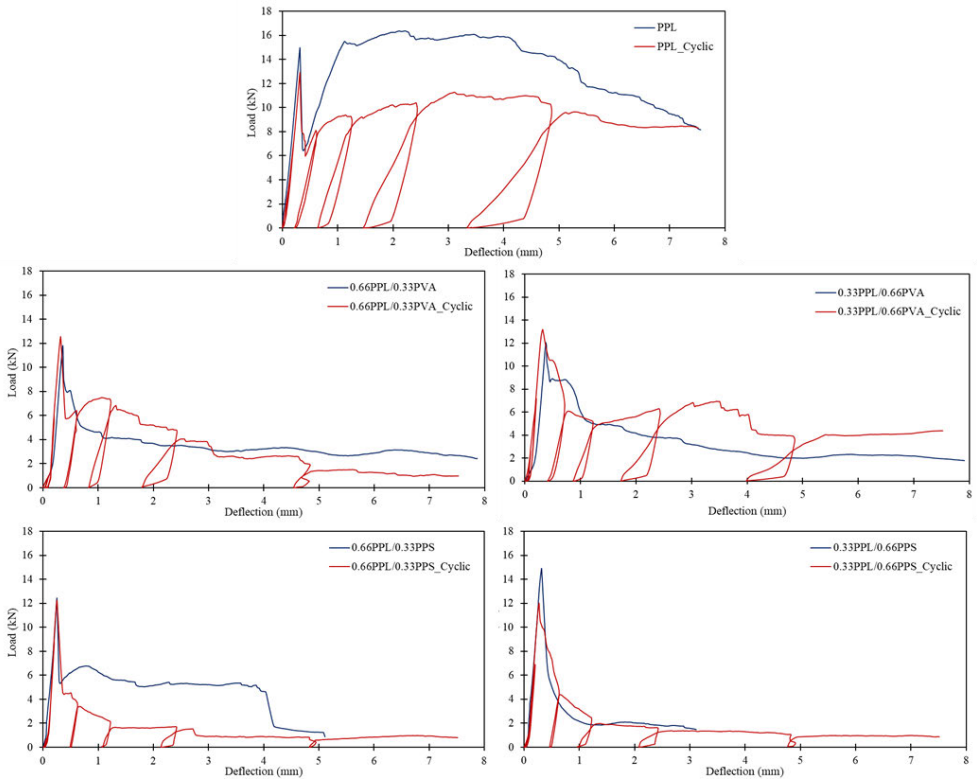


Figure 5-11 Monotonic and cyclic load-deflection behaviour of FR-SWSSC reinforced with PPL fibers and their hybridization with micro-fibers in flexural testing.

The partial substitution of PPL fibers with PVA fibers demonstrably improved their cyclic flexural performance. This enhancement could be attributed to the strengthened interfacial bonding facilitated by the incorporation of PVA fibers, ultimately leading to superior behaviour under repeated loading and unloading cycles. Moreover, a higher PVA fiber content within the PPL/PVA hybrid system yielded better performance at large deflections. A 66% substitution of TPPL fibers with PVA resulted in similar load-deflection behaviour under both cyclic and monotonic loading regimes. The 0.66TPPL/0.33BF hybrid showed similar performance in both loading conditions. This likely resulted from the strong chemical bonding strength of BF. However, higher BF content significantly reduced the load-bearing capacity after the peak under monotonic loading, possibly due to BF corrosion. PPL/PPS hybrids displayed negligible response modification under monotonic and cyclic loading owing to weak PPS fiber-matrix

adhesion. Consequently, increased PPS content resulted in a pronounced post-peak response weakening across both loading regimes.

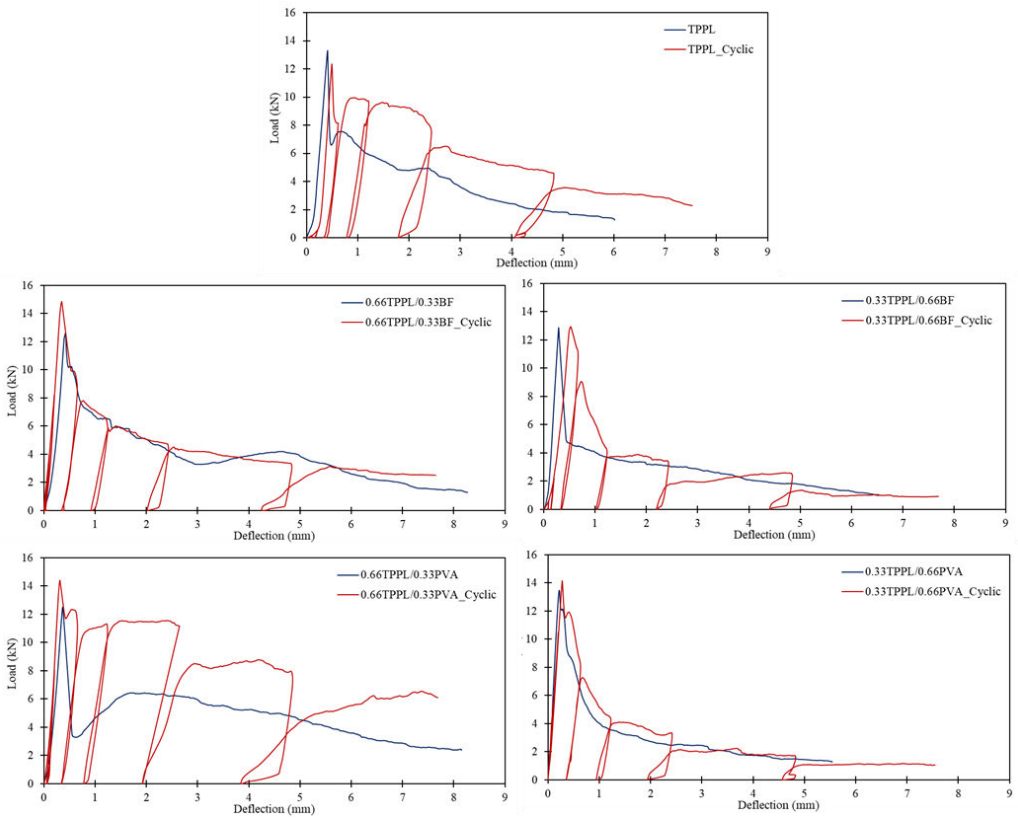


Figure 5-12 Monotonic and cyclic load-deflection behaviour of FR-SWSSC reinforced with TPPL fibers and their hybridization with micro-fibers in flexural testing.

5.3.1.5 Energy absorption capacity

To mitigate the risk of catastrophic and abrupt failure under dynamic loading scenarios, such as earthquakes, the incorporation of high-energy absorption materials becomes a critical design consideration (Shoaib *et al.* 2021; Gaddafi *et al.* 2023). This study investigated the energy absorption capacity as a key factor influencing the flexural behaviour of FR-SWSSC after concrete cracking by using backbone load-deflection results. The energy absorption capacity represents the amount of energy absorbed up to a specific deflection. In this study, T_{600}^{D} and T_{150}^{D} were evaluated as employed in previous study (Lee *et al.* 2017), representing the energy absorption capacity of FR-SWSSC up to deflection values of 0.50 mm (1/600 of the beam span) and 2 mm (1/150 of the beam span), respectively, as shown in **Figure 5-13**.

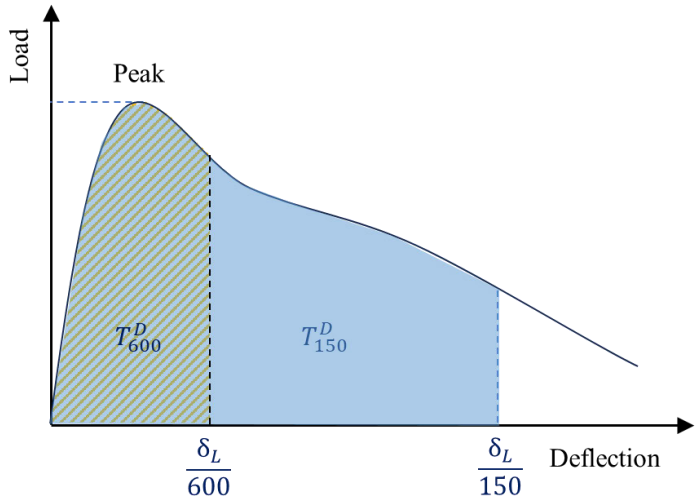


Figure 5-13 Characterization of peak load and energy absorption capacity (T_{600}^{D} and T_{150}^{D}) in typical backbone load-deflection behaviour.

Figure 5-14 demonstrates that SWSSC exhibited a significantly higher T_{150}^{D} (by about 67%) compared to FWNS, while its T_{600}^{D} is notably lower (by about 64%). This translated to a ratio of T_{150}^{D}/T_{600}^{D} of 5.36 for SWSSC and 1.15 for FWNS. This finding suggested that SWSSC promoted higher energy absorption at post-peak stage, likely due to its denser microstructure and stronger interlocking strength (**Figure 5-6**). Fiber addition significantly enhanced the energy absorption of SWSSC (T_{150}^{D} and T_{600}^{D}). This likely stemmed from micro- and macro-fibers bridging cracks at different stages during cyclic loading. While T_{150}^{D} showed minimal variation with micro-fiber type, PPS fibers yielded a 71% and 20% increase in T_{600}^{D} compared to BF and PVA, respectively. This translated to T_{150}^{D}/T_{600}^{D} ratios of 2.03, 2.47, and 3.29 for PPS, PVA, and BF, respectively. The corrosion of BF in SWSSC led to more brittle post-peak behaviour and the lowest T_{600}^{D} among all micro-fibers. PPL and TPPL fiber addition significantly improved post-peak energy absorption, as evidenced by increases of 128% and 132% in T_{150}^{D} for PPL and TPPL, respectively, compared to plain SWSSC. Similarly, T_{600}^{D} exhibited improvements of 136% and 32% for PPL and TPPL, respectively. These findings indicated the effectiveness of macro-fibers in bridging macro-cracks, resulting in a substantial increase in post-peak energy absorption. PPL and TPPL fibers exhibited similar T_{150}^{D} values, but PPL fibers displayed superior energy dissipation after peak load, resulting in a 79% higher T_{600}^{D} value. This difference translated to a T_{150}^{D}/T_{600}^{D} ratio of 9.43 for TPPL fibers and 5.19 for PPL fibers. This disparity likely originated from the stronger mechanical bonding

in PPL fibers, which mitigated the drop in load-bearing capacity and led to a lower T_{150}^{D}/T_{600}^{D} ratio.

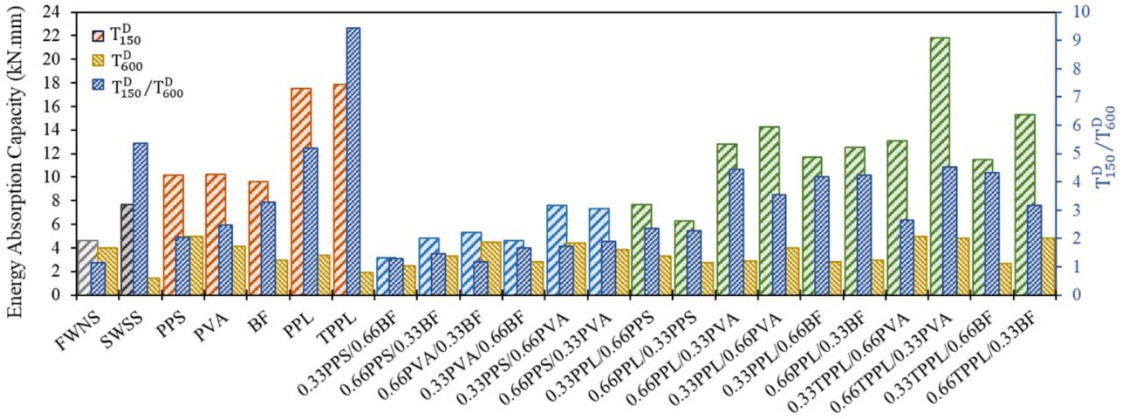


Figure 5-14 Energy absorption parameters of FR-SWSSC mixtures from backbone curves.

Micro-fiber hybridization decreased T_{150}^{D} but improved T_{600}^{D} compared to mono-fibers. For example, 0.66PPS/0.33BF hybridization yielded a 12% increase in T_{600}^{D} relative to mono BF. This positive synergy likely arises from improved bonding between PPS fibers due to BF incorporation, enhancing their contribution to bridging micro-cracks at low deflection cycles, thereby improving energy absorption. PVA/BF hybridization significantly enhanced T_{600}^{D} at low deflection cycles, with a 54% increase observed for 0.66PVA/0.33BF compared to mono BF. This result indicates that after the peak point, the synergy of PVA/BF hybridization improved ductility through the incorporation of PVA fibers, owing to their high tensile strength and strong bond with the concrete matrix. However, micro-fiber hybridization generally increased FR-SWSSC brittleness, although some combinations improved low-deflection performance.

Hybridizing macro/micro-fibers led to significant improvements in T_{150}^{D} compared to mono micro-fibers. Notably, 0.66PPL/0.33PVA and 0.33PPL/0.66PVA hybrids exhibited 25% and 39% higher T_{150}^{D}, respectively, compared to mono PVA fibers. Similarly, 0.66TPPL/0.33PVA and 0.33TPPL/0.66PVA hybrids achieved 113% and 28% enhancements in T_{150}^{D}, respectively, over mono PVA fibers. T_{150}^{D} increased by 31% and 22% for 0.66PPL/0.33BF and 0.33PPL/0.66BF hybrids, respectively, compared to mono BF fibers. Likewise, 0.66TPPL/0.33BF and 0.33TPPL/0.66BF hybrids exhibited T_{150}^{D} enhancements of 59% and 20%, respectively, compared to mono BF. TPPL fiber

hybridization with PVA and BF fibers significantly increased T_{600}^{D} compared to mono TPPL fibers. Notably, TPPL/PVA hybridization proved more effective, with 0.66TPPL/0.33PVA and 0.33TPPL/0.66PVA exhibiting 155% and 161% enhancements in T_{600}^{D}, respectively, over mono TPPL fibers. This suggests that PVA fibers reinforce micro-cracks, improving low-deflection energy dissipation, while TPPL fibers, due to their superior distribution, bridge macro-cracks, enhancing high-deflection energy absorption. Among macro/micro-fiber hybrids, 0.66TPPL/0.33PVA exhibited the most effective synergy, demonstrating significantly higher energy absorption at both T_{150}^{D} and T_{600}^{D} compared to PVA and TPPL mono-fibers.

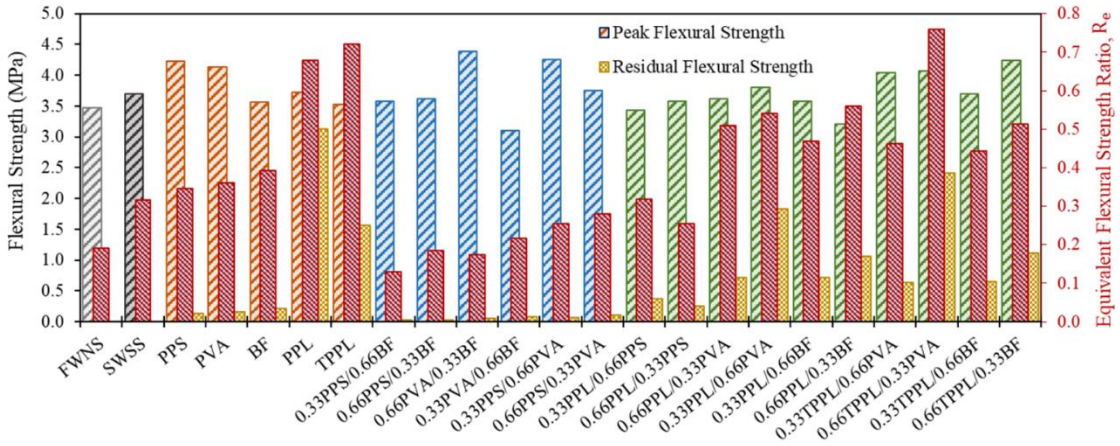


Figure 5-15 Flexural strength, residual strength, and equivalent flexural strength of all mixtures.

5.3.1.6 Flexural tensile strength

The flexural tensile behaviour of FRC is typically quantified by the equivalent flexural strength ratio, denoted as $R_{e,3}$ (SF 1984; Society 2003; Wei *et al.* 2024). This parameter is derived from the energy absorption capacity of FRC up to a deflection corresponding to 1/150 of the beam span and the initial peak load experienced during the flexural test (Astm 2007; Lee *et al.* 2017; Lee *et al.* 2018a; Lee *et al.* 2018b). As such, the value of $R_{e,3}$ can be determined through analysis of the backbone load-deflection curves in this study and can be calculated as:

$$R_{e,3} = \frac{T_{150}^{D}}{P_1 \delta_{\frac{L}{150}}} \quad (5\text{-}2)$$

where P_1 signifies the first peak load.

Figure 5-15 depicts the value of $R_{e,3}$ for all mixes and additionally presents the flexural strength at peak and residual, defined as the strength at 3.5 mm deflection. Eq. (5-3) was employed to calculate both peak and residual flexural strength. According to ASTM C1609 standard (Astm 2007), the first peak strength was identified as the cracking strength of FR-SWSSC.

$$f_u = \frac{P_u L}{b d^2} \quad (5\text{-}3)$$

where L, b, and d denote the span, width, and depth of the beam specimen, respectively.

Plain concrete mixes (FWNS and SWSSC), lacking fibers and exhibiting brittle behaviour, displayed no residual flexural strength. SWSSC exhibited 68% greater $R_{e,3}$ compared to FWNS. This aligns with other study results, suggesting that the denser microstructure of SWSSC and superior interlocking contribute to its enhanced flexural strength. Compared to plain SWSSC, micro-fibers marginally improved residual flexural strength. Macro-fibers, however, achieved significantly higher residual strength due to crack bridging and energy absorption. PPL fibers were more effective (99% higher strength than TPPL), possibly due to their stiffness and appropriate bond with the matrix. Conversely, TPPL fibers exhibited a 6% increase in $R_{e,3}$ compared to PPL fibers, likely due to their enhanced energy absorption capability facilitated by their flexibility. Furthermore, BF demonstrated the highest $R_{e,3}$ among the micro-fibers, exceeding plain SWSSC by 22%.

Micro-fiber hybridization decreased residual flexural strength and $R_{e,3}$ compared to mono micro-fibers. However, cracking strength in FR-SWSSC exhibited some improvement with hybridization, with 0.66PVA/0.33BF achieving 6% and 23% increases over mono-PVA and BF, respectively. This suggested a positive synergy from PVA/BF hybridization, potentially due to BF enhancing PVA fiber bonding and consequently improving cracking strength. Macro/micro-fiber hybridization significantly increased

residual flexural strength and $R_{e,3}$ compared to mono micro-fibers. For example, 0.33PPL/0.66PVA hybrid exhibited 10.8 times greater residual flexural strength and 50% higher $R_{e,3}$ than mono PVA fibers. Also, 0.66PPL/0.33BF hybridization yielded 382% and 44% higher residual flexural strength and $R_{e,3}$, respectively, compared to mono BF. This improvement was attributed to the ability of PPL fibers to bridge macro-cracks and enhance energy absorption. Interestingly, for PPL fiber hybridization, PVA was more effective at higher dosages, while the opposite was true for BF. This disparity was likely due to BF corrosion in SWSSC, leading to brittleness (Özkan *et al.* 2020; Wang, Qingxuan *et al.* 2021; Mashayekhi *et al.* 2024a). Therefore, lower BF content resulted in superior flexural performance when combined with PPL fibers. Moreover, the hybrid PPL/PPS fibers exhibited slightly higher residual strength than mono PPS fibers, attributed to the crack-bridging effect of PPL fibers. However, when the fiber dosage was reduced in the hybrid mix, the $R_{e,3}$ value decreased compared to both mono PPS and PPL fibers. This suggests a negative synergy and the inability of the fibers to complement each other effectively, likely due to the lower bonding strength of PPS and the reduced stiffness of PPL, negatively impacting stress distribution and flexural performance.

0.66TPPL/0.33PVA hybrid displayed a 54% and 15% increase in residual flexural and cracking strengths, respectively, compared to mono TPPL fibers. $R_{e,3}$ also improved by 6% and 111% for the hybrid relative to mono TPPL and PVA, respectively. This synergy was attributed to the strong interaction of PVA fibers with the concrete matrix, enhancing TPPL fiber bonding and promoting energy dissipation for improved flexural strength. Previous study on the hybridization of macro-BF and micro PVA fibers revealed similar results in FWNS concrete, indicating that a higher percentage of macro-BF was more effective under cyclic loading (Min *et al.* 2024). 0.66TPPL/0.33BF hybridization yielded a 20% increase in cracking strength compared to mono TPPL fibers. This enhancement was attributed to the ability of BF to improve TPPL fiber bonding strength. However, increasing the BF content resulted in a detrimental effect due to corrosion.

5.3.2 Damage characteristics

An evaluation of FR-SWSSC damage was conducted using damage index (DI), strength deterioration ratio (SDR), and degree of reversibility (R). These parameters were determined using Equations (5-4) to (5-6) from the data presented in **Figure 5-16**.

$$DI_i = 1 - {E_{d_i}}/{E_0} \tag{5-4}$$

$$SDR_i = {P_{rel_i}}/{P_{unl_i}} \tag{5-5}$$

$$R_i = 1 - {D_{residual_i}}/{D_{max_i}} \tag{5-6}$$

where E_{d_i} and E_0 denote the damage modulus and initial modulus, respectively. P_{rel_i} represents the reloading strength, and P_{unl_i} signifies the unloading strength. Additionally, $D_{residual_i}$ and D_{max_i} correspond to the residual deflection and maximum displacement experienced during each loading cycle (i). The results of the investigated damage parameters—DI, SDR, and R—are presented in **Figure 5-17** to **Figure 5-19**. The DI represents the reduction in concrete stiffness during unloading, caused by damage. The SDR value obtained from the cyclic flexural test provides a quantitative measure of the cyclically induced reduction in the load-bearing capacity during loading-unloading cycles. A lower SDR value corresponds to a more significant loss in capacity. The R factor signifies the degree of elastic recovery of concrete after a loading-unloading cycle. This reflects the resilience of concrete under repeated bending stresses. Higher R values indicate greater reversibility, suggesting more elastic behaviour and improved performance under cyclic loading due to reduced permanent deformation with each cycle.

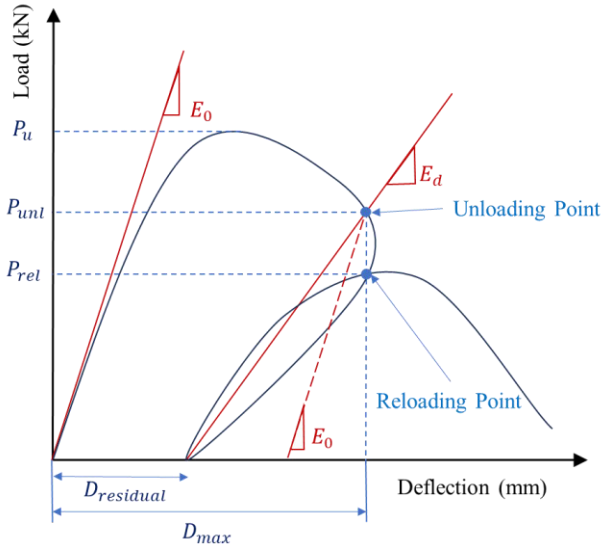


Figure 5-16 Cyclic damage parameters.

5.3.2.1 Plain concrete

The DI results for plain concrete mixes showed that both SWSS and FWNS exhibited similar damage indices across cycles, with FWNS having a slightly higher DI at deflections exceeding 1 mm. FWNS consistently exhibited up to 20% higher SDR than SWSS across all deflections. However, FWNS showed a higher R value at deflections below 0.4 mm, while SWSS outperformed FWNS at greater deflections. These results suggest that at lower deflections, the presence of salts in SWSS induced micro-cracks in the early cycles, exacerbated by its denser, more brittle microstructure (Wang, Junjie *et al.* 2018; Vafaei *et al.* 2022b; Yang *et al.* 2023). This led to higher residual deflections (lower R) and greater strength reduction (lower SDR) compared to FWNS. At higher deflections, the increased interlocking strength in SWSSC resulted in more reversibility and less residual deformation, leading to more elastic behaviour than FWNS. Although crack propagation reduced SDR, the preserved elasticity led to slightly lower stiffness degradation and DI in SWSS. Conversely, FWNS exhibited higher ductility due to the absence of salts, promoting distributed micro-cracking, which resulted in a higher SDR but lower R.

5.3.2.2 Mono-fibers

Mono micro-fibers primarily affected the early loading cycles due to their limited ability to bridge macro-cracks after peak strength, constrained by their short length. Their addition significantly improved the SDR of SWSSC by enhancing micro-crack bridging and reducing strength loss. PPS fibers increased both SDR and R values at deflections below 0.5 mm; however, beyond this point, the R value dropped sharply. This suggests that PPS fibers provided elastic recovery (high R) and retained strength (high SDR) at small deflections due to their better distribution, which improved the elastic modulus and initial stiffness. However, weak bonding with the concrete matrix and low tensile strength led to fiber pull-out after the peak deflection (0.3 mm), limiting crack bridging at larger deflections and causing reductions in both SDR and R for deflections above 0.5 mm. PVA fibers, with superior chemical bonding, maintained higher SDR at larger deflections, indicating better strength retention during cyclic loading. The R value for PVA fibers was comparable to PPS, likely due to similar stiffness and elastic modulus, resulting in similar elastic behaviour and residual deflections at larger deflections. Conversely, BF of PPS and PVA reinforced SWSSC, with its higher elastic modulus and strong bond with the matrix, provided better reversibility and higher R at large deflections, leading to lower

residual strength. This contributed to the lowest SDR among all mono micro-fibers, likely due to the elastic behaviour and low elongation BF, resulting in reduced strength retention. Consequently, BF showed a similar DI to plain SWSSC. PPS and PVA fibers, while improving initial stiffness, caused higher DI at all deflections. After peak deflection (approximately 0.3 mm for PPS and 0.4 mm for PVA), both fibers experienced a sharp drop in stiffness after crack formation, leading to greater DI due to the increased difference between unloading and initial stiffness.

The incorporation of PPL fibers resulted in a significantly higher DI than TPPL fibers at all deflections, and outperformed plain SWSSC for deflections below 1.2 mm. This is likely due to the better distribution and flexibility of TPPL fibers, which helped preserve initial stiffness during loading-unloading cycles, leading to a lower DI compared to PPL and plain SWSSC. Conversely, PPL fibers demonstrated higher SDR and R values across all deflections compared to TPPL fibers. Notably, PPL fibers improved SDR by 22% at low deflections, attributed to their superior mechanical bonding and stiffness, which minimized strength reduction and residual deflections. Both PPL and TPPL fibers enhanced SDR for deflections below 0.9 mm, likely due to crack bridging by macro-fibers. Regarding deflection reversibility, TPPL fibers resulted in lower R values than plain SWSSC for deflections below 0.9 mm, while PPL fibers exhibited higher R. However, for deflections exceeding 0.9 mm, both fiber types showed higher R values than plain SWSSC, likely due to the flexibility of TPPL, causing early micro-crack formation, leading to initial residual deflection. At larger deflections, the crack-bridging ability of TPPL fibers reduced residual deflections and increased R values.

5.3.2.3 Micro-fiber hybridization

Micro-fiber hybridization showed that PPS/BF and PVA/BF hybrids outperformed mono fibers in DI, particularly at low deflection cycles. This can be attributed to BF increasing the initial stiffness of the hybrid systems with PPS and PVA fibers, resulting in more elastic behaviour and increased brittleness. Consequently, the peak deflection decreased, followed by a sharper drop in the hybrids containing BF. The synergy of BF with PPS and PVA fibers led to higher DI at low deflections compared to mono PPS and BF, reducing residual deflection and R values in PPS/BF and PVA/BF hybrids. The 0.66PPS/0.33BF hybrid exhibited greater R than 0.33PPS/0.66BF, likely due to BF corrosion in SWSSC, which reduced ductility. The 0.66PVA/0.33BF hybrid achieved superior R values at higher deflections compared to mono PVA and BF, as hybridization

improved concrete ductility. BF enhanced PVA fiber bond strength, allowing full utilization of tensile capacity. The 0.33PVA/0.66BF hybrid showed better SDR at low deflections than mono PVA and BF, and at higher deflections compared to BF. This result indicated positive synergy which improved interlocking in SWSSC and strength recovery across all deflections. While a higher BF dosage aided strength recovery, PVA content improved elasticity compared to mono BF. In PPS/BF hybrids, the 0.66PPS/0.33BF hybrid was more effective for strength recovery, showing 22% and 35% higher SDR than mono PPS and BF. In PPS/PVA hybrids, the 0.33PPS/0.66PVA combination performed better, with lower DI at low deflections compared to mono PPS, improved R at large deflections, and reduced residual deflection. This effect can be attributed to a synergistic mechanism: PVA fibers bridged initial cracks, while the lower modulus of PPS facilitated uniform stress distribution, delaying damage, and improving cracking strength (**Figure 5-15**). This synergy also enhanced high-deflection SDR and load-bearing capacity during loading-unloading cycles, with the hybrid 0.33PPS/0.66PVA mix showing a 23% and 30% increase in SDR at failure compared to mono PPS and PVA, respectively.

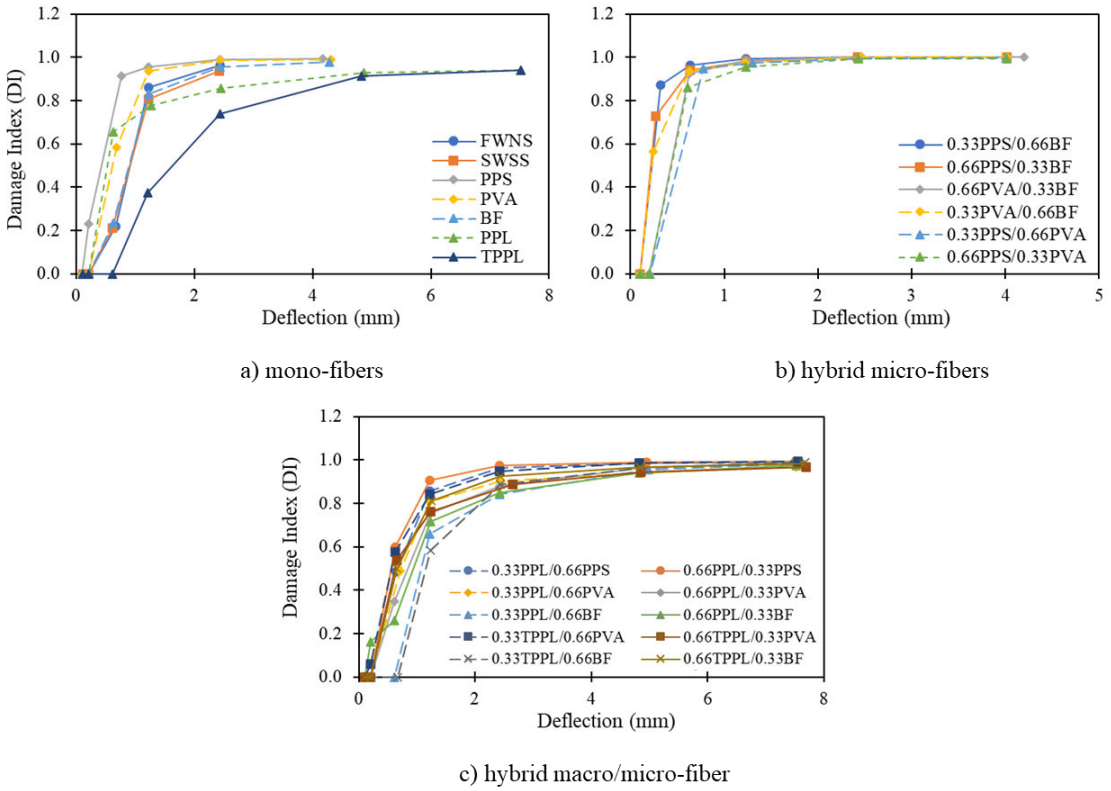


Figure 5-17 Damage index (DI) of FR-SWSSC mixtures per cycle with varying fiber reinforcements: (a) mono-fibers, (b) hybrid micro-fibers, and (c) hybrid macro/micro-fibers.

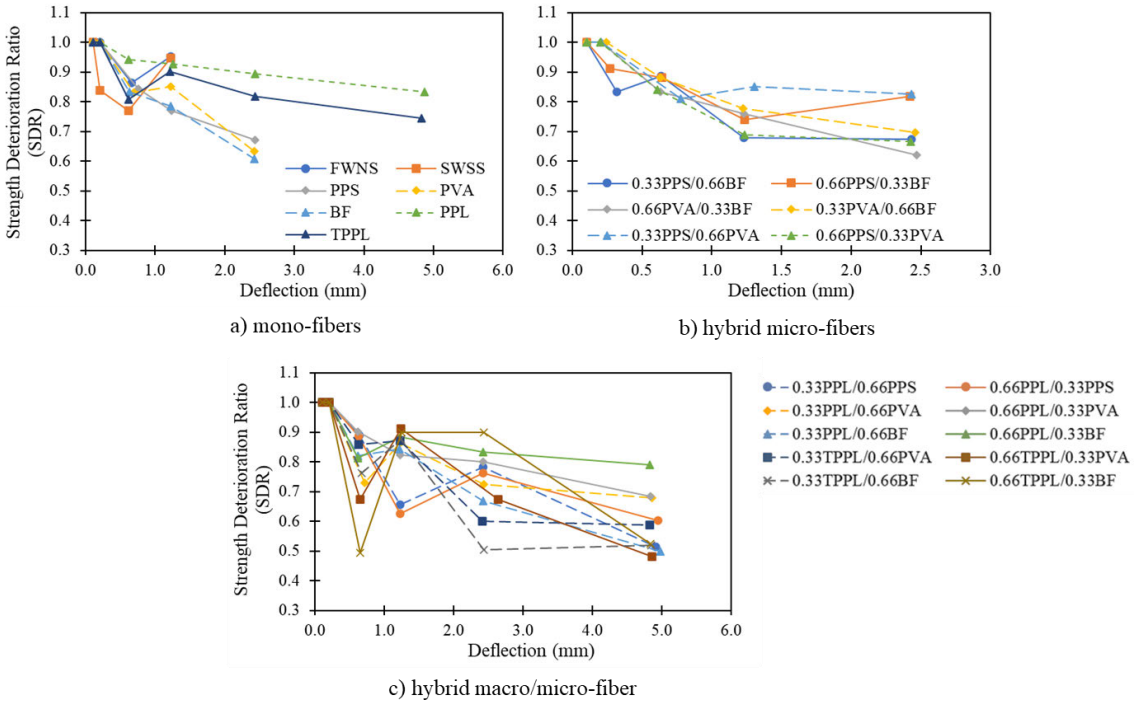


Figure 5-18 Strength degradation ratio (SDR) of FR-SWSSC mixtures per cycle with varying fiber reinforcements: (a) mono-fibers, (b) hybrid micro-fibers, and (c) hybrid macro/micro-fibers.

5.3.2.4 Macro/micro-fiber hybridization

The PPL/PPS hybrid exhibited a lower DI at low deflections compared to both mono PPL and PPS, and reduced DI relative to PPS at the post-peak stage, suggesting a synergistic effect in preventing initial micro-cracks and lowering early damage. The mechanical bonding and stiffness of PPL fibers helped preserve initial stiffness and reduced damage across all deflections compared to PPS, which showed stiffness degradation during cyclic loading. This effect was more pronounced in the 0.33PPL/0.66PPS combination. PPL/PPS hybridization also led to a 17% increase in SDR over mono PPS at 2.4 mm (the failure point for PPS), though it resulted in a 19% decrease in SDR at 1.2 mm in the post-peak stage. The pull-out of PPL fibers during large crack development at post-peak reduced strength recovery and SDR, but at higher deflections, PPL fibers more effectively bridged larger cracks, maintaining strength better than mono PPS fibers.

A higher proportion of PPL fibers led to significantly greater strength recovery and SDR than PPL/PPS hybridization, highlighting the importance of macro-fiber dosage for

maintaining strength during loading-unloading cycles. This trend was reflected in the R values, with mono PPL showing lower residual deflection than PPL/PPS. PPL/PPS hybridization also increased the R value compared to mono PPS at deflections over 1.2 mm, showing positive synergy in crack bridging and deflection recovery by PPL fibers. A similar effect was observed in PPL/PVA hybridization, which improved R values compared to PPL/PPS, attributed to enhanced bonding strength between PPL and PVA fibers and their positive synergy. The synergistic crack-bridging by PVA (micro-cracks) and PPL (macro-cracks) improved ductility and reversibility. This effect also resulted in higher SDR values than mono PVA fibers at large deflections, particularly with a 0.66PPL/0.33PVA combination, showing a 26% increase at 2.4 mm compared to 14% for 0.33PPL/0.66PVA. PPL/PVA hybridization maintained initial stiffness better, reducing damage and stiffness degradation compared to mono PVA. It also resulted in lower DI than mono PPL at deflections below 1.2 mm, likely due to improved bonding and stress distribution from PVA fibers, which reduced PPL fiber pull-out and subsequent damage.

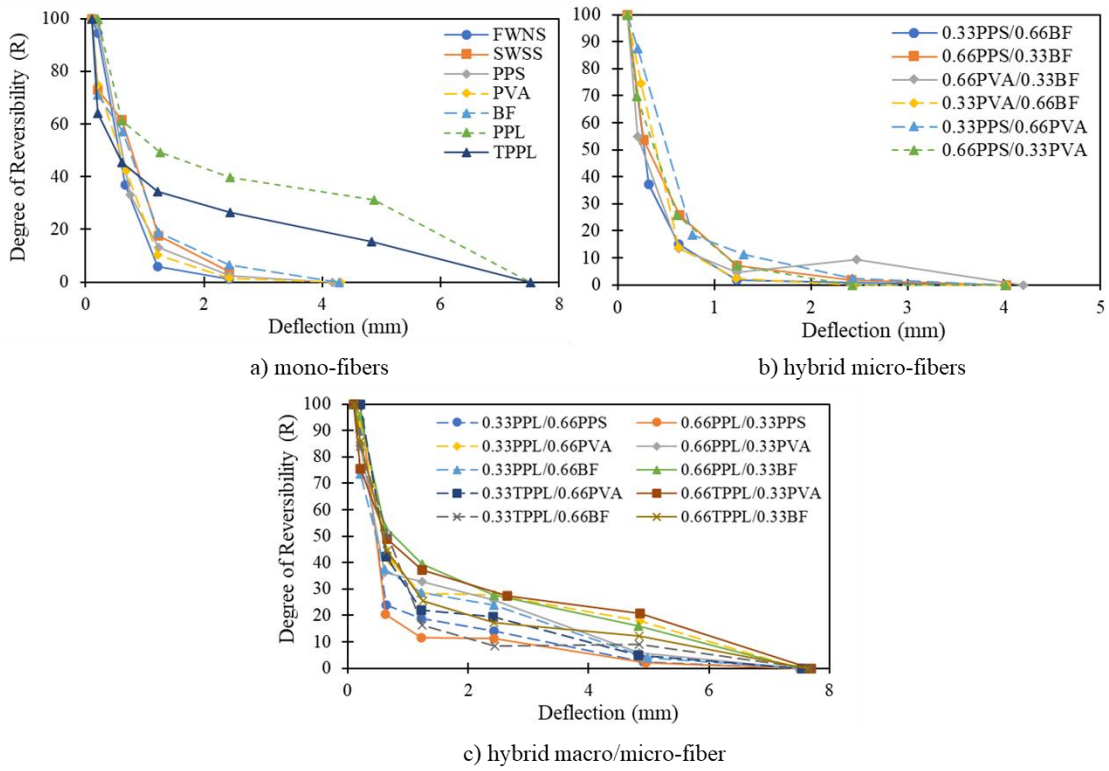


Figure 5-19 Degree of reversibility (R) of FR-SWSSC mixtures per cycle with varying fiber reinforcements: (a) mono-fibers, (b) hybrid micro-fibers, and (c) hybrid macro/micro-fibers.

The hybridization of PPL and BF fibers resulted in a lower DI compared to mono-fiber inclusions, with the 0.33PPL/0.66BF ratio being most effective at lower deflection cycles. This partial replacement improved concrete strength during crack initiation and propagation. The SDR showed strong dependence on fiber content, with 0.66PPL/0.33BF offering a 37% higher SDR than mono BF at 2.4 mm deflection (failure point of BF), while 0.33PPL/0.66BF showed a 10% improvement. Additionally, 0.66PPL/0.33BF provided a 59% increase in SDR compared to 0.33PPL/0.66BF, likely due to the synergy between PPL and BF. BF enhanced the bonding strength of PPL, improving the ability of the system to recover strength through the fiber bridging of PPL fibers in large cracks. This effect was also evident in deflection recovery, with 0.66PPL/0.33BF proving more effective, leading to lower residual strength and higher R than mono BF. However, increased BF content, due to its susceptibility to corrosion, resulted in greater brittleness and reduced strength recovery and SDR under cyclic loading.

Hybridizing TPPL with PVA or BF resulted in less damage than mono micro-fibers (PVA or BF) but more than mono TPPL. At 1.2 mm deflection, 0.66TPPL/0.33PVA and 0.33TPPL/0.66PVA increased DI by 103% and 125% compared to mono TPPL, while reducing it by 18% and 10% relative to mono PVA. This was likely due to PVA fibers enhancing the initial stiffness of the hybrid system. The TPPL/PVA synergy improved low-cycle SDR, particularly for 0.33TPPL/0.66PVA, compared to mono fibers. However, at higher deflections (2.4 mm), 0.66TPPL/0.33PVA showed superior load-bearing capacity, increasing SDR by 12% compared to 0.33TPPL/0.66PVA, likely due to PVA strengthening the TPPL bond. Additionally, 0.66TPPL/0.33PVA hybridization improved deflection recovery and increased R values compared to both mono TPPL and PVA, attributed to better crack bridging, lower residual deflection, and more elastic behaviour due to PVA inclusion.

The hybridization results of TPPL/BF showed that a lower BF content (0.66TPPL/0.33BF) was more effective, due to the brittleness caused by BF corrosion. At deflections greater than 1.2 mm, this mix exhibited higher SDR and R values, likely due to improved bonding strength of TPPL fibers. The presence of 0.33BF promoted more elastic behaviour after peak load, allowing TPPL fibers to bridge cracks more effectively, leading to higher SDR and R compared to mono BF. This elastic response, coupled with greater initial stiffness than mono TPPL or BF, resulted in higher DI in low-cycle

conditions. At 2.4 mm deflection, 0.33TPPL/0.66BF increased DI by 20% and decreased it by 7% compared to mono TPPL and BF, respectively.

In macro/micro-fiber hybridization, a higher dosage (66%) of macro-fibers resulted in lower SDR due to their superior bridging ability. Micro-fibers with chemical bonding properties, such as PVA and BF, enhanced performance, with PVA excelling at low deflections and BF at the post-peak stage. Hybrid macro/micro-fiber showed higher R values than mono micro-fibers but lower than mono macro-fibers in the post-peak stage. Notably, 0.66PPL/0.33BF had the highest R value for deflections below 2.0 mm, while 0.66TPPL/0.33PVA dominated above 2.0 mm.

5.4 Summary and conclusion

This study explored the impact of hybrid fiber reinforcement on the cyclic flexural response of fiber-reinforced seawater sea-sand concrete (FR-SWSSC). Five distinct fiber types were employed: micro-PPS, PVA, and BF alongside macro-PPL and TPPL. All fiber types were incorporated at a constant volume fraction of 0.25%. These fibers were incorporated into plain SWSSC in various combinations, including mono-fibers, hybrid micro-fibers, and hybrid micro-macro fiber configurations, to evaluate the synergistic effect of hybridization. The results elucidate the ability of hybrid fibers to improve the cyclic performance of FR-SWSSC. **Figure 5-20** and **Table 5-3** summarize the results of the parameters for all investigated mixtures, highlighting the synergistic effects of fibers in the hybrid systems and offering further clarification of the findings. **Figure 5-20** presents a heatmap of the various parameters analysed, normalized to the maximum value, resulting in a ratio ranging from 0 to 1.0. Based on the experimental observations, the following conclusions can be drawn:

- Micro-fibers enhanced the load-bearing capacity and minimized residual deflection at low deflections and initial cycles, with PPS fibers outperforming others. PPS fibers exhibited significantly higher energy dissipation (71% and 20% compared to BF and PVA) at 1/600th beam deflection, likely due to their micro-crack bridging and elongation capabilities. Conversely, PVA and BF displayed higher hysteretic damping at low deflections due to strong chemical bonds.

- Macro-fibers enhanced post-peak behaviour, particularly during large deflection cycles, by bridging macro-cracks. PPL fibers exhibited significantly superior

performance compared to TPPL fibers, with increases of 82% in cumulative energy dissipation, 99% in flexural strength, and 160% in hysteretic damping. This likely stemmed from the stiffness and mechanical bonding strength of PPL fibers. However, TPPL fibers demonstrated a significant reduction in damage index across all cycles, potentially due to their improved distribution and flexibility.

- Micro-fiber hybridization improved energy dissipation during initial cycles compared to mono-fibers, due to their complementary effects. However, micro/macro-fiber hybridization resulted in a more significant improvement during large deflection cycles, which can be attributed to their synergistic ability to bridge large cracks.

- In PPS/PVA hybrids, a positive synergy was observed, with PVA fibers bridging initial cracks while the lower modulus of PPS facilitated uniform stress distribution, delaying damage, and improving cracking strength. The 0.33PPS/0.66PVA combination performed better, exhibiting a lower damage index at low deflections compared to mono PPS and reduced residual deflection. It also increased the hysteretic damping ratio by 79% and 112% at low deflections, compared to mono PVA and PPS fibers, respectively.

- The 0.66TPPL/0.33PVA hybrid improved deflection recovery and increased cumulative energy dissipation by 105% and 664% over mono TPPL and PVA, respectively. Moreover, 0.33TPPL/0.66PVA improved hysteretic damping by 123% and 656% compared to mono PVA and TPPL, respectively. This improvement resulted from the enhanced bonding of TPPL by PVA, which strengthened the concrete matrix, improved crack bridging, reduced residual deflection, and promoted more elastic behaviour.

- PPL/PVA hybridization indicated that the 0.33PPL/0.66PVA hybrid showed a slight increase in ultimate strength and improved post-peak response compared to 0.66PPL/0.33PVA. Additionally, the 0.33PPL/0.66PVA hybrid provided a 39% increase in energy dissipation at 1/150th beam deflection, a 260% improvement in cumulative energy dissipation, and 10.8 times greater residual flexural strength than mono PVA fibers.

- A lower dosage of BF in a hybrid system with micro- or macro-fibers resulted in superior cyclic performance compared to higher BF content. This improvement was

attributed to the corrosion of BF in SWSSC, which led to increased brittleness. Conversely, incorporating higher dosage of PVA fibers in the hybrid system also led to better cyclic performance, likely due to the high chemical bonding strength of PVA fibers.

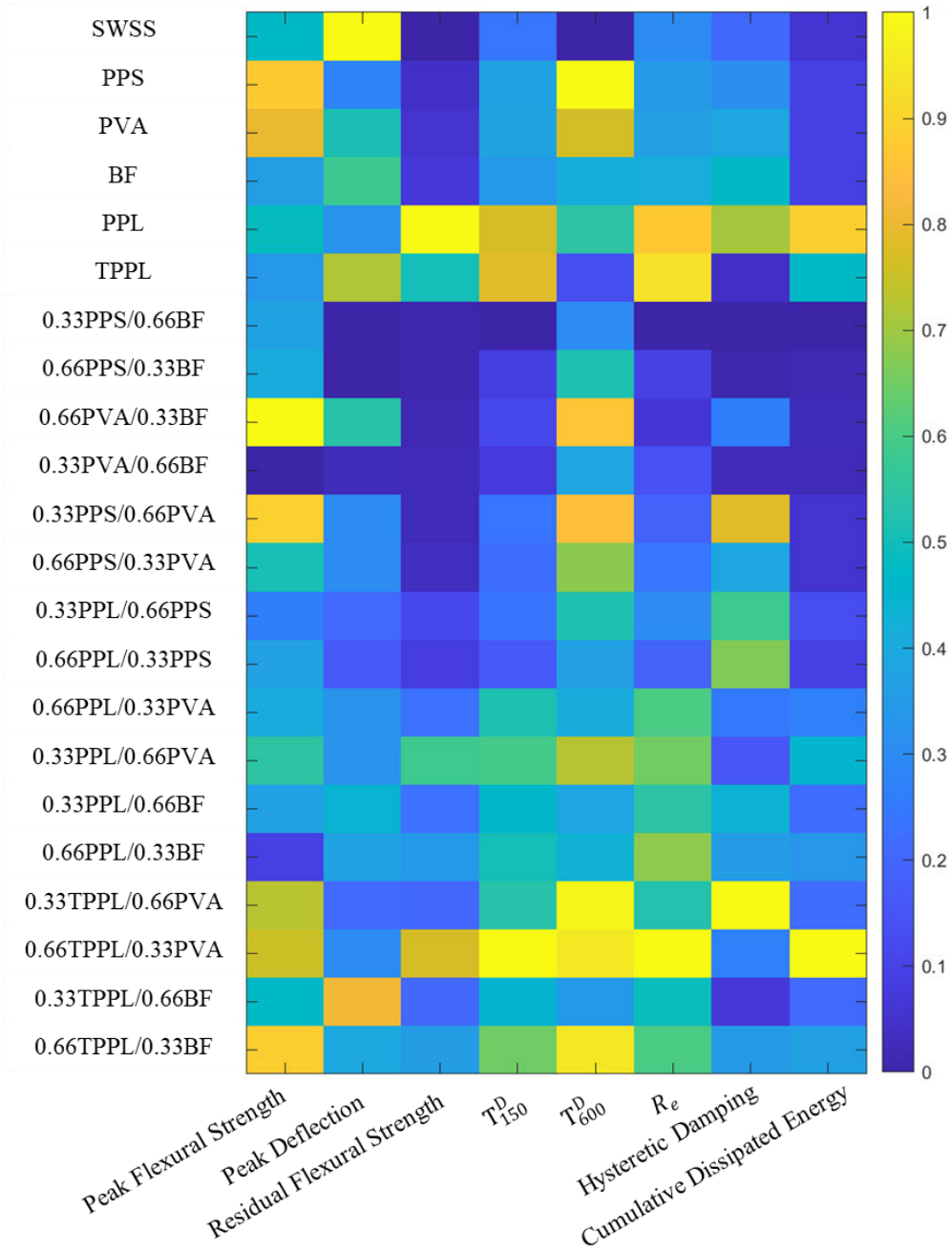


Figure 5-20 Heatmap of all investigated normalized parameters for different hybrid FR-SWSS mixes.

Table 5-3 The synergistic actions of fibers in the hybrid system of FR-SWSSC.

Groups	Hybrid FR-SWSSC mixes	Synergistic actions
Hybrid micro	PPS/PVA	• The synergy between PVA and PPS fibers enhanced bonding, crack prevention, and strength, with uniform stress distribution improving cracking strength. • Lower modulus of PPS promoted uniform stress distribution, delaying damage.
	PPS/BF	• BF incorporation improved the bonding strength of PPS fibers. • Synergistic effect enhanced PPS contribution to bridging micro-cracks at low deflection cycles. • Higher BF dosage had a negative effect, likely due to BF corrosion in SWSSC.
	PVA/BF	• Synergistic effect of PVA/BF improved bonding strength and elastic modulus, resulting in higher strength. • BF enhanced PVA fiber bond strength, enabling full utilization of tensile capacity.
Hybrid macro/micro	PPL/PPS	• PPL fibers effectively hinder crack initiation. • PPL fibers enhanced energy damping during lower cycles.
	PPL/PVA	• Enhanced bonding of PPL fibers was likely due to PVA addition. • Greater dosage of micro-fibers in the hybrid system was more effective. • Synergistic effect, maintained load-bearing capacity during cyclic loading.
	PPL/BF	• The chemical strength of BF improved the bonding strength of PPL fibers by reinforcing its surrounding matrix. • PPL fiber inclusion improved the performance of BF.
	TPPL/PVA	• TPPL fibers bridged macro-cracks; PVA fibers reinforced micro-cracks and improve bond strength of TPPL fibers. • Positive synergy increased the performance of PVA fibers, enhancing flexural strength, reducing damage, lower residual deflection and improving elastic behaviour.
	TPPL/BF	• Higher BF content negatively affected hybrid system performance, likely due to corrosion. • Synergistic effect improved performance through enhanced TPPL fiber bonding. • BF fibers were effective post-peak but reduced ductility.

This study explored the application of fiber hybridization in SWSSC and revealed its potential to enhance cyclic flexural performance. This improvement was attributed to synergistic effects within the hybrid fiber configuration. These findings suggest the suitability of hybrid FR-SWSSC for structures exposed to cyclic loading, such as those in coastal and offshore environments. The use of hybrid fibers improves ductility, energy dissipation, and crack control, resulting in more resilient and sustainable coastal structures. This study emphasizes the significance of understanding fiber interactions in hybrid systems under cyclic loading, offering insights for future design and construction

practices. As such, the findings are a valuable resource for engineers seeking to enhance performance and sustainability in practical applications. However, further research is necessary to fully understand the behaviour of FR-SWSSC under varying load conditions. Additionally, long-term performance and durability in marine environments warrant further evaluation. Overall, the study underscores the promising potential of hybrid fibers for creating more resilient SWSSC structures.

Acknowledgements

Financial support from the University of South Australia is gratefully acknowledged. The authors appreciate the technical expertise of the university's concrete laboratory technicians. We thank Adelaide Brighton Cement Ltd and Independent Cement and Lime Pty Ltd for donating OPC and GGBS, respectively, and TEXO company for their PPS and TPPL fiber donations. Additionally, the valuable instrumentation and expertise of Microscopy Australia at the Future Industries Institute (FII), University of South Australia are acknowledged.

Chapter 5 References

Abbas, YM, Hussain, LA & Khan, MI 2022, 'Constitutive compressive stress–strain behavior of hybrid steel-PVA high-performance fiber-reinforced concrete', Journal of Materials in Civil Engineering, vol. 34, no. 1, p. 04021401.

Abdel-Karim, AH, Khalil, GI, Ewis, AE & Makhlouf, MH 2023, 'Impact of developed hybrid polypropylene fiber inclusion on the flexural performance of concrete beams reinforced with innovative hybrid bars', Construction and Building Materials, vol. 409, p. 134113.

Ahmad, J, González-Lezcano, RA, Majdi, A, Ben Kahla, N, Deifalla, AF & El-Shorbagy, MA 2022, 'Glass fibers reinforced concrete: Overview on mechanical, durability and microstructure analysis', Materials, vol. 15, no. 15, p. 5111.

Ahmed, SFU & Mihashi, H 2011, 'Strain hardening behavior of lightweight hybrid polyvinyl alcohol (PVA) fiber reinforced cement composites', Materials and structures, vol. 44, no. 6, pp. 1179-91.

Ahmed, W & Lim, C 2023, 'Multicriteria performance assessment of sustainable recycled concrete produced via hybrid usage of basalt, polypropylene and glass fiber', Construction and Building Materials, vol. 397, p. 132462.

Alani, AM & Beckett, D 2013, 'Mechanical properties of a large scale synthetic fibre reinforced concrete ground slab', Construction and Building Materials, vol. 41, pp. 335-44.

Astm, C 2007, '1609', Standard test method for flexural performance of fiber-reinforced concrete (using beam with third-point loading), vol. 4.

Australia, S 1994, Methods of testing concrete-Preparation of concrete mixes in the laboratory, AS.

Australia, S 2000, 'Methods of testing concrete-Method 11: Determination of the modulus of rupture (AS 1012.11)', Sydney, NSW: Standards Australia.

Boulekbache, B, Hamrat, M, Chemrouk, M & Amziane, S 2016, 'Flexural behaviour of steel fibre-reinforced concrete under cyclic loading', Construction and Building Materials, vol. 126, pp. 253-62.

CAO, X-q, ZHANG, Y, HE, Y-j, JIANG, Y-c & YUAN, X-j 2008, 'Retrospect and discussion of surveys for construction sand in China offshore area', Marine Geology & Quaternary Geology, vol. 28, no. 3, pp. 121-25.

Çelik, Z & Bingöl, AF 2020, 'Fracture properties and impact resistance of self-compacting fiber reinforced concrete (SCFRC)', Materials and structures, vol. 53, no. 3, pp. 1-16.

Chenggong, Z, Zhiyuan, W, Zhenyu, Z, Qiuyu, G, Xinrui, W & Renda, Z 2023, 'Research on different types of fiber reinforced concrete in recent years: An overview', Construction and Building Materials, vol. 365, p. 130075.

de Alencar Monteiro, VM, Lima, LR & de Andrade Silva, F 2018, 'On the mechanical behavior of polypropylene, steel and hybrid fiber reinforced self-consolidating concrete', Construction and Building Materials, vol. 188, pp. 280-91.

De Smedt, M, Vrijdaghs, R, Van Steen, C, Verstrynge, E & Vandewalle, L 2020, 'Damage analysis in steel fibre reinforced concrete under monotonic and cyclic bending by means of acoustic emission monitoring', Cement and Concrete Composites, vol. 114, p. 103765.

de Souza Castoldi, R, de Souza, LMS & de Andrade Silva, F 2019, 'Comparative study on the mechanical behavior and durability of polypropylene and sisal fiber reinforced concretes', Construction and Building Materials, vol. 211, pp. 617-28.

Decision, C 2003, 'Council Decision 2003/33/EC of 19 December 2002 establishing criteria and procedures for the acceptance of waste at landfills pursuant to Article 16 and Annex II to Directive 1999/31/EC', Official Journal of the European Communities, vol. 16, no. 2003, pp. 27-49.

Deng, F, Ding, X, Chi, Y, Xu, L & Wang, L 2018, 'The pull-out behavior of straight and hooked-end steel fiber from hybrid fiber reinforced cementitious composite: Experimental study and analytical modelling', Composite Structures, vol. 206, pp. 693-712.

Dhondy, T, Remennikov, A & Shiekh, MN 2019, 'Benefits of using sea sand and seawater in concrete: a comprehensive review', Australian Journal of Structural Engineering, vol. 20, no. 4, pp. 280-89.

Du, X, Li, Y, Si, Z, Huang, L & Chen, X 2022, 'Effects of basalt fiber and polyvinyl alcohol fiber on the properties of recycled aggregate concrete and optimization of fiber contents', Construction and Building Materials, vol. 340, p. 127646.

Etxeberria, M, Fernandez, JM & Limeira, J 2016a, 'Secondary aggregates and seawater employment for sustainable concrete dyke blocks production: Case study', Construction and Building Materials, vol. 113, pp. 586-95.

Etxeberria, M, Gonzalez-Corominas, A & Pardo, P 2016b, 'Influence of seawater and blast furnace cement employment on recycled aggregate concretes' properties', Construction and Building Materials, vol. 115, pp. 496-505.

Fattah, KP, Al-Tamimi, AK, Hamweyah, W & Iqbal, F 2017, 'Evaluation of sustainable concrete produced with desalinated reject brine', International Journal of Sustainable Built Environment, vol. 6, no. 1, pp. 183-90.

Feng, J, Su, Y & Qian, C 2019, 'Coupled effect of PP fiber, PVA fiber and bacteria on self-healing efficiency of early-age cracks in concrete', Construction and Building Materials, vol. 228, p. 116810.

Feng, J, Jia, X, Dong, X, Wang, P, Xu, B & Wang, Z 2023, 'Cyclic compressive behavior of hook-end steel and macro-polypropylene hybrid fiber reinforced recycled aggregate concrete', Case Studies in Construction Materials, vol. 19, p. e02310.

Gaddafi, AKF, Alengaram, UJ, Bunnori, NM, Muhammad, SI, Ibrahim, S & Sumesh, M 2023, 'Mechanical properties, flexural behaviour, and ductility characteristics of fibre-reinforced geopolymer mortar', Construction and Building Materials, vol. 403, p. 133109.

Gu, L, Liu, Y, Zeng, J, Zhang, Z, Pham, PN, Liu, C & Zhuge, Y 2024, 'The synergistic effects of fibres on mechanical properties of recycled aggregate concrete: A comprehensive review', Construction and Building Materials, vol. 436, p. 137011.

Guo, M, Hu, B, Xing, F, Zhou, X, Sun, M, Sui, L & Zhou, Y 2020, 'Characterization of the mechanical properties of eco-friendly concrete made with untreated sea sand and

seawater based on statistical analysis', Construction and Building Materials, vol. 234, p. 117339.

Hassanli, R, Manalo, A, Vafaei, D, Yekrangnia, M, Elchalakani, M & Noël, M 2023, 'Cyclic behavior of GFRP-reinforced concrete one-way slabs with synthetic fibers', Journal of Building Engineering, vol. 65, p. 105741.

Hsie, M, Tu, C & Song, P 2008, 'Mechanical properties of polypropylene hybrid fiber-reinforced concrete', Materials Science and Engineering: A, vol. 494, no. 1-2, pp. 153-57.

Kai, C, Lihua, X, Tao, T, Le, H, Jian, L, Jian, H, Huan, L & Yin, C 2023, 'Mechanical behavior of multiscale hybrid fiber reinforced recycled aggregate concrete subject to uniaxial compression', Journal of Building Engineering, vol. 71, p. 106504.

Kaidi, J, Xin, W, Lining, D, Zhiyuan, C, Huang, H, Xia, L, Jianxun, L & Zhishen, W 2023, 'Mechanical properties of multi-scale mono/hybrid non-metallic fiber-reinforced ultra-high performance seawater sea-sand concrete', Construction and Building Materials, vol. 401, p. 132922.

Katano, K, Takeda, N, Ishizeki, Y & Iriya, K 2013, Properties and application of concrete made with sea water and un-washed sea sand, Proceedings of Third International conference on Sustainable Construction Materials and Technologies.

Lee, J-H, Cho, B & Choi, E 2017, 'Flexural capacity of fiber reinforced concrete with a consideration of concrete strength and fiber content', Construction and Building Materials, vol. 138, pp. 222-31.

Lee, J-H, Cho, B, Kim, J-B, Lee, K-J & Jung, C-Y 2018a, 'Shear capacity of cast-in headed anchors in steel fiber-reinforced concrete', Engineering Structures, vol. 171, pp. 421-32.

Lee, J-H, Lee, K-J & Choi, E 2018b, 'Flexural capacity and crack-closing performance of NiTi and NiTiNb shape-memory alloy fibers randomly distributed in mortar beams', Composites Part B: Engineering, vol. 153, pp. 264-76.

Li, M, Xing, D, Zheng, Q-B, Li, H, Hao, B & Ma, P-C 2022, 'Variation on the morphology and tensile strength of basalt fiber processed in alkali solutions', Construction and Building Materials, vol. 335, p. 127512.

Li, P, Li, W, Sun, Z, Shen, L & Sheng, D 2021, 'Development of sustainable concrete incorporating seawater: A critical review on cement hydration, microstructure and mechanical strength', Cement and Concrete Composites, vol. 121, p. 104100.

Li, Y, Zhang, J, He, Y, Huang, G, Li, J, Niu, Z & Gao, B 2022, 'A review on durability of basalt fiber reinforced concrete', Composites Science and Technology, vol. 225, p. 109519.

Li, Y, Liu, W, Mi, T, Ding, X, Tang, L & Xing, F 2024, 'Durability study of seawater and sea-sand concrete under the combined effects of carbonation and chloride redistribution', Journal of Building Engineering, p. 109294.

Ling, Y, Zhang, P, Wang, J & Chen, Y 2019, 'Effect of PVA fiber on mechanical properties of cementitious composite with and without nano-SiO2', Construction and Building Materials, vol. 229, p. 117068.

Lothenbach, B, Scrivener, K & Hooton, R 2011, 'Supplementary cementitious materials', Cement and concrete Research, vol. 41, no. 12, pp. 1244-56.

Ma, J, Yuan, H, Zhang, J & Zhang, P 2024, Enhancing concrete performance: A comprehensive review of hybrid fiber reinforced concrete, Structures.

Mashayekhi, A, Hassanli, R, Zhuge, Y, Ma, X & Chow, CW 2024a, 'Synergistic effects of fiber hybridization on the mechanical performance of seawater sea-sand concrete', Construction and Building Materials, vol. 416, p. 135087.

Mashayekhi, A, Hassanli, R, Zhuge, Y, Ma, X, Chow, CW, Bazli, M & Manalo, A 2024b, 'Synergistic Effects of Fiber Hybridization on the Fracture Toughness of Seawater Sea-Sand Concrete', Construction and Building Materials.

Mashayekhi, A, Hassanli, R, Zhuge, Y, Ma, X, Chow, CW, Bazli, M & Manalo, A 2024c, 'Synergistic effects of fiber hybridization on the fracture toughness of seawater sea-sand concrete', Construction and Building Materials, vol. 444, p. 137845.

Mehran, K, Mingli, C, Chaopeng, X & Majid, A 2022, 'Effectiveness of hybrid steel-basalt fiber reinforced concrete under compression', Case Studies in Construction Materials, vol. 16, p. e00941.

Meng, K, Xu, L & Chi, Y 2021, 'Experimental investigation on the mechanical behavior of hybrid steel-polypropylene fiber reinforced concrete under conventional triaxial cyclic compression', Construction and Building Materials, vol. 291, p. 123262.

Miller, SA, Horvath, A & Monteiro, PJ 2018, 'Impacts of booming concrete production on water resources worldwide', Nature Sustainability, vol. 1, no. 1, pp. 69-76.

Min, W-l, Jin, W-l, He, X-y, Wu, R-j, Chen, K-y, Chen, J-j & Xia, J 2024, 'Experimental study on the flexural fatigue performance of slag/fly ash geopolymer concrete reinforced with modified basalt and PVA hybrid fibers', Journal of Building Engineering, p. 109917.

Nguyen, D-L, Thai, D-K & Lam, MN-T 2022, 'Synergy in Flexure of High-Performance Fiber-Reinforced Concrete with Hybrid Steel Fibers', Journal of Materials in Civil Engineering, vol. 34, no. 6, p. 04022090.

Oyguc, R, Toros, C & Abdelnaby, AE 2018, 'Seismic behavior of irregular reinforced-concrete structures under multiple earthquake excitations', Soil Dynamics and Earthquake Engineering, vol. 104, pp. 15-32.

Özkan, Ş & Demir, F 2020, 'The hybrid effects of PVA fiber and basalt fiber on mechanical performance of cost effective hybrid cementitious composites', Construction and Building Materials, vol. 263, p. 120564.

Pakravan, H, Jamshidi, M & Latifi, M 2018, 'The effect of hydrophilic (polyvinyl alcohol) fiber content on the flexural behavior of engineered cementitious composites (ECC)', The Journal of The Textile Institute, vol. 109, no. 1, pp. 79-84.

Park, R & Paulay, T 1991, Reinforced concrete structures, John Wiley & Sons,

Ríos, J, Cifuentes, H, Leiva, C, Ariza, M & Ortiz, M 2020, 'Effect of polypropylene fibers on the fracture behavior of heated ultra-high performance concrete', International Journal of Fracture, vol. 223, no. 1, pp. 173-87.

Rostami, R, Zarrebini, M, Mandegari, M, Mostofinejad, D & Abtahi, SM 2020, 'A review on performance of polyester fibers in alkaline and cementitious composites environments', Construction and Building Materials, vol. 241, p. 117998.

SF, J 1984, 'Method of test for flexural strength and flexural toughness of fiber reinforced concrete', Japan Concrete Institute.

Sherif, MM, Khakimova, EM, Tanks, J & Ozbulut, OE 2018, 'Cyclic flexural behavior of hybrid SMA/steel fiber reinforced concrete analyzed by optical and acoustic techniques', Composite Structures, vol. 201, pp. 248-60.

Shoaib, A & Lubell, AS 2021, 'Effect of mix composition on the mechanical properties of SFRC', Construction and Building Materials, vol. 286, p. 122760.

Slowey, K 2018, 'Report: Global construction waste will almost double by 2025', Construction Dive.

Society, C 2003, Concrete industrial ground floors: A guide to design and construction, Concrete Society,

Şükrü, Ö & Ömer, Ç 2021, 'The hybrid effects of basalt and PVA fiber on properties of a cementitious composite: Physical properties and non-destructive tests', Construction and Building Materials, vol. 312, p. 125292.

Ting, MZY, Wong, KS, Rahman, ME & Selowara Joo, M 2020, 'Mechanical and durability performance of marine sand and seawater concrete incorporating silicomanganese slag as coarse aggregate', Construction and Building Materials, vol. 254, 2020/09/10/, p. 119195.

Tjaronge, MW & Irfan, UR 2015, 'Porosity, pore size and compressive strength of self compacting concrete using sea water', Procedia Engineering, vol. 125, pp. 832-37.

Vafaei, D, Hassanli, R, Ma, X, Duan, J & Zhuge, Y 2021, 'Sorptivity and mechanical properties of fiber-reinforced concrete made with seawater and dredged sea-sand', Construction and Building Materials, vol. 270, p. 121436.

Vafaei, D, Hassanli, R, Ma, X, Duan, J & Zhuge, Y 2022a, 'Fracture Toughness and Impact Resistance of Fiber-Reinforced Seawater Sea-Sand Concrete', Journal of Materials in Civil Engineering, vol. 34, no. 5, p. 04022038.

Vafaei, D, Ma, X, Hassanli, R, Duan, J & Zhuge, Y 2022b, 'Microstructural behaviour and shrinkage properties of high-strength fiber-reinforced seawater sea-sand concrete', Construction and Building Materials, vol. 320, p. 126222.

Vairagade, VS & Dhale, SA 2023, 'Hybrid fibre reinforced concrete–a state of the art review', Hybrid Advances, vol. 3, p. 100035.

Wang, C, Wu, H & Li, C 2022, 'Hysteresis and damping properties of steel and polypropylene fiber reinforced recycled aggregate concrete under uniaxial low-cycle loadings', Construction and Building Materials, vol. 319, p. 126191.

Wang, D, Ju, Y, Shen, H & Xu, L 2019, 'Mechanical properties of high performance concrete reinforced with basalt fiber and polypropylene fiber', Construction and Building Materials, vol. 197, pp. 464-73.

Wang, J, Liu, E & Li, L 2018, 'Multiscale investigations on hydration mechanisms in seawater OPC paste', Construction and Building Materials, vol. 191, pp. 891-903.

Wang, Q, Ding, Y & Randl, N 2021, 'Investigation on the alkali resistance of basalt fiber and its textile in different alkaline environments', Construction and Building Materials, vol. 272, p. 121670.

Wang, S, Xu, L, Chi, Y, Cui, K, Yin, C & Li, B 2023, 'Cyclic tensile behavior of ultra-high performance concrete with hybrid steel-polypropylene fiber: Experimental study and analytical model', Composite Structures, vol. 321, p. 117255.

Wei, J, Farzadnia, N & Khayat, KH 2024, 'Synergistic effect of macro synthetic fiber and shrinkage-reducing admixture on engineering properties of fiber-reinforced super-workable concrete', Construction and Building Materials, vol. 414, p. 134566.

Won, J-P, Jang, C-I, Lee, S-W, Lee, S-J & Kim, H-Y 2010, 'Long-term performance of recycled PET fibre-reinforced cement composites', Construction and Building Materials, vol. 24, no. 5, pp. 660-65.

Wu, H, Zhu, Z, Chen, Y, Li, H & Jiang, W 2023, 'Mechanical properties of short polypropylene fiber enhanced recycled concrete under cyclic compression', Structural Concrete, vol. 24, no. 4, pp. 4751-66.

Xiao, J, Qiang, C, Nanni, A & Zhang, K 2017, 'Use of sea-sand and seawater in concrete construction: Current status and future opportunities', Construction and Building Materials, vol. 155, pp. 1101-11.

Xie, F, Cai, D, Ji, L, Zhang, C & Ruan, J 2021, 'Experimental study on the mechanical properties of internally cured concrete with super absorbent polymer under monotonic and cyclic loads', Construction and Building Materials, vol. 270, p. 121495.

Xiong, Z, He, S, Kwan, A, Li, L & Zeng, Y 2021, 'Compressive behaviour of seawater sea-sand concrete containing glass fibres and expansive agents', Construction and Building Materials, vol. 292, p. 123309.

Yang, K-H, Jung, Y-B, Cho, M-S & Tae, S-H 2015, 'Effect of supplementary cementitious materials on reduction of CO2 emissions from concrete', Journal of Cleaner Production, vol. 103, pp. 774-83.

Yang, S, Zang, C, Xu, J & Fan, G 2020, 'Determination of Fracture Parameters of Seawater Sea Sand Concrete Based on Maximum Fracture Load', Journal of Materials in Civil Engineering, vol. 32, no. 1, p. 04019315.

Yang, Z, Zhan, X, Zhu, H, Zhang, B, Feng, P, Li, H & Kua, HW 2023, 'Performance-based alkali-activated seawater sea-sand concrete: Mixture optimization for mechanical, environmental, and economical objectives', Construction and Building Materials, vol. 409, p. 134156.

Younis, A, Ebead, U, Suraneni, P & Nanni, A 2018, 'Fresh and hardened properties of seawater-mixed concrete', Construction and Building Materials, vol. 190, pp. 276-86.

Yu, Y, Fang, G-H, Kurda, R, Sabuj, AR & Zhao, X-Y 2024a, 'An agile, intelligent and scalable framework for mix design optimization of green concrete incorporating recycled aggregates from precast rejects', Case Studies in Construction Materials, vol. 20, p. e03156.

Yu, Y, Zhou, L & Lin, L 2024b, 'Compressive stress–strain relationship and its variability of basalt fiber reinforced recycled aggregate concrete', AIP Advances, vol. 14, no. 7.

Zeng, L, Liang, X, Lu, H, Liu, S, Yuan, H & Mohamed, HS 2024, 'Compressive behavior of seawater and sea sand concrete-filled FRP-steel composite multi-tube hollow columns', Construction and Building Materials, vol. 438, p. 137133.

Zhang, ZH, Sang, ZQ, Zhang, LY, Ma, ZX & Zhang, Y 2013, Experimental research on durability of concrete made by seawater and sea-sand, Advanced Materials Research.

Zheng, Z & Feldman, D 1995, 'Synthetic fibre-reinforced concrete', Progress in Polymer Science, vol. 20, no. 2, pp. 185-210.

6 Shear performance of fibre reinforced seawater sea-sand concrete - fibre hybridization and synergy effects

Submitted for Publication:

Mashayekhi, A, Hassanli, R, Zhuge, Y, Ma, X, Chow, CW, Bazli, M & Manalo, A 'Fiber Hybridization and Synergy Effects on the Shear Performance of Seawater Sea-Sand Concrete', Available at SSRN 5036578.

Abstract

The shear performance of fiber-reinforced seawater sea-sand concrete (FR-SWSSC), a potential sustainable alternative to traditional concrete, requires comprehensive analysis of its shear behaviour to facilitate its integration into structural design practices. This study investigated the synergistic effects of fiber hybridization and its potential synergistic effects on the shear performance of SWSSC. Micro-fibers—basalt fibers (BF), polyvinyl alcohol (PVA), and short polypropylene (PPS)—and macro-fibers—twisted polypropylene (TPPL) and long polypropylene (PPL)—were utilized to explore the combined influence of fiber size and type. A modified shear test method, supported by experimental analysis and finite element modeling, was developed for improved accuracy. The results demonstrated a positive synergistic effect of PVA-based hybrids over mono-fibers. The PPL/PVA hybrid increased shear strength by 28% and 23% and shear toughness by 159% and 46% compared to mono PVA and PPL fibers, respectively. The high chemical bonding strength of PVA fibers improved concrete interlocking and reinforced the bonding of macro-fibers, contributing to this positive synergy. The TPPL/PVA hybrid also enhanced shear performance compared to plain SWSSC, making it the most effective hybrid system in this study. Moreover, the PVA/BF hybrid increased shear strength by 14%–24% and 6%–16% compared to mono PVA and BF fibers, respectively. These findings highlight fiber hybridization as a viable approach to improving the shear performance of SWSSC, addressing a key knowledge gap, and promoting its structural application.

Keywords

Shear strength, Shear toughness, Seawater, Sea-sand, Fiber-reinforced concrete, Hybrid fiber, Fiber synergy.

6.1 Introduction

The production of conventional concrete poses substantial environmental challenges, predominantly attributed to the extensive utilization of freshwater, natural sand, and cement. Annually, concrete production demands approximately 65.7 km³ of freshwater (Miller *et al.* 2018), thereby intensifying water scarcity in numerous regions already experiencing a burgeoning crisis (Huns 2020). Additionally, extensive sand mining contributes to ecological degradation, including the destruction of habitats (Vafaei *et al.* 2022a; Vafaei *et al.* 2022c). Excessive river sand extraction has led to significant depletion of sand resources and severe disruption of river ecosystems, causing long-term ecological damage (Soundarya 2022). Furthermore, cement production is a major contributor to global carbon dioxide emissions, accounting for 36% of emissions from the construction industry (Bajželj *et al.* 2013), thus significantly accelerating climate change. Additionally, the projected demand for aggregates expected to rise to 144.8 billion tons by 2030 (Xiong, Zhe *et al.* 2021). In addressing these concerns, seawater sea-sand (SWSS) concrete demonstrates significant potential for coastal construction, particularly in resource-scarce regions and remote areas where natural resources are not readily accessible. SWSS concrete utilizes readily available seawater and sea-sand as alternatives to freshwater and natural sand, thereby markedly reducing the environmental impacts associated with material procurement (Younis *et al.* 2018; Zhao *et al.* 2021). By mitigating resource limitations and enhancing sustainability, SWSS concrete emerges as a promising alternative for the development of coastal and offshore structures. SWSS concrete typically exhibits superior early-age compressive strength compared to conventional concrete, due to accelerated hydration induced by chloride ions in seawater and sea-sand (Vafaei *et al.* 2021a; Mashayekhi *et al.* 2024a). To address durability issues, the substitution of steel reinforcement with fiber-reinforced polymer (FRP) bars is often adopted, effectively eliminating the risk of steel corrosion in SWSS concrete (Chen *et al.* 2022; Zeng *et al.* 2022; Zhihao *et al.* 2022; Hassanli *et al.* 2023; Vafaei *et al.* 2023; Mashayekhi *et al.* 2024e; Amirhesam *et al.* 2025).

Ground Granulated Blast Furnace Slag (GGBS), an industrial by-product, is widely utilized as a supplementary cementitious material (SCM) to enhance the properties of SWSS concrete (Shi *et al.* 2015; Younis *et al.* 2018). While elevated salt concentrations and harmful ions in SWSS concrete could potentially compromise durability, the integration of SCMs like GGBS effectively mitigates these challenges, enhancing both

durability and mechanical performance (Li *et al.* 2015; Zhao *et al.* 2021). By reducing the tricalcium aluminate (C_3A) content in cement, GGBS functions as an alkali diluter, effectively lowering alkali levels (Hobbs 1982; Kwon 2005; Zhang *et al.* 2013). It also mitigates expansion caused by sulphate attacks and alkali-aggregate reactions by consuming calcium hydroxide through secondary hydration, preventing ettringite formation and improving concrete durability (Bai 2009; Vafaei *et al.* 2021a). Beyond durability, GGBS improves properties such as workability, chloride binding, seawater resistance (Wang *et al.* 2020), and long-term compressive strength (Wang *et al.* 2024), all while substantially decreasing CO_2 emissions (Lothenbach *et al.* 2011). Moreover, it demonstrates superior performance over conventional concrete with minimal impact on early-age and long-term compressive strength (Etxeberria *et al.* 2016b; Fattah *et al.* 2017).

The reinforcement of SWSS concrete with fibers, such as polypropylene (PP), basalt, or polyvinyl alcohol (PVA) fibers, substantially improves its mechanical characteristics, including fracture toughness, impact resistance, and ductility (Vafaei *et al.* 2022a; Mashayekhi *et al.* 2024d). For example, PP fibers contributed to increased ductility and residual strength of SWSS concrete, whereas PVA fibers enhanced pre-cracking properties, such as flexural strength, due to their chemical interaction with cementitious products (Vafaei *et al.* 2022a). This improvement in mechanical behaviour is particularly beneficial when combined with the use of FRP bars for SWSS concrete applications in marine and coastal infrastructure, where the material must withstand severe environmental conditions and sustained loading. Mono fibers, whether micro or macro, exhibit intrinsic limitations such as poor crack control, low tensile strength, limited toughness, and insufficient bonding with the concrete matrix (Vairagade *et al.* 2023; Mashayekhi *et al.* 2024a). Utilizing hybrid fibers in concrete is significant as they provide enhanced mechanical properties while addressing the limitations inherent in the use of mono fibers (Mohammadi *et al.* 2008; Mashayekhi *et al.* 2024a; Mashayekhi *et al.* 2024c, 2024d). The combination of various types of micro- and macro-fibers showed a synergistic effect that enhanced several mechanical properties including compressive strength, flexural strength, and the toughness of ultra-high-performance SWSS concrete (Kaidi *et al.* 2023). Furthermore, the incorporation of hybrid fibers in SWSS concrete showed that micro-fibers, such as PP and PVA, effectively controlled small cracks and ensured interfacial bonding, whereas macro-fibers, such as twisted polypropylene (TPPL) or long polypropylene (PPL), contributed to enhancing post-crack resistance

(Mashayekhi *et al.* 2024c, 2024d). This synergistic interaction facilitated improved crack bridging and more effective load distribution, thereby improving both energy absorption capacity and fracture toughness of SWSS concrete under monotonic and cyclic loading conditions (Mashayekhi *et al.* 2024c, 2024d). Although substantial research has focused on the impact of fibers on the mechanical properties of SWSS concrete, their impact on the shear strength of SWSS concrete remains unexplored.

Several investigations have highlighted the positive impact of fiber addition on increasing the shear strength of concrete. Most research primarily focused on steel fibers, showing improvements in shear strength and toughness (Boulekbache *et al.* 2012; Khanlou *et al.* 2012; Soetens *et al.* 2017; Simalti *et al.* 2020; Picazo *et al.* 2021). Steel fibers, depending on their geometric shape and quantity, were able to prevent diagonal tension failure (Jindal 1984; Jindal *et al.* 1987). Replacing vertical stirrups with different steel fibers effectively resisted shear failure, while increasing fiber content also reduced the shear span ratio (Batson *et al.* 1972). Previous studies have indicated that the incorporation of steel fibers at an appropriate dosage can lead to an increase in shear strength, by up to 65% (Boulekbache *et al.* 2012; Alimrani *et al.* 2023). Also, previous studies confirmed that fiber type and volume highly affected shear strength and toughness (González-Aviña *et al.* 2022), enhancing aggregate interlock, and thereby improving shear transfer (Cuenca *et al.* 2020). Adding 1%-vol of steel fibers led to a 229% increase in shear strength compared to plain concrete, while synthetic fibers with the same volume fraction enhanced shear strength by 27% (Charron *et al.* 2020). Hybrid PP and steel fibers improved shear strength by up to 58.9% compared to plain concrete (Alimrani *et al.* 2023). Additionally, incorporating steel and basalt fibers enhanced direct shear strength, shear toughness, and residual shear load (Li *et al.* 2017). The direct shear strength of ceramic concrete increased with glass fiber dosage, regardless of mix composition or fiber length (Tassew *et al.* 2014). However, incorporating up to 1% recycled polyvinyl chloride (PVC) fibers led to a 25.6% reduction in shear strength, likely due to the weak bond between the PVC fibers and the concrete matrix (Kurup *et al.* 2017). Hybrid macro-micro synthetic fibers improved shear strength by 24-44% compared to control specimens (Zainal *et al.* 2020). Navas et al. (Navas *et al.* 2018) and Zhang et al. (Zhang *et al.* 2014) confirmed the effectiveness of PP fibers as shear capacity and transfer mechanisms. Similar shear capacity improvements were observed with various fibers, including PP, PVA, and polyethylene (Jongvivatsakul *et al.* 2013).

Previous research has extensively explored the mechanical properties of fiber-reinforced seawater sea-sand concrete (FR-SWSSC), establishing its potential as an environmentally friendly construction material (Vafaei *et al.* 2021a, 2022a; Vafaei *et al.* 2022c, 2022b; Mashayekhi *et al.* 2024a; Mashayekhi *et al.* 2024c, 2024d; Yang *et al.* 2024a). While considerable attention has been given to compressive strength, tensile strength, and fracture toughness, a significant gap persists in understanding its shear strength—a critical property for structural stability and the prevention of sudden brittle failures. Moreover, the elevated levels of ions, such as sodium, potassium, chloride, sulphate, calcium, and magnesium, inherent in SWSS concrete present unique challenges—compared to traditional concrete (Vafaei *et al.* 2021a), particularly concerning their interaction with fibers in enhancing shear performance. Another significant limitation is the absence of a standardized testing method capable of isolating the shear strength of concrete without interference from tensile or flexural contributions, a concern highlighted in previous studies (Blanco *et al.* 2017; Tonon 2021). Existing methods often fail to provide pure shear strength measurements, which are essential for accurate assessment. To address this, the current study introduces a modified shear testing method based on the JSCE-SF6, adapted to align with Australian standards for greater applicability.

This research investigates the influence of hybrid fibers, combining micro- and macro-fibers of different types and sizes, on the direct shear strength of FR-SWSSC. By comparing the performance of hybrid fiber-reinforced mixes against mono-fiber alternatives, this study aims to bridge the gap in understanding the synergistic effects of fiber hybridization on shear performance. Through experimental investigations and finite element modelling, this work contributes to the development of a reliable shear test methodology and advances the knowledge of FR-SWSSC, supporting its application in sustainable coastal and offshore construction.

6.2 Experimental program

6.2.1 Materials

In this study, ordinary Portland cement (OPC) and ground granulated blast furnace slag (GGBS) were utilized as cementitious binders, comprising 35% OPC and 65% GGBS. Cement production significantly contributes to CO_2 emissions, and replacing 65% of cement with GGBS, a by-product of iron and steel production, has been shown to reduce emissions by approximately 50% (Yang *et al.* 2020). **Table 6-1** compares their chemical

compositions, showing that GGBS contains more silica, alumina, and magnesia, but less lime than OPC. Both materials mainly consist of SiO_2, Al_2O_3, Fe_2O_3, CaO, and MgO (Vafaei *et al.* 2021a). Seawater was collected from Adelaide, South Australia, and stored in a sealed container to prevent evaporation and contamination. Potable water from Adelaide's supply network was also used for conventional concrete. Ion Chromatography (IC) analysis showed that seawater contained chloride and sulphate concentrations of 19,810 mg/L and 2,824 mg/L, respectively, which were higher than those in tap water (Vafaei *et al.* 2021a). The coarse aggregate, consisting of crushed basalt (maximum size 14 mm), was obtained from South Australian quarries, while natural sand (NS) with a nominal size of 2.5 mm was used as fine aggregate. Additionally, sea sand, collected from Semaphore Beach, had uniform particles mostly below 0.5 mm. The physical characteristics of coarse and fine aggregates, including normal sand, and sea-sand are presented in **Table 6-2**. The sieve analysis results for the aggregates are presented in **Figure 6-1**.

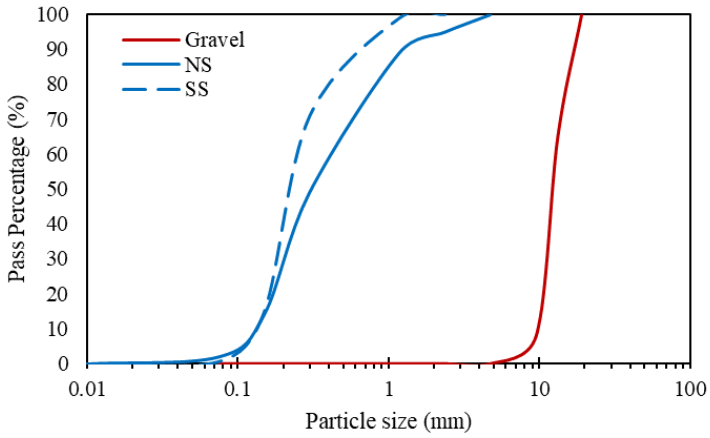


Figure 6-1 The sieve analysis of the aggregates.

Table 6-1 Chemical compositions of OPC and GGBS (Vafaei et al. 2022a).

	Chemical Compositions (%)								
Cementitious materials	CaO	SiO_2	Al_2O_3	Fe_2O_3	MgO	SO_3	K_2O	Cl	Na_2O
OPC	63.5	20.5	4.8	3.1	1.8	2.6	0.54	0.03	0.5
GGBS	42.70	33.01	13.05	0.36	5.91	2.03	—	0.00	—

Table 6-2 Physical properties of coarse and fine aggregates (Mashayekhi et al. 2024d).

Material	Bulk Density (kg/m^3)	Specific Gravity (kg/m^3)	Fineness Modulus
Gravel	1560	2.71	6.92
NS	1628	2.66	1.97

SS	1578	2.57	1.38

Elemental concentrations in sand (SS, NS) and water (SW, FW) were analysed using Inductively Coupled Plasma Optical Emission Spectroscopy (ICP-OES) after leaching with a solution. The results are summarized in **Table 6-3**. To assess the concentration of heavy metals, regulatory limits were referenced based on European standards for landfill (Decision 2003) and Australian standards for drinking water (Guidelines Version 3.8 Updated September 2022) in the case of SW. The results showed that the concentrations of lead (Pb) and selenium (Se) were found to be substantially higher in SS compared to NS. Sea-sand contained Pb and Se at concentrations of 1.05 mg/kg and 2.80 mg/kg, respectively, compared to 0.08 mg/kg and 0.17 mg/kg in normal sand. All observed concentrations were below the hazardous limits set by European standards for landfill, as detailed in **Table 6-3**.

In this study, SWSS concrete was reinforced using a combination of synthetic fibers—PVA, BF, and PP as a natural fiber. The properties of these fibers are summarized in **Table 6-4**. To investigate the effects of fiber hybridization, both micro-fibers (PPS, PVA, BF) and macro-fibers (PPL, TPPL) were utilized. The fibers were used in their untreated forms to keep manufacturing costs low. Notably, the PPL fiber employed in this study is eco-friendly, being entirely derived from recycled plastic. The polypropylene and polyvinyl alcohol fibers used in this research are readily available in the Australian market and are resistant to alkaline and corrosive environments, making them well-suited for application in SWSS concrete. Furthermore, these fibers are more cost-effective compared to other commercially available options such as polyethylene, glass, and carbon fibers.

Table 6-3 Concentration of elements determined from ICP-OES test.

Elements	Concentration of elements in leachate			Regulatory limit (mg/Kg) According to European Council directive			Regulatory limit by Australian Standard for Drinking Water (mg/L)
	Sea-sand (mg/Kg)	Normal Sand (mg/Kg)	Sea Water (mg/L)	Inert	Non-hazardous	Hazardous	
As	0.83	0.46	0.112	0.80	2.00	25.00	0.010
Cd	0.89	0.89	0.449	0.04	1.00	5.00	0.002
Cr	0.075	0.01	0.012	0.50	10.00	70.00	0.050
Cu	0.28	0.24	0.551	2.00	50.00	100.00	2.000
Hg	0.22	0.22	0.115	0.01	0.20	2.00	0.001
Mo	0.074	0.13	0.020	0.50	10.00	30.00	0.050

Ni	0.062	0.00	0.040	0.40	10.00	40.00	0.020
Pb	1.05	0.08	0.092	0.50	10.00	50.00	0.010
Sb	0.15	0.20	0.010	0.06	0.70	5.00	0.003
Se	2.80	0.17	0.113	0.10	0.50	7.00	0.010
Zn	1.01	1.57	0.845	4.00	50.00	200.00	0.010

During preliminary mix trials in the current study, it was observed that once BF was incorporated with other concrete constituents, the fibers dispersed evenly, making their identification within the mix challenging. Also, previous studies have highlighted the susceptibility of BF to corrosion in concrete (Wang, Qingxuan *et al.* 2021; Li, Meng *et al.* 2022). To further explore this phenomenon, a simple abrasion test was conducted on the BF using a mortar and pestle, simulating the mixing conditions typically encountered with concrete components. As shown in **Figure 6-2**, BF exhibited a tendency to break during mixing with sand and aggregate. Moreover, the alkaline resistance of BF was assessed by immersing it in a sodium hydroxide (NaOH) solution for more than 24 hours. In this test, BF was placed in a beaker containing NaOH solution and stirred continuously on a magnetic mixer for over 24 hours. The observation indicated that the fibers tended to merge and adhere to one another, forming an aggregate-like structure, as depicted in **Figure 6-3**.

6.2.2 Specimen preparation and mix proportions

Twenty-three distinct concrete mixes were prepared at the University of South Australia in accordance with AS 1012.2 (Australia 2014a). Two mixes consisted of plain concrete, whereas the remaining 21 included fiber reinforcement, all with a target compressive strength of 25 MPa, corresponding to the classification of normal-class concrete as defined by AS 1379 (Australia 2007). Mix proportions and 28-day compressive strengths are shown in **Table 6-5**. All mixes had the same proportions, except for the addition of fibers and the substitution of freshwater and natural sand with seawater and sea-sand. Fibers were added during the dry mixing of materials to ensure uniform dispersion and prevent clumping. The mixture was designed to be highly workable, targeting a slump range of 150-200 mm, without the addition of a superplasticizer. Specimens were demolded 24 hours after casting and cured in a 23°C ± 2°C fog room, then in lime-saturated water for 28 days.



Figure 6-2 Abrasion test of basalt fibers using mortar and pestle.

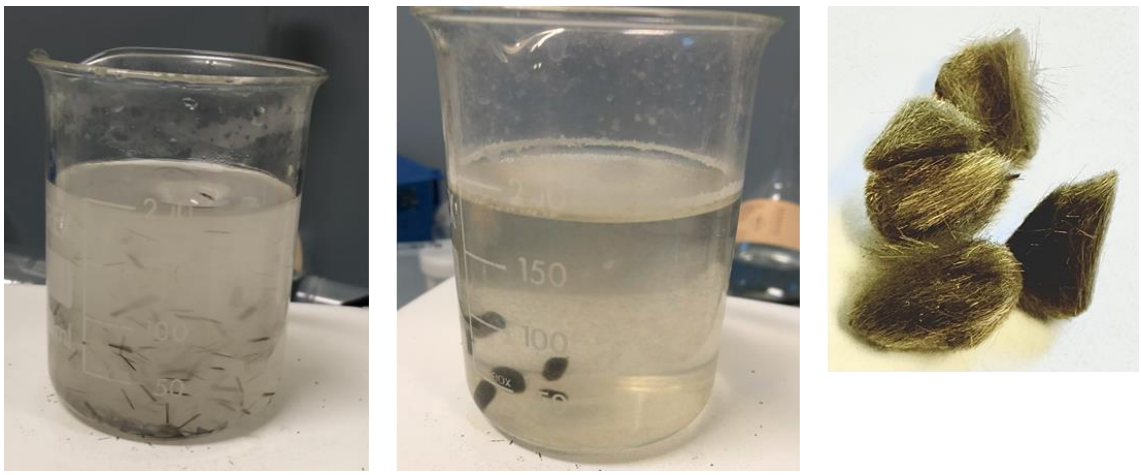


Figure 6-3 BF testing in NaOH solution using a magnetic stirrer and aggregate-shaped outcomes.

Research on optimal fiber content in FRC highlights that excessive fibers can increase viscosity and compromise workability, while insufficient content limits crack-bridging effectiveness (Pakravan *et al.* 2019; Zhang *et al.* 2020; Vafaei *et al.* 2021a). In this study, to enhance the performance of SWSS mixtures, micro-fibers (PPS, PVA, BF) and macro-fibers (PPL, TPPL) were added at 0.25% volume, both individually and in hybrid forms. This dosage, previously used to evaluate FRC properties in freshwater normal sand (FWNS) and SWSS concrete (Vafaei *et al.* 2021a, 2022a; Vafaei *et al.* 2022b), was chosen to minimize issues related to improper mixing. The hybrid mixtures included two ratios, 33% and 66% of each fiber type, such as 0.66PPL/0.33PVA and 0.33PPL/0.66PVA.

6.2.3 Shear strength test setup and specimen

The evaluation of concrete shear strength is a challenging aspect of structural engineering, as various testing methods possess inherent limitations. **Figure 6-4** presents the configurations of practical shear testing methods, including the Z-type push-off test, L-type test, ASTM D5607 (AC10520942 2008), and direct shear tests, such as those outlined by the Fédération Internationale de la Précontrainte (FIP) and the Japan Society of Civil Engineers (JSCE) (JSCE 1990). Despite their widespread use, these methods have limitations in accurately determining the pure shear strength of concrete.

The Z-type pushoff specimen, developed by Hoffbeck et al. (Hofbeck *et al.* 1969), is commonly used to evaluate shear strength but introduces tensile stresses at interface tips, leading to a mixed failure mode involving tensile and shear fractures (Jang *et al.* 2018). Additionally, due to being cast in two phases, it is more suitable for joint shear strength assessment rather than pure shear in homogeneous concrete (Hadi *et al.* 2022). The direct shear test method, JSCE-SF6 and JSCE-G553 are also commonly used to determine the shear strength of FRC beams (Boulekbache *et al.* 2012; Banthia *et al.* 2014; Tassew *et al.* 2014; Charron *et al.* 2020; Cuenca *et al.* 2020; Moghadam *et al.* 2020; Zainal *et al.* 2020; González-Aviña *et al.* 2022). However, the JSCE-SF6 test, which applies shear through knife-edge supports, often leads to a failure mode deviating from pure shear. So, its stress state does not represent true pure shear conditions, leading to inconsistencies in test outcomes, studies have thus suggested incorporating a shallow, all-around notch to predefine the failure plane, called modified JSCE-SF6 (Mirsayah *et al.* 2002). The fib shear test setup also introduces bending stresses that result in deviation from pure shear (Khanlou *et al.* 2012), while challenges such as friction at loading points and potential rotation of the cracking plane further complicate the interpretation of results (Cuenca *et al.* 2020). Also, shear strengths, τ_{cr} (cracking) and τ_{max} (maximum), measured using the JSCE-SF6 method were found to be 12.8%-33.3% and 21.7%-40% higher, respectively, compared to the FIP and Z-type methods, attributed to the presence of two shear planes without lateral displacement, enhancing shear resistance (Carrillo *et al.* 2024).

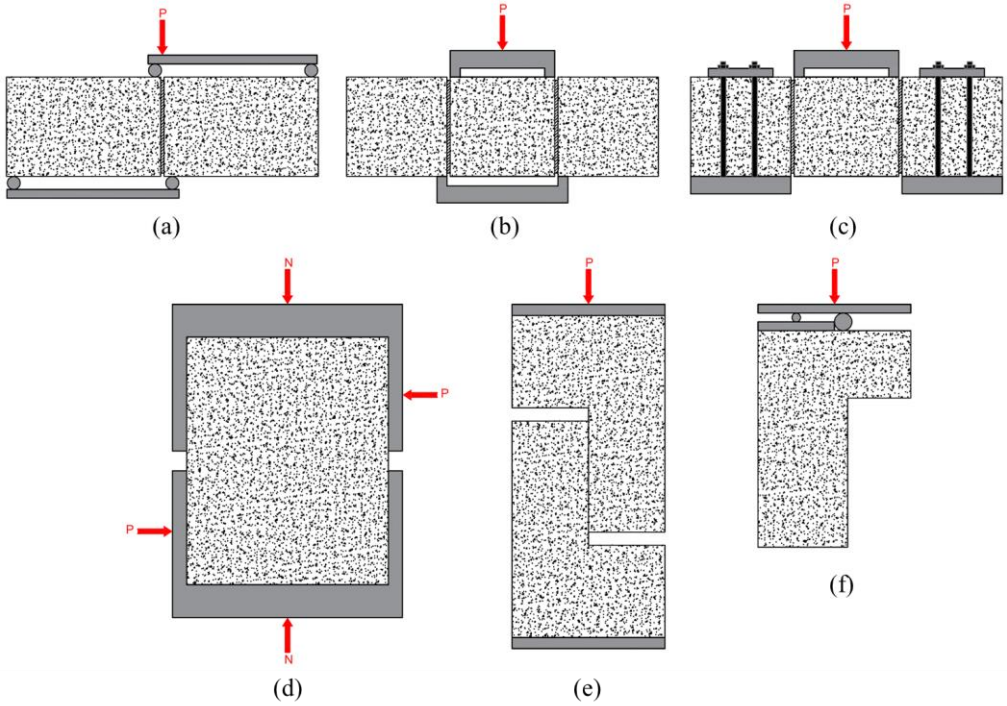
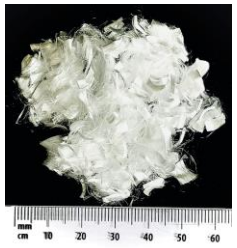
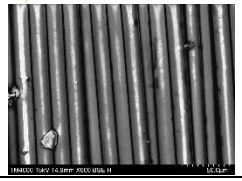
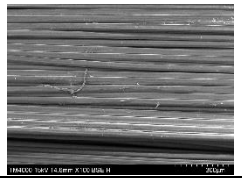
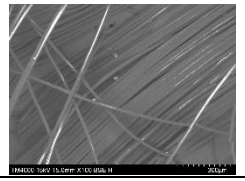
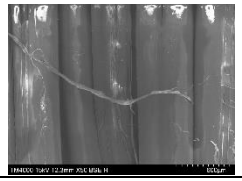
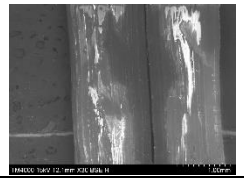


Figure 6-4 Typical concrete shear test methods: (a) FIB, (b) JSCE-SF6, (c) modified JSCE-G553, (d) ASTM D5607, (e) Z-type pushoff specimen, and (f) L-type specimen.

Given these challenges, this study aimed to refine the JSCE-SF6 shear test method by implementing targeted modifications and conducting 30 experimental trials to identify the most effective approach for achieving pure shear failure. The modified direct shear test method utilizes $100 \times 100 \times 350$ mm prismatic specimens, following the Australian standard (AS 1012.11) (Australia, Standard 2000) beam specifications for flexural strength, as illustrated in **Figure 6-5**. Also **Figure 6-5** presents the corresponding shear and bending moment diagrams. Based on Australian standard specimen dimensions, this modified method serves as a practical approach. As illustrated in **Figure 6-5**, the shear tests were standardized by positioning the specimen based on symmetry, using levels to ensure there was no torsion, and employing a torque wrench to apply consistent loading to all bolts, while a self-aligning platen facilitated uniform load distribution. The placement of notches, supports, and loading plates was optimized through experimental trials to achieve pure shear stress, as demonstrated in the shear diagram.

Table 6-4 Physical characteristics of various fibers (Mashayekhi et al. 2024a).

Property	BF[1]	PVA[2]	PPS[3]	TPPL[4]	PPL[5]
Specific gravity	2.8	1.3	0.91	0.91	0.91
Length (mm)	7	8	6	54	47
Diameter (μm)	15	38	180	800	—
Thickness (μm)	—	—	—	—	<500
Tensile strength (MPa)	2900	1600	600	620	400
Young's modulus (GPa)	85	40	9.5	9.5	6
Shape					
SEM					

[1] basalt fiber, [2] polyvinyl alcohol, [3] short polypropylene, [4] long twisted polypropylene, [5] long polypropylene.

A cutting machine was employed to produce notches with a width of 5 mm and a depth of 10 mm. Introducing notches after casting allowed for accurate depth control, minimized fiber misalignment, and ensured reliable shear performance evaluation. Cutting notches has been widely used in previous studies, particularly for evaluating the fracture toughness of concrete (Reis *et al.* 2004; Hoover *et al.* 2013; Mashayekhi *et al.* 2024d). Displacement of the specimen parallel to the shear plane, located at the center of specimen, was recorded using a Linear Variable Displacement Transducer (LVDT). The experiment was conducted with an INSTRON machine with a capacity of 100 kN, applying displacement control at a rate of 0.5 mm/min. This rate aligned with those employed in previous studies examining the performance of fiber-reinforced concrete (de Alencar Monteiro *et al.* 2018; Xie, Faxiang *et al.* 2021; Mashayekhi *et al.* 2024d, 2024c).The maximum shear strength ($\tau_{C,max}$) was calculated as follows:

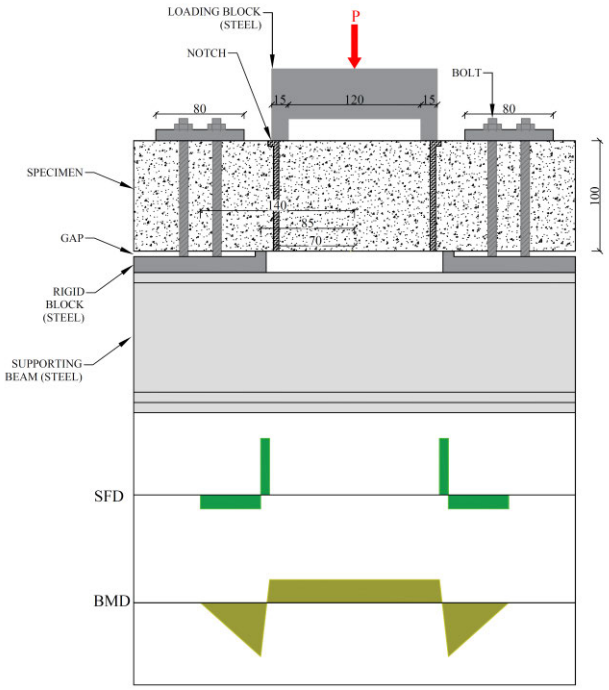
$$\tau_{C,max} = \frac{P_{max}}{2A} \tag{6-1}$$

where P_{max} represents the maximum load, and A denotes the area of the sliding planes.

6.2.4 Finite element method (FEM)

The finite element modelling of the concrete beam subjected to the shear test was conducted using ABAQUS, with a mesh size of 10 mm to achieve an optimal balance between computational efficiency and result accuracy. The model comprised over 3,500 elements, providing a detailed representation of the concrete beam geometry, with dimensions of 100 × 100 × 350 mm. Boundary conditions were applied using the displacement/rotation method to accurately simulate realistic constraints, accommodating the supports and rotation control system. The material properties of the FWNS concrete were defined using the Concrete Damaged Plasticity (CDP) model, incorporating key parameters such as concrete tension damage, concrete compression damage, tension stiffening, and compression hardening. These parameters were derived from the compression stress-strain results obtained in the experimental testing conducted in this study, ensuring an accurate representation of the nonlinear behaviour of FWNS concrete. The concrete beam was modelled with C3D8RH elements (8-node linear brick elements with reduced integration and hourglass control) using a solid section, while R3D4 elements (4-node bilinear rigid quadrilaterals) were utilized for the rotation control and

support plates. The interaction between the concrete and the rigid elements was defined as surface-to-surface contact, with a friction coefficient representative of the interface between steel and concrete.



(a)



(b)

Figure 6-5 Modified JSCE-SF6 concrete shear test setup.

6.3 Test results and discussion

6.3.1 Evaluation of the modified JSCE-SF6 using finite element

This section aims to evaluate the modified JSCE-SF6 shear test method through finite element method (FEM) analysis using ABAQUS and to investigate the effects of various

parameters on stress distribution and ultimate shear strength. To accomplish this, an ABAQUS model was developed for the FWNS concrete beam specimen and validated against experimental results. **Figure 6-6** illustrates the stress distribution in the specimen at different stages. At the initial stage, the stress originates from the loading points and transfers to the notches. As the load increases, the stress distributes through the notches and transfers to the supports. The stress continues to transfer and distribute over a larger portion of the notches until reaching maximum capacity. The stress distribution from the FEM analysis and the experimental failure mode of the FWNS specimen are presented in **Figure 6-7**. The figure combines these results to enable a direct comparison, providing a clearer understanding of the correlation between the experimental and numerical analyses. As shown, the experimentally determined failure mode closely aligns with the stress distribution obtained from the FEM analysis at the point of maximum load and failure. Shear failure occurred at the left-hand-side notch, followed by a subsequent and abrupt failure of the right-hand-side notch. The observed cracks also align with the stress distribution. Furthermore, the experimentally measured maximum load for the FWNS specimen was 71 kN, while the ABAQUS model predicted a maximum load of 70 kN, demonstrating strong agreement and successful validation of the model. All parameters investigated via FEM were applied to the validated specimen for comparative analysis, and the results are presented in the following sections.

6.3.1.1 Effect of concrete-steel plate friction

The research findings indicated that a primary limitation of the JSCE-SF6 method was the friction between the concrete and supporting steel plates, which induced axial pressure and confinement in the beams. This effect resulted in artificially elevated shear strength and compromising the accuracy of the shear testing results (Cuenca *et al.* 2020). Consequently, shear failure occurred outside the notched planes. This was corroborated by FEM results, where the friction coefficient between concrete and steel plates influenced the ultimate strength. For the FWNS specimen tested with the modified JSCE-SF6 method (**Figure 6-5**), the ultimate strength increased by approximately 45% (from 77 kN to 112 kN) when the friction coefficient was raised by around 70%. **Figure 6-8** illustrates the stress distribution at peak load for both specimens. As shown, an increased friction coefficient involved a larger portion of the section in stress transfer from the loading point to the supports, which enhanced the ultimate strength of the specimen but heightened the likelihood of failure outside the notches, thus inhibiting pure shear failure.

Table 6-5 Concrete mix designs and corresponding 28-day compressive strengths (Mashayekhi et al. 2024d).

	Binder (kg/m^3)		Gravel	Sand (kg/m^3)		Water (kg/m^3)		Fiber (kg/m^3)					28-day
Concrete Mix	OPC	GGBS	(kg/m^3)	NS	SS	FW	SW	PPS	PVA	BF	PPL	TPPL	f_c' (MPa)
FWNS	126	234	995	785	—	256	—	—	—	—	—	—	28.5
SWSS	126	234	995	—	785	—	256	—	—	—	—	—	27.6
PPS	126	234	995	—	785	—	256	2.28	—	—	—	—	27.2
PVA	126	234	995	—	785	—	256	—	3.25	—	—	—	28.9
BF	126	234	995	—	785	—	256	—	—	6.63	—	—	27.4
PPL	126	234	995	—	785	—	256	—	—	—	2.28	—	28.6
TPPL	126	234	995	—	785	—	256	—	—	—	—	2.28	29.0
0.33PPS/0.66BF	126	234	995	—	785	—	256	0.76	—	4.41	—	—	27.9
0.66PPS/0.33BF	126	234	995	—	785	—	256	1.52	—	2.21	—	—	28.2
0.66PVA/0.33BF	126	234	995	—	785	—	256	—	2.17	2.21	—	—	31.1
0.33PVA/0.66BF	126	234	995	—	785	—	256	—	1.08	4.41	—	—	27.0
0.33PPS/0.66PVA	126	234	995	—	785	—	256	0.76	2.17	—	—	—	27.3
0.66PPS/0.33PVA	126	234	995	—	785	—	256	1.52	1.08	—	—	—	26.9
0.33PPL/0.66PPS	126	234	995	—	785	—	256	1.52	—	—	0.76	—	27.2
0.66PPL/0.33PPS	126	234	995	—	785	—	256	0.76	—	—	1.52	—	26.4
0.66PPL/0.33PVA	126	234	995	—	785	—	256	—	1.08	—	1.52	—	31.9
0.33PPL/0.66PVA	126	234	995	—	785	—	256	—	2.17	—	0.76	—	31.1
0.33PPL/0.66BF	126	234	995	—	785	—	256	—	—	4.41	0.76	—	31.5
0.66PPL/0.33BF	126	234	995	—	785	—	256	—	—	2.21	1.52	—	31.5
0.33TPPL/0.66PVA	126	234	995	—	785	—	256	—	2.17	—	—	0.76	30.3
0.66TPPL/0.33PVA	126	234	995	—	785	—	256	—	1.08	—	—	1.52	30.5
0.33TPPL/0.66BF	126	234	995	—	785	—	256	—	—	4.41	—	0.76	28.5
0.66TPPL/0.33BF	126	234	995	—	785	—	256	—	—	2.21	—	1.52	29.6

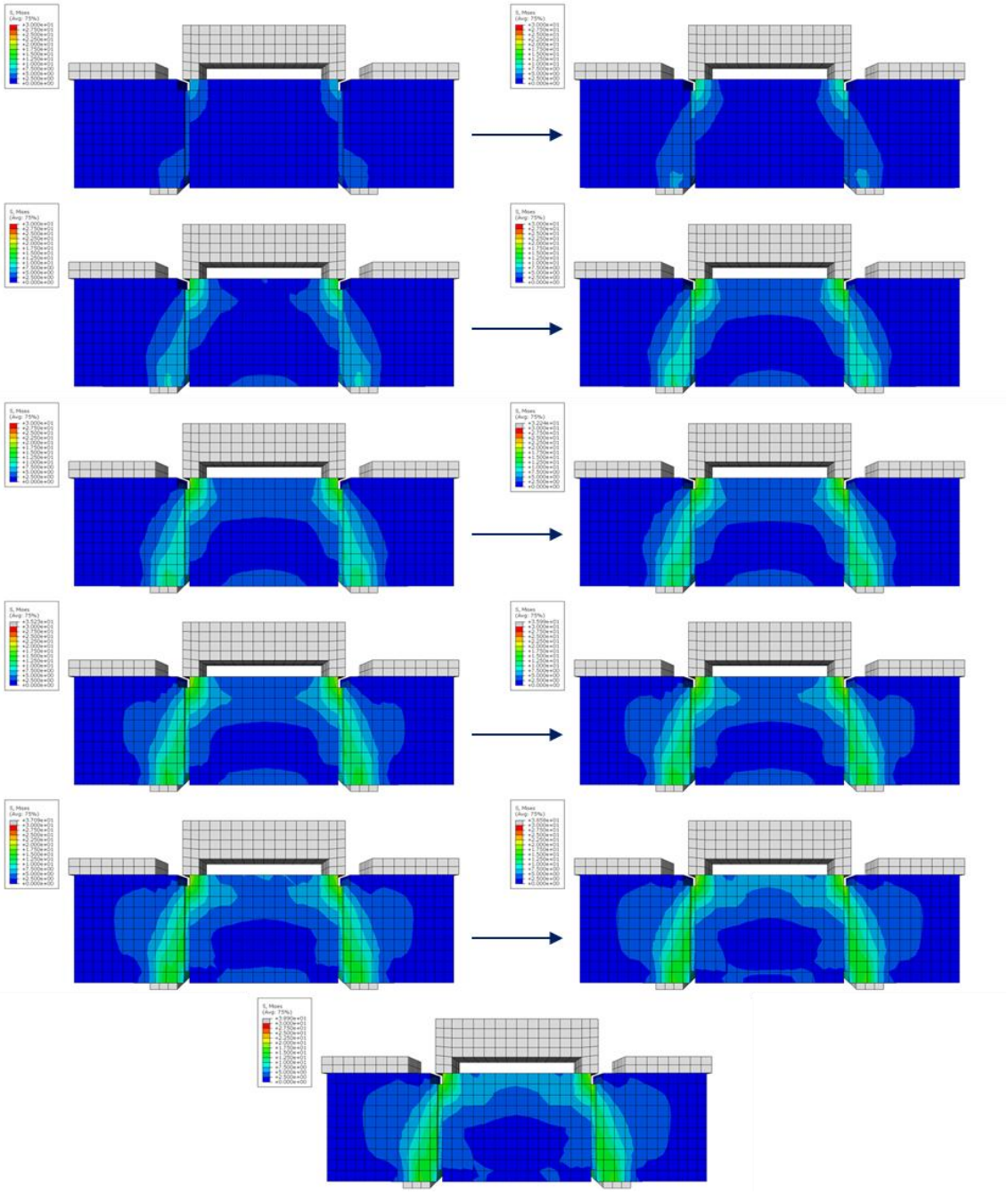


Figure 6-6 Stress distribution in various states.

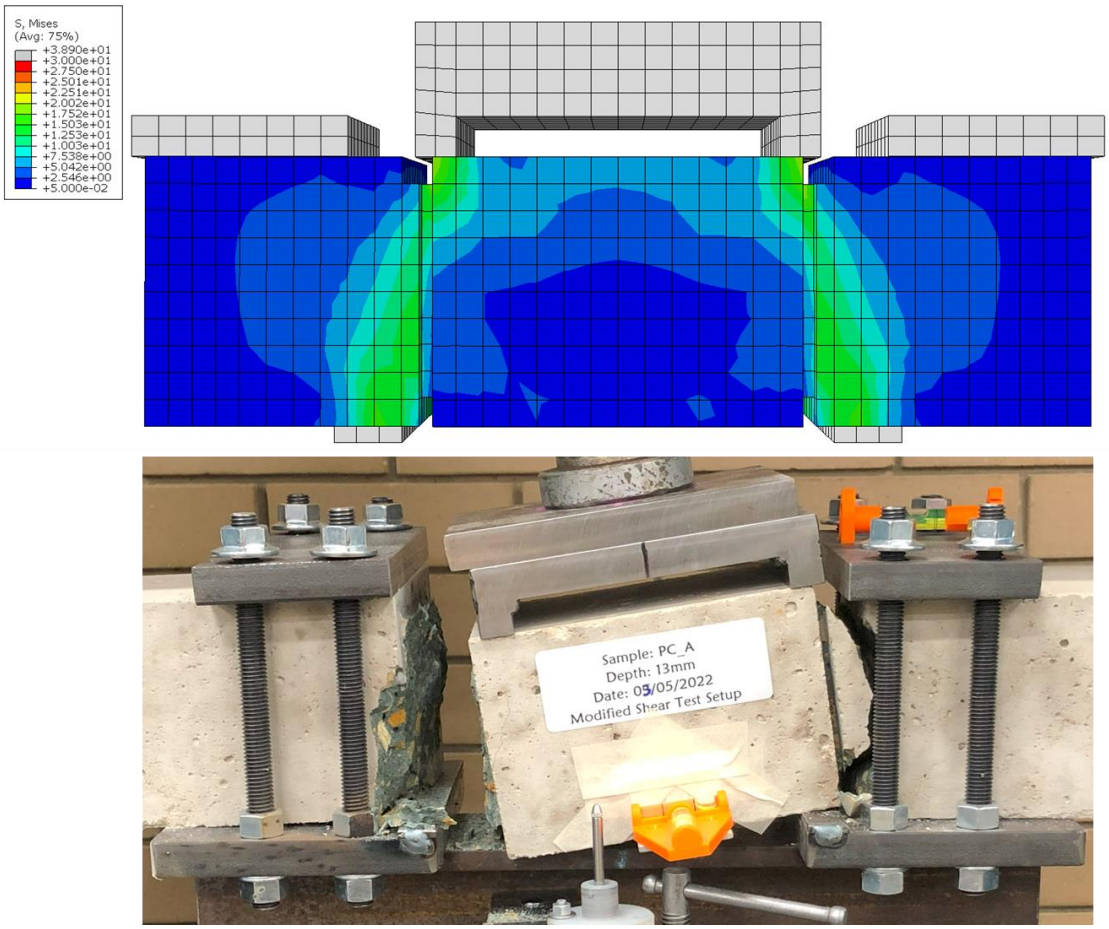


Figure 6-7 Comparison of FEM modeling and experimental results for the FWNS concrete specimen at peak load using the proposed shear test method.

6.3.1.2 Effect of support position

The FEM analysis of the FWNS concrete specimen, conducted using the modified JSCE-SF6, revealed stress concentration near the supports and notches (as shown in **Figure 6-9**), leading to failure outside of the notched areas and thus preventing pure shear failure. This behaviour was also observed in preliminary experimental tests. To mitigate this issue, the supports were relocated further from the notches, aiming to reduce stress concentration at these points. The support position impacts the internal stress distribution of the specimen. Closer support spacing results in higher reaction forces and localized shear stresses, while wider spacing reduces these forces but introduces larger bending moments, altering the interaction between shear and bending effects. The outcomes of this adjustment are presented in **Figure 6-9**. As illustrated, this modification enhances the test setup to achieve pure shear failure, as verified in subsequent experimental trials.

However, this adjustment also resulted in an approximate 7% reduction in the ultimate capacity of specimen.

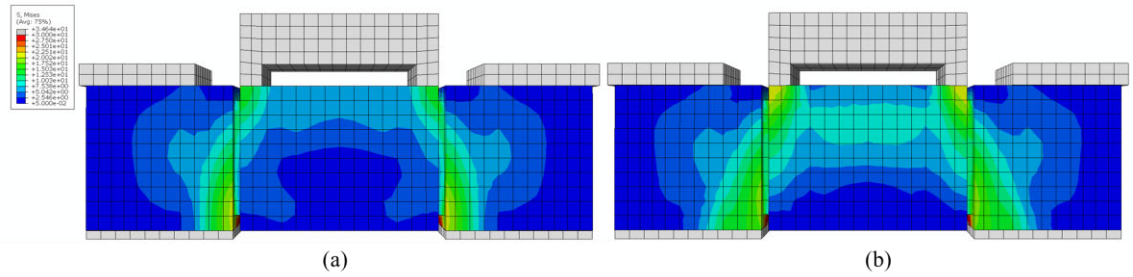


Figure 6-8 Stress distribution of FWNS concrete specimen in the modified JSCE-SF6 shear test method: (a) low friction coefficient, (b) high friction coefficient.

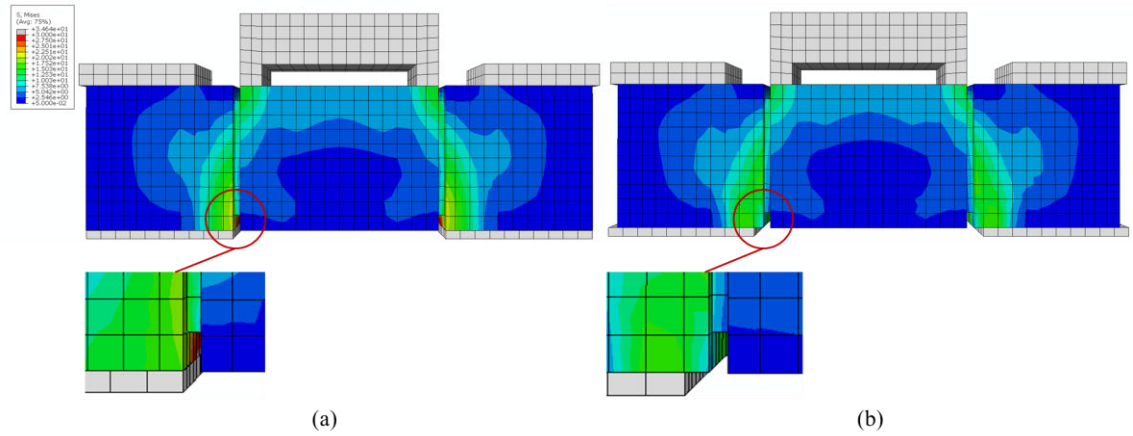


Figure 6-9 The effect of support location on stress distribution in FWNS concrete specimen using the modified JSCE-SF6 shear test method.

6.3.1.3 Effect of bolt prestressing

The prestressed loads applied to the supporting bolts influenced the results. Specifically, increasing the axial load on the bolts led to an enhancement in shear strength and prevented sudden failure, which is typically characteristic of shear failure observed in most specimens. This outcome can be attributed to the frictional force between the specimen and the supporting plates, which intensified as the pressure from the bolts and supporting plates increased. **Figure 6-10** illustrates the effect of rotation-control plates and the prestressed loads on the stress distribution. The results indicate that when the rotation plates allowed for upward movement, simulating a worst-case scenario where the bolts were tightened too loosely and leading to upward displacement during testing, the ultimate load capacity reached approximately 69 kN. Conversely, when the plates were

fixed to prevent upward movement—indicating a worst-case scenario of high prestressed loads applied to the bolts—the ultimate capacity increased to approximately 105 kN, representing a 52% increase in ultimate strength in this case. As shown in **Figure 6-10**, by restricting the upward movement of the rotation-control plates, a greater portion of the FWNS specimen was engaged, resulting in a higher ultimate capacity. These findings underscore the necessity of applying similar prestress loads to bolts for consistent comparison and shear strength calculation across different concrete specimens. In this study, this condition was maintained using a torque wrench to ensure uniform bonding conditions for all specimens.

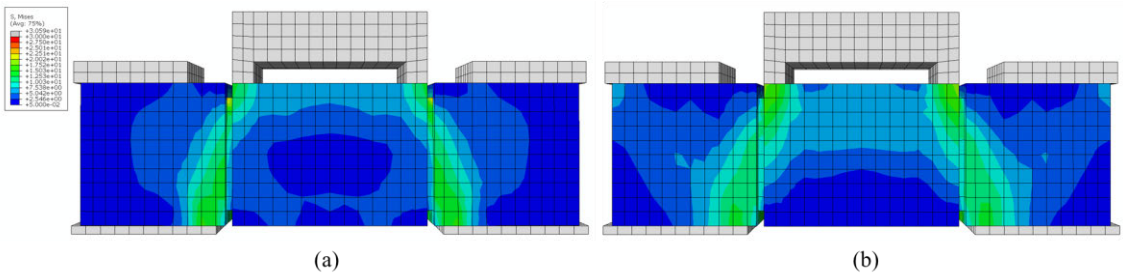


Figure 6-10 Stress distribution of FWNS concrete specimen using the modified JSCE-SF6 shear test method: (a) with released upward movement, (b) with fixed upward movement.

6.3.1.4 Proposed shear test method

Based on the experimental and FEM investigations of the modified JSCE-SF6 shear test method, a revised shear test method was developed using a concrete beam specimen aligned with the Australian standard (AS 1012.11) (Australia, Standard 2000). This proposed method aims to achieve enhanced shear performance and capture more realistic shear behaviour. The following modifications, illustrated in **Figure 6-5**, were applied:

- Two narrow steel plates were incorporated near the notches to direct the applied load and reaction forces from the supports through the sliding shear planes.
- Friction between the concrete and steel plates was minimized by attaching the two support plates.
- Notches were positioned at points of minimum bending moment and maximum shear force.

– The support plates were relocated away from the notches to prevent stress concentration.

Following these modifications, FEM results for the validated FWNS concrete specimen are presented in **Figure 6-7**. As observed, the proposed method produced stress concentration at the upper region of the notches, resulting in shear failure occurring at the notches and preventing failure progression toward the supports.

6.3.2 Failure mode

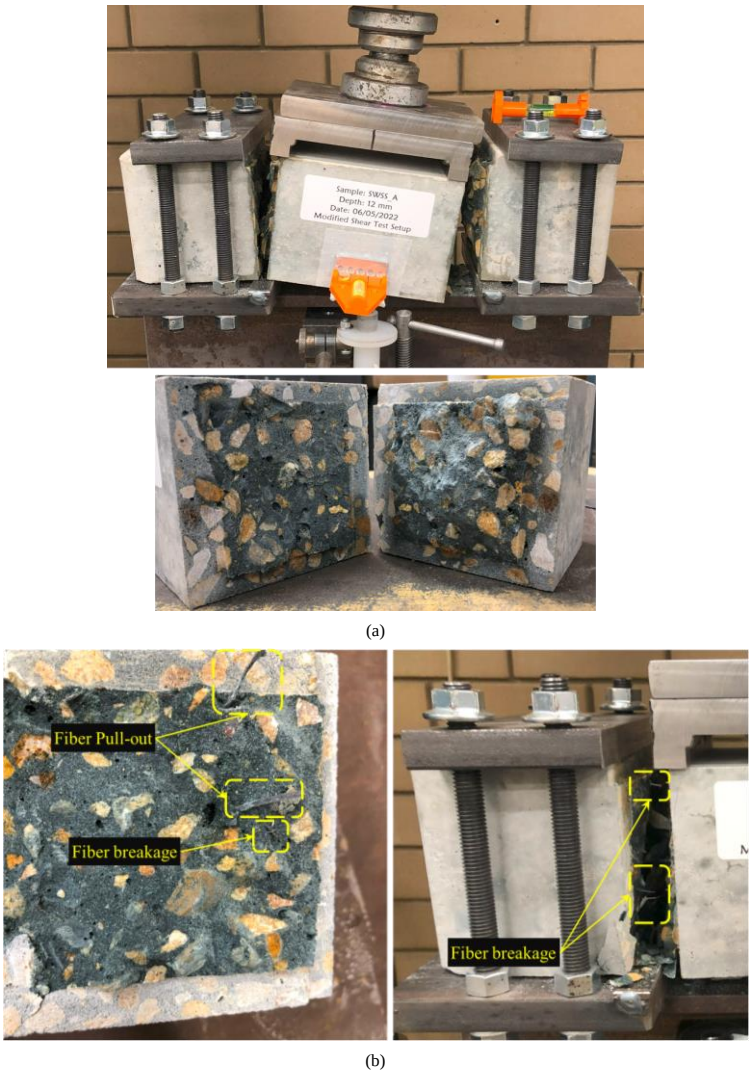
Figure 6-11 (a) presents the typical failure mode of the specimens, showing pure shear failure along the notches and sliding planes. Upon reaching the shear capacity, one sliding plane experienced shear failure, which subsequently triggered failure on the opposite plane, though this was not a shear failure. For example, in the specimen shown in **Figure 6-11** (a), failure began at the right-side notch and rapidly led to failure at the left-side notch. The shear failure section, also illustrated in **Figure 6-11** (a), revealed significant aggregate fracturing and failure concentrated at the predefined notch.

Pure shear failure was consistently observed in all 70 beams tested across all concrete mixes, characterized by abrupt failure along one sliding plane. Specimens containing macro-fibers, such as PPL and TPPL, exhibited sudden failure accompanied by fiber breakage and pull-out, as shown in **Figure 6-11** (b). The presence of both micro- and macro-fibers influenced the failure mode by enhancing shear strength and improving the interlocking strength of the concrete matrix. Fibers redistributed shear stress more uniformly at the notches, reducing localized stress concentrations.

Micro-fibers contributed by bridging cracks, allowing the concrete to absorb more shear stress and resist cracking. Macro-fibers, acting as small shear reinforcements, facilitated shear stress transfer across cracks. The number and distribution of macro-fibers in the shear plane were critical in preventing shear failure and influencing post-peak behaviour. Higher fiber dosages increased the number of macro-fibers within the shear plane, delaying shear failure and enhancing energy absorption. After cracking, shear strength peaked, with fibers contributing by either breaking—if adequately bonded—or pulling out to dissipate energy.

6.3.3 Load–deflection curves

The results of the typical shear load-deflection test conducted on mono-fiber, hybrid micro-fiber, and hybrid micro- and macro-fiber reinforced SWSS concrete are presented in **Figure 6-12**. The load- deflection curve progressed through several distinct stages as the load was applied, as depicted in **Figure 6-13**. The load-displacement behaviour of the specimen can be divided into four phases: the elastic phase, where linear deformation occurs; the plastic phase, marked by plastic deformation and micro-crack formation; the failure phase, characterized by maximum load and failure; and the post-peak phase, where deflection continues without further load increase. Each phase is distinguished by changes in the slope of the load-displacement curve, reflecting the response of specimens under increasing load.



(a)

(b)

Figure 6-11 Typical shear failure mode of the specimens: a) plain SWSS concrete, b) PPL reinforced specimen.

During the elastic phase, both SWSS and FWNS concrete exhibited a similar slope, indicating comparable stiffness. However, SWSS concrete demonstrated higher shear strength within this phase, suggesting greater interlocking strength compared to FWNS concrete, which is likely attributable to its denser microstructure, as reported in previous studies (Wang, Junjie *et al.* 2018; Vafaei *et al.* 2022b; Mashayekhi *et al.* 2024a). Following this stage, SWSS concrete experienced a broader plastic range, characterized by increasing deflection at a constant shear strength, in contrast to FWNS concrete. This behaviour could be attributed to the initiation and development of micro-cracks along sliding planes. Neither SWSS nor FWNS concrete exhibited post-peak behaviour, primarily due to the absence of fibers and the occurrence of sudden failure upon reaching the peak load.

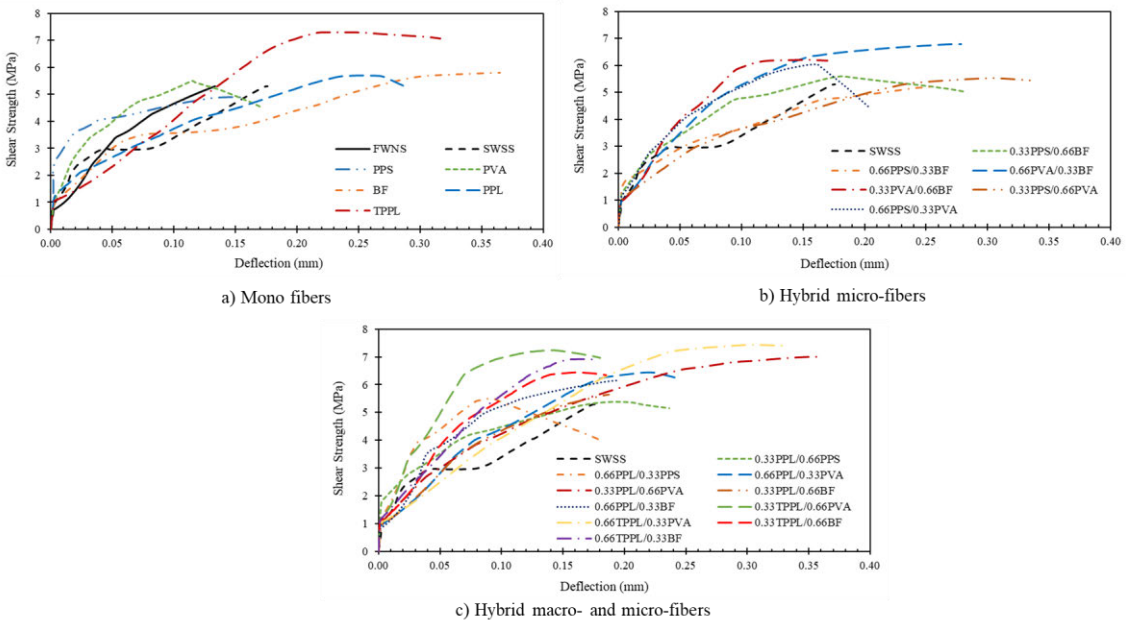


Figure 6-12 The typical stress-deflection curves of the shear strength test: a) Mono-fibers, b) Hybrid micro-fibers, and c) Hybrid macro- and micro-fibers.

The addition of micro-fibers increased the stiffness in the elastic phase of plain SWSS concrete by bridging microcracks and improving the interfacial bond with the matrix, restricting early crack propagation. However, BF slightly reduced stiffness due to their brittleness, which caused breakage during mixing. Abrasion testing (**Figure 6-2**) confirmed a significant reduction in the length of BF under high-shear mixing, which limited their crack-bridging capacity and ability to distribute stress effectively in larger cracks compared to other micro-fibers. SEM images in Figure 14 illustrate the shortened

BF in SWSSC, further highlighting the impact of breakage on their performance. Additionally, the incorporation of PPS and PVA fibers resulted in higher shear strength than plain SWSS concrete during this phase, which can be attributed to the enhanced interlocking strength provided by the fibers. Both PPS and PVA fibers exhibited an increasing trend in shear strength and facilitated a smoother transition from the elastic to the plastic phase. However, BF increased the deformation before failure, and considerably widened both the plastic and failure phases. This behaviour can be attributed to the distribution of BF within the concrete matrix. During mixing, BF fibers experienced breakage, leading to improved distribution with shorter fibers that can bridge micro-cracks but are not sufficiently long to restrain crack propagation. As a result, the length of the plastic phase increased due to the higher number of microcracks, and the stiffness of this phase decreased more rapidly compared to other microfibers. The dispersed BF fibers delayed the coalescence of microcracks and the attainment of the failure point, resulting in increased deflection and shear strength. As shown in **Figure 6-14**, PVA and BF exhibit better bonding strength compared to PPS fibers, which enhances the distribution of shear stress and results in higher shear capacity.

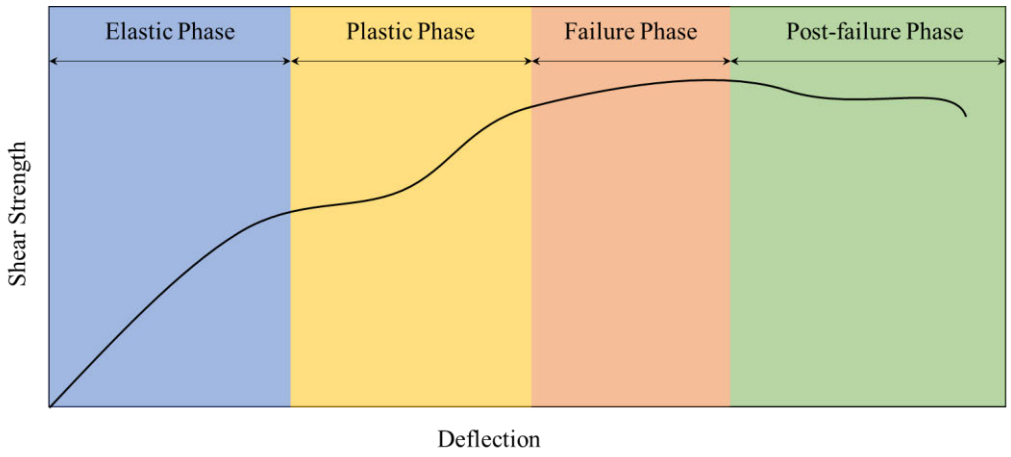


Figure 6-13 The typical load-displacement curves of the shear strength test.

The addition of macro-fibers slightly reduced stiffness during the elastic phase and resulted in lower shear strength compared to SWSS concrete. However, these fibers enhanced deflection prior to failure, contributing to an approximately stable slope before reaching the failure point and during the plastic phase. This indicates that before failure, the specimens experienced reduced plastic deformation. This behaviour can be attributed to the ability of PPL and TPPL fibers to bridge micro-cracks, thereby preventing their

propagation and maintaining stiffness during the plastic phase. Notably, TPPL fibers, due to their flexibility and better distribution, were more effective in bridging these cracks during the plastic phase, resulting in higher shear strength. Furthermore, the length of the failure phase for TPPL fibers was greater than for PPL fibers, demonstrating their superior performance in bridging primary shear cracks before failure.

The hybridization of PVA/PPS fibers demonstrated that, in comparison to mono PPS fibers, hybridization improved the stiffness of the specimens during the plastic and failure stages, resulting in a more stable slope of the load-deflection curve prior to failure. Although mono PVA fibers exhibited lower deflection at failure, partial replacement (66%) with PPS fibers led to higher deflection at the point of failure. Additionally, a 33% replacement of PVA fibers with PPS resulted in higher shear strength compared to both mono PPS and mono PVA fibers. This indicates that in the PVA/PPS hybridization, PVA fibers contributed to increased shear strength through their superior chemical bonding, while PPS fibers enhanced the deformation characteristics due to their greater elongation.

The PVA/BF hybridization led to increased stiffness compared to mono BF fibers and reduced the deflection at the failure point. Compared to mono PVA fibers, both the deflection at peak load and the shear strength improved. This enhancement could be attributed to the presence of PVA fibers in the hybrid system, which effectively bridged micro-cracks, mitigating the inherent weakness of the BF bridging effect and improving the stiffness during the plastic phase, thereby resulting in higher shear strength. The fiber synergy of the PVA/BF combination is illustrated in the SEM images provided in **Figure 6-15**. As shown, BF contributes to reinforcing the surrounding concrete matrix of PVA fibers, thereby enhancing the synergistic effect. The 0.66PVA/0.33BF hybridization demonstrated superior performance in terms of both failure deflection and ultimate shear strength, attributable to the positive synergy between these fibers.

The PPS/BF hybridization increased the deflection at failure compared to the mono PPS system, attributed to the improved bonding strength of PPS fibers due to the presence of BF fibers. In this hybrid system, BF fibers, with their superior bonding strength compared to PPS fibers, reinforced the surrounding concrete matrix of the PPS fibers, thereby contributing more effectively to bridging micro-cracks and increasing stiffness during the plastic phase compared to the mono BF system. In this case, a higher proportion of PPS fibers resulted in increased stiffness during the plastic phase.

PPL/PVA hybridization led to enhanced shear performance, with the 0.33PPL/0.66PVA combination exhibiting greater deflection at failure and higher shear strength compared to both mono PPL and PVA fibers. As observed in the SEM images provided in **Figure 6-15**, this enhancement might be attributed to the improved bonding strength of PPL fibers by the presence of PVA fibers, which reinforced the surrounding concrete matrix, thereby enhancing the crack bridging mechanism. In contrast, PPL/PPS hybridization increased stiffness and resulted in reduced deflection at the failure point compared to mono PPL fibers. Specifically, the 0.66PPL/0.33PPS hybridization exhibited higher shear strength within the hybrid system. A similar trend was observed with PPL/BF hybridization, which might be attributed to the effect of micro-fibers (PPS and BF) in enhancing the crack bridging mechanism by reinforcing micro-cracks, leading to increased stiffness during the plastic phase. In this scenario, incorporating 33% micro-fiber in hybridization with PPL fibers resulted in improved shear strength.

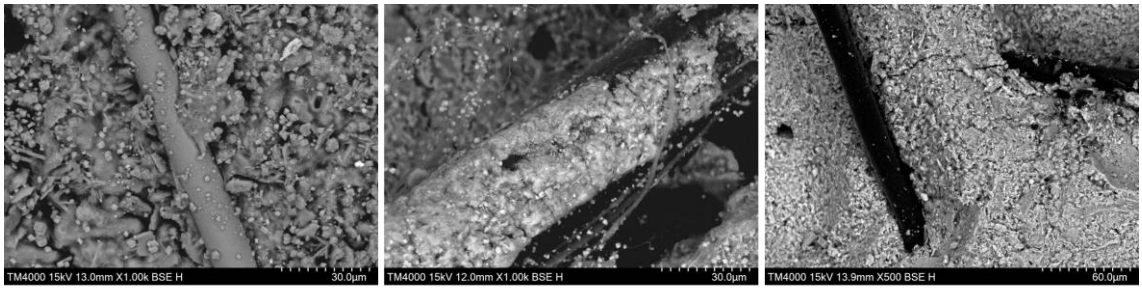


Figure 6-14 SEM images of micro-fibers, including BF, PVA, and PPS.

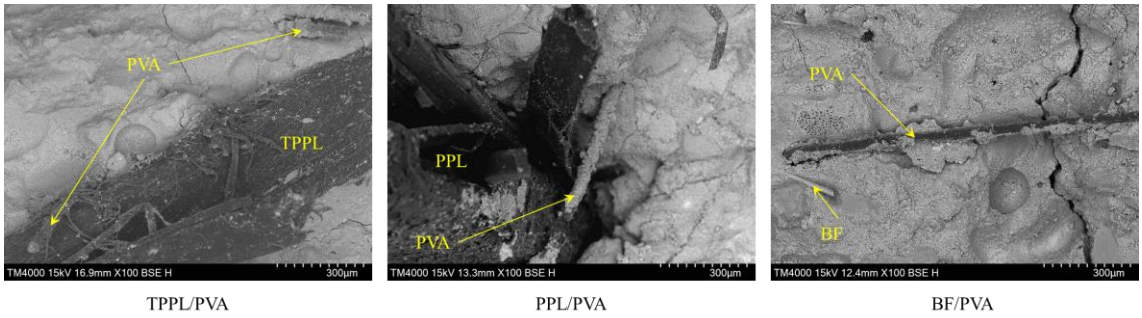


Figure 6-15 SEM images of PVA hybrid fibers combined with TPPL, PPL, and BF.

The incorporation of TPPL/BF resulted in reduced deflection at the failure point compared to both mono TPPL and BF fibers. This hybrid combination also enhanced stiffness and shear strength compared to mono BF incorporation. The observed improvements could be attributed to the presence of BF fibers, which enhanced the

bonding strength of TPPL fibers and effectively bridged micro-cracks, thereby improving stiffness during both the plastic and failure phases. Consequently, this led to a higher shear strength than the mono TPPL and BF fibers. Furthermore, TPPL/PVA hybridization led to improvements in both deflection at failure and shear strength compared to the mono PVA fiber. Notably, the 0.66 TPPL/0.33 PVA hybrid was more effective, achieving greater shear strength and deflection compared to both mono PVA and TPPL fibers. As observed in the SEM images provided in **Figure 6-15**, in this hybrid system, the PVA fibers contributed to increased stiffness and enhanced bonding strength of TPPL fibers, which consequently increased shear strength. The proportion of TPPL fibers played a crucial role in enhancing the deflection at failure, due to their effective bridging of primary shear cracks and resistance to failure. Like mono TPPL incorporation, TPPL/PVA hybridization resulted in an extended failure phase.

6.3.4 Shear strength and toughness

Figure 6-16 presents the mean shear strength (τ_C) of all mixes, accompanied by their standard deviations. Additionally, **Figure 6-17** illustrates the shear toughness (K_τ), defined as the area under the shear load-displacement curve up to the point of failure. The results indicate that the shear strength of FWNS and SWSS concrete was comparable, with a value of 5.3 MPa. However, the shear toughness of SWSS concrete was approximately 43% higher than that of FWNS. This could be attributed to the denser microstructure of SWSS concrete and the increased cohesion between its constituent materials, as also reported in previous studies (Wang, Junjie *et al.* 2018; Vafaei *et al.* 2022b; Mashayekhi *et al.* 2024a).

The incorporation of mono-fibers revealed that TPPL fibers provided the highest enhancement in shear strength, reaching 7.3 MPa—38% higher than plain SWSS concrete and 28% greater than PPL fibers, due to their flexibility and superior stress distribution. PPL fibers increased shear strength by 8%, while PPS fibers reduced it by 8%, and PVA fibers yielded a modest 3% improvement, attributed to the stronger chemical bonding of PVA within the concrete matrix, as noted in previous studies (Pakravan *et al.* 2019; Vafaei *et al.* 2021a; Mashayekhi *et al.* 2024e, 2024c). BF fibers increased shear strength by 10% due to their higher tensile and bonding strengths, also achieving the highest shear toughness, 132% higher than plain SWSS concrete. TPPL and PPL fibers improved shear toughness by 123% and 83%, respectively, by delaying crack initiation and propagation.

Micro-fiber hybridization with PVA and BF fibers demonstrated improved shear strength and toughness. A 0.66PVA/0.33BF mix increased shear strength (τ_C) by 28%, 24%, and 16% compared to plain SWSS, mono PVA, and mono BF, respectively, while the 0.33PVA/0.66BF mix achieved increases of 17%, 14%, and 6%, respectively. Higher PVA fiber content proved more effective in enhancing bonding strength and cohesion. Similar findings have been reported for the mechanical properties of SWSS concrete reinforced with hybrid PVA/BF fibers (Mashayekhi *et al.* 2024a; Mashayekhi *et al.* 2024e, 2024d, 2024c). Shear toughness of the 0.66PVA/0.33BF mix was 98% higher than plain SWSS and 81% higher than the 0.33PVA/0.66BF mix. This effect may be attributed to BF fiber corrosion in SWSS concrete, which increases brittleness. In this context, a higher proportion of PVA fibers in the hybrid system could provide greater resistance to shear crack development.

PPS/PVA hybridization exhibited superior shear performance compared to PPS/BF, with the 0.66PPS/0.33PVA mix achieving 9% and 24% higher shear strength than the 0.33PPS/0.66PVA mix and mono PPS, respectively. While its shear toughness was 17% lower than the 0.33PPS/0.66PVA mix, it was 80% higher than mono PPS. This improvement is attributed to the enhanced bonding strength from partial PVA fiber replacement (33%), which improved crack arresting and delayed crack initiation. Previous studies have also highlighted the positive effects of hybrid PPS/PVA fibers on SWSS concrete's mechanical properties (Mashayekhi *et al.* 2024a; Mashayekhi *et al.* 2024d, 2024c).

Micro- and macro-fiber hybridization with TPPL and PVA fibers significantly enhanced τ_C, making it the optimal combination studied. The 0.66TPPL/0.33PVA hybrid increased shear strength by 40% and 36% compared to plain SWSS and mono PVA fiber, respectively, while 0.33TPPL/0.66PVA achieved increases of 37% and 33%. Shear toughness also improved substantially, with 0.66TPPL/0.33PVA showing a 147% and 139% increase in K_τ relative to plain SWSS and mono PVA fiber. The partial replacement of TPPL fibers (33%) with PVA fibers enhanced bonding strength, delayed shear cracks, and inhibited their propagation, resulting in greater shear strength and toughness. This outcome is also confirmed by previous studies (Mashayekhi *et al.* 2024a).

Hybrid PPL/PVA fibers improved both τ_C and K_τ compared to mono fibers. The 0.66PPL/0.33PVA combination increased shear strength by 18% and 13% over mono

PVA and PPL fibers, while the 0.33PPL/0.66PVA hybrid achieved 28% and 23% increases. Additionally, the 0.33PPL/0.66PVA hybrid enhanced shear toughness by 159% and 46% compared to mono PVA and PPL fibers, outperforming the 0.66PPL/0.33PVA hybrid. Replacing 66% of PPL fibers with PVA fibers improved bonding strength of PPL fibers, enhancing both shear strength and toughness.

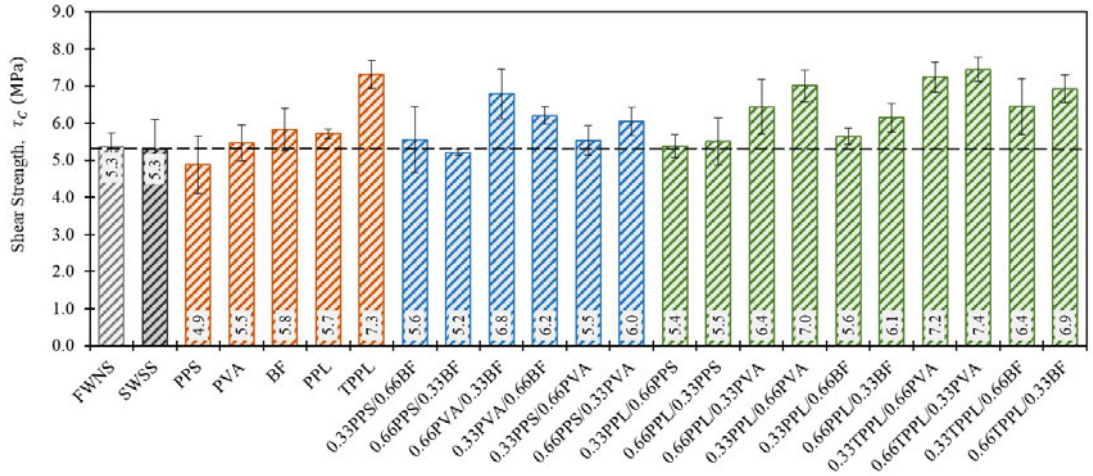


Figure 6-16 Comparison of mean shear strength (τ_C) for all mixtures.

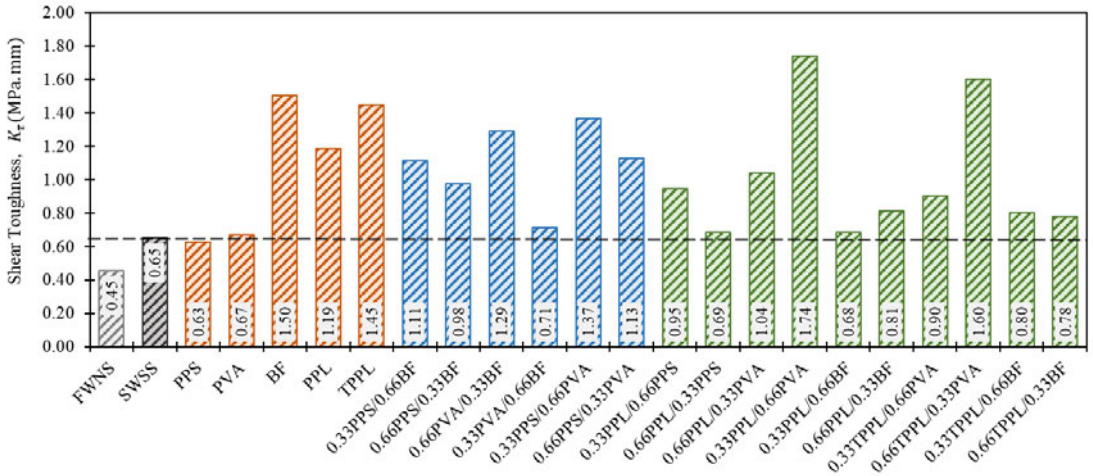


Figure 6-17 Comparison of mean shear toughness (K_τ) for all mixtures.

Partial replacement of PPS with PPL fibers enhanced shear strength and toughness, with the 0.66PPL/0.33PPS hybrid increasing shear strength by 13% and toughness by 9%, and the 0.33PPL/0.66PPS hybrid boosting shear strength by 10% and toughness by 50%, compared to mono PPS incorporation. While PPL/BF hybridization showed limited improvement, replacing 66% of BF with PPL increased shear strength by 5%. In contrast,

TPPL/BF hybridization significantly enhanced shear strength, with the 0.33TPPL/0.66BF and 0.66TPPL/0.33BF hybrids achieving 11% and 19% increases, respectively, over mono BF.

6.3.5 The synergy effect of fibers

The effectiveness of hybridization can be assessed by examining the synergistic effects among various hybrid fiber combinations. In this study, the synergistic coefficient (SC) was employed to evaluate the shear strength performance of hybrid fiber mixes in comparison to their mono fiber equivalents. Eq. (6-2) (Hoan *et al.* 2019; Nguyen *et al.* 2022) was used to calculate the SC, incorporating the shear strength characteristics of hybrid fiber-reinforced SWSS concrete and those of individual fibers, all at an identical fiber volume fraction (V_f = 0.25% by volume). A positive SC value indicates an enhancement in shear performance over individual fibers.

$$SC = \frac{R_{hybrid,a+b}^{(V_f)} - \max\left(R_{mono,a}^{(V_f)}, R_{mono,b}^{(V_f)}\right)}{\max\left(R_{mono,a}^{(V_f)}, R_{mono,b}^{(V_f)}\right)} \quad (6\text{-}2)$$

Here, $R_{hybrid,a+b}$ represents the shear strength and toughness of hybrid fiber-reinforced SWSS concrete, while $R_{mono,a}$ and $R_{mono,b}$ denote the corresponding values for mono-fibers, respectively.

Figure 6-18 illustrates the synergistic coefficients for the shear strength and toughness of SWSS concrete reinforced with hybrid fibers. As indicated, the PPS/BF fiber combination exhibited a negative synergy for both shear strength and toughness compared to single-fiber specimens. This observation can be attributed to the weak bonding strength of PPS fibers, as shown in the SEM images in **Figure 6-14**. In contrast, the PVA/BF fiber combination demonstrated positive synergy in enhancing shear strength, though it showed a negative effect on shear toughness. Conversely, the hybrid of PVA/PPS fibers demonstrated a positive synergistic effect, enhancing both shear strength and toughness.

The combined effects of micro- and macro-fiber hybridization indicated that PPL/PPS hybrid fibers exhibited a negative synergy in both shear strength and toughness. This outcome can be attributed to the weak bonding strength of PPS fibers and the absence of fibers with strong bonding properties to enhance the synergy. This aligns with previous

findings on the flexural strength and fracture toughness of PPL/PPS hybridization in SWSSC (Mashayekhi *et al.* 2024d). Conversely, the PPL/PVA hybrid showed positive synergy in both shear strength and toughness, except for the 0.66PPL/0.33PVA hybridization, which displayed negative synergy in shear toughness. Notably, the 0.33PPL/0.66PVA combination achieved a higher SC value and demonstrated a stronger complementary effect. TPPL/PVA hybridization produced positive synergy for both shear strength and toughness when using a 0.66TPPL/0.33PVA ratio. Similar results were observed for the fracture toughness and flexural strength of TPPL/PVA hybridization (Mashayekhi *et al.* 2024d). In contrast, TPPL/BF and PPL/BF combinations generally exhibited negative synergy for both parameters, except for the 0.66PPL/0.33BF hybridization, which yielded positive synergy for shear strength.

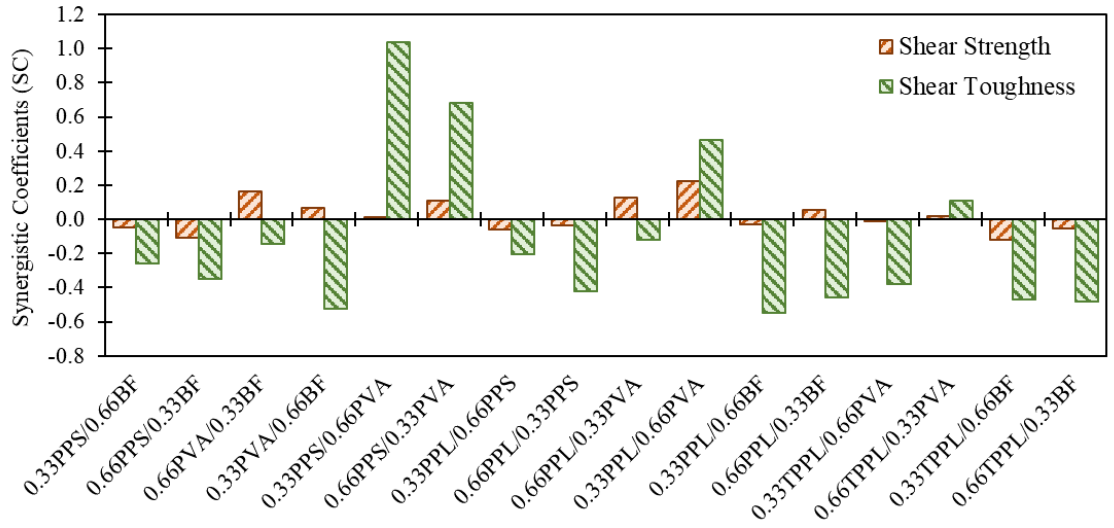


Figure 6-18 Synergistic effects of fiber hybridization on shear strength and toughness of FR-SWSS mixes.

An assessment of the synergistic coefficients for the examined shear parameters revealed that the influence of fiber addition varied across different fiber types and combination. Therefore, identifying the most suitable fiber-reinforced concrete mixture to optimize overall shear performance is essential. For this purpose, the combined mechanical performance (CMP) of each mixture was assessed compared to plain SWSS concrete, following Eq. (6-3) (Ali 2022). A CMP value exceeding 1.0 indicates an enhanced shear performance relative to plain SWSS concrete. In this study, all shear parameters were weighted equally, without considering the relative importance of individual properties.

$$CMP = \frac{\frac{\tau_{c,fiber}}{\tau_{c,SWSS}} + \frac{K_{\tau,fiber}}{K_{\tau,SWSS}}}{2} \quad (6\text{-}3)$$

where $\tau_{c,fiber}$ and $K_{\tau,fiber}$ represent the shear strength and toughness of FR-SWSSC, respectively, and $\tau_{c,SWSS}$ and $K_{\tau,SWSS}$ correspond to the shear strength and toughness of plain SWSS concrete.

Figure 6-19 presents the CMP results for all concrete mixes. The data indicate that BF, PPL, and TPPL exhibit enhanced performance, with CMP values exceeding 1.0, suggesting that these fibers contribute to improved overall shear properties. Among the mono fibers, TPPL achieves the highest CMP value (1.8), indicating superior performance relative to the other fibers. Hybrid micro-fibers showed notable improvements in CMP values, generally ranging from 3.4 to 4.4. The 0.66PVA/0.33BF mix achieved the highest CMP value among micro-fiber hybrids (4.4), highlighting a complementary interaction between these fibers that enhanced shear performance. Hybrid micro- and macro-fiber combinations exhibited the highest CMP values overall, ranging from 3.3 to 5.0. Notably, the 0.66TPPL/0.33PVA hybrid attained the highest CMP value of 5.0, demonstrating a substantial improvement in shear performance, compared to plain SWSS concrete.

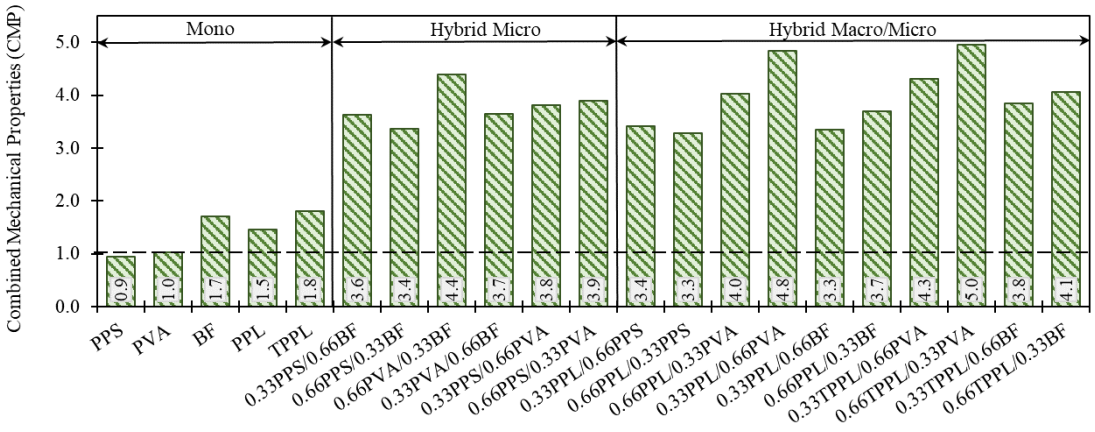


Figure 6-19 The combined mechanical performance (CMP) of FR-SWSS mixes.

6.4 Conclusion

This study evaluated the effect of fiber hybridization and its synergistic influence on the shear performance of seawater sea-sand concrete (SWSSC). A modified JSCE-SF6 direct

shear test method, based on the Australian standard specimen, was developed using both experimental and finite element modeling. Three types of micro-fibers— polyvinyl alcohol (PVA), basalt (BF), and polypropylene (PPS)—and two macro-fibers—twisted polypropylene (TPPL) and long polypropylene (PPL), each at a 0.25% volume fraction, were tested in mono and hybrid forms. The results provide insights into the optimal fiber types and configurations for improving the shear performance of concrete. The main findings are as follows:

- Hybridization of macro-fibers (TPPL or PPL) with PVA fibers showed positive synergy, as PVA enhanced macro-fiber bonding by reinforcing the surrounding concrete through strong chemical interaction with concrete.
- Due to its superior flexibility and distribution, TPPL fibers exhibited better synergy with PVA fibers than PPL fibers. The 0.66TPPL/0.33PVA hybrid increased shear strength by 36% and shear toughness by 139% compared to mono PVA fibers.
- The macro/micro-fiber hybridization positively delayed shear crack formation and propagation, enhancing shear performance. For instance, the 0.33PPL/0.66PVA combination increased shear strength by 28% and 23% and shear toughness by 159% and 46% compared to mono PVA and PPL fibers, respectively.
- The BF/PVA hybrid improved bonding strength and shear stress distribution, with 0.66PVA/0.33BF increasing shear strength by 24% and 16% over mono PVA and BF, respectively.
- SWSSC exhibited similar shear strength to normal concrete but 43% greater shear toughness due to its denser microstructure. Fiber addition improved stress distribution and crack resistance, with TPPL fibers being the most effective, increasing shear strength by 38% and toughness by 123%.
- The modified JSCE-SF6 shear test method effectively assessed shear strength, considering critical factors including concrete-steel friction, stress concentrations, and prestressed bolt loads, with specimen sizes aligned to Australian standards.

The investigation into hybrid fibers in SWSS concrete highlights their potential, showing improved shear performance over mono-fibers. However, further research is needed to optimize fiber content, evaluate performance under varying conditions, and assess long-

term durability in harsh environments such as chloride exposure, freeze-thaw cycles, and UV degradation. Future investigations should also include other fibers, such as carbon and glass fibers to further evaluate their compatibility and contribution to the performance of hybrid fiber-reinforced SWSSC.

Acknowledgements

The authors acknowledge the financial and laboratory support from the University of South Australia. Special thanks to the concrete laboratory technicians for their assistance. We are grateful to Adelaide Brighton Cement Ltd and Independent Cement and Lime Pty Ltd for donating OPC and GGBS, respectively, and to TEXO company for their donation of PPS and TPPL fibers. We recognize Dr. Murray Townsend, Mojtaba Karbasi from Department for Environment and Water (DEW), and Spiros Dimas from Department of Planning, Transport, and Infrastructure (DPTI), Government of South Australia, for providing sea-sand. Lastly, we acknowledge Microscopy Australia at the Future Industries Institute (FII), University of South Australia, for their expertise and instruments.

Chapter 6 References

AC10520942, A 2008, Standard test method for performing laboratory direct shear strength tests of rock specimens under constant normal force, ASTM Internat.,

Ali, B 2022, 'Development of environment-friendly and ductile recycled aggregate concrete through synergetic use of hybrid fibers', Environmental Science and Pollution Research, vol. 29, no. 23, pp. 34452-63.

Alimrani, NS & Balazs, GL 2023, 'Toughness and stiffness of fibre reinforced concrete in terms of shear capacity', Construction and Building Materials, vol. 389, p. 131711.

Amirhesam, M, Reza, H, Yan, Z, Xing, M, Christopher, WKC, Milad, B & Allan, M 2025, 'Cyclic performance of GFRP-reinforced seawater sea-sand concrete culverts reinforced with synthetic fibers', Structures, vol. 72, p. 108262.

Australia, S 2000, 'Methods of testing concrete-Method 11: Determination of the modulus of rupture (AS 1012.11)', Sydney, NSW: Standards Australia.

Australia, S 2007, AS 1379: Specification and Supply of Concrete, SAI Global Sydney.

Australia, S 2014, Methods for Testing Concrete, Preparation of Concrete Mixes in the Laboratory. AS 1012.2, Standards Australia Limited Sydney, Australia.

Bai, J 2009, 'Durability of sustainable concrete materials', Sustainability of construction materials, Elsevier, pp. 239-53.

Bajželj, B, Allwood, JM & Cullen, JM 2013, 'Designing climate change mitigation plans that add up', Environmental science & technology, vol. 47, no. 14, pp. 8062-69.

Banthia, N, Majdzadeh, F, Wu, J & Bindiganavile, V 2014, 'Fiber synergy in Hybrid Fiber Reinforced Concrete (HyFRC) in flexure and direct shear', Cement and Concrete Composites, vol. 48, pp. 91-97.

Batson, G, Jenkins, E & Spatney, R 1972, Steel fibers as shear reinforcement in beams, Journal Proceedings.

Blanco, A, Aire, C, Pujadas, P & Cavalaro, S 2017, 'Luong test for the characterization of the shear post-cracking response of fiber reinforced concrete', Construction and Building Materials, vol. 149, pp. 207-17.

Boulekbache, B, Hamrat, M, Chemrouk, M & Amziane, S 2012, 'Influence of yield stress and compressive strength on direct shear behaviour of steel fibre-reinforced concrete', Construction and Building Materials, vol. 27, no. 1, pp. 6-14.

Carrillo, J, Salcedo, E & Rojas, F 2024, 'Evaluating Direct Shear Performance of Steel Fiber–Reinforced Concrete', Journal of Materials in Civil Engineering, vol. 36, no. 2, p. 04023559.

Charron, J-P, Desmettre, C & Androuët, C 2020, 'Flexural and shear behaviors of steel and synthetic fiber reinforced concretes under quasi-static and pseudo-dynamic loadings', Construction and Building Materials, vol. 238, p. 117659.

Chen, Z, Li, S, Zhou, J, Xu, R & Dai, S 2022, 'Flexural behavior of GFRP bars reinforced seawater sea sand concrete beams exposed to marine environment: Experimental and numerical study', Construction and Building Materials, vol. 349, p. 128784.

Cuenca, E, Conforti, A, Monfardini, L & Minelli, F 2020, 'Shear transfer across a crack in ordinary and alkali activated concrete reinforced by different fibre types', Materials and structures, vol. 53, no. 2, pp. 1-15.

de Alencar Monteiro, VM, Lima, LR & de Andrade Silva, F 2018, 'On the mechanical behavior of polypropylene, steel and hybrid fiber reinforced self-consolidating concrete', Construction and Building Materials, vol. 188, pp. 280-91.

Decision, C 2003, 'Council Decision 2003/33/EC of 19 December 2002 establishing criteria and procedures for the acceptance of waste at landfills pursuant to Article 16 and Annex II to Directive 1999/31/EC', Official Journal of the European Communities, vol. 16, no. 2003, pp. 27-49.

Etxeberria, M, Gonzalez-Corominas, A & Pardo, P 2016, 'Influence of seawater and blast furnace cement employment on recycled aggregate concretes' properties', Construction and Building Materials, vol. 115, pp. 496-505.

Fattah, KP, Al-Tamimi, AK, Hamweyah, W & Iqbal, F 2017, 'Evaluation of sustainable concrete produced with desalinated reject brine', International Journal of Sustainable Built Environment, vol. 6, no. 1, pp. 183-90.

González-Aviña, J, Juárez-Alvarado, C, Terán-Torres, BT, Mendoza-Rangel, J, Durán-Herrera, A & Rodríguez-Rodríguez, J 2022, 'Influence of fibers distribution on direct shear and flexural behavior of synthetic fiber-reinforced self-compacting concrete', Construction and Building Materials, vol. 330, p. 127255.

Guidelines, ADW Version 3.8 Updated September 2022, Australian Drinking Water Guidelines,

Hadi, MN, Sajjad, U & Sheikh, MN 2022, 'Simple test method for determining shear strength of concrete', ACI Materials Journal, vol. 119, no. 1, pp. 173-80.

Hassanli, R, Manalo, A, Vafaei, D, Yekrangnia, M, Elchalakani, M & Noël, M 2023, 'Cyclic behavior of GFRP-reinforced concrete one-way slabs with synthetic fibers', Journal of Building Engineering, vol. 65, p. 105741.

Hoan, PT & Thuong, NT 2019, 'Shear resistance of ultra-high-performance concrete reinforced with hybrid steel fiber subjected to impact loading', Journal of Science and Technology in Civil Engineering (STCE)-HUCE, vol. 13, no. 1, pp. 12-20.

Hobbs, D 1982, 'Influence of pulverized–fuel ash and granulated blastfurnace slag upon expansion caused by the alkali–silica reaction', Magazine of concrete Research, vol. 34, no. 119, pp. 83-94.

Hofbeck, J, Ibrahim, I & Mattock, AH 1969, Shear transfer in reinforced concrete, Journal Proceedings.

Hoover, CG, Bažant, ZP, Vorel, J, Wendner, R & Hubler, MH 2013, 'Comprehensive concrete fracture tests: Description and results', Engineering Fracture Mechanics, vol. 114, pp. 92-103.

Huns, P 2020, '"Nature-Based Solutions" and Global Water Shortages: A Political Ecology of The United Nation's World Water Development Report 2018'.

Jang, H-O, Lee, H-S, Cho, K & Kim, J 2018, 'Numerical and Experimental Analysis of the Shear Behavior of Ultrahigh-Performance Concrete Construction Joints', Advances in Materials Science and Engineering, vol. 2018, no. 1, p. 6429767.

Jindal, RL 1984, 'Shear and moment capacities of steel fiber reinforced concrete beams', Special Publication, vol. 81, pp. 1-16.

Jindal, RL & Sharma, VR 1987, 'Behavior of steel fiber reinforced concrete knee-type beam-column connections', Special Publication, vol. 105, pp. 475-92.

Jongvivatsakul, P, Matsumoto, K & Niwa, J 2013, 'Shear capacity of fiber reinforced concrete beams with various types and combinations of fibers', Journal of JSCE, vol. 1, no. 1, pp. 228-41.

JSCE 1990, Method of test for shear strength of steel fiber reinforced concrete (SFRC). , Japan, Tokyo.

Kaidi, J, Xin, W, Lining, D, Zhiyuan, C, Huang, H, Xia, L, Jianxun, L & Zhishen, W 2023, 'Mechanical properties of multi-scale mono/hybrid non-metallic fiber-reinforced ultra-high performance seawater sea-sand concrete', Construction and Building Materials, vol. 401, p. 132922.

Khanlou, A, MacRae, G, Scott, A, Hicks, S & Clifton, G 2012, 'Shear performance of steel fibre-reinforced concrete'.

Kurup, AR & Senthil Kumar, K 2017, 'Effect of recycled PVC fibers from electronic waste and silica powder on shear strength of concrete', Journal of Hazardous, Toxic, and Radioactive Waste, vol. 21, no. 3, p. 06017001.

Kwon, Y-j 2005, 'A study on the alkali-aggregate reaction in high-strength concrete with particular respect to the ground granulated blast-furnace slag effect', Cement and concrete Research, vol. 35, no. 7, pp. 1305-13.

Li, M, Xing, D, Zheng, Q-B, Li, H, Hao, B & Ma, P-C 2022, 'Variation on the morphology and tensile strength of basalt fiber processed in alkali solutions', Construction and Building Materials, vol. 335, p. 127512.

Li, Q, Geng, H, Shui, Z & Huang, Y 2015, 'Effect of metakaolin addition and seawater mixing on the properties and hydration of concrete', Applied Clay Science, vol. 115, pp. 51-60.

Li, Z-X, Li, C-H, Shi, Y-D & Zhou, X-J 2017, 'Experimental investigation on mechanical properties of hybrid fibre reinforced concrete', Construction and Building Materials, vol. 157, pp. 930-42.

Lothenbach, B, Scrivener, K & Hooton, R 2011, 'Supplementary cementitious materials', Cement and concrete Research, vol. 41, no. 12, pp. 1244-56.

Mashayekhi, A, Hassanli, R, Zhuge, Y, Ma, X & Chow, CW 2024a, 'Synergistic effects of fiber hybridization on the mechanical performance of seawater sea-sand concrete', Construction and Building Materials, vol. 416, p. 135087.

Mashayekhi, A, Hassanli, R, Zhuge, Y, Ma, X, Chow, CW, Bazli, M & Manalo, A 2024b, 'Cyclic flexural performance of seawater sea-sand concrete reinforced with hybrid fibers', Construction and Building Materials, vol. 449, p. 138480.

Mashayekhi, A, Hassanli, R, Zhuge, Y, Ma, X, Chow, CW, Bazli, M & Manalo, A 2024c, 'Synergistic effects of fiber hybridization on the fracture toughness of seawater sea-sand concrete', Construction and Building Materials, vol. 444, p. 137845.

Mashayekhi, A, Hassanli, R, Zhuge, Y, Ma, X, Chow, CW, Bazli, M & Manalo, A 2024d, 'Structural behaviour of small GFRP-reinforced seawater sea-sand fiber reinforced concrete culverts', Structures.

Miller, SA, Horvath, A & Monteiro, PJ 2018, 'Impacts of booming concrete production on water resources worldwide', Nature Sustainability, vol. 1, no. 1, pp. 69-76.

Mirsayah, AA & Banthia, N 2002, 'Shear strength of steel fiber-reinforced concrete', Materials Journal, vol. 99, no. 5, pp. 473-79.

Moghadam, MA & Izadifard, RA 2020, 'Effects of steel and glass fibers on mechanical and durability properties of concrete exposed to high temperatures', Fire Safety Journal, vol. 113, p. 102978.

Mohammadi, Y, Singh, S & Kaushik, S 2008, 'Properties of steel fibrous concrete containing mixed fibres in fresh and hardened state', Construction and Building Materials, vol. 22, no. 5, pp. 956-65.

Navas, FO, Navarro-Gregori, J, Herdocia, GL, Serna, P & Cuenca, E 2018, 'An experimental study on the shear behaviour of reinforced concrete beams with macro-synthetic fibres', Construction and Building Materials, vol. 169, pp. 888-99.

Nguyen, D-L, Thai, D-K & Lam, MN-T 2022, 'Synergy in Flexure of High-Performance Fiber-Reinforced Concrete with Hybrid Steel Fibers', Journal of Materials in Civil Engineering, vol. 34, no. 6, p. 04022090.

Pakravan, HR & Ozbakkaloglu, T 2019, 'Synthetic fibers for cementitious composites: A critical and in-depth review of recent advances', Construction and Building Materials, vol. 207, pp. 491-518.

Picazo, A, Alberti, M, Gálvez, J & Enfedaque, A 2021, 'Shear slip post-cracking behaviour of polyolefin and steel fibre reinforced concrete', Construction and Building Materials, vol. 290, p. 123187.

Reis, J & Ferreira, A 2004, 'Assessment of fracture properties of epoxy polymer concrete reinforced with short carbon and glass fibers', Construction and Building Materials, vol. 18, no. 7, pp. 523-28.

Shi, Z, Shui, Z, Li, Q & Geng, H 2015, 'Combined effect of metakaolin and sea water on performance and microstructures of concrete', Construction and Building Materials, vol. 74, pp. 57-64.

Simalti, A & Singh, A 2020, 'Comparative study on direct shear behavior of manufactured and recycled shredded tyre steel fiber reinforced self-consolidating concrete', Journal of Building Engineering, vol. 29, p. 101169.

Soetens, T & Matthys, S 2017, 'Shear-stress transfer across a crack in steel fibre-reinforced concrete', Cement and Concrete Composites, vol. 82, pp. 1-13.

Soundarya, N 2022, 'A review on the physical & chemical properties of sea sand to be used a replacement to fine aggregate in concrete', Materials Today: Proceedings, vol. 51, pp. 1527-31.

Tassew, S & Lubell, A 2014, 'Mechanical properties of glass fiber reinforced ceramic concrete', Construction and Building Materials, vol. 51, pp. 215-24.

Tonon, F 2021, 'JSCE-SF6 Limitations for Shear Tests and ASTM D5607 Shear Tests on Fiber-Reinforced Concrete', ACI Materials Journal, vol. 118, no. 3.

Vafaei, D, Hassanli, R, Ma, X, Duan, J & Zhuge, Y 2021, 'Sorptivity and mechanical properties of fiber-reinforced concrete made with seawater and dredged sea-sand', Construction and Building Materials, vol. 270, p. 121436.

Vafaei, D, Hassanli, R, Ma, X, Duan, J & Zhuge, Y 2022a, 'Fracture Toughness and Impact Resistance of Fiber-Reinforced Seawater Sea-Sand Concrete', Journal of Materials in Civil Engineering, vol. 34, no. 5, p. 04022038.

Vafaei, D, Ma, X, Hassanli, R, Duan, J & Zhuge, Y 2022b, 'Microstructural and mechanical properties of fiber-reinforced seawater sea-sand concrete under elevated temperatures', Journal of Building Engineering, vol. 50, p. 104140.

Vafaei, D, Ma, X, Hassanli, R, Duan, J & Zhuge, Y 2022c, 'Microstructural behaviour and shrinkage properties of high-strength fiber-reinforced seawater sea-sand concrete', Construction and Building Materials, vol. 320, p. 126222.

Vafaei, D, Ma, X, Hassanli, R, Duan, J & Zhuge, Y 2023, 'Experimental study on cyclic flexural behaviour of GFRP-reinforced seawater sea-sand concrete slabs with synthetic fibres', Ocean Engineering, vol. 273, p. 114014.

Vairagade, VS & Dhale, SA 2023, 'Hybrid fibre reinforced concrete–a state of the art review', Hybrid Advances, vol. 3, p. 100035.

Wang, J, Liu, E & Li, L 2018, 'Multiscale investigations on hydration mechanisms in seawater OPC paste', Construction and Building Materials, vol. 191, pp. 891-903.

Wang, Q-z, Li, L-j, Zhao, Y-x, Song, Y & Zhang, C-l 2024, Feasibility assessment and application of sea sand in concrete production: A review, Structures.

Wang, Q, Ding, Y & Randl, N 2021, 'Investigation on the alkali resistance of basalt fiber and its textile in different alkaline environments', Construction and Building Materials, vol. 272, p. 121670.

Wang, Y, Shui, Z, Gao, X, Huang, Y, Yu, R & Song, Q 2020, 'Chloride binding capacity and phase modification of alumina compound blended cement paste under chloride attack', Cement and Concrete Composites, vol. 108, p. 103537.

Xie, F, Cai, D, Ji, L, Zhang, C & Ruan, J 2021, 'Experimental study on the mechanical properties of internally cured concrete with super absorbent polymer under monotonic and cyclic loads', Construction and Building Materials, vol. 270, p. 121495.

Xiong, Z, Wei, W, He, S, Liu, F, Luo, H & Li, L 2021, 'Dynamic bond behaviour of fibre-wrapped basalt fibre-reinforced polymer bars embedded in sea sand and recycled aggregate concrete under high-strain rate pull-out tests', Construction and Building Materials, vol. 276, p. 122195.

Yang, S, Zang, C, Xu, J & Fan, G 2020, 'Determination of Fracture Parameters of Seawater Sea Sand Concrete Based on Maximum Fracture Load', Journal of Materials in Civil Engineering, vol. 32, no. 1, p. 04019315.

Yang, Z, Lu, F, Zhan, X, Zhu, H, Zhang, B, Chen, Z & Zhang, H 2024, 'Mechanical properties and mesoscopic damage characteristics of basalt fibre-reinforced seawater sea-sand slag-based geopolymer concrete', Journal of Building Engineering, vol. 84, p. 108688.

Younis, A, Ebead, U, Suraneni, P & Nanni, A 2018, 'Fresh and hardened properties of seawater-mixed concrete', Construction and Building Materials, vol. 190, pp. 276-86.

Zainal, SIS, Hejazi, F, Aziz, FNA & Jaafar, MS 2020, 'Effects of hybridized synthetic fibers on the shear properties of cement composites', Materials, vol. 13, no. 22, p. 5055.

Zeng, J-J, Liao, J, Zhuge, Y, Guo, Y-C, Zhou, J-K, Huang, Z-H & Zhang, L 2022, 'Bond behavior between GFRP bars and seawater sea-sand fiber-reinforced ultra-high strength concrete', Engineering Structures, vol. 254, p. 113787.

Zhang, P, Yang, Y, Wang, J, Jiao, M & Ling, Y 2020, 'Fracture models and effect of fibers on fracture properties of cementitious composites—A review', Materials, vol. 13, no. 23, p. 5495.

Zhang, R, Matsumoto, K, Hirata, T, Ishizeki, Y & Niwa, J 2014, 'Shear behavior of polypropylene fiber reinforced ECC beams with varying shear reinforcement ratios', Journal of JSCE, vol. 2, no. 1, pp. 39-53.

Zhang, ZH, Sang, ZQ, Zhang, LY, Ma, ZX & Zhang, Y 2013, Experimental research on durability of concrete made by seawater and sea-sand, Advanced Materials Research.

Zhao, Y, Hu, X, Shi, C, Zhang, Z & Zhu, D 2021, 'A review on seawater sea-sand concrete: Mixture proportion, hydration, microstructure and properties', Construction and Building Materials, vol. 295, p. 123602.

Zhihao, W, Jianhe, X, Jianglin, L, Peng, L, Cuiqing, S & Zhongyu, L 2022, 'Flexural behaviour of seawater–sea sand concrete beams reinforced with GFRP bars: Effects of the reinforcement ratio, stirrup ratio, shear span ratio and prestress level', Journal of Building Engineering, vol. 54, p. 104566.

7 Structural behaviour of small GFRP-reinforced seawater sea-sand fiber reinforced concrete culverts

Reprinted and reformatted (including changes to the referencing style) with permission from Elsevier Ltd (see Appendix B).

Mashayekhi, A, Hassanli, R, Zhuge, Y, Ma, X, W. K. Chow, C, Bazli, M & Manalo, A 2024, 'Structural behaviour of small GFRP-reinforced seawater sea-sand fiber reinforced concrete culverts', Structures, vol. 69, p. 107492.

Abstract

This study investigates the structural behaviour of fiber-reinforced seawater sea-sand (FR-SWSS) concrete culverts employing glass fiber-reinforced polymer (GFRP) bars as internal reinforcements. Eighteen small concrete culverts with a total width of 470 mm and two different total heights of 425 mm and 365 mm, conforming to the Australian standard were subjected to experimental evaluation. The study investigated various parameters, including fiber type (macro polypropylene (PPL), macro twisted polypropylene (TPPL), micro polyvinyl alcohol (PVA), and micro basalt (BA) fibers), fiber hybridization, compression GFRP reinforcement, crown thickness, haunches, and concrete compressive strength. A comprehensive analysis of culvert behaviour was conducted, encompassing load at first crack, crack propagation, load-displacement response at the mid-span of the crown, ultimate load-carrying capacity, energy dissipation, ductility, and failure mode. The results showed that punching shear at the crown was the prevalent failure mode for FR-SWSS culverts. The ultimate shear capacity, cracking strength, and energy dissipation of culverts were significantly enhanced by the addition of fibers, particularly hybrid fibers (PVA/BA and PPL/PVA). Partial substitution of PPL fiber with PVA resulted in a substantial increase in ultimate strength compared to PPL fiber culvert. The performance and effectiveness of fibers, especially hybrid ones, were significantly influenced by the presence of compression GFRP reinforcement and reduced crown thickness. Haunches had a profound impact on the shear strength of GFRP-reinforced culverts and significantly altered the performance of fibers. This study demonstrates that FR-SWSS concrete culverts reinforced with GFRP bars and discrete fibres can serve as a sustainable alternative to conventional concrete culverts.

Keywords

Culverts; Hybrid fibers; GFRP; Shear capacity; Seawater; Sea-sand; Structural performance; Shear failure; PVA.

7.1 Introduction

Small concrete culverts (SCC), frequently used under driveways and sidewalks, play a critical role in stormwater management, flood prevention, and transportation network preservation. As shown in **Figure 7-1**, SCCs act as bridges over minor streams and drainage ditches, ensuring water flow. Despite their diverse applications, steel reinforced culverts face durability challenges. Exposed to harsh environments, they endure the detrimental effects of surrounding soil, water containing chemicals and salts, and other substances, leading to long-term damage and corrosion. This significantly reduces their service life and increases maintenance costs. While the prospect of using more sustainable alternatives with non-corrosive reinforcement is appealing, previous studies have predominantly focused on steel-reinforced large concrete culverts.



Figure 7-1 The application of small culverts.

Fiber-reinforced polymers (FRPs) offer a compelling alternative to steel in concrete structures due to their superior properties: low weight, high tensile strength, and exceptional corrosion resistance (Manalo *et al.* 2021; Xiao *et al.* 2023b; Mostafa *et al.* 2024). This eliminates corrosion, extending the lifespan of concrete, especially in harsh environments (Zhang, Pu *et al.* 2022). Among FRPs, glass fiber-reinforced polymer (GFRP) emerges as suitable for reinforcement due to their relative lower cost (Amran 2018; Xiao *et al.* 2023b). Studies on GFRP-reinforced culverts demonstrate their adequate load-carrying capacity through acceptable deflection and crack width and impressive long-term performance, maintaining microstructural integrity and mechanical

properties over time (Alkhrdaji *et al.* 2001; Gooranorimi *et al.* 2017b; Hassanli *et al.* 2022). With exceptional stability against saltwater, chemicals, and alkaline environments, GFRP proves ideal for sustainable concrete alternatives like seawater and sea-sand (SWSS) concrete (Wang *et al.* 2017b; D'Antino *et al.* 2018; Wang, Zike *et al.* 2018).

SWSS concrete made from abundant natural resources, a sustainable alternative with freshwater conservation, reduced transportation and maintenance cost, and exceptional marine environment resilience, proves ideal for coastal and environmental projects like artificial reefs (Tjaronge *et al.* 2015). Its cost-effectiveness makes it particularly attractive in water-scarce regions with limited high-quality aggregate access. While research exists on FRP bars in various SWSS concrete elements, studies on SWSS concrete culverts reinforced with FRP bars are scarce. Existing literature demonstrates that GFRP bars exhibit superior durability compared to basalt FRP (BFRP) bars when used in SWSS concrete (Wang *et al.* 2017b; Wang, Zike *et al.* 2018). Studies on GFRP-reinforced SWSS slabs and beams also indicate the viability of GFRP bars as a steel alternative with similar shear behaviour (Vafaei *et al.* 2023; Zhou *et al.* 2023). The ultimate load of these beams increased with both the reinforcement ratio and the shear span ratio (Wang, Zhihao *et al.* 2022). However, marine exposure can negatively impact bond behaviour, leading to reduced stiffness, ductility, and bond strength (Chen *et al.* 2022; Zhou *et al.* 2023).

Previous studies have investigated the use of fibers to enhance the mechanical properties of SWSS concrete. Polyvinyl alcohol (PVA)/basalt (BF) hybrid fibers have been shown to significantly improve the total energy absorption and residual strength of SWSS concrete under compression compared to mono BF (Mashayekhi *et al.* 2024a). While seawater sea-sand recycled aggregate concrete (SSRAC) generally exhibited higher compressive strength than ordinary concrete (Huang *et al.* 2018), the addition of stainless steel fibers (SSF) and polypropylene (PP) fibers increased compressive and splitting tensile strengths by an average of 17.30% and 2.87% (18.48% and 12.23%), respectively [19]. Micro-fiber hybridization, combining different types of fibers, has been found to significantly improve both flexural strength and fracture energy of SSRAC. Hybrid PP/BF and PP/PVA fibers have demonstrated notably improved fracture energy, with increases of 176% and 290% compared to PP fibers alone [20].

Previous studies employed fibers to improve the mechanical properties of SWSS concrete. Polyvinyl alcohol (PVA)/basalt (BF) hybridization significantly improved the total energy absorption and residual strength of SWSS concrete under compression by 44% and 181% compared to using mono BF incorporation (Mashayekhi *et al.* 2024a). While seawater sea-sand recycled aggregate concrete (SSRAC) generally exhibited higher compressive strength than ordinary concrete (Huang *et al.* 2018), reinforcing SSRAC with stainless steel fibers (SSF) and polypropylene (PP) fibers improved its mechanical performance. Studies reported that SSF-reinforced SSRAC and PP-reinforced SSRAC resulted in average compressive strengths that were 17.30% and 2.87% higher, respectively, compared to plain SSRAC. Additionally, the splitting tensile strengths of these fiber-reinforced SSRACs were 18.48% and 12.23% higher, respectively (Huang *et al.* 2022). Furthermore, research has indicated that hybridizing micro-fibers can significantly improve both the flexural strength and fracture energy of SWSS concrete. Hybrid combinations of PP/BF, or PP/PVA, have been shown to increase fracture energy by 176% and 290%, respectively, compared to using PP fibers alone (Mashayekhi *et al.* 2024d).

Multiple studies investigated the use of fibers to enhance the performance of FRP-reinforced SWSS concrete, particularly addressing bonding strength concerns. Incorporating 0.5% polyethylene (PE) fibers significantly increased bond strength by 3-10% (Zeng *et al.* 2022), while glass fibers improved bond stiffness without significantly impacting FRP bar bond strength (Xiong, Z *et al.* 2021). Though FRP bars offer advantages, their lower modulus results in wider cracks and larger deflections compared to steel bars (Amran 2018; Mahaini *et al.* 2023). However, PP and PVA fibers significantly reduced crack width and spacing in SWSS concrete slabs compared to plain concrete (Vafaei *et al.* 2023). Additionally, GFRP-RC slabs with plain SWSS concrete exhibited a 13% lower cracking moment than ACI 440.1R-15 (Institute 2015) predictions, but this was mitigated by adding fibers, particularly PP fibers (Vafaei *et al.* 2023). Furthermore, PP and PVA fibers improved ductility, tensile strength, and energy absorption, and reducing crack formation of SWSS concrete (Vafaei *et al.* 2021a, 2022a). However, limitations exist for mono-fibers, regardless of size, due to challenges in achieving uniform distribution and their limited impact on crack control, tensile strength, toughness, and bonding (Chenggong *et al.* 2023; Kaidi *et al.* 2023). This restricts their applicability and overall potential for enhancing mechanical properties.

Combining micro and macro fibers, chosen strategically for material, volume, aspect ratio, and bond strength, significantly enhances the mechanical performance, ductility, and long-term service life of both normal and SWSS concrete, overcoming limitations of single-fiber reinforcement (Chenggong *et al.* 2023; Kaidi *et al.* 2023). Specific fiber combinations like carbon/polypropylene/aramid significantly improved GFRP bar bonding (Huang *et al.* 2020), while steel/PVA fibers alongside GFRP bars resulted in substantial increases in bond strength, energy dissipation, and deformation capacity (Xiao *et al.* 2023a). Hybrid fibers also enhanced shear strength and ultimate load capacity of GFRP-reinforced concrete beams by 55% to 233% compared to non-fiber ones (Vakili *et al.* 2019). Hybrid steel/ polyolefin (PO) fibers effectively improved the shear strength and ductility of GFRP-reinforced beams, shifting failure modes from brittle to ductile (Dev *et al.* 2020a). Hybrid fibers outperformed mono fibers in enhancing post-cracking stiffness due to their combined crack resistance properties (Patil *et al.* 2020). Incorporating hybrid basalt/polyolefin fibers and a GFRP laminate into concrete beams with GFRP bars resulted in significant 59% and 49% enhancements in maximum yield and ultimate load, respectively, showcasing the effectiveness of hybrid fibers (Ramesh *et al.* 2020).

While previous research has demonstrated the potential application of GFRP bars as an alternative to steel in concrete culverts, limitations have been identified regarding crack width and deformation under load. Aiming to address this gap in knowledge and further enhance both structural performance and sustainability, this research investigates the combined use of non-corrosive GFRP bars and fibers with fiber-reinforced seawater and sea-sand concrete (FR-SWSSC). Employing mono- and hybrid-fibers in SWSSC, the study evaluates the mechanical properties, strength, and ductility of GFRP-reinforced culverts at both material and structural levels. Additionally, the research explores the influence of several parameters on performance, including compression reinforcement, slab thickness, haunches, and concrete strength. This study seeks to provide valuable insights into the behaviour of GFRP-reinforced concrete culverts using FR-SWSSC, demonstrating its potential as a viable, cost-effective, and sustainable alternative with enhanced performance.

7.2 Experimental program

7.2.1 Material properties and mixture proportions

SWSS concrete, designed for a 150 mm slump and 50 MPa compressive strength, adhering to the specifications outlined in AS 1379-2007 (Standard 2007) and AS 1597.2-2013 (AS1597.2-2013 2013), respectively, was employed for the culvert construction. Seawater from Adelaide coastal water with significantly elevated chloride and sulfate levels compared to tap water was utilized and carefully stored to prevent contamination. Sea-sand was obtained from Semaphore beach in Adelaide, and meticulously cleaned to remove impurities, served as the fine aggregate. Crushed basalt from a local quarry provided the coarse aggregate, with a maximum size of 14 mm. Ordinary Portland cement (OPC) and ground granulated blast furnace slag (GGBS) were employed as cementitious materials. To achieve the desired slump, a polycarboxylate ether-based superplasticizer was added to each mix.

This study investigated the use of mono/hybrid fibers (synthetic and natural) to improve the performance of SWSS concrete culverts. Untreated micro-fibers (polyvinyl alcohol and basalt) and macro-fibers (polypropylene and twisted polypropylene) were selected for cost-effectiveness. **Table 7-1** details the properties of these fibers provided by the manufacturer. Macro-fibers of similar length but varying aspect ratios and elastic modulus were utilized to evaluate their performance. An environmentally friendly recycled plastic PPL fiber, readily available in the Australian market, commercially named eMesh and manufactured by FIBERCON, was also chosen. Basalt fibers were selected for their high tensile strength, cost-effectiveness, and eco-friendliness. Uniform-length micro-fibers were used to minimize their influence on results.

Two GFRP bar shapes were used to manufacture the culverts: U-shaped and straight, both with a 10 mm diameter and manufactured via pultrusion. **Table 7-2** details the material properties of the GFRP bars, as specified by the manufacturer. The study utilized both mono-fiber and hybrid-fiber to investigate the influence of fibers on SWSS concrete culverts. Following the approach implemented in previous research (Mashayekhi *et al.* 2024a), four fiber-reinforced mixes were selected: PPL, TPPL, hybrid micro PVA/BA, and hybrid micro/macro PPL/PVA. For comparison, two additional mixes were included: plain SWSS and high-strength PPL-reinforced SWSS. **Table 7-3** details the specific mix proportions and **Table 7-4** details their corresponding

Table 7-1 Physical properties of different fibers.

Property	PVA[1]	BA[2]	PPL[3]	TPPL[4]
Specific gravity	1.3	1.57	0.91	0.91
Length (mm)	8	7	47	54
Diameter (μm)	38	15	—	800
Thickness (μm)	—	—	<500	—
Tensile strength (MPa)	1600	2900	400	620
Young's modulus (GPa)	40	85	6	9.5
Chemical resistance	Excellent	Excellent	Excellent	Excellent
Melting point (°C)	225	1450	160	160
Water absorption (% by weight)	<1	<1	Nil	Nil
Alkali resistance	Excellent	—	Excellent	Excellent
Corrosion resistance	Excellent	—	Excellent	Excellent
Shape				

[1] polyvinyl alcohol, [2] basalt fiber, [3] long polypropylene, [4] long twisted polypropylene.

Table 7-2 Physical properties of GFRP bars.

Property	Bar type	
	GFRP #3	
Nominal bar diameter (mm)	9.52	
Cross-sectional area (mm^2)	71	
Tensile elastic modulus (GPa)	60	
Ultimate tensile strength (MPa)	1000	
Strength of Bend (MPa)	Straight Portion	900
	Bend Portion	600
Ultimate tensile strain	0.017	
Glass Transition Temperature, T_g°	125 °c	

Table 7-3 Mix proportions of SWSS concrete.

Concrete mix	Total fiber volume fraction (%)	Mix proportions (kg/m^3)								
		Micro-fiber		Macro-fiber		Binder		Gravel	Seawater	Sea-sand
		PVA	BA	PPL	TPPL	OPC	GGBS			
Plain SWSS	—	—	—	—	—					
PPL	0.66	—	—	6.0	—					
TPPL	0.66	—	—	—	6.0	144	267	925	222	755
PPL/PVA	0.66	2.86	—	4.0	—					
PVA/BA	0.66	5.72	6.16	—	—					
HS-PPL	0.66	—	—	6.0	—	193	357	925	222	700

Table 7-4 Mechanical properties of different FR-SWSS concrete mixes.

Concrete mix	Compressive strength (MPa)	Splitting tensile strength (MPa)	Modulus of rupture (MPa)
Plain SWSS	47.7	4.34	4.4
PPL	50.5	4.88	4.9
TPPL	56.7	4.95	5.5
PPL/PVA	52.5	5.08	5.1
PVA/BA	55.2	4.80	5.4
HS-PPL	75.5	6.6	6.7

mechanical properties. The study employed a total fiber volume fraction of 0.66%, to provide a balance between optimal strength and workability. Increasing the dosage could lead to clumping, while a lower content might not significantly enhance properties as was experience by previous studies (Pakravan *et al.* 2019).

7.2.2 Test specimens and preparation

A total of 18 GFRP-reinforced concrete culverts were tested which were categorized into five groups as shown **Table 7-5**. Group I utilized five SWSSC mixes (**Table 7-3**), while

Table 7-5 Summary of culvert specimens.

Group	Culvert designation	Concrete mix	Slab thickness (mm)	GFRP reinforcement		Span	Height	Objective
				Bottom	Top			
I	C135-G1	SWSS	135	5 Ø 10	—	320	285	Effect of different fibers
	C135-G1-PL	PPL						
	C135-G1-TP	TPPL						
	C135-G1-PV/PL	PPL/PVA						
	C135-G1-BA/PV	PVA/BA						
II	C135-G2-PL	PPL	135	5 Ø 10	5 Ø 10	320	285	Effect of compression reinforcement
	C135-G2-TP	TPPL						
	C135-G2-PV/PL	PPL/PVA						
III	C80-G1-PL	PPL	80	5 Ø 10	—	320	285	Effect of crown thickness
	C80-G1-TP	TPPL						
	C80-G1-PV/PL	PPL/PVA						
	C80-G1-BA/PV	PVA/BA						
IV	C80-G1-PL-H	PPL	80	5 Ø 10	—	314	285	Effect of haunches
	C80-G1-TP-H	TPPL						
	C80-G1-PV/PL-H	PPL/PVA						
	C80-G1-BA/PV-H	PVA/BA						
V	C135-G1-PL.H	HS-PPL	135	5 Ø 10	—	320	285	Effect of concrete strength
	C135-G2-PL.H			5 Ø 10	5 Ø 10			

Groups II-V investigated the influence of compression reinforcement, crown thickness, haunches, and SWSS concrete strength, respectively. **Figure 7-2** presents the details of the culverts, including the size and spacing of the GFRP reinforcement. These dimensions comply with the Australian code for precast steel reinforced concrete box culverts (AS 1597.1-2010 (AS1597.1-2010 2010)).

Figure 7-3 illustrates the fabrication of culvert specimens. Plywood formworks were built and sealed with silicone for leak prevention (**Figure 7-3**a). GFRP cages were constructed and secured within the formwork using plastic chairs and ties, while lifting lugs were attached for ease of movement (**Figure 7-3**b). Strain gauges were mounted on longitudinal GFRP bars at mid-span for elongation measurement (**Figure 7-3**b). Concrete was vibrated for efficient compaction, especially for FRC culverts. After casting, culverts were covered in plastic for 24 hours and demolded after 48 hours, following the same curing process as cylindrical and beam specimens. All culverts were maintained under moisture curing conditions for over 45 days prior to testing, ensuring that all specimens reached their maximum strength. For enhanced crack visibility, culverts were painted white and marked with a grid pattern.

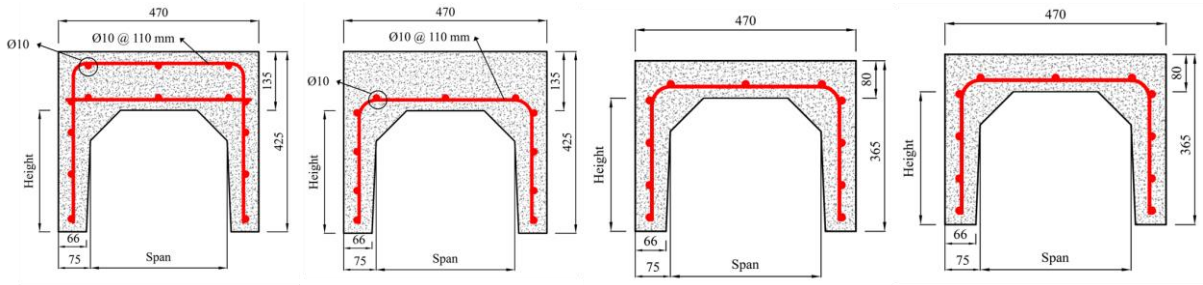


Figure 7-2 The details of culverts, a) group Ⅰ, Ⅱ, and Ⅴ, b) group Ⅲ, and c) group Ⅳ

Test setup, instrumentation, and testing procedure

Figure 7-4 depicts the culvert test setup, adhering to AS1597.1-2010 guidelines (AS1597.1-2010 2010). An 1,800-kN universal testing machine was used to apply load at 0.02 mm/s displacement rate until a 25% strength reduction was achieved. No lateral load was applied to simulate poor sidefill compaction to simulate the worst-case loading scenario, known to increase crown loads and compromise structural integrity (Ramadan *et al.* 2022b, 2022a). It is important to note that applying lateral load and providing additional support can potentially increase the ultimate strength of culverts (Hassanli *et al.* 2022). Two steel channels with about 10 mm clearance (**Figure 7-4**) simulated the

base slab behaviour and partially restrained leg lateral movements. Rubber pad strips between the legs and channels provided cushioning and prevented stress concentration as per AS1597.1-2010 (AS1597.1-2010 2010). A 10-mm rubber pad replicating a vehicle wheel and promoting even load distribution was placed on the culvert slab, followed by a rectangular steel bearing block (50 mm ×125 mm surface, 20 mm thickness). A LVDT positioned beneath the culvert midspan measured its vertical deflection. Two smaller LVDTs attached to the top of the legs (**Figure 7-4**) tracked the expected compression of the rubber pads placed under the culvert legs. Two strain gauges, capable of measuring large strains, were attached to the middle of GFRP bars (top and bottom) in the crown to monitor their strain behaviour. To protect them during concrete casting, the gauges were covered with duct tape and their wires carefully positioned.



(a) (b) (c)

Figure 7-3 The fabrication of culvert specimens, (a) plywood formwork sealed with silicone, (b) GFRP cage secured in formwork using plastic chairs and ties, and (c) casted SWSS concrete culverts.

7.3 Test results and observations

This section presents the results of two distinct parts of this study: (1) material testing of SWSS concrete, and (2) evaluation of the impact of different fibers on the performance of GFRP-reinforced culverts.

7.3.1 Behaviour of SWSS concrete

The results of material testing performed on fiber-reinforced SWSS concrete are presented in detail in Appendix A.

7.3.2 Behaviour of GFRP-reinforced SWSS concrete culverts

Five groups of GFRP-reinforced culverts were studied to assess the influence of various parameters on their performance. Group I examined the effect of fiber type (mono and hybrid), Group II investigated the impact of compression reinforcement, Group III focused on the influence of crown thickness, Group IV evaluated the role of haunches, and Group V studied the effect of concrete strength. The key observations from the testing of these culverts will be presented in the following sections.

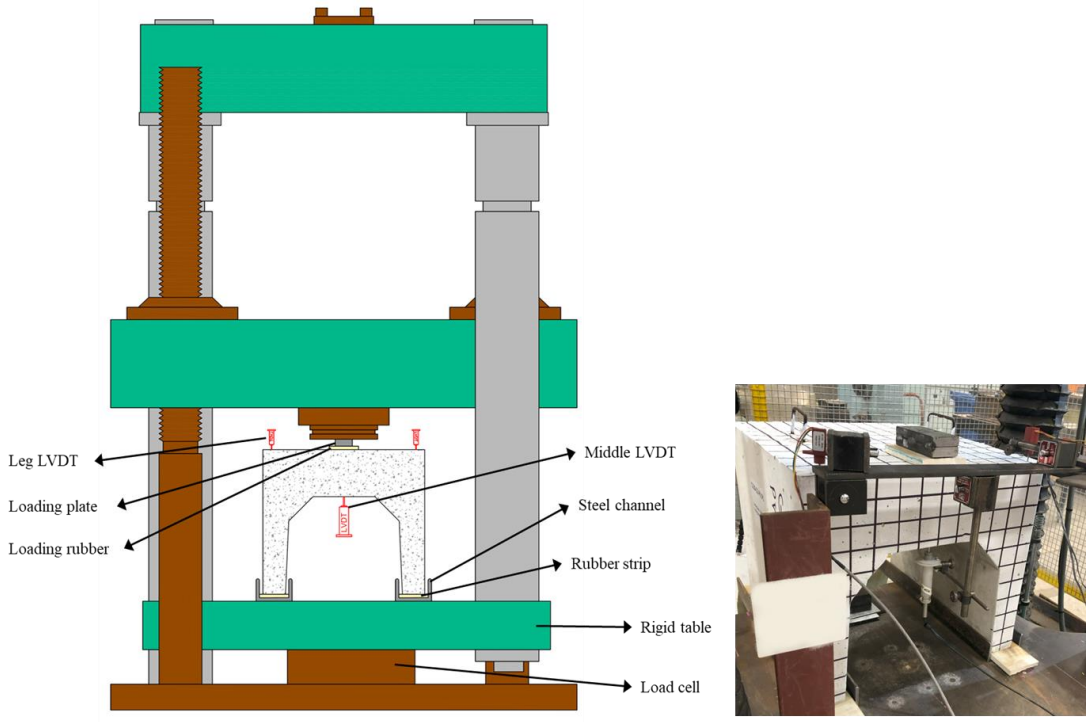


Figure 7-4 Test setup.

7.3.2.1 Crack pattern and failure mode

Figure 7-5 shows the crack pattern observed in the culverts at the failure point. The presence of a primary shear crack diagonally through the haunch, aligns with observations in the previous studies on GFRP culverts (Hassanli *et al.* 2022). Unlike steel-reinforced culverts, where flexural cracks are predominant (Abolmaali *et al.* 2008b), GFRP-reinforced culverts are more prone to shear cracks. This is primarily attributed to the lower modulus of elasticity of GFRP reinforcement, which significantly influences crack width limitations (Hassanli *et al.* 2022). Moreover, the dowel action of longitudinal reinforcement is negligible in GFRP bars due to their limited shear capacity in the transverse direction (Hassanli *et al.* 2022). Notably, all specimens initially exhibited

flexural cracks before transitioning to shear-dominant failure. This can be attributed to the high tensile stress at the bottom of the crown, which caused flexural cracks to form initially, as observed in previous studies on one-way and two-way GFRP-reinforced slabs (AlHamaydeh *et al.* 2021; Hassanli *et al.* 2023; Vafaei *et al.* 2023; Hassanli *et al.* 2024).

Fibers in Group I extended the length of the primary shear crack, initiating it from the load point and extending towards the end or middle of the haunch. Fiber-reinforced specimens typically failed with one dominant shear crack, except for the hybrid PPL/PVA fiber-reinforced concrete. This hybrid specimen developed two cracks, highlighting its ability to significantly increase shear strength. Additionally, this behaviour was also observed in Group III specimens with an 80 mm crown. This enhancement can be attributed to the synergistic effect of PPL/PVA hybridization, which resulted in a more uniform distribution of shear stresses. This, in turn, led to the formation of two primary shear cracks and a subsequent increase in the ultimate strength of culvert.

Reducing the crown thickness (group III) altered the shear failure path, increasing its angle and causing early failure before engaging the haunches, negating their influence on shear strength. Removing the haunches (group IV) further modified the path, directing it towards the leg tips with a single, dominant crack observed consistently. These findings suggest that haunches can significantly enhance the shear strength of concrete culverts, provided that the crown thickness is adequate. By reducing the effective span length, haunches lead to a lower span-to-depth ratio. This reduction in span-to-depth ratio is known to increase the ultimate shear strength of concrete culverts, similar to the behaviour of concrete beams (Guo 2014). PPL fibers effectively limited initial cracking in group IV, while replacing a portion of PPL with PVA fibers (hybrid PPL/PVA) resulted in more pronounced flexural cracks at mid-span. This suggested that the addition of PVA fibers resulted in a more uniform distribution of stress in the tensile portion of the section. TPPL fibers, due to their distribution, displayed a unique shear crack path with a higher angle and greater distance from the loading point. The uniform distribution of TPPL fibers and their strong bond with the concrete matrix effectively transferred shear stresses, preventing crack propagation, and resulting in a distinct shear crack path and angle.

Adding compression reinforcement (group II) considerably altered the shear crack behaviour of hybrid PPL/PVA fiber specimens, resulting in a single primary shear crack. In addition, PPL and TPPL fibers displayed contrasting crack patterns and angles. While

G135-G2-PL specimens exhibited a higher number of high-angle cracks compared to G135-G2-TP specimens, the crack lengths were shorter. These findings may be attributed to the presence of compression reinforcement, which can redistribute stresses within the section and potentially reduce the concentration of shear stresses at critical locations. This could potentially alter the failure mode of culverts reinforced with different fiber types. When concrete strength was increased (group V), G135-G1-PL.H developed more primary shear cracks. In contrast, G135-G2-PL.H displayed fewer cracks but fully utilized the haunch capacity. The primary crack shifted towards the haunch end and grew longer compared to G135-G2-PL.

7.3.2.2 Load–deflection behaviour

Figure 7-6 displays the load versus mid-span deflection curves for all culvert groups, revealing three distinct phases. The initial phase was linear and identical for all groups, followed by a second linear phase with a smaller slope, signifying reduced stiffness due to concrete cracking and lower effective inertia moment (Zhou *et al.* 2023). This slope was influenced by factors like fiber distribution, modulus, and length (Vakili *et al.* 2019). The final phase exhibited varying slopes in post-peak behaviour, influenced by the type and distribution of fibers.

Specimen C135-G1 with no fiber exhibited a significant (20%) decrease in load following initial cracking, attributed to the low GFRP bar elastic modulus replicating previous observations (Dev *et al.* 2020a; Patil *et al.* 2020; Abdel-Karim *et al.* 2023). This drop persisted after the peak load. Inclusion of fibers, both mono and hybrid, mitigated this drop and facilitated a smooth transition from each stage. Fibers achieved this by arresting major cracks, redistributing stresses, and enhancing the overall performance of culvert (Patil *et al.* 2020). Both fiber properties and quantity significantly influence this transition behaviour (Vakili *et al.* 2019; Patil *et al.* 2020). Prior research indicated that hybrid fibers were more effective than mono fibers in improving cracking strength (Akın *et al.* 2022), this finding confirmed in this study for GFRP-reinforced concrete culverts.

The addition of compression reinforcement significantly enhanced the culvert's stiffness, both before and after the peak load. This can be attributed to the improved axial stiffness provided by the compression reinforcement, which can substantially increase the overall stiffness. Replacing some PPL fibers with PVA fibers led to a notable increase in stiffness compared to using PPL fibers alone. This was likely due to the higher tensile strength of

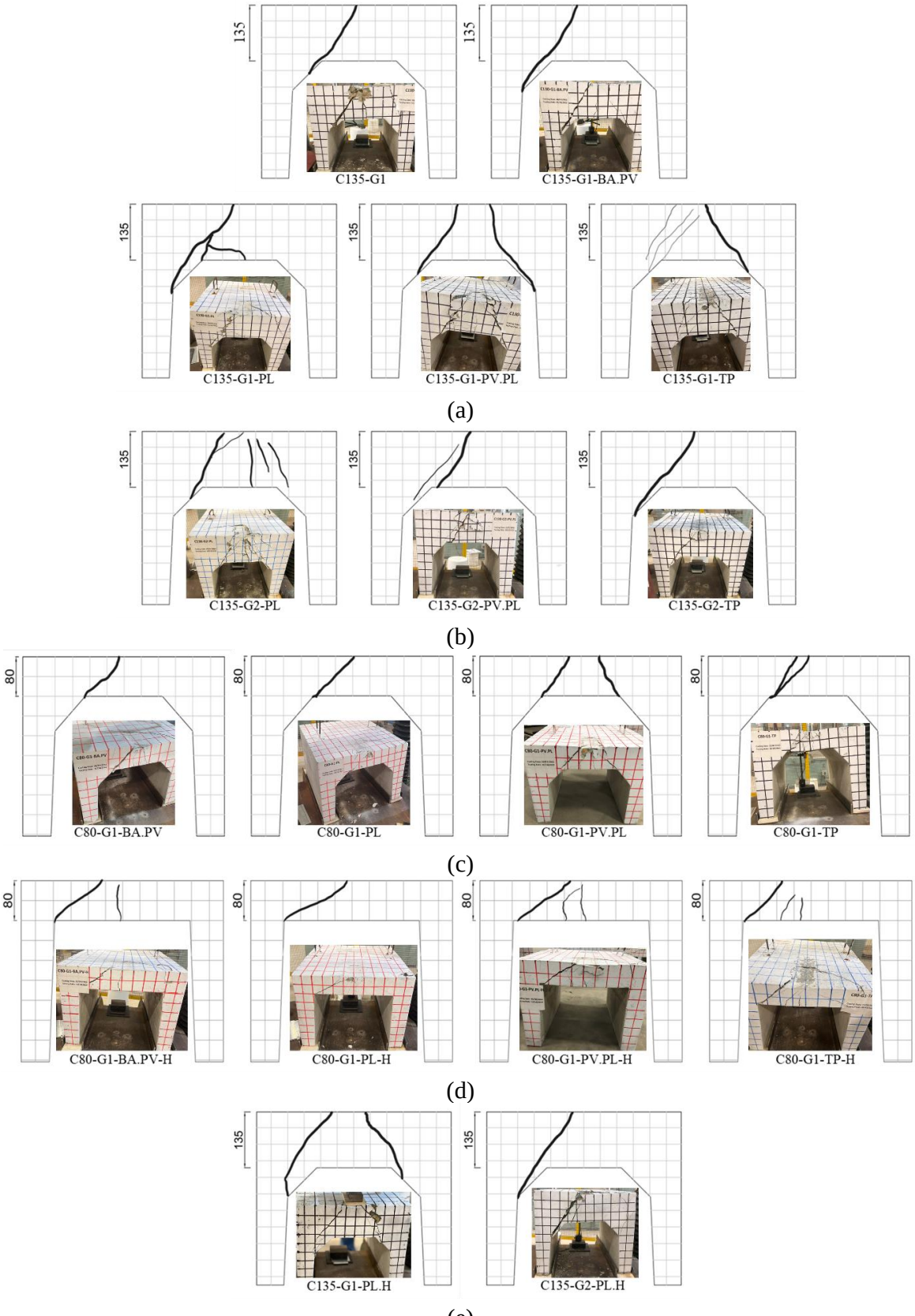


Figure 7-5 Failure mode of the fiber-reinforced SWSS concrete culverts, a) group Ⅰ, b) group Ⅱ, c) group Ⅲ, d) group Ⅳ, and e) group Ⅴ.

PVA fibers and their stronger bond with the concrete matrix, creating a positive synergy with PPL fibers that contributed to increased stiffness under tensile stresses. Comparing PPL and TPPL fibers, the top reinforcement effect on stiffness was more pronounced with TPPL fibers. Reducing the crown thickness by 40% considerably decreased pre-peak stiffness. This could be attributed to the smaller cross-sectional area, which results in a decrease in the bending moment capacity of culvert. Consequently, the overall stiffness was reduced. While specimens using different fibers exhibited a smooth transition to the post-peak phase, reduced thickness resulted in a sudden load drop after peak, except for specimens with TPPL fibers. This could be attributed to the improved distribution and flexibility of TPPL fibers, leading to a higher concentration of fibers in the failure plane and better post-peak behaviour.

The removal of haunches significantly impacted the pre-peak stiffness of C80 specimens, resulting in a decrease. This reduction could be attributed to the decreased section modulus, which ultimately leads to reduced stiffness. Partially replacing PPL fibers with PVA fibers improved the post-peak behaviour, offering better ductility. This enhancement could be attributed to the improved bonding strength between PPL fibers and the concrete matrix resulting from the addition of PVA fibers. This stronger bond contributed to enhanced crack bridging and improved ductility. TPPL fiber-reinforced culverts were more sensitive to haunch removal, experiencing a sudden drop in load-carrying capacity after reaching their peak. Deflection at peak point also decreased except for culverts reinforced with hybrid PPL/PVA fibers. Higher concrete strength increased pre-peak stiffness in both one and two-layer PPL fiber-reinforced culverts, but also resulted in a more abrupt post-peak drop. Specimens with only bottom reinforcement displayed drops during both pre-peak and post-peak phases, while those with top reinforcement exhibited less significant drops. This could be attributed to the higher bonding strength of PPL fibers with SWSS concrete at higher strengths, leading to prevent their pulling out during loading.

7.3.2.3 GFRP Strain

Figure 7-7 shows that all tested GFRP specimens experienced strains lower than their ultimate tensile capacity (17000 με), indicating non-rupture at failure. Group I specimens exhibited failure strains ranging from 47.2% to 73.8% of ultimate (8028 to 12556 με). Initially, strains were low but significantly increased after flexural crack initiation as GFRP bars took on tensile stress. During this stage, fibers in the tension section

effectively contributed to tensile stress reduction, lowering GFRP strain values (Dev *et al.* 2020a). Hybrid PPL/PVA decreased maximum bottom reinforcement strain by 20% compared to mono PPL fiber, despite increasing ultimate strength, suggesting a suitable reinforcing system of hybrid PPL/PVA that improves both shear and flexural strength. PPL and TPPL resulted in similar maximum GFRP strain, but TPPL offered higher shear strength. This enhancement could be attributed to the improved distribution and bonding strength of TPPL fibers, which led to a more uniform distribution of shear stresses. C135-G1-BA/PV had the lowest GFRP strain among all fibers, indicating that PVA/BA improved shear strength, allowing the culvert to carry more flexural strength by C135-G1-BA/PV.

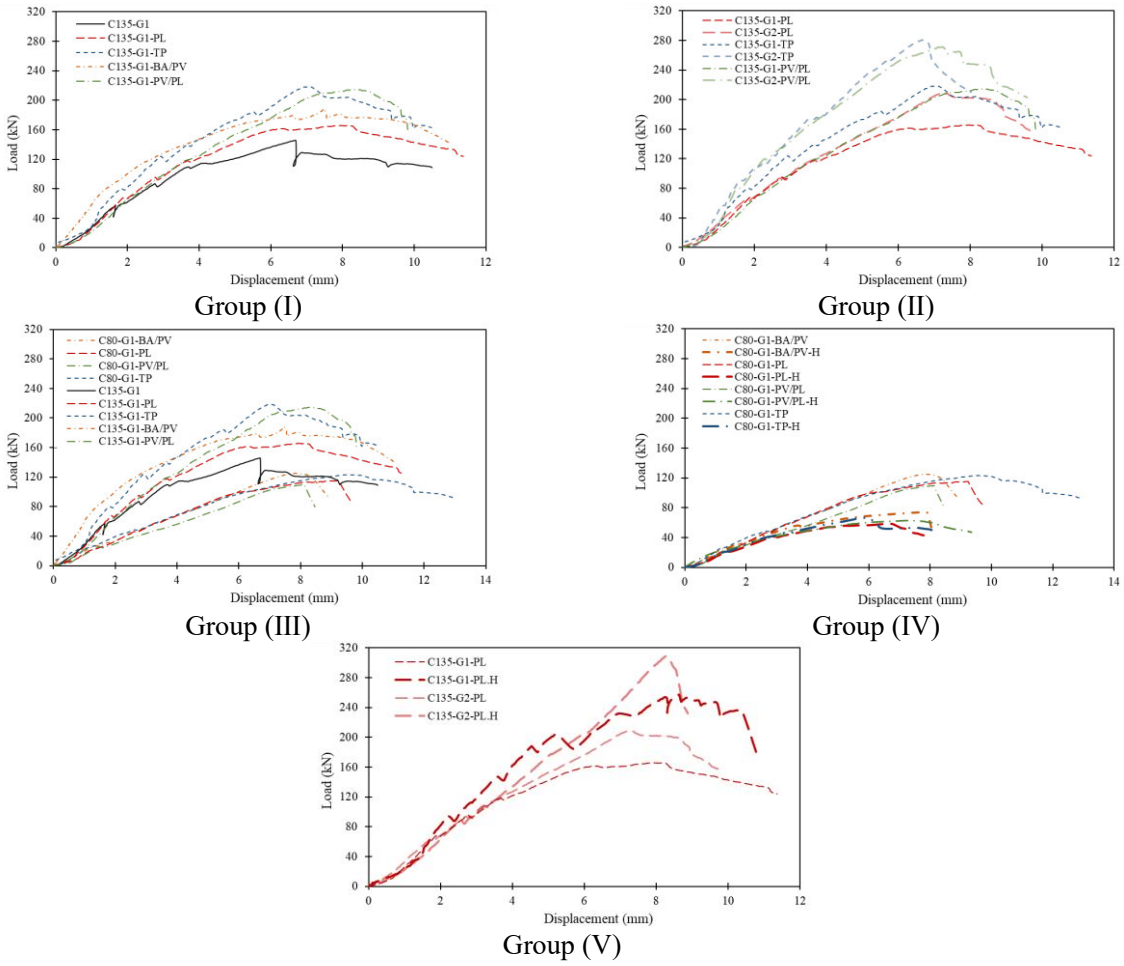


Figure 7-6 The load versus mid-span deflection curves for all culvert groups.

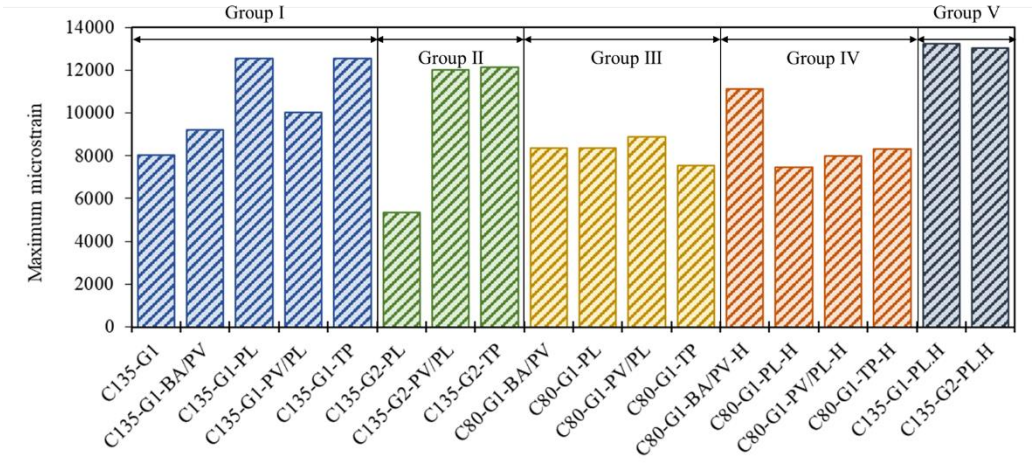


Figure 7-7 The maximum strain of GFRP bars for all culvert groups.

Adding top reinforcement significantly reduced the maximum bottom GFRP bar strain in C135-G2-PL specimens by 33%. This decrease stemmed from increased crown stiffness and reduced mid-span deflection, which led to lower tensile strain in the bottom GFRP reinforcement. The effect was consistent in both C135-G2-PL and C135-G2-PV/PL specimens. However, the tensile strain in the C135-G2-TP specimen remained like that of C135-G1-TP. This discrepancy between PPL and TPPL specimens likely arises due to the superior distribution and flexibility of TPPL fibers.

Removing haunches on C80 culverts had a contrasting effect on strain, increasing it for C80-G1-BA/PV-H while reducing it for others. Despite the expected increase in deflection due to the increased span length, shear failure occurred first and limited deflection, except for C80-G1-BA/PV-H where tensile strain increased instead. Similarly, increasing concrete strength led to a slight strain increase against the anticipated decrease. This was attributed to the improved shear strength, which resulted in higher tensile stress in the bottom GFRP bars.

7.4 Discussion

7.4.1 Group Ⅰ: Effect of mono and hybrid fibers

Figure 7-8 shows the typical stress and strain distribution of the crown section of culverts using ACI 440.1R-15 (ACI Committee 440 2015). The depth of neutral axis along with tensile and compression forces are also provided in **Table 7-6**. In this study the contribution of fibers in tension part was considered based on definition of ACI 544.4 R-

88 (ACI 1988) in Eq. (7-1), previously used for both steel and synthetic fibers (Shanour *et al.* 2018). Based on the design of the culverts according to ACI 440.1R-15 and AASHTO LRFD (AASHTO 2020), all culverts of group I had $\rho_f > \rho_{fb}$, indicating over reinforced section.

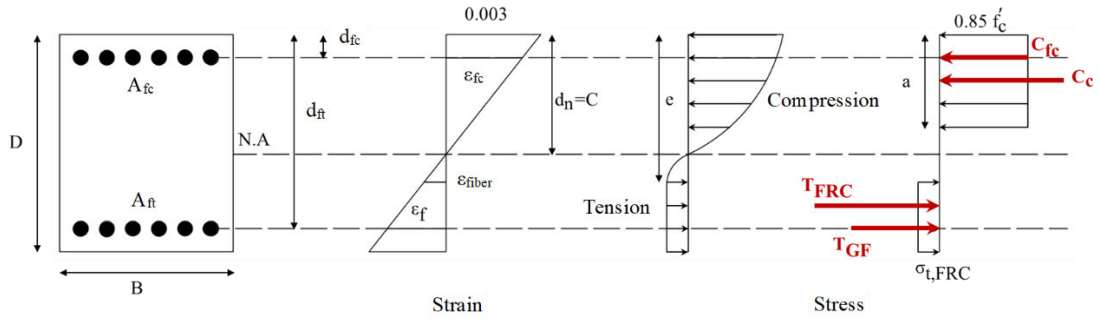


Figure 7-8 Typical distribution of stress and strain within the crown cross-section of GFRP fiber-reinforced culverts.

$$\sigma_{t,FRC} = 0.00772 \frac{l_{fiber}}{d_{fiber}} \rho_{fiber} F_{be} \ (MPa) \qquad (7\text{-}1)$$

where l_{fiber} is fiber length, d_{fiber} is fiber diameter, ρ_{fiber} is percent by volume of fibers and F_{be} is bond efficiency of the fiber which varies from 1.0 to 1.2 depending upon fiber characteristics.

7.4.1.1 Ultimate strength

Figure 7-9 demonstrates the significant effect of fiber addition on culvert strength. PPL fibers alone increased ultimate strength by 13.6%, while TPPL fibers offered a substantial 49.7% improvement. This aligns with prior research (Mostafazadeh *et al.* 2019) on the positive impact of macro PP fiber on shear strength of concrete culverts. TPPL exhibited a 31.8% higher ultimate strength over PPL fiber. This enhancement can be attributed to the superior distribution, flexibility, and bonding strength of TPPL, as observed in the scanning electron microscopy (SEM) analysis presented in **Figure A-9-5** Visualizing the bonding of PPL and TPPL fibers in SWSS concrete through SEM images., Appendix A. Additionally, the higher compressive strength achieved by TPPL-reinforced concrete at 45 days translated to increased shear and ultimate strength compared to PPL-reinforced concrete. Hybrid PPL/PVA fibers resulted in a 47.1% increase in ultimate strength

compared to plain culverts and a 29.5% increase compared to PPL-reinforced culverts. This improvement could be attributed to the potential synergistic effect of PVA fibers enhancing the bonding strength of PPL fibers, as was observed in the tensile and compressive strength tests of FR-SWSS mixtures. **Figure 7-10** presents scanning electron microscopy (SEM) images of hybrid PPL/PVA and hybrid PVA/BA, revealing that the chemical bonding of PVA fibers significantly improved the bond between PPL and BA with SWSS concrete, consistent with observations from previous studies (Mashayekhi *et al.* 2024a). As illustrated in **Figure 7-10**, the complementary action of PVA and PPL fibers in the hybrid system likely led to improved PPL fiber-matrix adhesion, resulting in enhanced tensile and compressive strength, ultimately contributing to increased shear strength of the concrete. The hydroxyl groups of PVA fiber contributed to chemical bonding and improved the inter-locking strength of concrete components (Hassanli *et al.* 2023; Vafaei *et al.* 2023). Micro-fiber hybridization (PVA/BA) achieved a 29% strength increase compared to plain culverts and a 13.6% increase over PPL fibers, highlighting the contribution of the superior strength and stiffness of BA fiber to culvert performance. Material testing revealed a significant increase in compressive strength for SWSS concrete containing a hybrid PVA/BA fiber compared to PPL fibers alone. This enhancement can be attributed to the synergistic behaviour of BA and PVA fibers, as observed in **Figure 7-10**. BA fibers likely improved the interfacial bonding strength of PVA fibers, aligning with findings from previous study (Mashayekhi *et al.* 2024a). This improved compressive strength, in turn, resulted in higher shear strength, which played a crucial role in achieving the observed increase in ultimate strength of the SWSS concrete culverts.

7.4.1.2 Cracking strength (P_{cr})

As shown in **Figure 7-11**, fiber inclusion significantly improved the cracking strength and serviceability of culverts, aligning with previous research on GFRP-reinforced beams (Patil *et al.* 2020). PVA/BA hybridization led to the highest increase (49.3%) compared to plain concrete, attributed to its strong ability to bridge micro-cracks. While PPL fibers exhibited superior tensile and flexural strength in material testing, PVA/BF achieved a 29.3% greater cracking strength. TPPL and PPL fibers increased cracking strength by 19.7% and 15.5%, respectively, with PPL/PVA hybridization demonstrating an 18% increase, exceeding mono PPL fibers. Similar results were observed in steel-reinforced beams, where hybrid fibers improved serviceability by reducing deflections and crack

widths (Abdel-Karim *et al.* 2023). PVA/BF incorporation further increased cracking strength by facilitating tensile stress transfer from GFRP reinforcement. Overall, fiber addition delays cracking and increases concrete tensile strength, as evidenced by the material testing results presented in **Figure A-9-4** Splitting tensile strength of concrete samples. (Appendix A), directly impacting the first crack appearance in culverts (Vakili *et al.* 2019).

Table 7-6 Values of key parameters in Figure 7-8.

Group	Culvert designation	d_n (mm)	e (mm)	C_C (kN)	T_{FRC} (kN)	T_{GF} (kN)	$\sigma_{t,FRC}$ (MPa)
I	C135-G1	18.8	18.8	324.0	–	324.0	–
	C135-G1-PL	22.0	22.2	432.0	84.2	347.9	1.49
	C135-G1-TP	20.4	20.9	351.7	27.3	324.4	0.48
	C135-G1-PV/PL	19.7	20.1	386.0	38.5	347.5	0.67
	C135-G1-BA/PV	18.2	18.4	381.0	20.1	360.9	0.34
II	C135-G2-PL	21.9	22.5	377.6	27.0	324.4	0.48
	C135-G2-TP	21.2	21.6	414.9	38.0	347.5	0.67
	C135-G2-PV/PL	19.9	20.1	416.8	19.8	360.9	0.34
III	C80-G1-PL	13.8	13.9	287.4	49.3	238.1	1.49
	C80-G1-TP	12.5	12.8	248.8	16.1	232.7	0.48
	C80-G1-PV/PL	13.0	13.3	249.3	22.3	226.9	0.67
	C80-G1-BA/PV	11.8	12.0	253.8	11.7	242.1	0.34
IV	C80-G1-PL-H	14.3	14.5	277.5	48.9	228.6	1.49
	C80-G1-TP-H	13.2	13.6	231.6	15.9	215.7	0.48
	C80-G1-PV/PL-H	13.4	13.6	242.8	22.2	220.5	0.67
	C80-G1-BA/PV-H	12.5	12.6	238.3	11.6	226.7	0.34
V	C135-G1-PL.H	16.3	16.7	444.3	28.3	416.0	0.48
	C135-G2-PL.H	18.0	18.5	490.9	27.9	416.0	0.48

7.4.1.3 Energy dissipation (E_{tot})

Energy dissipation capacity (E_{tot}), also known as toughness, is calculated as the area under the load-deflection curve up to the ultimate displacement (Abdel-Karim *et al.* 2023). The ultimate capacity is typically defined as the point where the load drops by more than 10%–30% of the peak load of the tested specimen (Dev *et al.* 2020a). In this study, 25% drop from the peak load was considered the ultimate capacity. Eq. (7-2) below was used to compute the energy absorption capacity, with results presented in **Figure 7-12**.

$$E_{tot} = \int_0^P P \, d\delta \tag{7-2}$$

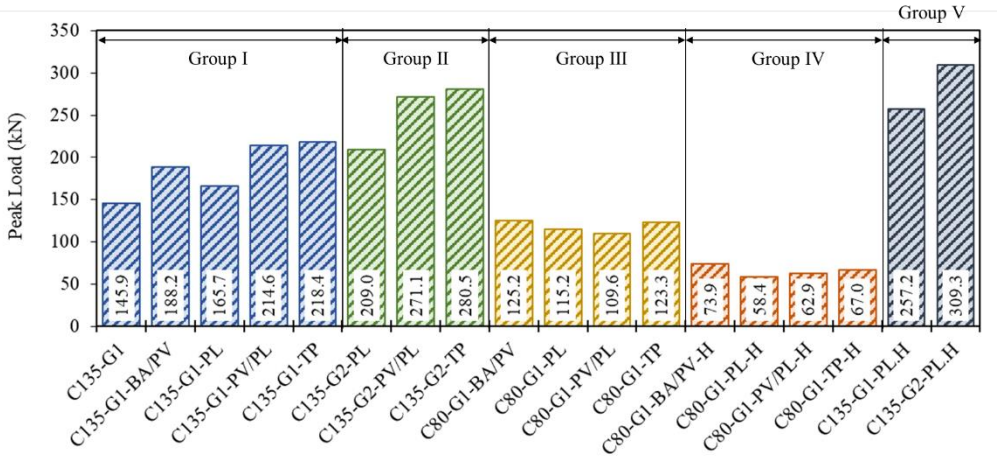


Figure 7-9 The ultimate strength of culverts for all groups.

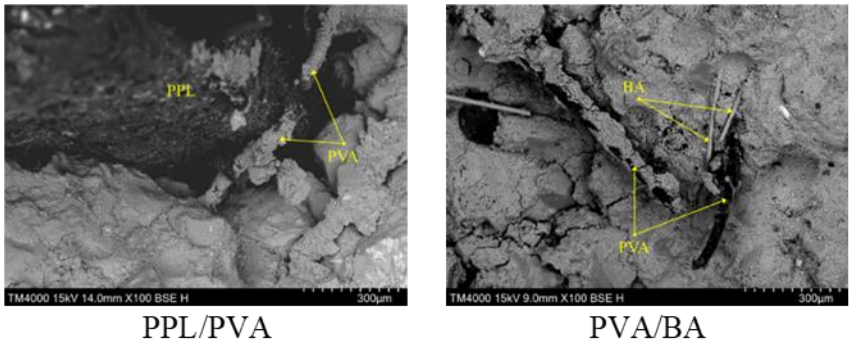


Figure 7-10 Synergistic hybridization of PPL/PVA and PVA/BA in SWSS concrete.

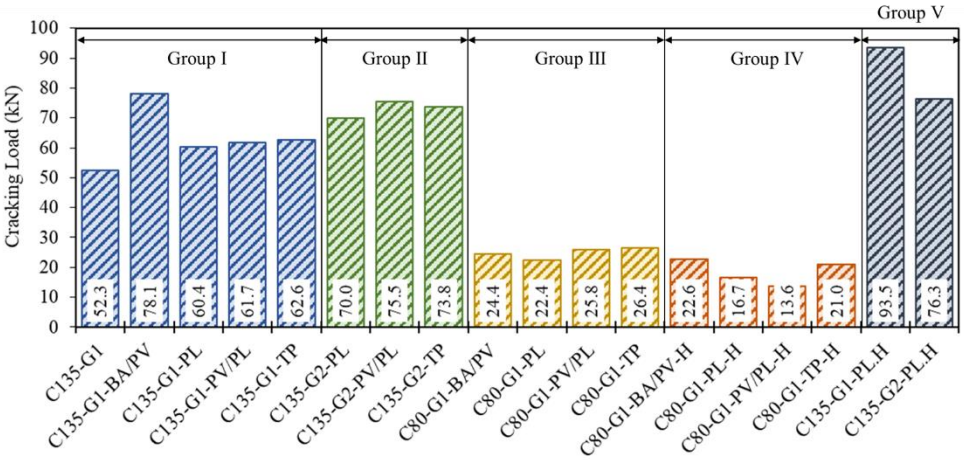


Figure 7-11 The cracking strength (P_{cr}) of culverts for all groups.

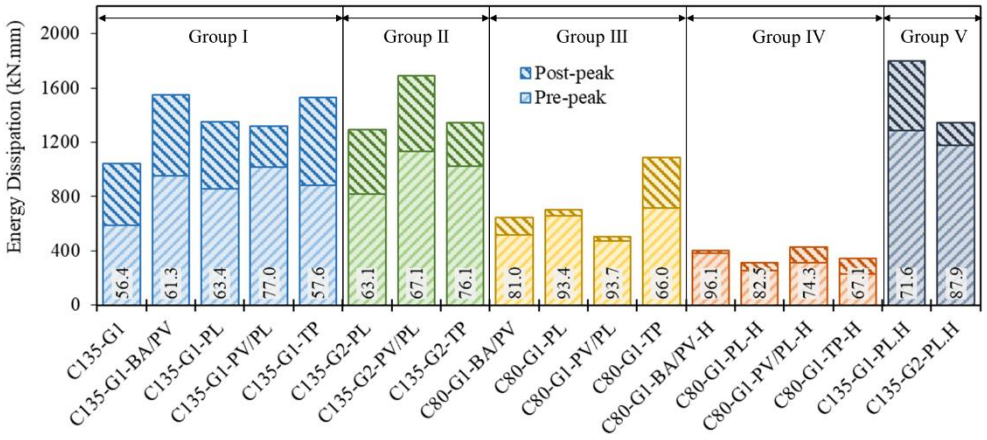


Figure 7-12 The energy dissipation (E_{tot}) of culverts for all groups (the values in each column represent the percentage of pre-peak energy dissipation to the total energy dissipation).

Adding fibers significantly increased the total energy dissipation of the specimens, with hybrid PVA/BA and TPPL fibers being the most effective, leading to increases of 49% and 47% respectively compared to the control specimen. TPPL fibers absorbed 13% more energy than PPL fibers, while partially replacing PPL with PVA maintained similar total energy absorption but shifted the distribution, increasing pre-peak energy by 18% and decreasing post-peak energy. Notably, hybrid PPL/PVA displayed the highest pre-peak energy dissipation, exceeding the control specimen by 73%, potentially due to the combined effect of the micro-crack bridging of PVA and its synergy with PPL in enhancing bonding strength. This aligns with previous research (Abdel-Karim *et al.* 2023). Hybridization of micro-fibers (PVA/BA) also led to significant energy absorption across both stages, surpassing PPL fibers by 21% and 11% in post-peak and pre-peak, respectively. This, along with its 14.6% higher total energy absorption compared to PPL, can be attributed to the improved shear capacity of PVA/BA and micro-crack bridging capabilities. Furthermore, the higher compressive strength and modulus of rupture exhibited by the hybrid PVA/BA fibers compared to PPL fibers contributed positively to achieving greater energy absorption capacity.

7.4.1.4 Ductility (μ_e)

Ductility, the ability to deform plastically before failure, cannot be measured using yielding for FRP-reinforced concrete members. In such cases, energy-based ductility serves as a toughness measure (Naaman *et al.* 1995; Patil *et al.* 2020). This study uses an

energy approach to measure ductility in GFRP-reinforced small culverts. Ductility factor (μ_e), an indirect measure for FRP-reinforced members, is defined as the ratio of total energy to elastic energy (Eq. 7-3).

$$\mu_e = \frac{1}{2}\left(\frac{E_{tot}}{E_{el}} + 1\right) \tag{7-3}$$

E_{el} represents elastic energy dissipated and is calculated as the area of the triangle formed at ultimate load by a line matching the initial linear portion of the load-deflection curve (Naaman *et al.* 1995). E_{tot} denotes total energy under the load-deflection curve (Abdel-Karim *et al.* 2023).

Figure 7-13 presents the ductility of culverts across different groups, highlighting the significant impact of fiber type, distribution, and bonding strength on ductility. While prior research on GFRP-reinforced beams suggested positive effects of fibers on ductility (Patil *et al.* 2020), this study reveals diverse responses in SWSS concrete culverts. Group I specimens showed the highest ductility (3.95) with hybrid PVA/BA fibers, exceeding plain concrete by 34%. This improvement stems from the even distribution of fibers, bridging micro-cracks and promoting inelastic energy absorption. PPL and TPPL fibers resulted in ductility values of 3.25 and 2.63, respectively. TPPL slightly increased elastic behaviour due to its improved distribution and bonding strength, leading to increased stiffness in the initial phase. Conversely, the lower bond strength of PPL favoured pull-out and enhanced inelastic behaviour. Partial replacement of PPL with PVA significantly reduced ductility by 36%. PVA improved the bonding strength of PPL and micro-crack bridging ability, enhancing elastic behaviour after the first crack (higher deflection at peak-point) than PPL. However, it led to lower ultimate deflection, indicating better inelastic behaviour in PPL-reinforced culverts.

7.4.2 Group Ⅱ: Effect of compression reinforcement

ACI 440.1R-15 (ACI Committee 440 2015) recommends neglecting the compressive strength of FRP bars due to its significant deviation from tensile strength. As shown in **Figure 7-8** and **Table 7-6**, adding top reinforcement increased the neutral axis depth (d_n), resulting in a reduced tension section and consequently, a decrease in the tensile force

(T_{FRC}) across all fibers. Additionally, the compression force of concrete (C_C) increased due to the enlarged compression section.

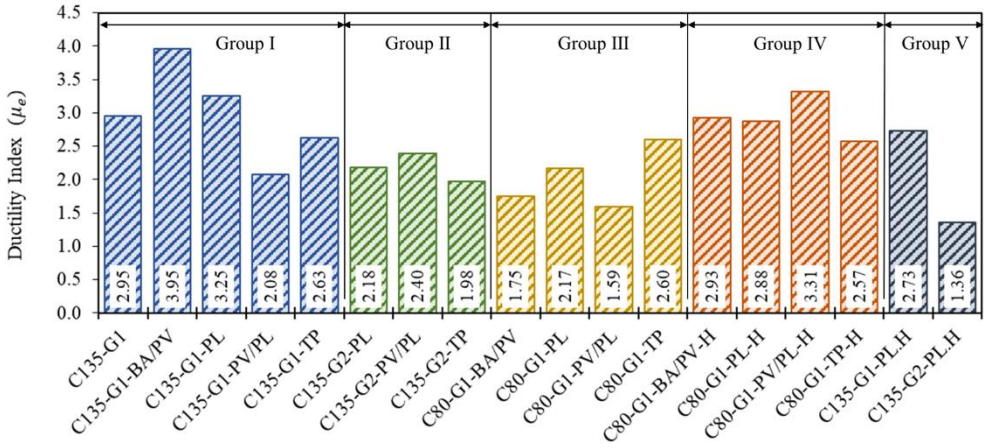


Figure 7-13 The ductility index (μ_e) of culverts for all groups.

Adding top reinforcement to culverts substantially improved their shear performance, with a 26.1%-28.4% increase in ultimate strength and a 15.9%-22.4% increase in first-cracking strength. While minimally impacting the influence of fibers on ultimate strength, it slightly increased first-cracking strength for hybrid PPL/PVA and TPPL fibers. However, top reinforcement addition resulted in a 4.3% to 12.3% decline in total energy dissipation and a 24.7% to 33% reduction in ductility for PPL and TPPL reinforced specimens, except for hybrid PVA/PPL fibers which resulted in a 28.1% and 15.3% increase, respectively. This was attributed to improved elastic energy and lower deflection at peak-point, leading to decreased inelastic energy and ultimately lower ductility. Additionally, PPL fibers, due to their inferior distribution and bonding, led to a more substantial reduction in inelastic energy and ultimate strength compared to TPPL fibers. While TPPL fibers absorbed more total energy than PPL fibers, adding top reinforcement reduced it more for TPPL fibers due to its better distribution and flexibility being more impacted by the reduced tension section.

Adding top reinforcement improved the ultimate strength of both PPL/PVA and PPL fiber-reinforced specimens by around 26%, attributed to the enhanced compression force and improved shear strength. However, its impact on ductility and energy absorption differed. While PPL/PVA experienced a 15% increase in ductility and a 28% increase in energy absorption, PPL fiber exhibited a 33% decrease in ductility and a 4.3% decrease in energy absorption. Notably, top reinforcement significantly increased the stiffness of

the culvert with hybrid PPL/PVA fibers by about 51%, highlighting the significant role of PVA fibers in enhancing stiffness and shear strength in small culverts. Furthermore, PVA fibers boosted both elastic and inelastic energy absorption, contributing to the improved ductility of hybrid PPL/PVA. Conversely, PPL fibers alone resulted in increased elastic energy without affecting stiffness, leading to decreased inelastic energy and ductility.

7.4.3 Group Ⅲ: Effect of crown thickness

Reducing the crown thickness (t_{top}) by 40% significantly reduced the cracking strength of fiber-reinforced SWSS concrete culverts, as evidenced by lower T_{GF}, T_{FRC}, and C_c values (**Figure 7-8**, **Table 7-6**). Both fiber type and crown thickness significantly influenced cracking, shear behaviour, energy absorption, and ductility. PVA/BA and PPL fibers caused the largest reductions in cracking strength (68.8% and 62.9%, respectively), while TPPL and hybrid PPL/PVA were less sensitive (57.8% and 58.2% reduction). Reducing the crown thickness also significantly decreased both the ultimate strength and the energy absorption capacity. The reduction in ultimate strength ranged from 30.5% to 48.9%, while the reduction in energy absorption ranged from 29.1% to 61.6%. These findings align with previous studies on GFRP-reinforced beams, which demonstrated that increasing the beam depth has a noticeable effect on energy absorption, ultimate shear capacity, and initial flexural cracking (Abdel-Karim *et al.* 2023; Zhou *et al.* 2023).

Comparing PPL and TPPL fibers, reducing slab thickness revealed interesting effects. While the gap in ultimate strength narrowed from 31.8% to 7%, the difference in cracking strength rose from 3.6% to 17.9%. This indicates that TPPL fibers, though less impactful on ultimate strength, significantly improve cracking strength when used in thinner slabs. Furthermore, TPPL exhibited superior total energy absorption (55% increase), a 7-fold increase in post-peak energy absorption, and a 19.7% higher μ_e compared to PPL. However, C135-G1-PL showed a higher μ_e than C135-G1-TP. This can be attributed to the superior distribution, flexibility, and bonding strength of TPPL fibers, leading to improved stress distribution and crack bridging in thinner slabs. Notably, reducing slab thickness significantly enhanced the post-peak behaviour and inelastic energy of TPPL-reinforced culverts, but considerably reduced their shear strength.

Replacing part of PPL with PVA in C80-G1-PV/PL significantly impacted its strength and energy absorption. While cracking strength increased by 15% compared to C80-G1-

PL, ultimate strength decreased by 4.9%. However, thicker crowns reversed this trend, with C135-G1-PV/PL exhibiting a 30% higher ultimate strength than C135-G1-PL. This suggests that PPL/PVA hybridization enhances cracking resistance but can compromise shear strength when used with thinner slabs. Hybridization led to a 27.9% decrease in E_{tot} and a 26.7% decrease in μ_e compared to C80-G1-PL, indicating increased elastic energy, and decreased inelastic energy due to partial replacement of PPL fibers. This suggests that for thinner crowns, the proportion of PPL fibers significantly influenced the ultimate shear strength, ductility, and energy absorption. However, for thicker crowns, PVA fibers demonstrated effectiveness in improving the bonding strength of PPL fibers and providing a positive synergistic effect.

Hybridization with PVA/BA improved the cracking strength of concrete slabs by 8.9% compared to using PPL alone, with the effect increasing for thicker slabs (135mm). Reducing the crown thickness by 40% significantly reduced the total, pre-peak, and post-peak energy absorption of PVA/BA by 59%, 45%, and 80%, respectively, highlighting its strong dependence on slab thickness. Notably, decreasing thickness also considerably lowered ductility for both PVA/BA and PPL, with reductions of 56% and 33% in μ_e, respectively. In conclusion, a strong correlation between ductility and crown thickness was observed for culverts reinforced with either hybrid PVA/BA or mono PPL fibers, as shown in **Figure 7-14**. This could be attributed to a more even distribution of stresses within the thicker crown section, which reduced stress concentrations. This allowed the fibers to be more effective in bridging and preventing cracks, resulting in higher ductility. When a thinner crown thickness was used, the increased stress concentration limited the effectiveness of the fibers. Accordingly, PVA/BA hybridization, due to the lack of long fibers, experienced a significant reduction in energy absorption and ductility. TPPL fibers exhibited better post-peak behaviour due to their better distribution compared to PPL fibers, which resulted in higher ductility for a lower crown thickness.

7.4.4 Group Ⅳ: Effect of haunches

Removing the haunches in the culverts increased the effective span of the crown, significantly reducing shear strength, as observed in GFRP-reinforced beams with increased shear-span ratios (Zhou *et al.* 2023). Among the investigated fibers, PVA/BA hybrid fibers exhibited the highest ultimate strength (41% reduction), suggesting their effectiveness in stress distribution under increased shear span. Ductility improved

significantly for all specimens by 32.5%-108% (except TPPL) after removing the haunches, indicating enhanced inelastic energy absorption. However, total energy absorption decreased by 16%-68% for all specimens due to reduced stiffness and ultimate strength. TPPL fibers outperformed PPL fibers in both ultimate strength (14.7% higher) and cracking strength (25.7% higher), potentially due to better stress transfer under shear. The post-peak energy dissipation difference between TPPL and PPL fibers became less significant after removing the haunches.

Removing haunches led to a significant decrease in ultimate strength and cracking strength for hybrid PPL/PVA (42.6% and 47.3% respectively), while the reduction for mono PPL was much smaller (7.7% and 18.6% higher than mono PPL). Total energy dissipation also decreased, with a 56% drop for PPL and a 16% reduction for hybrid PPL/PVA. Improved bonding between PPL and PVA fibers in the hybrid system helped distribute shear stresses, improve cracking strength, and absorb more energy, leading to superior ductility (3.31) compared to other fibers. This was attributed to improved micro-crack bridging by PVA fibers, enhancing inelastic behaviour. Removing haunches eliminated post-peak energy absorption for hybrid PVA/BA and significantly reduced total energy dissipation by 38%.

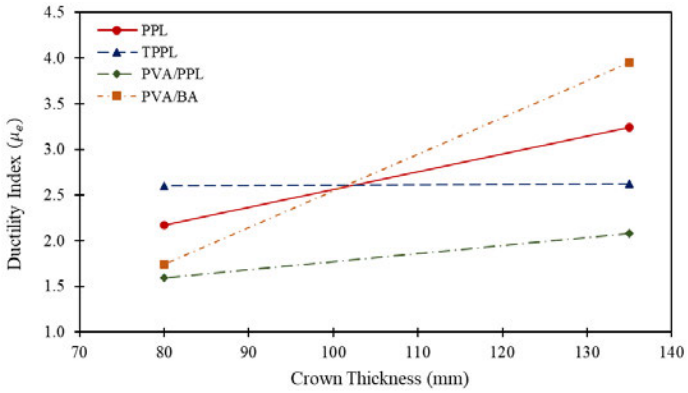


Figure 7-14 Influence of crown thickness on ductility index (μ_e) for various fibers.

7.4.5 Group V: Effect of SWSS concrete strength

The data presented in **Table 7-6** demonstrates that a 60% increase in concrete strength resulted in an elevation in the values of T_{GF}, T_{FRC}, and C_c, while simultaneously decreasing the depth of the neutral axis (d_n) compared to specimens with lower concrete strength. The introduction of compression reinforcement further contributed to an increase in d_n and a reduction in the tension zone of the cross-section. This effect

contributed to a more efficient utilization of the compressive strength of concrete and enhanced the overall shear behaviour of the culverts.

High-strength concrete significantly enhanced the ultimate strength and cracking strength (P_{cr}) of the C135-G1-PL.H specimen by 76.3% and 78.8%, respectively. For the C135-G2-PL.H specimen, the corresponding increases were 48% and 9%. This suggests that the impact of high-strength concrete on ultimate strength is more pronounced when only bottom reinforcement is employed. High-strength concrete also substantially improved the shear capacity of small culverts, leading to a notable increase in their ultimate bearing strength. This improvement was attributed to the increased compressive force exerted by the concrete within the compression zone of the crown section. The disparity in ultimate strength between C135-G1-PL.H and C135-G2-PL.H specimens was approximately 20% for high-strength concrete, compared to 26% for lower concrete strength, suggesting that top reinforcement was more effective with lower concrete strength. Compared to lower concrete strength, higher concrete strength allows the material to absorb a greater portion of the compressive load, reducing the reliance on top reinforcement. In contrast, for lower concrete strength, the addition of top reinforcement has a more significant impact on stress distribution and load-carrying capacity.

The C135-G1-PL.H specimen showed a significant 18% increase in cracking strength when high-strength concrete was employed, but a 16% decrease when lower-strength concrete was utilized. This difference was attributed to the improved bonding strength of PPL fibers with increasing concrete strength, facilitating enhanced tensile strength. Additionally, increasing concrete strength enhanced the total energy absorption (E_{tot}) of the C135-G1-PL.H specimen by about 33% but had no impact on the E_{tot} of the C135-G2-PL.H specimen. Interestingly, the pre-peak phase accounted for 71.6% of the E_{tot} for the C135-G1-PL.H specimen compared to 87.9% for the C135-G2-PL.H specimen. This suggests that increasing concrete strength and incorporating top reinforcement reduced the contribution of post-peak and inelastic behaviour, leading to a decrease in the ductility index (μ_e) of both specimens.

The contribution of the pre-peak stage to energy absorption increased significantly, from 63.4% to 71.6%, for the C135-G1-PL.H specimen due to the higher shear strength resulting from the use of high-strength concrete. The post-peak absorbed energy of the C135-G2-PL.H specimen improved by 66% compared to the C135-G2-PL specimen,

attributed to the enhanced bonding strength of PPL fibers in high-strength concrete, which facilitated crack bridging and energy dissipation. The difference in total energy absorption (E_{tot}) between the C135-G1-PL.H and C135-G2-PL.H specimens was 33.8%, while it was only 4.4% for the C135-G1-PL and C135-G2-PL specimens. This highlights the effectiveness of increasing concrete strength in improving energy absorption, particularly when compression reinforcement is present. Additionally, the combined effect of PPL fiber incorporation and increased concrete strength resulted in a 73% improvement in energy absorption compared to plain concrete culverts. However, the same combination led to only a 29% increase when the top reinforcement was utilized. This could be attributed to the improved bonding strength between PPL fibers and the concrete matrix when higher concrete strength was used. Additionally, adding top reinforcement caused stress redistribution within the section and increased axial stiffness, which reduced deflection. These factors collectively contributed to a decrease in the effectiveness of PPL fibers on energy absorption.

7.5 Shear capacity prediction models

Extensive research highlights ongoing debate regarding the shear capacity of concrete culverts. This has led to numerous studies on the shear behaviour of steel-reinforced counterparts, with findings indicating higher observed shear strengths than predicted by design codes (Yee 2004; Garg *et al.* 2007; Abolmaali *et al.* 2008b; Garg *et al.* 2009; Ghahremannejad *et al.* 2019b). This section evaluates the shear capacity of GFRP-reinforced fibrous SWSS concrete culverts using various standardized methods and presents a proposed shear capacity prediction. Five distinct approaches will be compared as described later. As the equations rely on steel reinforcement, an equivalent steel ratio ($\rho=\frac{E_{GFRP}}{E_s}\frac{A_{GFRP}}{bd}$) is employed to account for the GFRP bars.

7.5.1 Method-1: ACI 440.1R-15/RILEM TC-162

This method estimates the shear strength (V_n) of fiber-reinforced concrete without stirrups by summing the individual contributions from the concrete (V_c) and the fibers (V_f). This approach has been previously applied to concrete beams reinforced with both GFRP bars and synthetic fibers (Dev *et al.* 2020a). According to ACI 440.1R-15, the shear capacity of concrete with internal FRP reinforcement is calculated using Eq. (7-4) to Eq. (7-10):

$$V_c = \frac{2}{5}\sqrt{f_c'}\, b_w k d \tag{7-4}$$

$$k = \sqrt{2\rho_f n_f + \left(\rho_f n_f\right)^2} - \rho_f n_f \tag{7-5}$$

Furthermore, the shear resistance of fibers (V_{fc}) is determined according to Eq. (7-4), as recommended by RILEM TC-162 (TC162-TDF 2003).

$$V_{fc} = 0.7 k_f k_1 \tau_{fd} b d \tag{7-6}$$

The k_f and k_1 factors account for the contributions of the flanges in a T-section and the size effect, respectively. These factors can be calculated as follows:

$$k_1 = 1 + \sqrt{\frac{200}{d}} \leq 2 \tag{7-7}$$

$$k_f = 1 + n\left(\frac{h_f}{b_w}\right)\left(\frac{h_f}{d}\right) \leq 1.5 \tag{7-8}$$

$$n = \frac{b_f - b_w}{h_f} \leq 3 \tag{7-9}$$

$$\tau_{fd} = 0.12 f_{R,4} \tag{7-10}$$

where d is effective depth of the top slab (mm), b_f is width of the flanges (mm), h_f is height of the flanges (mm), b_w is width of the web (mm), τ_{fd} is shear strength due to fibers (MPa), and $f_{R,4}$ is residual flexural strength of fiber-reinforced concrete (FRC) at CMOD = 3.5 mm (MPa).

7.5.2 Method-2: AS 5100.5

This method utilizes simplified equations from AS 5100.5 (AS5100.5 2017), where the ultimate shear capacity (V_u) is attributed to both a concrete component (V_{uc}) and an

additional fiber-resisting component (V_{uf}). Consequently, V_u can be calculated using the following equations:

$$V_u = V_{uc} + V_{uf} \tag{7-11}$$

$$V_{uc} = k_v\sqrt{f_c'}bd_v \tag{7-12}$$

$$k_v = \frac{200}{1000 + 1.3d_v} \leq 0.1 \tag{7-13}$$

$$V_{uf} = 0.7k_\theta f_{1.5}' bd_v \tag{7-14}$$

$$k_\theta = \cot\theta_v \leq 1.28 \tag{7-15}$$

$$f_{1.5}' = 0.4f_{R,4}' - 0.07f_{R,2}' \tag{7-16}$$

The variables $f_{R,4}'$ and $f_{R,2}'$ denote the average residual flexural strengths corresponding to crack CMOD of 3.5 mm and 1.5 mm, respectively. The term $f_{1.5}'$ denotes the characteristic residual tensile strength of steel fiber-reinforced concrete (SFRC). The θ_v represents the angle created between the axis of the concrete compression strut and the longitudinal axis of member. The variable k_v represents the coefficient that measures the extent to which concrete contributes to shear strength, whereas d_v indicates the effective shear depth.

7.5.3 Method-3: AS 1597.2-2013

The Australian standard for steel-reinforced concrete culverts presents an alternative shear strength equation for culverts, derived from the following calculations applied to the critical shear section, where $\frac{M_u}{\emptyset V_u d} = 3.0$.

$$V_{uc} = v_b bdS_m \frac{F_D}{F_N}\ (N) \tag{7-17}$$

$$v_b = 4.98(0.018334 + \rho)\sqrt{f_c'} \leq 0.191\sqrt{f_c'}\ (MPa) \tag{7-18}$$

$$S_m = \frac{4}{\left(\frac{M_u}{\emptyset V_u d} + 1\right)} \tag{7-19}$$

$$F_D = 0.8 + \frac{40}{d} \leq 1.25 \tag{7-20}$$

$$F_N = 0.5 - \left(\frac{N_u}{6V_u}\right) + \sqrt{0.25 + \left(\frac{N_u}{6V_u}\right)^2} \tag{7-21}$$

where v_b denotes the nominal basic shear strength for locations where $\frac{M_u}{\emptyset V_u d} \geq 3.0$. F_D represents the depth factor, and F_N is the axial thrust factor.

7.5.4 Method-4: AASHTO LRFD 2020

a) The shear strength (V_c) in kN of slabs in steel-reinforced box culverts with a fill depth of 0.61 m (2.0 ft) or greater, subjected to one-way action, shall be evaluated according to the following AASHTO-recommended equations (AASHTO 2018, 2020):

$$V_c = \left(1.7756 \times 10^{-4}\lambda\sqrt{f_c'} + 0.03173\frac{A_s}{bd_e}\frac{V_u d_e}{M_u}\right) bd_e \tag{7-22}$$

where λ denotes the concrete density modification factor, A_s represents the area of reinforcement within the design width (mm²), b signifies the design width (mm), d_e stands for the effective depth (mm), V_u is the shear force due to factored loads (kN), and M_u represents the factored moment at the section (kN.mm). If normal-weight concrete is employed, λ should be assigned a value of 1.0.

b) For one-way action of steel-reinforced box culvert slabs under a fill depth less than 0.61 m (2.0 ft), AASHTO provides the following equation for concrete shear strength:

$$V_c = 8.3 \times 10^{-5}\beta\lambda\sqrt{f_c'}b_v d_v \tag{7-23}$$

$$\beta = \frac{4.8}{(1 + 750\varepsilon_f)} \frac{51}{(39 + s_{xe})} \quad (7\text{-}24)$$

$$\varepsilon_f = \frac{\frac{|M_u|}{d_v} + 0.5N_u + |V_u|}{E_f A_f} \leq 0.006 \quad (7\text{-}25)$$

$$s_{xe} = s_x \frac{1.38}{a_g + 0.63}; 304.8\, mm. \leq s_{xe} \leq 2032.0\, mm. \quad (7\text{-}26)$$

where b_v and d_v denote the effective web width and effective shear depth, respectively. The factor β represents the ability of diagonally cracked concrete to transmit tension and shear. ε_s signifies the net longitudinal tensile strain within the section at the centroid of the tension reinforcement, and s_{xe} denotes the crack spacing parameter influenced by aggregate size, while s_x stands for the crack spacing parameter.

c) For sections without transverse reinforcement, in the case of two-way action, the nominal shear resistance, V_c, of the concrete in kN, shall be determined as follows (AASHTO 2018):

$$V_c = 8.2933 \times 10^{-4}\, k \sqrt{f_c'} b_o d_v \quad (7\text{-}27)$$

where k denotes the ratio of depth of neutral axis to depth of flexural reinforcement. The perimeter of the critical section for shear (b_o) is expressed in mm.

7.5.5 Method-5: ACI 440.1R-15 punching shear strength

According to ACI 440.1R-15 (Institute 2015), Eq. (7-26) can be employed to calculate the punching shear capacity of two-way slabs. Given that the primary failure mode observed in the studied small culverts was punching shear, the applicability of this method was also investigated.

$$V_c = \frac{4}{5} \sqrt{f_c'} b_o k d \quad (7\text{-}28)$$

7.5.6 Comparison of the shear capacity prediction models

Figure 7-15 presents the ratio of experimental shear strength (V_{exp}) to predicted values (V_{pre}) obtained from various methodologies. The findings revealed that ACI 440.1R-15/RILEM TC-162 demonstrably underestimated the shear capacity of the GFRP-reinforced small SWSS concrete culvert without fibers (C135-G1), while AS 1597.2-2013 and AASHTO 4-c overestimated. Other methods exhibit a reasonable underestimation of the shear strength of C135-G1 specimen, where AASHTO 4-a, AASHTO 4-b and ACI 440.1R-15 punching shear methods resulted in more accurate estimations.

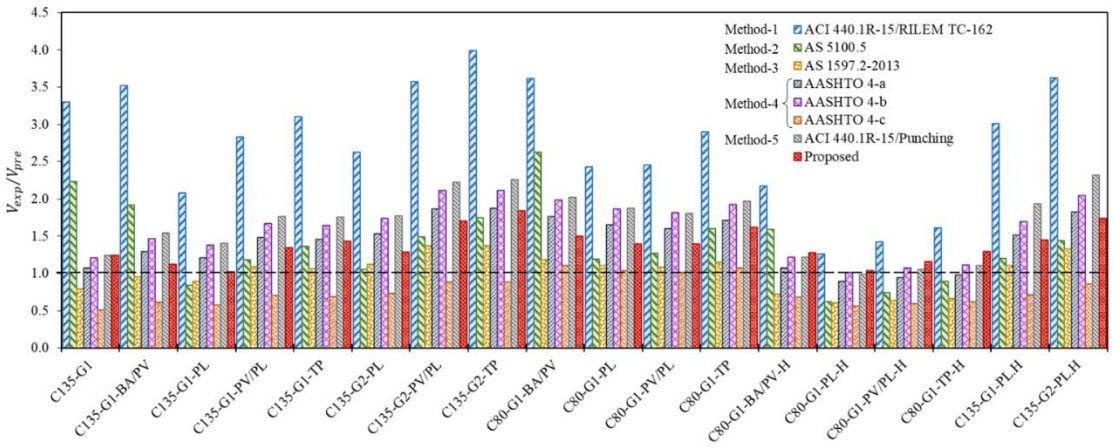


Figure 7-15 Comparison of experimental and predicted shear capacity for GFRP reinforced concrete culverts.

For FR-SWSS concrete culverts illustrated in **Figure 7-15**, the investigated methods demonstrated varying degrees of accuracy in predicting shear strength. The AASHTO 4-a, 4-b, and ACI 440.1R-15 punching shear methods consistently underestimated the capacity for all fiber types. In contrast, AASHTO 4-c significantly overestimated shear strength in culverts containing fibers, whether mono or hybrid. This could stem from the concept underlying this method, which is based on the two-way action of the crown. In contrast, the inverted U-shaped culverts investigated in this study exhibited one-way action due to the lack of lateral restraints, which aligns with the AASHTO 4-a and 4-b methods. Most methods underestimated shear strength for culverts with lower crown thickness (C80), with AS 1597.2-2013 and AASHTO 4-c providing the most accurate estimates. The removal of haunches yielded reasonable estimates, except for AS 5100.5 and ACI 440.1R-15/RILEM TC-162, which significantly underestimated, and AASHTO

4-c and AS 1597.2-2013, which significantly overestimated. For high-strength concrete, AS 5100.5 and AS 1597.2-2013 provided reliable predictions.

7.5.7 Proposed shear capacity prediction model

Based on a comparative analysis of various shear prediction models, this study proposes a modified model for GFRP-reinforced small SWSS concrete culverts. This proposed model incorporates two primary components: the punching shear strength of the crown with GFRP reinforcement (V_c) and that due to fiber-reinforced concrete (V_{uf}). The analysis revealed that ACI 440.1R-15 underestimates the shear capacity of the culverts, primarily due to neglecting fiber effects. By incorporating the fiber-reinforced concrete shear strength from AS5100.5 and adjusting for fiber type and hybridization, this study presents the proposed model. Eq. (7-27) to Eq. (7-31) outline the calculation method, where k_h represents the haunch effect and $f'_{R,1}$ denotes the residual flexural strength of FRC at CMOD = 0.5 mm in MPa.

$$V = V_c + V_{uf} \tag{7-29}$$

$$V_c = \frac{4}{5}\sqrt{f_c'}\, b_o k d \tag{7-30}$$

$$V_{uf} = 0.7 k_\theta k_h f'_{1.5} b d_v \tag{7-31}$$

$$f'_{1.5} = \begin{cases} 0.4f'_{R,4} - 0.07f'_{R,2}, & others \\ 0.3f'_{R,1}, & \dfrac{BA}{PV} \end{cases} \tag{7-32}$$

$$k_h = \begin{cases} 1.0, & with\ haunches \\ 0.7, & without\ haunches \end{cases} \tag{7-33}$$

Previous investigations have shown that hybrid BA/PV fibers exhibit superior performance in fracture toughness tests at low deflection levels and immediately following the peak load (Mashayekhi *et al.* 2024d). This suggests that a CMOD of 0.5 mm would be optimal for hybrid BA/PV fibers in such applications. Furthermore, this study revealed that for specimens without haunches, the V_{uf} should be reduced by 30% to account for the influence of haunches on the shear capacity of small concrete culverts.

7.6 Summary and conclusion

An experimental study examined the behaviour of small SWSS concrete culverts reinforced with GFRP bars and fibers. Eighteen FR-SWSS concrete culverts were tested according to AS 1597.2-2013. The study evaluated various parameters that affect culvert behaviour, including fiber type, compression GFRP reinforcement, crown thickness, haunches, and concrete strength. The experimental study yielded the following conclusions:

- Shear failure was the primary mode of failure in all culverts, characterized by a diagonal shear crack propagating from the load point to the haunch. This could be attributed to the limited shear capacity of GFRP bars in the transverse direction. Fiber incorporation potentially modified crack patterns and improved post-peak performance.

- TPPL fibers increased ultimate strength by 49.7% and energy dissipation by 47% over plain SWSS culverts, outperforming PPL fibers by 31.8% and 13%, respectively. TPPL and PPL fibers enhanced cracking strength by 19.7% and 15.5%. The improved performance was likely due to the better distribution and mechanical bonding of TPPL fibers, enhancing elasticity, while PPL fibers favoured pull-out and inelastic behaviour.

- PPL/PVA hybridization improved shear stress distribution and increased ultimate strength by 47.1% over SWSS culverts and 29.5% over PPL culverts. It also improved cracking strength by 18% compared to mono PPL fibers, preserved total energy dissipation, and achieved 73% higher pre-peak dissipation, but reduced ductility compared to the control specimen. This improvement was likely due to the higher tensile strength and strong chemical bond of PVA fibers with the concrete matrix, which, in synergy with PPL fibers, increased stiffness, reduced ductility, and enhanced pre-peak energy dissipation.

- Micro-fiber hybridization (PVA/BA) increased ultimate strength, first-cracking strength, and ductility by 29%, 49.3% and 34%, respectively, compared to plain SWSS concrete culvert. Additionally, it improved energy absorption and ultimate strength by 14.6% and 13.6%, respectively, over PPL fibers. This improvement was attributed to the positive synergy of PVA/BA hybridization and the superior strength

and stiffness of BA, which contributed to increased stiffness, effective distribution of shear stresses, and improved pre-peak behaviour of the culverts.

- The addition of top reinforcement increased ultimate strength (up to 28%) and first-cracking strength (up to 22%) but reduced ductility and energy dissipation. This could be attributed to the enhanced axial stiffness provided by the compression reinforcement. Hybridizing PPL/PVA fibers improved stiffness compared to PPL fibers alone, resulting in 15% higher ductility and 28% higher energy absorption, compared to specimens without top reinforcement, indicating enhanced performance in the presence of compression reinforcement.

- Reducing crown thickness by 40% significantly decreased the strength, energy absorption, and ductility of fiber-reinforced culverts. Thicker crowns distributed stress better, enhancing fiber performance and ductility, while thinner crowns concentrated stress, reducing effectiveness. TPPL fibers improved cracking strength in thinner slabs, increasing total energy absorption by 55%, with a sevenfold increase in post-peak absorption and 19.7% higher ductility than PPL fibers.

- Removing haunches increased the shear span and reduced stiffness, reducing shear strength and energy absorption by 16% to 68% but improving ductility by 32.5% to 108% (excluding TPPL). TPPL fibers showed 14.7% higher ultimate strength and 25.7% higher cracking strength than PPL fibers, likely due to better stress distribution. PVA/BA hybrid fibers had the highest ultimate strength and stress distribution, but energy dissipation decreased by 38% and post-peak absorption was eliminated after removing haunches.

- A 60% increase in concrete strength improved the ultimate and cracking strength of PPL-reinforced culverts by 76.3% and 78.8%, respectively, with only bottom reinforcement. This suggests that top reinforcement was more effective with lower concrete strength. Higher concrete strength enhanced PPL fiber bonding and compressive load absorption, reducing the need for top reinforcement. For lower concrete strength, top reinforcement significantly increased stress distribution and load-carrying capacity.

- The AASHTO equations for steel-reinforced concrete box culverts, based on one-way crown action, reliably predicted the shear capacity of small GFRP-reinforced concrete

culverts with fiber inclusions, though with some underestimation. This can be attributed to the one-way action observed in the crown of the investigated culverts, resulting from the lack of lateral restraint. The proposed model, considering GFRP bars, punching shear failure, haunches, and crown thickness, offered more accurate predictions.

Acknowledgements

The authors gratefully acknowledge the financial support provided by the University of South Australia. We extend our appreciation to the university's concrete laboratory technicians for their technical expertise. We also thank Adelaide Brighton Cement Ltd and Independent Cement and Lime Pty Ltd for their generous donations of OPC and GGBS, respectively, and TEXO for supplying TPPL fibers. Additionally, we recognize the valuable instrumentation and expertise provided by Microscopy Australia at the Future Industries Institute, University of South Australia.

Chapter 7 References

AASHTO 2018, AASHTO LRFD Bridge Design Guide Specifications for GFRP–Reinforced Concrete, American Association of State Highway & Transportation Officials (AASHTO),

AASHTO 2020, AASHTO LRFD Bridge Design Specifications, 9th Edition, American Association of State Highway and Transportation Officials (AASHTO),

Abdel-Karim, AH, Khalil, GI, Ewis, AE & Makhlouf, MH 2023, 'Impact of developed hybrid polypropylene fiber inclusion on the flexural performance of concrete beams reinforced with innovative hybrid bars', Construction and Building Materials, vol. 409, p. 134113.

Abolmaali, A & Garg, AK 2008, 'Effect of wheel live load on shear behavior of precast reinforced concrete box culverts', Journal of Bridge Engineering, vol. 13, no. 1, pp. 93-99.

ACI, A 1988, '544.4 R-88 Design considerations for steel fibre reinforced concrete, American concrete institute', ACI committee, vol. 544.

ACI Committee 440 2015, Guide for the Design and Construction of Structural Concrete Reinforced with Fiber-reinforced Polymer FRP Bars.

Akın, SK, Kartal, S, Müsevitoğlu, A, Sancıoğlu, S, Zia, AJ & Ilgün, A 2022, 'Macro and micro polypropylene fiber effect on reinforced concrete beams with insufficient lap splice length', Case Studies in Construction Materials, vol. 16, p. e01005.

AlHamaydeh, M & Anwar Orabi, M 2021, 'Punching shear behavior of synthetic fiber–reinforced self-consolidating concrete flat slabs with GFRP bars', Journal of Composites for Construction, vol. 25, no. 4, p. 04021029.

Alkhrdaji, T & Nanni, A 2001, 'Design, construction, and field-testing of an RC Box Culvert Bridge reinforced with GFRP bars', Non-Metallic Reinforcement for Concrete Structures-FRPRCS, vol. 5.

Amran, YM, Alyousef, Rayed, Rashid, Raizal SM, Alabduljabbar, Hisham, Hung, Chung-Chan 2018, Properties and applications of FRP in strengthening RC structures: A review, Structures.

AS1597.1-2010 2010, Precast reinforced concrete box culverts, Part 1: Small culverts (not exceeding 1200 mm span and 1200 mm height), Standards Australia,

AS1597.2-2013 2013, Precast reinforced concrete box culverts, Part 2: Large culverts (exceeding 1200 mm span or 1200 mm height and up to and including 4200 mm span and 4200 mm height), Standards Australia,

AS5100.5 2017, Bridge design, Part 5: Concrete, Standards Australia,

Chen, Z, Li, S, Zhou, J, Xu, R & Dai, S 2022, 'Flexural behavior of GFRP bars reinforced seawater sea sand concrete beams exposed to marine environment: Experimental and numerical study', Construction and Building Materials, vol. 349, p. 128784.

Chenggong, Z, Zhiyuan, W, Zhenyu, Z, Qiuyu, G, Xinrui, W & Renda, Z 2023, 'Research on different types of fiber reinforced concrete in recent years: An overview', Construction and Building Materials, vol. 365, p. 130075.

D'Antino, T, Pisani, M & Poggi, C 2018, 'Effect of the environment on the performance of GFRP reinforcing bars', Composites Part B: Engineering, vol. 141, pp. 123-36.

Dev, A, Chellapandian, M & Prakash, SS 2020, 'Effect of macrosynthetic and hybrid fibers on shear behavior of concrete beams reinforced with GFRP bars', Journal of Bridge Engineering, vol. 25, no. 7, p. 04020031.

Garg, AK, Abolmaali, A & Fernandez, R 2007, 'Experimental investigation of shear capacity of precast reinforced concrete box culverts', Journal of Bridge Engineering, vol. 12, no. 4, pp. 511-17.

Garg, AK & Abolmaali, A 2009, 'Finite-element modeling and analysis of reinforced concrete box culverts', Journal of Transportation Engineering, vol. 135, no. 3, pp. 121-28.

Ghahremannejad, M, Abolmaali, A & Mahdavi, M 2019, 'Shear strength of top slab of reinforced concrete box culverts', ACI Structural Journal, vol. 116, no. 6, pp. 63-74.

Gooranorimi, O & Nanni, A 2017, 'GFRP Reinforcement in Concrete after 15 Years of Service', Journal of Composites for Construction, vol. 21, no. 5, p. 04017024.

Guo, Z 2014, Principles of reinforced concrete, Butterworth-Heinemann,

Hassanli, R, Youssf, O, Manalo, A, Najafgholipour, MA, Elchalakani, M, del Rey Castillo, E & Lutze, D 2022, 'An experimental study of the behavior of GFRP-reinforced precast concrete culverts', Journal of Composites for Construction, vol. 26, no. 5, p. 04022043.

Hassanli, R, Manalo, A, Vafaei, D, Yekrangnia, M, Elchalakani, M & Noël, M 2023, 'Cyclic behavior of GFRP-reinforced concrete one-way slabs with synthetic fibers', Journal of Building Engineering, vol. 65, p. 105741.

Hassanli, R, Youssf, O, El-Naqeeb, MH, Yekrangnia, M, Elchalakani, M, Ghanbari-Ghazijahani, T & Bazli, M 2024, 'Investigation of punching shear performance in concrete slabs reinforced with GFRP and synthetic fibers: An experimental study', Engineering Structures, vol. 311, p. 118215.

Huang, H, Yuan, Y, Zhang, W, Hao, R & Zeng, J 2020, 'Bond properties between GFRP bars and hybrid fiber-reinforced concrete containing three types of artificial fibers', Construction and Building Materials, vol. 250, p. 118857.

Huang, Y, He, X, Wang, Q & Sun, Y 2018, 'Mechanical properties of sea sand recycled aggregate concrete under axial compression', Construction and Building Materials, vol. 175, pp. 55-63.

Huang, Y, Wang, T, Sun, H, Li, C, Yin, L & Wang, Q 2022, 'Mechanical properties of fibre reinforced seawater sea-sand recycled aggregate concrete under axial compression', Construction and Building Materials, vol. 331, p. 127338.

Institute, AC 2015, Guide for the Design and Construction of Structural Concrete Reinforced with FRP Bars (ACI-440.1R-15), American Concrete Institute,

Kaidi, J, Xin, W, Lining, D, Zhiyuan, C, Huang, H, Xia, L, Jianxun, L & Zhishen, W 2023, 'Mechanical properties of multi-scale mono/hybrid non-metallic fiber-reinforced ultra-high performance seawater sea-sand concrete', Construction and Building Materials, vol. 401, p. 132922.

Mahaini, Z, Abed, F, Alhoubi, Y & Elnassar, Z 2023, 'Experimental and numerical study of the flexural response of Ultra High Performance Concrete (UHPC) beams reinforced with GFRP', Composite Structures, vol. 315, p. 117017.

Manalo, A, Mendis, P, Bai, Y, Jachmann, B & Sorbello, C 2021, 'Fiber-reinforced polymer bars for concrete structures: State-of-the-practice in Australia', Journal of Composites for Construction, vol. 25, no. 1, p. 05020007.

Mashayekhi, A, Hassanli, R, Zhuge, Y, Ma, X & Chow, CW 2024a, 'Synergistic effects of fiber hybridization on the mechanical performance of seawater sea-sand concrete', Construction and Building Materials, vol. 416, p. 135087.

Mashayekhi, A, Hassanli, R, Zhuge, Y, Ma, X, Chow, CW, Bazli, M & Manalo, A 2024b, 'Synergistic effects of fiber hybridization on the fracture toughness of seawater sea-sand concrete', Construction and Building Materials, vol. 444, p. 137845.

Mostafa, IT, Mousa, S, Mohamed, HM & Benmokrane, B 2024, 'Experimental and Analytical Behavior of GFRP-Reinforced Concrete Box Girders under Pure Torsion', Journal of Composites for Construction, vol. 28, no. 1, p. 04023064.

Mostafazadeh, M, Abolmaali, A & Ghahremannejad, M 2019, 'Shear Strength of Synthetic Fiber-Reinforced Concrete Box Culverts', Journal of Bridge Engineering, vol. 24, no. 6, p. 04019039.

Naaman, A & Jeong, M 1995, 45 Structural ductility of concrete beams prestressed with FRP tendons, Non-Metallic (FRP) Reinforcement for concrete structures: proceedings of the second international RILEM symposium.

Pakravan, HR & Ozbakkaloglu, T 2019, 'Synthetic fibers for cementitious composites: A critical and in-depth review of recent advances', Construction and Building Materials, vol. 207, pp. 491-518.

Patil, GM, Chellapandian, M & Prakash, SS 2020, 'Effectiveness of Hybrid Fibers on Flexural Behavior of Concrete Beams Reinforced with Glass Fiber-Reinforced Polymer Bars', ACI Structural Journal, vol. 117, no. 5.

Ramadan, SH & El Naggar, MH 2022a, 'Design guidelines for reinforced concrete three-sided culverts', Tunnelling and Underground Space Technology, vol. 119, p. 104259.

Ramadan, SH & El Naggar, MH 2022b, 'Effect of large-span three-sided culvert configuration on its performance at service and ultimate loading conditions', Tunnelling and Underground Space Technology, vol. 122, p. 104346.

Ramesh, B, Eswari, S & Sundararajan, T 2020, 'Flexural behaviour of glass fibre reinforced polymer (GFRP) laminated hybrid-fibre reinforced concrete beams', SN Applied Sciences, vol. 2, pp. 1-10.

Shanour, AS, Said, M, Arafa, AI & Maher, A 2018, 'Flexural performance of concrete beams containing engineered cementitious composites', Construction and Building Materials, vol. 180, pp. 23-34.

Standard, A 2007, 'Specification and supply of concrete, AS 1379–2007, Australia'.

TC162-TDF, R 2003, 'Test and design methods for steel fibre reinforced concrete', Materials and structures, vol. 36, pp. 560-67.

Tjaronge, MW & Irfan, UR 2015, 'Porosity, pore size and compressive strength of self compacting concrete using sea water', Procedia Engineering, vol. 125, pp. 832-37.

Vafaei, D, Hassanli, R, Ma, X, Duan, J & Zhuge, Y 2021, 'Sorptivity and mechanical properties of fiber-reinforced concrete made with seawater and dredged sea-sand', Construction and Building Materials, vol. 270, p. 121436.

Vafaei, D, Hassanli, R, Ma, X, Duan, J & Zhuge, Y 2022, 'Fracture Toughness and Impact Resistance of Fiber-Reinforced Seawater Sea-Sand Concrete', Journal of Materials in Civil Engineering, vol. 34, no. 5, p. 04022038.

Vafaei, D, Ma, X, Hassanli, R, Duan, J & Zhuge, Y 2023, 'Experimental study on cyclic flexural behaviour of GFRP-reinforced seawater sea-sand concrete slabs with synthetic fibres', Ocean Engineering, vol. 273, p. 114014.

Vakili, SE, Homami, P & Esfahani, MR 2019, Effect of fibers and hybrid fibers on the shear strength of lightweight concrete beams reinforced with GFRP bars, Structures.

Wang, Z, Zhao, X-L, Xian, G, Wu, G, Raman, RS, Al-Saadi, S & Haque, A 2017, 'Long-term durability of basalt-and glass-fibre reinforced polymer (BFRP/GFRP) bars in seawater and sea sand concrete environment', Construction and Building Materials, vol. 139, pp. 467-89.

Wang, Z, Zhao, X-L, Xian, G, Wu, G, Raman, RS & Al-Saadi, S 2018, 'Effect of sustained load and seawater and sea sand concrete environment on durability of basalt-and glass-fibre reinforced polymer (B/GFRP) bars', Corrosion science, vol. 138, pp. 200-18.

Wang, Z, Xie, J, Li, J, Liu, P, Shi, C & Lu, Z 2022, 'Flexural behaviour of seawater–sea sand concrete beams reinforced with GFRP bars: effects of the reinforcement ratio, stirrup ratio, shear span ratio and prestress level', Journal of Building Engineering, vol. 54, p. 104566.

Xiao, L, Dai, S, Jin, Q & Peng, S 2023a, 'Bond performance of GFRP bars embedded in steel-PVA hybrid fiber concrete subjected to repeated loading', Structural Concrete, vol. 24, no. 1, pp. 1597-611.

Xiao, L, Hu, H, Peng, S, Du, Z & Xu, C 2023b, 'Compression behavior of GFRP reinforced hybrid fibre reinforced concrete short columns subjected to eccentric loading', Construction and Building Materials, vol. 393, p. 131985.

Xiong, Z, Zeng, Y, Li, L, Kwan, A & He, S 2021, 'Experimental study on the effects of glass fibres and expansive agent on the bond behaviour of glass/basalt FRP bars in seawater sea-sand concrete', Construction and Building Materials, vol. 274, p. 122100.

Yee, RA 2004, 'Shear behaviour of concrete box culverts', Dept. of Civil Engineering, Univ. of Toronto, Toronto.

Zeng, J-J, Liao, J, Zhuge, Y, Guo, Y-C, Zhou, J-K, Huang, Z-H & Zhang, L 2022, 'Bond behavior between GFRP bars and seawater sea-sand fiber-reinforced ultra-high strength concrete', Engineering Structures, vol. 254, p. 113787.

Zhang, P, Shang, J, Liu, Y, Shao, J, Gao, D, Dong, Z & Sheikh, SA 2022, 'Flexural behavior of GFRP bar-reinforced concrete beams with U-shaped UHPC stay-in-place formworks', Journal of Building Engineering, vol. 45, p. 103403.

Zhou, L, Zheng, Y, Di, B, Lv, J & Taylor, SE 2023, Shear behaviour of SWSS-SCC beams reinforced with GFRP bars and Stirrups: Experimental and analytical investigations, Structures.

8 Cyclic performance of GFRP-reinforced seawater sea-sand concrete culverts reinforced with synthetic fibers

Reprinted and reformatted (including changes to the referencing style) with permission from Elsevier Ltd (see Appendix B).

Mashayekhi, A, Hassanli, R, Zhuge, Y, Ma, X, W. K. Chow, C, Bazli, M & Manalo, A 2025, 'Cyclic performance of GFRP-reinforced seawater sea-sand concrete culverts reinforced with synthetic fibers', Structures, vol. 72, p. 108262.

Abstract

This study investigates the cyclic behaviour of glass fiber reinforced polymer (GFRP) reinforced seawater sea-sand (SWSS) concrete culverts with synthetic fibers. Five full-scale culverts with macro-polypropylene (PPL) and micro- polyvinyl alcohol (PVA) fibers (mono and hybrid) were tested under cyclic loading. To assess the influence of concrete and reinforcement types, two additional culverts -steel and GFRP-reinforced freshwater normal-sand (FWNS) concrete without fibers - were also tested. Different behavioural aspect of the culverts was studied, including failure mechanisms, load-deflection response, ultimate capacity, energy dissipation, hysteretic damping, damage parameters, strength degradation ratio, and self-resetting capacity. All tested culverts exhibited punching shear failure at the top slab, characterized by concrete crushing without longitudinal reinforcement rupture. The results indicated that incorporation of discrete fibers enhanced the ultimate shear capacity of GFRP-reinforced SWSS concrete culvert by 12-20% and reduced peak deflection by 13-28%. Fibers also improved hysteretic damping, energy dissipation, and damage resistance, particularly at high deflections. Hybrid PPL/PVA fibers exhibited superior performance compared to their mono-fiber counterparts, demonstrating enhanced energy dissipation, and damping at low deflection levels. Steel-reinforced concrete (RC) culvert exhibited a 17% lower peak deflection compared to GFRP-reinforced one. The evaluation of standard shear capacity prediction equations demonstrated that AASHTO equations effectively predict the shear capacity of GFRP-reinforced concrete (GFRP-RC) culverts. This study contributes to

both enhanced culvert performance and increased sustainability by employing GFRP bars, synthetic fibers, and SWSS concrete.

Keywords

Shear capacity; GFRP; Inverted U-shape culvert; Seawater; Sea-sand; Hybrid fibers.

8.1 Introduction

Precast or cast-in-place reinforced concrete (RC) three-sided culverts (TSCs) are cost-effective solutions for managing drainage beneath transportation infrastructures like roads and railways (**Figure 8-1**) (Von Handorf 2004; Marshall *et al.* 2014). However, their long-term performance is compromised by aggressive environmental conditions from surrounding soil and water. Inspection data revealed widespread degradation, with concrete cores showing inadequate strength and ductility under compression, and embedded steel reinforcement exhibiting severe corrosion, reducing tensile strength and ductility (Yazdani *et al.* 2013). Corrosion-induced expansion created internal stresses, leading to cracking, spalling, and debonding of steel reinforcement, which accelerates chemical ingress and further damage (Karim *et al.* 2021; Broomfield 2023; Hassanli *et al.* 2023). To address these challenges, the adoption of innovative and sustainable construction materials has gained increasing attention.



Figure 8-1 The application of concrete culverts.

Growing concerns about sustainable construction have prompted the exploration of environmentally friendly materials for concrete production. Seawater (SW) and sea-sand (SS) offer an abundant and sustainable alternative, conserving freshwater (Tjaronge *et al.* 2015), reducing reliance on transported resources in remote coastal areas, and enhancing

marine resilience, making it ideal for coastal and environmental projects (Guo *et al.* 2020; Ge *et al.* 2023; Zhu *et al.* 2023). SWSS concrete minimizes transportation costs in regions with local access to SW and SS, though its economic feasibility depends on distance. Despite this, it remains attractive in water-scarce areas for its freshwater conservation. Comparative life cycle assessments indicate that SWSS concrete reduces environmental impacts categories by 26.3% to 48.6% compared to conventional concrete in marine applications (Dong *et al.* 2021). Despite its sustainability advantages, the high chloride and sulphate content in SW and SS accelerate steel reinforcement corrosion (Zongao *et al.* 2024). Consequently, the use of SW and SS in concrete has been prohibited by all design codes due to concerns regarding corrosion of steel reinforcement caused by chloride ions (Vafaei *et al.* 2022c, 2023). This issue has prompted the investigation of alternative reinforcement materials, such as fiber-reinforced polymer (FRP), which exhibits higher chloride ion resistance, along with lower weight and greater strength (Micelli *et al.* 2004; Kamal *et al.* 2011; Al-Salloum *et al.* 2013). As a result, FRP bars have emerged as an alternative to steel reinforcement in SWSS concrete (Hu *et al.* 2022).

Experimental studies have shown that chloride ions have a relatively lower negative impact on the durability of FRP materials (Ahmed *et al.* 2020). Field investigations have also confirmed that FRP bars show excellent resistance to the chloride content in sea-sand and seawater (Raman *et al.* 2018). However, the mechanical properties of FRP (e.g., tensile strength, ultimate strain, and modulus of elasticity) can degrade when exposed to moisture, acidic or alkaline environments, salinity, extreme temperatures, or ultraviolet radiation (ACI Committee 440 2012; Yan *et al.* 2017; D'Antino *et al.* 2018). Additionally, the integration of supplementary cementitious materials (SCMs) into SWSS concrete enhances sustainability and performance (Vafaei *et al.* 2021a) while reducing alkali levels (Hobbs 1982; Kwon 2005), thereby improving the durability of FRP bars.

To further enhance the performance of SWSS concrete, industrial by-products like fly ash (FA), Ground Granulated Blast Furnace Slag (GGBS), silica fume, and metakaolin are used as SCMs. These materials not only reduce CO_2 emissions (Lothenbach *et al.* 2011) but also improve chloride binding, seawater resistance (Wang *et al.* 2020), workability, and long-term compressive strength (Wang *et al.* 2024). Among them, GGBS is particularly notable for its extensive use in seawater-mixed (SW) concrete (Shi *et al.* 2015; Younis *et al.* 2018). Its incorporation has minimal impact on both early-age and long-term compressive strength, often yielding superior performance compared to

conventional concrete (Etxeberria *et al.* 2016b; Fattah *et al.* 2017). Through secondary hydration, GGBS consumes calcium hydroxide, preventing ettringite formation and mitigating expansion caused by sulphate attacks and alkali-aggregate reactions, thereby enhancing durability (Bai 2009; Vafaei *et al.* 2021a). Additionally, GGBS reduces the tricalcium aluminate (C_3A) content in cement (Zhang *et al.* 2013), functioning as an alkali diluter that significantly lowers alkali levels (Hobbs 1982; Kwon 2005).

Glass fiber-reinforced polymer (GFRP) bars offer a viable alternative to steel reinforcement in concrete culverts. Despite its novelty, advancements have addressed the economic and environmental challenges of GFRP bars, increasing its cost-competitiveness and practical use for concrete structures (Hassanli *et al.* 2023). However, research on the performance of GFRP-reinforced concrete (GFRP-RC) culverts remains limited. Hassanli et al. (Hassanli *et al.* 2022) explored the application of GFRP-RC in precast culverts, recommending a focus on serviceability limits, including deflection and crack control, rather than ultimate strength in design. Furthermore, a long-term study of a precast GFRP-RC box culvert in service for over 16 years revealed no signs of GFRP microstructural deterioration (Gooranorimi *et al.* 2017a). This observation supports the suitability of GFRP bars for enhancing durability and service life while reducing maintenance demands.

Previous research has demonstrated improved synergy between SWSS concrete and GFRP bars compared to conventional reinforcement, leading to enhanced durability of GFRP-reinforced SWSS concrete beams exposed to chlorides (Wang, Zhihao *et al.* 2023). Furthermore, field assessment revealed no significant deterioration of GFRP bars in concrete structure subjected to accelerated marine conditions for six months (Bertola *et al.* 2017; Khatibmasjedi *et al.* 2017). Previous studies have also shown that GFRP bars demonstrate strong durability in marine environments (Kim *et al.* 2008; Wu, Weiwei *et al.* 2023). Five to eight years of field exposure did not reveal microstructural changes in GFRP bars. Consequently, these bars were presumed to retain 100% of their tensile strength after similar durations (Wang *et al.* 2017b). Studies have demonstrated that the failure modes and shear behaviour of SWSS concrete beams reinforced with GFRP bars are comparable to those of conventional concrete beams with GFRP reinforcement (Zhihao *et al.* 2022; Lingzhu *et al.* 2023). Research has shown that incorporating seawater into the concrete mixture does not significantly affect the interfacial behaviour between GFRP and concrete (Sena-Cruz *et al.* 2018). Moreover, the water absorption and

expansion of FRP contribute to an increase in bonding strength between FRP and SWSS concrete, temporarily enhancing structural performance (Hu *et al.* 2022). After long-term exposure to corrosive environments, FRP reinforced SWSS concrete beams demonstrate better performance compared to steel-reinforced beams (Hu *et al.* 2022). These findings support the potential of FRP bars for SWSS applications.

Unlike steel reinforcement, which exhibits elastoplastic behaviour and undergoes plastic deformation before failure, GFRP bars display linear elastic behaviour until rupture. Their lower elastic modulus (one-quarter to one-third of steel (Hassanli *et al.* 2023)) can result in wider cracks and greater deflections in GFRP-reinforced elements (Yuntao *et al.* 2020; Hu *et al.* 2023). Adding fibers to GFRP-reinforced concrete (GFRP-FRC) improved cracking behaviour, ductility, and energy absorption (Yang *et al.* 2012; Chellapandian *et al.* 2020; Dev *et al.* 2020b; Patil *et al.* 2020; AlHamaydeh *et al.* 2021; Hassanli *et al.* 2023), shifting failure modes from brittle to ductile (Chellapandian *et al.* 2020; Dev *et al.* 2020b). For example, steel and synthetic fibers increased GFRP beam ductility by up to 80% (Yang *et al.* 2012), while polyethylene (PE) fibers enhanced the bonding strength of GFRP bars in SWSS concrete (Zeng *et al.* 2022). Macro polypropylene (PP) fibers reduced creep, shrinkage, cracking, and deflection while increasing the effective moment of inertia and reducing strains in GFRP bars and concrete surfaces (Razan *et al.* 2023). Fiber-reinforced SWSS (FR-SWSS) slabs with macro polyolefin fibers showed slightly higher punching shear capacity and over twice the toughness of control specimens (AlHamaydeh *et al.* 2021). Macro synthetic fibers also improved shear strength, ductility, and altered crack patterns in RC beams (Altoubat *et al.* 2009).

Beyond static applications, the cyclic performance of GFRP-RC elements is critical for their design under dynamic loads, as it reveals potential vulnerabilities. Limited research exists on this topic, particularly for SWSS concrete. Previous studies explored the cyclic flexural response of GFRP-RC slabs with synthetic fibers including micro polypropylene (PP) and polyvinyl alcohol (PVA), demonstrating improved crack behaviour and reduced crack widths compared to steel-RC due to the lower modulus of GFRP (Hassanli *et al.* 2023). Additionally, fiber inclusion promoted elastic behaviour, with significant recovery of applied deflection observed after each loading cycle (Hassanli *et al.* 2023). While plain GFRP-SWSS slabs exhibited reduced cracking moments, fiber addition (especially PP) mitigated this decrease and enhanced both cracking moment and ultimate strength (Vafaei *et al.* 2023). Furthermore, fibers reduced crack width, spacing, and residual deflection

after load cycling (Vafaei *et al.* 2023). The cyclic flexural performance of hybrid fiber-reinforced SWSS concrete beams revealed that the hybridization of macro-PP and micro-PVA fibers resulted in a 260% increase in cumulative energy dissipation (Mashayekhi *et al.* 2024c). A review of the literature reveals a scarcity of research on the cyclic performance of GFRP-RC box culverts, particularly with the use of fibers. Notably, only one such study focusing on quasi-static loading has been identified (Alkhrdaji *et al.* 2001). Further investigations are necessary to comprehensively understand their behaviour, particularly with the incorporation of fibers.

Previous research has predominantly focused on steel-reinforced concrete culverts, leaving a significant knowledge gap concerning the performance of GFRP-RC culverts, particularly under cyclic loads. Addressing this gap necessitates a deeper understanding of the hysteretic behaviour of GFRP-RC concrete culverts for improved design and performance under dynamic loads. Synthetic fibers have also shown to improve the shear capacity of traditional concrete culverts (Mostafazadeh *et al.* 2019). However, the influence of fiber type and content on GFRP culvert performance and shear capacity remains unknown. This study aims to address this gap by investigating the shear capacity of GFRP-reinforced SWSS concrete culverts incorporating mono- and hybrid-fiber under cyclic loading. Also, the impact of fibers on culvert performance, including load capacity, post-peak behaviour, and ductility was examined. Additionally, it compared steel- and GFRP-RC culverts. Finally, the shear capacity results were compared to analytical methods from design codes. This study paves the way for further exploration of GFRP-reinforced FR-SWSS concrete culvert, a promising, cost-effective, and sustainable alternative with improved performance.

8.2 Experimental program

8.2.1 Raw materials

Seawater sourced from the Adelaide coastal area, containing 19,810 mg/L of chloride ions (Cl^-) and 2,824 mg/L of sulfate ions (SO_4^{2-})—360 and 76 times higher, respectively, than standard tap water—was used in the SWSS mix. Strict storage protocols were adhered to prevent contamination. The fine aggregate for the SWSS mix consisted of sea-sand from Semaphore Beach in Adelaide, thoroughly cleaned to minimize impurities. Crushed basalt with a maximum particle size of 14 mm, obtained from a local quarry, was used as the coarse aggregate. Ordinary Portland cement (OPC) and ground granulated

blast furnace slag (GGBS) were used as the cementitious binders, with a mix ratio of 35% OPC and 65% GGBS. Since cement production is a significant contributor to CO_2 emissions, substituting 65% of the cement with GGBS—a by-product of iron and steel manufacturing—can reduce emissions by approximately 50% (Yang *et al.* 2020).

Two configurations were tested to evaluate the impact of fiber reinforcement on SWSS concrete culverts: mono and hybrid (micro/macro) fibers. Micro PVA and macro PPL fibers were chosen for their cost-effectiveness (properties detailed in **Table 8-2**). Recycled PPL fiber (eMesh by FIBERCON) was employed to promote sustainability, reflecting the growing trend towards eco-friendly construction materials. Four FR-SWSS mixtures were utilized following prior research (Mashayekhi *et al.* 2024a). These included mono-fiber types (PPL, PVA) at 0.4% volume and hybrid macro/micro PPL/PVA combinations (66%/33%) at 0.4% and 0.6% total volume fractions. Fiber type and volume fraction selection aimed to balance optimal distribution within the concrete matrix with potential property improvements. Too much fiber can cause clumping, while insufficient amounts offer minimal benefit (Pakravan *et al.* 2019). The chosen 66%/33% PPL/PVA hybrid composition reflects an established optimum based on prior research (Mashayekhi *et al.* 2024a). Details on the mix proportions for each FRC are also provided in **Table 8-1**.

This investigation employed two distinct reinforcements for the culvert specimens GFRP bars (manufactured using a pultrusion process) and conventional steel rebars. Steel bars were sized the same as GFRP bars to directly compare the performance of steel- and GFRP-RC culverts aligned with the methodology adopted in prior research. Material properties of both GFRP and steel bars are provided in **Table 8-3**.

Table 8-1 Mix proportions of SWSS concrete.

Concrete mix	Mix proportions (kg/m^3)									
	Fiber			Binder		Gravel	Sand		Water	
	PVA	PPL	Total volume fraction (%)	OPC	GGBS		NS	SS	FW	SW
FWNS	—	—	—	250	150	1095	605	—	240	—
SWSS	—	—	—							
SWSS-PVA	5.20	—	0.40				—	605	—	240
SWSS-PPL	—	3.64								
SWSS-Hybrid 0.4	1.72	2.40								
SWSS-Hybrid 0.6	2.57	3.60	0.60							

8.2.2 Mix design and specimen preparation

Both SWSS and freshwater/normal sand (FWNS) concrete mixes were used in the manufacturing of culverts, with both designed to achieve a target slump of 120-140 mm and a compressive strength of 35 MPa. Plasticizers were intentionally excluded from the mix design to eliminate the effect of admixtures on the concrete properties and test results. FWNS concrete, with water and sand content matched to the SWSS mix, was used for comparative analysis. Detailed mix proportions are provided in **Table 8-1**.

A total of seven full-scale, inverted U-shaped concrete culverts were manufactured and tested under incremental cyclic loading. Details of the culverts and their concrete mixtures are provided in **Table 8-4**. Culvert design followed ACI 440.1R-15 (Institute 2015) for a single midspan W80 wheel load, applied at the midspan as specified in AS 1597.1-2010 (AS1597.1-2010 2010). The load was applied to the front face of the crown, consistent with (Hassanli *et al.* 2022) to replicate the worst-case scenario in terms of the location of vehicle's wheels. The reinforcement for the front face was designed accordingly and the same reinforcement configuration was applied throughout the entire length of the culvert. Additionally, the top slab incorporated two layers of reinforcement to efficiently transfer both negative and positive moments between the legs and the slab. Both serviceability and ultimate limit state criteria were considered in the design. The serviceability limit state of precast reinforced concrete three-sided structures, as specified by AASHTO LRFD (AASHTO 2018, 2020), was considered for the culverts in this study.

As denoted in **Table 8-4**, culvert designations define "GFSS" as GFRP-RC culverts with SWSS concrete, "GFNC" as GFRP-reinforced with FWNS concrete, and "STNC" as steel-reinforced with FWNS concrete. All tested culverts shared identical dimensions: 500 mm length, 1400 mm total width, 735 mm overall height, and 155 mm crown thickness. A clear concrete cover of 25 mm was maintained for the primary reinforcing bars. Five GFRP-RC culverts, designated CL1-CL5, were employed to assess the effect of fiber type and dosage on performance. These culverts incorporated FR-SWSS concrete with varying fiber reinforcement including PVA, PPL, and hybrid PPL/PVA at 0.4% and 0.6% dosages, respectively. Culvert CL5 served as the control, utilizing plain SWSS concrete. A single culvert (CL6) utilized GFRP bars with FWNS concrete to investigate the influence of concrete type. Finally, a steel-reinforced culvert with FWNS concrete (STNC) served as a benchmark for GFRP and steel reinforcement performance. Specific dimensions and reinforcement details are provided in **Figure 8-2**, adhering to the

Table 8-2 Physical properties of different fibers.

Property	Shape	Specific gravity	Length (mm)	Diameter/Thickness (μm)	Tensile strength (MPa)	Young's modulus (GPa)
PVA[1]		1.3	8	38	1600	40
PPL[2]		0.91	47	<500	400	6

Table 8-3 Mechanical properties of reinforcing bars.

Property	Bar type			
	GFRP #3	GFRP #5	Steel N10	Steel N16
Nominal bar diameter (mm)	9.5	15.9	10	16
Cross-sectional area (mm^2)	71	199	78.5	201
Tensile elastic modulus (GPa)	62.5	60.0	200	200
Tensile strength (MPa)	1315	1237	500	500
Ultimate tensile strain	0.023	0.021	—	—

Australian code for precast concrete box culverts (AS 1597.1-2010 (AS1597.1-2010 2010)). In addition, six 100 mm × 200 mm cylinders per mix were cured at ambient temperature and tested for compressive strength alongside the culvert specimens according to AS 1012.9-2014 (Committe 2014).

Custom plywood formwork was constructed and sealed with silicone to ensure water impermeability during concrete casting. Pre-assembled steel and GFRP reinforcing cages were positioned within the formwork using 25 mm chairs for precise placement. Lifting lugs were then attached to facilitate manipulation with a laboratory crane. After concrete placement, thorough vibration was employed to achieve proper compaction and eliminated air pockets. To prevent shrinkage and thermal cracks, the culverts were covered in plastic sheeting for a 24-hour cure. They were then demolded, re-covered with plastic to maintain humidity for complete curing before testing. The culverts were painted white and marked with a detailed grid to aid crack identification during testing.

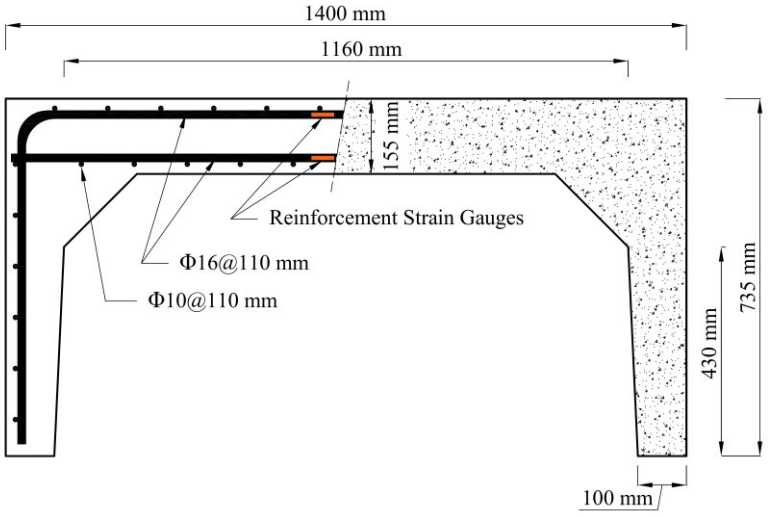


Figure 8-2 Dimensions and reinforcement details of the specimens.

8.2.3 Test setup, instrumentation, and testing procedure

To evaluate the compressive strength of the concrete, three cylindrical specimens (100 mm × 200 mm) were prepared for each mix and tested in accordance with AS 1012.9 (Committe 2014). The average compressive strength values are presented in **Table 8-4**. Additionally, the microstructure of the concrete mixes was analysed using scanning electron microscopy (SEM) to provide detailed insights into the microstructure and to further support the discussions.

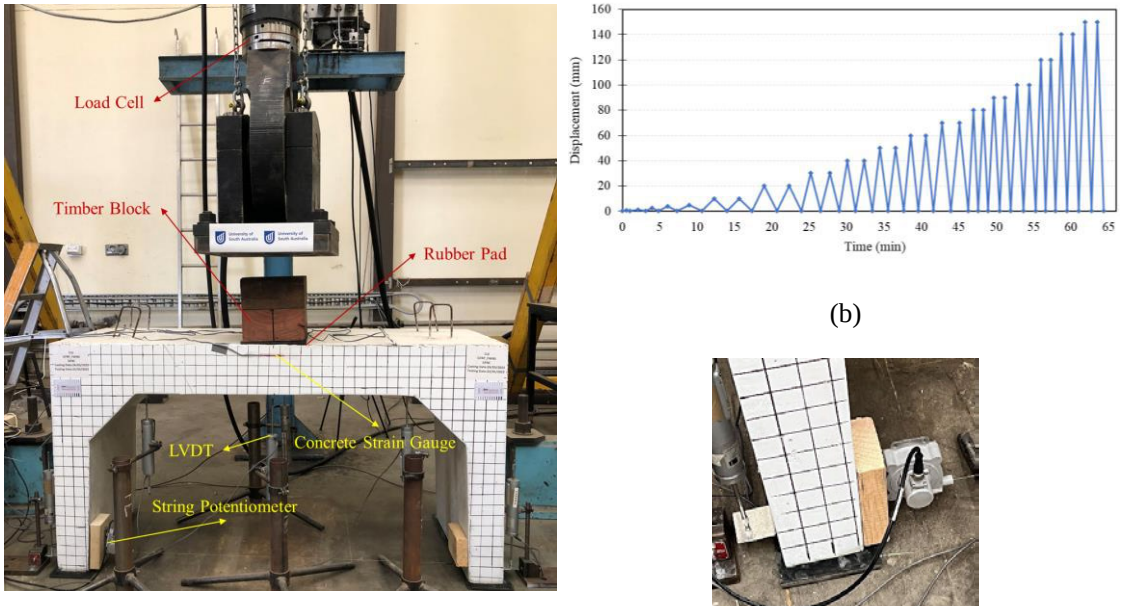
Table 8-4 Summary of culvert specimens.

Number	Culvert designation	Concrete mix	Reinforcement				Span (mm)	Height (mm)	Slab thickness (mm)	Concrete compressive strength (MPa)
			Type	Bottom	Top	Ratio				
CL1	GFSS-PVA0.4	SWSS-PVA	GFRP	5Ø16	5Ø16	0.0165	1160	580	155	39.8
CL2	GFSS-PPL0.4	SWSS-PPL								34.3
CL3	GFSS-Hy0.4	SWSS-Hybrid 0.4								35.1
CL4	GFSS-Hy0.6	SWSS-Hybrid 0.6								40.3
CL5	GFSS	SWSS								34.2
CL6	GFNC	FWNS								29.0
CL7	STNC	FWNS	Steel							25.9

Figure 8-3 illustrates the test setup designed to evaluate culvert behaviour according to AS 1597.1-2010 (AS1597.1-2010 2010). In practice, the installation of culverts involves placing them on a base slab to provide a simple connection and filling the gap with backfill materials. The stiffness of the backfill material plays an important role in controlling the lateral movement of the legs and providing lateral restraint. As can be seen in **Figure 8-3**, no lateral support was provided for the culverts to consider the worst-case scenario in real-life projects. A displacement-controlled half-cyclic increasing loading regime was applied at a constant rate of 1 mm/min. A hydraulic MTS machine equipped with a 1000 kN capacity jack having a maximum stroke of 75 mm was employed to apply the vertical load. A load cell integrated within the MTS system measured the force exerted on the culvert through the vertical jack (**Figure 8-3**a). A loss of 50% in specimen strength was designated as the failure criterion. Following AS 1597.1-2010 (AS1597.1-2010 2010), a 200 mm width rubber pad with 15 mm thickness was positioned on the crown of the culvert to simulate a vehicle wheel load, distributing it uniformly. A 200 mm × 100 mm × 200 mm timber block was placed on the pad. The load was applied at the mid-span and front face of the culvert to replicate the worst-case scenario in terms of the vehicle's wheel locations. This method has also been employed in previous studies on the structural performance of concrete culverts (Garg *et al.* 2007; Abolmaali *et al.* 2008a; Abolmaali *et al.* 2008b; Mostafazadeh *et al.* 2019; Hassanli *et al.* 2022; Mashayekhi *et al.* 2024e). The specific loading pattern is depicted in **Figure 8-3**b. It consisted of five individual cycles reaching a displacement of 5 mm, followed by some sets of repeated cycles at progressively larger displacements (Hassanli *et al.* 2017; Javadi *et al.* 2021; Hassanli *et al.* 2023; Saeed *et al.* 2024). It is important to note that assessing the performance of concrete culverts under repeated loads requires investigation through fatigue loading, which falls outside the scope of this paper.

Four Linear Variable Differential Transformers (LVDTs) were installed vertically as shown in **Figure 8-3**a to monitor the crown deflection of the culverts. These LVDTs had a stroke length of 100 mm and were positioned at two locations: (i) the culvert mid-span (one at the front and one at the back), and (ii) near the haunches at both ends of the crown. Rubber strips were placed between the culvert legs and the strong floor to comply with AS 1597.1-2010 (AS1597.1-2010 2010) and prevent stress concentration. These strips also ensured even distribution of the applied forces. In real-life projects, inverted U-shaped culverts are installed on a base slab with the bearing area cleaned and covered

with mortar or a damp proof course for uniform bearing. Additionally, when culverts are placed directly on the soil, flexible support should be considered in experimental studies to replicate this condition. The rubber pads mimic this practice by providing a flexible interface that facilitates uniform contact and load distribution. Two additional LVDTs were mounted at the corners of the culverts at their base to measure the vertical movement of the legs due to compression of the rubber pads. A string potentiometer was attached to the legs, as depicted in **Figure 8-3**c, to quantify the relative movement between them. Two strain gauges were also employed on each reinforcement layer (top and bottom) at mid-span to capture their strain behaviour during the test (see **Figure 8-2**). These gauges were secured with duct tape for protection. An additional strain gauge with a gauge length of 60 mm was also affixed to the face of the culvert to monitor the concrete strain at compression. Crack width gauges were strategically placed at various locations to measure crack development during each displacement cycle of the test.



(a) (b) (c)

Figure 8-3 Test setup and instrumentations along with cyclic loading pattern.

8.3 Results and discussion

8.3.1 Load-deflection behaviour under cyclic loading

The load-deflection response of the plain SWSS culvert exhibited distinct behavioural phases under cyclic loading, including linear elastic, linear plastic, nonlinear plastic, post

peak, and large plastic deflection, as shown in **Figure 8-4**. These phases are distinguished by the slope of the load-deflection curve during loading and unloading cycles. Fiber incorporation influenced these phases differently and significantly improved culvert performance, especially at larger displacements. The effects of fiber addition, reinforcement type, and concrete type (SWSS and FWNS) on the various stages will be discussed in the following paragraphs, as illustrated in **Figure 8-5**.

As shown in **Figure 8-5**a, during this initial phase, characterized by linear elastic behaviour up to approximately 4% of the peak deflection, fiber inclusion had no discernible effect on culvert behaviour. In the second phase, the culvert transitioned to a state of linear elastic-plastic behaviour. This is evidenced by a decrease in the material stiffness, quantified by the slope of the curve. The area enclosed by the hysteresis loops increased, indicating the formation of multiple cracks. Subsequently, material damage continued to progress, manifested by a gradual decline in the peak load for each loading cycle and the accumulation of residual deflection. The slopes of both the loading and unloading paths decreased with increasing cycle numbers, reflecting this stiffness degradation attributable to material damage. Notably, while the slope remained relatively constant throughout this phase, plastic deflection was observed and progressively increased with deflection. This phase extended up to 30% of the peak deflection. During this phase, fiber addition modestly increased culvert stiffness and delayed the transition from linear to nonlinear behaviour. Additionally, fibers reduced plastic deflection and extended the linear plastic behaviour phase to roughly 60% of the peak deflection. The inclusion of fibers likely mitigated crack growth and stress concentrations, preventing excessive plastic deformation in culverts. Additionally, fiber bridging and pull-out resistance helped the culvert retain its original shape under load, thus delaying permanent deformation and extending the linear elastic range. A closer examination of this phase reveals that fiber incorporation significantly improved the linear behaviour of culverts, with mono PPL and PVA fibers exhibiting greater effectiveness compared to GFSS-Hy0.4. Furthermore, increasing the dosage of hybrid fibers in GFSS-Hy0.6 resulted in a significant improvement in linear behaviour.

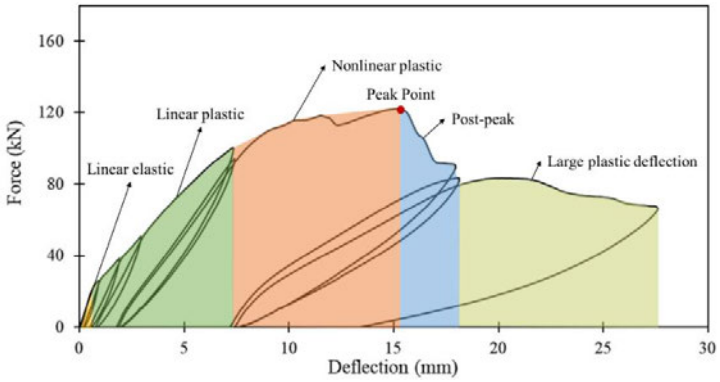
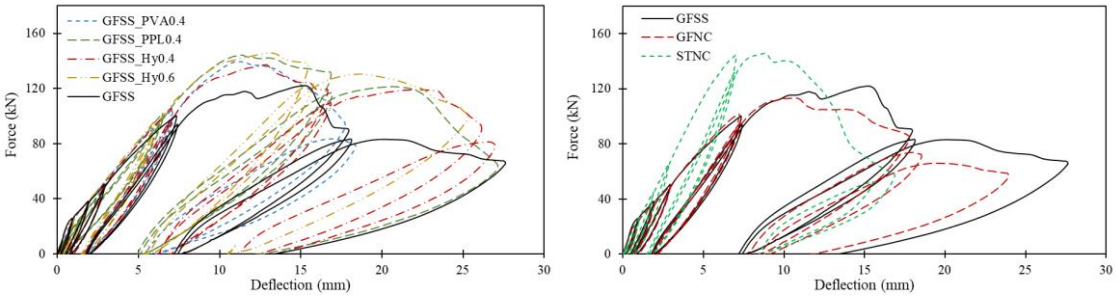


Figure 8-4 Load-deflection behaviour of GFRP-reinforced SWSS concrete culvert (GFSS).

The third phase exhibited nonlinear plastic behaviour, characterized by a continuous decrease in tangent stiffness until reaching the peak load point. During this phase, plastic deformation increased significantly. The addition of fibers significantly reduced plastic deflection and demonstrably enhanced the load-carrying capacity. This improvement can be caused by the crack-bridging effect of the fibers (Changqing *et al.* 2022; Hassanli *et al.* 2023; Vafaei *et al.* 2023). Notably, the incorporation of mono PPL fibers and hybrid fibers with a higher dosage (GFSS-Hy0.6) transformed the pre-peak behaviour of the culvert from nonlinear to linear. This observation suggests the superior effectiveness of PPL fibers due to their greater length and enhanced bonding strength with the concrete matrix. Consistent with (Mashayekhi *et al.* 2024a), partially replacing PPL fibers with PVA fibers enhanced the bonding strength, likely due to the inherent chemical bonding properties of PVA fibers, which strengthen the concrete matrix surrounding the PPL fibers. Previous research has shown that macro synthetic fibers improve the load capacity of concrete culverts (Mostafazadeh *et al.* 2019). These fibers bridge cracks, distribute stress, and prevent crack widening, thereby enhancing toughness and ductility. Consequently, culverts can withstand higher loads before failure. This finding aligns with the results of the present study, which also observed improved shear strength because of fiber inclusion. The fourth phase occurred immediately following the peak point, characterized by a sharp decline in capacity lasting approximately up to 20% after the peak deflection. In this phase, fibers demonstrably mitigated the sharp decline in loading capacity. Notably, both mono PPL and high-dosage hybrid fibers (GFSS-Hy0.6) exhibited greater efficacy. This enhanced performance can be stemmed from the bridging effect and superior bond strength offered by these fiber types. Following phase four, the

culvert transitioned to the final phase, characterized by significant plastic deflection and a gradual decrease in load capacity. Fiber incorporation significantly increased the load capacity of the culverts and reduced plastic deflection during this phase. This is consistent with previous research on the incorporation of macro synthetic fibers in concrete culverts utilizing FWNS concrete. The addition of 0.52% volume fraction of macro synthetic fibers was found to enhance both shear capacity and ductility (Mostafazadeh *et al.* 2019).



(a) (b)

Figure 8-5 Hysteretic behaviour of culverts: Effects of (a) fiber incorporation and (b) SWSS concrete and GFRP reinforcement.

Figure 8-5b compares the hysteretic behaviour of steel- and GFRP-RC culverts, as well as concrete types SWSS and FWNS. GFSS and GFNC exhibited similar behaviour under cyclic loading, while STNC with steel reinforcement displayed higher stiffness during linear plastic phase up to 65% of peak deflection. The observed behaviour was due to the higher elastic modulus of the steel bars. Consistently with the present findings, prior research also reported this effect in both GFRP and steel reinforced slabs (Hassanli *et al.* 2023). Comparing FWNS and SWSS culverts revealed that both GFSS and GFNC exhibited similar behaviour under cyclic loading. However, GFSS culverts demonstrated a higher load-bearing capacity at larger deflections. This phenomenon can likely be explained by the superior interlocking strength of SWSS concrete compared to FWNS concrete, as reported in (Mashayekhi *et al.* 2024a).

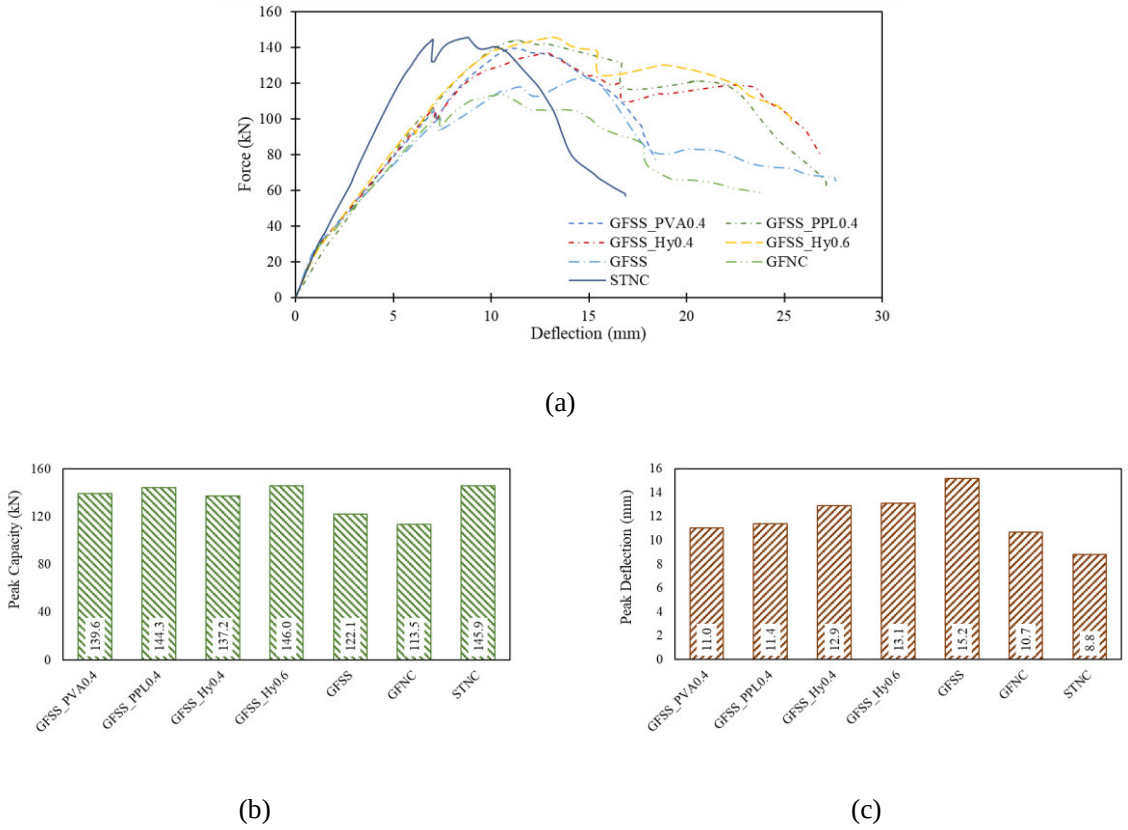
8.3.2 Backbone curve

Figure 8-6 presents the culvert backbone curves, peak capacities, and corresponding deflections. The results presented indicated that SWSS exhibited an 8% increase in ultimate capacity and a 42% increase in peak deflection compared to FWNS. This improvement may be attributed to the denser microstructure and more cohesive matrix of

SWSS concrete. This denser structure was likely responsible for the higher shear and tensile strengths in SWSS concrete (Mashayekhi *et al.* 2024a), ultimately improving the load-bearing capacity of the SWSS concrete culvert. Similar findings have been reported in previous research on concrete beams (Lingzhu *et al.* 2023). Additionally, fiber incorporation improved ultimate capacity by 12-20% compared to GFSS, with a significant decrease (13-28%) in peak deflection. Consequently, lower crown deflection was observed before failure. Mono PPL and PVA fibers increased ultimate capacity by 18% and 14%, respectively, while their hybrid form yielded a 12% increase. Increasing the dosage of hybrid fibers to 0.6% further improved the ultimate capacity by approximately 20%, without a significant change in peak deflection. This suggests that incorporating hybrid fibers at an optimal dosage has the potential to enhance the shear strength of GFRP-RC culverts compared to mono fibers. Previous studies have also confirmed that fiber hybridization can potentially enhance the mechanical properties of plain SWSS concrete (Mashayekhi *et al.* 2024a; Mashayekhi *et al.* 2024d, 2024e, 2024c). As this study lays the groundwork for incorporating hybrid macro/micro fiber in concrete culverts, further investigation is necessary to determine the optimal hybrid fiber dosage. Steel reinforcement provided a 29% ultimate capacity increase but caused a 17% deflection reduction relative to GFRP-RC (GFNC) culverts. The higher elastic modulus of steel reinforcement compared to GFRP (about 3.3 times) contributed to the observed behaviour. STNC culvert displayed a higher peak load ratio by about 1.3 and lower deflection ratio by about 0.8 compared to GFNC. This aligns with previous findings on peak deflection in cyclic loaded concrete slabs (Al-Zahrani *et al.* 2023; Hassanli *et al.* 2023). Similar GFRP and steel reinforcement ratios employed in this study yielded higher steel axial stiffness, resulting in greater peak load and lower deflection as expected from on previous study on concrete beams (Hu *et al.* 2023).

Figure 8-7 depicts the microstructural analysis of FWNS and SWSS concrete using a Hitachi TM4000 scanning electron microscope (SEM) to evaluate hydration products and structural features at the micro-scale. Samples were prepared by cutting into small sections and drying to remove residual moisture. SEM imaging was conducted at an accelerating voltage of 15 kV using secondary electron imaging (SEI) mode to capture surface morphology with high precision. The results show that SWSS concrete contained more needle-like ettringite crystals and hexagonal portlandite particles compared to FWNS concrete, attributed to the accelerated hydration induced by chlorides, which

resulted in a denser microstructure. These particles fill voids, leading to fewer micro-cracks in the structure, consistent with previous studies (Wang, Junjie *et al.* 2018; Yifan *et al.* 2021; Vafaei *et al.* 2022b; Mashayekhi *et al.* 2024a; Mashayekhi *et al.* 2024d, 2024c). A previous study revealed that the content of ettringite formed in a seawater system was 67% higher than that formed in a freshwater system at 28 days of curing (Li, Peiran *et al.* 2020a). The incorporation of GGBS also resulted in a higher content of ettringite in SWSS concrete compared to FWNS. A similar observation was reported in a previous study, where employing 50% GGBS resulted in 20%-30% higher ettringite content in seawater concrete than in freshwater concrete (Yifan *et al.* 2021).



(a)

(b)

(c)

Figure 8-6 Backbone curves of all investigated culverts with (b) peak capacity and (c) peak deflection.

Figure 8-8 depict the contribution of effective parameters to the shear strength of concrete culverts. including the uncracked concrete compression zone (V_{cc}), inclined shear stress from aggregate interlocking (V_{AI}), dowel force from tension reinforcement (V_d), and the vertical components of the fiber pull-out force (V_{uf}). The contribution of V_{AI} to total shear resistance was estimated to range between 25–50% (Kim *et al.* 1996). Moreover, the

denser microstructure and more cohesive matrix of SWSS concrete enhanced interparticle bonding, leading to a higher V_{AI} and greater aggregate interlocking compared to FWNS concrete, which is essential for resisting shear forces, as depicted in Figure 8. The inclusion of fibers increased the contribution of V_{uf} (see Figure 8), thereby improving the shear strength of the crown. In this case, fibers with stronger bonding strength, greater pull-out force, and higher dosage resulted in superior performance. This study aligns with prior research on the influence of synthetic fibers in concrete. It was found that macro-synthetic fiber addition enhanced both shear strength and ductility, along with modifying the cracking and failure patterns (Altoubat *et al.* 2009; Mostafazadeh *et al.* 2019). It was observed that addition of fibers altered the behaviour of the culverts during pre-peak phases, changing it from nonlinear to linear, attributable to an increase in stiffness.

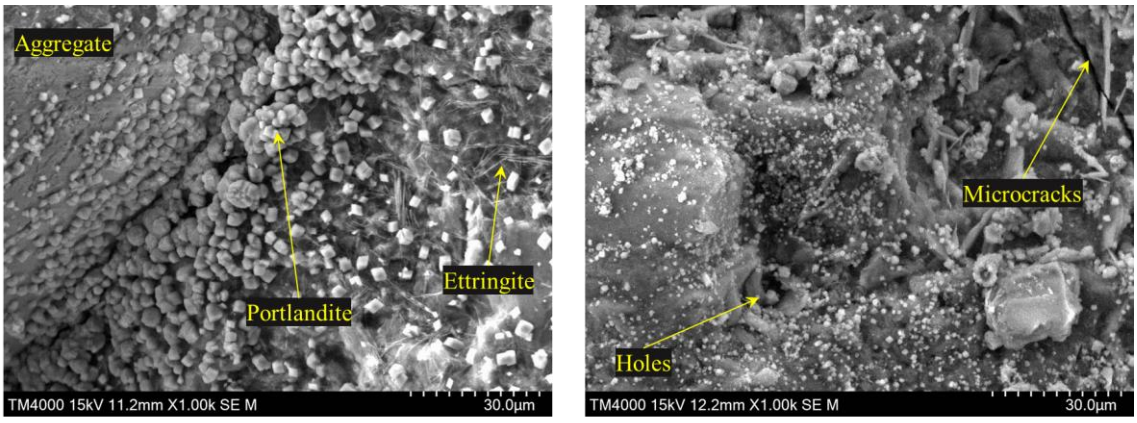


Figure 8-7 Microstructure analysis of SWSS and FWNS concrete.

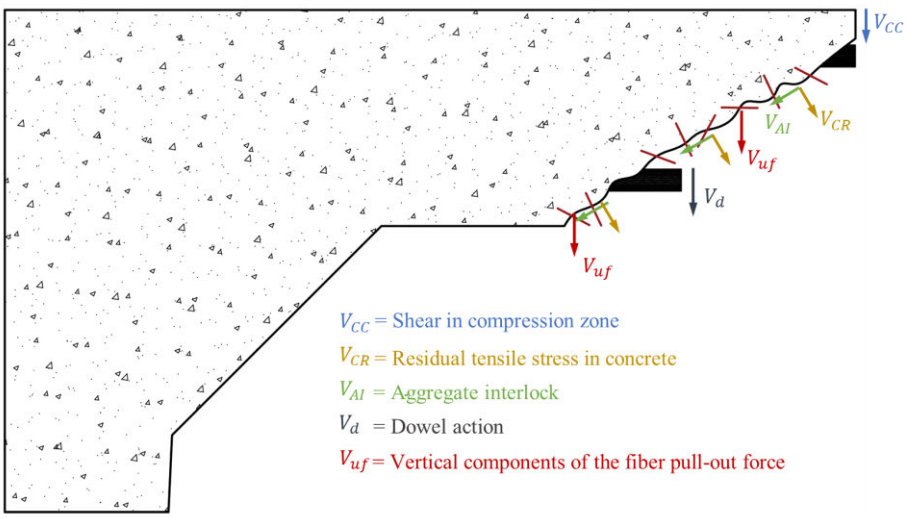


Figure 8-8 Shear transfer mechanism at the crown.

8.3.3 Failure mode and damage mechanism

All culverts exhibited punching shear failure at the crown, consistent with previous studies (Mostafazadeh *et al.* 2019; Hassanli *et al.* 2022), with large cracks propagating from the loading point through the haunch tip and the crown underside to the back (see **Figure 8-9**). This aligns with AS 1597.2-2013 (AS1597.2-2013 2013), which identifies the critical shear section for inverted U-shaped culverts with corner haunches at d_v (effective shear depth) from the haunch tip. This study confirms this concept by applying mid-span loading, previously identified as the worst-case scenario for GFRP-RC culvert strength (Hassanli *et al.* 2022). Under increasing load cycles, flexural cracks initiated, followed by propagation of narrow shear cracks from the loading point towards the haunches, ultimately resulting in shear failure (**Figure 8-9**). While the damage mechanism was similar for plain and fiber-reinforced concrete, fiber type influenced specific behaviours. Strain analysis showed no yielding in steel or rupture in GFRP reinforcements, indicating an over-reinforced designed section. This resulted in a shallow compression zone (depth of neutral axis=34 mm). At low deflections, the top reinforcement initially experienced compression. As the load and deflection increased, this behaviour generally shifted to tension, except in the case of GFSS-Hy0.6. Crack propagation in the concrete tension zone, followed by shear crack development, significantly reduced the depth of the compression zone, and shifted the neutral axis, resulting in tension in the top reinforcement. However, in the GFSS-Hy0.6 culvert, the higher fiber dosage enhanced crack bridging, effectively limiting crack propagation. This led to an increased compression zone depth, which maintained the top reinforcement in compression as the load and deflection increased.

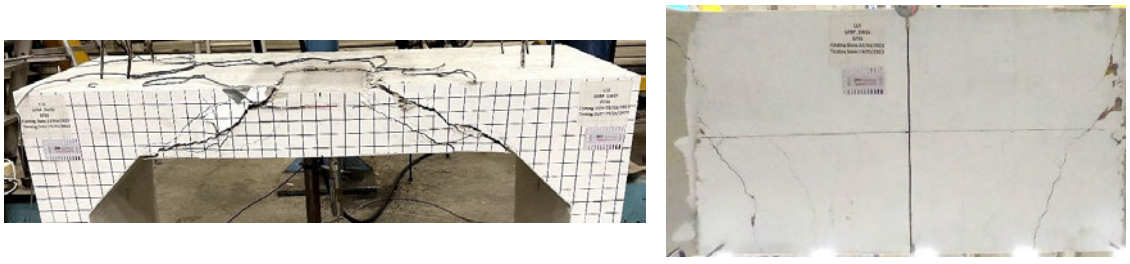
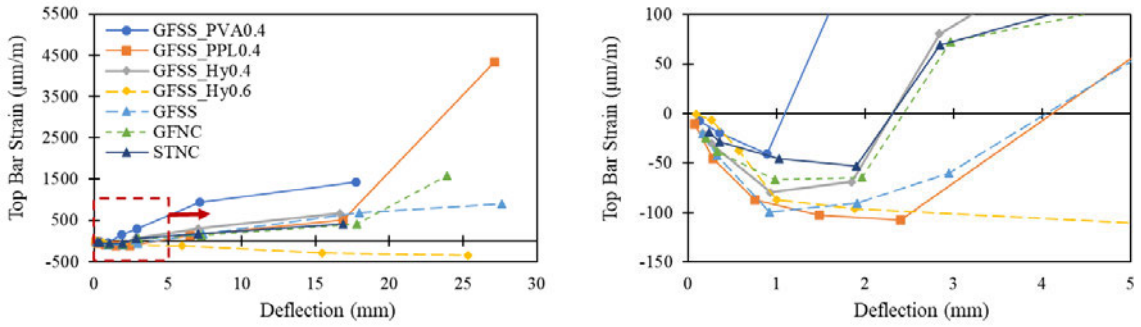


Figure 8-9 Typical failure mode of the investigated culverts.

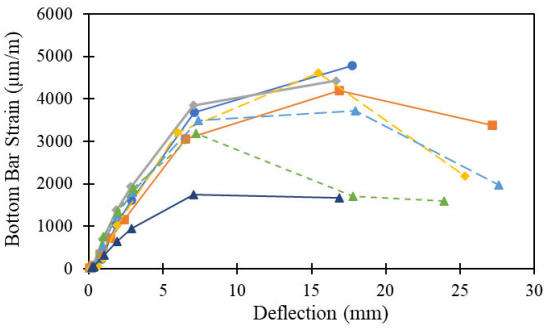
PVA fiber incorporation significantly increased compressive strength, leading to a deeper neutral axis and a larger compression zone, consistent with previous research

(Mashayekhi *et al.* 2024a). The incorporation of PVA fibers, characterized by high tensile strength, elastic modulus, and elongation (Amin *et al.* 2013), significantly enhanced the reinforcement properties of SWSS concrete (Mashayekhi *et al.* 2024a). Also, these dispersed micro-reinforcements effectively bridged micro-cracks, enhancing tensile strength, and reducing overall cracking (Vafaei *et al.* 2021a; Mashayekhi *et al.* 2024a). Compared to GFSS culverts, PVA reinforcement transferred more tensile force to the bottom reinforcement and less compressive force to the top (**Figure 8-10**). This is further confirmed by the significantly reduced concrete compressive strain in the PVA section (by approximately 73%) compared to GFSS (**Figure 8-11**). The higher load-bearing capacity can be due to the higher shear strength of PVA fiber-reinforced concrete, compared to plain concrete, as reported in previous study (Hassanli *et al.* 2024). This improvement was attributed to the strong chemical bonding of PVA fibers, which promoted superior inter-material interlocking (Mashayekhi *et al.* 2024a). This improved shear resistance allowed for a higher tension force in the bottom reinforcement at larger crown deflections before failure (**Figure 8-10**b).

The results showed a significant increase in shear capacity for SWSS concrete culvert with PPL fibers. Examining top/bottom reinforcement behaviour revealed significant enhancement of tensile force in both at large deflections (**Figure 8-10**). Notably, concrete compressive strain was also significantly higher (by approximately 27%) with PPL fibers (**Figure 8-11**). This could be arisen from PPL fibers bridging micro- and macro-cracks, particularly at large deflections, delaying crack propagation and leading to a higher load-bearing capacity for GFSS-PPL0.4. This bridging effect also delayed shear failure and allowed the top reinforcement to carry more tensile force at large deflections. GFSS-PPL0.4 exhibited lower tensile strains (top/bottom reinforcement) and higher compressive strain than GFSS-PVA0.4 at lower deflections. However, under larger deflections and wider cracks, the inability of PVA fibers to bridge cracks effectively resulted in a sudden shear failure upon reaching shear capacity. Conversely, the pullout and breakage of PPL fibers during cracking absorbed energy, enhancing the deformation capacity of crown, leading to the observed increase in tensile strain for both the top and bottom reinforcement.



(a)



(b)

Figure 8-10 Strain values in reinforcement per cycle: (a) top bar, and (b) bottom bar.

Partial replacement of PPL fiber with PVA in hybrid system significantly reduced concrete compressive strain by 41% and 51% compared to GFSS and GFSS-PPL0.4, respectively. This suggests a PVA/PPL positive synergy, with PVA enhancing PPL bond strength (Mashayekhi *et al.* 2024a), leading to improved stress distribution and a larger tensile zone (confirmed by higher tensile strain at bottom reinforcement in **Figure 8-10**b). Notably, while mono PVA fibers reduced plastic strain compared to GFSS, mono PPL fibers had minimal impact (**Figure 8-12**). The hybrid PPL/PVA significantly outperformed both in this regard. Increasing the hybrid fiber dosage from 0.4% to 0.6% increased peak compressive strain by 32% and resulted in continuously increasing strain with crown deflection. This higher dosage significantly enhanced top reinforcement performance, maintaining compression under all deflections due to superior crack control and minimized concrete damage. Notably, GFSS-Hy0.6 exhibited a 36% concrete strain reduction compared to GFSS-PPL0.4 (**Figure 8-11**).

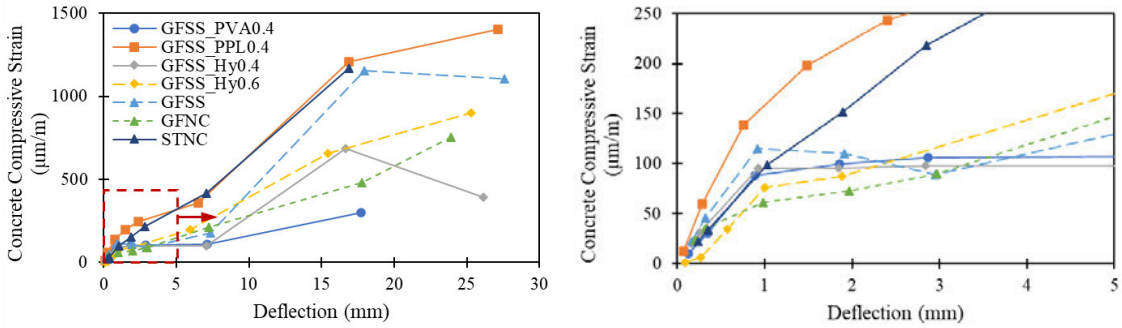


Figure 8-11 Concrete compressive strain of the culverts per cycle.

The SWSS culvert exhibited a 46% increase in concrete compressive strain compared to the GFNC. Furthermore, SWSS concrete resulted in higher top reinforcement strains at lower deflections, delaying the transition to tension (**Figure 8-10**a). At higher deflections, SWSS concrete experienced greater tensile strain. Notably, plastic strain remained lower in the GFNC culvert. This behaviour likely stemmed from the higher interlocking strengths and denser structure of SWSS concrete, enabling it to transfer compressive forces to the top reinforcement before tension developed. Additionally, the higher tensile strength of SWSS concrete minimized cracking, further promoting tensile force transferred to the reinforcement. Conversely, the lower tensile strength and extensive cracking observed in GFNC concrete at larger deflections led to increased top reinforcement tensile strain. Concrete culverts reinforced with steel bars (STNC) displayed a 55% increase in peak compressive strain at failure compared to GFRP-RC culverts, along with significantly lower tensile strain in the bottom reinforcement. Both exhibited similar behaviour for top reinforcement under varying crown deflections. The higher elastic modulus of steel in STNC culverts resulted in lower bar strain but correspondingly induced higher compressive strain in the surrounding concrete.

8.3.4 Relative leg-opening

The incorporation of fibers in concrete culverts can potentially affect the stiffness, ductility, and load transfer mechanisms of culverts. Investigating the leg-opening at different deflections can provide valuable insights into the effectiveness of the fibers. Additionally, inverted U-shaped culverts are usually placed on a base slab, and the legs are set in recesses with a gap between the culvert legs and the nibs, which are typically filled with cement mortar. In this case, investigating the horizontal displacement of the

legs provides valuable insights for determining the required gaps and the stiffness of the backfill material to ensure adequate support for the legs.

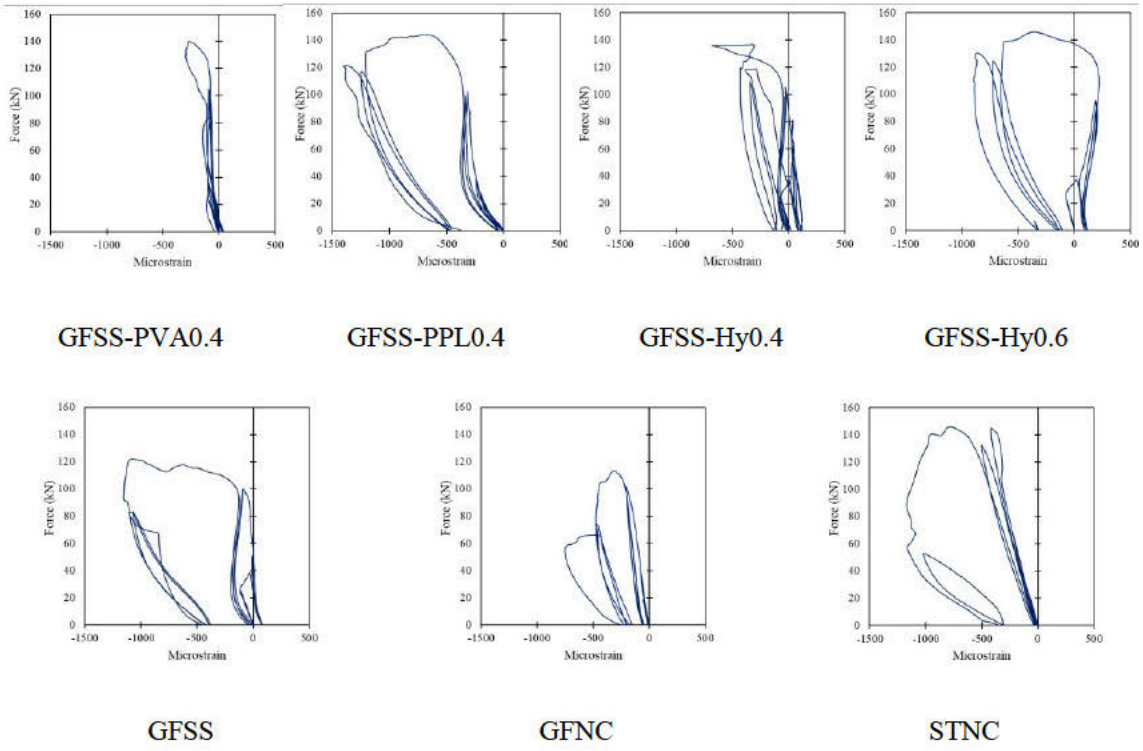


Figure 8-12 Hysteresis behaviour of concrete strain.

Figure 8-13 depicts the hysteretic behaviour of leg-opening (Δ_h) and **Figure 8-14** illustrates the leg-opening per cycle. As it can be observed the Δ_h of all investigated culverts was relatively similar for lower crown deflection. By increasing the crown deflection, the Δ_h of GFSS exhibited an increasing-decreasing trend. But by addition of the fibers, it steadily increased. The observed behaviour can be due to crown failure in the GFSS culvert at higher deflections. This failure resulted in a significant drop in the load-bearing capacity of the crown, leading to reduced load transfer to the legs and a corresponding decrease in Δ_h. The addition of fibers significantly improved the post-peak residual strength and ductility of the crown, leading to enhanced load transfer to the legs and a greater Δ_h. Partially replacement of PVA fiber with PPL ones led to a significant improvement in the Δ_h of the culvert compared to mono PVA fiber. Among the investigated fibers, mono PPL fibers exhibited the lowest residual Δ_h, while hybrid fibers resulted in the highest. This enhancement can be attributed to the improved distribution

and load transfer mechanisms facilitated by the synergistic behaviour of the PPL and PVA fiber combination.

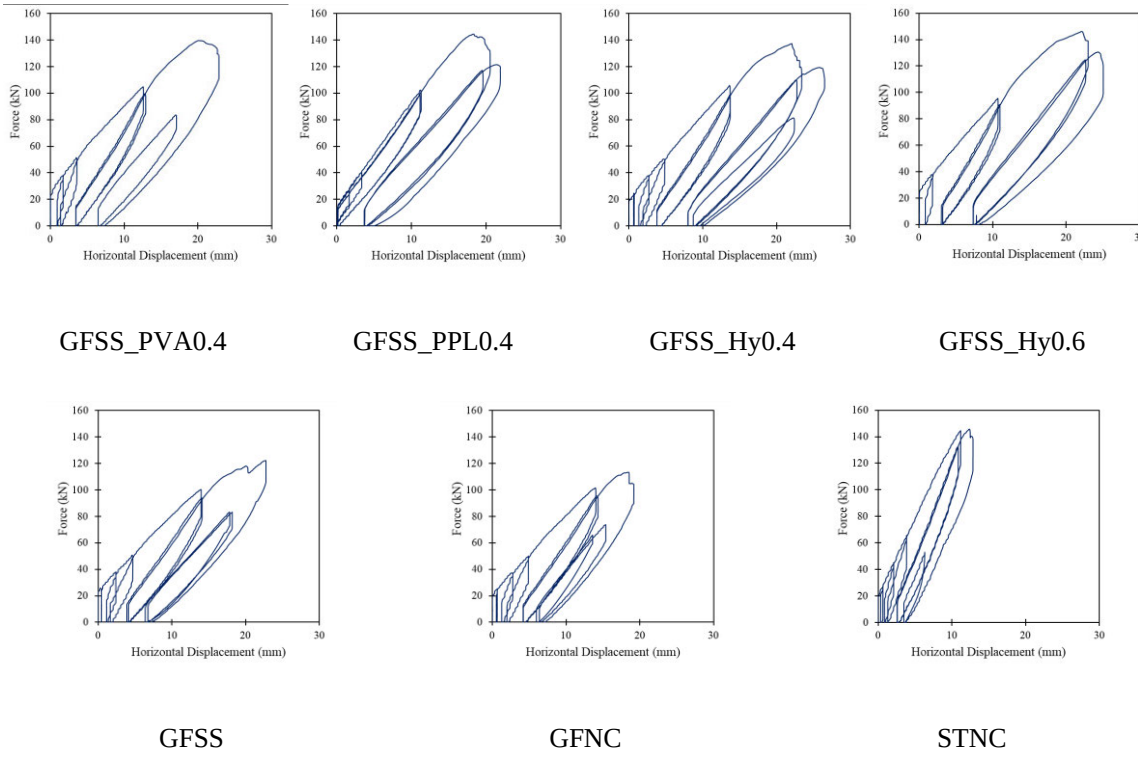


Figure 8-13 Hysteresis behaviour of leg-opening in the culverts.

When it comes to compare the effect of SWSS and FWNS concrete it was demonstrated that the Δ_h of GFSS was higher than GFNC, but similar pattern was observed by increasing the crown deflection. The higher shear strength of SWSS concrete likely explains the observed behaviour. This strength allowed the concrete to bear greater loads, resulting in increased crown deflection (observed in **Figure 8-6**) and consequently, a higher Δ_h value. Comparing GFRP and steel reinforcement demonstrated that steel bars led to significant reduction in Δ_h. Also, plastic Δ_h was significantly reduced by using steel reinforcement. The observed behaviour can be attributed to the higher elastic modulus of the steel reinforcement. This resulted in a reduction in crown deflection, which consequently led to a decrease in leg-opening.

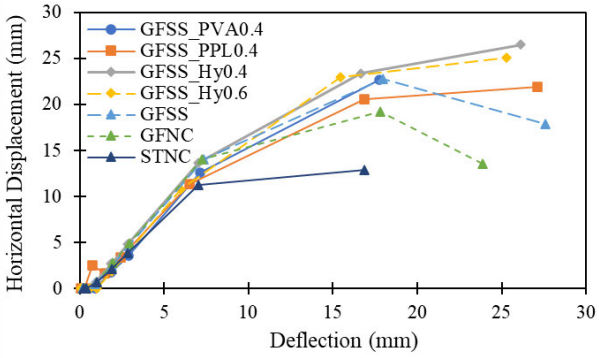


Figure 8-14 Leg-opening of the culverts per cycle.

8.3.5 Damage evaluation

The incorporation of hybrid fibers in concrete improves its damage tolerance (Mashayekhi *et al.* 2024c). Understanding how damage evolves is crucial for accurately predicting the performance of SWSSC culverts under cyclic loading. The damage assessment of the culverts was carried out using three key parameters: the damage index (DI), strength deterioration ratio (SDR), and self-resetting capacity (R). These parameters were determined using equations (8-1) to (8-3) and the data presented in **Figure 8-15**.

$$DI_i = 1 - {E_{d_i}}/{E_0} \tag{8-1}$$

$$SDR_i = {F_{rel_i}}/{F_{unl_i}} \tag{8-2}$$

$$R_i = 1 - {\Delta_{r_i}}/{\Delta_{m_i}} \tag{8-3}$$

where E_{d_i} and E_0 represent the damage modulus and initial modulus, respectively. F_{rel_i} denotes the reloading strength, and F_{unl_i} signifies the unloading strength. Additionally, Δ_{r_i} and Δ_{m_i} correspond to the residual deflection and maximum displacement for each cycle (i), respectively.

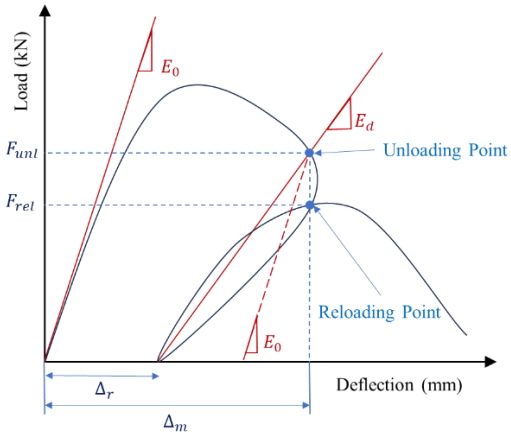


Figure 8-15 Cyclic damage parameters.

8.3.5.1 Damage index

Figure 8-16a presents the DI for each cycle. A positive correlation was observed between crown deflection and DI values. This indicates that an increase in crown deflection was associated with an increase in DI values. Mono PPL fibers initially increased DI for deflections below 5 mm compared to plain GFSS but resulted in lower DI for larger deflections. Conversely, PVA fiber addition significantly reduced DI by approximately 25% compared to GFSS. The observed behaviour can be explained by the reduced initial stiffness of the culvert reinforced with PPL fibers. This can be explained by the low elastic modulus of the PPL fibers as reported in prior studies (Issa *et al.* 2011; Shi *et al.* 2023). While fiber hybridization (GFSS-Hy0.4) slightly increased DI for deflections under 18 mm, it yielded lower DI for larger deflections compared to GFSS. Notably, the hybrid system exhibited lower DI than mono PPL fibers for low deflections, but higher DI than mono PVA fibers. The results suggest a beneficial effect of PVA fibers in reducing DI, although a higher dosage was necessary for a substantial impact. This was further evidenced by the significant decrease in DI observed when increasing the hybrid fiber content from 0.4% to 0.6%. These findings highlight the importance of optimizing fiber dosage in hybrid systems.

Regarding the influence of concrete type, the results revealed that utilizing SWSS concrete led to a slightly lower DI compared to FWNS concrete. This observation can be potentially related to the denser microstructure of SWSS concrete (**Figure 8-7**), which contributed to its increased stiffness and elastic modulus compared to FWNS concrete (Mashayekhi *et al.* 2024a). This resulted in greater shear strength (**Figure 8-8**) and

reduced damage. The denser microstructure improved mechanical interlocking and reduced porosity and voids (**Figure 8-7**), thereby strengthening the concrete matrix, and enhancing its overall stiffness. A comparison of steel and GFRP bars demonstrated that steel reinforcement produced a significantly lower DI compared to GFNC, attributing to the higher elastic modulus of steel bars. However, this benefit came at the cost of a 30% reduction in maximum achievable crown deflection. Moreover, the disparity in DI between GFNC and STNC was substantial at lower deflections but diminished significantly with increasing crown deflection.

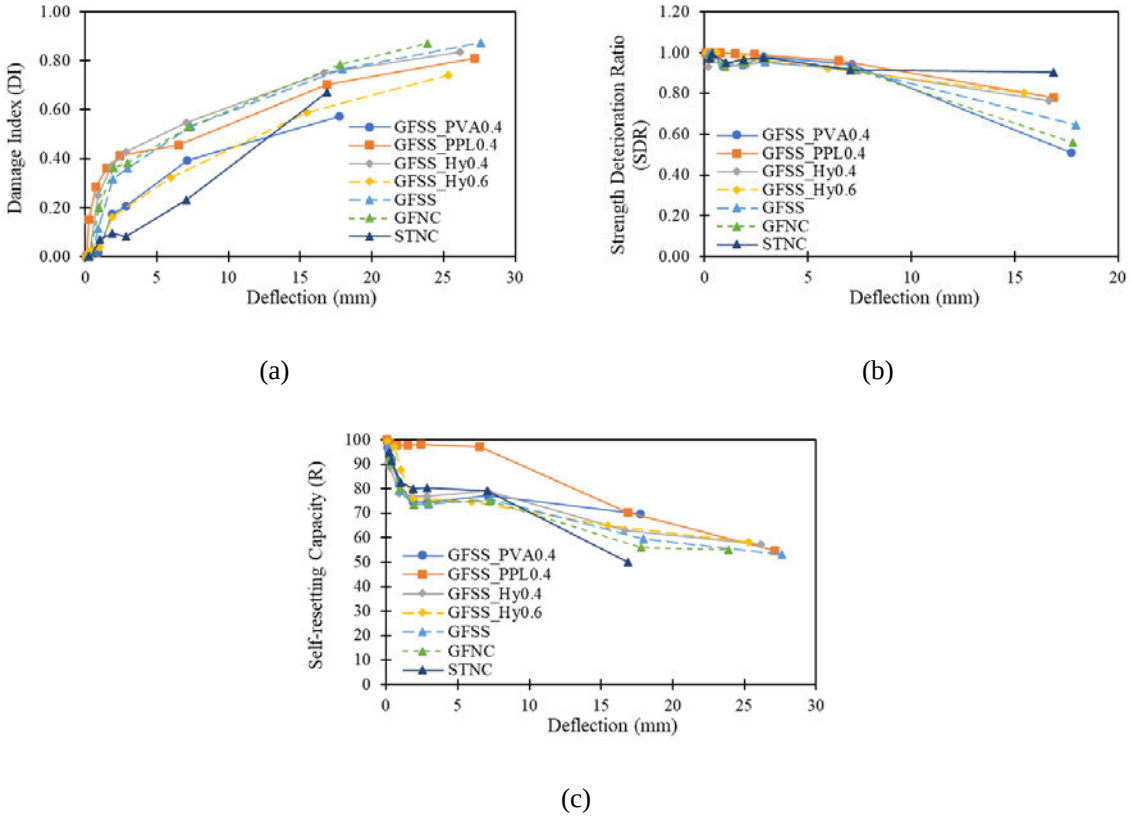


Figure 8-16 Damage parameters (a) damage index (DI), (b) stress deterioration ratio (SDR), and (c) self-resetting capacity (R).

8.3.5.2 Strength degradation ratio

The SDR for each cycle is presented in **Figure 8-16**b. A SDR value close to 1.0 indicates minimal strength reduction after reloading in cyclic loading. A negative correlation exists between crown deflection and the SDR value. This phenomenon can be arisen from the propagation of larger cracks with increasing crown deflection. Consequently, reloading after significant deflection leads to a greater reduction in strength. The incorporation of

mono PVA fibers resulted in higher SDR values for deflections below approximately 8 mm, though this effect diminished for larger deflections as well. This phenomenon can be due to the ability of PVA fibers to bridge and arrest microcracks, thereby minimizing strength reduction at lower deformations. However, for larger cracks exceeding the fiber length, the effectiveness of PVA fibers diminishes gradually. Conversely, the inclusion of PPL fibers consistently improved SDR values across all deflection levels compared to GFSS. This enhancement can be explained by the superior bridging ability of PPL fibers, owing to their greater length and stronger physical bond with the concrete matrix. Partial replacement of PVA fibers with PPL fibers significantly increased the performance of GFSS-PVA0.4. This was evidenced by higher SDR values observed at larger deflections. This enhancement can be stemmed from the synergistic effect of PPL and PVA fibers in enhancing crack-bridging capacity (Mashayekhi *et al.* 2024a).

Compared to FWNS, SWSS exhibited higher SDR values for larger deflections. This can be attributed to the superior interlocking strength of the concrete matrix in SWSS compared to FWNS ones. Furthermore, the use of steel reinforcement resulted in consistently higher SDR values across all deflection levels compared to GFRP bars. This effect was particularly pronounced at larger deflections due to the higher elastic modulus of steel compared to GFRP. The increased stiffness of steel reinforcement allows the sections to maintain a greater level of strength even under significant deformations.

8.3.5.3 Self-resetting capacity

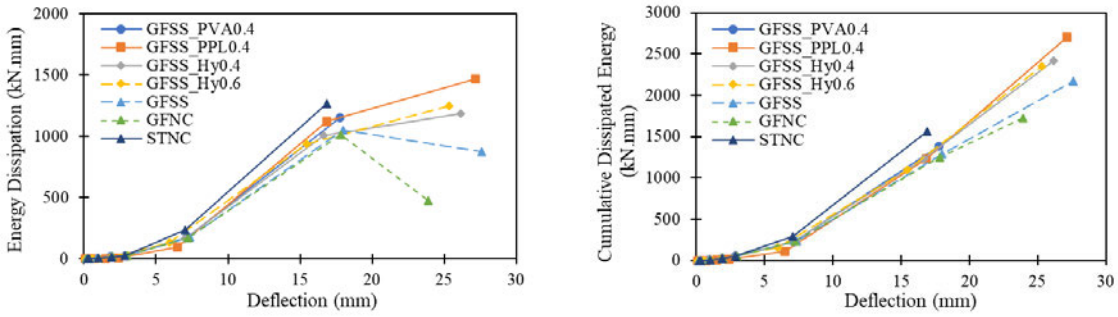
Figure 8-16c illustrates the R observed for each cycle. A negative correlation was observed between the R value and the crown deflection, indicating that the progressive damage of materials resulted in a decrease in the R value. The incorporation of mono PPL fibers significantly improved the R of GFSS for lower deflections due to the tensile strength and bridging effect of the PPL fibers. However, this effect diminished with increasing crown deflection. This phenomenon can be due to the widening of cracks within the concrete matrix as deflection increases. Consequently, the bridging effectiveness of the PPL fibers is compromised due to a decline in both fiber-matrix bond strength and the occurrence of fiber breakage. PVA fibers had no significant impact on R at lower deflections, but improved R at higher deflections. This phenomenon can be explained by the high chemical bonding and tensile strength of PVA fibers as reported in previous studies (Bo *et al.* 2010; Mashayekhi *et al.* 2024a). These properties enhanced the bridging effect within the concrete. However, the limited fiber length restricted their

ability to bridge larger cracks that developed at higher deflections. Fiber hybridization, combining PPL and PVA fibers, also enhanced the R of GFSS culverts. This improvement was more pronounced at higher deflections compared to mono PPL or PVA fibers alone, likely due to the enhanced bonding strength of PPL fibers within the hybrid system.

Culvert constructed with SWSS concrete (GFSS) exhibited higher R values compared to FWNS concrete at high deflections. This can be explained by higher inter-material cohesion properties and denser structure of SWSS concrete compared to FWNS concrete (Vafaei *et al.* 2021a; Mashayekhi *et al.* 2024a), resulting in superior shear strength compared to FWNS concrete. The R of culverts reinforced with steel bars exceeded that of GFRP-RC culverts for deflections less than approximately 10 mm. Conversely, GFRP reinforcement resulted in superior R at higher deflections. This difference in behaviour can be attributed to the higher elastic modulus of steel bars compared to GFRP bars, which aided the culvert in elastically recovering its original shape after unloading. At larger deflections, the lower deformability of GFRP bars compared to steel bars allowed for greater deflection without permanent deformation. Consequently, culverts reinforced with GFRP bars may had a better chance of regaining their original shape after the load was removed.

8.3.6 Energy dissipation

Figure 8-17a depicts the energy dissipation of the analysed culverts per cycle. The dissipated energy was determined by calculating the area enclosed by each hysteretic deflection loop. For the analysis, only the first cycle of each displacement series was considered. Also, the cumulative energy dissipation was calculated by summing the areas of all individual loops throughout the loading history. The energy dissipation of GFSS and GFNC was similar, increasing with crown deflection up to approximately 18 mm, after which it began to decrease. Beyond this point, the energy dissipation of both GFSS and GFNC decreased, with a more pronounced reduction in the GFNC culvert, resulting in higher cumulative energy dissipation for GFSS. This could be attributed to the better bonding strength of GFRP bars in SWSS concrete, as its superior interlocking strength and denser structure likely allowed it to undergo larger deflections and absorb more energy compared to FWNS concrete.



(a) (b)

Figure 8-17 Energy dissipation (a) per cycle, and (b) cumulatively.

A comparison of steel and GFRP reinforcing bars indicated that the STNC culvert displayed higher energy dissipation per cycle. This dissipation further increased with increasing crown deflection before failure. The GFNC (or GFSS) culvert demonstrated approximately 20% lower energy dissipation than the STNC culvert at approximately 17 mm of deflection (the failure point of the STNC), despite failing earlier than GFNC culvert. These findings are consistent with prior research on beams and slabs (Hassanli *et al.* 2023; Hu *et al.* 2023). This could be attributed to the higher elastic modulus of steel reinforcement, resulting in greater ultimate strength and energy dissipation at lower deflections. Nevertheless, following the peak point and due to punching shear failure in both culverts, a sharp decrease in ultimate strength was observed, resulting in significantly lower post-peak dissipation. The previous study also reported similar results, showing that GFRP-RC slabs exhibited larger deflections compared to steel-reinforced ones, allowing it to absorb more energy at higher deflections and consequently improve total energy dissipation (Hassanli *et al.* 2023).

The incorporation of fibers enhanced the energy dissipation of the GFSS culvert and reduced the difference in energy dissipation between the STNC and GFSS. Notably, PPL fibers resulted in the highest energy dissipation per cycle at a deflection of 17 mm compared to other fiber types, though it was approximately 12% lower than STNC and 18% higher than GFSS. This performance was likely attributed to their ability to bridge macro-cracks formed during large deflections. However, PPL fibers exhibited lower energy dissipation at deflections below about 7 mm. This behaviour can be explained by the reduced initial stiffness of the PPL fiber-reinforced culverts, due to its relatively low elastic modulus of PPL fibers (Issa *et al.* 2011; Shi *et al.* 2023). In contrast, partially

replacing PPL fibers with PVA fibers led to increased energy dissipation at lower deflections. This phenomenon can be attributed to the increased elastic modulus of SWSS concrete due to the synergistic effect of the fibers (Mashayekhi *et al.* 2024a).

Figure 8-17b illustrates the cumulative energy dissipation, showing that the incorporation of PVA fibers resulted in a 7% increase in cumulative energy dissipation compared to GFSS at 18 mm deflection, identified as the failure point of the PVA-reinforced culvert. While the addition of PVA fibers led to approximately 10% higher energy dissipation, it is noted that the PVA fibers also increased the shear strength, resulting in a 14% higher ultimate strength compared to GFSS. However, once shear cracks developed, the limited length of the PVA fibers likely contributed to premature failure at larger deflections due to the formation of larger cracks, which caused a sharp drop in loading capacity after the peak, resulting in lower deflection at the failure point. Partially replacing PVA fibers with PPL fibers did not change cumulative energy dissipation at 18 mm deflection compared to the PVA-reinforced specimen, but it resulted in an 11% increase in total cumulative energy dissipation at the failure point compared to GFSS. Conversely, PPL fibers led to an approximately 25% increase in total cumulative energy dissipation at the failure point compared to GFSS. This outcome confirms previous findings (Mostafazadeh *et al.* 2019; Mashayekhi *et al.* 2024e) that incorporation of macro fibers, such as PPL, in concrete culverts, either in mono or hybrid forms, resulted in enhanced energy dissipation capacity.

8.3.7 Hysteretic damping ratio

Hysteretic damping, ξ_{hys}, was calculated to further analyse the energy dissipation response of the tested culverts. Hysteretic damping reflects the ratio of dissipated energy to elastic energy (this is the energy stored within the material due to its deformation and the energy returned when the load is removed) within each deflection loop and is defined as follows (Hassanli *et al.* 2023):

$$\xi_{hys} = \frac{1}{4\pi}\frac{E_{hys}}{E_{el}} = \frac{A_l}{2\pi F_l d_l} \tag{8-4}$$

where for a specific deflection loop, E_{hys} represents the dissipated energy within the loop, E_{el} denotes the elastic strain energy, A_l refers to the enclosed area by the loop, while F_l

and d_l correspond to the maximum force experienced by the loop and its associated deflection, respectively, as depicted in **Figure 8-18**.

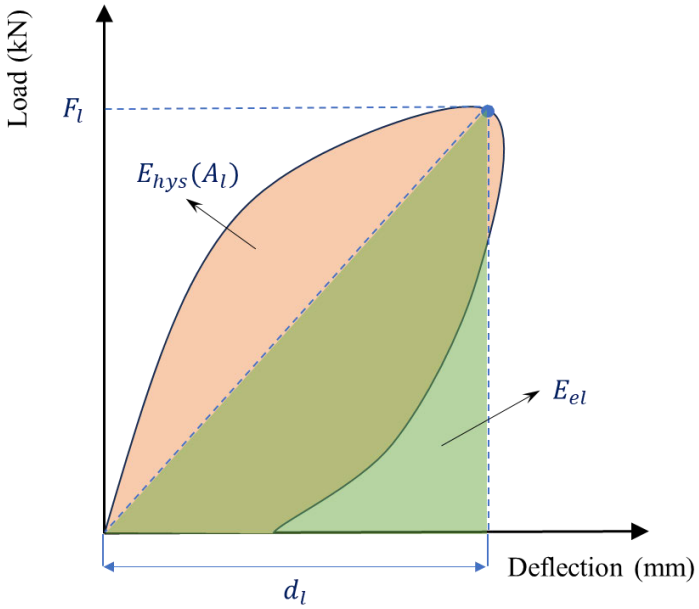


Figure 8-18 Hysteretic damping ratio parameters.

Figure 8-19 illustrates the hysteretic damping ratio for each loop. Both plain concrete culvert types (GFSS and GFNC) displayed a sharp decrease in hysteresis damping for deflections exceeding 18 mm. This behaviour was mitigated by the incorporation of various fiber types, leading to an overall increasing trend in damping. The incorporation of mono PVA fibers resulted in a similar trend of hysteresis damping before failure compared to GFSS culvert. Similar effects were observed for micro PVA fibers in concrete slabs subjected to cyclic loading (Hassanli *et al.* 2023). However, mono PPL fibers exhibited significantly lower hysteresis damping at lower deflection levels, with reductions reaching up to 77%. Conversely, at higher deflections, PPL fibers resulted in a significant increase in hysteresis damping coefficient by 70% compared to GFSS culverts. This contrasting behaviour can be attributed to the combined effects of PPL fiber length, tensile strength, and their ability to bridge wider cracks that develop at larger deflections. In contrast, at lower deflections, the incorporation of PPL fibers led to a significant improvement in elastic energy storage and a reduction in plastic deformation, resulting in a lower ξ_{hys}. This trend is consistent with the observations from other investigated parameters. Partial replacement of PVA fibers with PPL fibers yielded a higher hysteresis damping for deflections below approximately 2 mm, but this behaviour

diminished for larger deflections. Additionally, increasing the fiber dosage in the hybrid system further decreased hysteresis damping at high deflections and increased it for lower deflections. This outcome suggests that the synergistic behaviour of PPL and PVA fibers improved the inelastic behaviour at lower deflections, but conversely, it caused a more elastic deflection at higher deflections, leading to a lower ξ_{hys}.

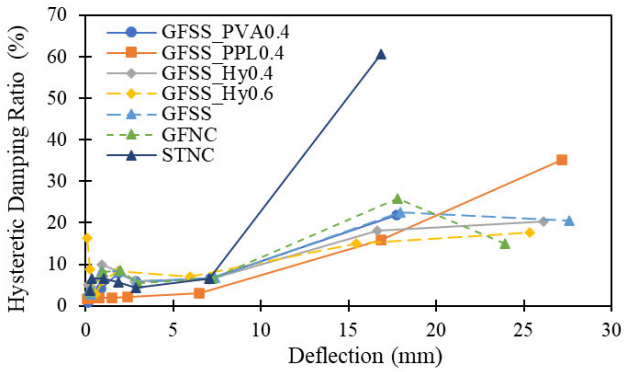


Figure 8-19 Hysteretic damping ratio (ζ) of the culverts per cycle.

A comparison of SWSS and FWNS revealed similar hysteresis damping behaviour for deflections below 7 mm. At higher deflections, SWSS concrete exhibited superior damping characteristics. This phenomenon can be explained by the increased friction and cohesion between materials within the SWSS matrix, leading to a higher damping ratio at larger deformation levels. While STNC displayed lower hysteresis damping than GFNC for deflections less than approximately 7 mm, it demonstrated a significant increase in damping compared to GFNC at higher deflection levels. This behaviour can be explained by the contrasting material properties of the reinforcing bars. At lower deflections, STNS exhibits a more elastic response due to the higher elastic modulus of steel bars. This results in the storage of a larger portion of the deformation energy, which is then released upon unloading, leading to a lower damping ratio. Conversely, at larger deflections, the superior deformability of steel reinforcements contributes to a higher damping ratio. In contrast, GFRP bars, due to their elastic behaviour, experience greater elastic deflection at higher deflections, consequently resulting in a lower hysteretic damping capacity.

8.4 Prediction models for shear capacity

Previous studies have reported considerable debate regarding the shear performance of steel-reinforced concrete culverts, leading to a series of investigations into their shear

behaviour. Notably, research has indicated that the shear strength of concrete culverts often exceeds the predictions provided by various design codes (Yee 2004; Garg *et al.* 2007; Abolmaali *et al.* 2008b; Garg *et al.* 2009; Ghahremannejad *et al.* 2019b). This section assesses the shear capacity of GFRP-reinforced SWSS concrete culverts by incorporating various fiber types and employing a range of standardized methodologies. A comparative analysis is conducted using five distinct approaches, which are outlined in the following sections. Since the equations traditionally rely on steel reinforcement, an equivalent steel reinforcement ratio ($\rho=\frac{E_{GFRP}}{E_s}\frac{A_{GFRP}}{bd}$) is applied to account for the use of GFRP bars as longitudinal reinforcement. In this context, E_{GFRP} and E_s denote the elastic modulus of GFRP and steel bars, respectively, while A_{GFRP} represents the GFRP reinforcement area, b the section width, and d the effective depth.

8.4.1 ACI 440.1R-15/RILEM TC-162

This method calculates the shear strength (V_n) of fiber-reinforced concrete without stirrups by considering the combined contributions from the concrete matrix (V_c) and the fibers (V_f). This method has been previously utilized for concrete beams reinforced with both GFRP bars and synthetic fibers (Dev *et al.* 2020a). As outlined in ACI 440.1R-15 (Institute 2015), the shear capacity of concrete with internal FRP reinforcement is determined using Eq. (8-5) to Eq. (8-11):

$$V_c = \frac{2}{5}\sqrt{f_c'}\,b_w k d \tag{8-5}$$

$$k = \sqrt{2\rho_f n_f + \left(\rho_f n_f\right)^2} - \rho_f n_f \tag{8-6}$$

where b_w denotes the web width (mm), k represents the neutral axis depth ratio, d signifies the distance (mm) from the extreme compression fiber to the tension reinforcement centroid, ρ_f represents the GFRP reinforcement ratio, and n_f denotes the modulus of elasticity ratio (GFRP bars to concrete).

Moreover, the shear resistance contribution from fibers (V_{fc}) is calculated in accordance with Eq. (8-7), following the RILEM TC-162 (TC162-TDF 2003) guideline.

$$V_{fc} = 0.7 k_f k_1 \tau_{fd} b d \quad (8\text{-}7)$$

The factors k_f and k_1 represent the influence of the flanges in a T-section and the size effect, respectively. Their values are determined through the following equations:

$$k_1 = 1 + \sqrt{\frac{200}{d}} \leq 2 \quad (8\text{-}8)$$

$$k_f = 1 + n\left(\frac{h_f}{b_w}\right)\left(\frac{h_f}{d}\right) \leq 1.5 \quad (8\text{-}9)$$

$$n = \frac{b_f - b_w}{h_f} \leq 3 \quad (8\text{-}10)$$

$$\tau_{fd} = 0.12 f_{R,4} \quad (8\text{-}11)$$

In this context, d represents the effective depth of the top slab (mm), b_f denotes the width of the flanges (mm), h_f indicates the height of the flanges (mm), and b_w refers to the width of the web (mm). The parameter τ_{fd} signifies the shear strength attributed to the presence of fibers (MPa), while $f_{R,4}$ represents the residual flexural strength of fiber-reinforced concrete (FRC) at a crack mouth opening displacement (CMOD) of 3.5 mm.

8.4.2 ACI 440.1R-15

The punching shear capacity of two-way slabs can be calculated using Eq. (8-12) in accordance with ACI 440.1R-15 (Institute 2015).

$$V_c = \frac{4}{5}\sqrt{f_c'} b_o k d \quad (8\text{-}12)$$

8.4.3 AASHTO LRFD

AASHTO LRFD (AASHTO 2018, 2020) provides the following equations to calculate the shear strength (V_c) in kN for steel-reinforced box culvert slabs, depending on the slab type and loading conditions.

a) For one-way action of steel-reinforced box culvert slabs under a fill depth of 0.61 m (2.0 ft) or greater:

$$V_c = \left(1.7756 \times 10^{-4}\lambda\sqrt{f_c'} + 0.03173\frac{A_s}{bd_e}\frac{V_u d_e}{M_u}\right) bd_e \quad (8\text{-}13)$$

In this context, λ represents the concrete density modification factor, A_s indicates the area of reinforcement within the specified design width (mm²), b denotes the design width (mm), and d_e refers to the effective depth (mm). Furthermore, V_u corresponds to the shear force resulting from factored loads (kN), while M_u signifies the factored moment at the specified section (kN.mm). When utilizing normal-weight concrete, a value of 1.0 should be assigned to λ.

b) For one-way action of steel-reinforced box culvert slabs under a fill depth less than 0.61 m (2.0 ft):

$$V_c = 8.3 \times 10^{-5}\beta\lambda\sqrt{f_c'}b_v d_v \quad (8\text{-}14)$$

$$\beta = \frac{4.8}{(1 + 750\varepsilon_f)}\frac{51}{(39 + s_{xe})} \quad (8\text{-}15)$$

$$\varepsilon_f = \frac{\frac{|M_u|}{d_v} + 0.5N_u + |V_u|}{E_f A_f} \leq 0.006 \quad (8\text{-}16)$$

$$s_{xe} = s_x\frac{1.38}{a_g + 0.63}; 304.8\ mm. \leq s_{xe} \leq 2032.0\ mm. \quad (8\text{-}17)$$

where b_v and d_v refer to the effective web width and the effective shear depth, respectively. The parameter β indicates the capacity of diagonally cracked concrete to transmit both tension and shear forces. ε_s represents the net longitudinal tensile strain occurring at the centroid of the tension reinforcement within the section. Additionally, s_{xe} signifies the crack spacing parameter influenced by the size of the aggregate (a_g), while s_x denotes the crack spacing parameter.

c) For sections without transverse reinforcement and exhibiting two-way action, the nominal shear resistance, V_c of the concrete in kN, should be calculated according to the following equation (AASHTO 2018):

$$V_c = 8.2933 \times 10^{-4}\, k\, \sqrt{f_c'}\, b_o d_v \tag{8-18}$$

where k represents the ratio of the neutral axis depth to the depth of the flexural reinforcement. The perimeter of the critical section for shear, denoted as b_o (mm), while d_v signifies the effective shear depth.

8.4.4 AS 1597.2-2013

The Australian Standard for steel-reinforced concrete culverts (AS 1597.2-2013 (AS1597.2-2013 2013)) introduces an alternative equation for calculating shear strength in culverts. This equation is based on specific calculations performed at the critical shear section, where the ratio of $\frac{M_u}{\emptyset V_u d}$ is equal to 3.0.

$$V_{uc} = v_b b d S_m \frac{F_D}{F_N}\ (N) \tag{8-19}$$

$$v_b = 4.98(0.018334 + \rho)\sqrt{f_c'} \leq 0.191\sqrt{f_c'}\ (MPa) \tag{8-20}$$

$$S_m = \frac{4}{\left(\frac{M_u}{\emptyset V_u d} + 1\right)} \tag{8-21}$$

$$F_D = 0.8 + \frac{40}{d} \leq 1.25 \tag{8-22}$$

$$F_N = 0.5 - \left(\frac{N_u}{6V_u}\right) + \sqrt{0.25 + \left(\frac{N_u}{6V_u}\right)^2} \tag{8-23}$$

Here,v_b signifies the nominal basic shear strength applicable at locations where $\frac{M_u}{\emptyset V_u d} \geq$ 3.0. Additionally, F_D and F_N denote the factors related to depth and axial thrust, respectively. M_u is the flexural moment (N.mm), N_u is the axial thrust (N), V_u is the shear

force (N), ∅ is the shear capacity reduction factor (0.7), and ρ is the proportion of tensile steel.

8.4.5 AS 5100.5

This approach employs simplified equations from AS 5100.5 (AS5100.5 2017), wherein the ultimate shear capacity (V_u) is divided into a concrete component (V_{uc}) and an additional fiber-reinforced component (V_{uf}). Therefore, the ultimate shear capacity can be determined using the following equations:

$$V_u = V_{uc} + V_{uf} \tag{8-24}$$

$$V_{uc} = k_v \sqrt{f_c'} b d_v \tag{8-25}$$

$$k_v = \frac{200}{1000 + 1.3 d_v} \leq 0.1 \tag{8-26}$$

$$V_{uf} = 0.7 k_\theta f_{1.5}' b d_v \tag{8-27}$$

$$k_\theta = \cot \theta_v \leq 1.28 \tag{8-28}$$

$$f_{1.5}' = 0.4 f_{R,4}' - 0.07 f_{R,2}' \tag{8-29}$$

In this context, k_v signifies the coefficient that quantifies the concrete's contribution to shear capacity, while d_v denotes the effective shear depth. $f_{1.5}'$ refers to the characteristic residual tensile strength of steel fiber-reinforced concrete (SFRC). Additionally, $f_{R,4}'$ and $f_{R,2}'$ represent the mean residual flexural strengths at CMOD of 3.5 mm and 1.5 mm, respectively. θ_v indicates the angle formed between the axis of the concrete compression strut and the longitudinal axis of the member.

8.4.6 Assessing the accuracy of different shear capacity prediction models

Figure 8-20 compares the ratio of experimental shear strength (V_{exp}) to predicted values (V_{pre}) obtained from various methods. Among the investigated methods, AS 1597.2-2013 provided the most accurate estimates for steel-reinforced concrete culverts (STNC), with

a reasonable factor of safety. This method incorporates the effects of axial thrust and relies on steel reinforcement, leading to good predictions for STNC. However, it overestimated the shear capacity of both plain and fiber-reinforced GFRP-RC culverts. This overestimation could be due to the higher elastic modulus of steel bars compared to GFRP bars. GFRP bars exhibit lower strength and stiffness in the transverse direction compared to steel bars. As a result, their contribution to dowel action is assumed to be less than that of an equivalent steel area (Institute 2015). Consequently, the AS 1597.2-2013 method might require modification with a reduction factor to account for the effect of lower axial stiffness of GFRP bars on shear capacity predictions.

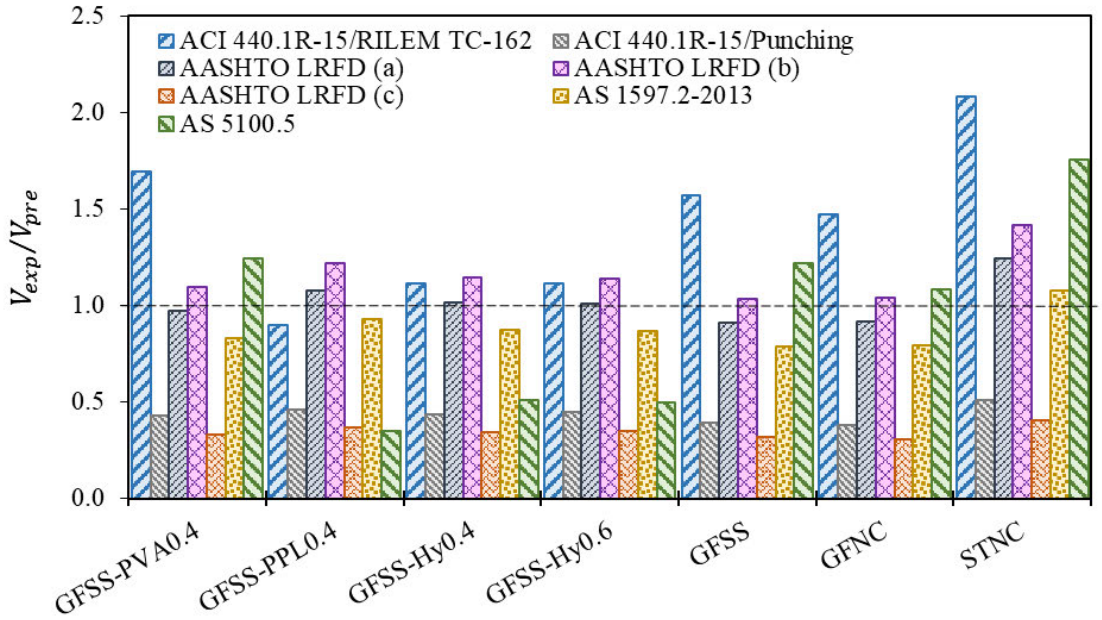


Figure 8-20 Experimental vs. predicted shear capacity of concrete culverts.

In contrast, the AASHTO LRFD (c) and ACI 440.1R-15 methods significantly overestimated the shear strength of these large culverts. Both methods assume of two-way action in concrete slabs. Additionally, ACI 440.1R-15 specifically predicts punching shear in two-way slabs supported by interior columns or subjected to concentrated loads. However, the crown of concrete culverts is primarily supported by the side walls, making it more likely to behave in one-way action rather than two-way. The absence of lateral movement restrictions and the use of inverted u-shaped culverts significantly amplify this effect. This leads to increased deflection in the crown of the culvert, further promoting one-way action behaviour. This is further supported by the results of AASHTO LRFD (a)

and AASHTO LRFD (b), which are based on one-way action and provided more accurate predictions for both plain and fiber-reinforced GFRP-RC culverts. This finding was also supported by a previous study on fiber-reinforced small GFRP-RC culverts, which reported that AASHTO equations based on one-way crown action provided reliable predictions of shear capacity (Mashayekhi *et al.* 2024e).

The ACI 440.1R-15/RILEM TC-162 method underestimated the shear capacity of plain concrete culverts but was more accurate for GFRP-RC culverts containing macro fibers, especially those with macro/micro hybrid fibers. This is likely because the RILEM TC-162 method is primarily based on steel fibers, which can be extended to macro synthetic fibers with some reliability. Conversely, the AS 5100.5 method provided reliable predictions for both plain and PVA fiber-reinforced GFRP-RC culverts but overestimated the capacity of culverts containing macro fibers, whether mono or hybrid. This overestimation might be due to the assumption that the proportion of shear strength contributed by fibers is based on steel fibers, requiring a reduction factor for synthetic fibers in this method.

8.5 Summary and conclusion

This study investigated the cyclic performance of GFRP-reinforced seawater sea-sand (SWSS) concrete culverts incorporating mono/hybrid long polypropylene (PPL) and polyvinyl alcohol (PVA) fibers. It also examined the effect of reinforcement type (GFRP vs. steel) and analysed the influence of concrete type (SWSS and conventional) on the structural response of the culvert. The research aimed to address key deficiencies in GFRP-RC culverts (wide cracks, large deflections, and poor ductility) by incorporating mono/hybrid fibers and evaluating their performance under cyclic loading. Based on the experimental observations, the following conclusions can be drawn:

- The incorporation of mono PPL fibers enhanced the shear strength of the culvert by approximately 18%, attributed to the length and mechanical bonding of fibers with the concrete matrix. This resulted in superior performance under larger crown deflections by bridging macro cracks, improving the damage mechanism of the culvert, and contributing to a higher damping ratio and greater energy dissipation during cyclic loading.

- The inclusion of mono PVA fibers led to a 14% enhancement in the shear capacity of the culvert. This improvement could be attributed to the capability of PVA fibers to strengthen the interlocking and reinforce the SWSS concrete matrix, primarily through their strong chemical bonding. This enhanced bonding also significantly improved the damage behaviour of the culvert, resulting in a 25% reduction in the damage index.

- The combination of PPL and PVA fibers (hybrid PPL/PVA) resulted in a synergistic improvement in the ultimate shear capacity and damage mechanism of the culvert. The chemical bonding provided by PVA fibers enhanced the bonding of PPL fibers by reinforcing the surrounding concrete, which facilitated more effective crack bridging and shear capacity. This was evident in cyclic parameters like energy dissipation and damping ratio.

- Incorporating SWSS concrete in GFRP-RC culverts resulted in significant performance improvements, including an 8% increase in ultimate shear capacity and a substantial 42% increase in peak deflection compared to conventional concrete. The enhanced cohesion and interlocking properties of SWSS concrete increased initial crack resistance, resulting in higher shear and tensile strengths. These improvements also facilitated better energy dissipation and damage control, especially under large crown deflections.

- The Steel-RC culvert demonstrated a 29% increase in ultimate shear capacity compared to the GFRP-RC culvert, while exhibiting a 17% reduction in peak crown deflection. This behaviour could be attributed to the modulus of elasticity of steel being approximately 3.3 times that of GFRP, which significantly enhanced the bending stiffness and led to reduced crown deflection.

- AASHTO shear strength equations, originally developed for one-way action in steel-reinforced concrete box culverts, reliably predicted the shear capacity of inverted U-shape GFRP-RC culverts in this study. The lack of lateral restraint in these culverts suggests a propensity for one-way behaviour in the crown slabs.

Acknowledgements

This research was made possible by the generous support of the University of South Australia, who provided essential laboratory facilities and financial support. We are also

thankful to Adelaide Brighton Cement Ltd and Independent Cement and Lime Pty Ltd for their kind donations of OPC and GGBS, respectively. We are grateful to Mr. Jason Quinn and Dr. Murray Townsend from the Department for Environment and Water (DEW) for their invaluable support in providing the sea-sand used in this research. We extend our gratitude to Inconmat Australia for supplying the GFRP reinforcement used in this project. Additionally, the valuable instrumentation and expertise of Microscopy Australia at the Future Industries Institute (FII), University of South Australia are acknowledged.

Chapter 8 References

AASHTO 2018, AASHTO LRFD Bridge Design Guide Specifications for GFRP–Reinforced Concrete, American Association of State Highway & Transportation Officials (AASHTO),

AASHTO 2020, AASHTO LRFD Bridge Design Specifications, 9th Edition, American Association of State Highway and Transportation Officials (AASHTO),

Abolmaali, A & Garg, A 2008a, 'Shear behavior and mode of failure for ASTM C1433 precast box culverts', Journal of Bridge Engineering, vol. 13, no. 4, pp. 331-38.

Abolmaali, A & Garg, AK 2008b, 'Effect of wheel live load on shear behavior of precast reinforced concrete box culverts', Journal of Bridge Engineering, vol. 13, no. 1, pp. 93-99.

ACI Committee 440 2012, Guide test methods for fiber-reinforced polymer (FRP) composites for reinforcing or strengthening concrete and masonry structures.

Ahmed, A, Guo, S, Zhang, Z, Shi, C & Zhu, D 2020, 'A review on durability of fiber reinforced polymer (FRP) bars reinforced seawater sea sand concrete', Construction and Building Materials, vol. 256, p. 119484.

Al-Salloum, YA, El-Gamal, S, Almusallam, TH, Alsayed, SH & Aqel, M 2013, 'Effect of harsh environmental conditions on the tensile properties of GFRP bars', Composites Part B: Engineering, vol. 45, no. 1, pp. 835-44.

Al-Zahrani, MM, Rahman, MK, Fasil, M, Al-Abduljabbar, S, Nanni, A, Al-Osta, MA, Najamuddin, SK & Al-Gahtani, HJ 2023, 'Punching shear capacity of GFRP bar-reinforced concrete slabs-on-ground', Engineering Structures, vol. 289, p. 116285.

AlHamaydeh, M & Anwar Orabi, M 2021, 'Punching shear behavior of synthetic fiber–reinforced self-consolidating concrete flat slabs with GFRP bars', Journal of Composites for Construction, vol. 25, no. 4, p. 04021029.

Alkhrdaji, T & Nanni, A 2001, 'Design, construction, and field-testing of an RC Box Culvert Bridge reinforced with GFRP bars', Non-Metallic Reinforcement for Concrete Structures-FRPRCS, vol. 5.

Altoubat, S, Yazdanbakhsh, A & Rieder, K-A 2009, 'Shear behavior of macro-synthetic fiber-reinforced concrete beams without stirrups', ACI Materials Journal, vol. 106, no. 4, p. 381.

Amin, N, Bijan, S & Kirk, V 2013, 'Effect of polyvinyl alcohol (PVA) fibre on dynamic and material properties of fibre reinforced concrete', Construction and Building Materials, vol. 49, pp. 374-83.

AS1597.1-2010 2010, Precast reinforced concrete box culverts, Part 1: Small culverts (not exceeding 1200 mm span and 1200 mm height), Standards Australia,

AS1597.2-2013 2013, Precast reinforced concrete box culverts, Part 2: Large culverts (exceeding 1200 mm span or 1200 mm height and up to and including 4200 mm span and 4200 mm height), Standards Australia,

AS5100.5 2017, Bridge design, Part 5: Concrete, Standards Australia,

Bai, J 2009, 'Durability of sustainable concrete materials', Sustainability of construction materials, Elsevier, pp. 239-53.

Bertola, F, Canonico, F & Nanni, A 2017, SEACON Project: sustainable concrete using seawater, salt-contaminated aggregates, and non-corrosive reinforcement, XIV DBMC-14th International Conference on Durability of Building Materials and Components.

Bo, X, Houssam, AT & John, G 2010, 'Impact resistance of poly(vinyl alcohol) fiber reinforced high-performance organic aggregate cementitious material', Cement and concrete Research, vol. 40, no. 2, pp. 347-51.

Broomfield, JP 2023, Corrosion of steel in concrete: understanding, investigation and repair, Crc Press,

Changqing, W, Huixia, W & Chunxiang, L 2022, 'Hysteresis and damping properties of steel and polypropylene fiber reinforced recycled aggregate concrete under uniaxial low-cycle loadings', Construction and Building Materials, vol. 319, p. 126191.

Chellapandian, M, Mani, A & Prakash, SS 2020, 'Effect of macro-synthetic structural fibers on the flexural behavior of concrete beams reinforced with different ratios of GFRP bars', Composite Structures, vol. 254, p. 112790.

Committe, SA 2014, AS 1012.9 Methods of Testing Concrete-Method 9: Determination of the Compressive Strength of Concrete Specimens, Australian Standards Sydney.

D'Antino, T, Pisani, M & Poggi, C 2018, 'Effect of the environment on the performance of GFRP reinforcing bars', Composites Part B: Engineering, vol. 141, pp. 123-36.

Dev, A, Chellapandian, M & Prakash, SS 2020a, 'Effect of macrosynthetic and hybrid fibers on shear behavior of concrete beams reinforced with GFRP bars', Journal of Bridge Engineering, vol. 25, no. 7, p. 04020031.

Dev, A, Chellapandian, M, Prakash, SS & Kawasaki, Y 2020b, 'Failure-mode analysis of macro-synthetic and hybrid fibre-reinforced concrete beams with GFRP bars using acoustic emission technique', Construction and Building Materials, vol. 249, p. 118737.

Dong, S, Li, C & Xian, G 2021, 'Environmental impacts of glass-and carbon-fiber-reinforced polymer bar-reinforced seawater and sea sand concrete beams used in marine environments: An LCA case study', Polymers, vol. 13, no. 1, p. 154.

Etxeberria, M, Gonzalez-Corominas, A & Pardo, P 2016, 'Influence of seawater and blast furnace cement employment on recycled aggregate concretes' properties', Construction and Building Materials, vol. 115, pp. 496-505.

Fattah, KP, Al-Tamimi, AK, Hamweyah, W & Iqbal, F 2017, 'Evaluation of sustainable concrete produced with desalinated reject brine', International Journal of Sustainable Built Environment, vol. 6, no. 1, pp. 183-90.

Garg, AK, Abolmaali, A & Fernandez, R 2007, 'Experimental investigation of shear capacity of precast reinforced concrete box culverts', Journal of Bridge Engineering, vol. 12, no. 4, pp. 511-17.

Garg, AK & Abolmaali, A 2009, 'Finite-element modeling and analysis of reinforced concrete box culverts', Journal of Transportation Engineering, vol. 135, no. 3, pp. 121-28.

Ge, L, Feng, Z, Sayed, U & Li, H 2023, 'Research on the performance of seawater sea-sand concrete: A review', Construction and Building Materials, vol. 409, p. 133921.

Ghahremannejad, M, Abolmaali, A & Mahdavi, M 2019, 'Shear strength of top slab of reinforced concrete box culverts', ACI Structural Journal, vol. 116, no. 6, pp. 63-74.

Gooranorimi, O, Myers, J & Nanni, A 2017, GFRP reinforcements in box culvert bridge: A case study after two decades of service, Symposium on Concrete Pipe and Box Culverts.

Guo, M, Hu, B, Xing, F, Zhou, X, Sun, M, Sui, L & Zhou, Y 2020, 'Characterization of the mechanical properties of eco-friendly concrete made with untreated sea sand and seawater based on statistical analysis', Construction and Building Materials, vol. 234, p. 117339.

Hassanli, R, Youssf, O & Mills, JE 2017, 'Experimental investigations of reinforced rubberized concrete structural members', Journal of Building Engineering, vol. 10, pp. 149-65.

Hassanli, R, Youssf, O, Manalo, A, Najafgholipour, MA, Elchalakani, M, del Rey Castillo, E & Lutze, D 2022, 'An experimental study of the behavior of GFRP-reinforced precast concrete culverts', Journal of Composites for Construction, vol. 26, no. 5, p. 04022043.

Hassanli, R, Manalo, A, Vafaei, D, Yekrangnia, M, Elchalakani, M & Noël, M 2023, 'Cyclic behavior of GFRP-reinforced concrete one-way slabs with synthetic fibers', Journal of Building Engineering, vol. 65, p. 105741.

Hassanli, R, Youssf, O, El-Naqeeb, MH, Yekrangnia, M, Elchalakani, M, Ghanbari-Ghazijahani, T & Bazli, M 2024, 'Investigation of punching shear performance in concrete slabs reinforced with GFRP and synthetic fibers: An experimental study', Engineering Structures, vol. 311, p. 118215.

Hobbs, D 1982, 'Influence of pulverized–fuel ash and granulated blastfurnace slag upon expansion caused by the alkali–silica reaction', Magazine of concrete Research, vol. 34, no. 119, pp. 83-94.

Hu, X, Xiao, J, Zhang, K & Zhang, Q 2022, 'The state-of-the-art study on durability of FRP reinforced concrete with seawater and sea sand', Journal of Building Engineering, vol. 51, p. 104294.

Hu, X, Xiao, J, Zhang, K & Zhang, Q 2023, 'Evaluation of cracking and deflection of GFRP bar reinforced recycled concrete beams with seawater and sea sand', Journal of Building Engineering, vol. 80, p. 108092.

Institute, AC 2015, Guide for the Design and Construction of Structural Concrete Reinforced with FRP Bars (ACI-440.1R-15), American Concrete Institute,

Issa, MS, Metwally, IM & Elzeiny, SM 2011, 'Influence of fibers on flexural behavior and ductility of concrete beams reinforced with GFRP rebars', Engineering Structures, vol. 33, no. 5, pp. 1754-63.

Javadi, M, Hassanli, R, Rahman, MM & Karim, MR 2021, 'Experimental study on cyclic behavior of post-tensioned segmental retaining walls (PSRWs)', Engineering Structures, vol. 229, p. 111619.

Kamal, A & Boulfiza, M 2011, 'Durability of GFRP rebars in simulated concrete solutions under accelerated aging conditions', Journal of Composites for Construction, vol. 15, no. 4, pp. 473-81.

Karim, R & Shafei, B 2021, 'Performance of fiber-reinforced concrete link slabs with embedded steel and GFRP rebars', Engineering Structures, vol. 229, p. 111590.

Khatibmasjedi, M & Nanni, A 2017, Durability of GFRP reinforcement in SEACON, The Fifth International Conference on Durability of Fiber Reinforced Polymer (FRP) Composites for Construction and Rehabilitation of Structures (CDCC 2017).

Kim, H-Y, Park, Y-H, You, Y-J & Moon, C-K 2008, 'Short-term durability test for GFRP rods under various environmental conditions', Composite Structures, vol. 83, no. 1, pp. 37-47.

Kim, J-K & Park, Y-D 1996, Prediction of shear strength of reinforced concrete beams without web reinforcement.

Kwon, Y-j 2005, 'A study on the alkali-aggregate reaction in high-strength concrete with particular respect to the ground granulated blast-furnace slag effect', Cement and concrete Research, vol. 35, no. 7, pp. 1305-13.

Li, P, Li, W, Yu, T, Qu, F & Tam, VW 2020, 'Investigation on early-age hydration, mechanical properties and microstructure of seawater sea sand cement mortar', Construction and Building Materials, vol. 249, p. 118776.

Lingzhu, Z, Yu, Z, Bo, D, Jiamei, L & Susan, ET 2023, 'Shear behaviour of SWSS-SCC beams reinforced with GFRP bars and Stirrups: Experimental and analytical investigations', Structures, vol. 56, p. 104946.

Lothenbach, B, Scrivener, K & Hooton, R 2011, 'Supplementary cementitious materials', Cement and concrete Research, vol. 41, no. 12, pp. 1244-56.

Marshall, JD, Anderson, JB, Meadows, RL & Jensen, TJ 2014, 'Full-scale testing of three-sided precast concrete arch sections', Journal of Bridge Engineering, vol. 19, no. 12, p. 04014051.

Mashayekhi, A, Hassanli, R, Zhuge, Y, Ma, X & Chow, CW 2024a, 'Synergistic effects of fiber hybridization on the mechanical performance of seawater sea-sand concrete', Construction and Building Materials, vol. 416, p. 135087.

Mashayekhi, A, Hassanli, R, Zhuge, Y, Ma, X, Chow, CW, Bazli, M & Manalo, A 2024b, 'Structural behaviour of small GFRP-reinforced seawater sea-sand fiber reinforced concrete culverts', Structures.

Mashayekhi, A, Hassanli, R, Zhuge, Y, Ma, X, Chow, CW, Bazli, M & Manalo, A 2024c, 'Cyclic flexural performance of seawater sea-sand concrete reinforced with hybrid fibers', Construction and Building Materials, vol. 449, p. 138480.

Mashayekhi, A, Hassanli, R, Zhuge, Y, Ma, X, Chow, CW, Bazli, M & Manalo, A 2024d, 'Synergistic effects of fiber hybridization on the fracture toughness of seawater sea-sand concrete', Construction and Building Materials, vol. 444, p. 137845.

Micelli, F & Nanni, A 2004, 'Durability of FRP rods for concrete structures', Construction and Building Materials, vol. 18, no. 7, pp. 491-503.

Mostafazadeh, M, Abolmaali, A & Ghahremannejad, M 2019, 'Shear Strength of Synthetic Fiber-Reinforced Concrete Box Culverts', Journal of Bridge Engineering, vol. 24, no. 6, p. 04019039.

Pakravan, HR & Ozbakkaloglu, T 2019, 'Synthetic fibers for cementitious composites: A critical and in-depth review of recent advances', Construction and Building Materials, vol. 207, pp. 491-518.

Patil, GM, Chellapandian, M & Prakash, SS 2020, 'Effectiveness of Hybrid Fibers on Flexural Behavior of Concrete Beams Reinforced with Glass Fiber-Reinforced Polymer Bars', ACI Structural Journal, vol. 117, no. 5.

Raman, RS, Guo, F, Al-Saadi, S, Zhao, X-L & Jones, R 2018, 'Understanding fibre-matrix degradation of FRP composites for advanced civil engineering applications: an overview', Corrosion and Materials Degradation, vol. 1, no. 1, pp. 27-41.

Razan, H, Muhammad, KS & Emilio, G-T 2023, 'Flexural and deflection behaviour of synthetic fibre reinforced concrete beams reinforced with glass fibre reinforced polymers bars under sustained service load', Structures, vol. 54, pp. 946-55.

Saeed, FH, Hejazi, F & Rashid, RSM 2024, 'Strengthening of reinforced concrete slabs using carbon fiber reinforced polymers rods and concrete jacket with a mechanical anchorage system', Construction and Building Materials, vol. 440, p. 137464.

Sena-Cruz, J, Pereira, E, Freitas, N, Pereira, E & Soares, SRR 2018, 'Bond behaviour between GFRP rods and concrete produced with seawater: an experimental research'.

Shi, F, Pham, TM, Tuladhar, R, Deng, Z, Yin, S & Hao, H 2023, 'Comparative performance analysis of ground slabs and beams reinforced with macro polypropylene fibre, steel fibre, and steel mesh', Structures, vol. 56, p. 104920.

Shi, Z, Shui, Z, Li, Q & Geng, H 2015, 'Combined effect of metakaolin and sea water on performance and microstructures of concrete', Construction and Building Materials, vol. 74, pp. 57-64.

TC162-TDF, R 2003, 'Test and design methods for steel fibre reinforced concrete', Materials and structures, vol. 36, pp. 560-67.

Tjaronge, MW & Irfan, UR 2015, 'Porosity, pore size and compressive strength of self compacting concrete using sea water', Procedia Engineering, vol. 125, pp. 832-37.

Vafaei, D, Hassanli, R, Ma, X, Duan, J & Zhuge, Y 2021, 'Sorptivity and mechanical properties of fiber-reinforced concrete made with seawater and dredged sea-sand', Construction and Building Materials, vol. 270, p. 121436.

Vafaei, D, Ma, X, Hassanli, R, Duan, J & Zhuge, Y 2022a, 'Microstructural behaviour and shrinkage properties of high-strength fiber-reinforced seawater sea-sand concrete', Construction and Building Materials, vol. 320, p. 126222.

Vafaei, D, Ma, X, Hassanli, R, Duan, J & Zhuge, Y 2022b, 'Microstructural and mechanical properties of fiber-reinforced seawater sea-sand concrete under elevated temperatures', Journal of Building Engineering, vol. 50, p. 104140.

Vafaei, D, Ma, X, Hassanli, R, Duan, J & Zhuge, Y 2023, 'Experimental study on cyclic flexural behaviour of GFRP-reinforced seawater sea-sand concrete slabs with synthetic fibres', Ocean Engineering, vol. 273, p. 114014.

Von Handorf, J 2004, 'Clear-span culverts: Economical designs', Better Roads, vol. 74, no. 2.

Wang, J, Liu, E & Li, L 2018, 'Multiscale investigations on hydration mechanisms in seawater OPC paste', Construction and Building Materials, vol. 191, pp. 891-903.

Wang, Q-z, Li, L-j, Zhao, Y-x, Song, Y & Zhang, C-l 2024, Feasibility assessment and application of sea sand in concrete production: A review, Structures.

Wang, Y, Shui, Z, Gao, X, Huang, Y, Yu, R & Song, Q 2020, 'Chloride binding capacity and phase modification of alumina compound blended cement paste under chloride attack', Cement and Concrete Composites, vol. 108, p. 103537.

Wang, Z, Zhao, X-L, Xian, G, Wu, G, Raman, RS, Al-Saadi, S & Haque, A 2017, 'Long-term durability of basalt-and glass-fibre reinforced polymer (BFRP/GFRP) bars in seawater and sea sand concrete environment', Construction and Building Materials, vol. 139, pp. 467-89.

Wang, Z, Xie, J, Mai, Z, Liu, P, Lu, Z & Li, L 2023, 'Durability of GFRP bar-reinforced seawater–sea sand concrete beams: Coupled effects of sustained loading and exposure to a chloride environment', Engineering Structures, vol. 283, p. 115814.

Wu, W, He, X, Yang, W, Wei, B & Alam, MS 2023, 'Durability and microstructure degradation mechanism of FRP-seawater seasand concrete structures: A review', Construction and Building Materials, vol. 391, p. 131825.

Yan, F, Lin, Z, Zhang, D, Gao, Z & Li, M 2017, 'Experimental study on bond durability of glass fiber reinforced polymer bars in concrete exposed to harsh environmental agents: Freeze-thaw cycles and alkaline-saline solution', Composites Part B: Engineering, vol. 116, pp. 406-21.

Yang, J-M, Min, K-H, Shin, H-O & Yoon, Y-S 2012, 'Effect of steel and synthetic fibers on flexural behavior of high-strength concrete beams reinforced with FRP bars', Composites Part B: Engineering, vol. 43, no. 3, pp. 1077-86.

Yang, S, Zang, C, Xu, J & Fan, G 2020, 'Determination of Fracture Parameters of Seawater Sea Sand Concrete Based on Maximum Fracture Load', Journal of Materials in Civil Engineering, vol. 32, no. 1, p. 04019315.

Yazdani, N, Hossain, S, Hossain, J & Shumac III, W 2013, 'Forensic Investigation of Deteriorated Concrete in Plantation East Culverts, City of Benbrook, Texas', Journal of Performance of Constructed Facilities, vol. 27, no. 4, pp. 468-76.

Yee, RA 2004, 'Shear behaviour of concrete box culverts', Dept. of Civil Engineering, Univ. of Toronto, Toronto.

Yifan, Z, Xiang, H, Caijun, S, Zuhua, Z & Deju, Z 2021, 'A review on seawater sea-sand concrete: Mixture proportion, hydration, microstructure and properties', Construction and Building Materials, vol. 295, p. 123602.

Younis, A, Ebead, U, Suraneni, P & Nanni, A 2018, 'Fresh and hardened properties of seawater-mixed concrete', Construction and Building Materials, vol. 190, pp. 276-86.

Yuntao, H, Shiping, Y & Zhangtao, P 2020, 'Crack development and calculation method for the flexural cracks in BFRP reinforced seawater sea-sand concrete (SWSSC) beams', Construction and Building Materials, vol. 255, p. 119328.

Zeng, J-J, Liao, J, Zhuge, Y, Guo, Y-C, Zhou, J-K, Huang, Z-H & Zhang, L 2022, 'Bond behavior between GFRP bars and seawater sea-sand fiber-reinforced ultra-high strength concrete', Engineering Structures, vol. 254, p. 113787.

Zhang, ZH, Sang, ZQ, Zhang, LY, Ma, ZX & Zhang, Y 2013, Experimental research on durability of concrete made by seawater and sea-sand, Advanced Materials Research.

Zhihao, W, Jianhe, X, Jianglin, L, Peng, L, Cuiqing, S & Zhongyu, L 2022, 'Flexural behaviour of seawater–sea sand concrete beams reinforced with GFRP bars: Effects of the reinforcement ratio, stirrup ratio, shear span ratio and prestress level', Journal of Building Engineering, vol. 54, p. 104566.

Zhu, M, Chen, B, Wu, M & Han, J 2023, 'Preparation and mechanical characterization of cost-effective low-carbon engineered cementitious composites with seawater and sea-sand', Cement and Concrete Composites, vol. 136, p. 104883.

Zongao, L, Fuming, D, Hui, Q, Peifan, Q & Yifei, S 2024, 'Shear performance of seawater sea-sand concrete beams reinforced with shape memory alloy longitudinal and stirrup bars', Construction and Building Materials, vol. 421, p. 135685.

9 Conclusions and future research recommendations

9.1 Conclusions

This study comprehensively investigated the impact of fiber hybridization and its synergy on the mechanical properties of seawater sea-sand concrete (SWSSC). Additionally, it evaluated the performance of glass fiber reinforced polymer (GFRP)-reinforced concrete culverts incorporating hybrid fiber-reinforced SWSSC (FR-SWSSC). Discrete fibers are effective in controlling cracks and enhancing structural integrity, particularly in challenging environments. However, mono-fibers have inherent limitations due to their physical and chemical properties. Hybrid fibers address these limitations by combining the complementary characteristics of micro- and macro-fibers, resulting in improved overall performance. Additionally, fiber-reinforced polymer (FRP) reinforcement mitigates the primary concern of using SWSSC in concrete structures—the risk of steel reinforcement corrosion—making it particularly suitable for applications in harsh conditions such as culverts. A detailed literature review was conducted, examining the performance of concrete culverts, FR-SWSSC, and the application of FRP bars in SWSSC structural elements.

Incorporating seawater (SW) and sea-sand (SS) reduces the environmental impact of concrete by conserving freshwater and natural river sand resources. This approach further lowers transportation costs in remote areas where SW and SS are readily available, making it a cost-effective and sustainable solution. Previous studies have demonstrated the beneficial impact of fiber incorporation on the mechanical performance of SWSSC. However, the synergistic effects of hybrid fibers and their influence on mechanical behaviour of SWSSC under varying loading conditions have not been thoroughly investigated. While the use of FRP-reinforced SWSSC structural elements in has been explored to some extent, their application in concrete culverts—critical components of transport and road infrastructure in diverse environmental conditions—remains largely unexamined. Utilizing GFRP-reinforced SWSSC in culverts offers significant advantages, including better corrosion resistance, enhanced durability, and reduced maintenance needs, particularly in aggressive environments such as coastal and marine areas. This study contributed to addressing these gaps by advancing knowledge on hybrid

fibers and GFRP reinforcement in SWSSC for sustainable and durable infrastructure solutions.

The research was divided into two phases: Phase I focused on the fresh and mechanical properties of hybrid FR-SWSSC to understand the synergistic interaction of fibers in SWSSC. A total fiber volume fraction of 0.25% was considered to assess slump, air content, compressive strength, stress-strain behaviour, tensile strength, elastic modulus, fracture toughness, cyclic flexural performance, and direct shear behaviour. Both micro-fibers—including polypropylene (PPS), polyvinyl alcohol (PVA), and basalt (BF)—and macro-fibers, such as long polypropylene (PPL) and twisted polypropylene (TPPL), were used to examine the combined effects of fiber size and type on the mechanical properties of SWSSC. Hybrid fiber reinforcements were applied in two configurations: micro-fibers only, and a combination of micro- and macro-fibers. Ground granulated blast furnace slag (GGBS) was also used to reduce the environmental impact of concrete by minimizing CO_2 emissions. The results of Phase I were presented as four separate studies (Studies 1 to 4). Phase II evaluated the structural performance of GFRP-reinforced culverts with hybrid fibers, examining both small- and large-scale culverts to determine their effectiveness across diverse applications. Based on the results of Phase I, the most effective hybrid systems were selected for evaluating FR-SWSSC culverts reinforced with GFRP bars. The results of Phase II were presented as two separate studies (Studies 5 and 6). The following conclusions are drawn from each of these studies.

9.2 Phase I: Synergistic effects of fiber hybridization on material characteristics

9.2.1 Study 1: Mechanical properties

Limited research has addressed the role of hybridizing fibers, especially micro-fibers, in SWSS concrete. This study addressed this gap by exploring the potential of hybrid fibers to enhance the compressive and tensile strength, and ductility of SWSSC. Various combinations—mono-fibers, hybrid micro-fibers, and hybrid micro- and macro-fibers—were tested to understand their synergistic effects on the fresh and hardened characteristics of hybrid FR-SWSSC. The primary findings are presented below:

- The inclusion of fibers generally led to a reduction in slump, apart from macro-fibers. The impact of micro-fibers on slump was more pronounced, primarily due to their uniform distribution, greater surface area, and enhanced water absorption properties.

- As the W/B ratio increased, the difference in slump between plain SWSS and FWNS mixtures became less significant. This was because at lower W/B ratios, SWSS exhibited higher cohesion, restricting workability. However, with increased water content, the cohesion reduced, leading to a more comparable slump behaviour between the two mixtures.
- PVA fiber concrete exhibited a sharp slump increase with higher water content, which can be attributed not only to its hydrophilic nature but also to its smooth surface texture and superior dispersion efficiency. Unlike basalt fibers (BF), which are also hydrophilic, PVA fibers distribute more evenly, reducing internal friction and enhancing workability.
- The incorporation of PPS and BF fibers increased the air content of the mixture due to their hydrophobic characteristics, which facilitated the formation of air pockets. In contrast, the combination of BF and PVA fibers in a 66:33 ratio reduced the air content by 33% compared to using BF alone. This reduction can be attributed to the hydrophilic nature of PVA fibers, which effectively prevents air pocket formation and facilitates the release of entrapped air.

- The corrosion of BF in SWSS concrete led to a reduction in compressive strength (f_{cm}) at both 28 and 365 days. In contrast, the incorporation of PVA fibers enhanced the compressive strength, which can be attributed to their high tensile strength, elevated elastic modulus, and superior chemical bonding, collectively improving the fiber-matrix interlocking.

- The observed weakness of BF in SWSS concrete, primarily due to corrosion, was effectively mitigated by hybridizing with PVA fibers, resulting in a significant improvement in f_{cm}. Notably, the optimal hybrid combination of 66:33 PVA to BF yielded a 13% increase in compressive strength compared to plain SWSS concrete.

- The incorporation of PPL in combination with PVA or BF fibers significantly enhanced the compressive strength of SWSS concrete by 13% to 16% compared to plain concrete. This improvement was attributed to the superior bonding and effective stress transfer mechanisms between the fibers and the matrix.

- After 365 days, the incorporation of PVA fibers led to an increase in compressive energy absorption by 17% for $CTI_{0.8}$ and by 35% for $CTI_{0.2}$. In contrast, the use of

BF fibers resulted in reduced ductility and decreased energy absorption, attributed to corrosion, which subsequently increased the brittleness.

- The combination of 0.66PVA and 0.33BF fibers led to a notable 44% improvement in $CTI_{0.2}$. Although the use of PPL fibers independently showed minimal impact on energy absorption, hybridizing PPL with PVA fibers in a 66:33 ratio resulted in a 59% increase in $CTI_{0.2}$ compared to using only PPL fibers.

- The addition of fibers significantly influenced the residual strength (f_{res}) of SWSS concrete, with notable variations depending on the fiber type. Incorporating PPS and PVA fibers led to significant improvements, increasing residual strength by 98% and 80%, respectively. On the other hand, BF fibers exhibited a 36% decrease in residual strength, attributed to issues related to corrosion.

- The incorporation of a 66:33 hybrid PVA/BF fibers led to a remarkable enhancement in f_{res}, exhibiting an increase of 181% relative to the mono BF fiber mixture. Although the influence of PPL fibers on f_{res} was less significant compared to that of PVA fibers, primarily due to the limited bonding strength of PPL fibers under elevated compression strain, substituting 66% of PPL with PVA resulted in notable gains. The residual strength improved by 65% and 19% compared to mono PPL and mono PVA, respectively.

- The impact of micro-fiber hybridization has highlighted the importance of the fibers with high elastic modulus, tensile strength, and bonding properties on the compressive elastic modulus (E_c). It was observed that incorporating micro-fibers resulted in a decrease in E_c, primarily due to the rise in air void content and the subsequent reduction in material stiffness.

- The influence of hybrid micro-fibers on the splitting tensile strength (f_{st}) of SWSS concrete was found to be minimal when compared to mono-fibers. A notable synergy was achieved with the hybridization of PPS and either PVA or BF fibers (in a 66:33 ratio), as the enhanced elongation properties of PPS and the strong bonding ability of PVA or BF fibers contributed to improved inter-fiber bonding and crack-bridging performance.

- The CMP analysis indicated that all mono-fiber concretes exhibited a CMP greater than 1.0, except for BF, which had a CMP of 0.87. Among all mono-fiber concretes,

PVA fiber demonstrated the highest CMP at 1.20. Hybrid PVA/BF in a 66:33 ratio achieved the highest CMP value of 1.44 among all micro-fiber combinations.

- The 66:33 hybridization of PPL/PVA exhibited the highest CMP among all FR-SWSS concretes. TPPL fibers showed a notable synergy with 66% PVA, attributed to improved distribution and flexibility. This increased PVA dosage enhanced TPPL bonding, improving both strength and ductility.

9.2.2 Study 2: Fracture toughness

To complement the mechanical performance investigation in Study 1, Study 2 aimed to investigate the influence of hybrid fibers on the fracture behaviour of FR-SWSSC, focusing on crack resistance, ductility, and overall fracture performance. There is a knowledge gap in understanding the fracture properties of FR-SWSSC, specifically with the effects of hybrid fibers and their synergy. The main results are summarized as follows:

- The incorporation of macro-fibers, specifically PPL and TPPL, significantly enhanced the post-peak behaviour of SWSSC. Compared to plain SWSSC, the addition of PPL and TPPL fibers increased fracture energy by 144% and 93%, respectively, at a CMOD of 3.5 mm. This improvement was primarily due to the length of the macro-fibers and their effective capability to bridge macro-cracks during the post-peak phase, facilitated by their superior mechanical bonding strength.

- The incorporation of micro-fibers into SWSSC had only a marginal effect on post-crack performance, whereas hybridization significantly improved fracture behaviour. The combination of PPS with either BF or PVA fibers increased fracture energy at CMOD 3.5 mm by 176% and 290%, respectively, compared to mono PPS. This improvement was attributed to the weak bond strength of PPS fibers, which BF and PVA fibers effectively reinforced, creating a synergistic effect that reduced micro-cracking and enhanced overall fracture performance.

- The fracture energy at a CMOD of 3.5 mm was significantly enhanced by hybridizing PPL fibers with PPS, PVA, or BF, resulting in improvements of 244%, 66%, and 68%, respectively, compared to mono micro-fibers. Similarly, hybridizing TPPL fibers with PVA or BF increased fracture energy by 80% and 93%. This was due to the effective macro-crack bridging by PPL and TPPL fibers, which activated the

micro-fibers for synergistic performance. Additionally, the strong chemical bonding of PVA and BF strengthened the concrete matrix and macro-fiber bonding.

- The inclusion of fibers substantially extended the fracture process zone length (Δa_c) of SWSSC. Specifically, PVA, BF, PPL, and TPPL fibers increased Δa_c by approximately 30, 19, 39, and 21 times, respectively. This enhancement was also reflected in cohesion toughness (K_{IC}^{C}), with PVA and PPL fibers increasing K_{IC}^{C} by roughly 54 and 93 times, respectively. This improvement was due to effective micro-crack bridging, which facilitated better tensile stress distribution and engaged a larger concrete section compared to plain SWSSC.

- The initial fracture toughness (K_{IC}^{ini}) of SWSSC was significantly enhanced by fiber hybridization. The 0.66PVA/0.33BF hybrid achieved the greatest improvement among micro-fiber combinations, exceeding the performance of mono BF and PVA by 22% and 17%, respectively. This improvement was attributed to the synergistic effect of the PVA/BF, resulting in better matrix bonding and more effective reinforcement.

- The 0.66PPL/0.33PVA hybrid exhibited a 25% and 32% increase in initial fracture toughness (K_{IC}^{ini}) compared to mono PVA and PPL, respectively. This synergy improved bond strength and reinforcement within the concrete matrix, enhancing the resistance of PPL fibers to crack initiation.

9.2.3 Study 3: Cyclic flexural performance

Following the investigation of mechanical and fracture properties, understanding the cyclic flexural behaviour of FR-SWSSC is crucial to evaluate its suitability for structures exposed to repeated loading, such as culverts and coastal infrastructure. There was a lack of information in the literature regarding the flexural behaviour of FR-SWSSC under cyclic loading, especially considering the impact of hybrid fibers. Therefore, this study aimed to address this gap by evaluating the flexural performance of FR-SWSSC with hybrid fibers under cyclic loading. The focus was on understanding the influence of both micro and macro fibers hybridization on the flexural behaviour, as compared to mono-fiber systems. The key outcomes are summarized below:

- The inclusion of micro-fibers improved load-bearing capacity and reduced residual deflection, at early loading stages and small deflections. PPS fibers outperformed

other types, with energy dissipation values 71% higher than BF fibers and 20% greater than PVA fibers at 1/600th beam deflection. This was attributed to the micro-crack bridging ability and elongation of PPS fibers. On the other hand, PVA and BF fibers displayed enhanced hysteretic damping at low deflections, which can be explained by their strong chemical bonding.

- The addition of macro-fibers improved post-peak performance by bridging macro-cracks, which was particularly beneficial during large deflection cycles. PPL fibers exhibited significantly better results compared to TPPL fibers, including an 82% increase in cumulative energy dissipation, a 99% enhancement in flexural strength, and a 160% rise in hysteretic damping. This was due to the stiffness and mechanical bonding capabilities of PPL fibers. In contrast, TPPL fibers resulted in a lower damage index throughout all cycles, which can be attributed to their enhanced distribution and greater flexibility.

- Micro-fiber hybridization has demonstrated enhanced energy dissipation performance during initial loading cycles, attributed to the synergistic effects between fibers. Conversely, a combination of micro and macro fibers showed superior improvements during larger deflection cycles. This improvement was primarily due to the complementary behaviour of micro and macro fibers, which work together to bridge larger cracks more efficiently.

- The analysis of PPS/PVA hybrid fibers highlighted a synergistic interaction, where the PVA fibers effectively bridged early-stage cracks, while the lower modulus of PPS fibers facilitated a more even distribution of stress. This interaction delayed the initiation of damage and led to an increase in the cracking strength of the composite.

- The 0.33PPS/0.66PVA hybrid mixture demonstrated enhanced performance, evidenced by a lower damage index at smaller deflections compared to the mono PPS. In addition, this hybrid mixture led to a substantial increase in the hysteretic damping ratio, outperforming the mono PVA and PPS fibers by 79% and 112%, respectively, at low deflection levels.

- The hybrid combination of 0.66TPPL and 0.33PVA fibers yielded a remarkable enhancement in deflection recovery and cumulative energy dissipation, achieving improvements of 105% and 664% over mono TPPL and PVA, respectively.

Additionally, the 0.33TPPL/0.66PVA hybrid displayed an increase in hysteretic damping by 123% and 656% in comparison to mono PVA and TPPL, respectively.

- These results highlight the enhanced bonding effect of PVA, which effectively strengthened the concrete matrix, improved crack-bridging performance, reduced residual deflection, and promoted a more elastic structural response.
- The hybridization of PPL and PVA fibers revealed that the 0.33PPL/0.66PVA combination led to a slight enhancement in ultimate strength and a notable improvement in the post-peak behaviour compared to the 0.66PPL/0.33PVA configuration.
- The 0.33PPL/0.66PVA hybrid demonstrated a 39% increase in energy dissipation at a beam deflection of 1/150th, a 260% improvement in cumulative energy dissipation, and a residual flexural strength 10.8 times higher than that of mono PVA fibers.
- In hybrid fiber systems containing micro- or macro-fibers, a reduced dosage of BF demonstrated superior cyclic performance compared to using higher BF content. This effect could be attributed to the susceptibility of BF to corrosion in SWSSC, leading to greater brittleness. Conversely, increasing the dosage of PVA fibers enhanced cyclic performance, likely due to their high chemical bonding strength.

9.2.4 Study 4: Shear performance

The mechanical, fracture, and cyclic performance studies provided foundational insights into hybrid FR-SWSSC and the synergistic effects of hybrid fibers. However, evaluating its shear strength is vital for comprehensive design applications, particularly to ensure compliance with Australian standards. No information was previously available on the shear strength of SWSSC, especially when reinforced with fibers (FR-SWSSC). Therefore, this study aimed to address this gap by developing an effective shear test method aligned with Australian standards through modifications to the JSCE-SF6 method and investigating the impact of hybrid fibers on the shear performance of FR-SWSSC. The experimental work provided insights into the shear behaviour of FR-SWSSC, supporting sustainable concrete applications, especially in coastal environments. The main outcomes are presented below:

- The synergy analysis revealed that incorporating PVA/PPS fibers significantly improved shear strength and toughness. Furthermore, the hybrid combinations of TPPL/PVA and PPL/PVA, when applied in suitable ratios, displayed positive synergistic effects, demonstrating the effective role of PVA fibers in enhancing shear performance.

- The hybrid combination of macro and micro-fibers enhanced shear strength and toughness compared to using mono-fibers alone. The 0.66TPPL/0.33PVA hybrid showed a 40% and 36% increase in shear strength, along with a 147% and 139% increase in shear toughness, compared to plain SWSS and mono PVA fibers, respectively. These enhancements were primarily due to the improved bonding strength of TPPL, facilitated by the presence of PVA fibers, which delayed the formation and propagation of shear cracks and, in turn, boosted overall shear performance.

- The hybridization of PPL and PVA fibers led to notable enhancements in both shear strength and toughness. Specifically, the combination of 0.33PPL/0.66PVA resulted in a 28% and 23% increase in shear strength, and a 159% and 46% increase in shear toughness, compared to mono PVA and PPL fibers, respectively. This improvement was attributed to the enhanced bonding strength resulting from the partial substitution of PPL fibers with PVA fibers, thereby providing superior performance in comparison to mono fiber systems.

- The inclusion of hybrid micro-fibers significantly enhanced the shear performance compared to mono-fiber systems. Specifically, the 0.66PVA/0.33BF hybrid composition demonstrated a 24% and 16% increase in shear strength over mono PVA and BF fibers, respectively. Furthermore, this hybrid combination exhibited a remarkable 98% improvement in shear toughness compared to plain SWSS and an 81% increase over the 0.33PVA/0.66BF. This enhanced performance could be attributed to the role of BF in strengthening the bonding strength of PVA fibers, thereby promoting improved shear stress distribution.

- SWSS concrete demonstrated comparable shear strength to conventional concrete, while exhibiting approximately 43% greater shear toughness. This improvement could be attributed to a denser microstructure that enhanced cohesion and interlocking strength. Among the mono-fiber types evaluated, TPPL fibers were found to be the

most effective, increasing shear strength by 38% and shear toughness by 123%. This substantial improvement was due to the enhanced stress distribution provided by TPPL fibers, which also serve to delay the propagation of cracks.

- The modified JSCE-SF6 shear test method presented in this study has proven to be an effective tool for assessing shear strength with specimen dimensions aligned with Australian standards. The performance of the modified JSCE-SF6 method in pure shear testing was influenced by several key factors, including friction between concrete and steel plates, stress concentrations near supports and notches, and prestressed forces on the supporting bolts.

9.3 Phase Ⅱ: Structural performance of GFRP-reinforced SWSSC culverts incorporating hybrid fibers

9.3.1 Study 5: Structural behaviour of small GFRP-reinforced FR-SWSSC culverts

To provide a comprehensive understanding of the structural performance of GFRP-reinforced SWSSC culverts, separate studies on small and large culverts are essential due to their distinct design requirements and applications. There was no comprehensive research available regarding the structural performance of GFRP-reinforced SWSSC culverts. Therefore, this study focused on small culverts, evaluating the performance of GFRP-reinforced concrete culverts incorporating mono- and hybrid-fibers in SWSSC. The aim was to enhance strength, ductility, and sustainability, with the key outcomes summarized below:

- All culverts primarily exhibited shear failure, characterized by a diagonal crack extending from the load point to the haunch. This was mainly due to the limited shear capacity of GFRP bars under transverse forces. The addition of fibers influenced crack propagation and enhanced structural performance beyond the peak load.

- The addition of TPPL fibers significantly enhanced the performance of SWSS culverts, increasing ultimate strength by 49.7% and energy dissipation by 47%. These improvements were notably greater than those achieved with PPL fibers, outperforming them by 31.8% in strength and 13% in energy dissipation.

- Cracking strength increased by 19.7% with TPPL fibers and 15.5% with PPL fibers. The superior performance of TPPL fibers was due to their enhanced mechanical

bonding and uniform distribution, which improved elasticity. In contrast, PPL fibers favoured a pull-out mechanism, leading to more inelastic behaviour.

- The hybridization of PPL and PVA fibers significantly enhanced the shear stress distribution of SWSS culverts, achieving a 47.1% improvement in ultimate strength compared to SWSS culverts without fiber reinforcement, and a 29.5% increase over those reinforced with mono PPL fibers.

- While TPPL-reinforced culverts exhibited slightly higher shear strength, the hybridization of PPL/PVA fibers contributed to a more uniform distribution of shear stresses, enhancing stress redistribution and crack control. This improved stress transfer mechanism reduced localized stress concentrations, resulting in a single dominant shear crack failure, as evidenced by the higher pre-peak energy dissipation observed in PPL/PVA specimens.

- The hybrid PPL/PVA specimen showed an 18% increase in cracking strength compared to the mono PPL specimen, while maintaining total energy dissipation capacity. Pre-peak energy dissipation improved by 73%, though at the cost of reduced ductility compared to the control specimen. These improvements were attributed to the higher tensile strength and strong chemical bond of PVA fibers with the concrete matrix. The combination of PVA and PPL fibers enhanced stiffness and pre-peak energy dissipation but resulted in decreased ductility.

- The hybridization of micro-fibers (PVA/BA) significantly enhanced the mechanical properties of SWSS concrete culverts. The introduction of PVA/BA fibers resulted in improvements of 29%, 49.3%, and 34% in ultimate strength, first-cracking strength, and ductility, respectively, when compared to plain SWSS concrete culverts. In addition, energy absorption and ultimate strength were increased by 14.6% and 13.6%, respectively, relative to PPL fiber reinforcement. These advancements were attributed to the synergistic interaction between PVA and BA fibers, as well as the superior strength and stiffness of BA. This combination improved stiffness, facilitated effective shear stress distribution, and enhanced the pre-peak response of the concrete culverts.

- Adding top reinforcement increased ultimate strength by up to 28% and first-cracking strength by up to 22%, but reduced ductility and energy dissipation, likely due to the increased axial stiffness from the compression reinforcement.

- The hybrid use of PPL and PVA fibers in specimens with top reinforcement significantly improved stiffness compared to using PPL fibers alone, resulting in a 15% increase in ductility and a 28% increase in energy absorption compared to specimens without top reinforcement. These findings highlight the positive effect of hybrid fibers on structural performance under compression reinforcement conditions.

- A 40% reduction in crown thickness notably compromised the strength, energy absorption, and ductility of fiber-reinforced culverts. Thicker crowns were more efficient at distributing stress, thereby enhancing fiber performance and ductility, while thinner crowns exhibited stress concentration, reducing their overall efficacy. The incorporation of TPPL fibers into thinner slabs significantly increased cracking strength, resulting in a 55% boost in total energy absorption, a sevenfold increase in post-peak energy absorption, and a 19.7% improvement in ductility compared to PPL fibers.

- Removing haunches increased the shear span, which subsequently decreased stiffness, leading to reductions in shear strength and energy absorption between 16% and 68%. However, ductility improved significantly by 32.5% to 108%, except in the case of TPPL fibers. TPPL fibers were found to achieve 14.7% greater ultimate strength and 25.7% higher cracking strength than PPL fibers, possibly due to their superior stress distribution capabilities. PVA/BA hybrid fibers showed the highest ultimate strength and stress distribution, though removing haunches reduced energy dissipation by 38% and eliminated post-peak absorption.

- An increase of 60% in concrete strength led to significant improvements in the ultimate and cracking strength of PPL-reinforced culverts, with gains of 76.3% and 78.8%, respectively, using only bottom reinforcement. This suggests that top reinforcement was more beneficial when concrete strength is lower. Higher concrete strength enhanced the bonding of PPL fibers and allowed for better compressive load absorption, reducing the need for top reinforcement. Conversely, with lower concrete strength, top reinforcement was essential for effective stress distribution and increased load-carrying capacity.

- The AASHTO equations, traditionally used to predict the shear capacity of steel-reinforced concrete box culverts through one-way crown action, were effective for small GFRP-reinforced culverts with fiber additions, although they tended to underestimate shear capacity. This underestimation likely results from the one-way crown action caused by insufficient lateral restraint. In contrast, the proposed model, which considers GFRP bars, punching shear failure, haunches, and crown thickness, provided more accurate predictions.

9.3.2 Study 6: Cyclic performance of GFRP-reinforced FR-SWSSC culverts

Building on the findings from the small culvert testing presented in the previous section, this study addresses the lack of information on the performance of large GFRP-reinforced concrete culverts under cyclic loading, particularly regarding the influence of hybrid fiber and content. To fill this gap, the shear capacity and overall performance of GFRP-reinforced SWSSC culverts, incorporating mono- and hybrid-fibers, were investigated under cyclic loading conditions. The study evaluated load capacity, post-peak behaviour, and ductility, while also comparing the performance with steel-reinforced culverts. These findings provide valuable insights into the potential of GFRP-reinforced SWSSC culverts as a sustainable and durable alternative for infrastructure applications. The key results are summarized below:

- The inclusion of fibers in GFRP-reinforced SWSS concrete culverts enhanced the ultimate shear capacity by 12% to 20%, while peak crown deflection was notably reduced by 13% to 28%. This enhancement was attributed to the improved stiffness provided by the fiber reinforcement within the concrete matrix. The fibers effectively bridged micro- and macro-cracks, which helped shift the pre-peak behaviour from nonlinear to linear, thus reducing crown deflection significantly before failure occurred.

- The incorporation of mono PPL fibers resulted in a significant enhancement of the shear strength capacity of the culvert by approximately 18%, attributed to the length and strong mechanical bonding of PPL fibers with the concrete matrix. These fibers demonstrated excellent performance under larger crown deflections by effectively bridging macro cracks, which improved the overall damage mechanism of the culvert.

Consequently, this led to a notable increase in the damping ratio and enhanced energy dissipation during cyclic loading.

- The incorporation of PVA fibers into the SWSS concrete matrix resulted in substantial improvements in interlocking and reinforcement due to the strong chemical bonding of the fibers, thereby enhancing shear strength. This enhancement was demonstrated by an approximately 14% increase in the shear capacity of the culvert. Furthermore, the ability of PVA fibers to bridge micro-cracks, combined with their robust bonding strength, significantly reduced the damage sustained by the culvert, achieving a 25% reduction in the damage index.

- The use of hybrid PPL and PVA fibers exhibited a synergistic effect, improving both the ultimate shear capacity and the damage resistance of the culvert. The PVA fibers, with their strong chemical bonding, strengthened the concrete matrix, which enhanced the effectiveness of PPL fibers in crack bridging and load bearing. This synergistic interaction was further reflected in cyclic loading conditions, showing enhanced energy dissipation and damping ratios across a wide range of crown deflections.

- The use of SWSS concrete in GFRP-reinforced culverts has demonstrably enhanced their overall performance compared to conventional concrete counterparts. The superior cohesion and interlocking properties of SWSS concrete were found to improve initial crack resistance, resulting in greater shear and tensile strength. As a result, the SWSS concrete culverts exhibited an 8% increase in ultimate shear capacity, along with a remarkable 42% improvement in peak deflection. These enhancements contributed to increased energy dissipation capacity and more effective damage mechanisms, especially at larger crown deflections.

- The steel-reinforced concrete culvert showed a 29% improvement in ultimate shear capacity compared to its GFRP counterpart, though it also experienced a 17% reduction in peak crown deflection. This behaviour could be explained by the modulus of elasticity of steel being roughly 3.3 times that of GFRP bars, contributing to enhanced stiffness in bending and lower crown deflection.

- GFRP-reinforced culvert benefited from the linear elastic behaviour of GFRP bars, which provided greater self-resetting ability at large deformations. Additionally,

despite the superior energy dissipation capacity of steel-RC culvert, the GFRP-RC culvert demonstrated better performance beyond the peak load.

- This study showed that the AASHTO shear strength equations, originally intended for one-way action in steel-reinforced concrete box culverts, can accurately predict the shear capacity of inverted U-shaped GFRP-RC culverts. The findings suggest that the inherent lack of lateral restraint in the GFRP-reinforced culverts leads to one-way behaviour in the crown slabs.

Overall, these studies demonstrate that hybrid fibers significantly enhance the mechanical and structural performance of SWSSC, addressing key limitations and challenges associated with using seawater and sea-sand in concrete production. Hybrid fiber reinforcement improves the compressive strength, ductility, fracture toughness, shear resistance, and cyclic performance of SWSS concrete, leading to better crack control and enhanced energy dissipation under various loading conditions. The synergy between different types of fibers—such as micro- and macro-fibers—promotes more efficient bonding within the concrete matrix, resulting in improved structural integrity and resilience compared to mono-fiber systems. Furthermore, hybrid fiber reinforcement enhances the load-bearing capacity and crack control of both small and large GFRP-reinforced SWSSC culverts, providing greater strength and resilience under static and cyclic loading conditions. This approach effectively compensates for the individual weaknesses of mono-fiber systems, thereby enhancing structural integrity in challenging environments compared to conventional reinforcement strategies.

9.4 Future research

The present study aimed to evaluate the impact of hybrid fiber addition on SWSSC to enhance its mechanical properties and address the limitations associated with mono-fiber use. Additionally, the structural performance of both small and large GFRP-reinforced concrete culverts incorporating mono- and hybrid-fiber reinforced SWSSC was assessed under monotonic and cyclic loading. This research requires further exploration of the following aspects:

- This study indicated that fibers in SWSS concrete, such as BF, can be susceptible to corrosion, which negatively affects compressive strength and ductility. Therefore, conducting long-term durability tests to evaluate the effects of environmental

conditions, such as exposure to seawater, freeze-thaw cycles, and chemical attack, on SWSS concrete containing hybrid fibers is essential.

- The study indicated that different combinations of fibers led to considerable improvements in compressive and residual strength. However, the total fiber content was kept constant at 0.25% for all fiber hybridizations. Investigating the effect of different total hybrid fiber dosages on the mechanical and durability properties of SWSSC is crucial to determine the optimal dosage that balances improvements in strength, toughness, and workability.

- The study employed recycled PPL fibers to improve the sustainability of hybrid FR-SWSSC but did not consider other recycled materials. Exploring the effects of recycled materials, such as recycled aggregates, rubber, and plastic, on the performance of SWSSC with and without fibers could contribute to the development of more sustainable construction materials.

- The study introduced a modified JSCE-SF6 method for shear testing but did not experimentally compare it with other methods. Conducting a comprehensive experimental evaluation of various concrete shear test methods is essential to determine the most suitable approach for assessing the shear capacity of concrete.

- The experimental studies provided valuable insights into the behaviour of hybrid FR-SWSS GFRP-reinforced culverts; however, parametric variations were not fully explored. Developing FEM models of GFRP-reinforced concrete culverts to perform parametric studies will help in understanding the effects of geometry, loading conditions, reinforcement details, and boundary conditions, thereby complementing the experimental results of this study.

- The results demonstrated the effectiveness of GFRP bars and hybrid fibers in enhancing the structural performance of culverts. A comprehensive study to develop practical design tables for GFRP-reinforced culverts, incorporating different fiber combinations, would further promote the use of GFRP and hybrid fibers in practice by providing engineers with clear, practical guidelines.

- The results did not explore the behaviour of hybrid FR-SWSSC at elevated temperatures, which is crucial for fire-prone applications. Therefore, investigating the

behaviour of hybrid FR-SWSSC at high temperatures will provide insights into its thermal stability and residual mechanical properties.

- The impact behaviour of SWSS concrete was not addressed in the study. Conducting impact testing on hybrid FR-SWSSC will help evaluate the impact resistance and energy absorption capacity of GFRP-reinforced SWSSC culverts with hybrid fibers.
- The study provided short-term experimental results; however, long-term field data is still lacking. Conducting field studies to assess the real long-term performance of SWSSC culverts reinforced with hybrid fibers and GFRP bars will provide valuable insights into their behaviour under service conditions.
- The results demonstrated improvements in SWSSC culvert performance; however, other structural elements were not investigated. Extending the investigation of hybrid fibers and FRP bars to other structural elements, such as beams, columns, and slabs, will help assess their performance in different structural configurations.
- The results highlighted the effects of reinforcement on culvert performance, but boundary conditions were not comprehensively evaluated. Performing an evaluation of boundary conditions, such as lateral support and surrounding soil properties, on the performance of FRP-reinforced concrete culverts will improve understanding of real-world culvert behaviour.
- Future research should incorporate analytical modeling, finite element simulations, and parametric studies to further investigate the structural behaviour of full-scale SWSS fiber-reinforced culverts. Additionally, developing a shear strength equation based on experimental and numerical findings would enhance predictive accuracy and optimize design parameters.

Appendix A Supplementary Information for Chapter 7

A.1 Behaviour of SWSS concrete

SWSSC material samples underwent both short-term and long-term tests (**Table A-1**). Short-term tests assessed compressive and flexural strength of 45-day-old samples, coinciding with the culvert testing date, using a 100-kN universal testing device. Long-term evaluations on 365-day-old samples utilized a 100-kN displacement control machine to evaluate compressive stress-strain behaviour, splitting tensile strength, and flexural behaviour. This included both monotonic and cyclic flexural tests, with the cyclic scheme following a seven-cycle loading regime up to 7 mm displacement (**Figure A-9-1**) (Zhang *et al.* 2021). Compressive stress-strain characteristics were determined using an 1800-kN universal testing machine at a constant displacement rate of 0.001 mm/s. Linear variable displacement transducers (LVDTs) positioned between the platens measured axial shortening during compression.

The material testing phase evaluated the mechanical properties of SWSS concrete mixtures, including compressive strength, stress-strain behaviour, splitting tensile strength, and flexural strength. This comprehensive assessment is aimed to understand the behaviour of fiber-reinforced SWSS concrete culverts from a material characteristics perspective. To account for age and investigate both short-term and long-term behaviour, concrete samples were tested at 45 days (at the time of culvert testing) and 365 days. Recognizing cyclic loading in culverts, flexural strength testing incorporated both monotonic and cyclic loading schemes to investigate fiber performance in SWSS concrete.

A.1.1 Compressive stress-strain behaviour

Figure A-9-2 depicts the compressive strength results of fiber-reinforced SWSS (FR-SWSS) concrete. Fiber incorporation significantly enhanced short-term compressive strength (f_{cm}) compared to plain SWSS concrete. This enhancement was attributed to the ability of fibers to bridge micro-cracks, enhance interlocking strength, and facilitate even stress distribution within the concrete matrix. TPPL fibers exhibited the most pronounced effect, increasing f_{cm} by 19% after 45 days, primarily due to their superior distribution

and flexibility compared to PPL fibers, enabling a more effective fiber-matrix bond. Hybridization of micro- and macro-fibers (PPL/PVA) and micro-fibers (PVA/BA) also improved f_{cm} by 10% and 16%, respectively, attributed to the synergistic effects of enhanced bonding strength when combined. Previous study revealed that the chemical bonding of PVA fibers significantly improved the bond between PPL and BA with SWSS concrete (Mashayekhi *et al.* 2024a). These findings suggest that combining fibers with different properties can provide synergistic benefits in SWSS concrete. PPL fibers uniquely maintained f_{cm} after 365 days, increasing by 5.5%, indicating their effectiveness in preserving long-term strength of SWSS concrete. Among TPPL, PPL/PVA, and PVA/BA, TPPL fibers exhibited the greatest reduction in long-term compressive strength, decreasing by 6.4%, likely due to bond degradation and increased porosity.

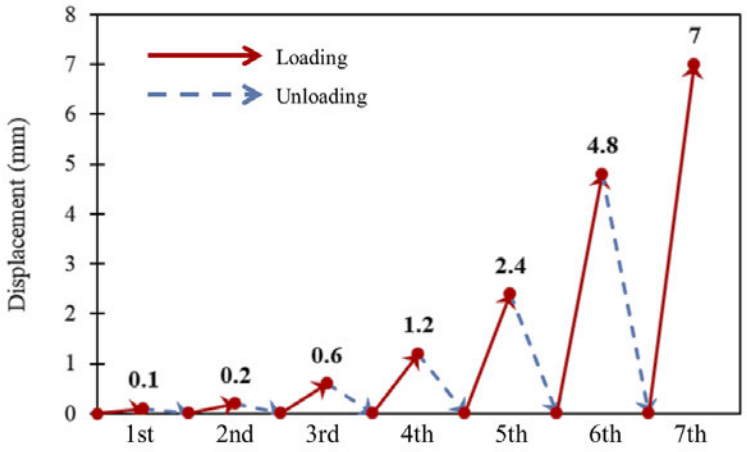


Figure A-9-1 Cyclic loading regime used in flexural testing.

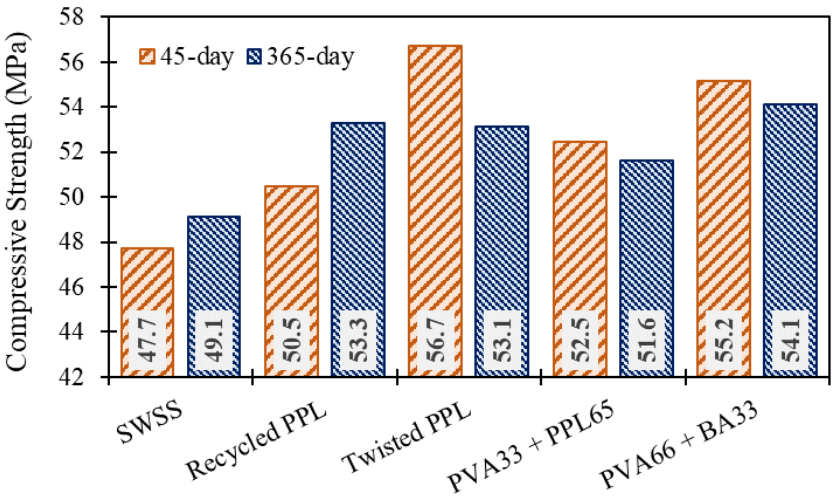
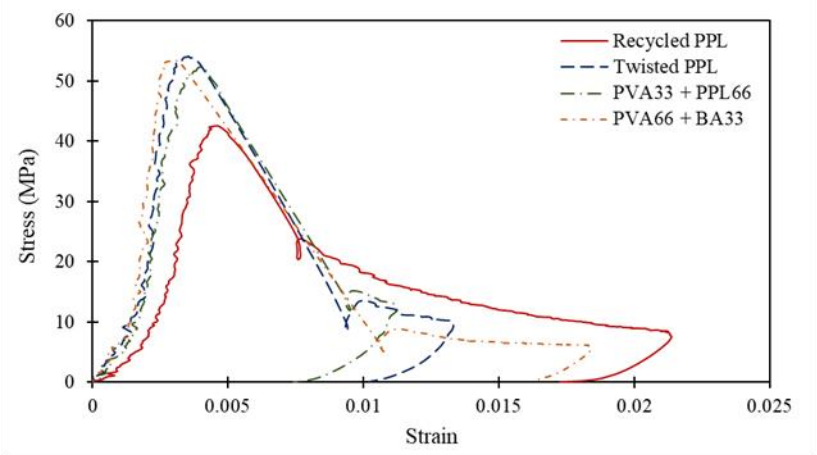


Figure A-9-2 Compressive strength of concrete samples.

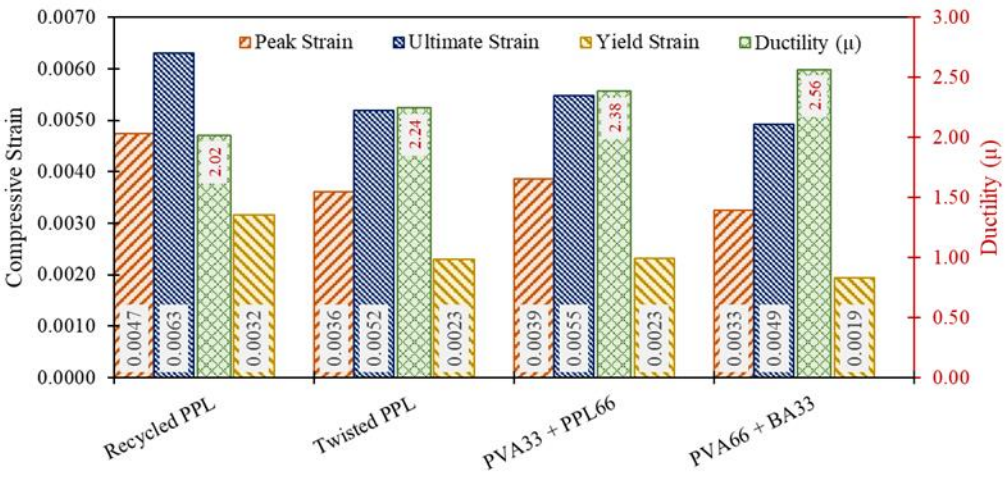
The compressive stress-strain behaviour of 365-day samples (**Figure A-9-3**) revealed that PPL fiber exhibited higher strain capacity, but lower ductility (μ) compared to other investigated fibers. This can be attributed to the lower modulus of elasticity of PPL fibers, which promoted inelastic behaviour over elastic behaviour. Notably, the superior flexibility and distribution of TPPL fibers resulted in an 11% increase in ductility. PVA/BA hybridization demonstrated the lowest strain values but the highest toughness, owing to its ability to bridge micro-cracks and dissipate energy effectively. Furthermore, PV/BA hybridization exhibited the greatest ductility, attributed to its enhanced stiffness during pre-peak behaviour and reduced yielding strain. This contributed to improved inelastic behaviour through the transition from the yielding point to the ultimate point. Partial replacement of PPL fibers with PVA fibers resulted in lower strain values but increased ductility, presumably due to the enhanced crack-bridging ability of PVA fiber and contribution to inelastic behaviour. However, this replacement negatively impacted post-peak toughness, likely due to the reduced content of PPL fibers and the higher modulus of elasticity of PVA fibers, which favoured elastic behaviour. Nevertheless, the hybrid PPL/PVA combination achieved an 18% increase in ductility, highlighting the effectiveness of PVA fibers in improving inelastic behaviour and crack-bridging capabilities.

A.1.2 Splitting tensile strength

The tensile strength results of 365-day samples are presented in **Figure A-9-4**. The incorporation of fibers significantly enhanced the tensile strength (f_{st}) of SWSS concrete. The addition of PPL and TPPL fibers increased f_{st} by 12% and 14%, respectively, compared to plain SWSS concrete. TPPL fibers exhibited superior distribution, flexibility, and bonding strength compared to PPL fibers, enabling them to bridge cracks and provide reinforcement in multiple directions. SEM images in **Figure A-9-5** demonstrate the stronger fiber-matrix bond of TPPL fibers. PPL/PVA hybridization resulted in a 17% increase in f_{st}, while PVA/BA hybridization improved f_{st} by 10%. Hybrid PPL/PVA provided both strength and toughness due to enhanced bonding strength of PPL fibers facilitated by PVA fibers. PVA/BA hybridization provided a balance of strength and ductility, with BA fibers contributing strength and PVA fibers enhancing ductility. PVA fibers also improved the bonding strength of BA fibers in SWSS concrete.



(a)



(b)

Figure A-9-3 Compressive behaviour of FR-SWSS concrete: a) stress-strain curves and b) key parameters (e.g., strain values and ductility).

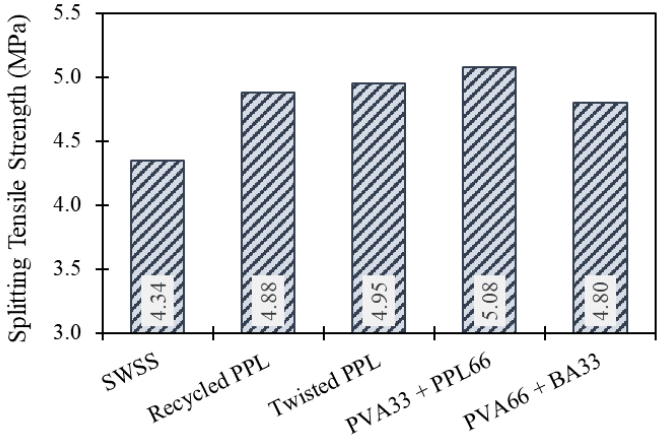


Figure A-9-4 Splitting tensile strength of concrete samples.

A.1.3 Flexural strength

The inclusion of fibers significantly enhanced the modulus of rupture (MOR) of SWSS concrete, as demonstrated in **Figure A-9-6**. Macro-fibers, PPL and TPPL, exhibited the most notable improvement, with increases in 45-day/365-day MOR of 11%/45% and 26%/61%, respectively, compared to plain SWSS. PPL/PVA and PVA/BA hybrids offered moderate increases (15%/17% and 23%/14%). This enhancement was attributed to the effective crack bridging of macro-fibers, evidenced by a substantial long-term energy absorption increase (PPL: 31 times, TPPL: 30 times). The superior distribution and flexibility of TPPL fibers further enhanced reinforcement, while the higher tensile strength of PPL fibers contributed to greater energy absorption.

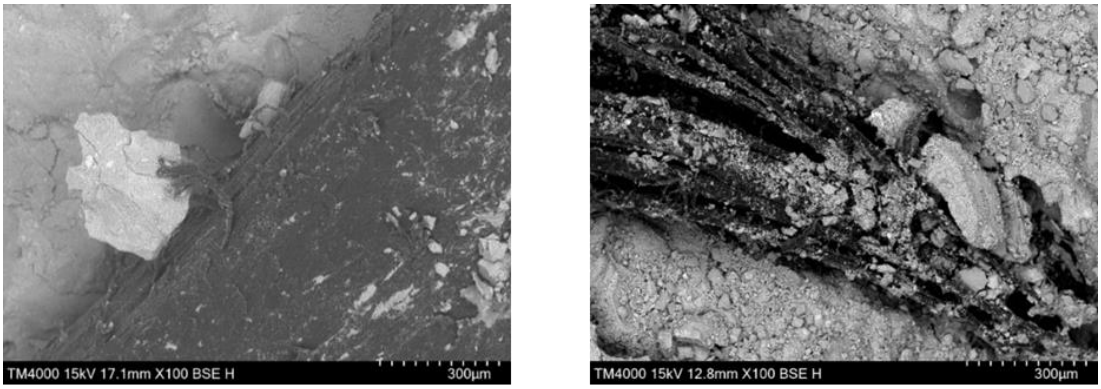


Figure A-9-5 Visualizing the bonding of PPL and TPPL fibers in SWSS concrete through SEM images.

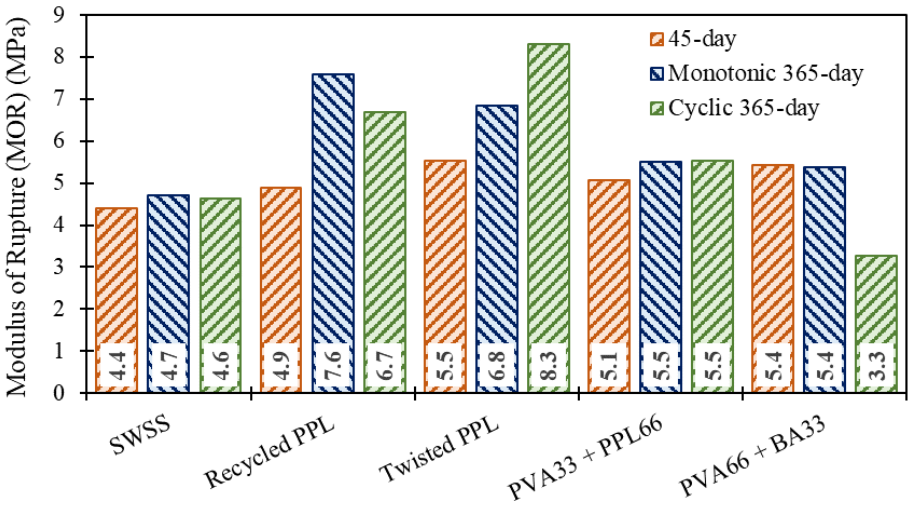


Figure A-9-6 Modulus of rupture values of concrete samples under flexural test.

Table A-1 Material level test methods used to determine concrete mechanical properties.

Sample age	Target properties	Method	Testing type	Sample shape	Sample dim. (mm)	Test setup
Short-term 45-day	Compressive strength	AS 1012.9	Load-control	Cylinder	100×200	
	Flexural strength	AS 1012.11	Load-control	Prism	100×100×350	
Long-term 365-day	Flexural strength	AS 1012.11	Monotonic displacement-control Cyclic displacement-control	Prism	100×100×350	
	Compressive stress-strain	RILEM (Committee 1970)	Displacement-control	Cylinder	100×200	
	Splitting tensile strength	AS 1012.10	Load-control	Cylinder	100×200	

The long-term increase in compressive strength of SWSS concrete further improved macro-fiber bonding, leading to significant flexural strength enhancement. Notably, PPL/PVA hybridization resulted in a remarkable 95.7 kN.mm of energy absorption, 26 times that of plain SWSS concrete. PVA/BA hybridization also improved energy absorption by 44%. While PPL/PVA hybridization, due to reduced PPL content, displayed lower flexural strength and energy absorption, the PVA fibers enhanced the bonding strength of PPL fibers.

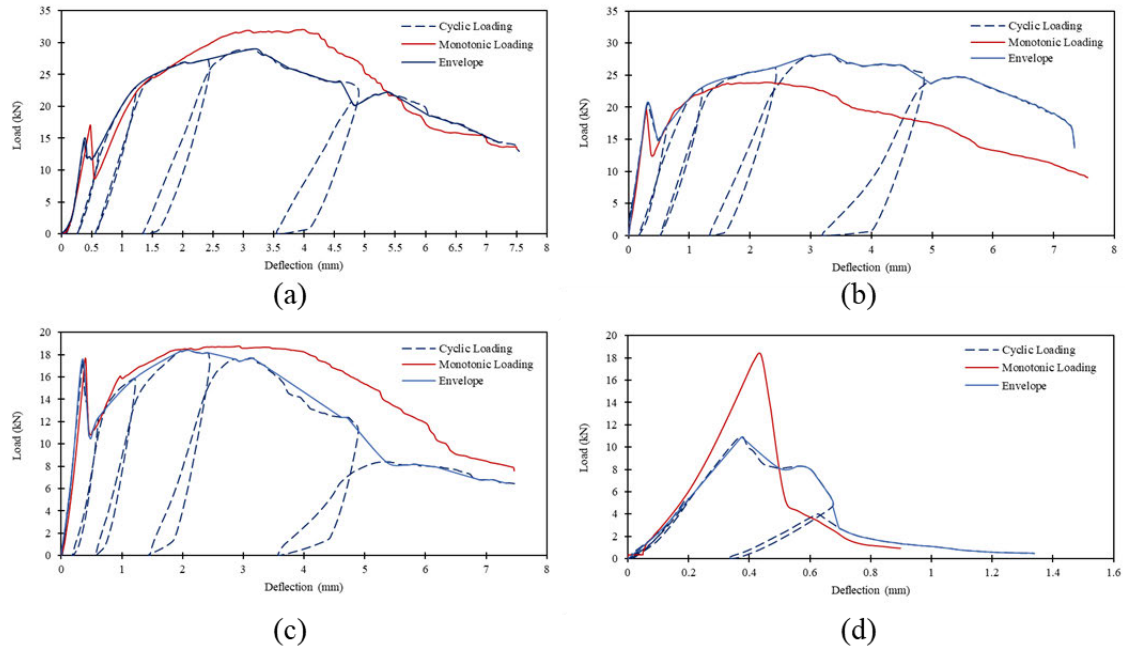


Figure A-9-7 Comparison between flexural behaviour of a) PPL, b) TPPL, c) hybrid PPL/PVA, and d) hybrid PVA/BF under monotonic and cyclic loading.

Fiber performance diverged under monotonic and cyclic loading (**Figure A-9-7**). As shown in **Figure A-9-8**, TPPL fibers demonstrated superior energy absorption under cyclic loading, as calculated by the area under the backbone curves. In this case, TPPL fibers outperformed PPL fibers by 15% in terms of energy absorption. This advantage stemmed from its superior flexibility, more even distribution, and stronger matrix bond, which facilitated efficient stress transfer and microcrack bridging. Conversely, PPL fibers, with their inherent rigidity and high tensile strength, dominated under monotonic loading in terms of flexural strength. Partial replacement of PPL fibers with PVA, however, enhanced bonding, leading to comparable performance under both loading regimes. Hybrid PVA/BA exhibited higher MOR under monotonic loading but

demonstrated superior ductility under cyclic loading, attributable to fiber rupture and pull-out.

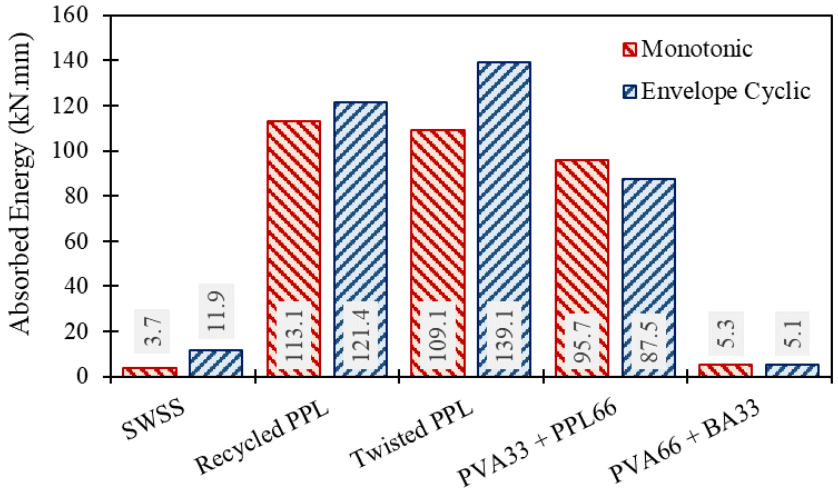


Figure A-9-8 Energy absorption under monotonic and cyclic flexural tests.

Appendix B Copyright permissions

B.1 Copyright permission for Chapter 3

Mashayekhi, A, Hassanli, R, Zhuge, Y, Ma, X & Chow, CW 2024a, 'Synergistic effects of fiber hybridization on the mechanical performance of seawater sea-sand concrete', Construction and Building Materials, vol. 416, p. 135087.

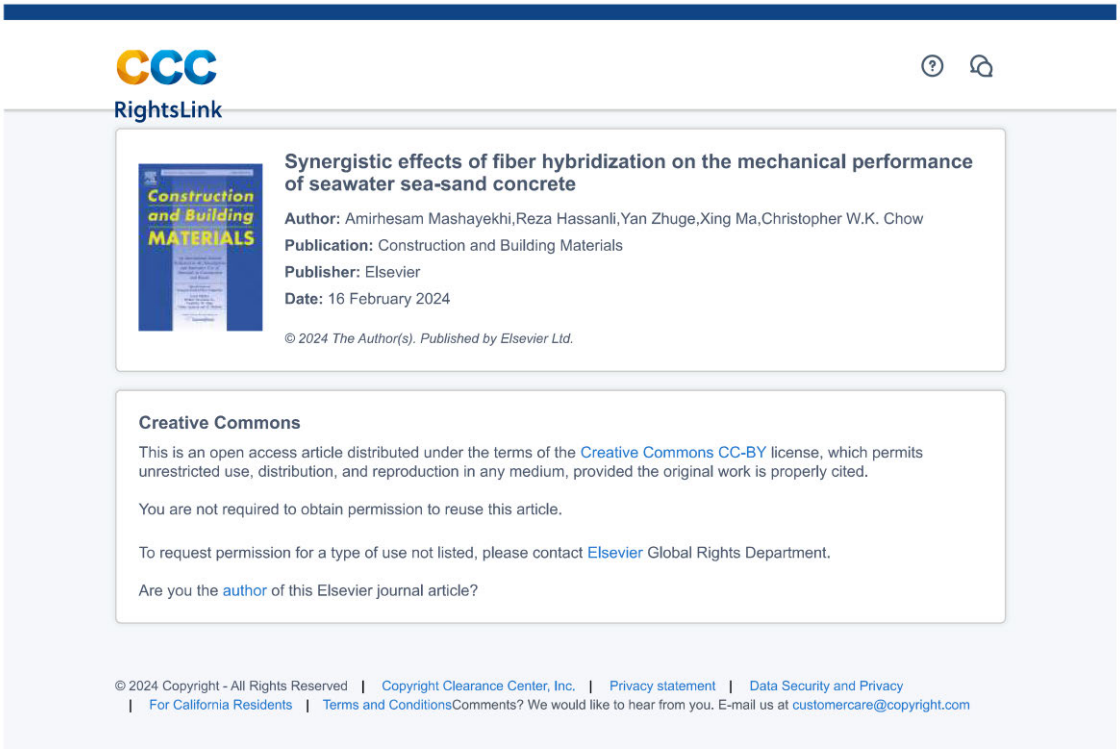


Figure B-1 Copyright permission for Chapter 3.

B.2 Copyright permission for Chapter 4

Mashayekhi, A, Hassanli, R, Zhuge, Y, Ma, X, Chow, CW, Bazli, M & Manalo, A 2024c, 'Synergistic effects of fiber hybridization on the fracture toughness of seawater sea-sand concrete', Construction and Building Materials, vol. 444, p. 137845.



Figure B-2 Copyright permission for Chapter 4.

B.3 Copyright permission for Chapter 5

Mashayekhi, A, Hassanli, R, Zhuge, Y, Ma, X, Chow, CW, Bazli, M & Manalo, A 2024d, 'Cyclic flexural performance of seawater sea-sand concrete reinforced with hybrid fibers', Construction and Building Materials, vol. 449, p. 138480.

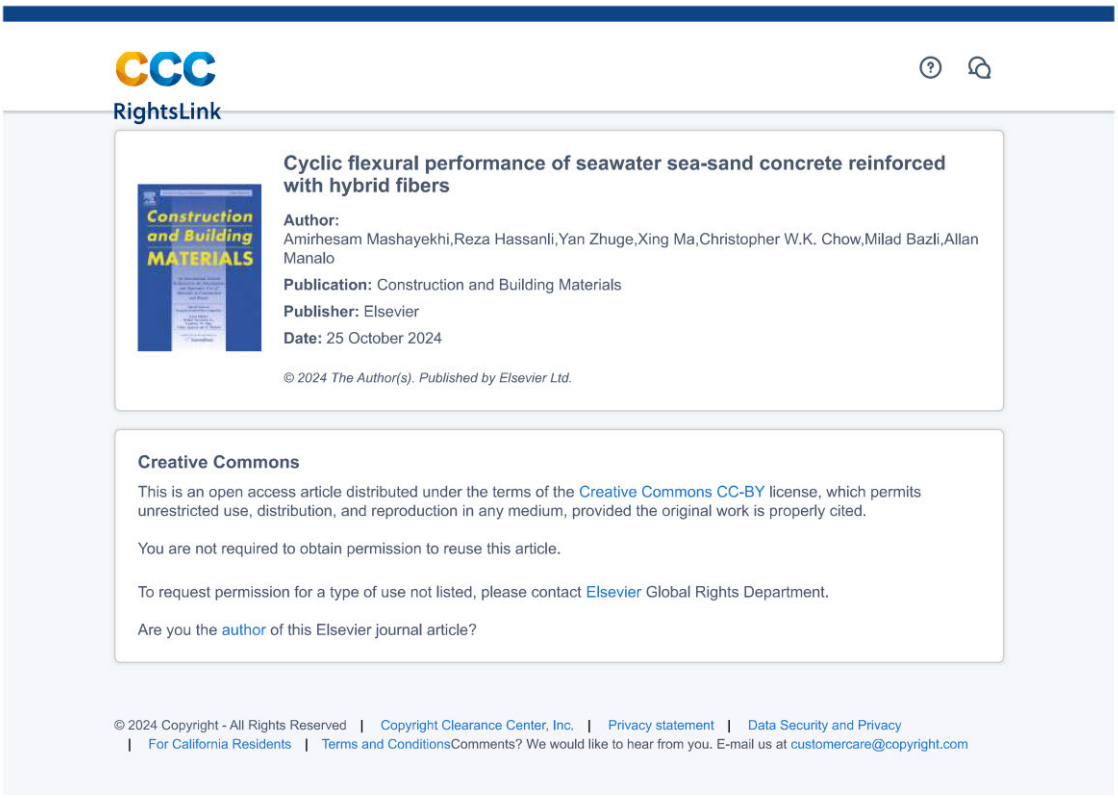


Figure B-3 Copyright permission for Chapter 5.

B.4 Copyright permission for Chapter 7

Mashayekhi, A, Hassanli, R, Zhuge, Y, Ma, X, W. K. Chow, C, Bazli, M & Manalo, A 2024, 'Structural behaviour of small GFRP-reinforced seawater sea-sand fiber reinforced concrete culverts', Structures, vol. 69, p. 107492.



Figure B-4 Copyright permission for Chapter 7.

B.5 Copyright permission for Chapter 8

Amirhesam, M, Reza, H, Yan, Z, Xing, M, Christopher, WKC, Milad, B & Allan, M 2025, 'Cyclic performance of GFRP-reinforced seawater sea-sand concrete culverts reinforced with synthetic fibers', Structures, vol. 72, p. 108262.



Figure B-5 Copyright permission for Chapter 8.

Appendix C Statements of authorship

University of South Australia

Statement of Authorship

Title of Paper	Cyclic flexural performance of seawater sea-sand concrete reinforced with hybrid fibers
Publication Status	■ Published ☐ Accepted for Publication ☐ Submitted for Publication ☐ Unpublished and Unsubmitted work written in manuscript style
Publication Details Relevant reference details	Construction and Building Materials 449 (2024) 138480 https://doi.org/10.1016/j.conbuildmat.2024.138480
PRINCIPAL AUTHOR	
Name of Principal Author (Candidate)	Amirhesam Mashayekhi
Contribution to the Paper Brief description of your work in this publication	– Conceptualized the research objectives and designed the experimental study. – Prepared and set up the experimental apparatus for the study. – Conducted a comprehensive series of tests and ensured accurate data collection. – Analyzed experimental data and interpreted results to derive meaningful insights. – Presenting the experimental methodology and results.
Overall Percentage (%)	75%
Certification	This paper reports on original research I conducted during the period of my Higher Degree by Research candidature and is not subject to any obligations or contractual agreements with a third party that would constrain its inclusion in this thesis. I am the primary author of this paper.
Signature *Signatures will be redacted by the Library at the time of publication*	[redacted] Date 5-Dec-24
CO-AUTHOR CONTRIBUTIONS	
By signing the Statement of Authorship, each author certifies that: I. the candidate's stated contribution to the publication is accurate (as detailed above); II. permission is granted for the candidate in include the publication in the thesis; and III. the sum of all co-author contribution is equal to 100% less the candidate's stated contribution.	
Name of Co-Author 1	Reza Hassanli

The University of South Australia

www.unisa.edu.au
CRICOS Provider No. 00121B

Last updated: May 2023

University of South Australia

% Contribution to the Paper	10%	
Signature *Signatures will be redacted by the Library at the time of publication*	[redacted]	Date 06/12/2024
Name of Co-Author 2	Yan Zhuge	
% Contribution to the Paper	3%	
Signature *Signatures will be redacted by the Library at the time of publication*	[redacted]	Date 13/12/2024
Name of Co-Author 3	Xing Ma	
% Contribution to the Paper	3%	
Signature *Signatures will be redacted by the Library at the time of publication*	[redacted]	Date
Name of Co-Author 4	Christopher W.K. Chow	
% Contribution to the Paper	3%	
Signature *Signatures will be redacted by the Library at the time of publication*	[redacted]	Date
Name of Co-Author 5	Milad Bazli	
% Contribution to the Paper	3%	
Signature *Signatures will be redacted by the Library at the time of publication*	[redacted]	Date
Name of Co-Author 6	Allan Manalo	
% Contribution to the Paper	3%	
Signature *Signatures will be redacted by the Library at the time of publication*	[redacted]	Date
Name of Co-Author 7		
% Contribution to the Paper		

The University of South Australia
www.unisa.edu.au
CRICOS Provider No. 00121B

University of South Australia

Statement of Authorship

Title of Paper	Structural behaviour of small GFRP-reinforced seawater sea-sand fiber reinforced concrete culverts
Publication Status	■ Published ☐ Accepted for Publication ☐ Submitted for Publication ☐ Unpublished and Unsubmitted work written in manuscript style
Publication Details Relevant reference details	Structures 69 (2024) 107492 https://doi.org/10.1016/j.istruc.2024.107492
PRINCIPAL AUTHOR	
Name of Principal Author (Candidate)	Amirhesam Mashayekhi
Contribution to the Paper Brief description of your work in this publication	– Conceptualized the research objectives and designed the experimental study. – Prepared and set up the experimental apparatus for the study. – Conducted a comprehensive series of tests and ensured accurate data collection. – Analyzed experimental data and interpreted results to derive meaningful insights. – Presenting the experimental methodology and results.
Overall Percentage (%)	75%
Certification	This paper reports on original research I conducted during the period of my Higher Degree by Research candidature and is not subject to any obligations or contractual agreements with a third party that would constrain its inclusion in this thesis. I am the primary author of this paper.
Signature *Signatures will be redacted by the Library at the time of publication*	[redacted] Date 5-Dec-24
CO-AUTHOR CONTRIBUTIONS	
By signing the Statement of Authorship, each author certifies that: I. the candidate's stated contribution to the publication is accurate (as detailed above); II. permission is granted for the candidate in include the publication in the thesis; and III. the sum of all co-author contribution is equal to 100% less the candidate's stated contribution.	
Name of Co-Author 1	Reza Hassanli

University of South Australia

% Contribution to the Paper	10%	
Signature *Signatures will be redacted by the Library at the time of publication*	[redacted]	Date 06/12/2024
Name of Co-Author 2	Yan Zhuge	
% Contribution to the Paper	3%	
Signature *Signatures will be redacted by the Library at the time of publication*	[redacted]	Date 13/12/2024
Name of Co-Author 3	Xing Ma	
% Contribution to the Paper	3%	
Signature *Signatures will be redacted by the Library at the time of publication*	[redacted]	Date 13/12/24
Name of Co-Author 4	Christopher W.K. Chow	
% Contribution to the Paper	3%	
Signature *Signatures will be redacted by the Library at the time of publication*	[redacted]	Date 11/12/24
Name of Co-Author 5	Milad Bazli	
% Contribution to the Paper	3%	
Signature *Signatures will be redacted by the Library at the time of publication*	[redacted]	Date 7/12/24
Name of Co-Author 6	Allan Manalo	
% Contribution to the Paper	3%	
Signature *Signatures will be redacted by the Library at the time of publication*	[redacted]	Date 11/12/24
Name of Co-Author 7		
% Contribution to the Paper		

The University of South Australia
www.unisa.edu.au
CRICOS Provider No. 00121B

University of South Australia

Statement of Authorship

Title of Paper	Synergistic effects of fiber hybridization on the fracture toughness of seawater sea-sand concrete
Publication Status	■ Published ☐ Accepted for Publication ☐ Submitted for Publication ☐ Unpublished and Unsubmitted work written in manuscript style
Publication Details Relevant reference details	Construction and Building Materials 444 (2024) 137845 https://doi.org/10.1016/j.conbuildmat.2024.137845
PRINCIPAL AUTHOR	
Name of Principal Author (Candidate)	Amirhesam Mashayekhi
Contribution to the Paper Brief description of your work in this publication	– Conceptualized the research objectives and designed the experimental study. – Prepared and set up the experimental apparatus for the study. – Conducted a comprehensive series of tests and ensured accurate data collection. – Analyzed experimental data and interpreted results to derive meaningful insights. – Presenting the experimental methodology and results.
Overall Percentage (%)	75%
Certification	This paper reports on original research I conducted during the period of my Higher Degree by Research candidature and is not subject to any obligations or contractual agreements with a third party that would constrain its inclusion in this thesis. I am the primary author of this paper.
Signature *Signatures will be redacted by the Library at the time of publication*	[redacted] Date 5-Dec-24
CO-AUTHOR CONTRIBUTIONS	
By signing the Statement of Authorship, each author certifies that: I. the candidate's stated contribution to the publication is accurate (as detailed above); II. permission is granted for the candidate in include the publication in the thesis; and III. the sum of all co-author contribution is equal to 100% less the candidate's stated contribution.	
Name of Co-Author 1	Reza Hassanli

University of South Australia

% Contribution to the Paper	10%	
Signature *Signatures will be redacted by the Library at the time of publication*	[redacted]	Date 06/12/2024
Name of Co-Author 2	Yan Zhuge	
% Contribution to the Paper	3%	
Signature *Signatures will be redacted by the Library at the time of publication*	[redacted]	Date 13/12/2024
Name of Co-Author 3	Xing Ma	
% Contribution to the Paper	3%	
Signature *Signatures will be redacted by the Library at the time of publication*	[redacted]	Date 13/12/24
Name of Co-Author 4	Christopher W.K. Chow	
% Contribution to the Paper	3%	
Signature *Signatures will be redacted by the Library at the time of publication*	[redacted]	Date 11/12/24
Name of Co-Author 5	Milad Bazli	
% Contribution to the Paper	3%	
Signature *Signatures will be redacted by the Library at the time of publication*	[redacted]	Date 7/12/24
Name of Co-Author 6	Allan Manalo	
% Contribution to the Paper	3%	
Signature *Signatures will be redacted by the Library at the time of publication*	[redacted]	Date 11/12/24
Name of Co-Author 7		
% Contribution to the Paper		

The University of South Australia
www.unisa.edu.au
CRICOS Provider No. 00121B

University of South Australia

Statement of Authorship

Title of Paper	Synergistic effects of fiber hybridization on the mechanical performance of seawater sea-sand concrete
Publication Status	■ Published ☐ Accepted for Publication ☐ Submitted for Publication ☐ Unpublished and Unsubmitted work written in manuscript style
Publication Details Relevant reference details	Construction and Building Materials 416 (2024) 135087 https://doi.org/10.1016/j.conbuildmat.2024.135087
PRINCIPAL AUTHOR	
Name of Principal Author (Candidate)	Amirhesam Mashayekhi
Contribution to the Paper Brief description of your work in this publication	– Conceptualized the research objectives and designed the experimental study. – Prepared and set up the experimental apparatus for the study. – Conducted a comprehensive series of tests and ensured accurate data collection. – Analyzed experimental data and interpreted results to derive meaningful insights. – Presenting the experimental methodology and results.
Overall Percentage (%)	75%
Certification	This paper reports on original research I conducted during the period of my Higher Degree by Research candidature and is not subject to any obligations or contractual agreements with a third party that would constrain its inclusion in this thesis. I am the primary author of this paper.
Signature *Signatures will be redacted by the Library at the time of publication*	[redacted] Date 5-Dec-24
CO-AUTHOR CONTRIBUTIONS	
By signing the Statement of Authorship, each author certifies that: I. the candidate's stated contribution to the publication is accurate (as detailed above); II. permission is granted for the candidate in include the publication in the thesis; and III. the sum of all co-author contribution is equal to 100% less the candidate's stated contribution.	
Name of Co-Author 1	Reza Hassanli

University of South Australia

% Contribution to the Paper	10%	
Signature *Signatures will be redacted by the Library at the time of publication*	[redacted]	Date 06/12/2024
Name of Co-Author 2	Yan Zhuge	
% Contribution to the Paper	5%	
Signature *Signatures will be redacted by the Library at the time of publication*	[redacted]	Date 13/12/2024
Name of Co-Author 3	Xing Ma	
% Contribution to the Paper	5%	
Signature *Signatures will be redacted by the Library at the time of publication*	[redacted]	Date 13/12/24
Name of Co-Author 4	Christopher W.K. Chow	
% Contribution to the Paper	5%	
Signature *Signatures will be redacted by the Library at the time of publication*	[redacted]	Date 11/12/24
Name of Co-Author 5		
% Contribution to the Paper		
Signature *Signatures will be redacted by the Library at the time of publication*		Date
Name of Co-Author 6		
% Contribution to the Paper		
Signature *Signatures will be redacted by the Library at the time of publication*		Date
Name of Co-Author 7		
% Contribution to the Paper		

University of South Australia

Statement of Authorship

Title of Paper	Cyclic performance of GFRP-reinforced seawater sea-sand concrete culverts reinforced with synthetic fibers
Publication Status	☒ Published ☐ Accepted for Publication ☐ Submitted for Publication ☐ Unpublished and Unsubmitted work written in manuscript style
Publication Details Relevant reference details	Structures 72 (2025) 108262 https://doi.org/10.1016/j.istruc.2025.108262
PRINCIPAL AUTHOR	
Name of Principal Author (Candidate)	Amirhesam Mashayekhi
Contribution to the Paper Brief description of your work in this publication	– Conceptualized the research objectives and designed the experimental study. – Prepared and set up the experimental apparatus for the study. – Conducted a comprehensive series of tests and ensured accurate data collection. – Analyzed experimental data and interpreted results to derive meaningful insights. – Presenting the experimental methodology and results.
Overall Percentage (%)	75%
Certification	This paper reports on original research I conducted during the period of my Higher Degree by Research candidature and is not subject to any obligations or contractual agreements with a third party that would constrain its inclusion in this thesis. I am the primary author of this paper.
Signature *Signatures will be redacted by the Library at the time of publication*	[redacted] Date 5-Dec-24
CO-AUTHOR CONTRIBUTIONS	
By signing the Statement of Authorship, each author certifies that: I. the candidate's stated contribution to the publication is accurate (as detailed above); II. permission is granted for the candidate in include the publication in the thesis; and III. the sum of all co-author contribution is equal to 100% less the candidate's stated contribution.	
Name of Co-Author 1	Reza Hassanli

University of South Australia

% Contribution to the Paper	10%	
Signature *Signatures will be redacted by the Library at the time of publication*	[redacted]	Date 6/12/2024
Name of Co-Author 2	Yan Zhuge	
% Contribution to the Paper	3%	
Signature *Signatures will be redacted by the Library at the time of publication*	[redacted]	Date 13/12/2024
Name of Co-Author 3	Xing Ma	
% Contribution to the Paper	3%	
Signature *Signatures will be redacted by the Library at the time of publication*	[redacted]	Date 13/12/24
Name of Co-Author 4	Christopher W.K. Chow	
% Contribution to the Paper	3%	
Signature *Signatures will be redacted by the Library at the time of publication*	[redacted]	Date 11/12/24
Name of Co-Author 5	Milad Bazli	
% Contribution to the Paper	3%	
Signature *Signatures will be redacted by the Library at the time of publication*	[redacted]	Date 7/12/24
Name of Co-Author 6	Allan Manalo	
% Contribution to the Paper	3%	
Signature *Signatures will be redacted by the Library at the time of publication*	[redacted]	Date 11/12/24
Name of Co-Author 7		
% Contribution to the Paper		

The University of South Australia
www.unisa.edu.au
CRICOS Provider No. 00121B

University of South Australia

Statement of Authorship

Title of Paper	Shear performance of fibre reinforced seawater sea-sand concrete - fibre hybridization and synergy effects
Publication Status	☐ Published ☐ Accepted for Publication ☒ Submitted for Publication ☐ Unpublished and Unsubmitted work written in manuscript style
Publication Details Relevant reference details	Construction and Building Materials
PRINCIPAL AUTHOR	
Name of Principal Author (Candidate)	Amirhesam Mashayekhi
Contribution to the Paper Brief description of your work in this publication	– Conceptualized the research objectives and designed the experimental study. – Prepared and set up the experimental apparatus for the study. – Conducted a comprehensive series of tests and ensured accurate data collection. – Analyzed experimental data and interpreted results to derive meaningful insights. – Presenting the experimental methodology and results.
Overall Percentage (%)	75%
Certification	This paper reports on original research I conducted during the period of my Higher Degree by Research candidature and is not subject to any obligations or contractual agreements with a third party that would constrain its inclusion in this thesis. I am the primary author of this paper.
Signature *Signatures will be redacted by the Library at the time of publication*	[redacted] Date 5-Dec-24
CO-AUTHOR CONTRIBUTIONS	
By signing the Statement of Authorship, each author certifies that: I. the candidate's stated contribution to the publication is accurate (as detailed above); II. permission is granted for the candidate in include the publication in the thesis; and III. the sum of all co-author contribution is equal to 100% less the candidate's stated contribution.	
Name of Co-Author 1	Reza Hassanli

University of South Australia

% Contribution to the Paper	10%	
Signature *Signatures will be redacted by the Library at the time of publication*	[redacted]	Date: 06/12/2024
Name of Co-Author 2	Yan Zhuge	
% Contribution to the Paper	3%	
Signature *Signatures will be redacted by the Library at the time of publication*	[redacted]	Date 13/12/2024
Name of Co-Author 3	Xing Ma	
% Contribution to the Paper	3%	
Signature *Signatures will be redacted by the Library at the time of publication*	[redacted]	Date 13/12/24
Name of Co-Author 4	Christopher W.K. Chow	
% Contribution to the Paper	3%	
Signature *Signatures will be redacted by the Library at the time of publication*	[redacted]	Date 11/12/24
Name of Co-Author 5	Milad Bazli	
% Contribution to the Paper	3%	
Signature *Signatures will be redacted by the Library at the time of publication*	[redacted]	Date 7/12/24
Name of Co-Author 6	Allan Manalo	
% Contribution to the Paper	3%	
Signature *Signatures will be redacted by the Library at the time of publication*	[redacted]	Date 11/12/24
Name of Co-Author 7		
% Contribution to the Paper		